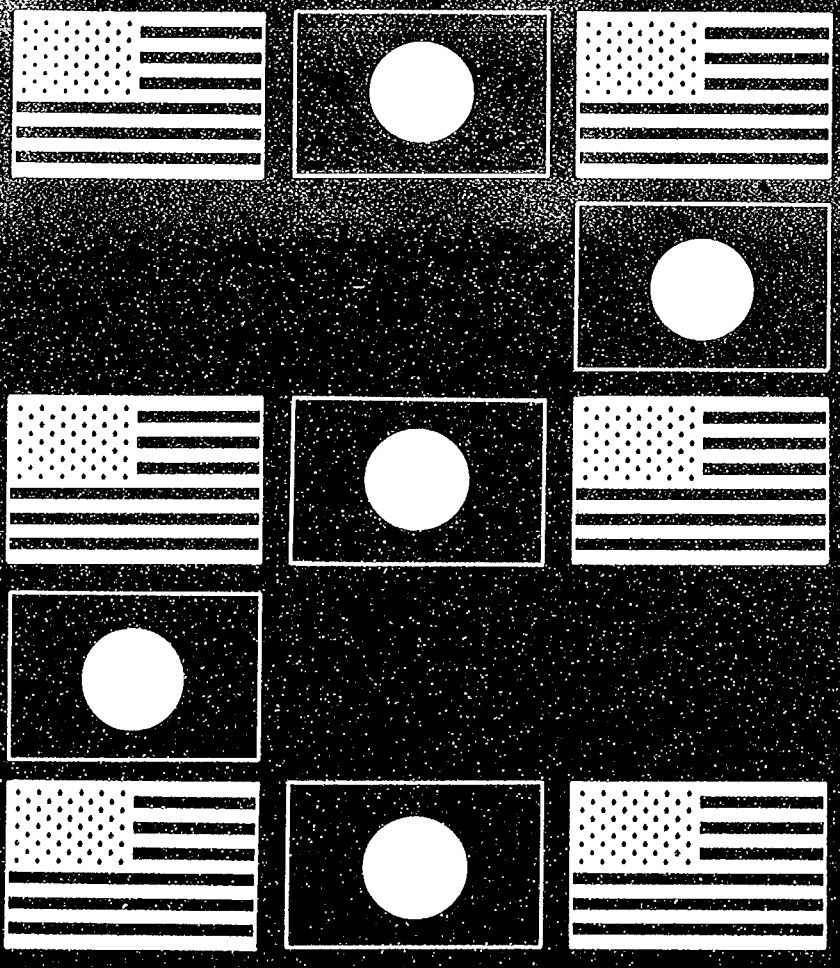
ISSN 0386-5878
Technical Memorandum
of PWRI No. 3196

THE SECOND U.S.-JAPAN WORKSHOP ON EARTHQUAKE PROTECTIVE SYSTEMS FOR BRIDGES



DECEMBER 7-8, 1992
PUBLIC WORKS RESEARCH INSTITUTE
TSUKUBA SCIENCE CITY, JAPAN

Copyright © (1993) by P. W. R. I.

All rights reserved. No part of this book may be reproduced by any means, nor transmitted, nor translated into a machine language without the written permission of the Director General of P. W. R. I.

この報告書は，土木研究所長の承認を得て刊行したものである。したがって，本報告書の全部又は一部の転載，複製は，土木研究所長の文書による承認を得ずしてこれを行ってはならない。

Technical Memorandum
of PWRI No. 3196

PROCEEDING OF THE SECOND U.S.-JAPAN WORKSHOP ON EARTHQUAKE PROTECTIVE SYSTEMS FOR BRIDGES

DECEMBER 7 AND 8, 1992
PUBLIC WORKS RESEARCH INSTITUTE
TSUKUBA SCIENCE CITY, JAPAN

by
Kazuhiko KAWASHIMA
Shigeki UNJOH
Hiroyuki IIDA
and
Hidetoshi MUKAI

Synopsis:

This proceedings document the results of the Second U.S.-Japan Workshop on Earthquake Protective Systems for Bridges. The workshop was held at PWRI in Tsukuba Science City, Japan, between December 7 and 8, 1992, and was organized by the task Committee G "Passive, Active and Hybrid Control Systems", Panel on Wind and Seismic Effects, UJNR.

Key word: Earthquake Protective Systems, Bridges, Passive, Active and Hybrid Control, UJNR

FORWARD

This proceedings documents the results of the Second U.S.-Japan Workshop on Earthquake Protective Systems for Bridges which was held at the Public Works Research Institute, Tsukuba Science City, Japan, on December 7 and 8, 1992 under the auspices of the Panel on Wind and Seismic Effects, UJNR. The Workshop was organized by the Task Committee G "Passive, Active and Hybrid Control Systems" of the Panel. The Workshop was coordinated by Dr. I. Buckle, Deputy Director, National Center for Earthquake Engineering Research, State University of New York at Buffalo, and Dr. K. Kawashima, Head of Earthquake Engineering Division of the Public Works Research Institute, Ministry of Construction.

The aims of the Workshop were : (1) to bring together experts from both countries to exchange technical information on current research and practical efforts being made in the area of earthquake protective systems for bridges, and (2) to identify future needs and opportunities between the two countries for cooperative research.

A broad range of special technical topics were presented at the Workshop. These included :

- ○ Testing of Seismic Isolation Hardware
- ○ Seismic Isolation Design
- ○ Design Applications
- ○ Dynamic Characteristics of Base-Isolated Bridges
- ○ Active and Hybrid Control for Bridges
- ○ Comparative Design Example

In total, thirty-three papers were presented in the two days of plenary sessions ; 22 papers from Japan, 10 papers from the United States, and 1 paper from New Zealand.

The material in the proceedings includes (1) all technical papers in the order in which they were presented during the Workshop, (2) resolutions that were unanimously approved by the participants during the closing session of the Workshop, and (3) the Workshop program and list of participants.

In concluding the forward, we wish to express our profound gratitude and sincere appreciation to all participants in the Workshop for supporting the Workshop by active presentations and discussion. In particular, we would like to thank Dr. S. C. Liu, Dr. I. Buckle, Mr. J. Cooper and Professor M. Shinozuka for leading the discussion. Participation of Dr. W. H. Robinson from New Zealand was also very much

appreciated for active discussion on the application of lead rubber bearings.

Grateful thanks are also extended to the Japan side members. Sincere appreciation goes to the members of the Joint Research Program between PWRI and 28 private companies. Special appreciation also goes to Shizuoka ken, Tochigi ken, Japan Highway Public Corporation, Metropolitan Expressway Public Corporation, Hanshin Expressway Public Corporation, and Trans-Tokyo Bay Crossing Highway Corporation for the generous cooperation in the workshop and during the study-tour. We also would like to thank the assisting staff members, Messrs. H. Sugita, J. Hoshikuma, T. Nakajima, K. Nagaya, and K. Tamura, and Misses. M. Ikeda and K. Saito at PWRI for the smooth progress of the schedule.

Kazuhiko KAWASHIMA,
Shigeki UNJOH,
Hiroyuki IIDA, and
Hidetoshi MUKAI

Earthquake Engineering Division
Earthquake Disaster Prevention Department
Public Works Research Institute

February 8, 1993

TABLE OF CONTENTS

Session-1 : Testing of Seismic Isolation Hardware-1 1

J-1) Approving Test Procedure for Menshin Devices
(Kawashima, K., Makiguchi, Y., Suizu, Y. and Endo, K.) 3

U-1) Mechanical Characteristics of Elastomeric Seismic Isolation Bearings
(Aiken, I.D., Clark, P.W. and Kelly, J.M.) 21

J-2) Approving Test Results on Four High Damping Rubber Bearings
(Kawashima, K., Endo, K., Doro, N., Sudoh, C. and Nishikawa I.) 31

Session-2 : Testing of Seismic Isolation Hardware-2 57

J-3) Hybrid Earthquake Loading Tests of Various Types of Base Isolation Bearings
(Iemura, H., Yamada, Y., Tanzo, W. and Nanjo, A.) 59

U-2) Seismic Response Variability of Bridges on Friction Controllable Isolators
(Feng, M.Q.) 79

J-4) Shake Table Test of A Model Bridge with Sliding Isolation System
(Okamoto, S., Constantinou, M., Tsopelas, P., Fujii, S. and Ozaki, D.) 89

Session-3 : Testing of Seismic Isolation Hardware-3 113

J-5) Evaluation of Shear Modulus of High Damping Rubber Bearings and Lead Rubber Bearing during Low-Rate Load Reversals
(Kawashima, K., Koshitoge, M., Sudo, C., Makiguchi, Y. and Endo, K.)
..... 115

J-6) Loading Facilities for Menshin Devices
(Makiguchi, Y., Endo, K., Kawai, N., Suizu, Y. and Nishikawa, I.) . 139

J-7) Temperature-Dependency of Base-Isolated Bearings
(Nakano, O., Nishi, H., Shirono, T. and Kumagai, K.) 151

J-8) Load Durability Test for Highway Bridge Rubber Bearing Pads
(Matsuda, T., Maeda, Y. and Murayama, A.) 167

Session-4 : Seismic Isolation Design-1 183

NZ-1) Seismic Isolation of Bridges in New Zealand
(Robinson, W.H.) 185

J-9) Manual for Menshin Design of Highway Bridges
(Kawashima, K.) 195

U-3) Application of AASHTO Seismic Isolation Design and Analysis Requirements
(Mayes, R.L.) 221

Session-5 : Seismic Isolation Design-2 239

U-4) Stability of Elastomeric Base Isolators
(Buckle, I.G. and Liu, H.) 241

J-10) Development of Expansion Joint, Stopper and Knock-off Abutment for Menshin Bridges
(Goto, Y., Kikuchi, T., Kimishima, T., Matsumoto, F., Ozaki, D. and Tsukamoto, A.) 255

U-5) Development and Application of Simple Analytical Models of Lead Rubber Base Isolated Bridges
(Maragakis, E. and Saiidi, M.) 275

J-11) Design of 9-span Continuous Prestressed Concrete Girder Bridge with Base Isolation
(Kubota, N., Shikauchi, S., Osaki, H., Mitake, Y. and Arai, H.) 285

Session-6 : Design Applications-1 309

U-6) A Simplified Preliminary Design Approach for Base-Isolated Bridges
(Mahin, S.A.) 311

J-12) Preliminary Analysis of the Effects of Spatially Correlated Input Motions on the Response of Multiple-Span Continuous Bridges
(Tokida, K., Tamura, K. and Fukada, H.) 321

U-7) Recent Developments in Seismic Isolation at CALTRANS
(Yashinsky, M.) 337

J-13) Seismic Design of the Trans-Tokyo Bay Highway Bridges
(Shioi, Y., Yoshida, O. and Homma, M.) 347

Session-7 : Design Applications-2 367

J-14) Menshin Design and Construction of Multi-Span Continuous Prestressed Concrete Bridge
(Uzuka, T., Kawakami, K., Kumakura, K. and Tani, H.) 369

U-8) Two Shake Tables Experimental Studies of the Effectiveness of Damping-Augmentation Devices in Cable-Stayed Bridges
(Abdel-Ghaffar, A., Masri, S.F. and Ali, H.) 391

J-15) Improvement of Earthquake Resistance of Prestressed Concrete Cable-Stayed Bridges by Hysteresis Damper
(Ichinomiya, T., Takeda, T. and Kanda, K.) 401

J-16) Development of Jointless System with Menshin Bearing for Existing Simple-Spanned Steel Bridges
(Naganuma, T., Mizobuchi, S. and Uno, H.) 411

Session-8 : Dynamic Characteristics of Base-Isolated Bridges 427

J-17) Vibration Tests of A Menshin Designed Prestressed Concrete Bridge
(Goto, Y., Kikuchi, T., Ina, Y. and Sakakibara, N.) 429

J-18) Report on Vibration Experiments for an Actual Steel Bridge Supported with Menshin-Type Bearings
(Komatsu, I., Yasuda, F. and Nishibayashi, M.) 445

J-19) Response Analysis of Miyagawa Bridge Based on A Measured Acceleration Record
(Kawashima, K., Nagashima, H., Masumoto, S. and Hara, K.) 467

Session-9 : Active and Hybrid Control for Bridges 477

J-20) Effectiveness of the Variable Damper for Reducing Seismic Response of Highway Bridges
(Kawashima, K., Unjoh, S., Iida, H. and Mukai, H.) 479

J-21) Active Control of Seismic Response of Structures with Base Isolation System
(Sato, T. and Toki, K.) 495

U-9) Use of Variable Dampers for Earthquake Protection of Bridges
(Shinozuka, M. and Ghanem, R.) 507

U-10) Hybrid Control of Sliding Isolated Bridges
(Reinhorn, A.M., Nagarajaiah, S., Riley, M.A. and Subramaniam, R.) . 517

Session-10 : Comparative Design Example 525

U-11) Bridge Design Example-1
(Mayes, R.L.) 527

U-12) Bridge Design Example-2
(Constantinou, M.C., Tsopelas, P.C. and Ozaki, D.) 537

J-22) Design Example of A Highway Bridge Based on The Manual for Menshin Design of Highway Bridges
(Kawashima, K., Okado, M. and Horikawa, M.) 561

U-13) Directory of Seismially Isolated Bridges in North America 579

Resolution 587

Appendices 591

Workshop Program 593

Participants 598



Session-1

Testing of Seismic Isolation Hardware-1

J-1) Approving Test Procedure for Menshin Devices
(Kawashima, K., Makiguchi, Y., Suizu, Y. and Endo, K.)

U-1) Mechanical Characteristics of Elastomeric Seismic Isolation Bearings
(Aiken, I. D., Clark, P. W., Kelly, J. M.)

J-2) Approving Test Results on Four High Damping Rubber Bearings
(Kawashima, K., Endo, K., Doro, N., Sudoh, C. and Nishikawa, I.)

APPROVING TEST PROCEDURE FOR MENSHIN DEVICES

Kazuhiko KAWASHIMA[1], Yutaka MAKIGUCHI[2], Yoji SUIZU[3], Kazuo ENDO[4]

[1] Public Works Research Institute, Ministry of Construction, Tukuba-shi, Ibaraki, Japan
[2] Oiles Corporation, Fujisawa-shi, Kanagawa, Japan
[3] Bridgestone Corporation, Kodaira-shi, Tokyo, Japan
[4] The Yokohama Rubber Co., Ltd., Hiratsuka-shi, Kanagawa, Japan

SUMMARY

This report explains the results of the study described in the "Manual for Menshin Design of Highway Bridges (draft)." This cooperative study was conducted by the Ministry of Construction's Public Works Research Institute and twelve private firms. They developed not only approval test procedures for menshin devices to be used with highway bridges, but also evaluation procedures for certifying the performance of menshin devices. The manual describes two test procedures: one related to dynamic characteristics and the other to static characteristics of menshin devices. The dynamic characteristics test procedure includes an evaluation of characteristic values, fatigue resistance against repeatedly applied loads, residual displacement, and performance stability against variations in load, temperature, and other environmental parameters. The static characteristics test procedure includes an evaluation of the following properties: 1) durability under daily repetition of displacements that result from factors such as temperature change, 2) compressive deformation caused by creep, 3) effective stiffness with temperature change, and 4) horizontal reaction force in reaction to long-term loads such as temperature change.

INTRODUCTION

A wide variety of materials and structures are used in menshin devices. Some have a simply defined mechanism to achieve longer vibration periods and better damping performance. Others employ complex mechanisms such as high damping rubber bearings to absorb vibration energy. The specifications that govern the devices basic materials and allowable strain are important. Furthermore, it is especially important before installation to test both the dynamic and static mechanical properties of the menshin device.

Approval test procedures for menshin devices have been developed in order to unify quality standards for all types of menshin devices. This approval test procedure is applicable not only to menshin devices developed in the joint research program between PWRI and twelve private firms, but also to other menshin devices. In determing the test procedures, the above-menthioned mechanical properties required for use with menshin-designed highway bridges were also considered. These results were reported in the Menshin Design of Highway Bridges (draft).

Menshin devices are very important elements for menshin designed bridges,

so the menshin devices must remain stable despite wide variations in environmental condistions and the application of repeated loads. Therefore, in the joint group's preparation of the approval test procedures, they established a basic rule, that menshin devices which satisfy the approval test must be selected during the design stage of a menshin highway bridge.

When applying the Manual to a menshin device, the following specifications and requirements must be considered:

① It is not necessary to conduct all items of the approval test for all menshin devices to be used in a menshin-designed highway bridge. Test items that have already been conducted and for which there is a well-defined description of characteristics can be omitted. Whether each of the test items should be conducted for all menshin devices or only for randomly sampled devices depends on the operational record of the particular device.

② The Manual also describes the evaluation procedures used to certify the performance of menshin devices. These procedures include a specification of the devices with respect to yield strength, durability, and reliability and a specification with respect to mechanical characteristics. The first specification requires the menshin device to pass the approval test. On the other hand, the specification on mechanical properties is simply designed to make menshin design easier, and it is not an absolute requirement. In other words, if the mechanical characteristics of a menshin device are known and stable, they can be reflected in the menshin design no matter how complicated they are.

③ There are many energy absorption mechanisms used in menshin devices. The Manual classifies them as dependent on displacement, friction, or velocity. There are three types of approval test procedures according to which of these absorption mechanisms is used.

CHARACTERISTICS VALUE OF MENSHIN DEVICES

In the menshin design, the displacement assumed in design fro the devices u_B (design displacement of menshin device), the equivalent stiffness k_B and the equivalent damping ratio h_B of the menshin device are the key factors. They are evaluated as:

(1) Design Displacement of Menshin Device

The design displacement of menshin device is evaluated as

$$u_B = \frac{k_h \cdot W_u}{k_B} \quad \text{(S. C. Method)} \qquad (1)$$

$$u_B = \frac{k_{he} \cdot W_u}{k_B} \quad \text{(S. C. Method)} \qquad (2)$$

where,

u_B : Design displacement (m) of menshin device
k_h : Lateral force coefficient Method
k_{he} : Lateral force coefficient Bearing Capacity Method

k_B : Equivalent stiffness (tf/m) of menshin device
W_u : Weight of superstructure (tf) supported by the menshin device

(2) Equivalent Stiffness and Equivalent Damping Ratio

The equivalent stiffness and the equivalent damping ratio of menshin device are evaluated from the hysteresis loops as

$$k_B = \frac{F(u_{Be}) - F(-u_{Be})}{2\,u_{Be}} \qquad (3)$$

$$h_B = \frac{\Delta W}{2\,\pi\,W} \qquad (4)$$

where,

k_B : Equivalent stiffness (tf/m) of menshin device (refer to Fig. 1)
h_B : Equivalent damping ratio of menshin device
u_{Be} : Effective design displacement (m) of menshin device, and is given as

$$u_B = c_E \cdot u_B \qquad (5)$$

u_B : Design displacement (m) of menshin device
c_E : Modification coefficient for evaluating the effective design displacement (=0.7)
$F_{(u)}$: Lateral force required to produce μ for the menshin device
E : Strain energy induced in menshin device associated with u_{Be} displacement (refer to Fig. 1)
ΔW : Energy dissipated in menshin device per cycle (refer to Fig. 1)

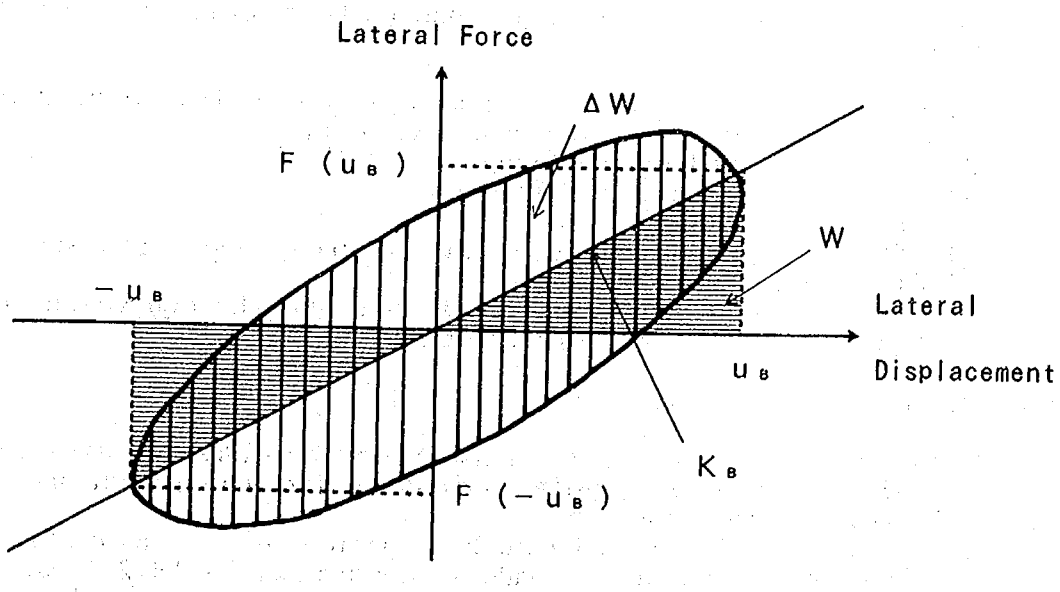


Fig. 1 Definition of Equivalent Stiffness and Equivalent Damping Ratio of Menshin Device for Approving Tests

REQUIREMENTS FOR MENSHIN DEVICES

(1) Requirements for Dynamic Load

Menshin devices have to be designed and fabricated so that their equivalent stiffness k_B and equivalent damping ratio h_B within ± 20% of the design values. The equivalent stiffness k_B and equivalent damping ratio h_B for this requirement have to be evaluated by Eqs. (3) and (4), and they shall be the ones averaged over k_B and h_B from 4th to 10th loading hystersiss among 10 cyclic loading reversals with harmonic displacement of u_{Be}. This is because deck acceleration and displacement are within tolerable range when the scatter of equivalent stiffness and the equivalent damping ratio are within ± 20% of the design values. However, the devices which produce unstable hysteretic behavior should not be adopted.

Menshin devices have to be stable against 50 cycles of harmonic loading with displacement ofu_B. The number of 50 was determined from the fact that number of load reversals developed during a major earthquake may be about 30. About 50% tolerance was included in 50.

Deck should return to the rest position even after it was subjected to a large earthquake. Therefore the residual displacement developed in menshin devices after smoothly releasing from the deformed displacement of u_B by Eq. (2) has to satisfy

$$u_{BR} \leqq 0.1 \cdot u_B \qquad (6)$$

where,

u_{BR} : Residual displacement (cm)

u_B : Design displacement (cm) of menshin device by Eq. (2)

The equivalent stiffness and the equivalent damping ratio of menshin devices have to be stable against the change of load condition at normal time, change of natural environment such as the temperature change and cyclic loading developed by an earthquake. Stability has to be examined against the following requirements:

1) cyclic loading due to elongation and shrinkage of deck due to the temperature change and the active load
2) effect of loading hysteresis
3) variation of vertical loading
4) effect of loading rate
5) effect of pre-deformation due to creep and shrinkage
6) direction of excitation
7) change of the equivalent stiffness and the equivalent damping ratio depending on the temperature change

(1) Requirements for Static Load

Materials and mechanism of menshin devices have to give credit to long term use. They have to be stable against cyclic elongation and shrinkage of deck due to temperature change.

Menchin devices have to be stable against local shear strain. Check of the local shear strain has to be made in accordance of "4.2.4 Design of rubber Bearings" of the Manual for Menshin Design of Highway Bridge".

For rubber-type menshin devices, the creep of rubber in vertical direction due to dead weight of superstructure shall not exceed 5% of total thickness of the rubber.

The equivalent stiffness of menshin device at -10 ℃ normalized by the equivalent stiffness at 40 ℃ shall not exceed 1.5. Because the temperatures of -10 ℃ and 40 ℃ is for moderate climate area, at cold area they have to be decided based on the appropriate site condition.

Menshin devices have to have appropriate initial stiffness so that harmful displacement of deck due to non-seismic lateral force such as wind effects be avoided.

APPROVING TESTS OF MENSHIN DEVICES

(1) General

Because the menshin device is one of the important structural components of menshin bridges, their requirements have to be well approved by the tests. There are various types of menshin devices for use of bridges. Based on the mechanism for producing the energy dissipation, the devices may be classified into three groups as

(a) displacement dependent type,
(b) friction force type, and
(c) velocity dependent (viscous) type.

The approving tests for the menshin devices are presented in the Manual for each of the three types.

(2) Approving Tests for Dynamic Loads

For approving the requirements for dynamic loads, the following approving tests are provided in the Manual.

1) Approving test for confirming the equivalent stiffness and the equivalent damping ratio

(a) For displacement dependent type

At the temperature of 20℃ apply 10 cycles of harmonic lateral load to the menshin device with loading displacement of u_{Be} computed by Eq. (2) and with the frequency equivalent to the natural period of menshin bridge. The vertical load equivalent to the design load shall be simultaneously applied. The averaged equivalent stiffness and the averaged damping ratio of the menshin device are defined by Eq. (7) and Eq. (8) respectively.

$$K_{Bm} = \frac{1}{7}\sum_{j=1}^{10} K_{Bj} \qquad (7)$$

$$h_{Bm} = \frac{1}{7}\sum_{j=1}^{10} h_{Bj} \qquad (8)$$

where,

K_{Bm} : Averaged equivalent stiffness (tf/m)
K_{Bj} : Equivalent stiffness at j-th load reversal by Eq. (3) (tf/m)
h_{Bm} : Averaged damping ratio
h_{Bj} : Equivalent damping ratio at j-th load reversal by Eq. (4)

The averaged equivalent stiffness K_{Bm} and the averaged damping ratio h_{Bm} should be within ± 10% of the design values.

(b) For friction force type

If the menshin device of friction force type has a friction damper and an isolator as separate components and their functions are definitely distinguishable, then they may be tested independently. When only the friction damper is tested, the friction coefficient can be applied for the characteristic value because it is not always possible to evaluate the equivalent stiffness and equivalent damping ratio.

At the temperature of 20℃ apply 10 cycles of harmonic lateral load to the menshin device with loading displacement of u_{Be} computed by Eq. (2) and with the frequency equivalent to the natural period of menshin bridge. The vertical load equivalent to the design load shall be simultaneously applied. The averaged friction coefficient of the menshin device are defined by Eq. (9).

$$u_m = \frac{1}{7}\sum_{j=1}^{10} u_j \qquad (9)$$

where,

u_m : Averaged friction coefficient

u_j : Friction coefficient at j-th load reversal

The averaged friction coefficient u_m should be within ± 10% of the design value.

(c) For velocity dependent (viscous) type

If the menshin device of velocity dependent type has a viscous damper and an isolator as separate components and their functions are definitely distinguishable, then they may be tested independently. When only the viscous damper is tested, the equivalent coefficient of viscosity can be applied for the characteristic value.

At the temperature of 20℃ apply 10 cycles of harmonic lateral load to the menshin device with loading displacement of u_{BE} computed by Eq. (2) and with the frequency equivalent to the natural period of menshin bridge.

The averaged equivalent coefficient of viscosity of the menshin device are defined by Eq. (10).

$$C_m = \frac{1}{7}\sum_{j=1}^{10} C_j \qquad (10)$$

where,

C_m : Averaged equivalent coefficient of viscosity (tf· sec/m)

C_j : Equivalent coefficient of viscosity (tf· sec/m)

The averaged equivalent stiffness and the averaged damping ratio computed by using the averaged equivalent coefficient of viscosity should be with± 10% of the design values.

Table 1 gives a summarized description of the approving test for confirming the equivalent stiffness and the equivalent damping ratio.

Table 1 Approving Test for Confirming the Equivalent Stiffness and the Equivalent Damping Ration

Type of menshin device and characteristic values for evaluation	Test procedures		Evaluation procedures
(1) Displacement-dependent menshin device: Equivalent stiffness and equivalent damping ratio (2) Friction-type menshin device: Friction coefficient (3) Rate-dependent menshin device: Equivalent coefficient of viscosity	Temperature condition	+20℃	The average of the effective stiffness and equivalent damping ratio should be within ± 10% of the design values.
	Vertical loading	Load equivalent to the design bearing stress	
	Horizontal loading	Ten cycic loadings with the effective design displacement of the menshin device (u_{Be}) at a seismic force level for an ultimate ductility check at a frequency equivalent to the natural period of the bridge.	

Each characteristic value used in the evaluation procedure is an average obtained from the hysteresis curves of the fourth through tenth loading cycles. This averaging process is particularly effective for some menshin devices that have variable (or decreasing) effective stiffness and equivalent damping ratios upon initial loading and that need several cycles to generate stable readings. This characteristic is too complicated to simplify the menshin design. But it is unavoidable due to the characteristics of menshin devices available on the market.

Throughout the test procedures, the temperature setting is held at 20℃ in temperate regions. For expected use in cold weather regions, the test temperature may be lowered accordingly.

2) Approving Test for Confirming Stableness Against 50 cycles Harmonic Load Reversals with the Design Displacement u_B

At the temperature of 20℃ apply 50 cycles of harmonic lateral load to the menshin device with loading displacement of u_B computed by Eq. (2) and with the frequency equivalent to the natural period of menshin bridge. The vertical load equivalent to the design load shall be simultaneously applied. The menshin device has suffered no structural damage that could affect its performance during the test.

Since the frequency is not a significant factor in this test, it may be as low as 0.1 Hz if the test equipment so allows.

3) Approving Test for confirming Residual Displacement Requirement

A menshin device is subject to the vertical load equivalent to the design load at the temperature of 20 ℃. Forced lateral displacement of u_B computed by Eq. (2) is administered to the munshin device. Five seconds after relieving the displacement, the residual displacement has to satisfy.

$$u_{BR} \leqq 0.1 u_B \qquad (11)$$

where,

u_{BR} : residual displacement (cm)
u_B : design displacement (cm) of menshin device by Eq. (2)

4) Approving Tests for Confirming Stableness against Variation of Load Condition at Normal Time, Change of Natural Environment such as the Temperature Change and Cycle Loading Developed by an Earthquake.

(a) Stableness against Cycle Load Reversals

At the room temperature of 20℃ apply 10 cycles of harmonic lateral load to the menshin device with loading displacement of u_B computed by Eq. (2) or smaller and with the frequency of 0.5 Hz. The vertical load equivalent to the design dead load shall be simultaneously applied. The equivalent stiffness and the equivalent damping ratio from the test have to satisfy Eqs. (12) and (13).

$$R_{Kc} = \frac{|K_{Bj} - K_{Bm}|}{K_{Bm}} \leqq \begin{cases} 0.3 \ (j=1,2,3) \\ 0.1 \ (j=4,5 \cdots 10) \end{cases} \qquad (12)$$

$$R_{hc} = \frac{|h_{Bj} - h_{Bm}|}{h_{Bm}} \leqq \begin{cases} 0.3 \ (j=1,2,3) \\ 0.1 \ (j=4,5 \cdots 10) \end{cases} \qquad (13)$$

where,

R_{Kc} : Variation ratio of equivalent stiffness
R_{hc} : Variation ratio of equivalent damping ratio
K_{Bj} : Equivalent stiffness at j-th load reversal (tf/m)
K_{Bm} : Averaged equivalent stiffness by Eq. (7)
h_{Bj} : Equivalent damping ratio at j-th load reversal
h_{Bm} : Averaged damping ratio by Eq. (8)

Some menshin devices have the dependence of the equivalent stiffness and the equivalent damping ratio on number of cyclic loading. Because considerable change of these parameters during an earthquake produces bridge response significantly different from the one assumed in design, it is not desirable.

(b) Stableness against Load Hysteresis

Conduct two series of rests, each series consisting of the loadings listed in Table 1. The equivalent stiffness and the equivalent damping ratio from the test have to satisfy Eqs. (14) and (15).

$$R_{kR} = \frac{|K_{Bm1} - K_{Bm2}|}{K_{Bm1}} \leqq 0.1 \qquad (14)$$

$$R_{hR} = \frac{| h_{Bm1} - h_{Bm2} |}{h_{Bm1}} \leqq 0.1 \qquad (15)$$

where,

R_{kR} : Variation ratio of averaged equivalent stiffness
R_{hR} : Variation ratio of averaged damping ratio
K_{Bm1} : Averaged equivalent stiffness (tf/m) by Eq. (7) for the displacement equivalent to the effective design displacement of u_{Be} by Eq. (5) at Ist series
K_{Bm2} : Averaged equivalent stiffness (tf/m) by Eq. (7) for the displacement equivalent to the effective design displacement of u_{BE} by Eq. (5) at 2st series
h_{Bm1} : Averaged damping ratio by Eq. (8) for the displacement equivalent to the effective design displacement of u_{BE} by Eq. (5) at 1st series
h_{Bm2} : Averaged damping ratio by Eq. (8) for the displacement equivalent to the effective design displacement of u_{BE} by Eq. (5) at 2nd series

In some menshin devices, the equivalent stiffness and the equivalent damping ratio depend on the past experience, in particular, the largest deformation ever experienced. Such dependence of K_B and h_B on the hysteresis ever experienced is significant, it produces different bridge response during an earthquake. Therefore, effect of load hysteresis has to be examined.

(c) Stableness against Change of Compression Force

At the temperature of 20℃ apply 10 cycles of harmonic lateral load with the displacement equivalent to either 100% of the total thickness of rubber or ± 15cm and with the frequency of 0.5Hz. The compression force shall be the force equivalent to design load, half of design load and the bearing stress of 80 kgf/cm². The equivalent stiffness and the equivalent damping ratio have to satisfy Eqs. (16) and (17).

$$R_{kb} = \frac{| K_{Bm1} - K_{Bm2} |}{K_{Bm1}} \leqq 0.2 \qquad (16)$$

$$R_{hb} = \frac{| h_{Bm1} - h_{Bm2} |}{h_{Bm1}} \leqq 0.2 \qquad (17)$$

where,

R_{kb} : Variation ratio of averaged equivalent stiffness
R_{hb} : Variation ratio of averaged damping ratio
K_{Bm1} : Averaged equivalent stiffness (tf/m) by Eq. (7) at compression force equivalent to the design load
K_{Bm2} : Averaged equivalent stiffness (tf/m) by Eq. (7) at compression force equivalent to the half of design load and the bearing stress of 80 kgf/cm²

h_{Bm1} : Averaged damping ratio by Eq. (8) at compression force equivalent to the design load

h_{Bm2} : Averaged damping ratio by Eq. (8) at compression force equivalent to the half design load and the bearing stress of 80 kgf/cm²

Compression force applied to the menshin device due to dead weight of superstructure may change associated with the error involved in construction stage and settlement of substructure. If the menshin device shows significantly due to such change of compression force, it brings different structural response. Therefore, stableness of the equivalent stiffness and the equivalent damping ratio of menshin devices have to be checked.

(d) Approving Test for Confirming the Stableness against Loading Rate

At the temperature of 20℃ apply 10 cycles of harmonic load with the displacement equivalent to either 100% of tha total thickness of rubber or ± 15cm .Frequency of the load reversal shall be 0.1Hz, 0.5Hz and 1.0Hz. The equivalent stiffness and the equivalent damping ratio have to satisfy Eqs.(18) and (19).

$$R_{kr} = \frac{| K_{Bm1} - K_{Bm2} |}{K_{Bm1}} \leqq 0.2 \qquad (18)$$

$$R_{hr} = \frac{| h_{Bm1} - h_{Bm2} |}{h_{Bm1}} \leqq 0.2 \qquad (19)$$

where,

R_{kr} : Variation ratio of averaged equivalent stiffness

R_{hr} : Variation ratio of averaged damping ratio

K_{Bm1} : Averaged equivalent stiffness (tf/m) by Eq. (7) at frequency of 0.5Hz

K_{Bm2} : Averaged equivalent stiffness (tf/m) by Eq. (7) at frequency of 0.1Hz and 1.0Hz

h_{Bm1} : Averaged damping ratio by Eq. (8) at frequency of 0.5Hz

h_{Bm2} : Averaged damping ratio by Eq. (8) at frequency of 0.1Hz and 1.0Hz

Because loading ratio to the menshin devices is not the same during excitation, dependence of the equivaqlent stiffness and the equivalent damping ratio on the loading rate has to be examined.

(e) Stableness against Pre-deformation

At the temperature of 20℃ apply 10 cycles of harmonic lateral load to the menshin device with loading displacement of u_{BE} computed by Eq.(5) or smaller and with the pre-deformation equivalent to 30% of u_{BE}. The equivalent stiffness and the equivalent damping ratio from the test have to satisfy Eqs.(20) and (21).

Table 2 shows test conditions and evaluation criteria in verifying the above six items. The test is conducted mainly on the displacement dependent menshin devices.

Table 2 Test to Certify Stability Against Changing Loads and Environmental Conditions (such as temperature)

Items to verify	Test conditions		Evaluation criteria
① Repeated loadings	Temperature condition	+20℃	At the first through third loadings, the equivalent stiffness and equivalent damping ratio should be within ± 30% of the corresponding average equivalent values, and within ± 10% at the fourth through 10th loadings.
	Vertical loading	Load equivalent to the design bearing stress	
	Frequency	0.5 Hz	
	Horizontal displacement	Repetition of positive and negative loadings with the effective design displacement of the menshin device (u_{Be}) at a seismic force level for an ultimate ductility check.	
	Number of loading repetitions	10 loadings	

② Hysteresis experience	Conduct two series of test, each series consisting of the loadings listed in Table 1.		Both the average equivalent stiffness and the average equivalent damping ratio in the first series should be within ± 10% of those in the second series.
③ Change in bearing stress	Temperature condition	+20℃	Both the average equivalent stiffness and the average equivalent damping ratio under a vertical load equivalent to half the design bearing stress and to 80 kgf/cm² should be within ± 20% of those under avertical load equivalent to the design bearing stress.
	Vertical loading	Vertical loads equivalent to half the design bearing stress and to 80 kgf/cm² .	
	Frequency	0.5 Hz	
	Horizontal displacement	Displacement equivalent to either ± 100% of the strain or ± 15 cm in displacement.	
	Number of loading repetitions	10 loadings at each stress.	
④ Change in deformation rate	Temperature condition	+20℃	Both the average equivalent stiffness and the average equivalent damping ratio at frequency of 0.1 Hz and 1.0 Hz should be within ± 20% of those at frequency of 0.5 Hz.
	Vertical loading	Load equivalent to the design bearing stress.	
	Frequency	0.1 Hz, 0.5 Hz, 1.0 Hz	
	Horizontal displacement	Displacement equivalent to either ± 100% of the strain or ± 15 cm in displacement.	
	Number of loading repetitions	10 loadings at each frequency.	

⑤ Static deformation	Temperature condition	+20℃	Both the average equivalent stiffness and the average equivalent damping ratio after having received static deformation should be within ± 20% of those that have not received static deformation.
	Vertical loading	Load equivalent to the design bearing stress	
	Frequency	0.5 Hz	
	Static deformation	① No static deformation before a test. ② Static deformation equivalent to 30% of the design displacement (u_D).	
	Horizontal displacement	Displacement equivalent to either ± 100% of the strain or ± 15 cm in displacement.	
	Number of loading repetitions	10 loadings for cases ① and ②.	
⑥ Change in temperature	Temperature condition	-10℃, +20℃, +40℃	The average equivalent stiffness at -10℃ and +40℃ should be within ± 30% of that at +20℃. The average equivalent damping ratio at -10℃ and +40℃ should be within ± 20% of that at +20℃.
	Vertical loading	Load equivalent to the design bearing stress.	
	Frequency	0.5 Hz	
	Horizontal displacement	Displacement equivalent to either ± 100% of the strain or ± 15 cm in displacement.	
	Number of loading repetitions	10 loadings at each temperature.	

The evaluation criteria described in Table 2 are fundamental rules. The primary object of these procedures is to obtain the mechanical characteristics of a menshin device. Therefore, unsatisfactory results do not necessarily lead to the rejection of the device.

Each of the evaluation criteria divides the 10 loadings into two groups, that is, the first three and the last seven. This serves to determine whether the characteristic value of the menshin device tends to reach a steady state, as shown in Figure 1. If there is such a tendency, the value can vary during the test. However, the broken line shown in Fig. 1 does not become steady, but tends to change more as the test advances, which is not acceptable behavior for a menshin device. Such a device should not be used.

Fig. 2 shows the procedure for evaluating how stability is affected by hysteresis experience. Some menshin devices show differences in behavior between the two series, and this test evaluates such differences.

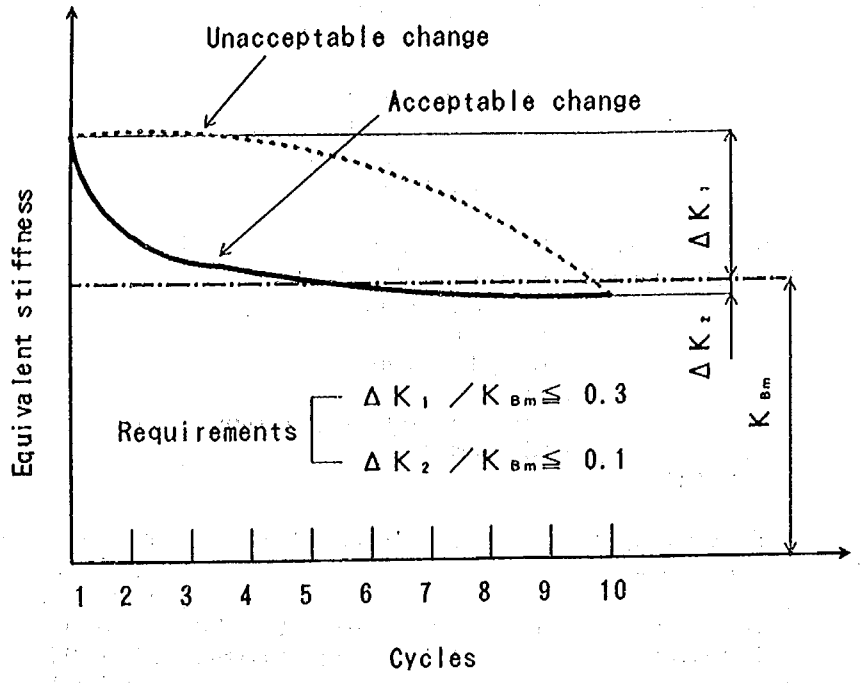


Fig. 2 Change of equivalent stiffness during cyclic loadings

Table 2 shows test procedures for displacement-dependent menshin devices. In addition, the "Manual for Menshin Design of Highway Bridges (draft)" describes procedures for friction-type and rate-dependent devices. For rate-dependent devices subjected to the deformation rate, static deformation, and temperature change conditions given in Table 2, the Manual sets the displacementrate at 50 cm/s. Displacement relates to the displacement rate as follows:

$$v = 2 \cdot \pi \cdot f \cdot u \qquad (1)$$

where v denotes the displacement rate in cm/s, f the frequency in Hz, and u the displacement in cm. From Eq. (1) we find that v is approximately 50 cm/s for f = 0.5 Hz and u = 15 cm.

STATIC MECHANICAL PROPERTIES OF MENSHIN DEVICES

There are three tests used to evaluate the static properties of a menshin device:

① Tests for approving the durability of the device against repeated ordinary displacement due to temperature change;
② Tests for approving compressive deformation caused by creep
③ Tests for approving the equivalent stiffness of the device at temperatures between -10° and +40℃ .

The Manual also describes test procedures for obtaining the horizontal reaction force of a menshin device for slow deformation of its superstructure caused by creep, shrinkage, and temperature change.

Table 3 shows the evaluation procedures for certifying the static properties of a menshin device.

Table 3 Evaluation Procedures for Certifying the Static Properties of a Menshin Device

Environmental change and properties to be evaluated	Test procedure		Evaluation procedure
① Durability against repeated ordinary deformation due to temperature variation	Temperature condition	+20℃	(1) Both the average equivalent stiffness and the average equivalent damping ratio after having received repeated deformation should be within ± 10% of those yet to receive the repeated deformation. (2) No damage to the menshin device.
	Vertical loading	Load equivalent to the design bearing stress	
	Horizontal displacement	Displacement equivalent to 20% of shear strain	
	Number of loadings	20,000 loadings	
② Compressive deformation by creep	Temperature condition	+20℃	The creep deformation estimated for service life (in years) by using the creep characteristic equation should be 5% or less of the total rubber thickness.
	Vertical loading	Load equivalent to the design bearing stress	
	Duration	1,000 hours	
	Estimation of creep deformation	Estimate the creep deformation for the service life (in years) by using the time-based creep characteristic equation obtained from the vertical displacements after 100 hours and 1,000 hours of loading.	
③ Equivalent stiffness at temperature of -10℃ and +40℃	Temperature condition	-10 ℃ and +40℃	The average equivalent stiffnes at +40℃ should be 1.3 times or less than that at -10℃ .
	Vertical loading	Load equivalent to the design bearing stress	
	Horizontal displacement	The effective design displacement of the menshin device ($\pm u_{be}$).	
	Number of loadings	10 loadings at each temperature	

A temperature change of 5℃ in a day may displace the bearing at a rate of about 1.4×10^{-4} cm/s for an expansion beam having an effective length of 50 m in an upper structure. This value is significantly lower than the displacement rate due to seisnic loads. Accordingly, some menshin devices operate differently depending on the horizontal reaction force at a small displacement rate or at a large rate during an earthquake. They require measurements of horizontal reaction force during slow deformation caused by a temperature change or other similar effects.

There is no problem if it is possible to recreate in tests the displacement rate caused by temperature change or other similar effects. It is generally difficult to simulate such a small displacement rate by means of repeated loading. Thus, the manual proposes two methods for estimating the horizontal reaction force during slow deformation. According to these methods, an ordinary exciter is used to simulate slow deformation. It has been confirmed that these two methods produce nearly the same reaction force values. We describe the methods in the following:

(a) Extrapolation Method

The extrapolation method is applicable to all types of menshin devices. When using this method, the excitation rate ranges from 0.002 to 5.0 cm/s, which is the rate that can be created by an ordinary shaken. Then, to estimate the horizontal reaction force for a long-term loads, the method extrapolates the measured force-rate relationship to a smaller deformation rate in the natural environment. Fig. 3 shows an example of extrapolation from the measured equivalent shear modulus-rate for a high-damping rubber bearing;

(b) Relaxation Method:

The relaxation method is applicable to menshin devices in which the relaxation of internal stress advances as time passes. Such devices include a high-damping rubber bearing and a lead plug-impregnated rubber bearing. The method assumes that it takes six hours (one quarter of a day) for the temperature to rise from its average to its highest level and the horizontal deformation during this period to be shear strain γ_d. Then, the method applies a first load to cause deformation of 1/4 γ d, then leaves the subject as it is for 1.5 hours (one quarter of six hours). This step is repeated four times so that the total shear stress reaches γ d in six hours. In the obtained hysteresis curve of a the relationship between a horizontal reaction force and shean strain, a smoothed curve is drawn through the points of the smallest reaction force at the four values for shear strain. This method uses the smoothed curve to estimate a characteristic horizontal force in slow deformation. Fig. 4 is an example of test result for a high-damping rubber bearing.

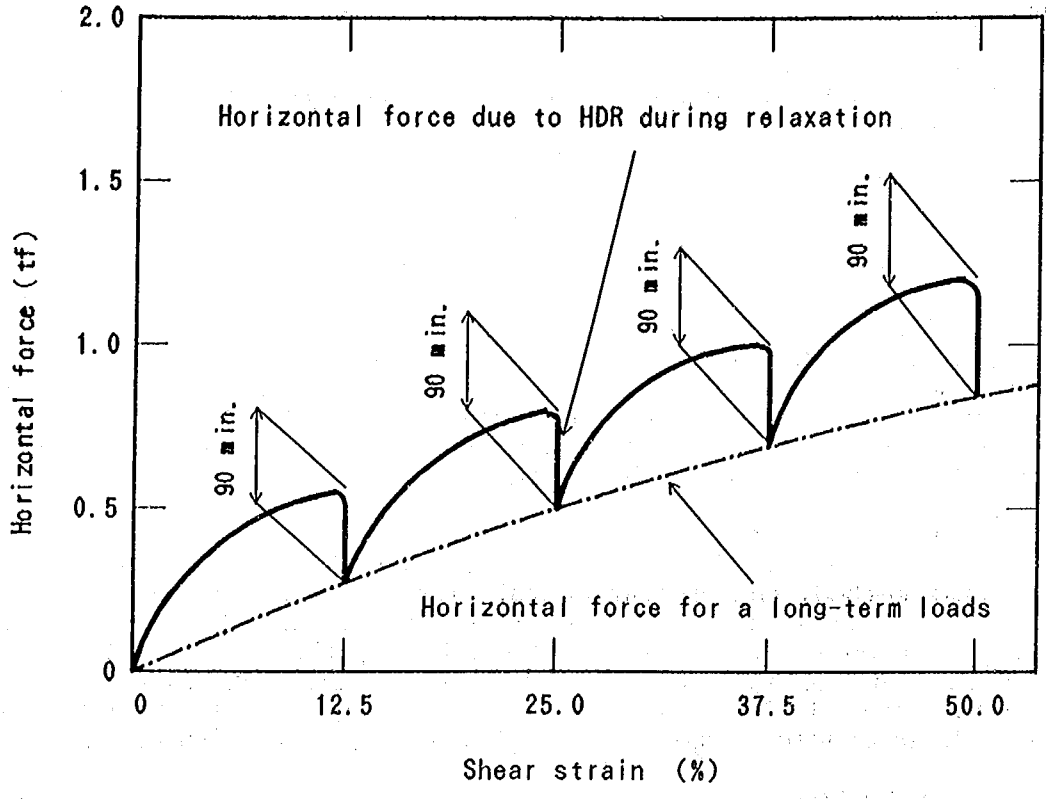


Fig. 5 Forizontal Force due to High Damping Rubber Bearing during Relazation for Six Hours

ACKNOWLEDGEMENTS

This study was made as part of the joint research on "Development of the Menshin System for Highway Bridges" conducted by PWRI and 28 private firms in Japan.

REFERENCES

1) PWRI and 28 private firms: Development of Menshin Systems for Highway Bridges, Report No. 3, 1992 (in Japanese)
2) PWRI and 28 private firms: Manual of Menshin Design of Highway Bridges (Draft), 1992 (in Japanese)
3) W.H. Robinson. "Lead-Rubber Hysteretic Bearings Suitable For Protecting Structures During Earthquakes," Earthquake Engineering and Structural Dynamics, Vol. 10, 593-604, 1982.

MECHANICAL CHARACTERISTICS OF ELASTOMERIC SEISMIC ISOLATION BEARINGS

Ian D. Aiken, Peter W. Clark, and James M. Kelly

Earthquake Engineering Research Center
University of California at Berkeley, CA 94720, USA

ABSTRACT

The results of an extensive series of experimental tests to identify the mechanical characteristics of three types of seismic isolation bearings are presented. Two types of high-damping rubber bearings and one type of lead-rubber bearing were studied. Cyclic horizontal displacement tests, varying the test parameters of shear displacement amplitude, axial load, and loading frequency were performed on all of the bearings. Bearing shear stiffness and damping properties were investigated in terms of the different test parameters. Additional tests investigated the influence of strain history on the performance of the bearings at moderate and high strain amplitudes. Ultimate-level tests consisted of monotonic shear loading to failure at several different axial loads, and tension failure tests of the bearings with bolted connections. Roll-out instability tests of the doweled bearings were conducted. Comparisons are made between experimental results and available analytical relationships for material and bearing properties.

1 INTRODUCTION

Elastomeric bearings are now the most commonly-used type of system for seismic isolation. Accurately characterizing bearing mechanical properties is a very important aspect of the design process for an isolated bridge or building structure, and this experimental program was aimed at verifying and refining existing analytical models for this purpose.

An extensive series of tests of three types of seismic isolation bearings was carried out with the objective of fully identifying their mechanical characteristics. Two types of high-damping rubber bearings and one type of lead-rubber bearing were studied.

The three types of bearings tested in this program were developed for earthquake simulator tests of a large-scale model of a three-story reinforced-concrete building located in Sendai, Japan (Saruta et al., 1988). The full-size building was constructed to study the performance of different isolation systems under real earthquake excitations. Since its completion in 1985, several different systems have been installed under the building, including the two types of high-damping bearings studied in this investigation. To date no isolation systems incorporating lead-rubber bearings have been installed under the full-size building.

2 BEARING DESIGNS

The high-damping A and high-damping B designs described below are both reduced-scale designs of bearings which have been used in the full-size building. The model constructed for the earthquake simulator tests has a (geometric) scale factor of 2.5, and this is the scale factor that was used to determine the size of the reduced-scale bearings. Because no full-size lead-rubber bearings have been installed in the building in Japan, the scaled lead-rubber bearings were designed to have the same stiffness characteristics as the high-damping A bearings.

The reduced-scale bearings were subjected to axial loads of approximately 49.0 kN and 78.5 kN under the model structure. These loads were the basis for defining the axial loads used in

this study. With a few exceptions, only the results for the 78.5 kN tests are presented and discussed in this paper.

The designs of the 1/2.5-scale bearings are described in the following sections.

2.1 Design 1: High-Damping A

These bearings were made from a blend of filled natural rubber and a synthetic rubber. The compound is called KL301 by the manufacturer, Bridgestone Corporation, Ltd., Japan, and is one of a suite of high-damping elastomers that they have developed for seismic isolation applications. KL301 has a shear modulus of about 4300 kPa at very small strains, which decreases to 650 kPa at 50 percent strain, 430 kPa at 100 percent strain, and 340 kPa at 150 percent strain. The bearings consist of twenty layers of 2.2 mm thick rubber at 176 mm diameter (shape factor = 20), nineteen 1.0 mm steel shims, and 12 mm top and bottom plates (Figure 1). The design axial pressure is 3.23 MPa. The bearings were designed with flange-type end plates to permit bolted structure and foundation connections. Fifteen bearings of this design were tested in this study.

2.2 Design 2: High-Damping B

These bearings were made from a low-modulus, filled natural rubber compound, designated HDNR-S by the manufacturer, Rubber Consultants, Ltd., England. The shear modulus of this material varies from about 800 kPa at a shear strain of 5 percent to about 480 kPa at 50 percent strain and 400 kPa at 100 percent strain. The bearings consist of twelve layers of 4.0 mm thick rubber at 140 mm diameter (shape factor = 8.75), eleven 1.6 mm steel shims, and 20 mm top and bottom plates (Figure 2). The design axial pressure is 5.10 MPa. Bearing-structure and foundation connections are bolted. Instead of using flange-type end plates, the bearings are connected by bolting directly into the top and bottom end plates. Twelve bearings of this design were tested in this study.

2.3 Design 3: Lead-Rubber

These bearings were made from an unfilled natural rubber compound, and contained a 25.4 mm diameter lead plug. For design purposes, the rubber shear modulus was assumed to have a constant value of 590 kPa. The bearings consist of 21 layers of 3.0 mm thick rubber at 180 mm diameter (shape factor = 15), twenty 1.0 mm steel shims, and 15 mm top and bottom plates (Figure 3). The design axial pressure is 3.08 MPa. These bearings had shear dowel end plate connections. The bearings were manufactured by Oiles Industries, Ltd., Japan. Fifteen bearings of this design were tested in this study.

3 TYPES OF TESTS

All of the tests were performed in a machine developed for general testing of small-to-moderate sized isolation bearings. The machine is capable of subjecting a bearing to simultaneous generalized horizontal and vertical dynamic loading. It has limits of 1335 kN vertical force, 534 kN horizontal force, and ± 250 mm horizontal displacement.

In addition to the horizontal shear tests, a large number of vertical tests were performed on the bearings. The results of these tests are not discussed in this paper.

3.1 Characteristic Tests

1. Basic Test The basic type of test performed on all of the bearings of each design was a 25 cycle sinusoidal horizontal displacement signal incorporating 5 cycles at each shear strain amplitude of 5, 25, 50, 75, and 100 percent. The axial loads during these basic tests were constant at either 49.0 kN or 78.5 kN corresponding to the axial loads to which the bearings were subjected in the earthquake simulator tests of the 1/2.5-scale model of the full-size

isolated building. The frequency of loading was 1 Hz for all of these tests.

2. Axial Load Varied The basic test was also performed at a number of different axial loads. The load was constant during each test, and tests were performed at loads of $3P_{des}$, $2P_{des}$, P_{des}, $P_{des}/2$, 0, and $-P_{des}/10$, where P_{des} was 49.0 kN or 78.5 kN. The rate of loading and the strain increments were otherwise the same as for the basic test described above.

3. Frequency Varied The basic test was also performed at frequencies of 0.1, 0.3, 0.5, 1.0, and 2.0 Hz. The other test variables were the same as those for the basic test.

4. Strain/Load History The sequence of cycles in the basic test was modified to investigate the effect of strain (load) history on bearing properties.

(a) Moderate Amplitude Tests

Five cycles of loading at each strain amplitude were imposed, and the tests were all performed at a frequency of 1 Hz and at axial loads of 49.0 kN and 78.5 kN. The following sequences were used:

1. Strain Sequence 1: 5-25-50-75-100 percent
2. Strain Sequence 2: 25-50-75-100-5 percent
3. Strain Sequence 3: 50-75-100-5-25 percent
4. Strain Sequence 4: 75-100-5-25-50 percent
5. Strain Sequence 4: 100-5-25-50-75 percent

The displacement control signal for the Strain Sequence 3 test is shown in Figure 4.

(b) Large Amplitude Tests

Large-strain sequences of 50-200-50 percent and 200-50-200 percent were also imposed (Figure 5). These tests were performed at a loading frequency of 1 Hz for the design 1 and 2 bearings, and 0.5 Hz for the design 3 bearings. Axial loads were 49.0 kN and 78.5 kN.

3.2 Ultimate Tests

1. Large-Strain Cyclic Large-strain sinusoidal cycles at strain amplitudes of 100, 150, 200, 250, 300, and 350 percent were performed. (Maximum strain for the design 3 bearings was 200 percent, limited by the onset of roll-out instability; loading frequency was 0.5Hz for the 250, 300, and 350 percent tests).

2. "Extra-Loop" Cyclic These tests consisted of large-strain sinusoidal cycles with a superimposed set of additional smaller cycles around the points of maximum and minimum amplitude. The test was defined as $\pm\gamma(+-\gamma/4)$, where γ = 100, 150, 200, 250 percent for the extra-loop1 test and γ = 200, 250, 300, 350 percent for the extra-loop2 test. The displacement control signal for the extra-loop2 test is shown in Figure 6. These tests were only performed on the design 1 and 2 bearings, and at a frequency of 1 Hz for the extra-loop1 test and 0.5 Hz for the extra-loop2 test. Axial loads were 49.0 kN and 78.5 kN.

3. Monotonic Shear Failure Two bearings of designs 1 and 2 were failed in shear under monotonic loading. One bearing was tested under zero axial load, and the other at 78.5 kN axial load. The ultimate-level shear tests of the design 3 bearings consisted of determining the roll-out displacement of the bearings under different axial loads. Roll-out tests were performed at axial loads of 0, 49.0, 78.5, and 156.9 kN.

4. Monotonic Tension Failure One bearing each of designs 1 and 2 was tested to break under monotonic tension loading. (The doweled connection detail of the design 3 bearings did not permit tension load to be applied to these bearings).

4 TEST RESULTS

Typical hysteresis loops for the three types of bearings under sinusoidal shear displacement loading are presented in Figure 7. The loops shown for the high-damping A bearing are at shear strains of 200, 250, 300, and 350 percent, those for the high-damping B bearing are at strains of 100, 150, 200, and 250 percent, and those for the lead-rubber bearing are at strains of 50, 100, 150, and 200 percent. Beyond a certain strain level, the high-damping bearings exhibit a clear stiffening behavior. Various results are presented and discussed in the following sections.

4.1 Characteristic Tests

Bearing effective stiffness and damping were calculated from the experimental hysteresis loops using the following relationships:

$$k_{eff} = \frac{F_{max} - F_{min}}{d_{max} - d_{min}} \tag{1}$$

$$\xi = \frac{W_d}{4\pi W_s} \tag{2}$$

where:

F_{max}, F_{min} = peak values of shear force

d_{max}, d_{min} = peak values of shear displacement

W_d = hysteresis loop area

$W_s = \frac{1}{2} F_{max} d_{max}$

These properties are plotted as a function of shear strain for each type of bearing in Figure 8. The design 1 and 3 bearings show very similar effective stiffness-strain relationships. This is to be expected, as the original design intent for these two types of bearings was that their stiffness properties be the same. The design 2 bearings, however, show a much lower stiffness, about one-third of the stiffness of design 1 or 3 over the entire strain range. The damping ratios of the three bearing designs show greater differences. For design 1, the damping ratio decreases gradually from 12 percent at small strains to about 10 percent at strains above 200 percent. The design 2 bearings have an almost constant damping ratio of about 9-10 percent for strains up to 150 percent, which increases to about 14 percent at 250 percent strain. The design 3 bearings have the highest damping ratio: nearly 19 percent at small strains, about 16 percent at 100 percent shear strain, and reducing to about 11 percent at 200 percent strain.

The manufacturer's curves for the shear modulus of the KL301 compound used in the high-damping A bearings was compared with the experimental stiffness-strain relationship of Figure 8(a). Reasonable agreement was obtained, although the predicted bearing stiffness slightly underestimated the observed stiffness. A similar comparison of predicted and measured damping ratio-strain relationships did not show close agreement. It is believed that the reason for the difference is that the manufacturer uses a different definition than that used here for the calculation of the damping ratio from the measured data (Kelly, 1991).

Experimental force-displacement relationships for the design 3 bearings were compared with a set of design equations for lead-rubber bearings (Ministry of Works and Development, 1983). Refinements to certain parameters led to reasonable results (Figure 9).

The influence of axial load variation on the shear stiffness for all bearing designs is shown in Figure 10. Using k_{eff} at P = 78.5 kN as the reference stiffness, the stiffness variations at 25 and 100 percent strain for the design 1 and 3 bearings is only about ±5 percent of the 78.5 kN stiffness. The variation for the design 2 bearings is somewhat greater, being about ±20 percent of the 78.5 kN stiffness. Axial load variations influence damping ratios more than stiffness for all three bearing designs. The design 1 bearing damping ratio varies from 11 to 14 percent at 25 percent strain, and from 10 to 12 percent at 100 percent strain, and the design 3 bearing damping ratio varies from 15 to 21 percent at 25 percent strain, and from 13 to 16 percent at 100 percent strain. The design 2 bearing damping ratio varied more, from 8 to 14 percent at 25 percent strain, and from 6 to 15 percent at 100 percent strain.

Loading frequency effects on stiffness and damping ratio are shown in Figure 11 for the design 3 bearings. Stiffness is negligibly affected by the variation in loading frequency for all of the three designs. Using k_{eff} at 0.5 Hz as the reference stiffness, the lead-rubber bearing stiffness variation at 25 and 100 percent shear strain is only about ±2 percent of the 0.5 Hz stiffness. The variation for the high-damping bearings is about ±10 percent, and about ±6 percent of the 0.5 Hz stiffness for designs 1 and 2, respectively. Damping ratio is influenced less by load frequency than by axial load. The variation is about ±5 to 10 percent for all three bearing types, when compared to the damping ratio at 0.5 Hz.

Moderate Amplitude Tests The variation in k_{eff} for each of the bearing designs during the Strain Sequence 1—5 tests is shown in Figure 12. In each of these tests the effective stiffness was calculated for each "group" of five cycles (see Figure 4). Each curve in Figure 12 represents the variation in the calculated k_{eff} at a single strain amplitude as a function of group number (or load history). At the large strain levels (100 percent, for example) the dependence of k_{eff} on the group number is not significant. However, at lower strain amplitudes the effective stiffness is significantly reduced from its "group 1" value when preceded by cycles at higher amplitudes. For example, the results for the design 1 bearings at a strain amplitude of 25 percent show a k_{eff} of approximately 0.65 kN/mm for the Strain Sequence 1 and 2 tests, while this stiffness is reduced to approximately 0.38 kN/mm in the Strain Sequence 3—5 tests in which the 25 percent strain group comes after the 100 percent strain group.

Large Amplitude Load History Effects The results at larger strain amplitudes were similar to those obtained at moderate amplitudes. For the 50-200-50 and 200-50-200 tests, the bearing k_{eff}s were determined for the middle three cycles of each test "group" (see Figure 5). Significant changes in stiffness were seen in the 50-200-50 tests for all three bearing types — the group 3 k_{eff} was about 40 percent less than the group 1 k_{eff} (range: 37.6 to 40.1 percent). However, in the 50-200-50 tests the group 1 versus group 3 k_{eff}'s dropped only about 6 percent (range: 4.7 to 7.5 percent). Clearly the large-strain deformations in the 50-200-50 test have a significant influence on the bearing properties in subsequent smaller deformations, while the intermediate lower-level deformations in the 200-50-200 test do not much affect the large-strain behavior.

1. Large-Strain Cyclic Large-strain cyclic tests up to 350 percent shear strain were performed on the design 1 bearings, up to 250 percent on the design 2 bearings, and up to 200 percent on the design 3 bearing. Hysteresis loops for these tests are shown in Figure 7. Both types of high-damping bearings exhibit a stiffening characteristic at large strains. The high-damping A bearings begin to stiffen at about 250 percent and the high-damping B bearings at about 200 percent shear strain. High-strain stiffening is a material property of filled rubbers. The lead-rubber bearing, which is made from unfilled natural rubber and has doweled shear connections (which permit instability in the bearing before it can sustain extreme lateral displacements) does not show this stiffening effect at large strains.

2. "Extra-Loop" Cyclic The shear force-displacement response of a design 1 bearing in the extra-loop2 test is shown in Figure 13. For the initial excursion to a new maximum deformation, the bearing exhibits a force higher than for subsequent cycles. This phenomenon is the same as seen for more conventional sinusoidal tests. The subsequent "quarter-amplitude" cycles lie within the initial force-deformation envelope, and show no further stiffness reduction.

3. Monotonic Shear Failure Shear failure force-displacement curves for a design 1 and a design 2 bearing under zero axial load are shown in Figure 14. The design 1 bearing failed at a strain of 739 percent, and the design 2 bearing at about 510 percent. The peak shear forces at failure were 274 kN and 116 kN for the design 1 and 2 bearings, respectively. These forces correspond to shear stresses of 11.2 MPa for the design 1 bearing, and 7.5 MPa for the design 2 bearing. The failure mechanisms for both bearings involved tensile material rupture..Elastomer-shim bond separation was not observed in any of the bearing shear failures. These results are consistent with results of failure tests reported by Ishida (1991).

Roll-out strains ranged from 133 to 200 percent, reached in the 0 and 78.5 kN axial load tests, respectively. The calculated roll-out displacements for the 49.0 and 78.5 kN axial loads agree well with the experimental results, however, agreement is not so good for the 0 and 156.9 kN loads.

4. Monotonic Tension Failure Tensile stress versus tensile strain curves for the failure tests of one design 1 and one design 2 bearing are plotted in Figure 15. The sharp reduction in stiffness in both curves at a stress of about 2 MPa indicates the onset of cavitation in the elastomer. The design 1 bearing reached a stress of 7.7 MPa and a strain of 514 percent at failure, while the design 2 bearing reached a stress of 8.0 MPa and a strain of 408 percent. These failure stresses represent a tension load of about two times the design compression load for the bearings. Future ultimate-level tests under combined large shear deformation and tension loading are planned. This type of test will more closely represent, than the pure tension tests described here, the type of extreme loading condition in which tensile stresses may develop in isolators.

5 CONCLUSIONS

All of the bearings performed well in the large range of tests conducted. This experimental investigation has provided an extensive database for the confirmation and refinement of existing analytical models for isolation bearing properties.

Fundamental bearing characteristics of stiffness and damping were studied in terms of shear strain, axial load, and rate of loading. In general, it was found that variations in axial load and rate of loading did not significantly affect bearing stiffness and damping properties for moderate shear strain levels. The understanding of the failure mechanisms of seismic isolators has been enhanced by the various ultimate-level tests performed. The ultimate-level shear tests achieved bearing shear strains in excess of 500 percent before failure occurred. The tension failure tests revealed the very large tension capacity of the bolted high-damping bearings.

The results and conclusions will directly benefit the designers of isolation systems utilizing these types of bearings, providing a greater understanding of and confidence in bearing properties and behavior.

ACKNOWLEDGEMENTS

The authors wish to recognize the financial support of Shimizu Corporation, Tokyo, Japan, for this research. In addition, the assistance and advice of M. Kikuchi and M. Saruta are acknowledged. The views expressed in this paper are those of the authors, and do not necessarily reflect the opinions of the sponsor.

REFERENCES

Ministry of Works & Development, 1983. Design of lead-rubber bridge bearings. *CDP 818/A*, Wellington, New Zealand.

Saruta, M., H. Watanabe, & M. Izumi, 1989. Proof test of base-isolated building using high damping rubber bearing. *Proc. SMIRT-10, vol. K:* 631-636, Los Angeles, USA.

Ishida, K., H. Shiojiri, M Iizuka, K. Mizukoshi, and K. Takabayashi, 1991. Failure tests of laminated rubber bearings. *Proc. SMIRT-11, vol. K:* 241-246, Tokyo, Japan.

Kelly, J.M., 1991. Dynamic and failure characteristics of Bridgestone isolation bearings. *Report No. UCB/EERC-91/04,* EERC, Univ. of Calif. at Berkeley, USA.

Aiken, I.D., J.M. Kelly, P.W. Clark, K. Tamura, M. Kikuchi, and T. Itoh, 1992. Experimental studies of the mechanical characteristics of three types of seismic isolation bearings. *Proc. 10th WCEE, vol. 4:* 2281-2286, Madrid, Spain.

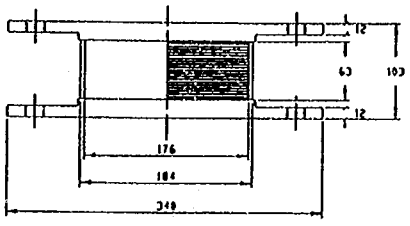


Fig. 1 Bearing Design 1: High-Damping A

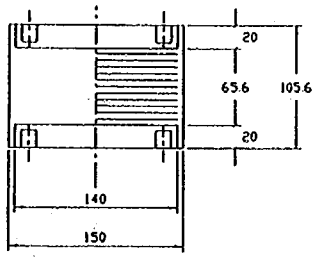


Fig. 2 Bearing Design 2: High-Damping B

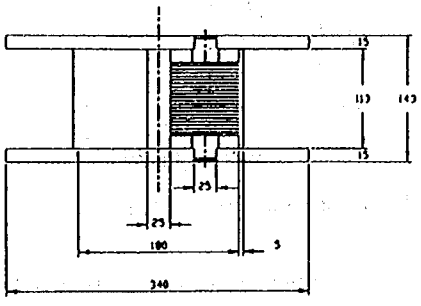


Fig. 3 Bearing Design 3: Lead-Rubber

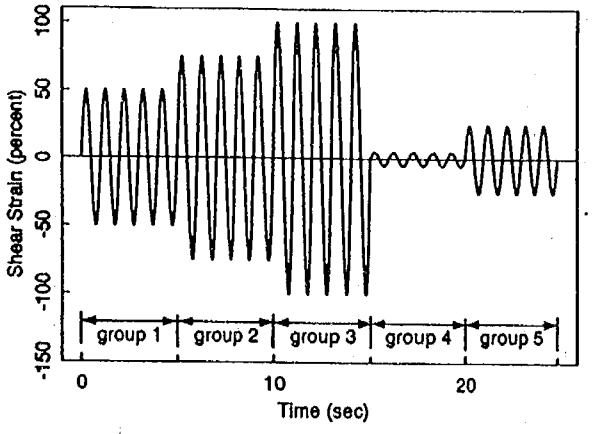


Fig. 4 Strain Sequence 3 Test Displacement Control Signal

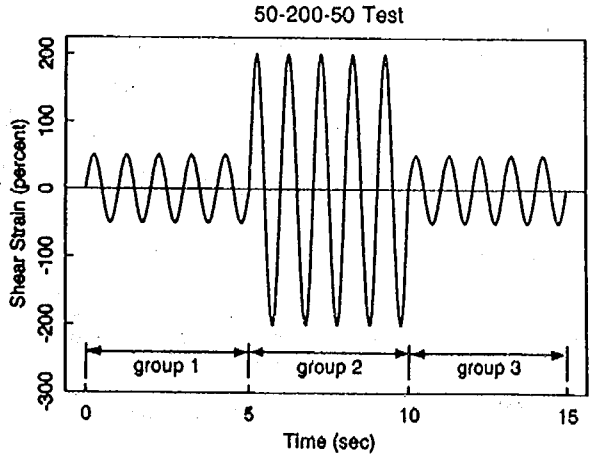


Fig. 5 Large-Amplitude Strain History Test

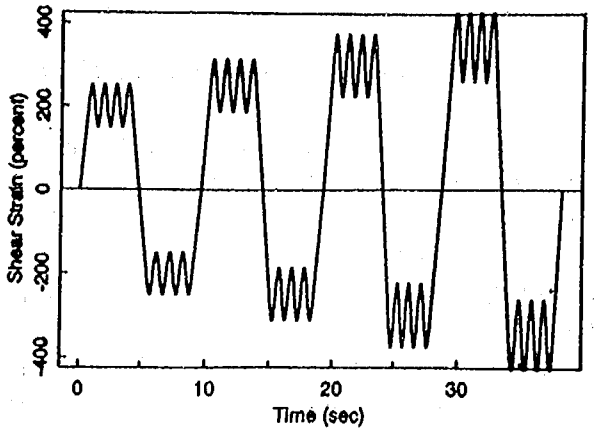
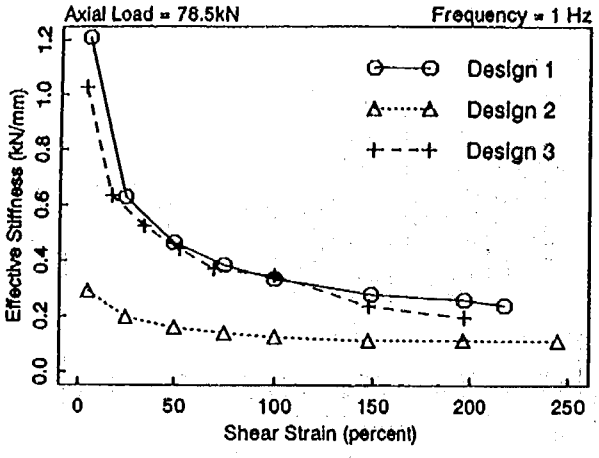
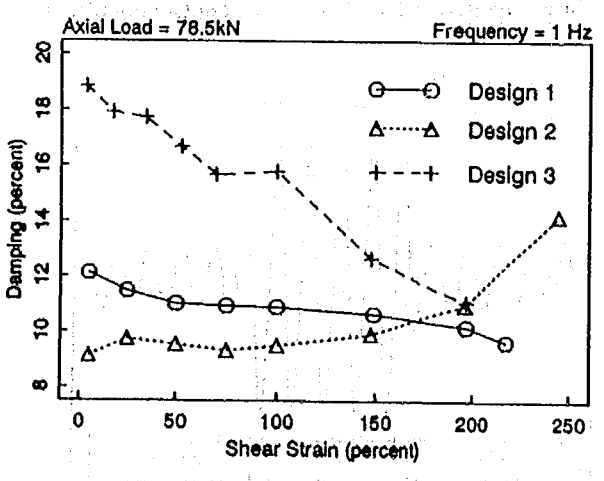


Fig. 6 Extra-Loop2 Test Displacement Control Signal

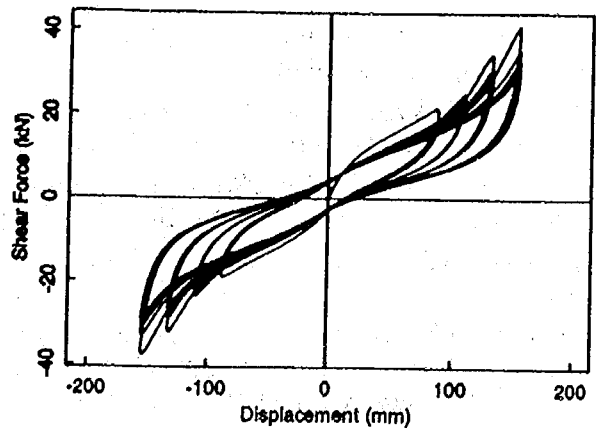


(a) Effective Stiffness vs. Shear Strain

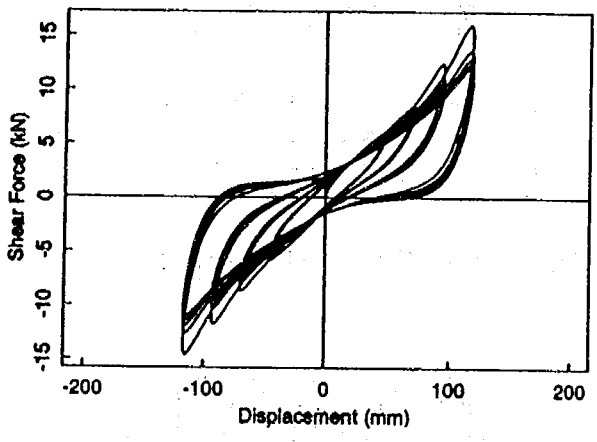


(b) Damping Ratio vs. Shear Strain

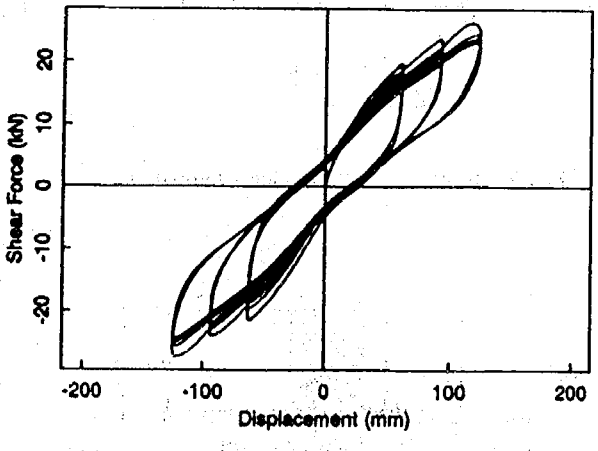
Fig. 8 Bearing Stiffness and Damping Ratio, All Designs



(a) Design 1, 200-350% Shear Strain Sequence

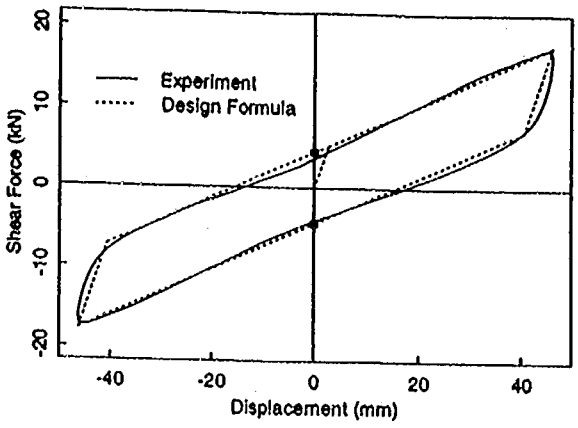


(b) Design 2, 100-250% Shear Strain Sequence



(c) Design 3, 100-200% Shear Strain Sequence

Fig. 7 Shear Force-Displacement Hysteresis Loops



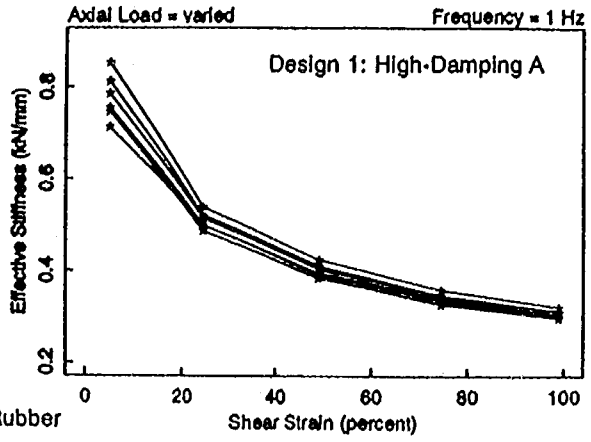
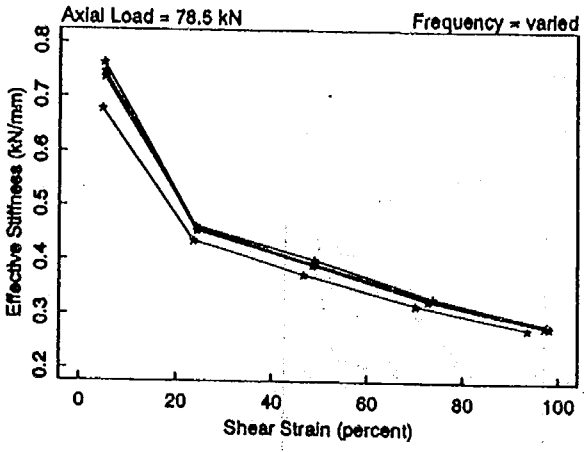
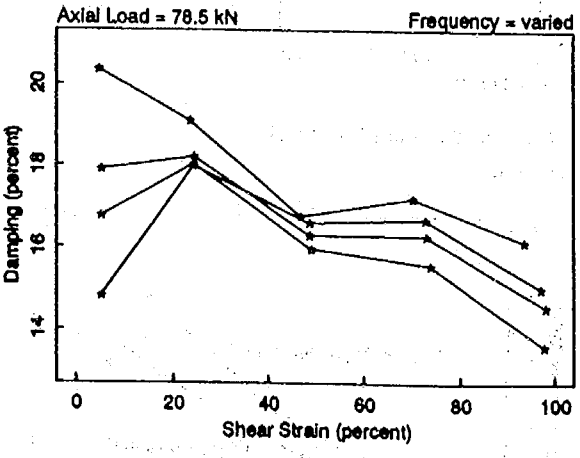


Fig. 9 Experimental and Design Formula Hysteresis Loops, Lead-Rubber Bearing, 75 Percent Shear Strain

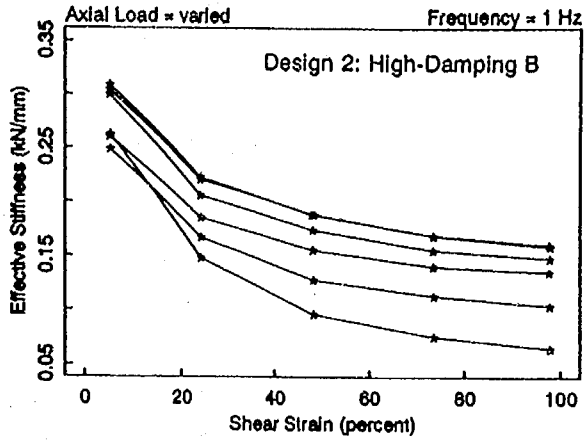


(a) Effective Stiffness vs. Shear Strain



(b) Damping Ratio vs. Shear Strain

Fig. 11 Effect of Loading Frequency on Bearing Properties, Design 3



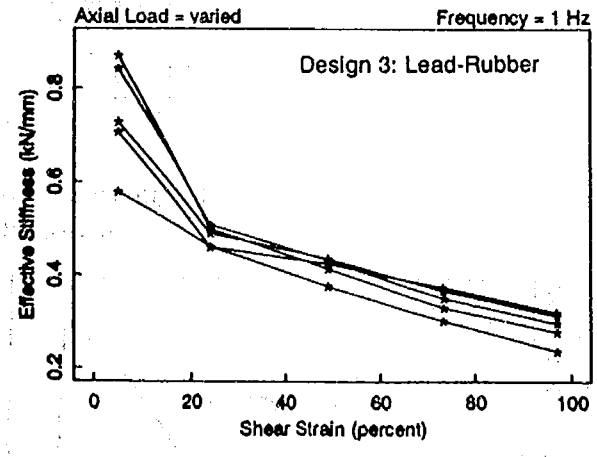


Fig. 10 Effect of Axial Load on Effective Stiffness, All Designs

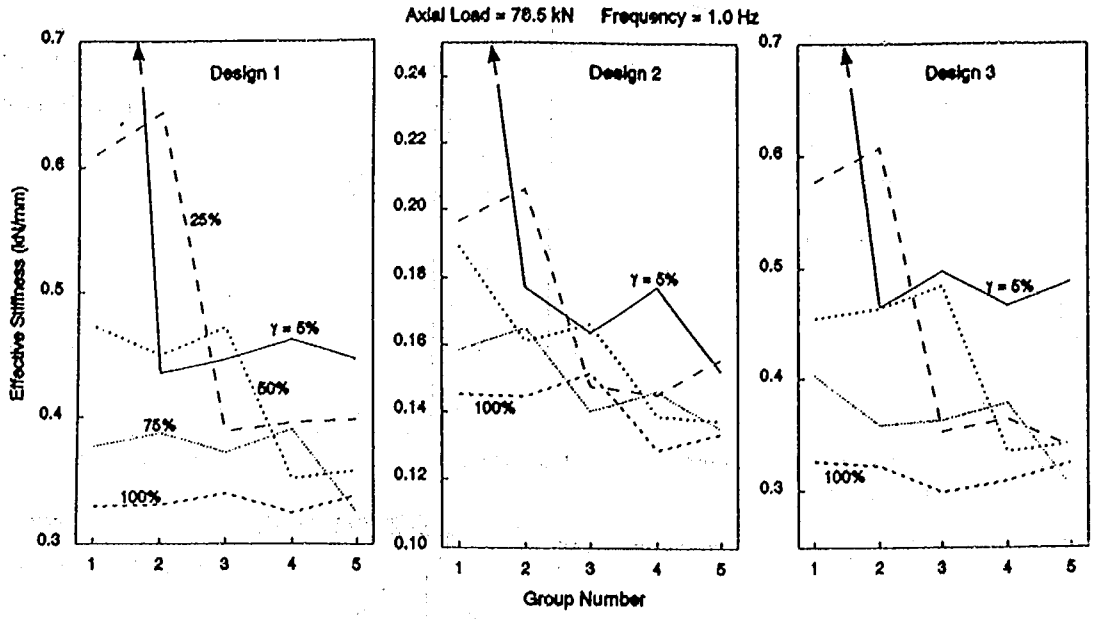


Fig. 12 Effect of Strain History on Effective Stiffness, All Designs

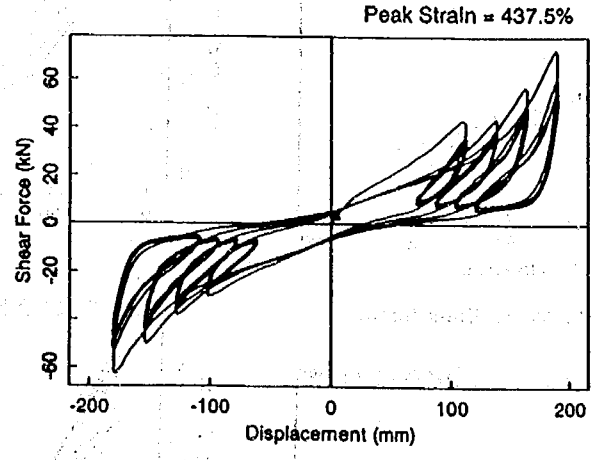


Fig. 13 Design 1 Shear Force-Displacement Hysteresis Loops, Extra-Loop2 Test

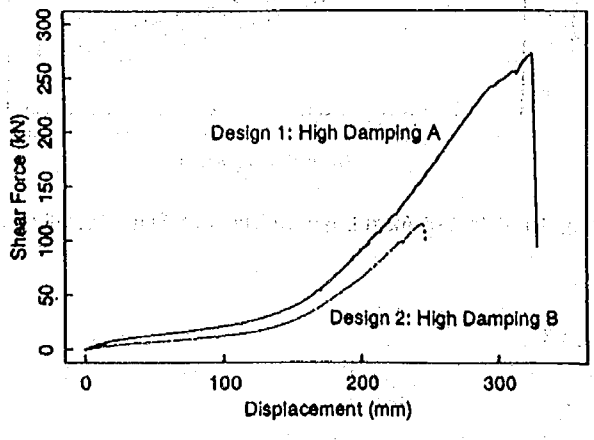


Fig. 14 Monotonic Shear Failure, Designs 1 and 2

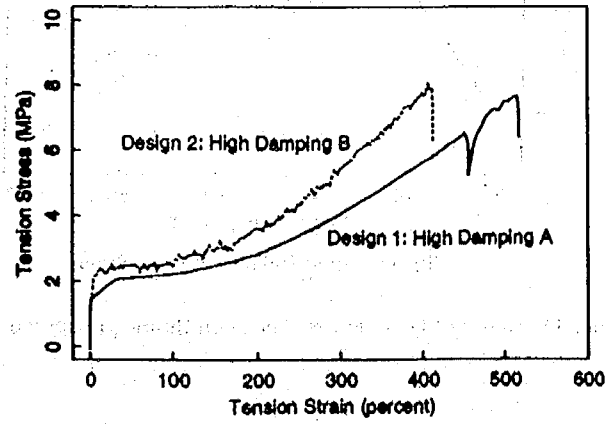


Fig. 15 Tension Failure, Designs 1 and 2

APPROVING TEST RESULTS ON FOUR HIGH DAMPING RUBBER BEARINGS

Kazuhiko KAWASHIMA[1], Kazuo ENDO[2], Nobuyuki DORO[3], Chiaki SUDO[4], Ichiro NISHIKAWA[5]

[1] Head, Earthquake Engineering Division, Public Works Research Institute, Tsukuba-shi, Ibaraki, Japan
[2] Chief Engineer, Construction Materials Dept., The Yokohama Rubber Co.,Ltd., Hiratsuka-shi, Kanagawa, Japan
[3] Manager, Technical Dept., Chemical/Industrial Products Division, Toyo Tire & Rubber Co.,Ltd., Iruma-shi, Saitama, Japan
[4] Chief Engineer, New Products Dept. (Seismic isolation), Bridgestone Corporation, Yokohama-shi, Kanagawa, Japan
[5] Manager, Vibration & Control Dept., Showa Electric Wire & Cable Co.,Ltd., Sagamihara-shi, Kanagawa, Japan

SUMMARY

Through the Joint Research Program between Public Works Research Institute and 28 private companies for the past three years, 4 High Damping Rubber Bearings were developed. Because the standard Approving Test Methods were also developed in the Joint Research Program, a series of loading tests were made for the 4 bearings. The approving tests results were effectively used for developing design method of the devices. This paper briefly presents the performance of the 4 High Damping Rubber Bearings through the Standard Approving Test Methods.

INTRODUCTION

The high damping laminated rubber bearing (HDR) is a maintenance-free and isotropic Menshin device, which has full functions required to a Menshin device of bridges, namely vertical load-bearing capacity, horizontal restoring force and energy dissipation capacity, by its simple structure without any additional dampers. These are the excellent characteristics as the Menshin devices for bridges, and they have been increasingly adopted to bridges in Japan (Refs.5 and 6).

In the Joint Research Program on "Development of Menshin System of Highway Bridges" between PWRI and 28 corporations, 4 HDRs were developed. The corporations in charge of the development in cooperation with the Pub-

lic Works Research Institute are The Yokohama Rubber Co.,Ltd (HDR-1), Toyo Tire & Rubber Co.,Ltd (HDR-2), Bridgestone Corporation (HDR-3) and Showa Electric Wire & Cable Co.,Ltd (HDR-4). Various targets were set for each HDR which differs considerably in performance and character, although the structures are almost the same.
In the first year, an examination into the fundamental structure of the HDRs was made. Simultaneously, a target to develop the characteristics and performance was set up and the development of material was made (Ref.1). In the 2nd year, a series of tests to confirm the HDRs was made by the corporations, before the Dynamic Loading Tests for aiming at confirming the performance were made at PWRI. These tests were performed under almost the same conditions following the Standard Approving Tests Methods which were developed separately in the Joint Research Programs (Ref.2).
In the tests, the fundamental and indispensable performance of the Menshin devices for bridges was confirmed. In the 3rd year, some following-up tests were made and a practical design method was developed (Ref.3).

STRUCTURAL CHARACTERISTICS

HDR-1, HDR-2 and HDR-3 are characterized by a typical laminated structure in which the side of inner steel plates used as reinforcements of rubber are covered by rubber as shown in Fig.1. On the other hand, in HDR-4, the steel plates project their own edges from the surface of the rubber, as shown in Fig.2. The HDR-4 has an advantage that the dimensional stability can be maintained during vulcanization by keeping hold of the projected steel plates. The shape of HDR-4 is, however, restricted to a circle because of the structural peculiarity of the bearing.

CHARACTERISTICS OF HIGH DAMPING RUBBER

In order to compare the performance of the 4 types of high damping rubber, the shear modulus, equivalent damping ratio, ultimate elongation and tensile strength were evaluated. They are summarized as shown in Table 1. These are essential for understanding the characteristics and performance of HDR. The shear modulus is directly related to the equivalent stiffness of the Menshin device, and also has an influence on the economical aspect, because the higher shear modulus can make the device smaller. The equivalent damping ratio is an important factor which contributes to the reduction in seismic force. The ultimate elongation and tensile strength are also important factors relating to the ultimate strength of the device. The characteristics of each HDR can be summarized as follows;

The shear modulus of HDR-1 is about 8.8 kgf/cm^2, the minimum of the 4 types, while the equivalent damping ratio, ultimate elongation and tensile strength are the maximum of the 4 types. In HDR-2, both of the shear

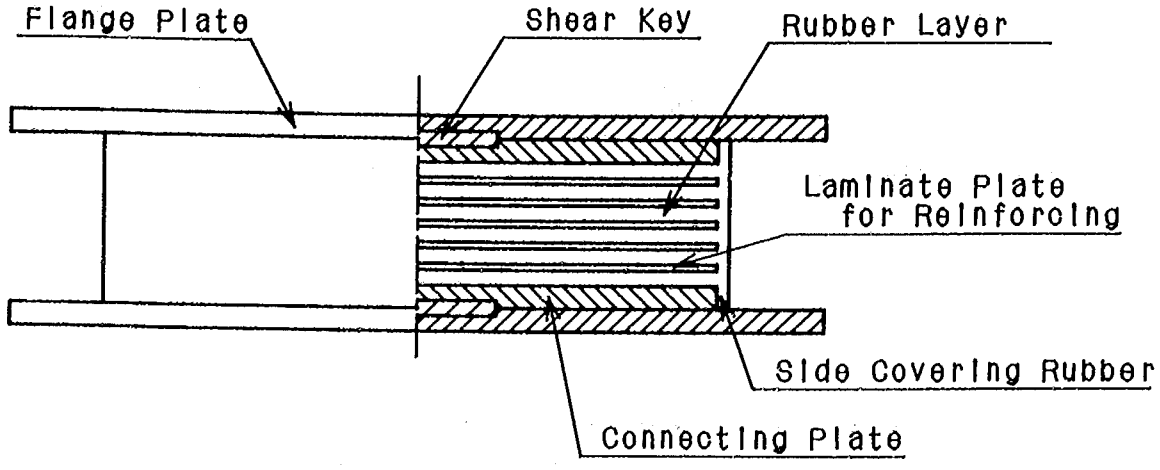


Fig. 1 Fundamental Structure of HDR-1, HDR-2 and HDR-3

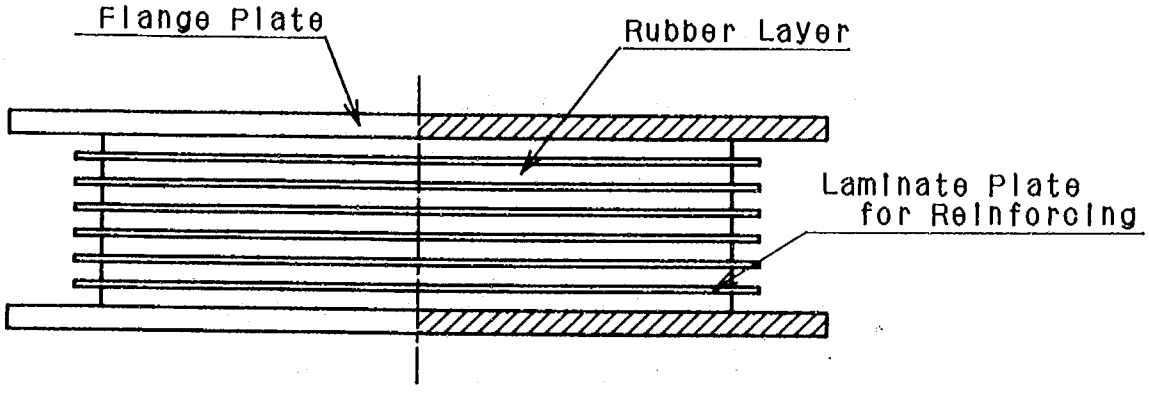


Fig. 2 Structure of HDR-4

Table 1 Characteristic Values of High Damping Rubber

	HDR-1	HDR-2	HDR-3	HDR-4
Shear modulus (kgf/cm^2)	8.8	12.0	12.0	11.3
Equivalent damping ratio (%)	15.3	14.5	14.5	12.3
Ultimate elongation (%)	680	510	666	650
Tensile strength (kgf/cm^2)	210	162	122	110

Notes:

1. The value of Shear modulus and Equivalent damping ratio is obtained by lateral loading tests using a small-sized laminated model at 150% shear strain.
2. The value of ultimate tension and tensile strength is obtained by the testing method presented in JIS K 6301 using a dumbbell type test piece.

modulus and the equivalent damping ratio are comparatively higher. The ultimate elongation is, however, 510 % or the minimum of the 4 types. In HDR-3, the shear modulus, equivalent damping ratio and ultimate elongation are all high. The tensile strength is, however, 122 kgf/cm² or low. In HDR-4, the ultimate elongation is 650 % or comparatively larger, while the equivalent damping ratio is the minimum of the 4 types.

DYNAMIC LOADING TESTS AT PWRI

A series of dynamic loading tests were made at the Public Works Research Institute for all the divices developed. The same loading procedure was adopted for the test. An actuator with dynamic loading capacity of 125 tf with the maximum loading rate of 100 cm/sec was used (Photo.1). Because the stiffness of HDR bearings depends on the temperature, the tests were made in a room with the constant temperatures (20°C). Fig.3 and Photo.2 show the specimens used for the tests.

Table 2 shows a comparison of the 4 HDR Bearings obtained from the Dynamic Loading Tests at the Public Works Research Institute.

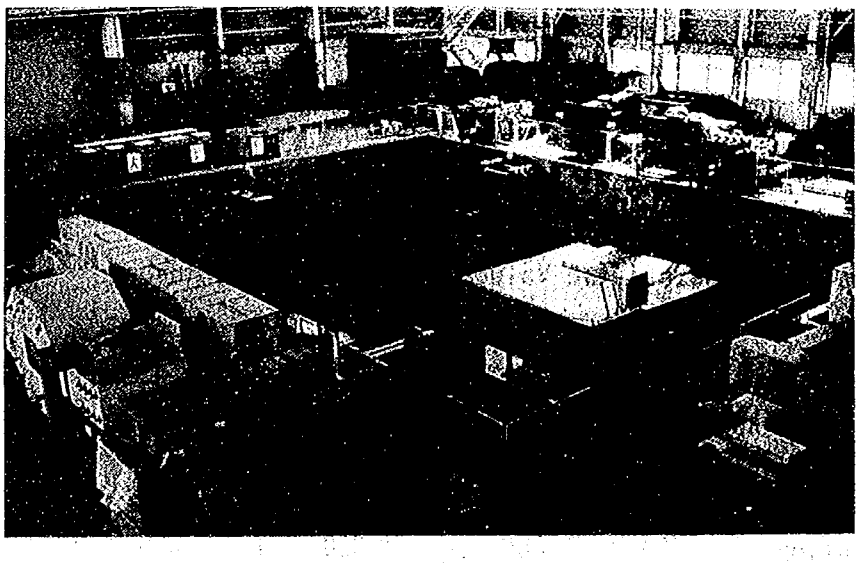
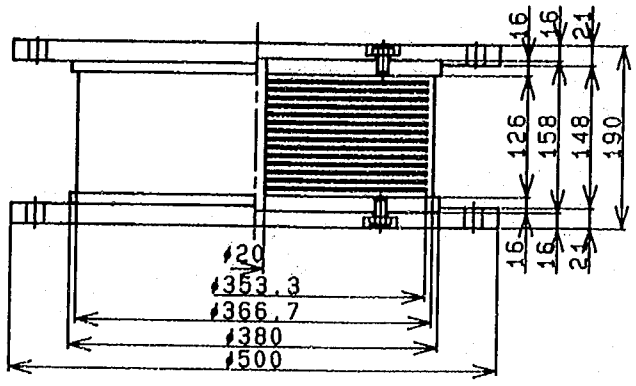
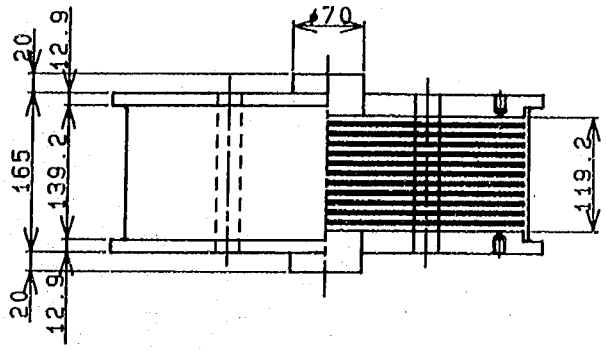


Photo. 1 Testing Facilities of the Dynamic Loading Tests at Public Works Research Institute



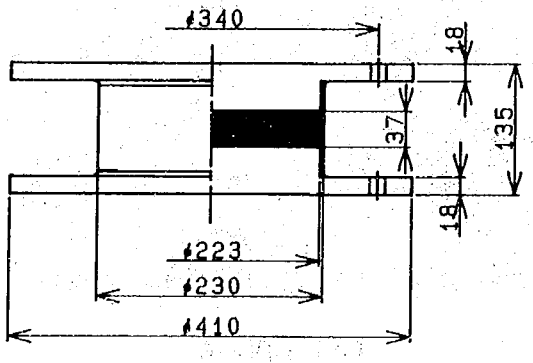
Rubber Layer 6. 33mmX15=95mm
Steel Plate 2. 21mmX14=31mm

(a)HDR-1



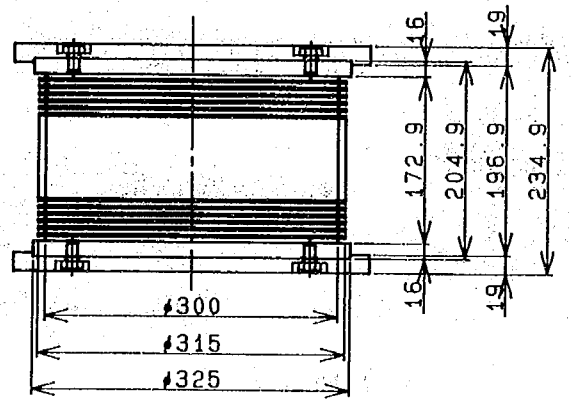
Rubber Layer 7 mmX12=84 mm
Steel Plate 3. 2mmX11=35. 2mm

(b)HDR-2



Rubber Layer 3. 75mmX8=30mm
Steel Plate 1 mmX7= 7mm

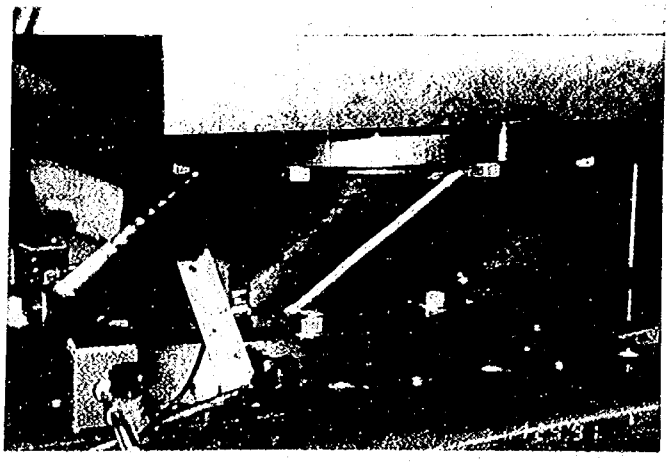
(c)HDR-3



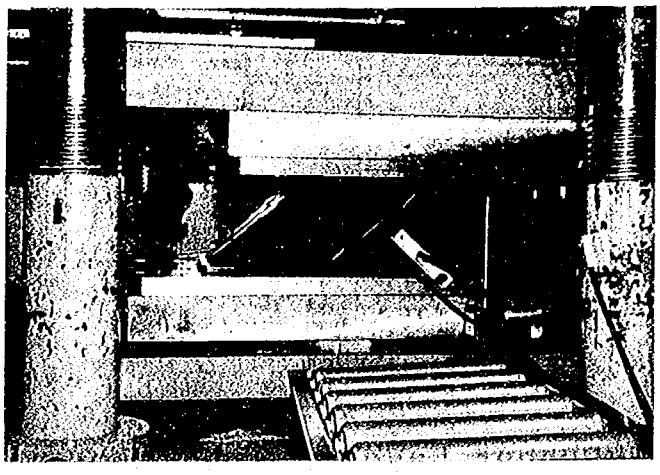
Rubber Layer 5 mmX24=120 mm
Steel Plate 2. 3mmX23= 52. 9mm

(d)HDR-4

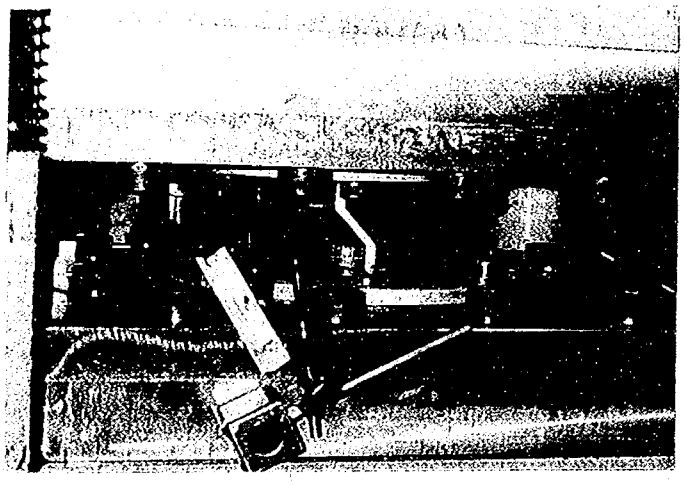
Fig. 3 Specimens used for Dynamic Loading Test at Public Works Research Institute



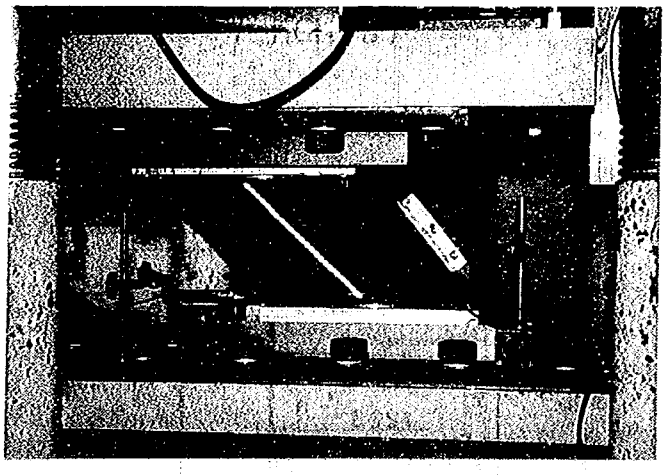
(a) HDR-1



(b) HDR-2



(c) HDR-3



(d) HDR-4

Photo. 2 HDRs under the Dynamic Loading Test at Public Works Research Institute

Table 2 Results of the Dynamic Loading Tests at Public Works Research Institute

Characteristics				HDR-1	HDR-2	HDR-3	HDR-4
①Basic characteristics	Shear modulus: G (kgf/cm²) (mean value at γ = 150%)			8.6	12.5	11.9	6.5
	Equivalent damping ratio: h (%) (mean value at γ = 150%)			14.0	7.3	13.4	10.8
②Stability against cyclic loadings The ratio of the 1st and the 10th value to the mean value during the continuous 10 cycles lateral loadings (γ = 150%, loading frequency 1.0Hz)		G_1/G_m		1.18	1.14	1.17	1.20
		G_{10}/G_m		0.98	0.98	0.98	0.99
		h_1/h_m		1.06	1.09	1.10	1.08
		h_{10}/h_m		0.95	0.93	0.95	0.91
③Stability against past loading hysteresis The ratio of the Characteristic Values of the 2nd series to those of the 1st series at γ=100and150% (Maximum loading γ=200%)		G_2/G_1	γ = 100%	0.79	0.79	0.62	0.80
		G_2/G_1	γ = 150%	0.85	0.79	0.74	0.86
		h_2/h_1	γ = 100%	1.03	1.06	1.10	1.11
		h_2/h_1	γ = 150%	1.01	1.15	1.07	1.04
④Influence of static pre-displacement The ratio of the Characteristic Values with 50% pre-displacement to those without pre-displacement (The values at γ=100, 150%)		G_{50}/G_0	γ = 100%	1.01	1.04	1.07	1.08
		G_{50}/G_0	γ = 150%	1.10	1.18	1.21	—
		h_{50}/h_0	γ = 100%	0.97	0.96	0.95	1.02
		h_{50}/h_0	γ = 150%	0.90	0.85	0.85	—
⑤Fatigue resistance characteristics The ratio of the Characteristic Values of the 40th loading of 1st series and 2nd series to the mean value of each series. The ratio of the mean Values of 2nd series to ones of 1st series. Each series consists of 40 times loadings with 3 hours interval between the series		$(G_{40}/G_m)_{1sr}$		0.84	0.86	0.85	0.86
		$(G_{40}/G_m)_{2sr}$		0.87	0.89	0.90	0.89
		$(G_m)_{2sr}/(G_m)_{1sr}$		0.96	0.94	0.93	0.93
		$(h_{40}/h_m)_{1sr}$		0.90	0.81	0.85	0.92
		$(h_{40}/h_m)_{2sr}$		0.95	0.84	0.94	0.94
		$(h_m)_{2sr}/(h_m)_{1sr}$		0.92	0.92	0.88	0.95
Testing specimens	Dimension (mm)			○367	□400	○230	○300
	Total rubber thickness(mm)			95	84	30	120

Notes: 1. G_m, h_m: in ①, The mean value of the 4th cycle ~ the 10th cycle
in ⑤, The mean value of 40 cycles
2. G_i, h_i: Suffix expresses "i-th cycle", "i-th series" and "pre-displacement(in strain)" respectively.
3. "1sr", "2sr" expresses "1st series", "2nd series" respectively.
4. ○, □ expresses circular shape and square shape respectively.

Basic Characteristics

A comparison of the equivalent stiffness and equivalent damping ratio from the Dynamic Loading Tests at PWRI with the corresponding results of an element test shown in Table 1 has revealed that there is little difference between the HDR-1 and HDR-3. There is, however, approximately 50 % decrease in the equivalent damping ratio in HDR-2. And there are 40 % decrease in the equivalent stiffness and 12 % decrease in the equivalent damping ratio in HDR-4. Some of them were caused by the effect that the specimens used for the Dynamic Loading Tests at PWRI were larger than those for the element test, and also rubber compounding and vulcanization condition were different.

Stability against Cyclic Loadings

The cyclic lateral loading tests, 150 % in shear strain and 10 times loadings without interruption, were carried out. In the 4 HDRs, the shear modulus and equivalent damping ratio (hereafter both are called "Characteristic Values") in the process take their maximum value at the first loading and decrease with the number of loading cycle.
In the shear modulus, the ratio of the value of the first loading to the average value over 10 loadings becomes minimum or +14 % in the HDR-2, while that of HDR-4 does maximum or increases by +20 %. And in every HDR, the Characteristic Values at the 10th loading is almost equal to the average value over 10 loadings. As the number of loadings increases, the Characteristic Value converges to some constant value. A change in the equivalent damping Ratio resulting from 10 times loading do not exceed 10 % of the average value over 10 loadings.

Stability against Past Loading Hysteresis

In order to confirm the influence of past loading experience to the Characteristic Values, two series of lateral loading tests were carried out as follows; In the virgin state, loading shear strains were increased from 25 %, 50 %, 100 %, 150 % up to 200 % stage by stage (1st series). Then the specimen had returned to the original point, the state of a zero shear strain, immediately after the 1st series, the same process of loading was repeated in the 2nd series.
This experiment has indicated that the shear modulus in the 2nd series tends to become smaller than that in the 1st series, while the equivalent damping ratio tends to become larger. The equivalent damping ratio in the 2nd series for HDRs is likely to increase. Therefore it is unnecessary to take the change rate into consideration because it is very small.
However, the shear modulus in the 2nd series decreases approximately 20-30 % at 100 % in shear strain, and 15-25 % at 150 % in shear strain. The change rate of the shear modulus between the 1st series and the 2nd series was 14-20 % at the minimum for the HDR-4. However, this fact can be just a

reference because the value of the shear modulus itself is very small. The maximum of this rate was 26-32 % for the HDR-3. The reason is that the rubber has been compounded so that the shear modulus might be relatively high. Attention should be paid to a change in the shear modulus because it directly affects a change in the equivalent stiffness of bridge bearings.

Influence of Static Pre-displacement

Under pre-displacement (50 % in shear strain), the shear modulus becomes 10-21 % larger, and the equivalent damping ratio becomes 0-15 % smaller in comparison with those under no pre-displacement. As no test was made on the HDR-4 subjected to 150 % shear strain under pre-displacement, the change rate of the Characteristic Values are not given in the Table 2.

There can be considered two main reasons why the shear modulus increases under pre-displacement: One is that a decrease in the effective bearing area due to the existence of static displacement causes the bearing stress to increase, which causes the intermolecular bonding strength of rubber to increase. This is a general tendency observed in rubber bearings. The other reason is that the existence of static pre-displacement makes the total shear strain increase and the influence of the resistance of rubber to tensile deformation more dominant, i.e., hardening phenomenon. The addition of 100 % of the dynamic strain amplitude to 50 % of the static strain gives rise to 150 % of the strain in total, and this does not cause a hardening phenomenon to occur. And an increase in the shear modulus is limited to about 8 %, and 150 % of the dynamic strain amplitude leads to 200 % of the shear modulus in total, which makes the hardening phenomenon more noticeable. This process causes 20 % increase in the shear modulus of the HDR-2 and HDR-3. The increase in the HDR-1 is relatively small, or 10 %. This reason is that the absolute value of the shear modulus is small (the hardness of rubber is small), and there is a delay in the occurrence of a hardening phenomenon. In the HDR under pre-displacement, whose shear modulus has a large rate of increase, the equivalent damping ratio is likely to have a large rate of decrease. This means that an increase in the shear modulus or equivalent stiffness leads to an increase in potential energy. But the changing rate of the equivalent damping ratio is limited to about 15 % even in the HDR-2 and HDR-3 which have a relatively high rate of change among the HDRs.

Fatigue Resistance Characteristics

In the Dynamic Loading Tests at PWRI, an investigation into the fatigue resistance characteristics of HDRs subjected to a series of repetitions of earthquake motion due to a significant earthquake and sequent aftershocks was made. The one series of tests consisted of 40 times lateral cyclic loading of 150 % in shear strain with a period of 2 seconds. Two series were carried out sequentially with a break of 3 hours taken between them

to investigate a change in the Characteristic Values during the test and whether there are change in the appearance or not. The fatigue resistence characteristics of HDRs were also examined on the basis of a rise in the surface temperature of the bearings for reference.

Concerning a change in the shear modulus, the ratio of the shear modulus at the 40th loading to the average value over 40 loadings in the first series is about 0.85 for the HDRs. On the other hand, the same ratio in the second series is about 0.90. This means that the rate of decrease in the second series is smaller than that in the first series. The rate of change of the shear modulus averaged over 40 loadings in the second series in comparison with that in the first series is only 5 % for all the 4 HDRs.
The rate of change of the equivalent damping ratio is much smaller than that of the shear modulus. And these were nothing unusual in the appearance of any of the HDRs after loadings. The rise in the surface temperature of the HDRs was about 10° C, and this hardly becomes a serious problem.

Changes in the Characteristic Values were investigated when the loading frequency changed from 0.1 Hz to 1.0 Hz, although the result was not referred to in Table 2. There was no significant change in either of the Characteristic Values. Furthermore, vertical displacement due to vertical dead loads was examined only to find no abnormal changes in any of the HDRs.
These experimental results have revealed that the fatigue resistance charactreristics of the 4 HDRs are excellent against a series of earthquakes including large earthquakes.

OTHER EXAMINATIONS BESIDES THE DYNAMIC LOADING TESTS AT PWRI

In the Dynamic Loading Tests at PWRI, the fundamental characteristics and performance of 4 types of HDR have been confirmed, and by making a comparison of the characteristics and performance of HDRs, their features have been revealed. However, some problems to be solved for practical applications are remained as;

a) During the tests, the temperature was kept constant.
b) No test to verify the ultimate strength of the Menshin devices was made.
c) Comparatively small specimens were used.

Thus, some additional examinations were made for the 4 HDRs individually on the following thema;

1) Confirmation of the Characteristic Values over a wide range of temperature (-10 - +40° C);
2) Confirmation of the ultimate breaking shear strain from the breaking test;

3) Confirmation of the characteristic of shear force caused by a slow rate of displacement due to the temrerature change;
4) Estimation of the long term changes in the Characteristic Values by heating accelerating test;
5) Confirmation of the performance of large-scale bearings;
6) Establishing the design method;

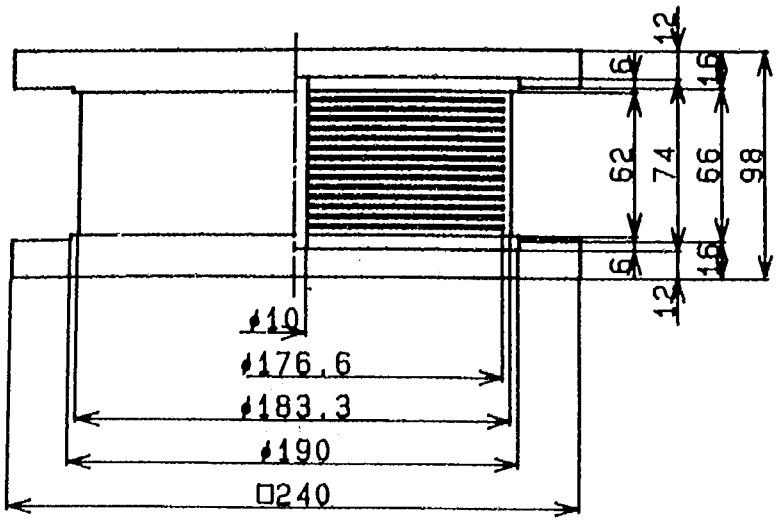
These results are shown in Table 3.

Table 3 Other Examinations besides the Dynamic Loading Tests at Public Works Research Institute

Characteristics		HDR-1	HDR-2	HDR-3	HDR-4
①The ratio of the Characteristic Values under -10℃ to those under 40℃.	G_{-10}/G_{40}	1.40	—	—	1.44
	h_{-10}/h_{40}	1.34	—	—	—
②Ultimate breaking shear deflection (%)		610	—	649	confirmed up to 350
③Shear modulus by a slow rate of displacement		cf. Eqs. (1)	—	—	—
④Long term changes in the Characteristic Values comparing with original values.	G_{40year}	—	—	—	+9.8%
	h_{40year}	—	—	—	−3.4%
⑤Performance of the large-scale specimen	Dimension (mm)	—	□1500 × H216	□805 × H280	—
	Max. shear def. (%)	—	150	230	—

For changes in the Characteristic Values resulting from temperature changes, the HDR-1 and HDR-4 have been examined. But the latter has never been examined for the equivalent damping ratio so far. The results have proved that there is 30 % or more difference in the Characteristic Values between 40° C and -10° C in each case, and the values are sensitive to temperature change.

The HDR-1 (Figs.4,5 and Photo.4) and HDR-3 (Figs.6,7 and Photo.4) have been examined for the ultimate strength by a lateral breaking test. The HDR-4 (Figs.8,9 and 10) has been examined only for the ability of large deflection up to 350 % of the shear strain. The ultimate strength of the HDR-2 has never been tested. It has been confirmed that the breaking shear strain of the HDR-1 and HDR-3 are over 600 % respectively. And further examination is necessary to apply these results to the design of the large-scale



Rubber Layer 3.17mm×15=47.5mm
Steel Plate 1.04mm×14=14.5mm

Fig.4 Specimen of HDR-1

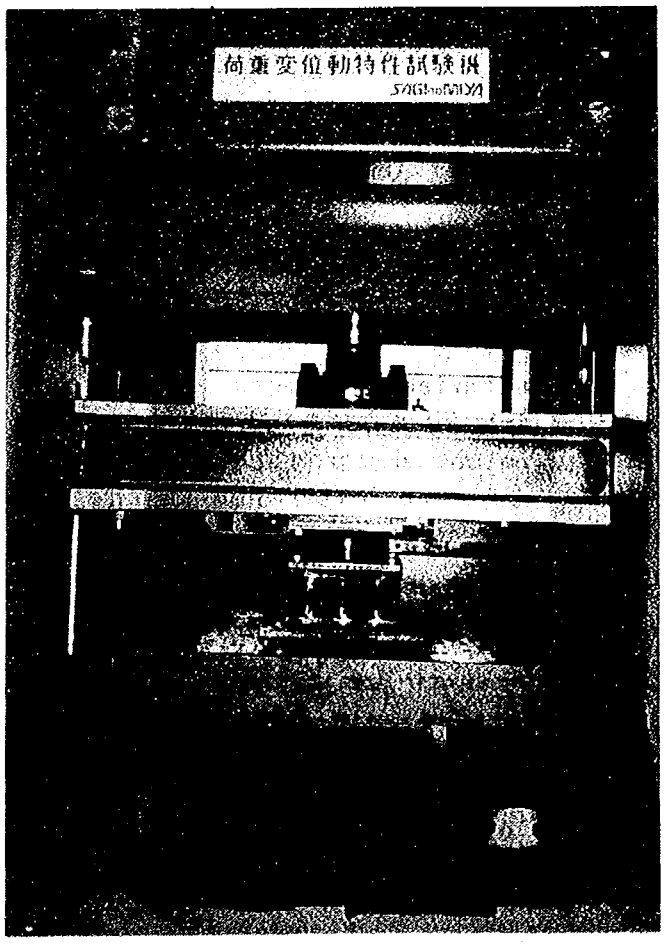
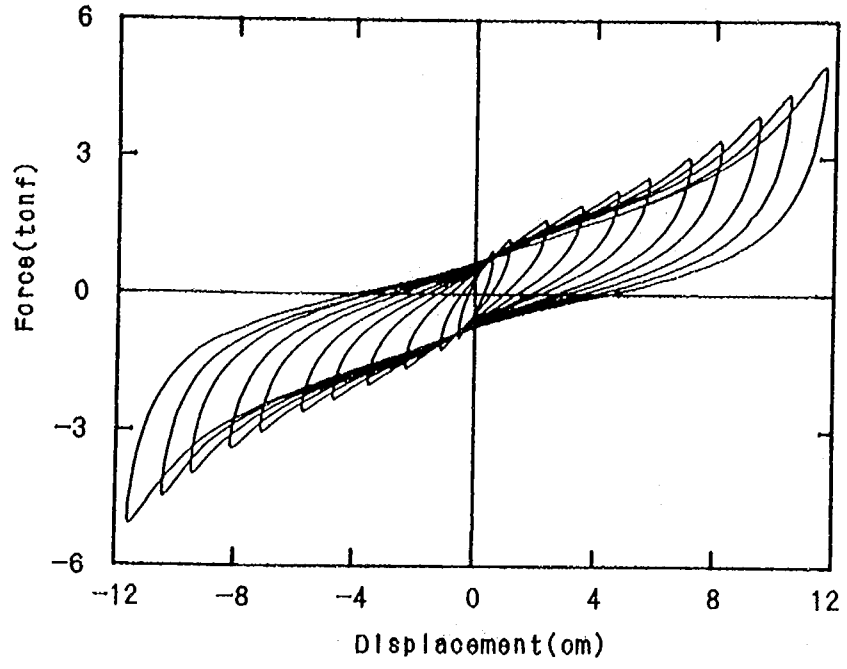
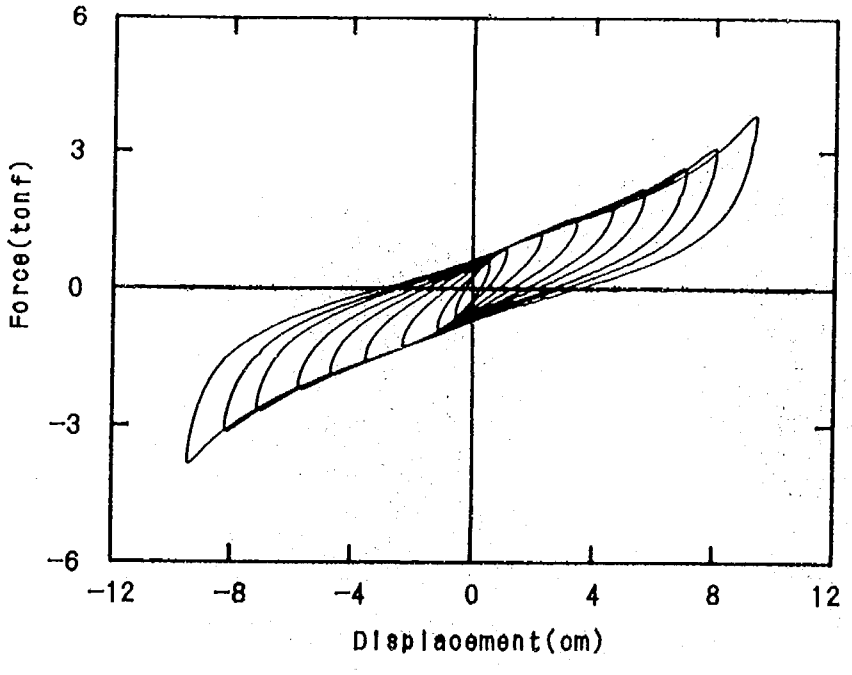


Photo.3 Testing Facility for HDR-1



Bearing Stress
60kgf/cm²
Frequency
0.5Hz
Sine Wave
Shear Strain
Min ±12.5%
Max ±250%
Loading Cycle
3Cycles
Specimen
Scale Model
Temp.
20℃

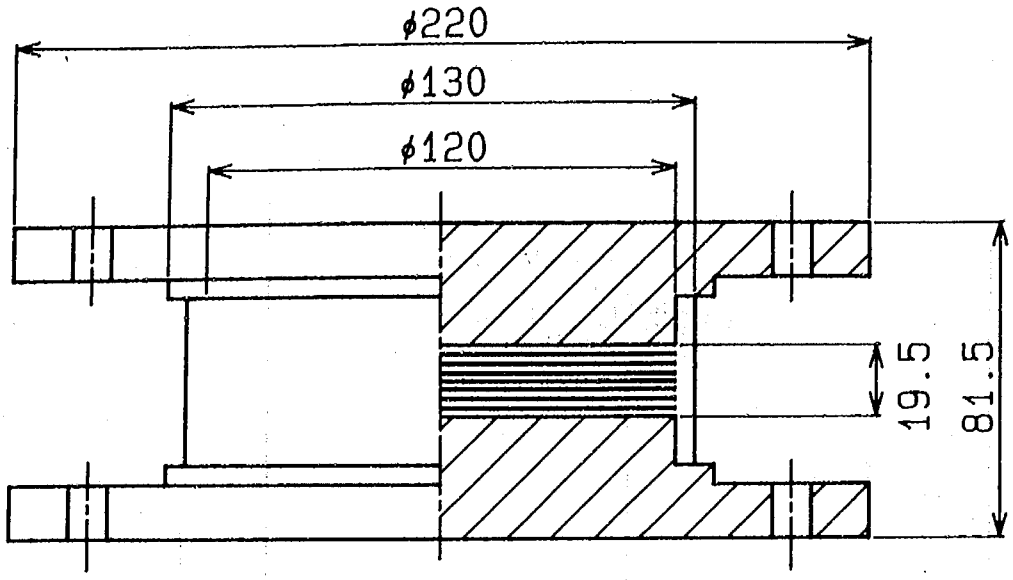
(a)1st Series



Bearing Stress
60kgf/cm²
Frequency
0.5Hz
Sine Wave
Shear Strain
Min ±12.5%
Max ±200%
Loading Cycle
3Cycles
Specimen
Scale Model
Temp.
20℃

(b)2nd Series

Fig.5 Hysteresis Loop of HDR-1



Rubber Layer 2 mm×8=16 mm
Steel Plate 0.5mm×7= 3.5mm

Fig. 6 HDR-3 Specimen used for Ultimete Lateral Loading Test

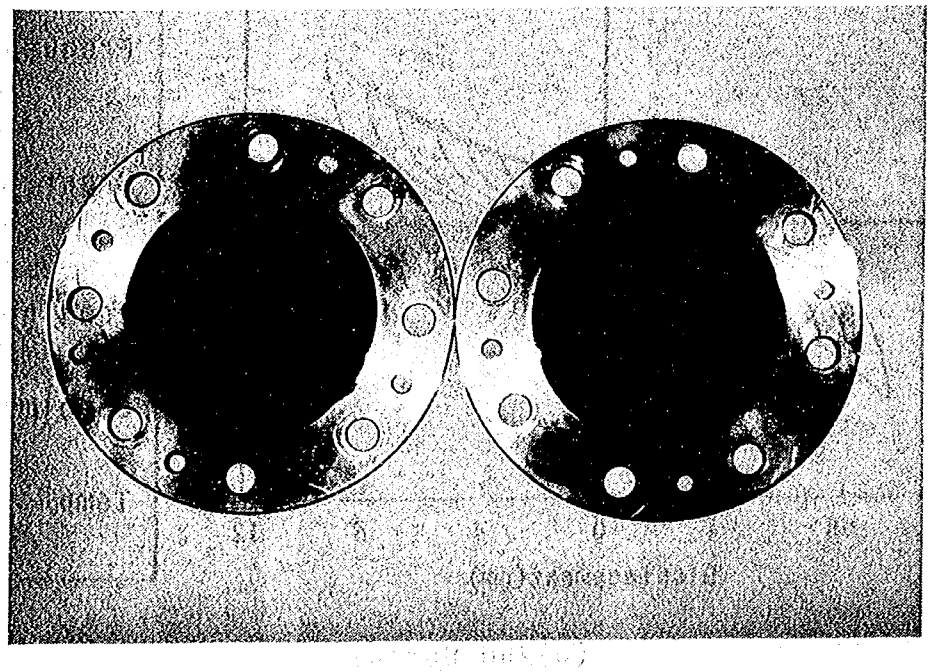
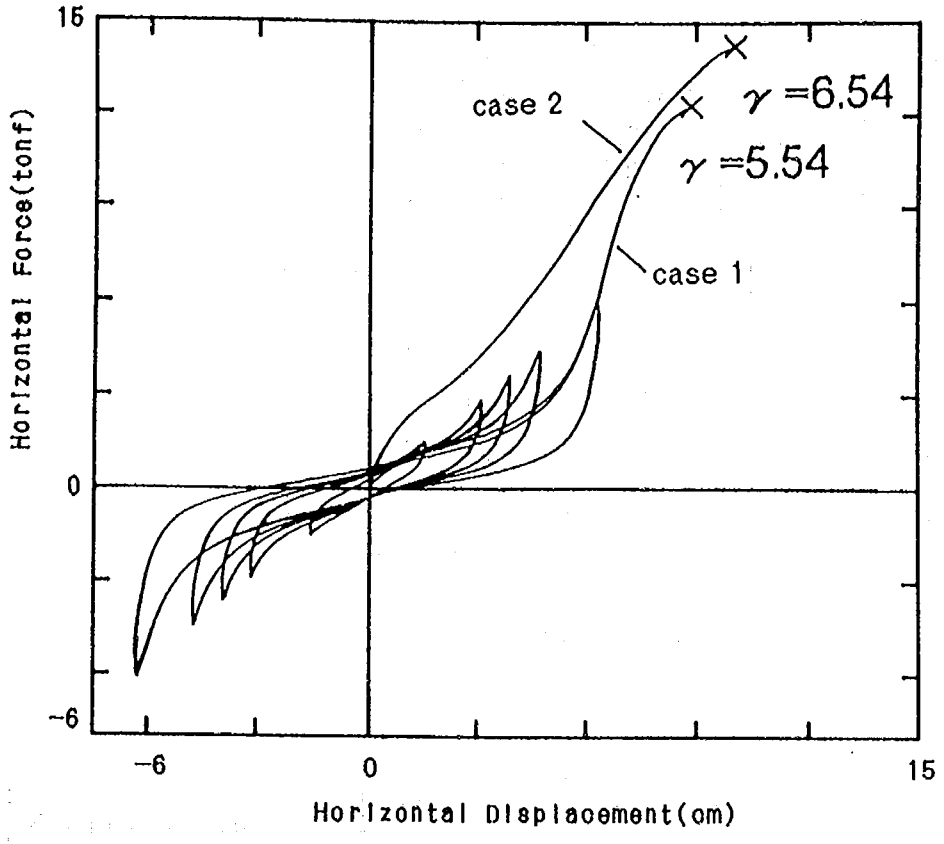


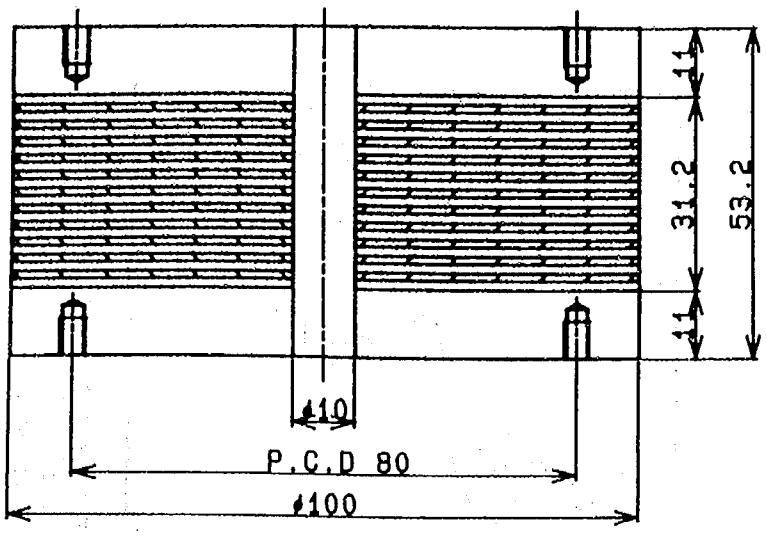
Photo. 4 HDR-3 Specimen for Lateral Breaking Test



Case 1	
Bearing Stress	60kgf/cm²
Load Velocity	4mm/sec
Shear Strain	±100% ±200% ±250% ±300% ±400% Ultimate
Loading Cycle	3Cycles
Specimen	φ180XH81.5
Temp.	Room Temp.

Case 2	
Bearing Stress	60kgf/cm²
Load Velocity	32mm/sec
Shear Strain	Ultimate
Loading Cycle	1Cycle
Specimen	φ180XH81.5
Temp.	Room Temp.

Fig. 7 Ultimate Lateral Loading Test



Rubber Layer 1.5mmX12=18 mm
Steel Plate 1.2mmX11=13.2mm

Fig. 8 Specimen of HDR-4

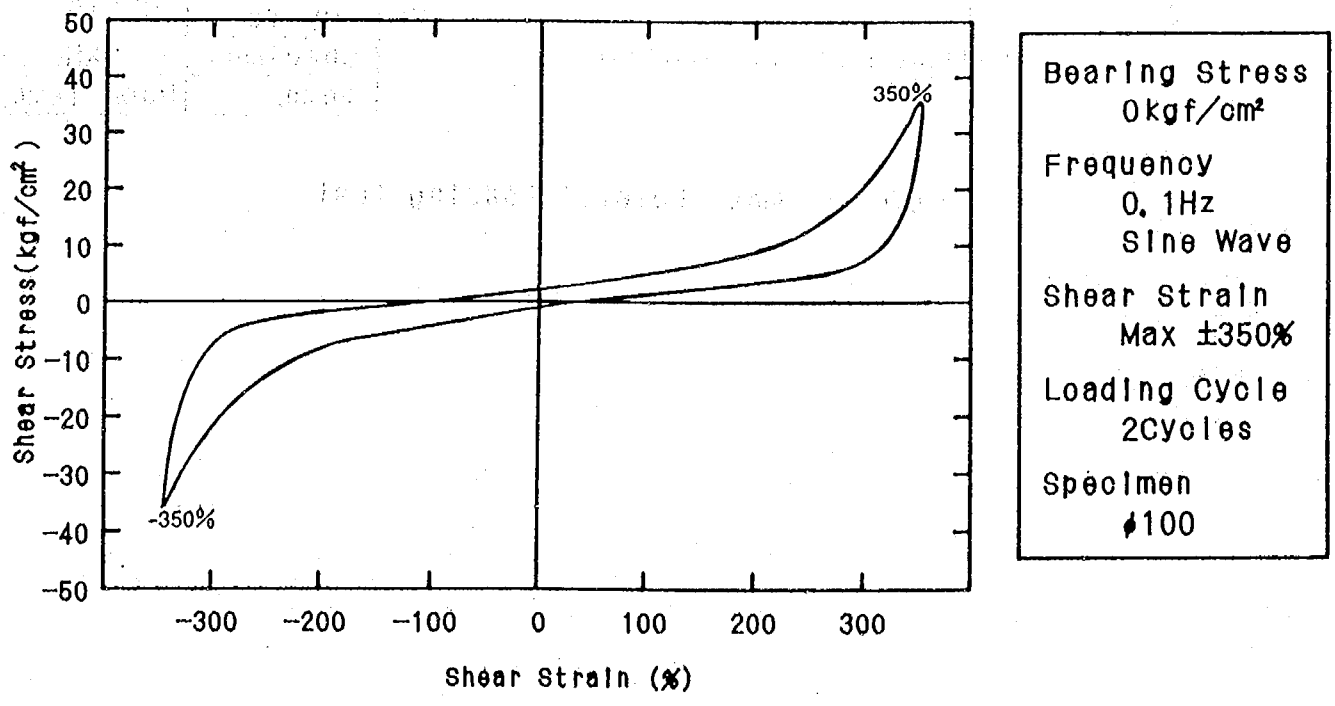
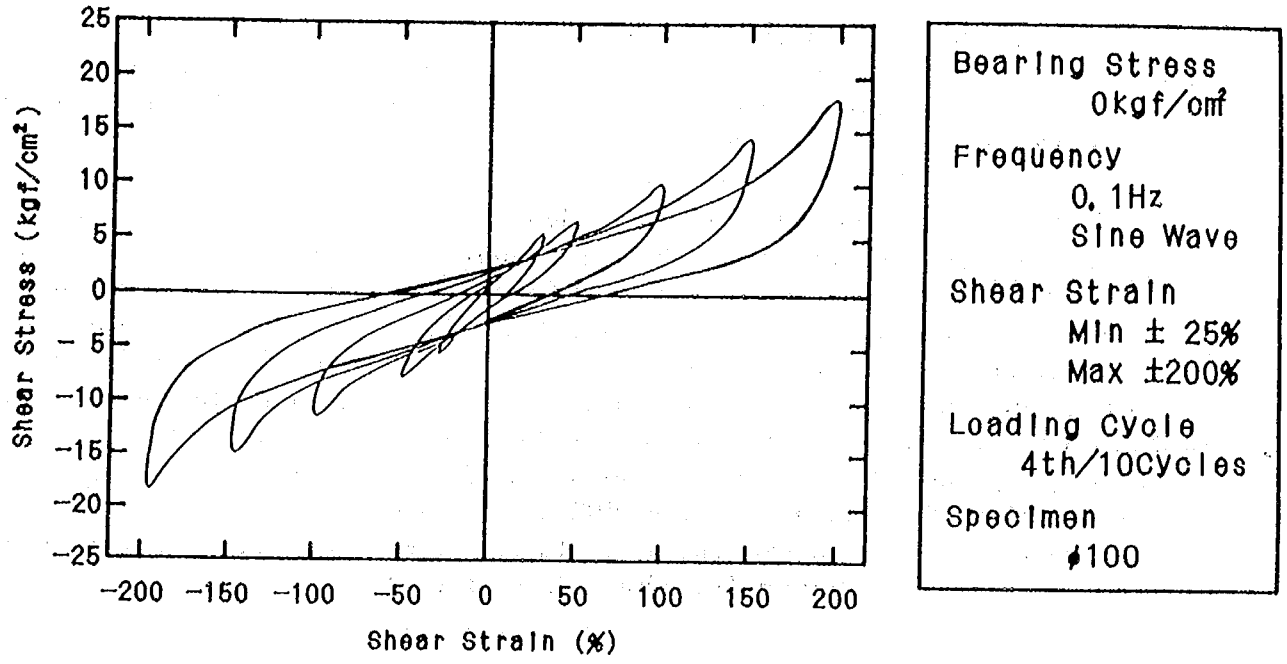
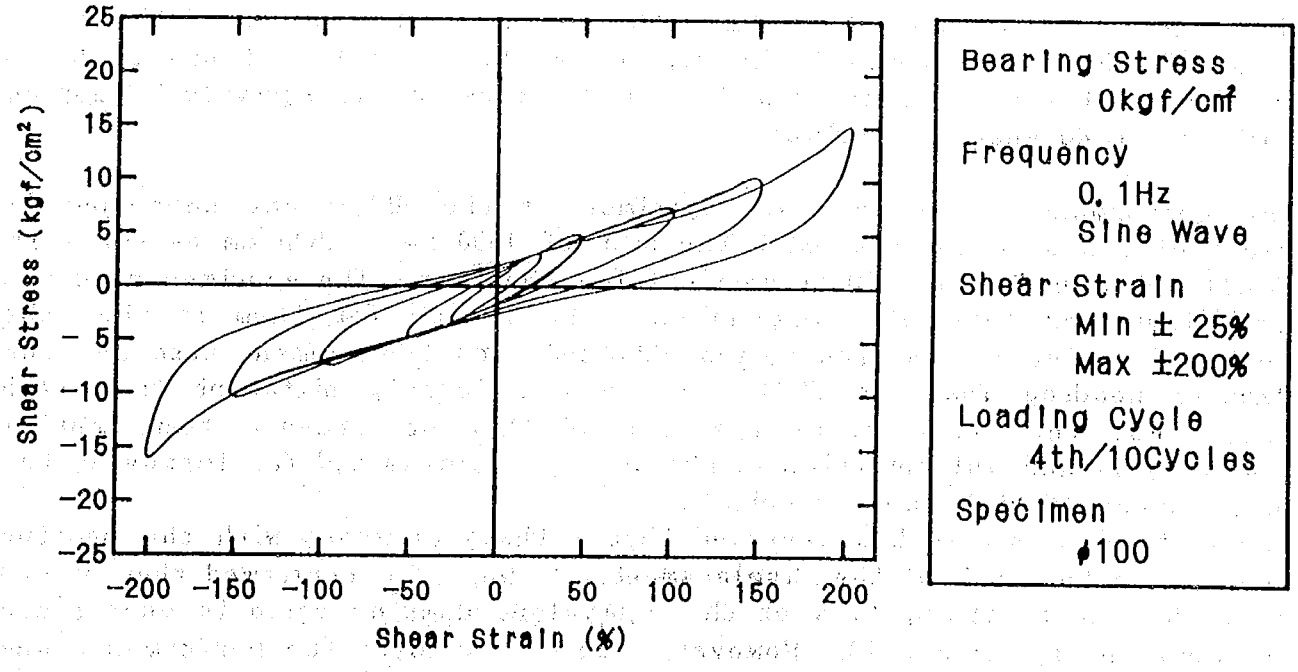


Fig. 10 Large-Displasement of HDR-4



(a)1st Series



(b)2nd Series

Fig. 9 Hysteresis Loop of HDR-4

bearing, because these results have been obtained using relatively small specimens with the diameter between 100 mm to 190mm. It will be possible to use them considering some safety factor (for example, 500 % for design purpose) for the present.

The characteristic of shear force of a Menshin device by a slow rate of displacement due to temperature change becomes an important factor in designing super multi-span continuous bridges in particular. Only the HDR-1 has been tested to make clear a characteristic of shear forces due to slow displacements, by means of the extrapolation and stress relaxation methods provided in "Manual for Menshin Design of Highway Bridges, 7.3.5 Horizontal Restoring Force due to Slow Deflection Caused by Such Effects as Creep, Drying Shrinkage and Temperature Changes" (Ref.4). The shear force due to slow deflection in the HDR-1 is about 60 % of that during dynamic loading. An expression for calculating the shear modulus for slow rate of displacements proposed for the HDR-1 is as ;

$$G_s = 5.94 \times \gamma_s^{-0.2335} \qquad (1)$$

where

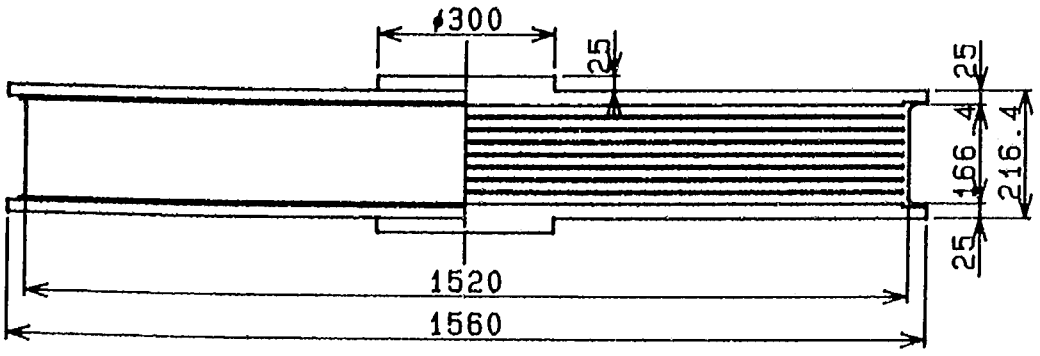
G_s: Shear modulus for slow rate of displacements (kgf/cm^2)

γ_s: Shear strain

Heat Aging Test was made to examine the Characteristic Values of the HDR-4 after 40 years of service. The result has revealed that there is 9.8 % increase in the shear modulus and 3.4 % decrease in the equivalent damping ratio after 40 years of service.

The performance of large-scale specimen of the HDR-2 was confirmed by means of a square specimen with the size of 1500 mm x 1500 mm as shown in Fig.11 , designed as a 1500 tf vertical load bearing. The specimen used was made from new type of compounding. The reason for them is that the observed equivalent damping ratios obtained from the element test and the Dynamic Loading Tests at PWRI have been noticeably different from each other. For the large scale specimen of this performance test, rubber compounding and vulcanization condition were re-examined for improving the performance of high damping rubber.
The test conclusively has revealed that nothing is wrong with the bearing even at up to 175 % of the displacement. It was also confirmed that at 100 % of the shear strain, 15 % of the equivalent damping ratio is guaranteed as shown in Figs.12 and 13. However, a test to confirm the performance was not conducted under the same conditions as those of the Dynamic Loading Tests at PWRI.

For the HDR-3, using a square specimen with the size of 805 mm x 805 mm as shown in Fig.14 and Photo.5, it was proved that nothing unusual was noticed in the bearing subjected to the large deflection or 230 % in the shear



Rubber Layer 18mm×8=144mm

Steel Plate 3.2mm×7=22.4mm

Fig. 11 Large-Scale Specimen of HDR-2

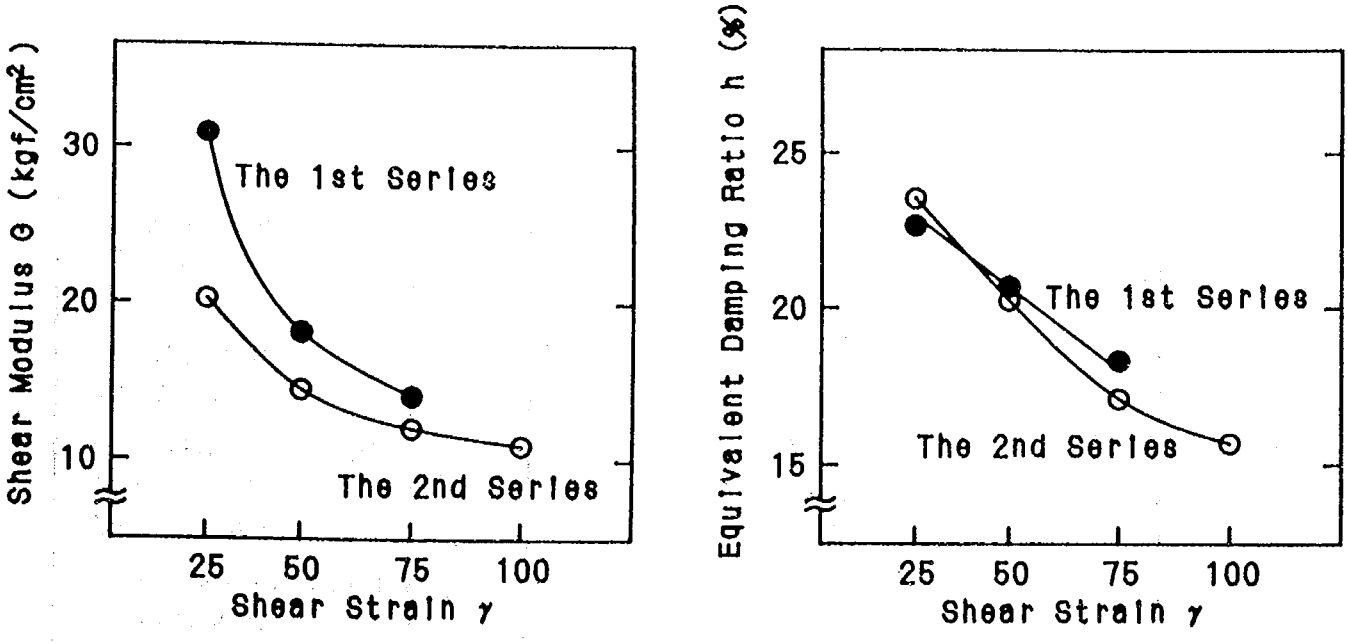
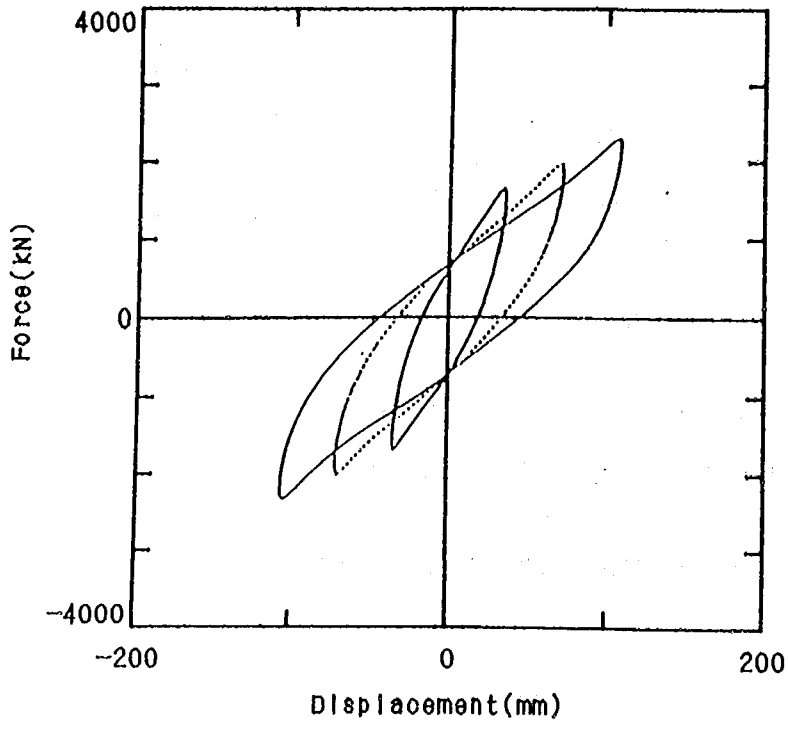
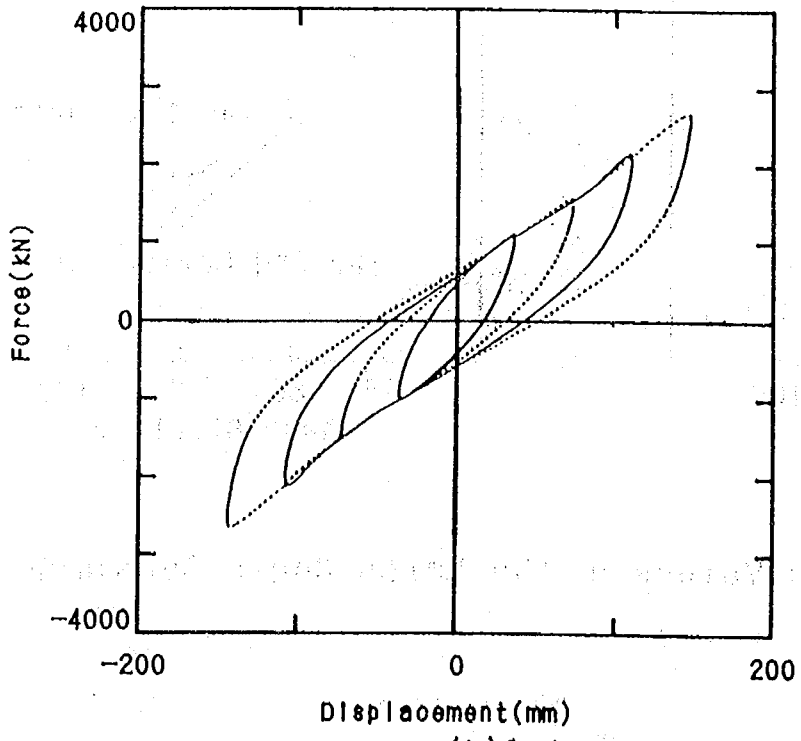


Fig. 13 Characteristic Values of the Large-Scale Specimen of HDR-2



Bearing Stress
60.7kgf/cm²
Frequency
0.003Hz
Sine Wave
Shear Strain
Min ± 20%
Max ± 75%
Loading Cycle
3Cycles
Specimen
□1500XH216

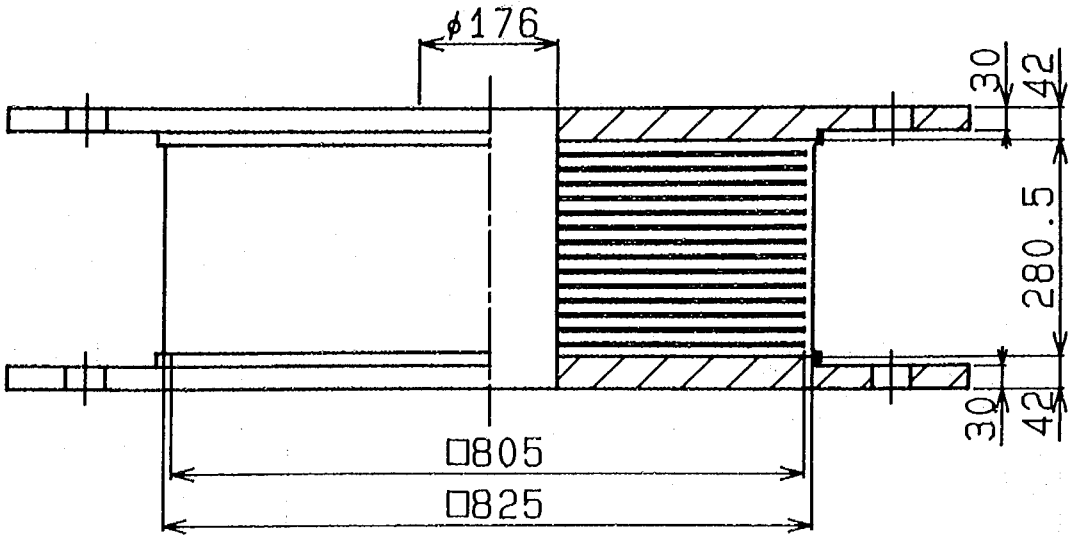
(a)1st Series



Bearing Stress
60.7kgf/cm²
Frequency
0.003Hz
Sine Wave
Shear Strain
Min ± 20%
Max ± 75%
Loading Cycle
3Cycles
Specimen
□1500XH216

(b)2nd Series

Fig. 12 Hysteresis Loop of the Large-Scale Specimen of HDR-2



Rubber Layer 14.5mm×15=217.5mm
Steel Plate 4.5mm×14= 63 mm

Fig.14 Large-Scale Specimen of HDR-3

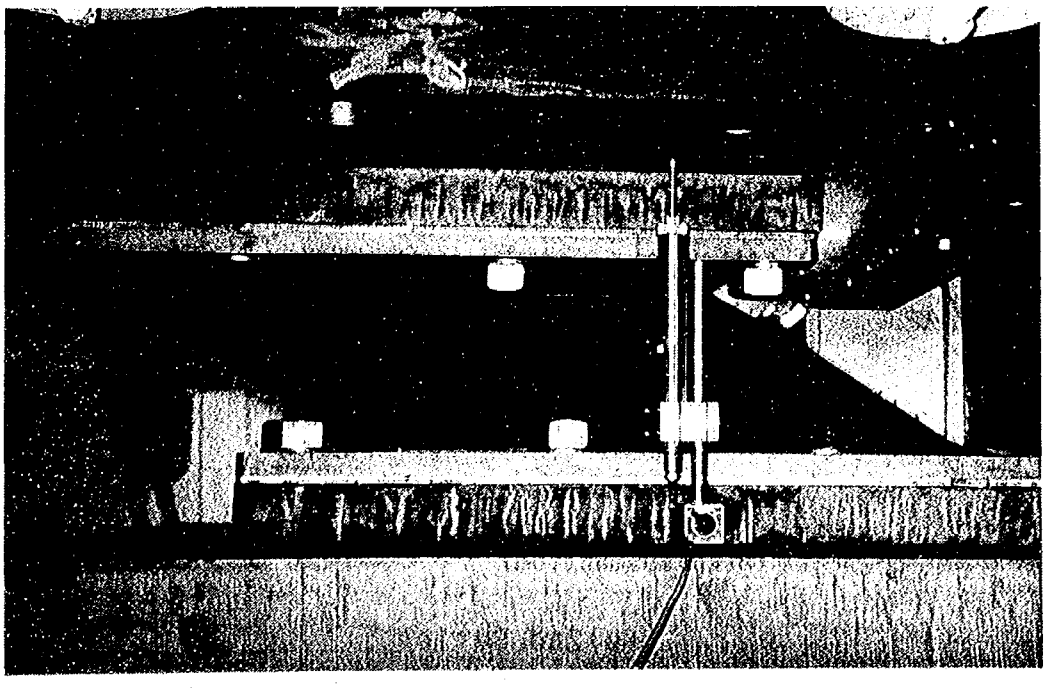
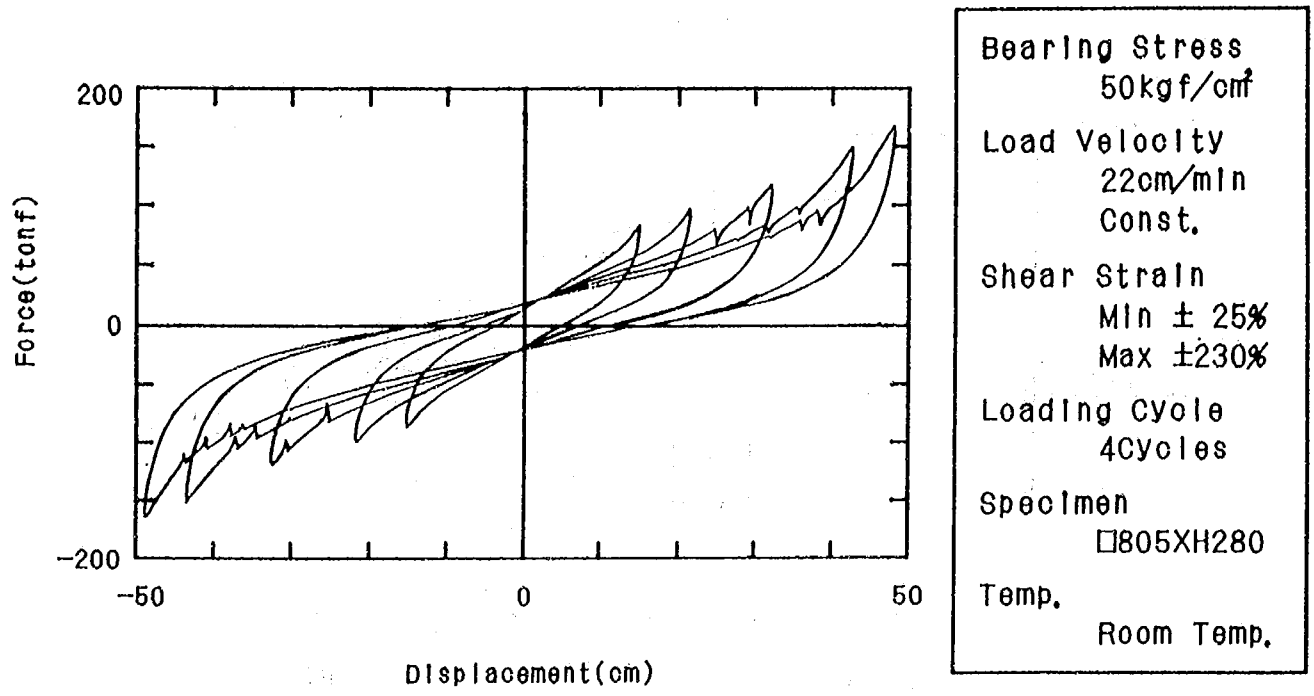
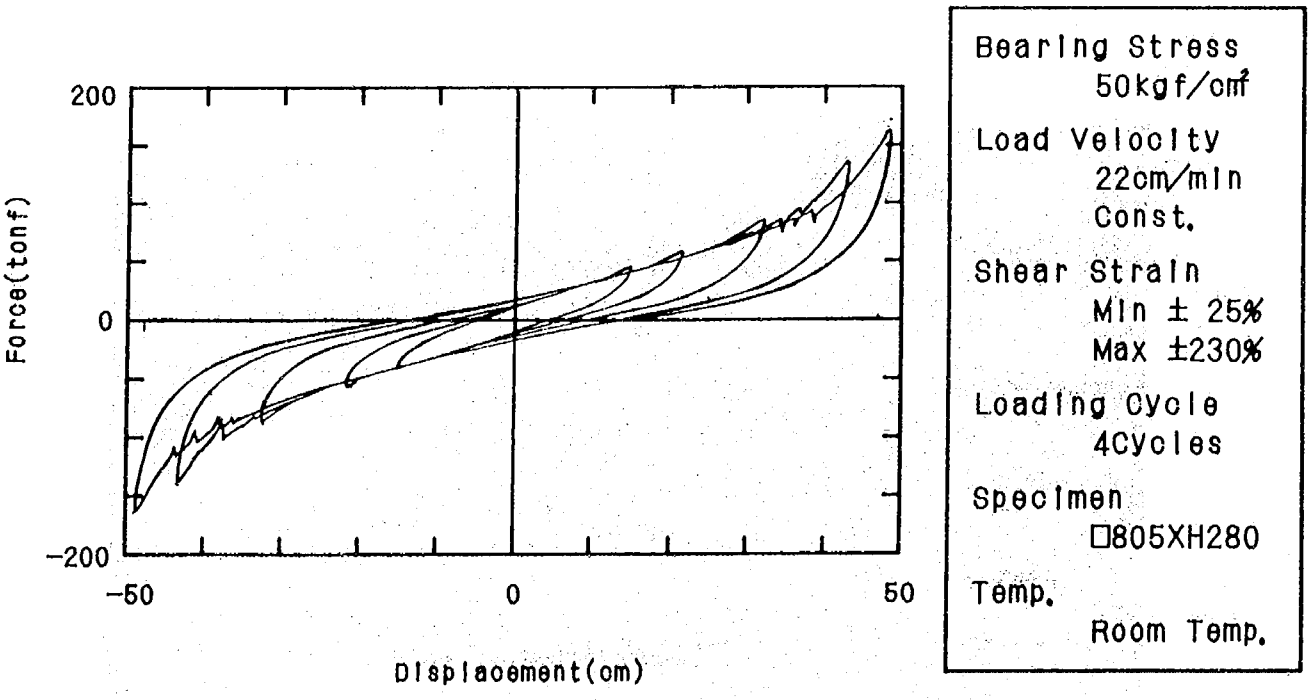


Photo.5 Large-Scale Specimen HDR-3



(a)1st Series



(b)2nd Series

Fig. 15 Hysteresis Loop of the Large-Scale Specimen of HDR-3

strain as shown in Fig.15, and also the Characteristic Values were almost the same as the values obtained already by the Dynamic Loading Test at PWRI.

The expressions for calculating the shear modulus and the equivalent damping ratio have been established considering all the examination above as follows:

$$G = a_0 + a_1\gamma + a_2\gamma^2 + a_3\gamma^3 + a_4\gamma^4 + a_5\gamma^5 \quad (2)$$

$$h = b_0 + b_1\gamma + b_2\gamma^2 + b_3\gamma^3 \quad (3)$$

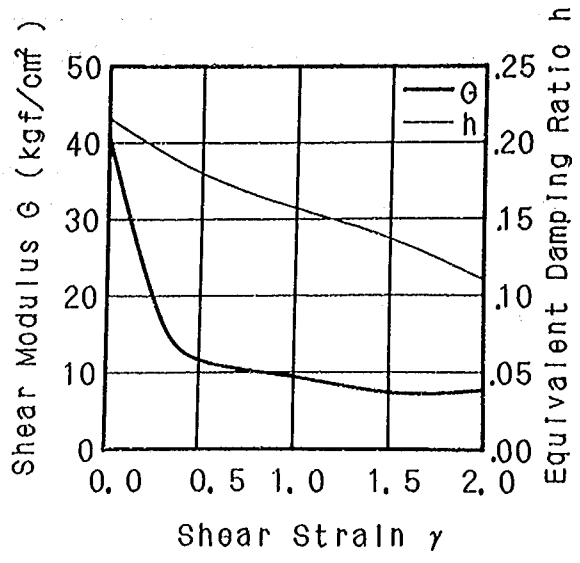
where

G : Shear modulus (kgf/cm^2)
h : Equivalent damping ratio
γ: Shear strain
a_i(i=0-5): Coefficients peculiar to each of the HDRs, and available from Table 4.
b_i(i=0-3): Coefficients peculiar to each of the HDRs, and available from Table 4.

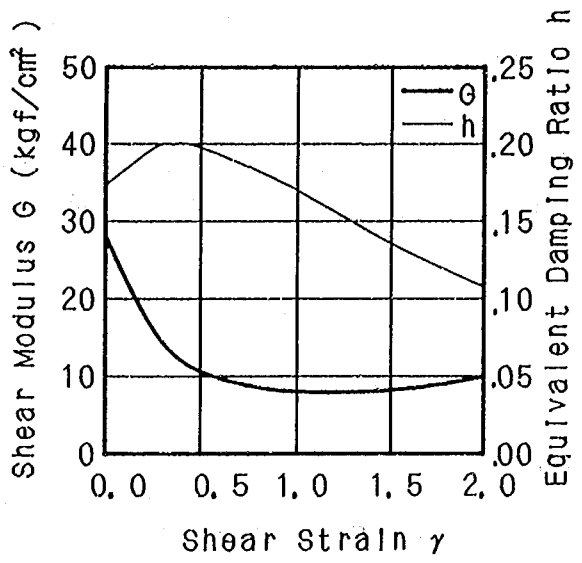
Eqs.(2) and (3) can be applied for the 4 HDRs except HDR-3 so long as the shear strain up to 200 %. For HDR-3, it can be applied up to 300 % in shear strain. The calculation results for the 4 HDRs are shown in Fig.16.

Table 4 Coefficients a_i and b_i for Eqs.(2) and (3)

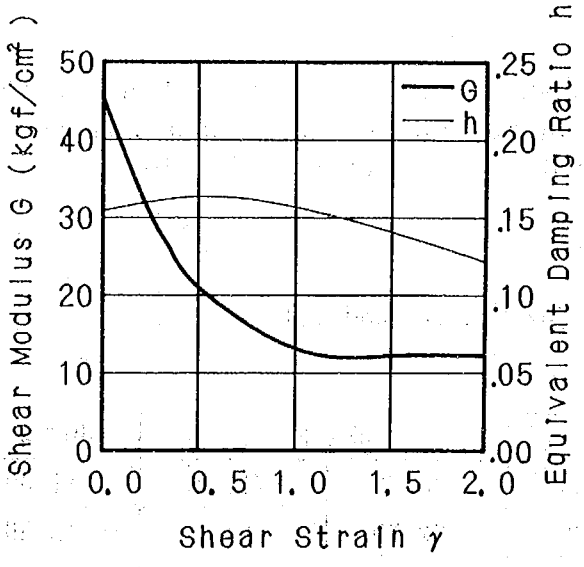
Coefficients	HDR-1	HDR-2		HDR-3		HDR-4
a_0	43.58	28.1	6.62	45.30	12.20	11.66
a_1	−155.36	− 69.7	11.2	− 72.70	−	− 12.80
a_2	286.21	98.1	− 19.1	57.33	−	8.70
a_3	−257.90	− 65.8	11.4	− 18.99	−	− 1.70
a_4	110.72	17.2	− 2.12	2.18	−	−
a_5	− 18.07	−	−	−	−	−
b_0	0.2159	0.173	0.2040	0.1543	0.1543	0.1544
b_1	− 0.0870	0.162	0.0152	0.03834	0.03834	− 0.0693
b_2	0.0397	− 0.287	− 0.0671	− 0.04448	− 0.04448	0.0695
b_3	− 0.0113	0.122	0.0177	0.00858	0.00858	− 0.0307
Range for application	$0 \leqq \gamma \leqq 2.0$	$0 \leqq \gamma \leqq 1.0$	$1 < \gamma \leqq 2.0$	$0 \leqq \gamma < 2.0$	$2 \leqq \gamma \leqq 3.0$	$0 \leqq \gamma \leqq 2.0$



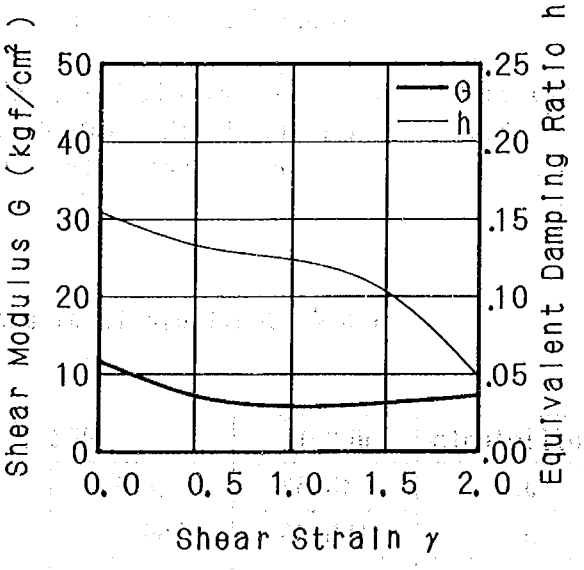
(a) HDR-1



(b) HDR-2



(c) HDR-3



(d) HDR-4

Fig. 16 Characteristic Values of 4 types of HDRs

CONCLUSIONS

Through the three years Joint Research Program, four types of High Damping Rubber Bearings have been examined intensively not only fundamental properties but also practical characteristics. The remarkable results are summarised as follows;

(1) Each type of these HDRs has its own characteristic horizontal restoring force properties. However, equivalent damping ratio of every HDR is larger than 10 %. Every type of HDR can be used as a Menshin device without any additional dampers.

(2) The applicability to the large scale bearings, the durability to the large displacement and the estimation of the long term changes in the Characteristic Values were examined and satisfactory results were obtained. Especially, the characteristic of shear force caused by a slow rate displacement is so remarkable that the HDRs are good for the super multi-span continuous bridges.

(3) The Characteristic Values of the 4 types of HDRs can be described in the same form of polynomial equations. Any of them can be designed by the same algorithm.

ACKNOWLEDGMENT

The developments of these four types of High Damping Rubber Bearings were made as a part of the Joint Research Program on "Development of Menshin System of Highway Bridges" between PWRI and 28 private companies in Japan.

REFERENCES

1) PWRI: The Report of The Joint Research Program on Development of Menshin Systemof Highway Bridges (No.1), PWRI Joint Research Report, 1990 (in Japanese)
2) PWRI: The Report of The Joint Research Program on Development of Menshin Systemof Highway Bridges (No.2), PWRI Joint Research Report, 1991 (in Japanese)
3) PWRI: The Report of The Joint Research Program on Development of Menshin Systemof Highway Bridges (No.3), PWRI Joint Research Report, 1992 (in Japanese)
4) PWRI and 28 Private Firms: Manual for Menshin Design of Highway Bridges, 1992
5) Ikeda,T., Kumakura,K., Ozeki,K. and Abe,N. : Design of Karasuyama No.1 Bridge (Base Isolated Bridge), Bridge and Foundation Engeneering, Vol.25

No.6 1991 (in Japanese)
6) Anzai,K., Kikuchi,T., Goto,Y. : Vibration experiment of the Menshin designed PC Highway Bridge, The 47 th Annual Meeting, Japan Society of Civil Engineers, 1992 (in Japanese)

Session-2

Testing of Seismic Isolation Hardware-2

J-3) Hybrid Earthquake Loading Tests of Various Types of Base Isolation Bearings
(Iemura, H., Yamada, Y., Tanzo, W. and Nanjo, A.)

U-2) Seismic Response Variability of Bridges on Friction-Controllable Isolators
(Feng, M. Q.)

J-4) Shake Table Test of A Model Bridge with Sliding Isolation System
(Okamoto, S., Constantinou, M., Tsopelas, P., Fujii, S. and Ozaki, D.)

HYBRID EARTHQUAKE LOADING TESTS OF VARIOUS TYPES OF BASE ISOLATION BEARINGS

Hirokazu IEMURA
Dept. of Civil Engineering
Kyoto University

Yoshikazu YAMADA
Dept. of Civil Engineering
Kyoto University

William TANZO
Dept. of Civil Engineering
Saitama University

Atsushi NANJO
Engineering Department
Hanshin Expressway Public Corp.

ABSTRACT

Under a joint research program between Kyoto University and the Hanshin Expressway Public Corporation, five isolation bearings of different damping mechanisms were tested under identical test conditions in order to evaluate their suitability and applicability to different types of bridges. The isolation bearings, including the lead-rubber bearing, 2 types of high-damping rubber bearings, sliding rubber bearing, and a conventional rubber bearing were tested under cyclic loading and hybrid earthquake (pseudo-dynamic) test methods. In addition to the fundamental cyclic load-deformation behavior, earthquake and resonant response behavior of the five isolation bearings were obtained. From the test results, equivalent damping ratios are evaluated based on the usual cyclic loading tests as well as from earthquake response of equivalent linear elastic models. In addition, effectiveness of isolation is evaluated based on acceleration and displacement amplifications using earthquake response results obtained using the hybrid earthquake loading tests. In order to evaluate the effect of initial first-cycle stiffness of rubber bearings on the earthquake response, a second identical specimen of each type of isolation bearings was tested for its virgin earthquake response behavior.

INTRODUCTION

Research and development of seismic isolation bearings for bridges in Japan have dramatically intensified in the past two years. In Japan, several base-isolated buildings have already been designed and constructed. Many of these were initiated by big construction companies and serves as company research centers or company dormitories. Acceptance of seismic isolation concept to bridges will be easier since bridges are basically designed to be supported on bearings, unlike in building structures which are conventionally designed fixed to the base.

There will be more application of base isolation technology to bridges in the next few years with the completion of several fundamental and feasibility studies. An intensive test program

between the Public Work Research Institute of the Japanese Ministry of Construction and 28 private companies [PWRI 1991; 1990] was conducted with the main objectives of developing menshin devices for bridges and formulating design guidelines. The Hanshin Expressway Public Corporation also initiated a research on applying seismic isolation to bridges and expressways under its management. Recently, menshin-type bearings have been installed to a steel box-girder bridge along the Bay Route in Osaka. A hybrid earthquake loading system had been developed at the Dept. of Civil Engineering, Kyoto University and was used to test a high-damping rubber isolation bearing for its fundamental cyclic behavior and earthquake response behavior [Iemura et al, 1991].

Under a joint research program between Kyoto University and the Hanshin Expressway Public Corporation, five isolation bearings of different isolation mechanisms were tested using this loading system in order to evaluate their suitability and applicability to different types of bridges. In this paper, the experimental results of the completed first phase of the research project will be presented.

VARIOUS TYPES OF BASE ISOLATION DEVICES

In buildings, base isolation devices are installed at the base to uncouple the whole building structure from destructive effects of earthquake ground motion; whereas in bridges, the plane of isolation is below the girder superstructure so that inertial forces from the heavy superstructure that are transmitted to the critical pier supports can be reduced by the base isolation system (or more appropriately, seismic isolation system).

Many types of devices have been proposed to achieve seismic isolation. Several of these isolation systems use combinations of rubber bearings and complementary damping devices and have been used in buildings where these have the luxury of a whole basement story devoted to house several isolation devices spaced at considerable distances. But in bridges where the bridge seats may not offer enough space, single-unit compact isolation devices are desirable. In addition, these devices must be made of robust construction due to exposure to harsher environmental conditions.

In recent years, many seismic isolation devices satisfying the above requirements for bridge application have been developed. Among these are the lead-rubber bearing, high-damping rubber bearing, and sliding rubber bearing. In a single unit are contained the necessary mechanisms to achieve seismic isolation: flexibility to lengthen natural period of supported structure, damping to limit excessive deformation, vertical stiffness to support heavy superstructure, and sufficient stiffness at low loads for serviceability against ambient vibrations. In the above-mentioned seismic isolation bearings, laminated elastomers made of rubber materials provide the required flexibility and interleaved steel plates give vertical stiffness. These bearings differ largely in

the way damping mechanism is achieved. The lead-rubber bearing, which was developed in New Zealand, has a lead core at the center and utilize plastic yielding of the lead core for hysteretic damping. The high-damping rubber bearings use special rubber compounds that are inherently high damping. For the sliding rubber bearing, sliding friction provides the damping mechanism. Many other ways of providing damping have been proposed and developed, e.g., flexural yielding of steel bars, lead extrusion, torsional beam, high-yielding rubber core, etc. As base isolation concept gains more acceptance, new isolation techniques and configurations will continue to be developed. Excellent state-of-the-art reviews of base isolation concept since its inception up to the present time can be found in Kelly [1986], Izumi [1988], Buckle and Mayes [1990].

For these isolation devices to be widely accepted by the structural engineering profession, their fundamental mechanical properties and their expected behavior during strong earthquakes should be well established. Extensive experimental tests are very much needed to study their behavior and provide data for analytical modeling and design.

The most fundamental test being done on seismic isolators is the repeated cyclic loading test (or quasi-static test). This is a test procedure to establish some mechanical properties of the isolators, such as hysteretic load-deformation behavior, cyclic energy absorption capacity, performance deterioration under repeated loads, ...

Effectiveness of seismic isolators are very much dependent on the characteristics of the input earthquake motion and the supported structures. Most dynamic testing of seismic isolators have been done on shaking tables. However, the requirement of applying high vertical loads due to the high dependence of isolation characteristics on axial bearing pressure would necessitate a large-capacity table for a full-scale specimen; or specimens would have to be drastically scaled down in order to accommodate them in most shaking tables. Due to the limitation of shaking tables, one test was done using explosively simulated earthquake about 10 years ago [cited in Kelly, 1986].

During the last two decades, online hybrid test method (pseudo-dynamic test method) has become a very powerful tool to test for inelastic earthquake response of structures. Online hybrid test method is a computer-controlled experimental technique in which direct step-by-step time integration is used to solve the equations of motion. The computed displacement at each step is statically imposed on a specimen through computer-controlled load actuators in order to measure its restoring forces at the current deformation state. The measured restoring forces are then fed into the equations of motion to compute the next set of displacements. The numerical time integration process and the online loading process are carried out for a given earthquake ground motion history.

With the various types of isolation devices tested under different test methods and conditions, it is very difficult for the bridge designers to evaluate suitable isolation devices for a particular bridge. In addition, most of the tests conducted on large-scale specimens give only cyclic load-deformation characteristics and very few earthquake response tests (mostly shaking-table tests). It is necessary to evaluate and verify the seismic performance of seismic isolation devices under earthquake excitations and for different structural configurations.

BENCHMARK TEST PROGRAM FOR VARIOUS ISOLATION BEARINGS

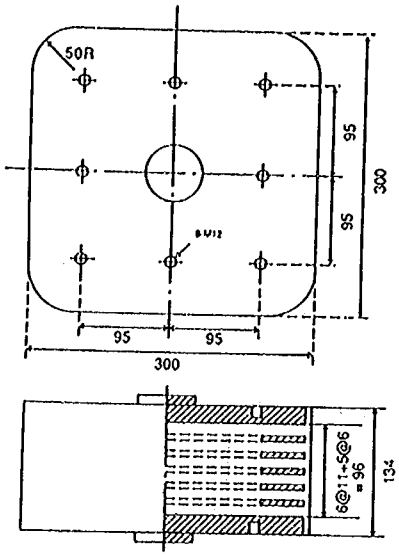
In order to evaluate suitable isolation devices for different types of bridges of the Hanshin Expressway Public Corporation, a joint research has been initiated with the Earthquake Engineering Laboratory of the Department of Civil Engineering of Kyoto University to evaluate the fundamental mechanical properties and earthquake response behavior of various isolation devices of different mechanisms tested under similar conditions.

The isolation bearings tested were lead-rubber bearing (LRB), 2 types of high-damping rubber bearings (HDR1, HDR2), and sliding rubber bearing (SRB). In addition, a conventional rubber bearing (CRS) was also tested and used for comparison with the base isolation devices. Two identical specimens were made for each type of bearings. The details of the specimens are shown in Fig. 1.

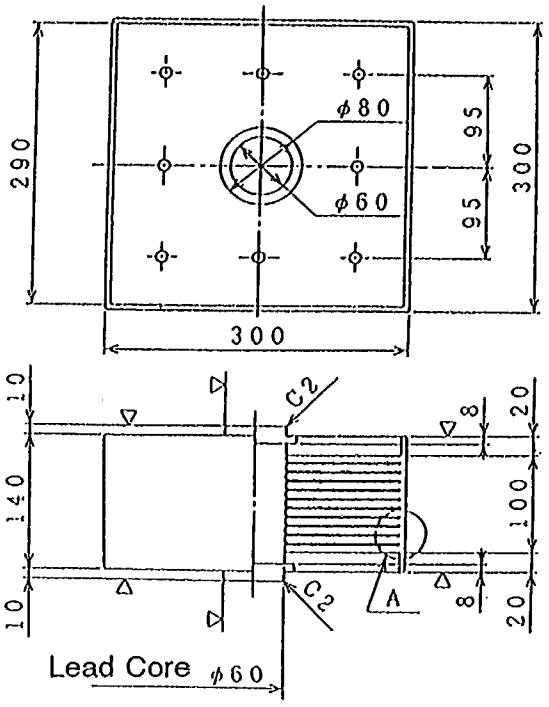
The test set-up used in this experiment is shown in Fig. 2. The specimen is bolted to the underside of the rigid load-transfer beam and to a rigid platform that is fixed to the rails of the strong reaction floor. Different heights of isolator specimens could be accommodated by inserting filler plates between the specimen and the test platform.

The actuator for horizontal motion (labeled no. 1) has a maximum stroke of ± 125 mm and a maximum load capacity of 40 tonf. Each of the vertical actuators (no. 2 and no. 3) has load capacity of 40 tonf; hence, vertical load as high as 80 tonf can be applied on a specimen. Under the present set-up, specimens can be loaded to about $\pm 150\%$ shear strain. This will be extended to more than $\pm 250\%$ in the next phase of the experimental program with the procurement of a loading jack with larger stroke capacity.

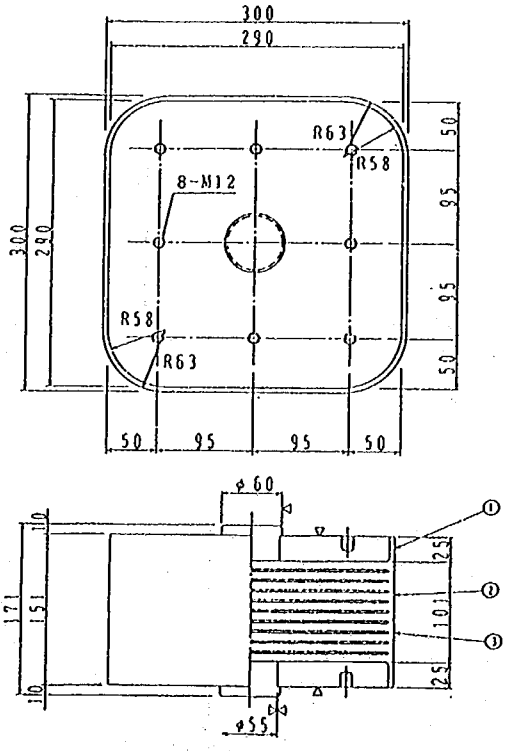
The test methods adopted into the benchmark test program for this investigative study are mainly the cyclic loading tests and the hybrid earthquake loading tests. The notation for the test methods used for the discussion is shown in Table 1. For the earthquake response test, a 2-second SDOF system was assumed and subjected to the three earthquake records prescribed in the Specifications for Highway Bridges (S.H.B.) of Japan [1990]. The central difference time integration scheme is used for solving the equation of motion in this test. In the next phase of the research project where substructured hybrid earthquake loading method will be used to test



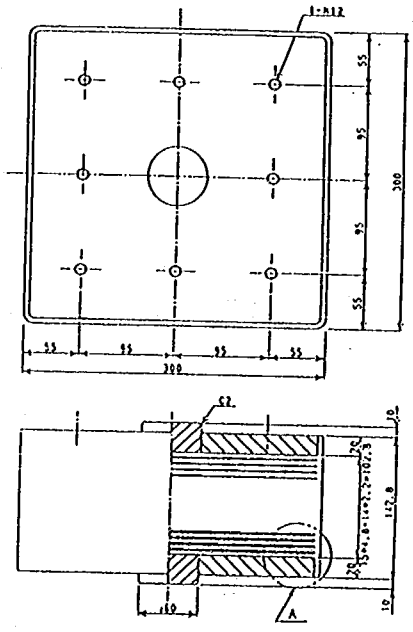
(a). Conventional Rubber Bearing



(b). Lead-Rubber Bearing

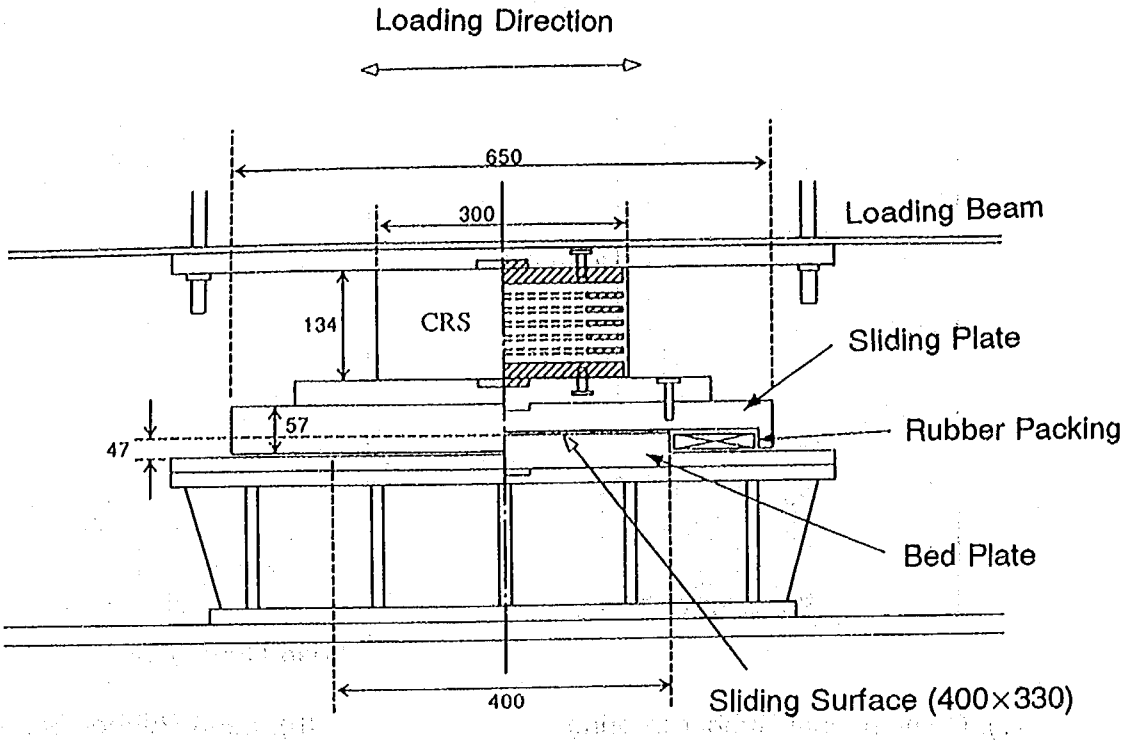


(c). High-Damping Rubber Bearing No. 1



(d). High-Damping Rubber Bearing No. 2

Figure 1 Tested Specimens (continuation next page)



(e). Sliding Rubber Bearing No. 1

Figure 1 Tested Specimens (continued)

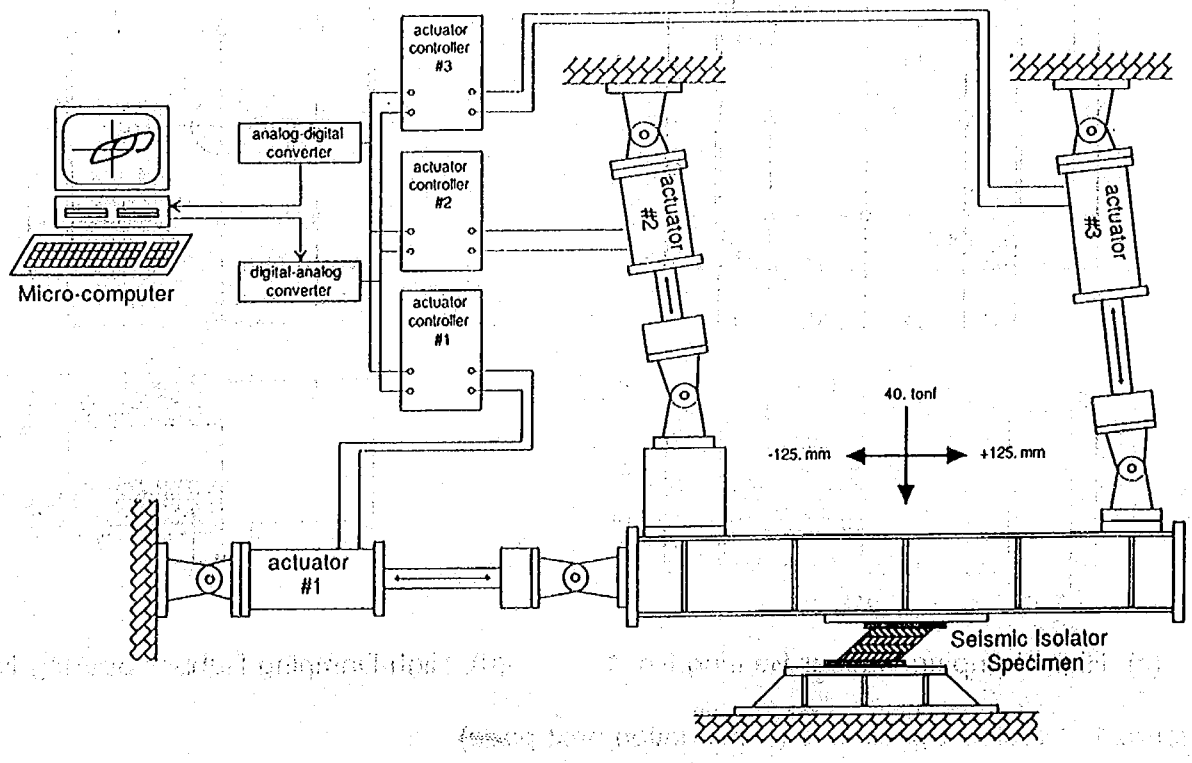


Figure 2 Test Set-up, Control and Measurement Systems

for earthquake response of seismically-isolated MDOF bridge system, a mixed explicit-implicit time integration scheme is used for numerical stability and accuracy considerations.

Table 1 Test Methods and Notation

BCL	Bipolar Cyclic Loading Test	Cyclic Alternating Positive–Negative Loading
UCL	Unipolar Cyclic Loading Test	Cyclic Positive Loading
HE	Hybrid Earthquake Loading Test	Input Earthquakes from S.H.B.
HS	Hybrid Sweep Loading Test	Input Frequency-Sweeping Sine Base Acceleration

The sequence of tests is summarized in Table 2. Two specimens were fabricated for each type of isolation bearing. All tests can be done under one test set-up which enabled a series of test to be completed within a few hours and giving both fundamental mechanical properties and earthquake response behavior. To test for virgin earthquake response, the second specimen of each type was subjected to Type-3 Earthquake of S.H.B. This is especially important in that some rubber bearings exhibit exceptionally high stiffness during first displacement excursions. Due to this high initial stiffnesses, isolation effect might be diminished and consequently transmitting large forces to the pier supports.

Table 2 Sequence of Tests

	Test Sequence
Reloaded	BCL-1 BCL-2 HE-1 HE-2 HE-3 HS UCL-1 UCL-2
Virgin	HE-3 (×2) BCL (×2) HE-3

TEST RESULTS AND DISCUSSIONS

Only a few representative results of the tests will be briefly described in this section. A more complete report on the test results is given in DPRC [1992].

Fundamental Cyclic Load-Deformation Behavior

First, results of first two sequences of cyclic loading tests for each type of isolation bearings are given in Figs. 3–7. Load-deformation behavior for SRB can be easily divided into that exhibited by the rubber bearing and that of the sliding surface as shown in Fig. 7. At the end of the first test series (Table 2), the rigid load-transfer beam is offset by 80 mm and fixed to enable large deformation in one orientation (UCL test). Figure 8 shows the results of the second UCL test for each type of isolation bearings. These serve as the tests for fundamental mechanical properties from which the usual equivalent shear moduli and equivalent damping ratios are computed. Fig. 9 gives the equivalent elastic shear moduli for each type of isolators, while Fig. 10 gives the equivalent damping ratios. The values G_{eq} and h_{eq} are both plotted

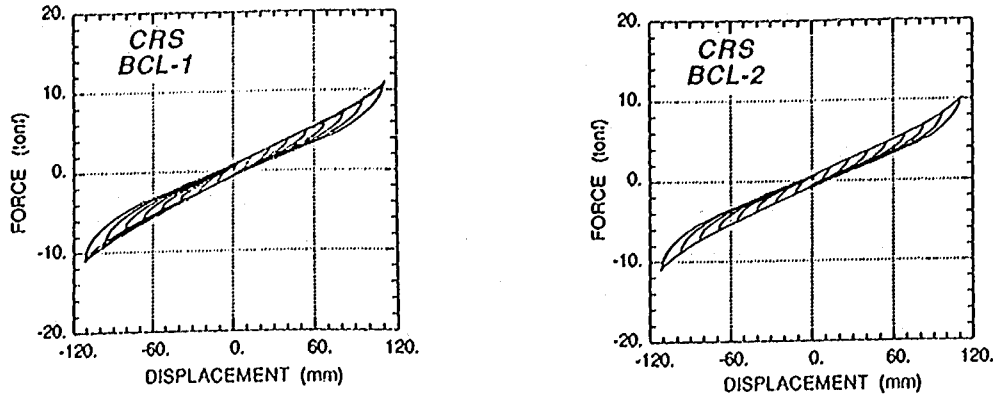


Figure 3 Cyclic (BCL) Load-Deformation Behavior for Conventional Rubber Bearing

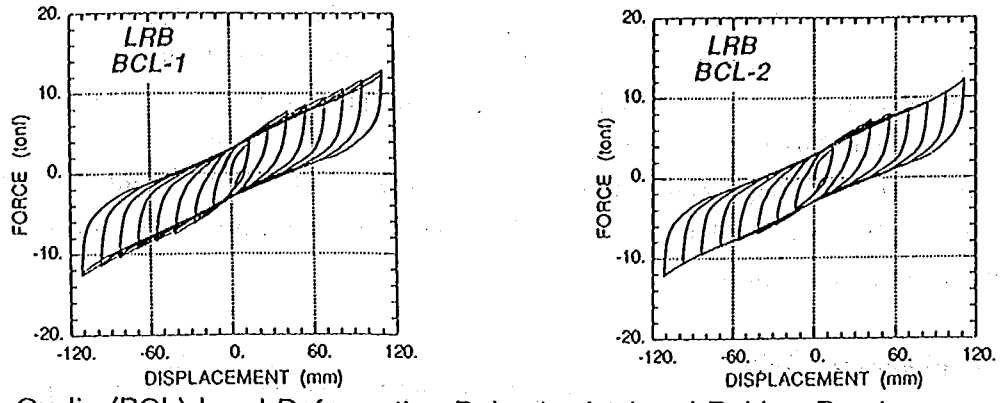


Figure 4 Cyclic (BCL) Load-Deformation Behavior for Lead-Rubber Bearing

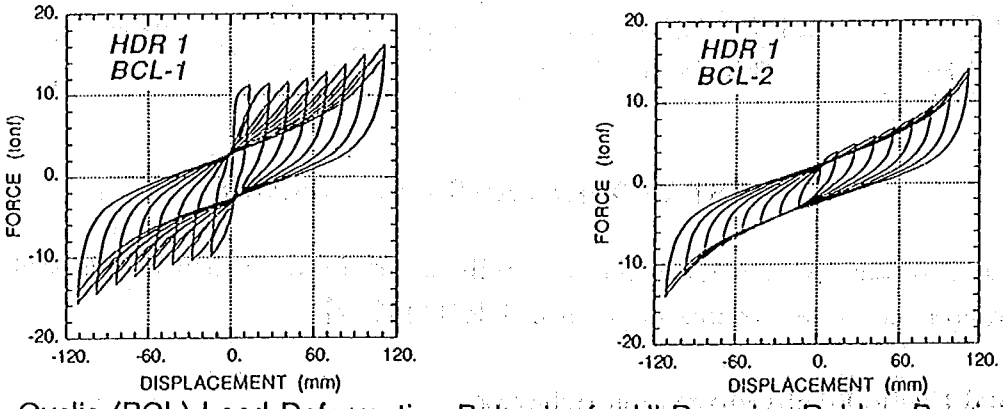


Figure 5 Cyclic (BCL) Load-Deformation Behavior for Hi-Damping Rubber Bearing No. 1

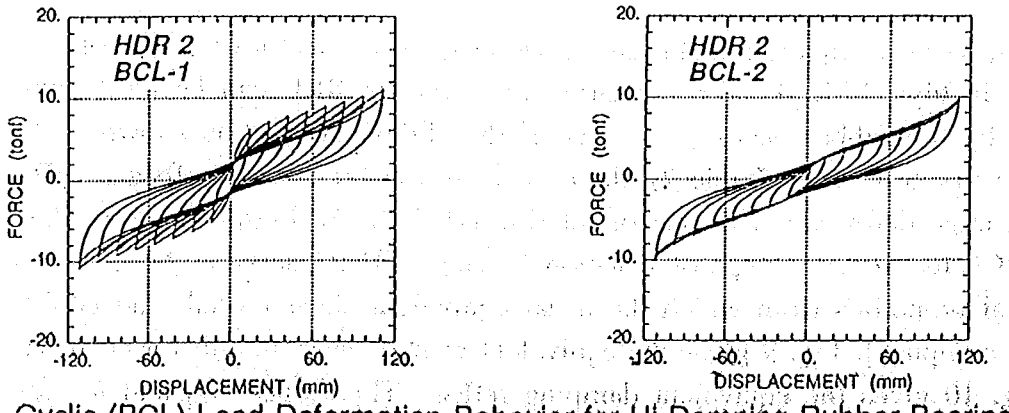


Figure 6 Cyclic (BCL) Load-Deformation Behavior for Hi-Damping Rubber Bearing No. 2

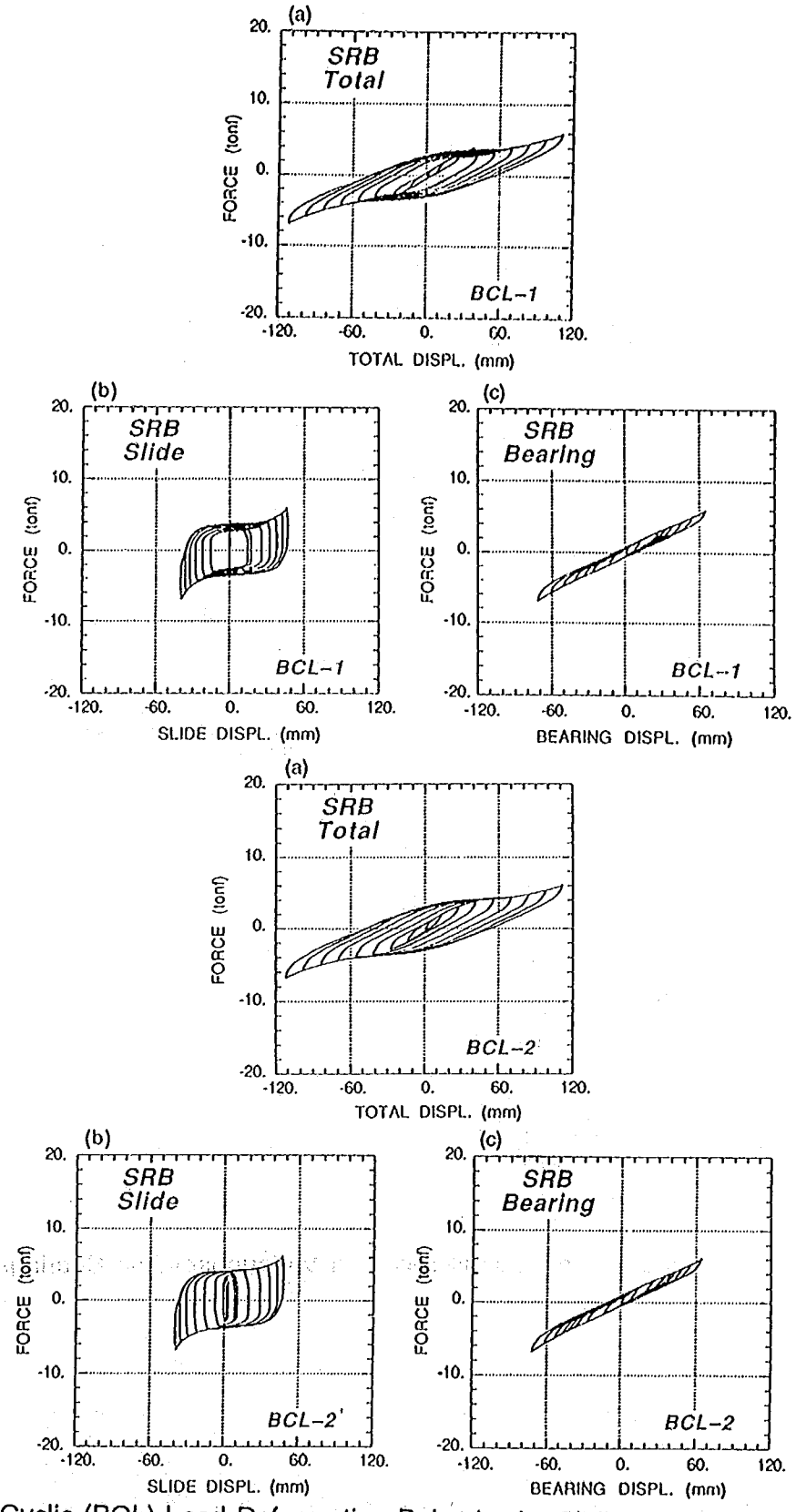


Figure 7 Cyclic (BCL) Load-Deformation Behavior for Sliding Rubber Bearing

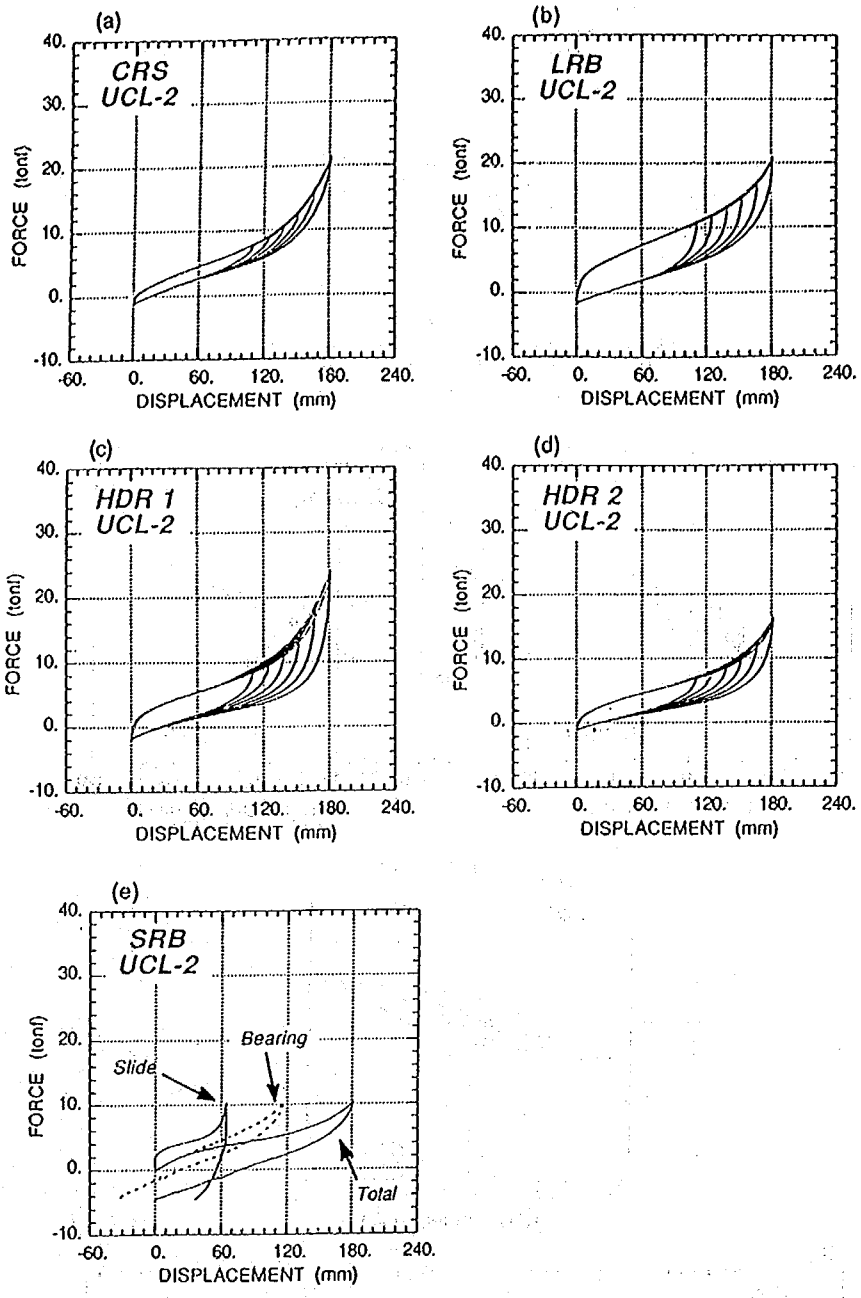


Figure 8 Cyclic (UCL) Load-Deformation Behavior of Various Isolation Bearings

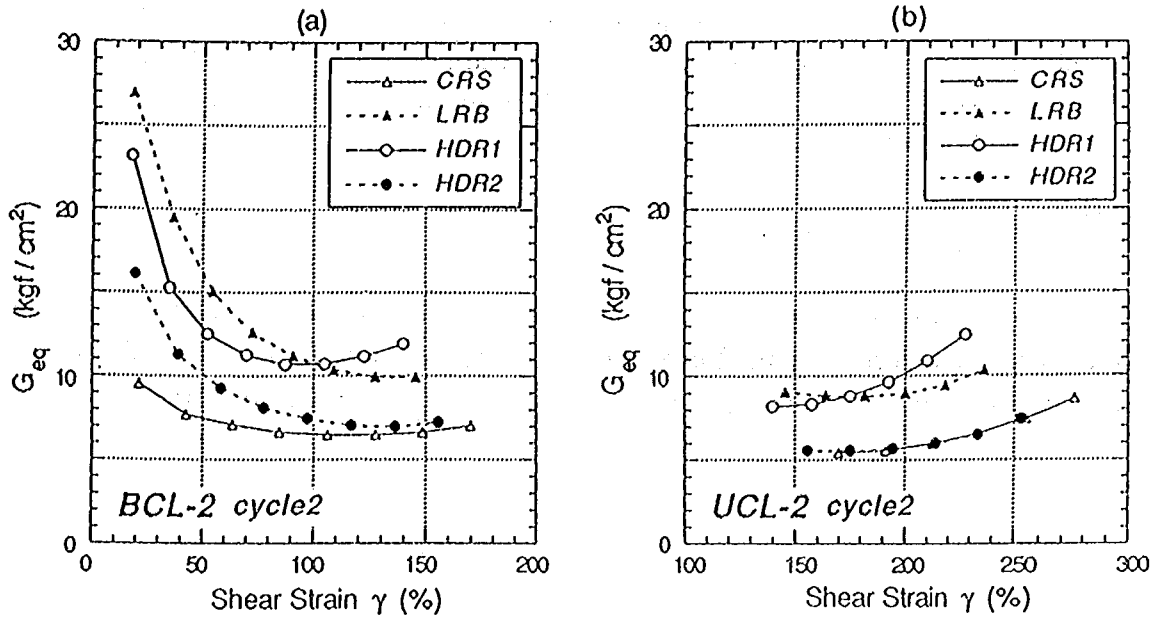


Figure 9 Equivalent Elastic Shear Moduli

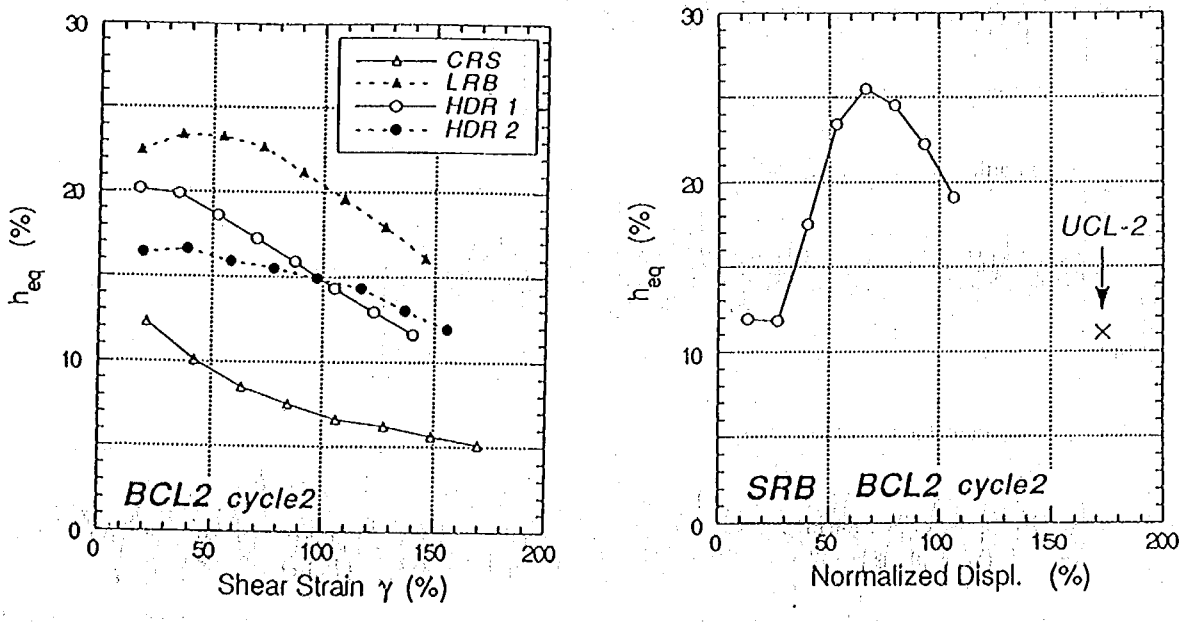


Figure 10 Equivalent Damping Ratios

against the shear strain ratio (total deformation divided by total height of rubber layers), except for the sliding rubber bearing in which the shear strain ratio is not defined. Instead, a normalized displacement parameter (total deformation divided by the design displacement specified) is used as shown in Fig. 10(b).

Earthquake Response Behavior

To evaluate earthquake response behavior, a 2-second SDOF system is subjected to the three earthquake records specified in S.H.B. (Fig. 11). Maximum ground acceleration amplitudes were scaled for each type of isolators to give shear strain ratios in the 100% - 150% range.

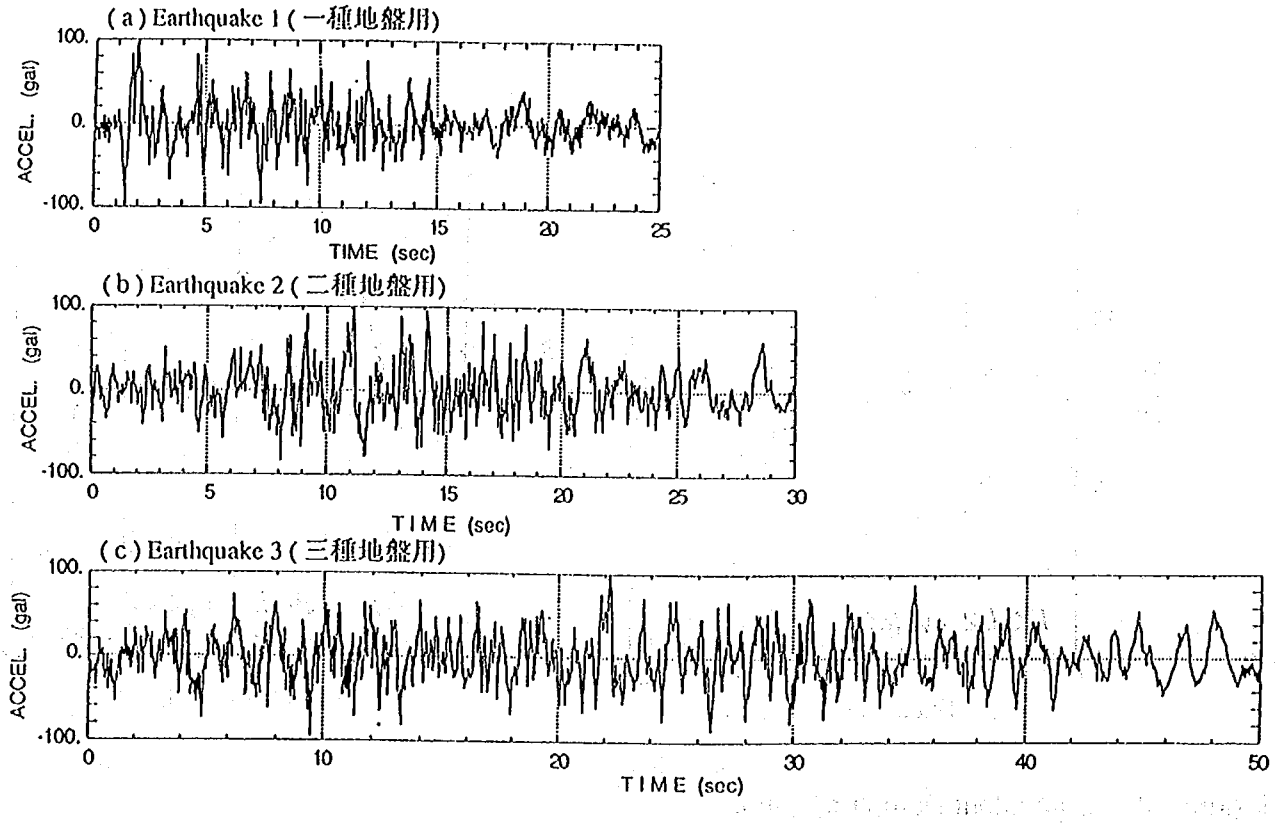


Figure 11 Earthquakes Records From the Specifications for Highway Bridges and Used in the Hybrid Earthquake Loading Tests

Representative results of earthquake response tests for each isolator type are given in Figs. 12-16. With these results, effectiveness of isolation can be evaluated directly in terms of earthquake response characteristics, or more specifically, the displacement and acceleration response time histories. From these, response reduction factors for both displacement and acceleration are computed and given in Table 3. In addition, linear elastic response is computed to match the maximum displacement and acceleration values from hybrid earthquake loading tests and obtain the equivalent damping ratios based on earthquake response behavior. Table 4 summarizes the equivalent damping ratios based on earthquake response tests.

For the second specimen of each isolation type, earthquake record no. 3 was used as input excitation (first test of second test series in Table 2) and virgin earthquake response for all isolation bearings were obtained. The main objective is to evaluate the effect of high initial stiffnesses during first displacement excursions on earthquake response of seismically isolated bridge structures. This is specially pronounced in some types of rubber materials. Fig. 17 shows virgin earthquake response for one of the specimens. Comparison with the response of a preloaded specimen is indicated in Table 4.

Resonant Response Behavior

The same 2-second SDOF model was tested for resonant response when subjected to a sweeping sine-wave acceleration excitation (Fig. 18). Maximum input acceleration amplitudes were scaled to give resonant response also in the 100% - 150% range. The same technique as in hybrid earthquake loading test can be applied. Fig. 19 gives resonant response under sweeping waves for one of the specimens. Results for all of the types tested are summarized in Table 5.

CONCLUSIONS AND FURTHER CONSIDERATIONS

A benchmark test program for testing various seismic isolators with different damping mechanisms under similar conditions was adopted. Using cyclic loading test and hybrid earthquake loading test methods, it is possible to test for fundamental mechanical properties, earthquake response behavior and resonant response behavior. Effectiveness of isolation can be evaluated directly in terms of earthquake response values.

In the next phase of this research project, a loading jack with larger horizontal strokes ($\pm$250 mm) is procured for the purpose of further examining the behavior at larger shear strain (above 200%). In addition, the seismic safety of the total structure will be investigated by substructured hybrid earthquake loading test to obtain earthquake response of MDOF system. Using this technique, it will be possible to examine the effect of the isolation system on the response behavior of the other components of bridge structure, especially the critical bridge piers.

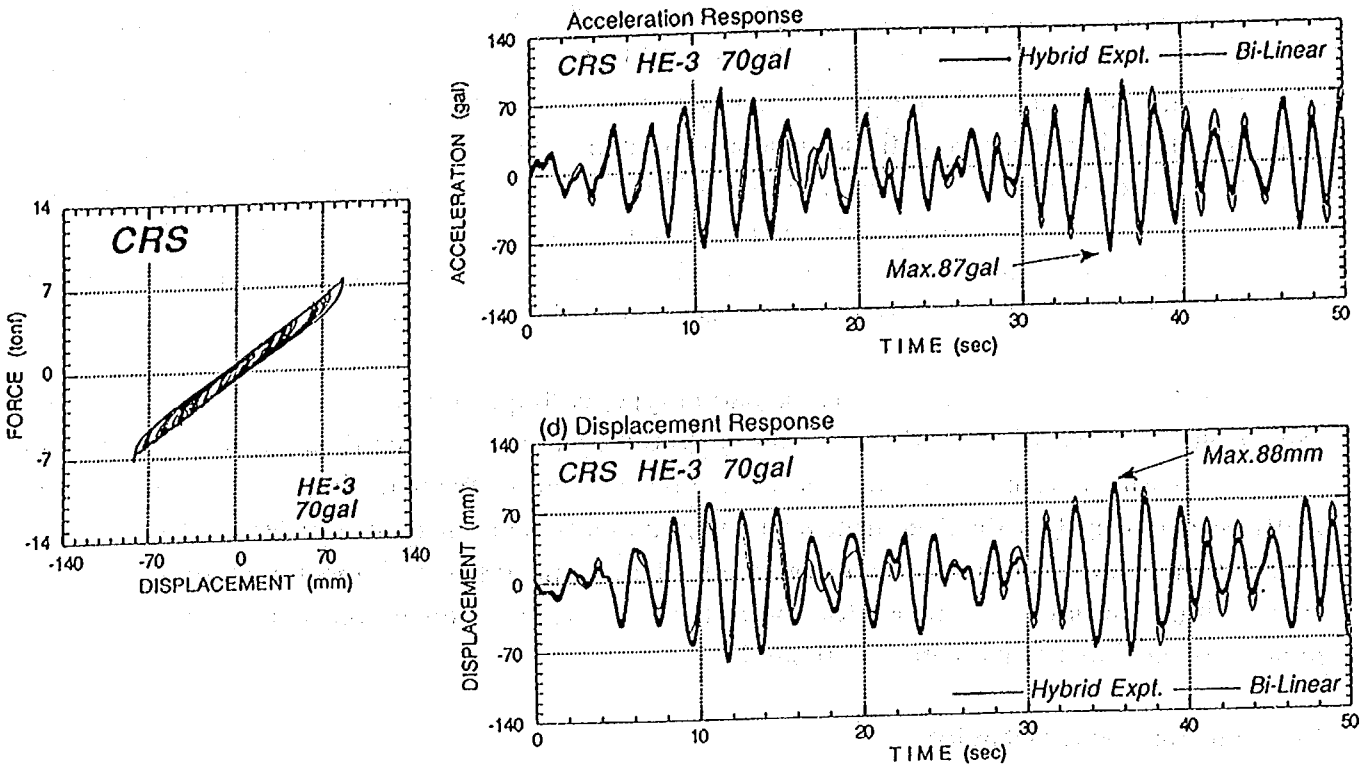


Figure 12 Earthquake Response from Hybrid Earthquake Loading Test (CRS, HE-3)

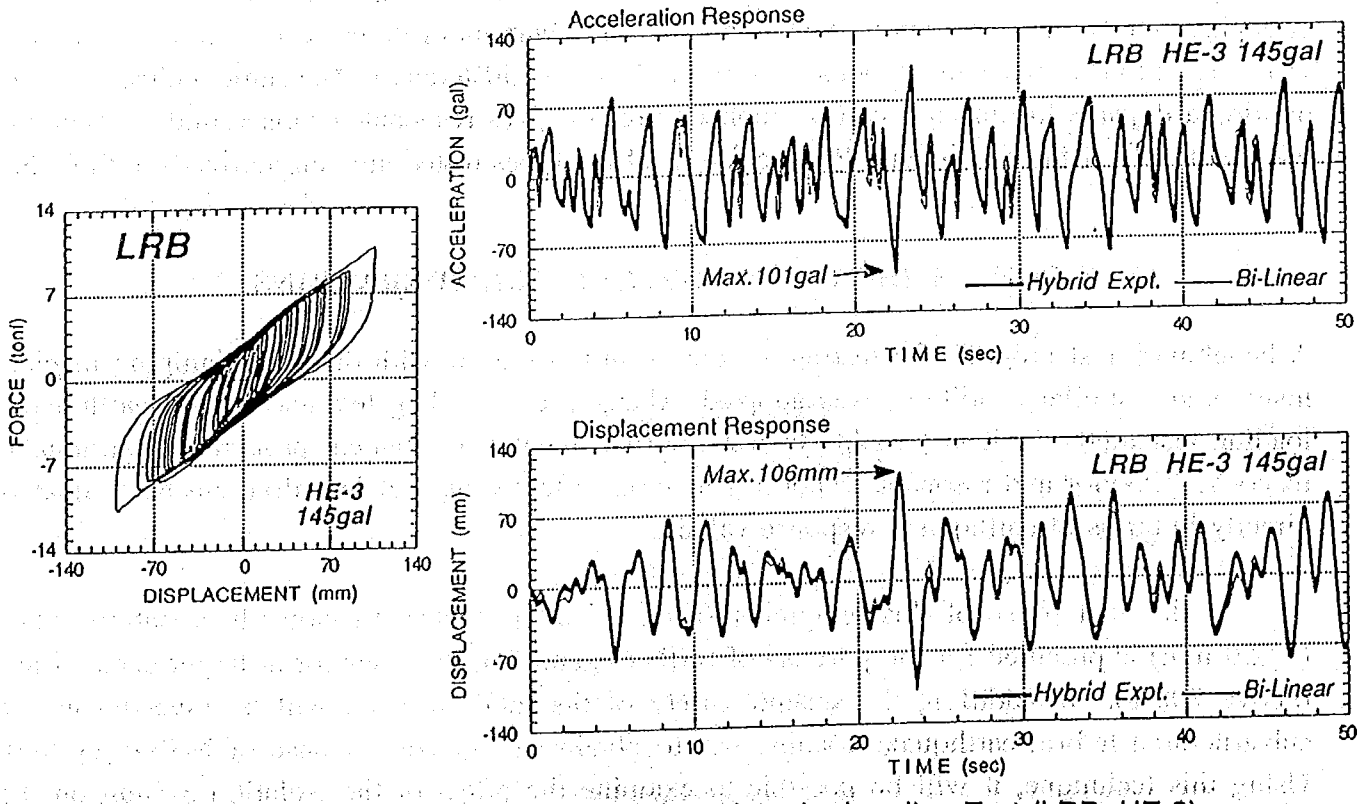


Figure 13 Earthquake Response from Hybrid Earthquake Loading Test (LRB, HE-3)

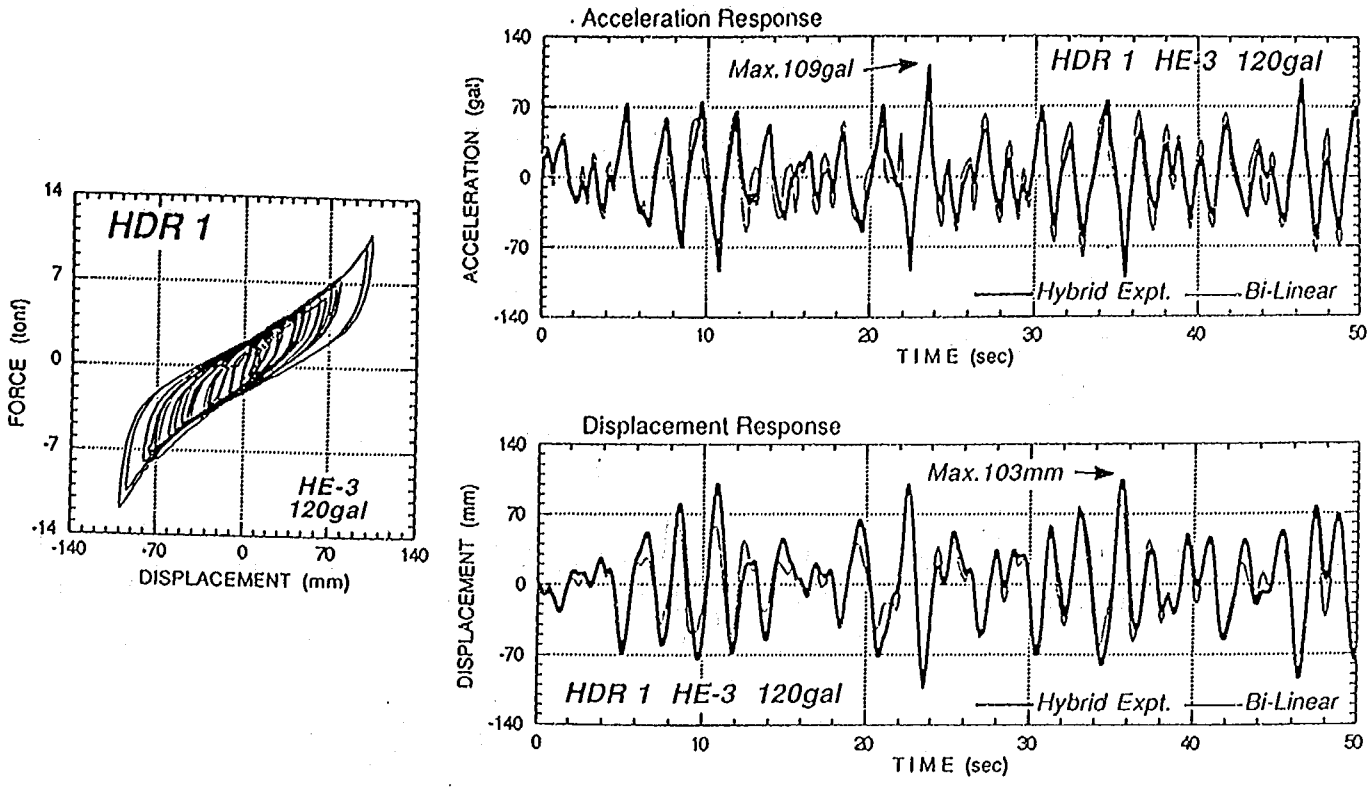


Figure 14 Earthquake Response from Hybrid Earthquake Loading Test (HDR1, HE-3)

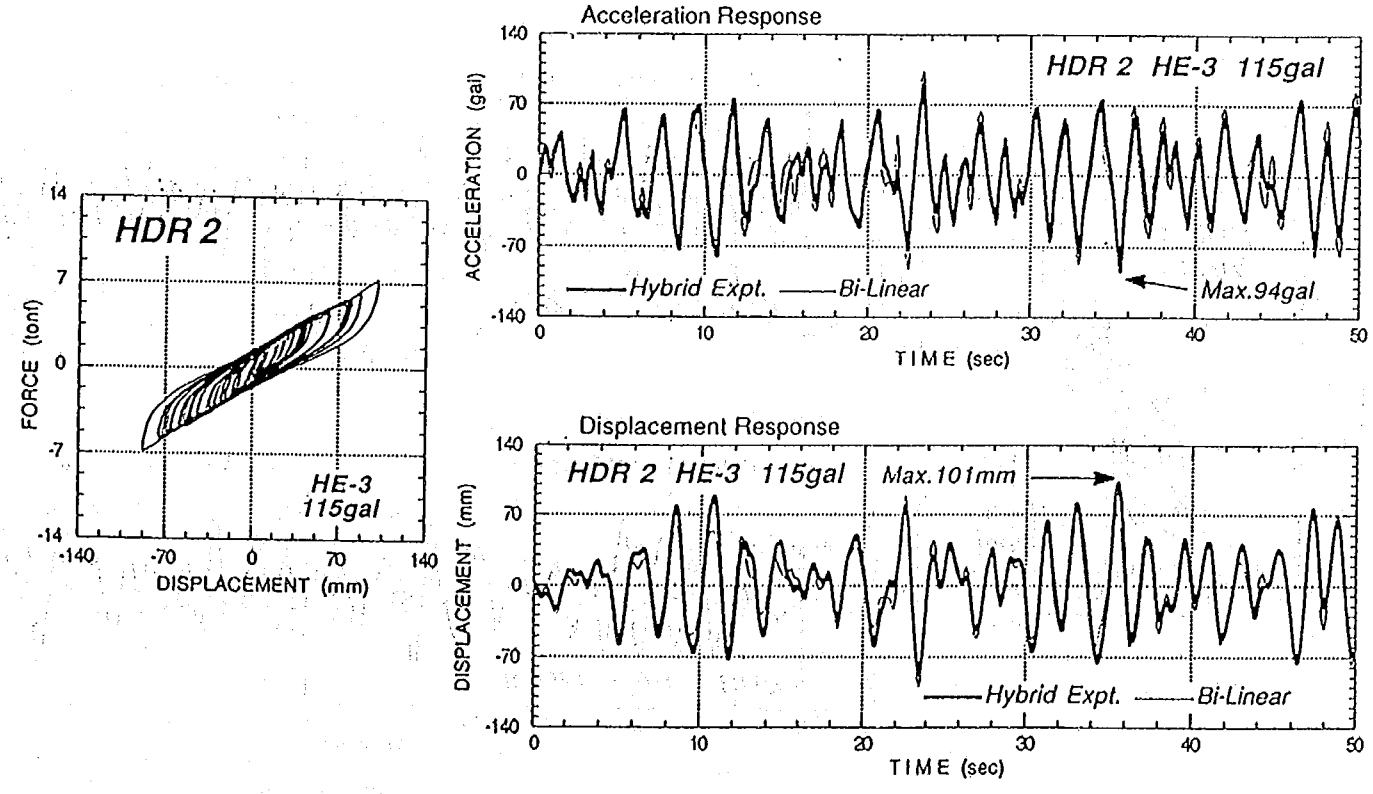


Figure 15 Earthquake Response from Hybrid Earthquake Loading Test (HDR2, HE-3)

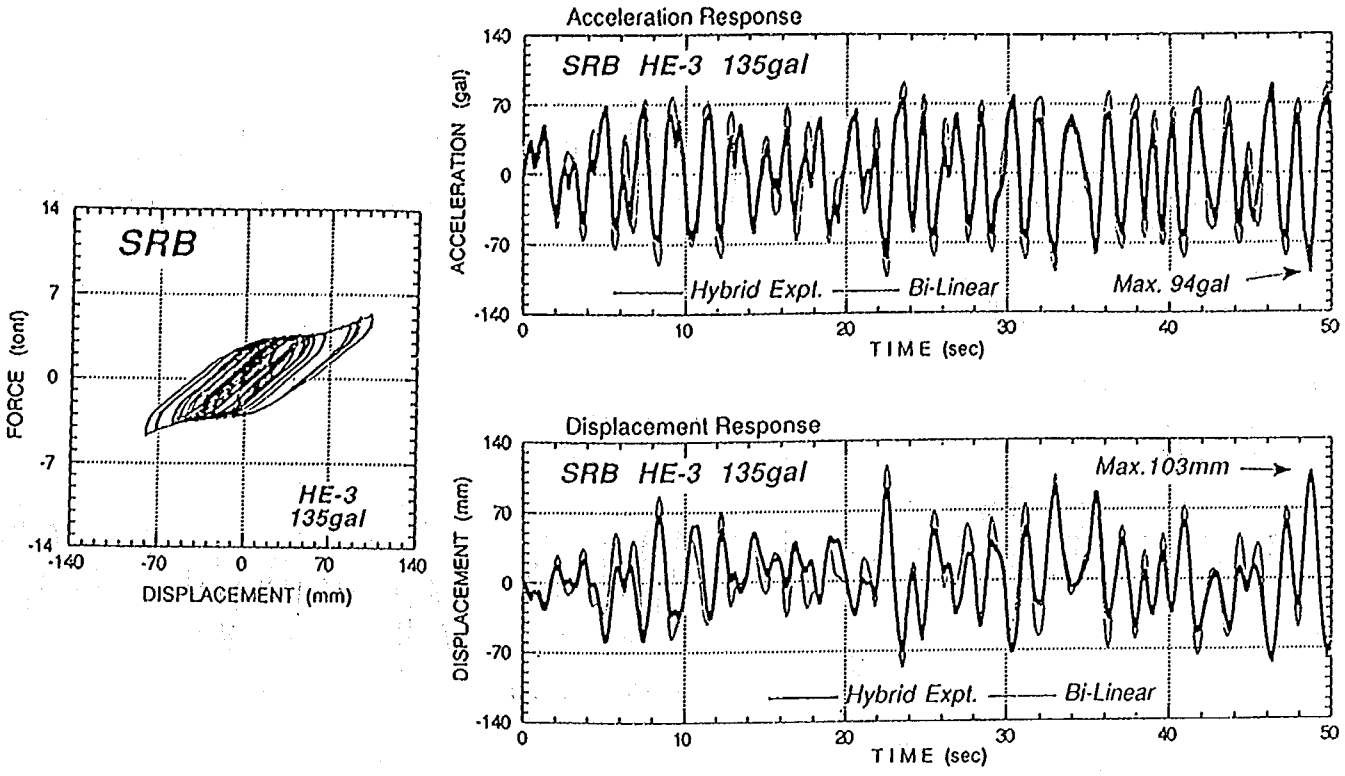


Figure 16 Earthquake Response from Hybrid Earthquake Loading Test (SRB, HE-3)

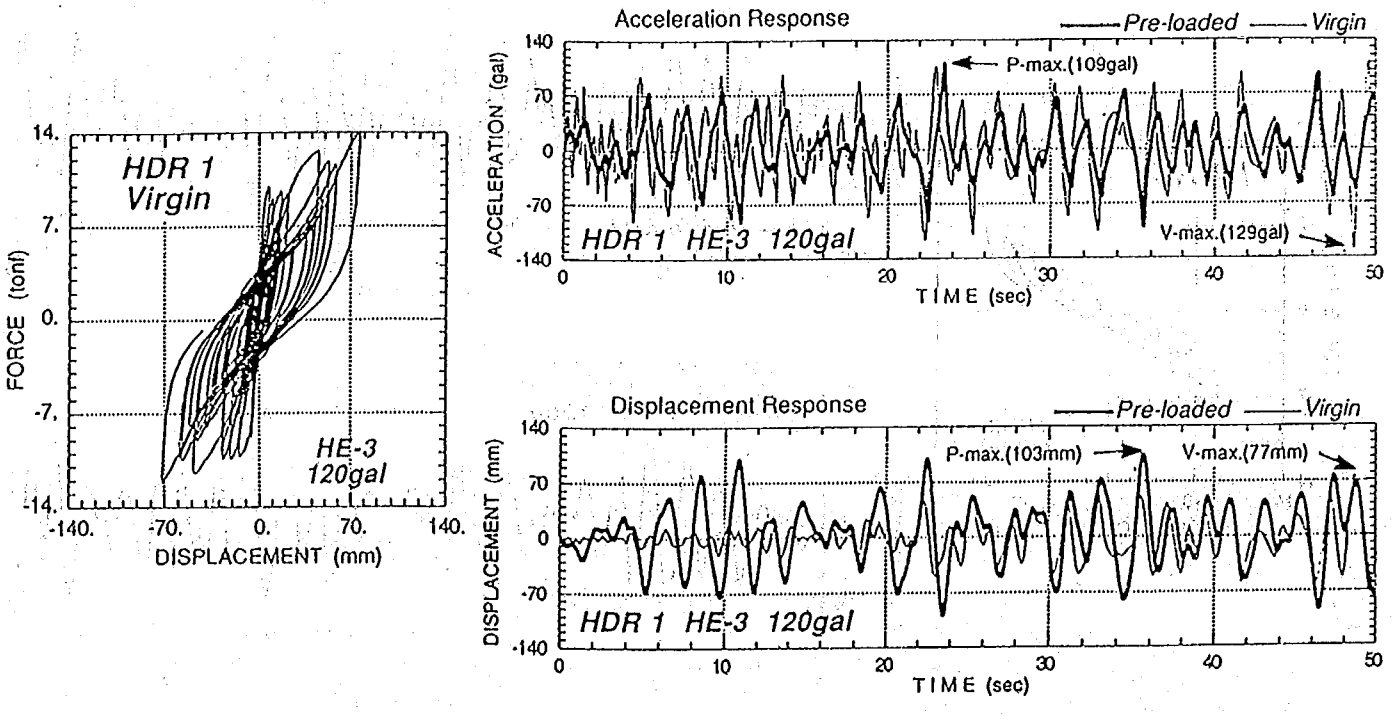


Figure 17 Virgin Earthquake Response from Hybrid Earthquake Loading Test

(a) CRS

Experiment	Input Accel. (gal)	Acceleration Response		Displacement Response		
		Max.Response (gal)	Amplification (%)	Max.Response (mm)	Shear Strain (%)	Magnification (%)
HE-1	100	101.1	101	97	147	96
HE-2	80	99.1	124	97	147	119
HE-3	70	86.8	124	87	132	123
HE-3 Virgin	70	88.9	127	83	126	117

(b) LRB

Experiment	Input Accel. (gal)	Acceleration Response		Displacement Response		
		Max.Response (gal)	Amplification (%)	Max.Response (mm)	Shear Strain (%)	Magnification (%)
HE-1	150	123.9	83	124	161	82
HE-2	140	98.9	71	103	134	73
HE-3	145	100.5	69	106	138	72
HE-3 Virgin	145	111.1	77	96	125	65

(c) HDR 1

Experiment	Input Accel. (gal)	Acceleration Response		Displacement Response		
		Max.Resp. (gal)	Amplification (%)	Max.Resp. (mm)	Shear Strain (%)	Magnification (%)
HE-1	120	119.8	100	113	141	93
HE-2	130	96.2	74	102	128	77
HE-3	120	109.4	91	103	129	85
HE-3 Virgin	120	129.2	108	77	96	63

(d) HDR 2

Experiment	Input Accel. (gal)	Acceleration Response		Displacement Response		
		Max.Resp. (gal)	Amplification (%)	Max.Resp. (mm)	Shear Strain (%)	Magnification (%)
HE-1	105	89.9	86	99	137	93
HE-2	105	86.2	82	93	129	87
HE-3	115	94.1	82	101	140	87
HE-3 Virgin	115	110.0	96	84	117	72

(e) SRB

Experiment	Input Accel. (gal)	Acceleration Response		Displacement Response		
		Max.Resp. (gal)	Amplification Factor (%)	Max.Resp. (mm)	Normalized Displ. (%)	Magnification (%)
HE-1	125	99.0	79	106	101	84
HE-2	130	102.6	79	105	100	80
HE-3	135	93.8	69	103	98	75
HS	48	108.9	227	113	108	232

Table 3 Response Reduction Under Earthquake Loading

(a) CRS

Experiment	Maximum Response Matching: Accel.match h_{eq} (%)	Maximum Response Matching: Displ.match h_{eq} (%)	Substitute Damping: h_s (%)
HE-1	5	6	9.0
HE-2	6	7	9.1
HE-3	7	7	9.1
HE-3 Virgin	7	8	–
HS	7	7	10.2

(b) LRB

Experiment	Maximum Response Matching: Accel.match h_{eq} (%)	Maximum Response Matching: Displ.match h_{eq} (%)	Substitute Damping: h_s (%)
HE-1	14	12	30.5
HE-2	> 30	20	28.6
HE-3	> 30	18	28.2
HE-3 Virgin	18	21	–
HS	20	18	28.9

(c) HDR 1

Experiment	Maximum Response Matching: Accel.match h_{eq} (%)	Maximum Response Matching: Displ.match h_{eq} (%)	Substitute Damping: h_s (%)
HE-1	5	6	21.8
HE-2	30	18	18.7
HE-3	12	13	18.3
HE-3 Virgin	9	22	–
HS	13	14	20.6

(d) HDR 2

Experiment	Maximum Response Matching: Accel.match h_{eq} (%)	Maximum Response Matching: Displ.match h_{eq} (%)	Substitute Damping: h_s (%)
HE-1	11	6	22.1
HE-2	20	14	20.4
HE-3	15	12	18.3
HE-3 Virgin	11	17	–
HS	15	14	20.2

(e) SRB

Experiment	Maximum Response Matching: Accel.match h_{eq} (%)	Maximum Response Matching: Displ.match h_{eq} (%)	Substitute Damping: h_s (%)
HE-1	19	11	25.2
HE-2	23	17	24.4
HE-3	29	16	25.8
HS	24	22	30.6

Table 4 Equivalent Damping Ratios Based on Earthquake Response

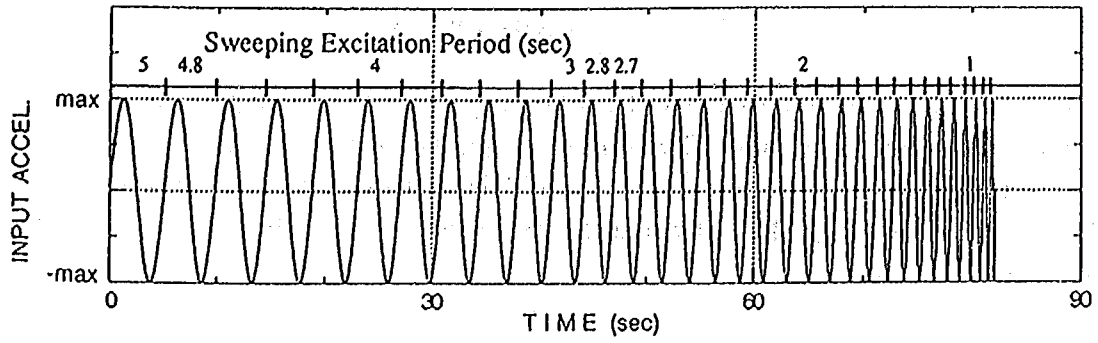


Figure 18 Input Frequency-Sweeping Sine Ground Acceleration Excitation

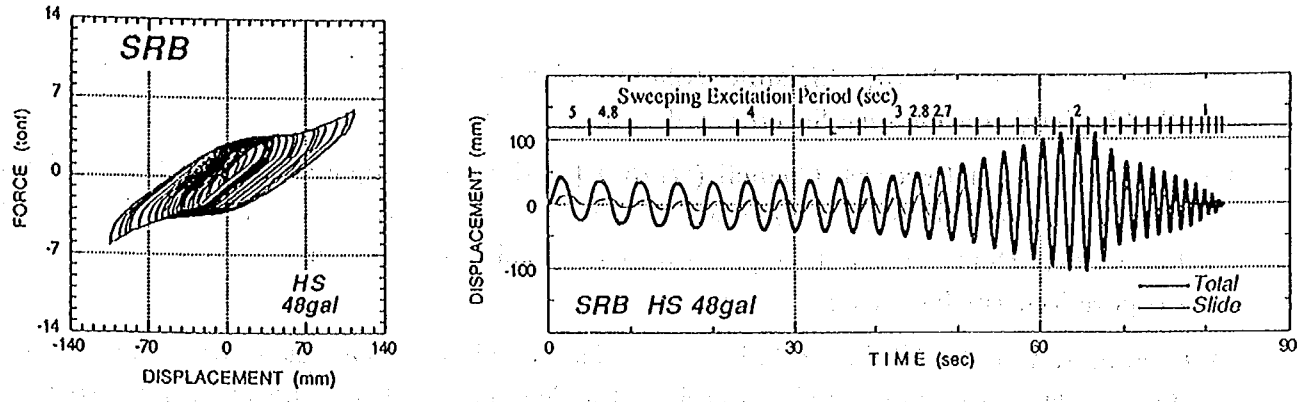


Figure 19 Resonant Response under Sweeping Excitation Input

Table 5 Response Reduction/Amplication Under Sweep Excitation

HS – Experiment		Acceleration Response		Displacement Response		
Specimen	Input Accel. (gal)	Max.Response (gal)	Amplification (%)	Max.Response (mm)	Shear Strain (%)	Magnification (%)
CRS	15	87.0	580	88	133	580
LRB	37	98.6	266	105	136	280
HDR 1	28	103.5	370	100	125	352
HDR 2	30	102.9	343	104	144	342
SRB	48	108.9	227	113	★ 108	232

★ : Normalized Displ. (%)

ACKNOWLEDGEMENTS

The authors would like to acknowledge the following staff and students of the Earthquake Engineering Laboratory, Department of Civil Engineering, Kyoto University for their assistance and contribution to this research project: Mr. Shinji Nakanishi (laboratory engineer), Mr. Kazuyuki Izuno (research associate), Mr. Masaaki Tanaka (former graduate student), and Mr. Norio Watanabe (graduate student).

REFERENCES

I. Buckle, R. Mayes [1990]: "Seismic Isolation: History, Application, and Performance — A World View," *Earthquake Spectra,* Vol. 6, No. 2, 161-201.

Disaster Prevention Research Council (DPRC) [1992]: "Investigative Research on Seismic Isolation Design of Highway Bridges," Report submitted by the Earthquake Engineering Laboratory, Dept. of Civil Engg., Kyoto University to the Hanshin Expressway Public Corporation. (in Japanese)

H. Iemura, Y. Yamada, W. Tanzo, Y. Uno, S. Nakamura [1991]: "On-line Earthquake Response Tests of High-Damping Rubber Bearings for Seismic Isolation," *1st US-Japan Workshop on Earthquake Protective Systems for Bridges,* Buffalo, New York, Sept.

M. Izumi [1988]: "State-of-the-Art Report on Base Isolation and Passive Seismic Response Control," *Proc., 9th WCEE,* Tokyo-Kyoto.

Japan Road Association [1990]: *Specifications for Highway Bridges,* Part V - Seismic Design. (in Japanese)

J. Kelly [1986]: "Aseismic Base Isolation: Review and Bibliography, *Soil Dynamics and Earthquake Engineering,* Vol. 5, No. 3.

PWRI [1991, 1990]: "Report of Joint Research Between PWRI and 28 Private Firms on Development of Menshin Devices for Highway Bridges," *Technical Report of Cooperative Research,* No. 44 and No. 60, Public Work Research Institute.

W. Tanzo, Y. Yamada, H. Iemura [1992]: "Substructured Computer-Actuator Hybrid Loading Tests for Inelastic Earthquake Response of Structures," *Research Report 92-ST-01,* Kyoto University, January.

SEISMIC RESPONSE VARIABILITY OF BRIDGES ON FRICTION CONTROLLABLE ISOLATORS

Maria Q. Feng
Department of Civil Engineering
University of California, Irvine
Irvine, California 72717

ABSTRACT

The present author collaborating with others developed earlier a prototype hybrid base isolation system using friction controllable sliding bearings and demonstrated its effectiveness in circumventing the shortcomings of passive counterparts by means of shaking table tests and numerical analysis under the 1940 El Centro earthquake record linearly scaled to various levels of intensity. The purpose of the present paper is to show that the same hybrid system exhibits similar degree of effectiveness over a practical range of parameters that define the ground acceleration characteristics. These parameters include spectral shape, dominant frequency and duration of the ground motion. For this purpose, artificial earthquake ground acceleration histories representing different sets of these parameter values are generated using a modified Kanai-Tajimi spectrum. The bridge responses under these earthquakes are evaluated numerically when the bridge is isolated by passive and hybrid sliding systems. The results demonstrate that the hybrid system indeed more effectively isolates the bridge under the variety of ground motion characteristics.

INTRODUCTION

Isolation performance of conventional sliding systems for reduction of seismic response of structures has some limitaitons. If the frictional coefficient is small, excellent isolation performance is expected due to correspondingly small rate of transmission of ground acceleration to the structure. In this case, however, the structure tends to suffer from an unacceptably large displacement between its base and ground. On the other hand, if the frictional coefficient is large, the structure will be isolated only under correspondingly large earthquakes and the sliding system will not be activated under small to moderate earhquakes that occur more often. This ineffectiveness of the passive sliding system with a large coefficient of friction for small to moderate earthquakes is considered to be a significant shortcoming of the sliding system. Furthermore, since the system will remain inactive in this case over a prolonged period of time, the system will not be tested until a strong earthquake strikes, thus giving rise to justifiable reliability concern.

Providing a restoring device to develop a strong-enough restoring force in order to reduce unacceptably large sliding displacement creates another set of problems, since such a restoring device usually increases the overall stiffness of the isolated structure to the detriment of the advantage of the essential sliding base isolation system.

In order to substantialy alleviate these difficulties, the author in collaboration with others developed a hybrid sliding base isolation system using friction controllable bearings, where the frictional force can be controlled by adjusting the fluid pressure in the fluid chamber located inside the bearings. The effectiveness of this system for controlling a bridge model has been verified by means of shaking table tests and numerical simulation under the El Centro earthquakes with various linearly scaled peak accelerations.

The present study evaluates the bridge response under artificially generated earthquakes when the bridge is isolated by such a hybrid system and by passive systems. The results are compared to indicate that the hybrid system does perform better as a base isolator regardless of the spectral shape, dominant frequency, and duration that characterize the artificial earthquakes. In doing so, the statistical variablities of maximum values of response acceleration and of sliding displacement and residual displacement are computed in the Monte Carlo approach. While these variabilities are not necessarily small, they are nevertheless small enough to confirm the trend that indicates the better isolation performance of the hybrid system.

HYBRID SYSTEM AND SHAKING TABLE TESTS

The hybrid isolation system using friction controllable bearings is conceptually depicted in Fig. 1 with a bridge girder resting on the bearings. Each bearing has a fluid chamber which is connected to a pressure control system composed of a servo valve, an accumulator and a computer. The friction on the interface between the bearing and the ground is controlled by adjusting the fluid pressure in the chamber. The computer calculates an appropriate signal to control the fluid pressure based on the observed structural response, such as response acceleration and sliding displacement, and sends it to the pressure control device.

The idealized section view of the friction controllable sliding bearing is given in Fig. 2. The steel disk-shaped bearing contains a fluid chamber which is sealed by a rubber O-ring around the circular perimeter just inside the sliding interface. A sliding material, such as teflon-based materials, is placed on the sliding surface.

The word "HYBRID" is used for this friction controllable sliding isolation system, since it is a combination of the passive sliding isolation system and the active control device. The system can be a passive sliding isolation system as long as the pressure of the bearing chamber, and thus the friction is kept at a constant value. At the same time, the system can be an active system when the pressure is controlled so that the friction is controlled.

This hybrid isolation system has the following general advantages: (a) Changing friction force through controlling pressure requires smaller amounts of energy and power than the corresponding actuator-driven active base isolation system, and as a consequence, (b) the use of accumulators for the source of energy is possible, thus eliminating the necessity of emergency energy supply system and (c) it has a fail safe feature.

In order to examine the performance of the hybrid isolation system, a prototype system with friction controllable sliding bearings has been developed and shaking table tests have been performed earlier on a shaking table at The Taisei Technology Research Center in Yokohama, Japan. Figure 3 shows a prototype bearing developed for the tests. A rigid bridge girder model weighing 12 tonf is supported equally by four friction controllable sliding bearings on the shaking table. No restoring force device is used in order to study the effect of friction force only. A servo valve is located at the center of the girder model from which the pressurized fluid is distributed to each sliding bearing.

Experiments were performed first to identify the dynamic characteristics of the bearing pressure control device, and to identify the relationship between the pressure and the coefficient of friction on the sliding interface. Then, shaking table tests were carried out on the hybrid system in which the friction is controlled under the bang-bang control or instantaneous optimal control algorithm which is especially developed for this hybrid system [1,2,3], and also on the passive system in which the coefficient of friction is kept constant at several different values. The isolation performance of the hybrid and passive systems are then compared.

The El Centro (NS, 1940) earthquake record was used as ground input motion for most of the test cases, by linearly adjusting the peak acceleration to 100, 200, 300 400 and 450 gal. Figure 4 shows the maximum response acceleration, maximum sliding displacement, and the residual displacement of the structural model with passive or hybrid isolation system under the El Centro records of different peak ground acceleration. The dashed lines represent the passive isolation systems with three different coefficients of friction, 1.6%, 5.3%, and 10.2%, while the solid line represents the hybrid isolation system in which the coefficient of friction is controlled between 1.6% and 10.2%. Hybrid isolation results shown in these figures are those under instantaneous optimal control algorithm.

In the passive isolation, if a small friction coefficient, for example 1.6%, is used, a high level of isolation performance is expected since the response acceleration is reduced to a small level. In this case, however, the maximum displacement becomes excessive very rapidly as the input earthquake becomes more intense. On the other hand, if a large friction coefficient, such as 10.2%, is used, the sliding displacement can be confined within a relatively small range. However the isolation performance in this case is limited in the sense that the acceleration can not be satisfactorily reduced. Particularly for small to medium earthquakes with peak acceleration less than 100 gal, this passive sliding isolation system does not function at all, thus the response accleration equals to the input acceleration.

The hybrid isolation system, however, can alleviate these problems associated with the passive isolation system. For small to medium earthquakes, the friction can be controlled to a very small level to make the structure slide easily, so that the response acceleration can be considerably reduced. For large earthquakes, the friction is controlled to prevent the excessive sliding displacement, while the response acceleration can also be kept at a small level. Another advantage of the hybrid system is clearly seen in Fig. 4 where the residual sliding displacement can be maintained almost at zero level.

Shaking table tests, as well as numerical simulations, verify that under the El Centro type ground motion, the sliding isolation sytem will become effective for all intensities of earthquake

if its sliding bearings are modified to be friction controllable as proposed. However, the influence of the frequency content and time duration of the earthquake on the effectiveness of the proposed hybrid system needs to be further investigated before the same claim can be made under a wider class of ground accelerations.

ARTIFICIAL EARTHQUAKES

While recorded ground accelerations are often used for response calculation, they are recorded at specific locations under specific earthquakes. Therefore, these accelerograms may not be appropriate for the use in the response analysis of structures located in different locations and for future earthquakes. Furthermore, the records severe enough to be used for a meaningful response analysis are scarce particularly in the eastern United States. In view of these, the use of artificial earthquake ground motion is much more appropriate for a systematic examination of the effects of major parameters of ground acceleration histories on the structural response. In the present study, the artificial earthquake acceleration history $\ddot{z}(t)$ is generated in the form of product of a specified peak ground acceleration PGA and the normalized nonstationary time history $a_m(t)$

$$\ddot{z}(t) = PGA \times a_m(t) \tag{1}$$

The normalized nonstationary time history $a_m(t)$ is obtained by applying an envelop function $f(t)$ to an underlying stationary time history $a_s(t)$ with mean zero, and then normalized by the absolute maximum of the time history a_{max} observed in $a_s(t)$;

$$a_m(t) = \frac{a_s(t)f(t)}{a_{max}} \tag{2}$$

The envelope function $f(t)$ has a trapezoidal shape with the unit height (see Fig. 5)

The stationary acceleration time history $a_s(t)$ is simulated by the following expression [4]:

$$a_s(t) = \sqrt{2}\sum_{k=1}^{N_f}\sqrt{S_g(\omega_k)\Delta\omega}\cos(\omega_k t + \phi_k) \tag{3}$$

where $S_g(\omega)$=one-sided power spectrum of $a_s(t)$; N_f=number of frequency intervals; $\Delta\omega = \omega_u/N_f$ with ω_u being upper cutoff frequency; $\omega_k = k\Delta\omega$, and ϕ_k=k-th random phase angle uniformly distributed between 0 and 2π.

The spectral density function $S_g(\omega)$ is assumed to take the following form [5]:

$$S_g(\omega) = S_{K-T}(\omega)m(\omega) \tag{4}$$

$$S_{K-T}(\omega) = S_0\frac{\omega_g^4 + 4\zeta_g^2\omega_g^2\omega^2}{(\omega_g^2 - \omega^2)^2 + 4\zeta_g^2\omega_g^2\omega^2} \tag{5}$$

and

$$m(\omega) = \begin{cases} \sin^2(\frac{\omega T_r}{2}), & for \quad \omega < \frac{\pi}{T} \\ 1, & for \quad \omega > \frac{\pi}{T} \end{cases} \tag{6}$$

Table 1: Parameters of Artificial Earthquakes

Soil	ω_g	ζ_g	d_E (sec)
Rock	8π	0.60	15
Stiff	5π	0.60	20
Soft	2.4π	0.85	25

In Eqs. 4 through 6, $S_{K-T}(\omega)$ is the Kanai-Tajimi spectrum and $m(\omega)$ is derived from seismological consideration with T_r representing the rise time of slip function, characterizing the shear dislocation of seismic source. In the present study, T_r is assumed to be 1 *sec.* From engineering point of view, the function $m(\omega)$ is significant in the following sense; It modifies the Kanai-Tajimi spectrum of underlying stationary acceleration process in such a way that the corresponding stationary velocity process now has a finite variance. Also, in Eq. 5, S_0 is the amplitude of the spectrum representing the intensity of earthquake; ω_g and ζ_g are the dominant ground frequency and the damping coefficient respectively, which depend on the site soil condition. The parameters ω_g and ζ_g for the power spectra corresponding to three soil conditions are tabulated in Table 1 [6]. The strong motion duration d_E used in this study is also included in the table. Alghough the strong motion duration is taken to be different for different soil conditions as shown in Table 1, the rise and decay time are respectively taken to be $T_r = 2.5sec$ and $T_d = 7.5sec$ for all the cases. Figure 6 shows the one-sided power spectrum $S_g(\omega)$ with $S_0 = 1(cm^2/sec^3)$ for three cases of soil condition.

Utilizing the artificial acceleration histories thus generated, a Monte Carlo analysis of the bridge response is performed. For this purpose, 200 artificial earthquake histories are generated for each set of *PGA* and soil condition. Since five (5) levels of *PGA* (50, 100, 200, 300 and 400 *gal*) and three (3) types of soil condition are considered here for the Monte Carlo analysis, a total of $5 \times 3 \times 200 = 3,000$ artificial acceleration histories are generated. One artificial history under stiff soil condition and with PGA = 100 *Gal* is plotted in Fig. 7 as an example.

MONTE CARLO SIMULATION

The equation of motion of a rigid bridge girder supproted by the friction controllable sliding system is as follows:

1. Sticking Phase — Phase I

$$\dot{x} = 0, \quad x = const. \tag{7}$$

2. Sliding Phase — Phase II

$$\ddot{x} = -\ddot{z} - f \, \mathrm{sgn}(\dot{x}), \tag{8}$$

3. Criterion for transition from Phase I to Phase II

$$|\ddot{z}| > f \tag{9}$$

Table 2: Parameters of Hybrid System

T_i	29 ms	c_1	2.4 $cm^3/(s^2kgf)$
T_d	35 ms	c_2	124.1 cm/s^2
k^2	0.1 cm^2/s^2		

4. Criteria for transition from Phase II to Phase I

$$\dot{x} = 0, \quad |\ddot{z}| < 2f \tag{10}$$

where x=sliding displacement of mass relative to ground, $\ddot{z}$=input earthquake acceleration, f=friction force per unit mass defined as $f = \mu g$, μ=coefficient of friction on sliding interface.

It is assumed that the identical hybrid system with the following characteristics which were experimentally identified with the prototype system is used for this study. The dynamic characteristics of the pressure control device of the hybrid system follows the first order time delay model,

$$T\dot{p} + p = u \tag{11}$$

where p=pressure in bearing chamber, u=pressure control signal, T=time constant (T_i for increasing and T_d for decreasing pressure). The relationship between the pressure p in the fluid chamber and the friction force f on the sliding interface depends on the sliding velocity of the structure,

$$f = (-c_1 p + c_2)\frac{k^2}{\dot{x}^2 + k^2} \tag{12}$$

where k, c_1 and c_2 are constants defined previously. The parameters identified from the previous test are shown in Table 2.

The analytical models shown in Eqs.7 through 12 are numercically integrated in the time domain using Nemark's β-method (in which $\beta = 1/6$). For a frictional system, the high precision is crucial to the accuracy of the response evaluation particularly when the motion of the structure switches between the sticking phase and the sliding phase and when the sliding velocity reverses its direction. For this reason, the computational algorithm adopts a time step Δt ($\Delta t = 0.002sec$) when the system is in continuous sticking or sliding phase, whereas a much smaller time step Δt_i ($\Delta t_i = 0.0002sec$) is used whenever a phase change is in progress or when the velocity reverses its direction.

This integration is repeated two hundred (200) times, each repetition under a different acceleration history, however having one of the five PGA values and representing one of the three soil conditions. Two hundred (200) response time histories are obtained, thus giving three sets of 200 values each of the absolute maximum response acceleration as well as sliding displacement, and residual displacement.

The mean values and standard deviations of these three sets of response values are computed. Upon repeating the same procedure for all PGA values, the mean values and standard deviations

are plotted as functions of the PGA values as shown in Fig. 8, for stiff soil where the range of standard deviation is also indicated. Similarly, Fig. 9 show the same response quantities as functions of PGA under rock condition, respectively.

Observation of Figs. 8 and 9 suggests that:

1. Whether it is passive or the hybrid, the same trend is observed for isolation performance under three different types of soil conditions (the results under the soft soil are not shown here);

2. The sliding displacement under passive system with small frictional coefficient has relatively large standard deviation range. Hybrid system can reduce this range;

3. The standard deviation range of the response accleration under hybrid control is not necessarily small, but it is nevertherless small enough to confirm that the trend of the hybrid system performance under the statistical variability of response quantities.

Hence, it is concluded that the advantage of the hybrid system demonstrated by shaking table tests under the El Centro earthquake as shown in Fig. 4 essentially prevail also for the earthquakes regardless of frequency content, damping effect, and strong motion duration of their acceleration histories.

CONCLUDING REMARKS

The proposed hybrid system has been shown by a Monte Carlo analysis to perform much better than its passive counterparts not just under El Centro type ground motions as indicated by shaking table tests but also under a wider class of ground motions. In fact, under artificial ground acceleration histories characterized by the underlying power spectral density function of the modified Kanai-Tajimi form with three sets of dominant frequency, damping coefficient, and strong motion duration values and within a wide range of seismic intensity, the hybrid system has been shown

1. to make the bridge girder slide easily so that the the bridge response acceleration is reduced significantly even for small to moderate earthquakes;

2. to prevent excessive sliding displacement while the response acceleration is kept at an acceptably small level;

3. to reduce the residual sliding displacement to almost zero level;

Finally, the following comments appear to be in order: while the present study primarily depended on Monte Carlo simulations in demonstrating the effectiveness of the hybrid system, the author recognizes the desirability to have analytical solutions for the bridge response under stochastic excitations as considered here. In collaboration with others, she has begun her effort in this direction as demonstrated in Ref. [7] where the analytical solution under the stationary input is derived. Further attempts will be made to derive the analytical solution under more realistic nonstationary input. Some of the earlier efforts [8, 9, 10] by others dealing with passive systems may be extendable to the analysis of the proposed hybrid system.

ACKNOWLEDGEMENT

This work was supported by the National Center for Earthquake Engineering Research under Contract No. 925001G. The author is grateful to Prof. M. Shinozuke of Princeton University for his valuable comments. She also wishes to acknowledge the partial support of Taisei Corporation in the course of this study.

References

[1] Feng, M. Q., Fujii, S. and Shinozuka, M., "Experimental and analytical study of a hybrid isolation system using friction controllable sliding bearings," *Technical Report NCEER-92-0009*, 1992.

[2] Feng, M. Q., Shinozuka, M., and Fujii, S., "A friction controllable sliding isolation system," Accepted for publication in *ASCE Journal of Engineering Mechanics.*

[3] Yang, J.N., Long, F. X., and Wong, D., 1988b, "Optimal control of nonlinear structure," *Journal of Applied Mechanics,* Vol. 110, pp. 931-938.

[4] Shinozuka, M. and Deodatis G., "Simulation of stochastic processes by spectral representation," *Applied Mechanics Reviews*, Vol. 44, No. 4, April 1991, pp.191-204.

[5] Shinozuka, M., Zhang R., and Deodatis G., "Sinesquare modification to Kanai-Tajimi earthquake ground motion spectrum," a paper submitted for ICOSSAR '93.

[6] Ellingwood, B.R., and Batts, M.E., "Characterization of earthquake forces for probability-based design of nuclear structures," *NUREG/CR-2945*, U.S. Nuclear Regulatory Commission, Washington, DC.

[7] Zhang R., Feng, Q., and Shinozuka, M., "Statistical analysis of hybrid sliding isolation system with new stochastic linearization approach," a paper submitted for ICOSSAR '93.

[8] Papageorgiou, A. S. and Constantinou, M. C., "Response of sliding structures with restoring force to stochastic excitation," Probabilistic Engineering Mechanics, Vol. 5, No. 1, 1990, pp. 19-26.

[9] Constantinou, M. C. and Papageorgiou, A. S., "Stochastic response of practical sliding isolation systems," Probabilistic Engineering Mechanics, Vol. 5, No. 1, 1990, pp. 27-34.

[10] Lin S., Ahmadi, G., and Tadjbakhsh, I. G., "Response of base-isolated shear beam structures to random excitations," Probabilistic Engineering Mechanics, Vol. 5, No. 1, 1990, pp. 35-46.

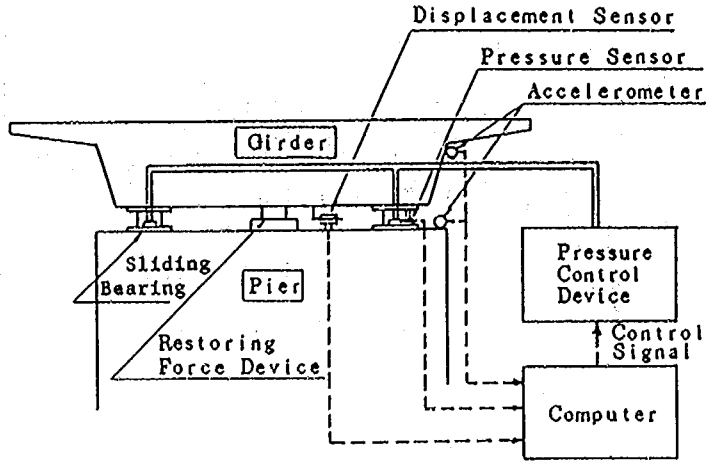


Figure 1: Concept of Isolated Bridge

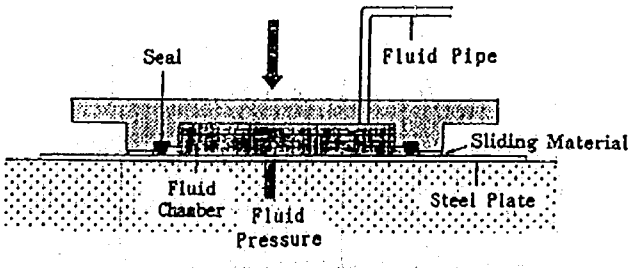


Figure 2: Idealized View of Bearing

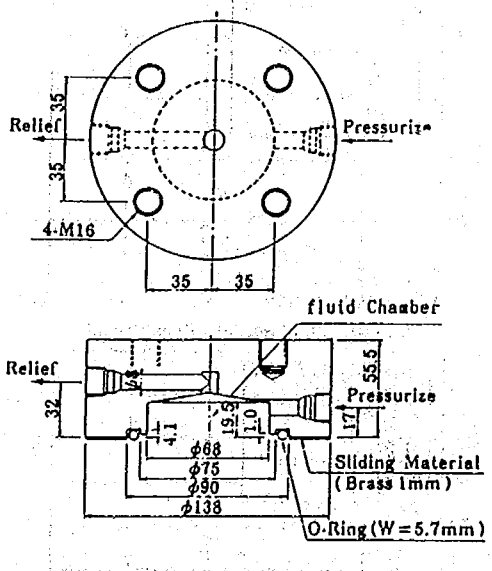


Figure 3: Prototype Bearing

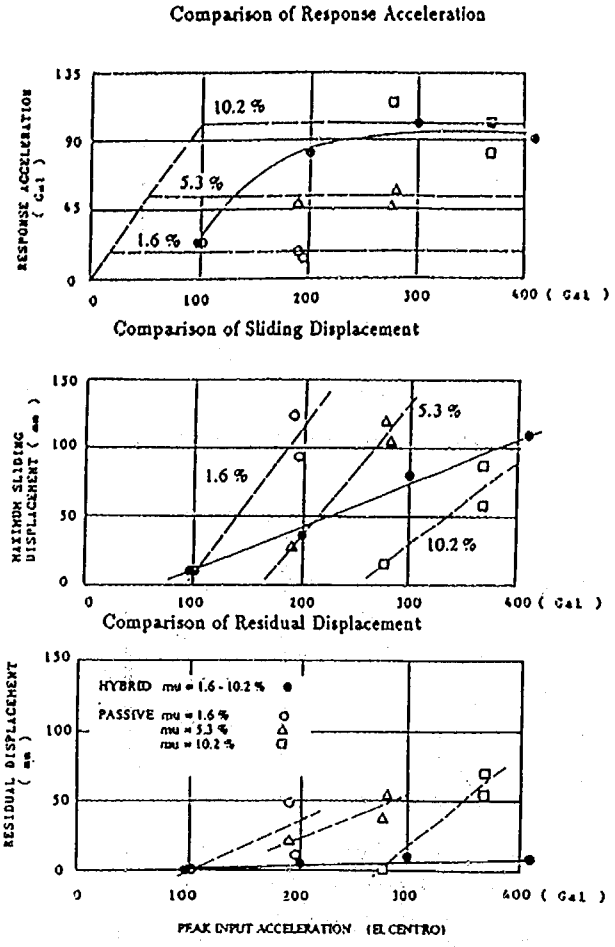


Figure 4: Experimental Results

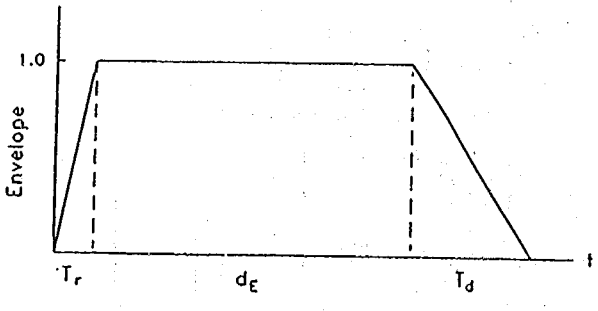


Figure 5: Envelop Function

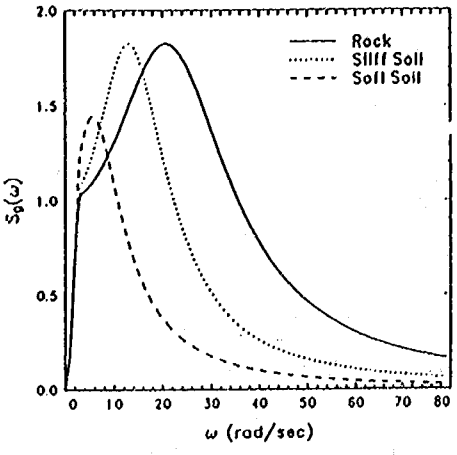


Figure 6: One-sided Power Spectrum

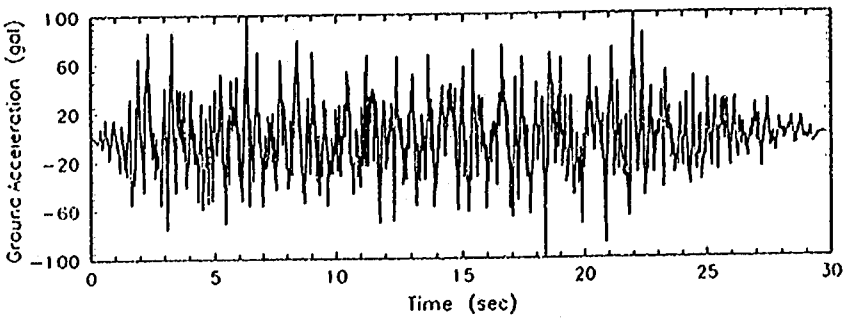


Figure 7: Artificial Earthquake

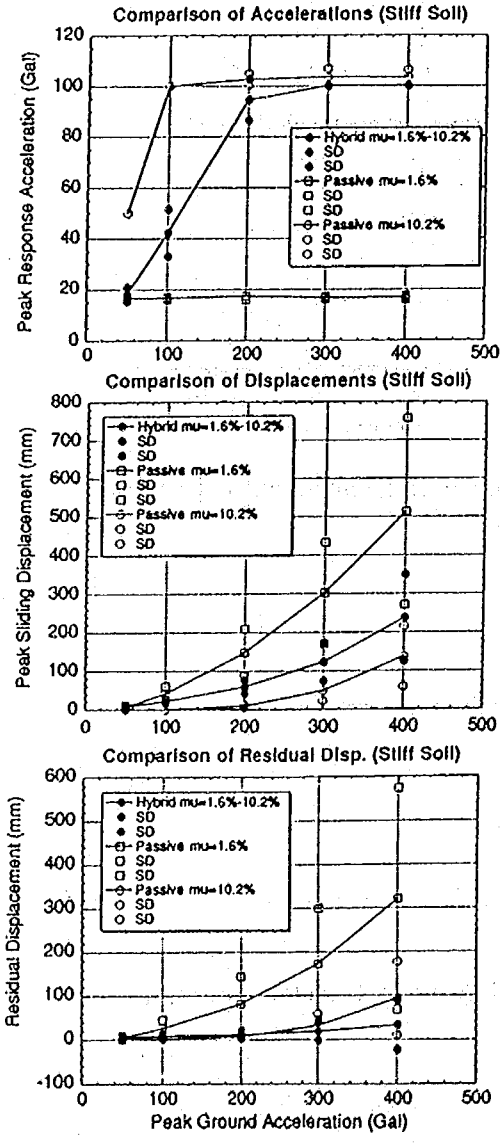


Figure 8: Simulation Results (Stiff Soil)

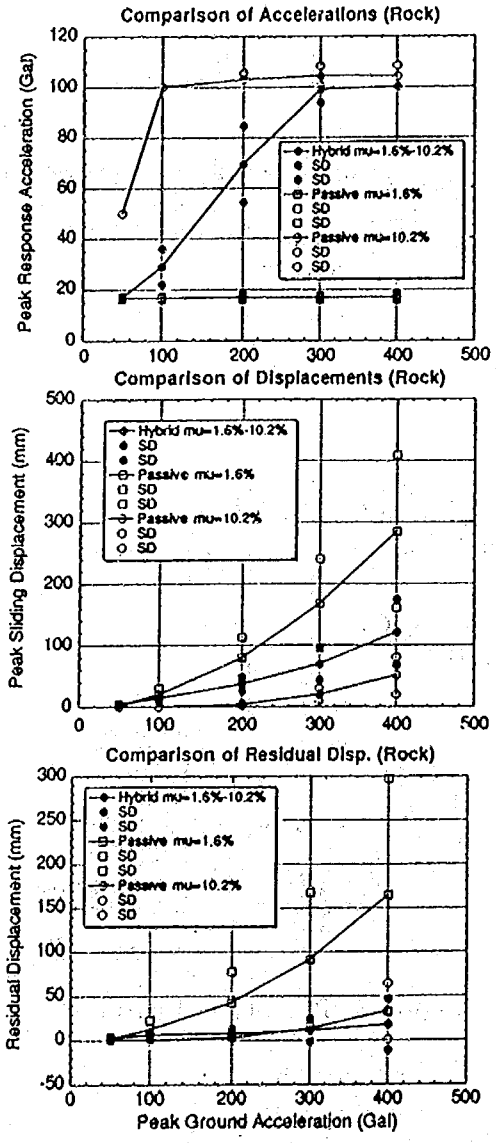


Figure 9: Simulation Results (Rock)

Shake Table Test of A Model Bridge with Sliding Isolation System

Susumu Okamoto[1], Michael Constantinou[2], Panos Tsopelas[3], Shunji Fujii[4] and Daisuke Ozaki[1]

1) Research Engineer, Earthquake and Wind Engineering Research Group,
Technology Research Center, Taisei Corporation

2) Associate Professor, Department of Civil Engineering,
State University of New York at Buffalo

3) Student, Department of Civil Engineering,
State University of New York at Buffalo

4) Senior Research Engineer, Technology Planning Department,
Taisei Corporation

ABSTRACT

The sliding type seismic isolation system composed of a sliding bearing and a horizontal spring is already used for buildings[1]. The application of the similar sliding system to bridges are considered. The proposed isolation system for bridges consists of a sliding bearing and a rubber restoring force device, which acts also as a displacement restrainer. The system is installed between the deck and the pier. A shake table tests were performed using a model bridge to confirm the fundamental characteristics of the isolation system. This report outlines the proposed system and describes the test results. Some noticeable points related to the design of the system which were derived from the tests, are also summarized.

INTRODUCTION

In recent years, several types of seismic isolators for bridges have been developed, such as the lead laminated rubber bearing and the high damping laminated rubber bearing, in New Zealand, United States, Japan and some other countries. Sliding type isolation systems have also been developed, and used for buildings[1]. In the application of the sliding system to bridges, the following points must be carefully considered :

1) isolation effect of the proposed system,
2) appropriate level of the restoring force and
3) prevention of the falling of a deck during an unexpected strong earthquake.

The above consideration led to an isolation system that consists of a sliding bearing, composed of a teflon plate that slides on a stainless steel plate, and a rubber restoring force device, which also acts as a displacement restrainer (or stopper) during strong earthquake. Viscous damper may also be added.

Shake table tests were performed to confirm the performance of bridges isolated with the

proposed system during earthquakes. One-fourth scale bridge models with seven different system properties were shaken by fourteen different motions, which include famous recorded waves and artificial waves used in design.

As a result of these tests, the isolation effect of the proposed system was confirmed and also some useful information needed in design were pointed out.

SLIDING TYPE SEISMIC ISOLATION SYSTEM FOR BRIDGES

Sliding Type Seismic Isolation System

The sliding type isolation system has been selected based on the following advantageous features;

1) The sliding system does not have any predominant period, so it is free from resonant vibration.
2) Maximum inertia force transmitted to the deck from the pier is limited to the total of the maximum friction force on the sliding interface and the restoring force.
3) A large energy dissipation is expected due to the friction at the sliding bearing.

However, the following points must be carefully considered in the development of the system for bridges;

1) The relative displacement during the earthquake and the residual relative displacement after the earthquake between the deck and the pier tend to become larger compared to the elastomeric systems.
2) An appropriate displacement restrainer (or stopper) has to be developed.

The proposed sliding type seismic isolation system then is composed of a sliding bearing and a rubber restoring force device; sometimes, the system may contain a viscous damper.

The sliding bearing supports the weight of the deck and the vertical live load. The energy dissipation is expected by the friction at the sliding interface. The rubber restoring force device works as a horizontal spring during the expected design earthquake, and as a displacement restrainer (or stopper) during the unexpected earthquake stronger than the design earthquake. If additional energy dissipation is necessary, a viscous damper is also used. The system is effective in all directions.

Sliding Bearing

The sliding bearing is composed of a teflon plate set to the pier and a stainless steel plate set to the deck. **Figure1** shows an example of the dynamic friction coefficient versus the velocity and pressure when an unfilled teflon is used[2]. Some basic characteristics are as follows.

1) When the velocity on the sliding interface is less than 10cm/sec (4in/sec), the friction coefficient increases with the increases in the velocity. Above the 10cm/sec (4in/sec) velocity, the friction coefficient is almost constant.
2) The maximum friction coefficient in the high velocity range increases from 5% to 14% as the pressure decreases from 44.9MPa (6500psi) to 6.9MPa (1000psi).
3) The minimum friction coefficient in the low velocity range equals to a few percent.

These fundamental characteristics are qualitatively applicable to other sliding bearings composed of any kind of teflon pate and the stainless steel plate, as in this experiment.

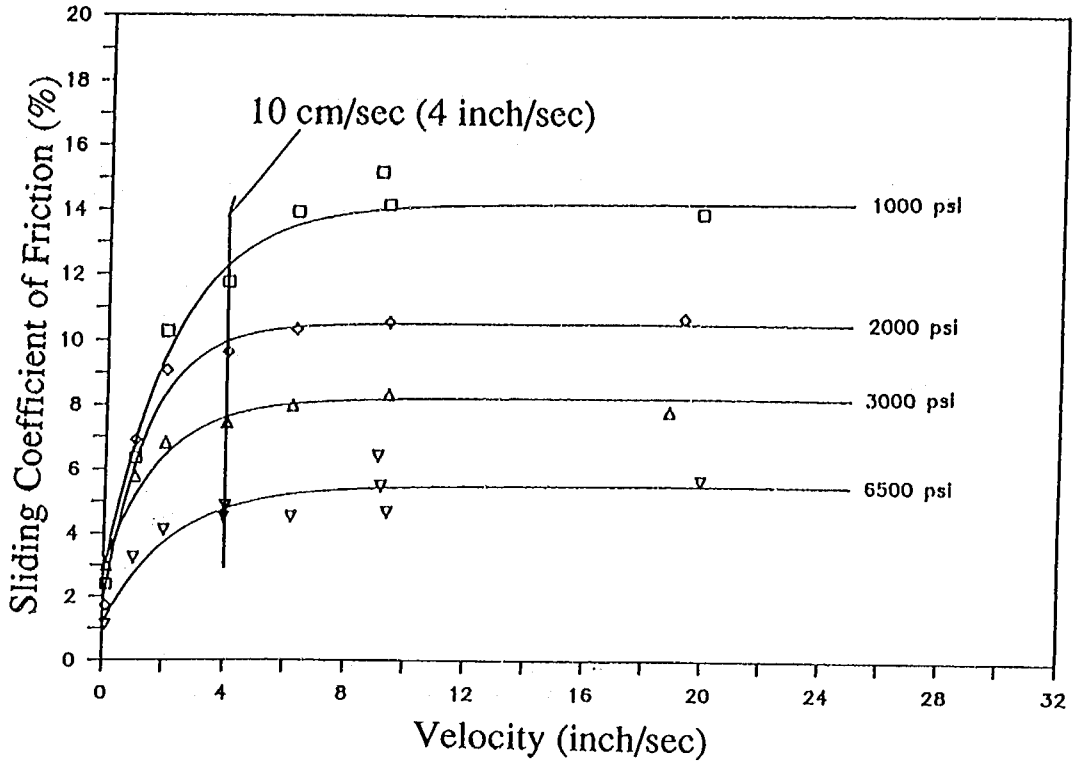


Fig.1 Variation of Maximum Sliding Coefficient of Friction With Velocity and Pressure on Sliding Interface of Unfilled Teflon (After Constantinou et al [2])

Rubber Restoring Force Device

The rubber restoring force device works as a horizontal spring and as a displacement restrainer (or stopper). **Figure2** shows the composition of the rubber restoring force device. It is composed of an anchor bar and a spoke type rubber block. The anchor bar, which is set to the pier, is inserted into the center hole of the rubber block, which itself is set to the deck. **Figure3** shows the general view of the element test and **Fig.4** shows one example of the test result. When the displacement is below 3.5cm, the rubber plates, with induced tension, works as a linear horizontal spring. Above the 3.5cm displacement, the cavity between the adjacent rubber plates is filled by the rubber plates themselves because the plates buckle and fold into the cavity. Then the reaction force increases steeply, and the device acts as a displacement restrainer.

Viscous Damper

If the energy dissipation of the system composed of the sliding bearing and the rubber restoring force device is not enough, a viscous damper may be used to augment the energy dissipation. Damping coefficient of the viscous damper is almost proportional to the velocity.

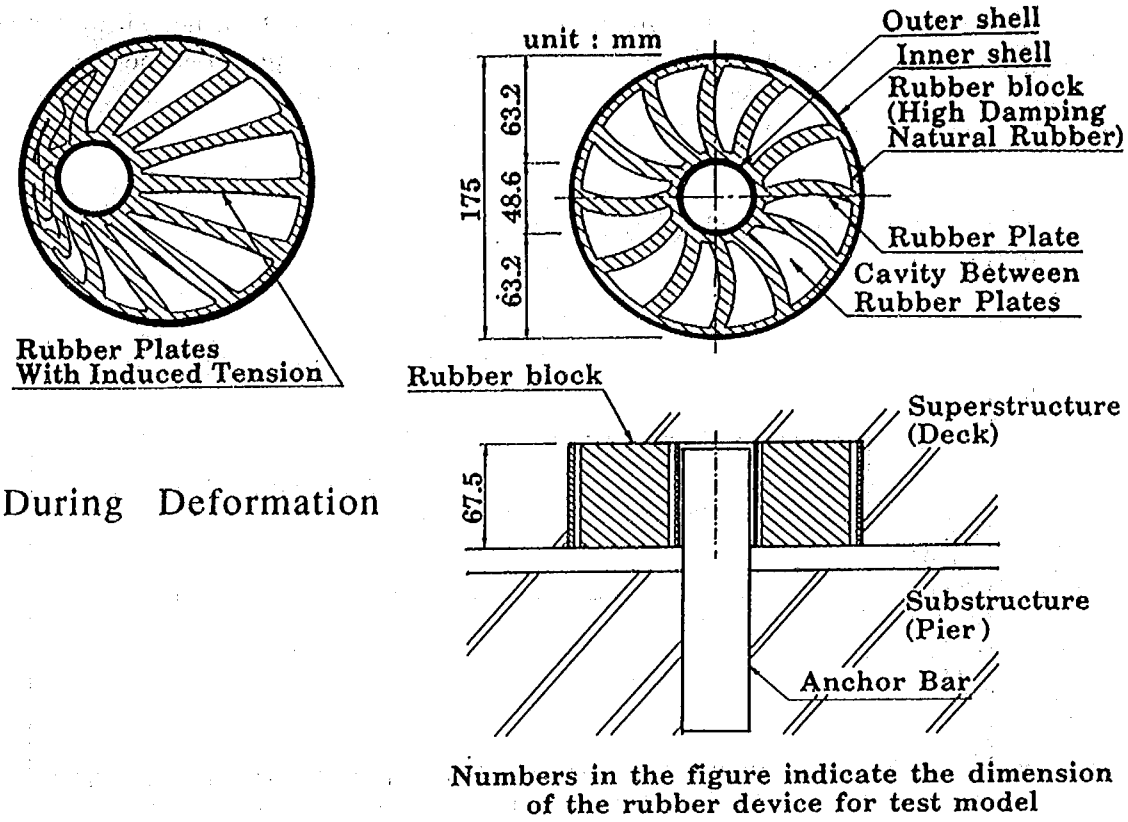


Fig. 2 Composition of Rubber Restoring Force Device

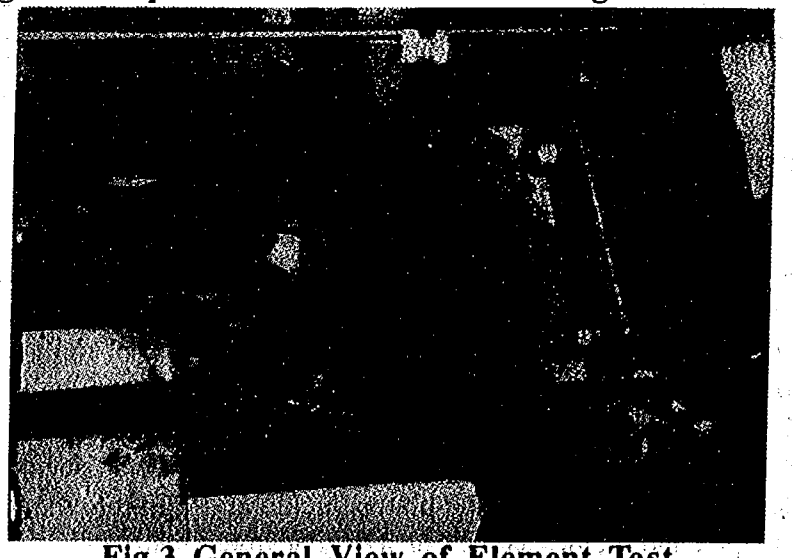


Fig.3 General View of Element Test

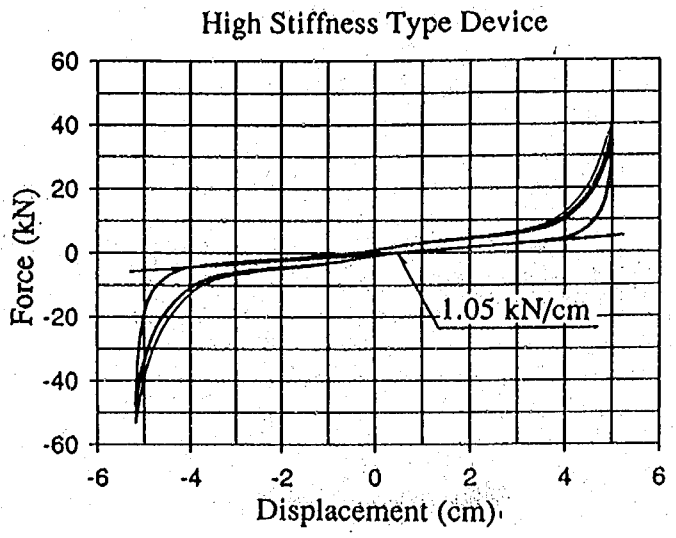


Fig.4 Results of Element Test of Rubber Restoring Force Device

EXPERIMENTAL SETUP AND MODEL STRUCTURES

Bridge Model

A bridge model with one span is used in this test as shown in **Fig.5**. The scale factors for acceleration and unit weight are set to 1/1 so as to achieve a same ratio of the inertia force and the friction force for the model and prototype. The scale factor for time is set to 1/2 after considering the ability of the shake table. The scale factors for other properties are automatically defined as shown in **Table1**. For example, the scale factor is 1/4 for length, 1/2 for velocity, and so on.

Main properties of the model are shown in **Table2.** The span length is 4.8m. The model pier is made of steel with the height of 1.4m. The predominant period of the model pier obtained from the resonant excitation test is 0.096 second (10.4Hz) which is equal to the value evaluated from the stiffness. The deck is made of a steel frame, and the weight including additional mass is 143kN.

The predominant period of the model bridge when the sliding of the bearing is constrained, is 0.26 second in the white noise excitation test, it is 0.52 second in the prototype. Damping ratio of the model bridge is about 1~3% estimated from the peak value of the transfer function in the white noise excitation.

Four sliding bearings are installed between the deck and the load cells on each columns of the pier. Two rubber restoring force devices are installed between the deck and the beam of each pier. In this test, anchor bars are set to the deck and the rubber blocks are set to the pier.



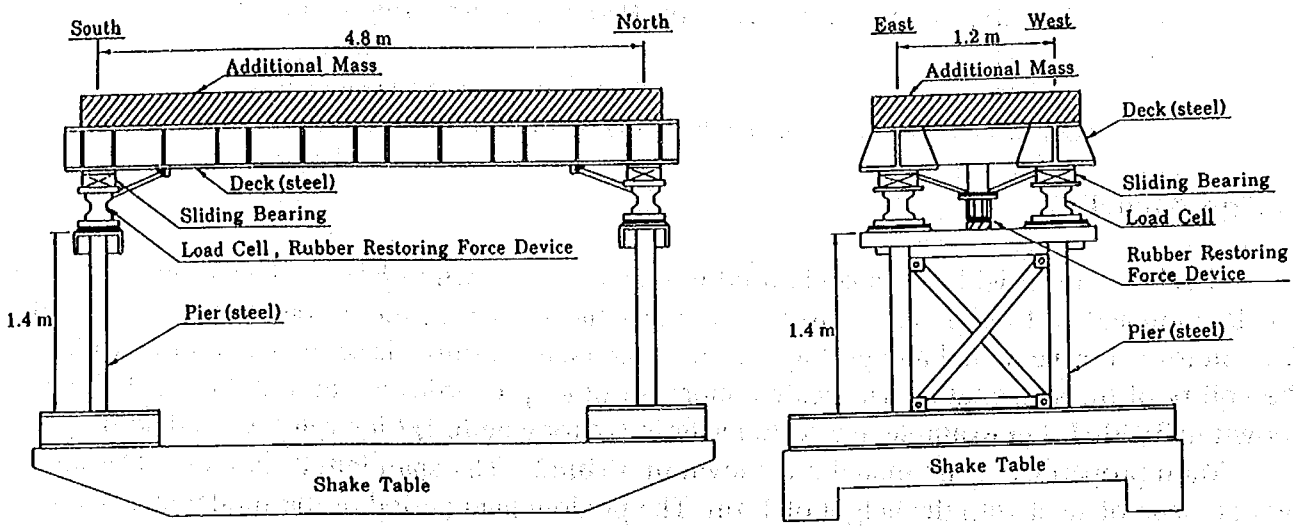


Fig.5 Construction of Model Bridge

Table 1 Scale Factor of Test

Property	Unit	Rule of the Similitude	Scale Factor
Time	sec	T	1 / 2
Length	m	L	1 / 4
Acceleration	m / sec^2	L / T^2	1 / 1
Velocity	m / sec	L / T	1 / 2
Displacement	m	L	1 / 4
Unit Weight	N / m^3	F / L^3	1 / 1
Mass	$N * sec^2 / m$	FT^2 / L	1/64
Force	N	F	1/64

Table 2 Main Properties of Model

Property	Quantity (Model Scale)	Quantity (Prototype Scale)
Span of the Deck	4.8 m	19.2 m
Height of the Pier	1.4 m	5.6 m
Weight of the Deck	143 kN	9,152 kN
Weight of the Pier(per 2 piers)	8.9 kN	570 kN
Predominant Period of the Free Standing Pier	0.096 sec (10.4Hz)	0.192 sec (5.2Hz)
Predominant Period of the Bridge (Non-Isolated Case)	0.26 sec (3.8Hz)	0.52 sec (1.9Hz)

Friction Coefficient of Sliding Bearing

Three types of teflon plates with different friction coefficient are used in this test as shown in **Table3**. **Figure6** shows one example of the relationship between the force and the displacement on the sliding interface during the identification test. **Figure7** shows the friction coefficient on the sliding interface at different velocity level. The maximum friction coefficient of the unfilled type teflon plate, which is obtained in the velocity range between 5 and 15 cm/sec in all cases, is 13% to 16%, which is almost the same as of the filled type teflon plate. The maximum friction coefficient of the low friction composite is 6% to 7%. **Figure7** also shows the friction coefficient of the case when two filled type teflon plates are set to one pier and two low friction composites are set to the other pier. The maximum friction coefficient is 9% to 10%, which is almost the same as the average value of the friction coefficients of the filled type teflon plate and the low friction composite. The friction coefficient during tests under earthquake motions is larger than those during identification tests because the velocity on sliding interface was larger during tests under earthquake motions. The minimum friction coefficient of each type of teflon plate in the low velocity range is 4% to 9%, which is not excessive in the slow sliding caused by the elongation of the deck due to temperature change.

Table 3 Friction Coefficient of Each Teflon Plate

Type of the Teflon	Unfilled Type Teflon	Filled Type Teflon	Low Friction Composite
Contact Area	70.9 cm^2	20.4 cm^2	3.2 cm^2
Pressure on Sliding Interface	5.0 MPa	17.5 MPa	111.7 MPa
Friction Coefficient in Velocity Range between 5 and 15 cm/sec	13% to 16%	13% to 14%	6% to 7%
Friction Coefficient in Low Velocity Range	4% to 9%		

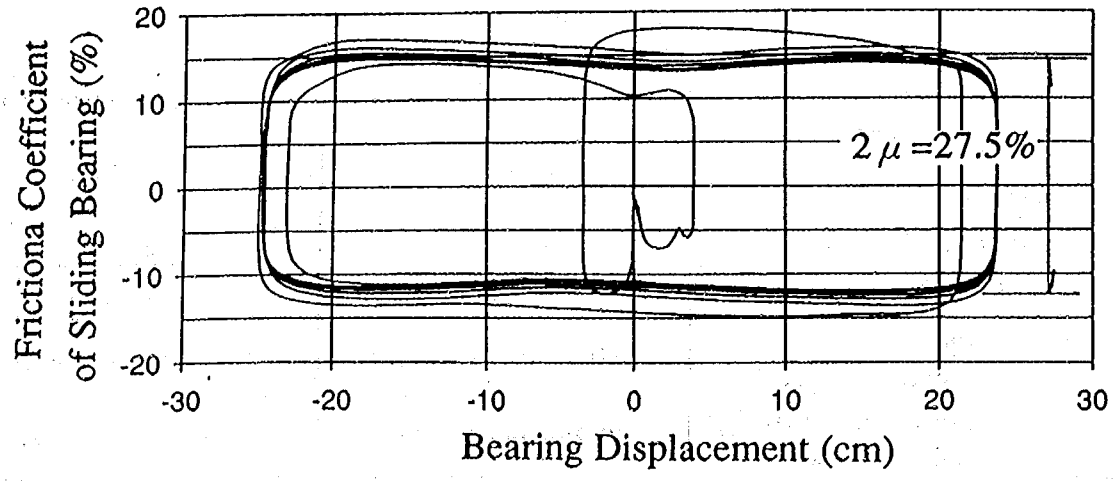


Fig.6 Relation between Force and Displacement on Sliding Interface (Filled Type Teflon, 1Hz, Amplitude : 2.5cm)

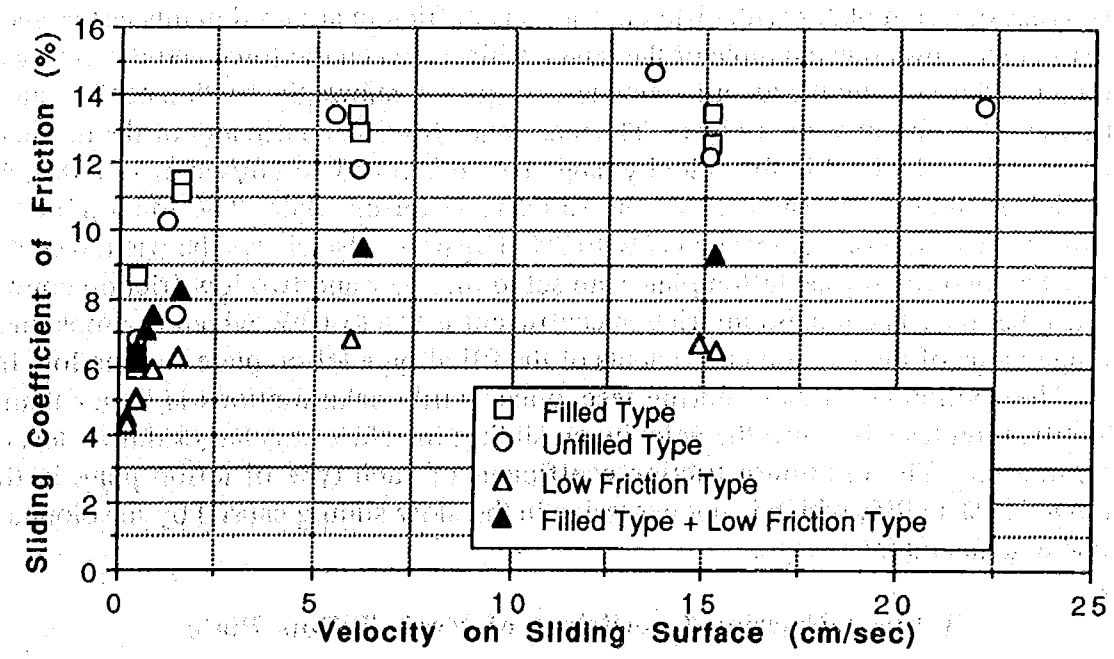


Fig.7 Relation Between Friction Coefficient and Velocity on Sliding Interface

Stiffness and Damping Ratio of Rubber Restoring Force Device

The rubber restoring force device used in the test is made of high damping natural rubber. The outer diameter of the rubber block is 17.5cm, as shown in **Fig.2**, which allows 5cm relative displacement between the deck and the pier. The maximum relative displacement allowed in the prototype bridge thus is 20cm.

Three types of rubber restoring force device with different stiffness are used in this test. The stiffness does not vary with velocity of input motion.The stiffness in the small displacement range, less than 3.5cm, is almost linear and then the stiffness increases, as shown in **Fig.4.** The stiffness of the devices used in the linear range are 0.51, 1.34 and 2.10kN/cm, as shown in **Table4.** The predominant periods of the system with the rubber devices after sliding, are 2.38, 1.47 and 1.17second, respectively.

Figure8 shows the damping ratio which is defined as the ratio of the restoring energy of each loop and the elastic storage energy (refer to **Equation 1**).

$$h=\frac{1}{2\pi}\cdot\frac{\Delta W}{W} \qquad (1)$$

where , h : damping ratio

ΔW : dissipated energy

W : elastic storage energy in one cycle

The damping ratios of the low, medium and high stiffness devices with the displacement amplitude of 3.5cm are about 7.3%, 5.0%, and 3.5%, respectively.

Table 4 Stiffness of Rubber Device

Type of Rubber Device	Low Stiffness Type	Medium Stiffness Type	High Stiffness Type
Hardness in JIS	HS45	HS67	HS80
Young's Modulus of the Rubber Piece[1)]	1.6 MPa	3.2 MPa	5.6 MPa
Stiffness of the Device as a Horizontal Spring[2)]	0.26 kN / cm	0.67kN / cm	1.05 kN / cm
Predominant Period without Sliding Interface	2.38 sec	1.47 sec	1.17 sec
Damping Ratio[3)]	3.5%	5.0%	7.3%

1) Secant modulus at 50% strain
2) Secant modulus of stiffness when the displacement amplitude is 3.5cm
3) Damping Ratio when the displacement amplitude is 3.5cm

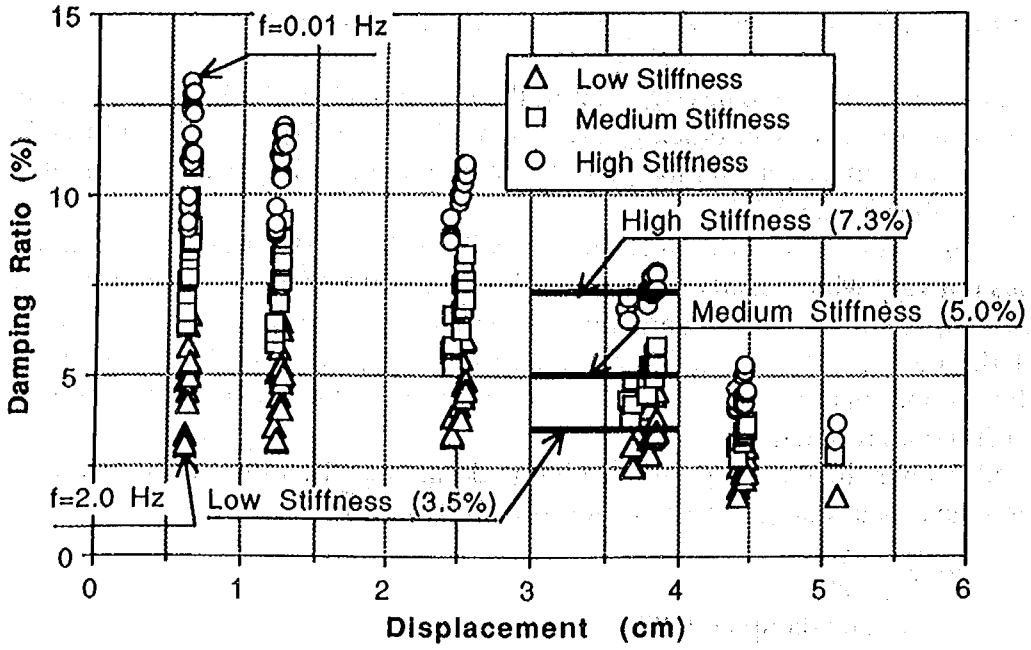


Fig.8 Relation Between Damping Ratio and Displacement of Rubber Restoring Force Device

Damping Ratio of Viscous Damper

The viscous damper filled with compressible silicon fluid is used in the test. The damping coefficient of the damper in the laboratory temperature range (about 22℃～25℃) is around 0.15 kN sec/cm (88 lb sec/in), as shown in **Fig.9**. Four dampers are installed. The damping ratio of the viscous dampers is evaluated as 48% when the system is assumed to be composed of four viscous dampers and two rubber restoring force devices with medium stiffness (T=1.47sec).

Test Program

The shaking is applied only in the longitudinal direction, though the system is effective in all directions. The input motions, as listed in **Table5**, are eight famous observed records and the six artificial motions which are used in the bridge design as per the "Japanese Specification of Highway Bridges". The artificial motions are classified according to three ground conditions, and for each ground condition two motions are defined. The level 1 motion is used for allowable stress design, and the level 2 motion is used to check the ultimate strength of the pier. During the test, the maximum acceleration is increased until the sliding displacement reaches 4.5cm, which is the limit considering the safety. In the case of Pacoima S16E motion, unscaled motion could not be applied because the maximum amplitude of this motion is too large for the system.

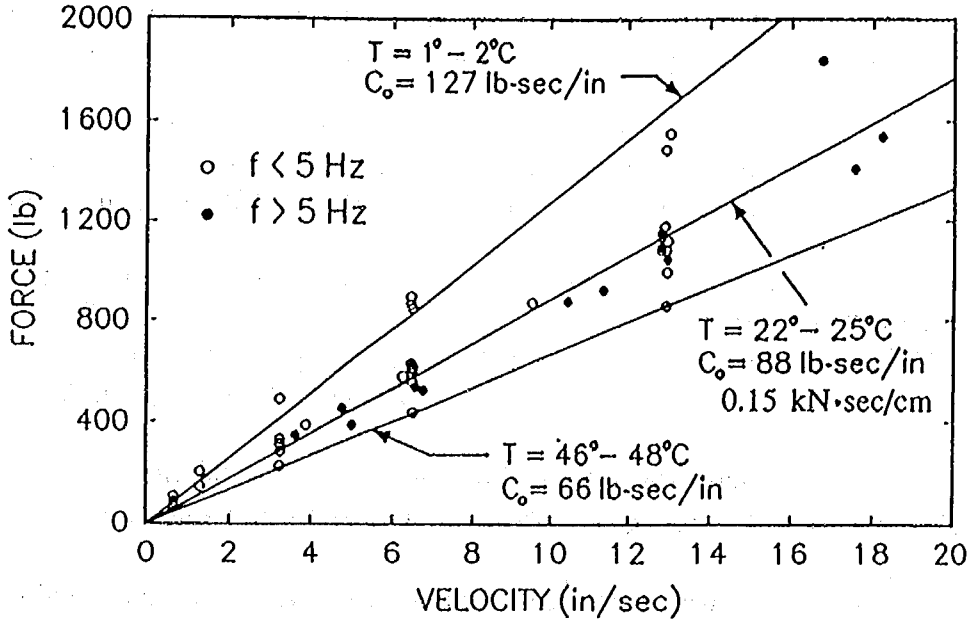


Fig.9 Force-Velocity Relationship of Viscous Damper

Table 5 Input Motions

Component of Input Motion		Maximum Value		
		Acceleration (g)	Velocity[1] (cm / sec)	Displacement[1] (cm)
El Centro S00E		0.35	16.8	2.3
Taft N21E		0.16	7.4	1.7
Pacoima S74W		1.08	28.8	3.4
Pacoima S16E		1.17	57.4	8.5
Mexico N90W		0.17	29.8	5.3
Hachinohe NS		0.23	17.1	2.8
Miyagiken-Oki EW		0.16	6.9	1.6
Akita NS		0.19	14.6	3.6
Japanese Level 1	G.C. 1[2]	0.10	10.8	2.3
	G.C. 2[2]	0.12	12.6	1.7
	G.C. 3[2]	0.14	13.7	3.3
Japanese Level 2	G.C. 1[2]	0.37	43.4	13.2
	G.C. 2[2]	0.43	49.9	13.2
	G.C. 3[2]	0.36	44.8	14.0

1) These values are derived in model scale.
(Velocity : 1/2 of prototype , Displacement : 1/4 of prototype)
2) G.C.1 : Ground Condition 1, Rock Site
G.C.2 : Ground Condition 2, Soil Deposit except for G.C.1 and G.C.2
G.C.3 : Ground Condition 3, Soft Alluvial Soil Deposit

Properties to be measured during the test are shown in **Table6**. They include the acceleration response of the deck and the pier, the shear forces of the pier and the bearing, and the relative displacement between the deck and the pier.

Table7 shows the test program. A series of tests with three kinds of teflon plates, three kinds of rubber restoring force devices, and with or without viscous damper were performed. The cases with fixed bearing were also performed to evaluate the effects of the system. Following points were clarified from these tests.

1) The isolation effect of the system was confirmed by comparing with the non-isolated case (Case1) and the fundamental case II (Case3).

2) Influences of the stiffness of the device was examined by comparing with the fundamental case I (Case2,T=1.47sec), the high stiffness case (Case4,T=1.17sec) and the low stiffness case (Case5,T=2.38sec).

3) Influences of the friction coefficient was examined by comparing with the high stiffness case (Case4, μ=13%~14%), the low friction case (Case7, μ=6%~7%) and the average friction case(Case6, μ=9%~10%).

4) Influences of the viscous damper was examined by comparing with the fundamental case II (Case3,he=10.0%) and the high damping case(Case8,he=10.0%,hv=48%).

Table 6 Instrumentations

	Table		Pier		Deck			Sliding Bearing		Rubber Device
	L[2]	V[4]	L[2]	T[3]	L[2]	T[3]	V[4]	L[2]	V[4]	L[2]
Acceleration	1	2	4	2	2	2	4	---	---	-----
Absolute Displacement	1	---	2	---	1	---	---	---	---	-----
Relative Displacement[5]	---	---	---	---	---	---	---	4	---	2
Shear Force	---	---	4	---	---	---	---	4	---	-----
Vertical Force	---	---	---	---	---	---	---	---	4	-----

1) Number in the table means the number of the instruments
2) L : Longitudinal direction of the model bridge
3) T : Transverse direction of the model bridge
4) V : Vertical direction
5) Relative displacement between the deck and the pier

Table 7 Test Program

Case No.		1	2	3	4	5	6	7	8
Case Name		Non Isolated Case	Fundamental Case I	Fundamental Case II	High Stiffness Case	Low Stiffness Case	Average Friction Case	Low Friction Case	High Damping Case
Type of Sliding Bearing[1]	FX	○	-----	-----	-----	-----	-----	-----	-----
	LW	-----	-----	-----	-----	-----	○[8]	○	-----
	FL	-----	○	-----	○	○	○[8]	-----	-----
	UF	-----	-----	○	-----	-----	-----	-----	○
Type of Rubber Device[2]	No	○	-----	-----	-----	-----	-----	-----	-----
	LS	-----	-----	-----	-----	○	-----	-----	-----
	MS	-----	○	○	-----	-----	○[9]	-----	○
	HS	-----	-----	-----	○	-----	○[9]	○	-----
Viscous Damper[3]	No	○	○	○	○	○	○	○	-----
	Yes	-----	-----	-----	-----	-----	-----	-----	○
Friction Coefficient[4] (%)		-----	13 to 14	13 to 16	13 to 14	13 to 14	9 to 10	6 to 7	13 to 16
Predominant Period[5] (sec)		0.26	1.47	1.47	1.17	2.38	1.29	1.17	1.47
Equivalent Damping Ratio[6] he		-----	10.0%	10.0%	14.6%	7.0%	12.3%	14.6%	10.0%
Damping Ratio of Viscous Damper[7] hv		-----	-----	-----	-----	-----	-----	-----	48.0%

1) FX : Bearing is Fixed, LW : Low Friction Composites (friction Coefficient : 6% to 7%),
FL : Filled Type Teflon Plates (friction Coefficient : 13% to 14%),
UF : Unfilled Type Teflon Plates (friction Coefficient : 13% to 16%)
2) No : No Rubber Device, LS : Rubber Device with Low Stiffness
MS : Rubber Device with Medium Stiffness, HS : Rubber Device with High Stiffness
3) No : Without Viscous Damper, Yes : With Viscous Damper
4) Expected friction coefficient of the system in the velocity range between 5 and 15cm/sec
5) Expected predominant period of the system without sliding interface
6) Expected equivalent damping ratio exerted by rubber device
7) Expected damping ratio exerted by viscous damper
8) Two low friction composites are set to one pier and two filled type teflon plates are set to the other pier
9) One medium stiffness rubber device is set to one pier and one high stiffness rubber device is set to the other pier

FUNDAMENTAL CHARACTERISTICS OF PROPOSED SLIDING TYPE ISOLATION SYSTEM

Advantages of Sliding Type Seismic Isolation System

Figures10 and **11** show the relationships between the displacement and the normalized shear force of the isolation system. **Figures12** and **13** show the time histories of the pier and the deck acceleration, the normalized shear force of the pier, the bearing displacement between the deck and the pier, and the table acceleration. The normalized force is defined as the ratio of the force and the weight of the deck. These figures illustrate the results of the case composed of the unfilled type teflon and of the medium stiffness devices(Fundamental Case Ⅱ) comparing with those of the non-isolated case during the level 1 and the level 2 motions defined on the rock site. **Figure14** shows the time histories in the case with viscous damper (High Damping Case) under the level 2 motion. In the non-isolated case, all time histories are scaled to get the same table acceleration of the isolated case under the assumption that the responses of the non-isolated case are proportional to the input acceleration.

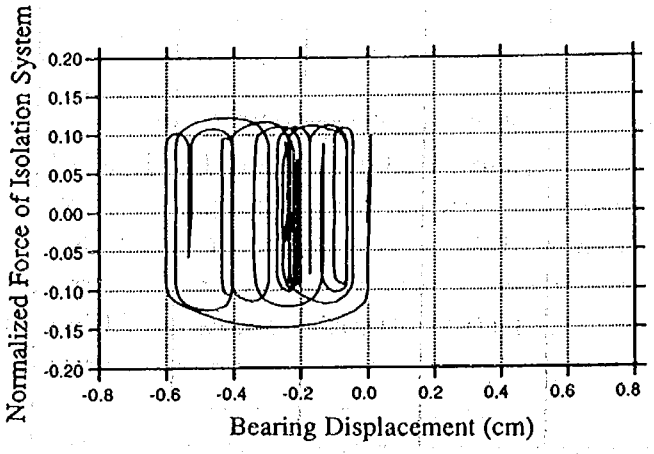


Fig.10 Relationship between Normalized Force of Isolation System and Displacement (Under Level 1 Motion, Rock Site, Fundamental Case Ⅱ)

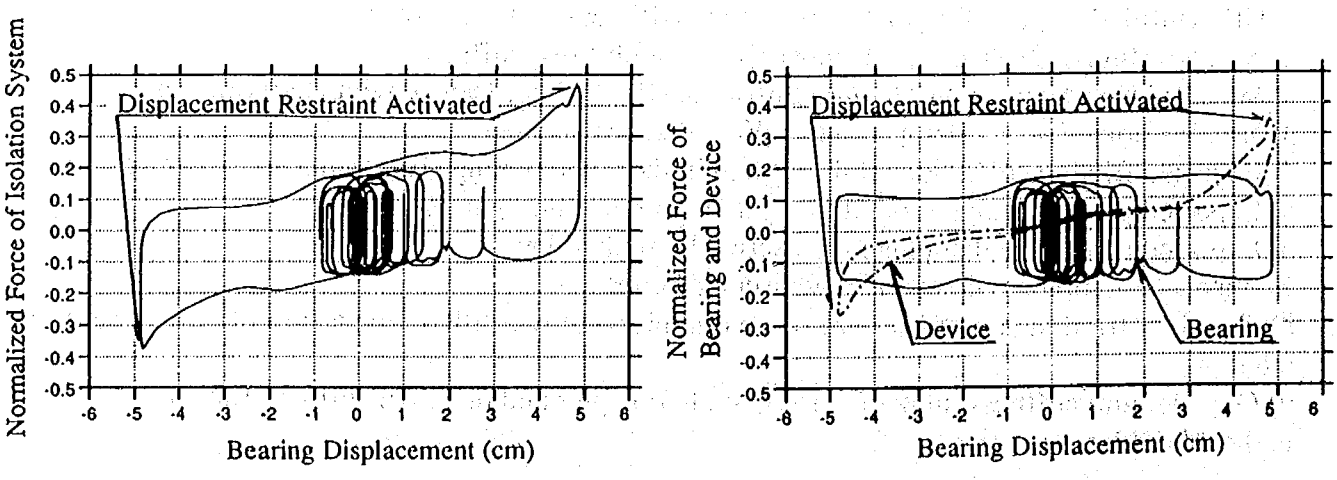


Fig.11 Relationship between Normalized Force of Isolation System and Displacement (Under Level 2 Motion, Rock Site, Fundamental Case Ⅱ)

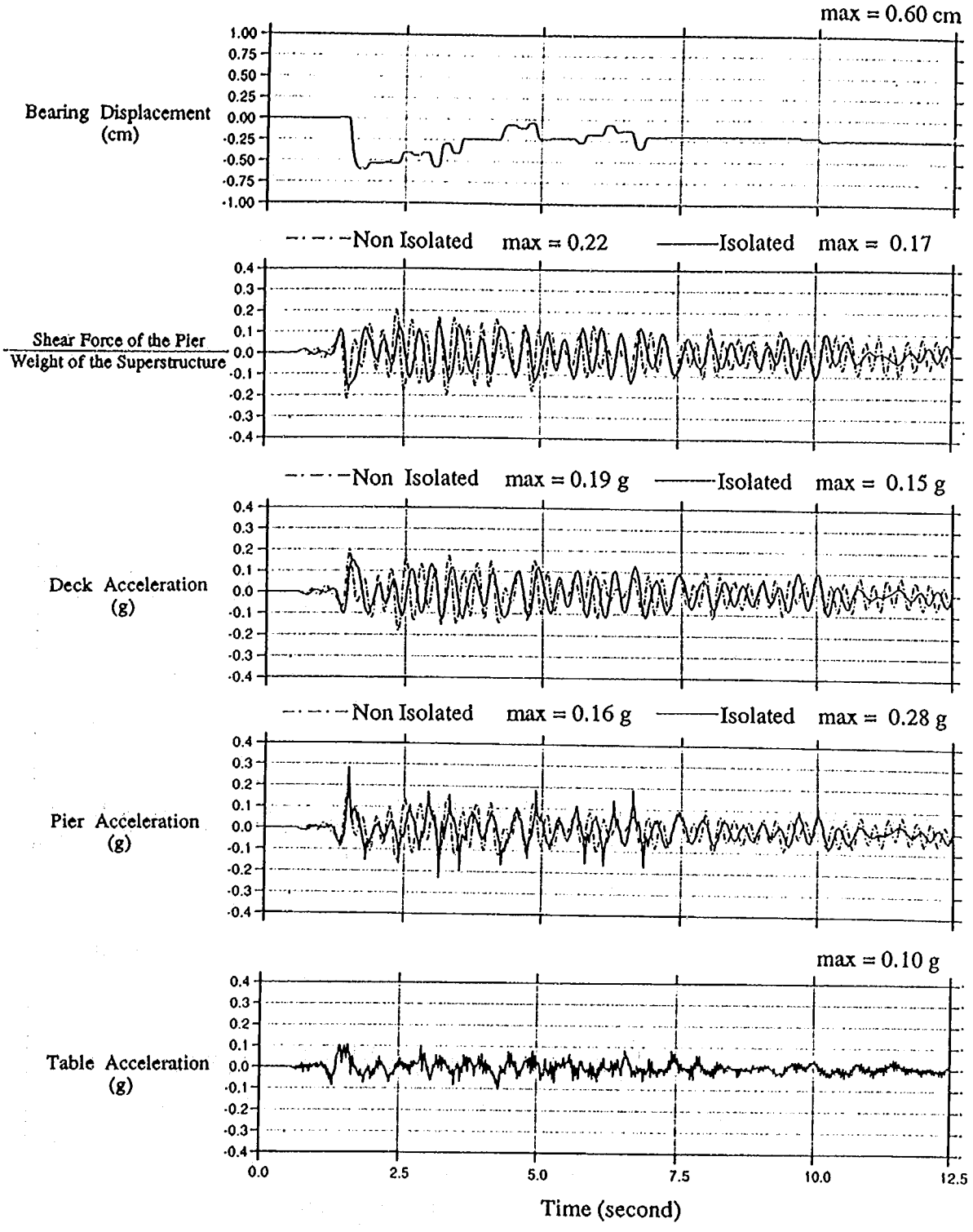


Fig.12 Time Histories of Table, Pier and Deck Acceleration, Normalized Shear force of Pier and Bearing Displacement (Under Level 1 Motion, Fundamental Case II)

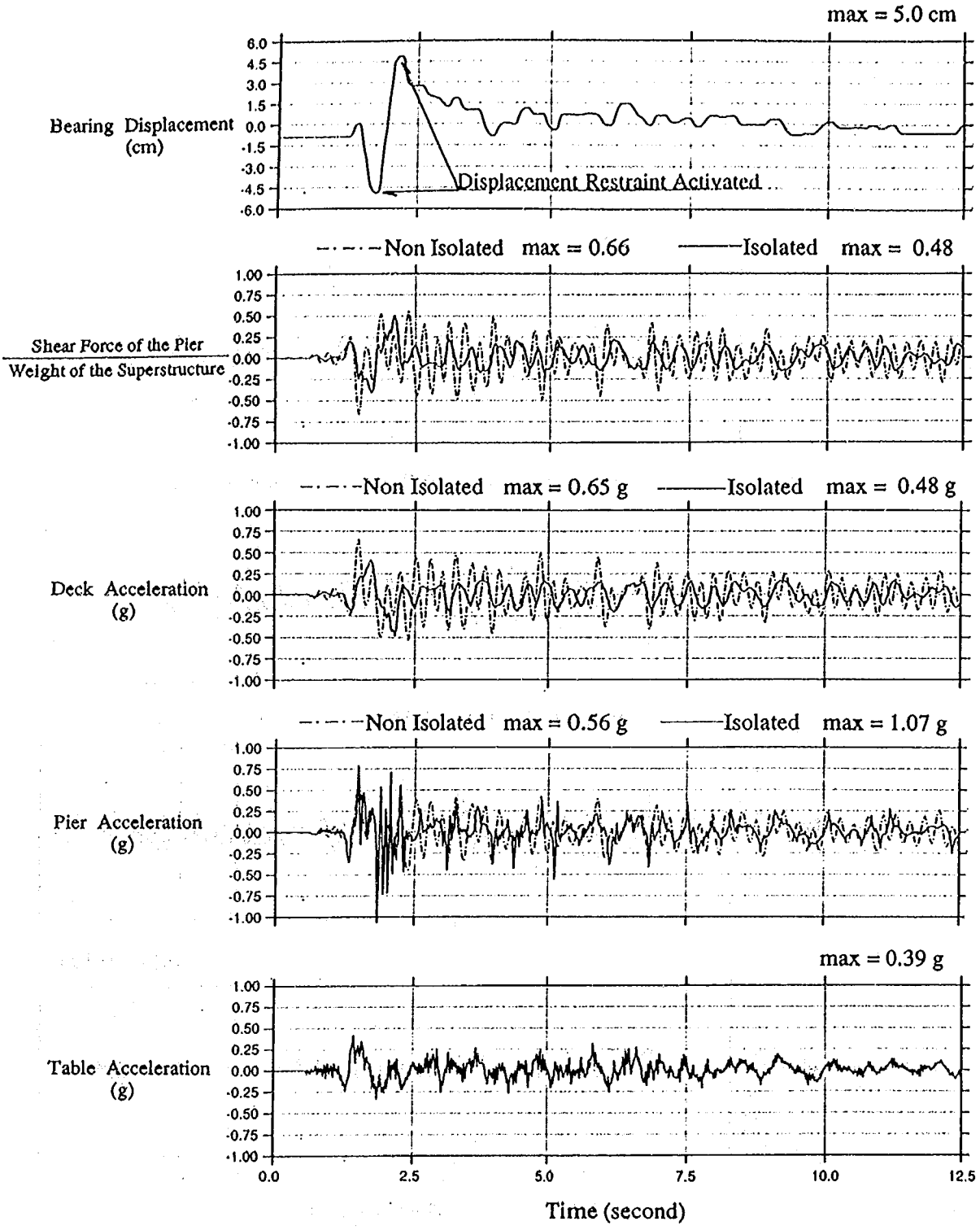


Fig.13 Time Histories of Table, Pier and Deck Acceleration, Normalized Shear force of Pier and Bearing Displacement (Under Level 2 Motion, Fundamental Case Ⅱ)

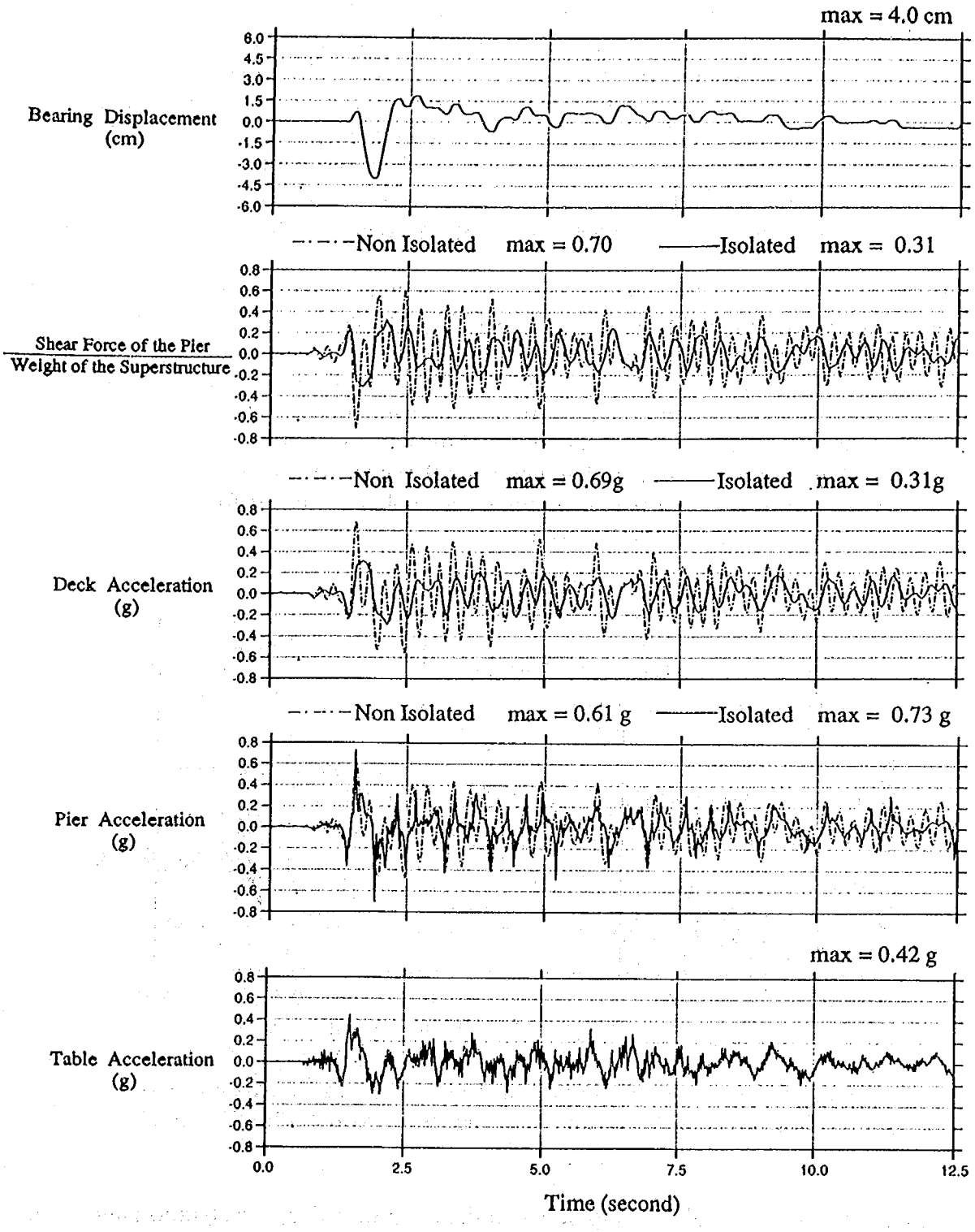


Fig.14 Time Histories of Table, Pier and Deck Acceleration, Normalized Shear force of Pier and Bearing Displacement (Under Level 2 Motion, High Damping Case)

The deck acceleration and the normalized shear force of the pier of the base isolated case are less than those of the non-isolated case. The reduction factors of the deck acceleration and the normalized shear force of the pier under the level 1 motion are 0.77 to 0.79 and the factors under the level 2 motion are 0.73 to 0.74. But the pier acceleration of the isolated case is larger than that of the non-isolated case. Especially, under the level 2 motion, the pier acceleration of the isolated case exceeds the gravity acceleration (1g), because the rubber restoring force device at this moment acts as a displacement restrainer, as shown in **Fig.11**. In the case with the viscous damper, the deck acceleration and the normalized shear force show large reduction of 45% of those for the non-isolated case.

Figure11 indicates that the energy dissipation is induced mainly on the sliding interface. Even under the level 1 motion, the deck begins to slide when the normalized friction force is larger than 0.10.

Figure15 shows the relationship between the peak value of the deck and the table acceleration under thirty different input motions. The average amplification factor of the deck acceleration with respect to the table acceleration of the non-isolated case is about 2.15. The peak and average deck acceleration of the isolated case are 0.48g and 0.23g, respectively. The case that the deck acceleration reaches to 0.48g, is when the rubber restoring force device works as a displacement restrainer under the level 2 motion.

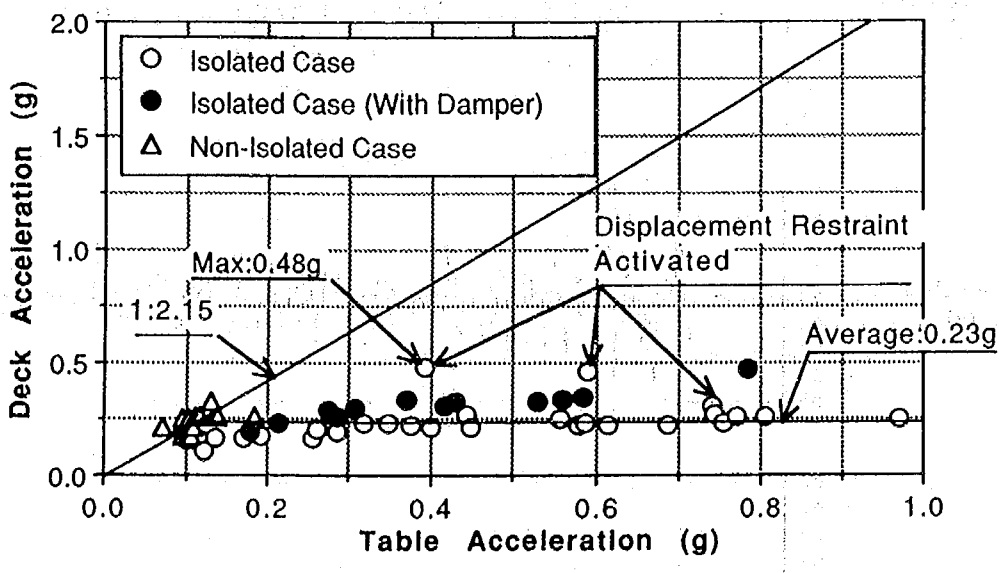


Fig.15 Relationship between Deck and Table Acceleration (Comparison between Isolated and Non-Isolated Case)

Figure16 shows the relationship between the maximum deck acceleration and the bearing displacement. The solid line in the figure indicates the predicted ratio of the inertia force and the weight of the deck. The inertia force is computed as the summation of the friction force and the restoration force of the device assuming of 18% friction coefficient. In the displacement range below 4cm, the peak deck acceleration is almost constant and the peak value is at most 0.3g. But when the bearing displacement exceeds 4cm, the deck acceleration increases quickly because then

the device acts as a displacement restrainer, as shown in **Fig.11**. The important point for the design of the proposed system is that the bearing displacement between the deck and the pier must be less than the critical displacement when the device starts to act as a displacement restrainer. For the device used in this experiment, the critical bearing displacement in model scale is 4.5cm and in prototype scale 18cm. The critical displacement can be easily changed by changing the diameter of the device.

Figures15 and **16** also show results of the case with viscous damper. The deck acceleration of the case with viscous damper is larger than that of the case without viscous damper, except for the cases when the device is activated as a displacement restrainer.

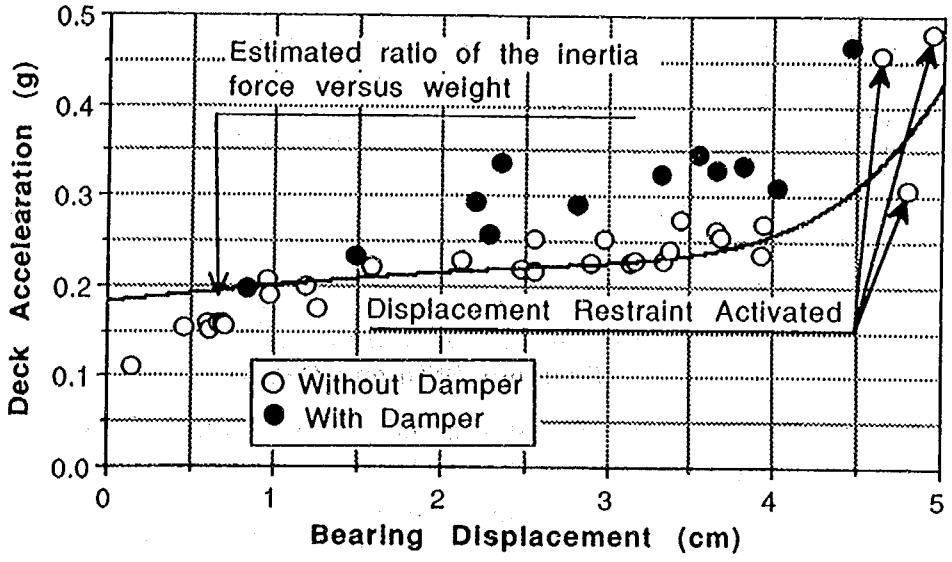


Fig.16 Relationship between Deck Acceleration and Bearing Displacement (Fundamental Case II and High Damping Case)

Influences of Device Stiffness

Figures17 and **18** show the comparisons of the peak normalized shear force of the pier and the bearing displacement between the deck and the pier, of three cases with different stiffness of the device. These figures show the results under twenty seven different input motions.

The normalized shear force of the pier increases as the stiffness of the device increases. But the difference of the normalized shear force is not so large. On the other hand, the bearing displacement decreases as the stiffness increases. The average ratios of the bearing displacement of the cases with high and low stiffness device versus that of the case with medium stiffness device are 1.17 and 0.91, respectively. Especially, with the low stiffness device, the bearing displacement sometimes is larger than 4.5 cm and the device acts as a displacement restrainer resulting in the extremely large reaction force as shown in **Fig.19**. It should be noted that both the bearing displacement and the normalized shear force of the pier are decrease as the stiffness increases. Use of high stiffness device is one powerful resolution to decrease the bearing displacement, without increasing the shear too much.

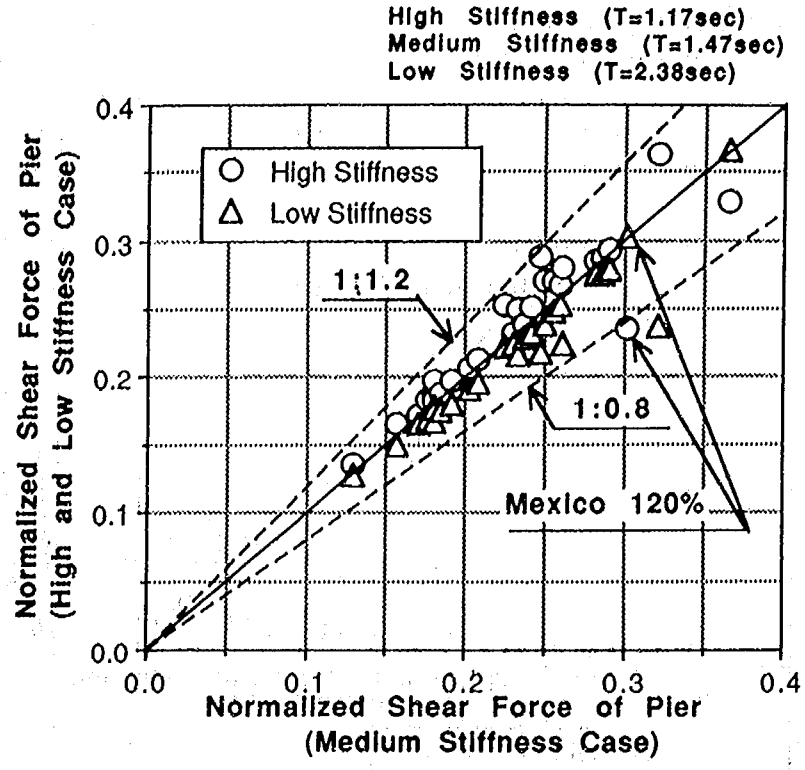


Fig.17 Comparison of Normalized Shear Force of Pier (Three Different Stiffness Cases)

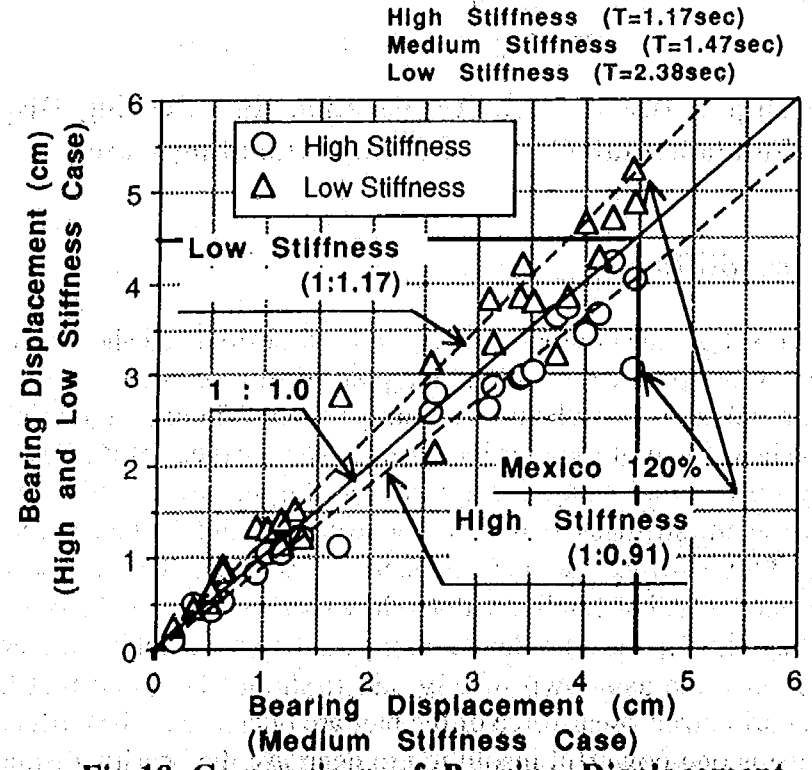


Fig.18 Comparison of Bearing Displacement (Three Different Stiffness Cases)

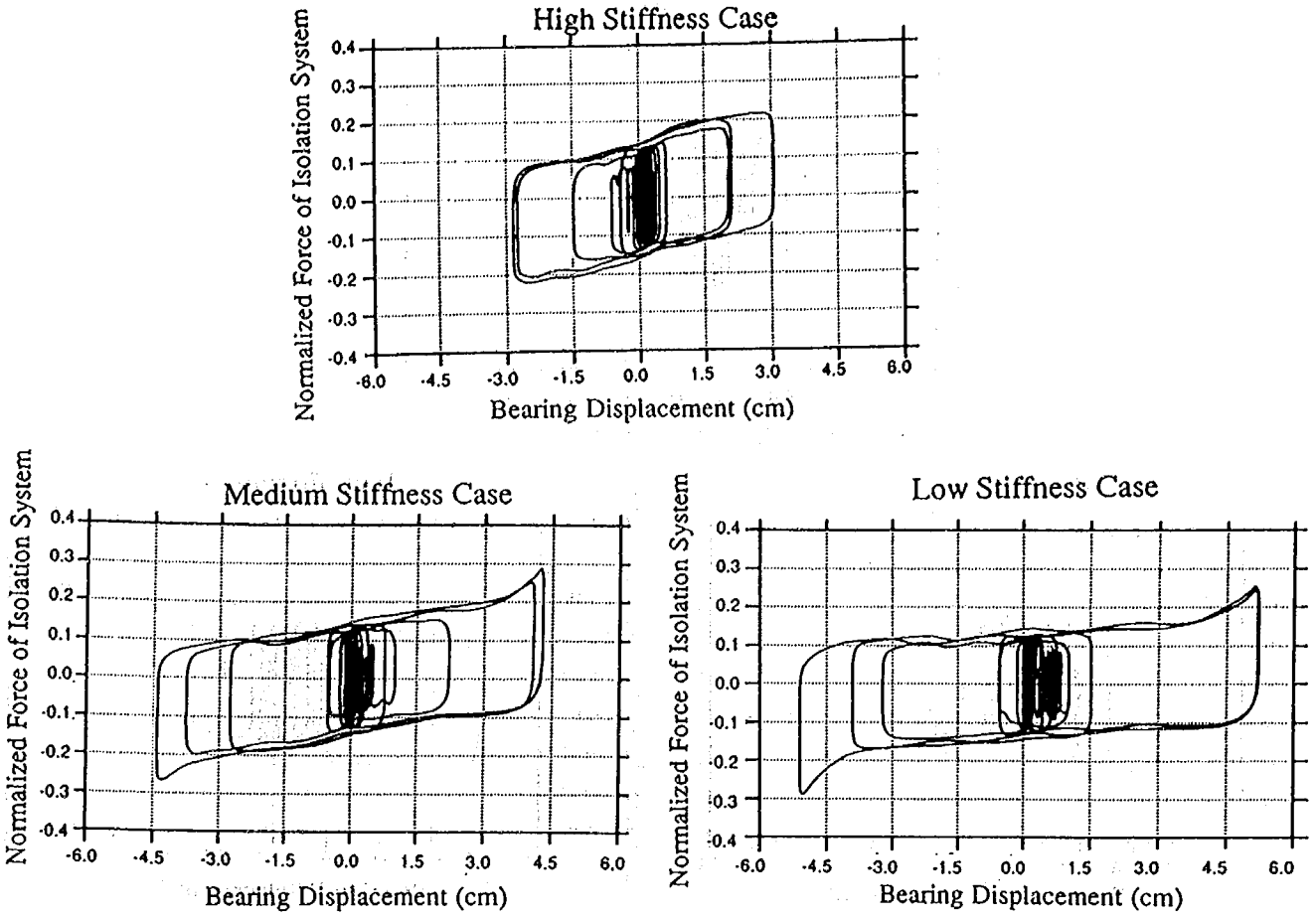


Fig.19 Relationship between Normalized Force of Isolation System and Bearing Displacement (Under Mexico N90W, 120%, Three Different Stiffness Cases)

Influences of Sliding Interface and Viscous Damper

Influences of the friction coefficient is examined comparing with the cases of the filled teflon (μ=13% to 14%) and of the low friction composite (μ=6% to 7%). Also, the case when the filled teflon is set to one pier and the low friction composite is set to the other pier (μ=9% to 10%), is studied. In this case, the stiffness of device is a little different from the other two cases.

Figure20 shows one example of the relationship between the normalized force of the isolation system and the bearing displacement for three cases under the level 1 motion on rock site. The force-displacement behavior is mainly governed by the friction coefficient of the bearing. The displacement can be confined in small level when the filled teflon is used.

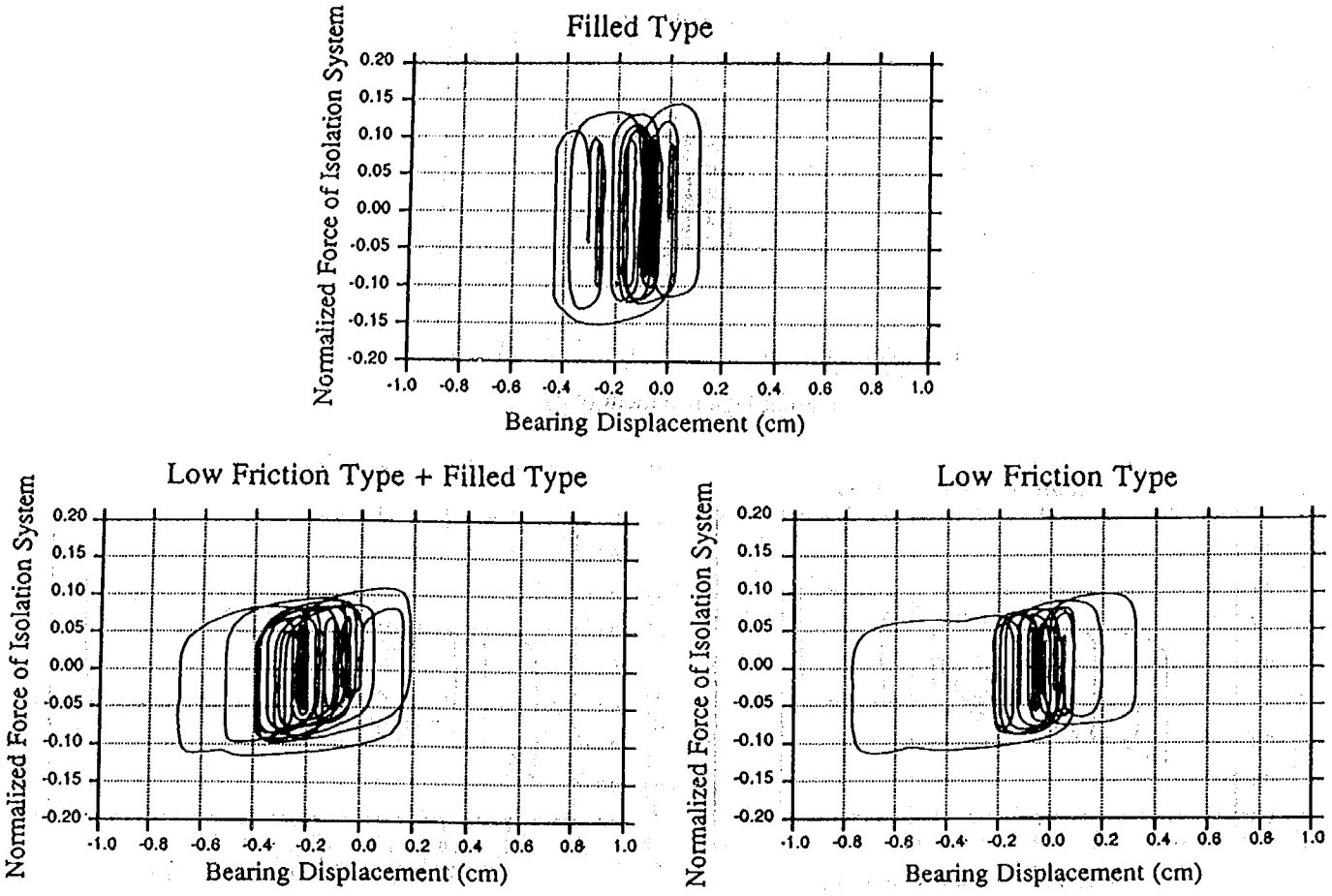


Fig.20 Relationship between Normalized Force of Isolation System and Bearing Displacement (Under Level 1 Motion, Rock Site, Three Different Friction Coefficient Cases)

Figures21 and **22** show comparisons of the normalized shear force of the pier and the bearing displacement between the system, with and without damper under relatively strong motions. Damping ratio of the viscous damper is evaluated as 48% when the system is assumed to be composed of four viscous dampers and two medium stiffness devices. The normalized shear force of the system with damper is almost the same value (0.30~0.35), while that of the system without damper varies in the range 0.25 to 0.50. The bearing displacement of the system with damper is less than that of the system without damper. **Figure23** shows the relationship between the normalized force of the system and the bearing displacement under the level 2 motion. For the system without damper, the bearing displacement exceeds 4.5cm, so the normalized shear force of the pier becomes larger. But for the system with damper, the maximum normalized shear force reaches only 0.30 because the bearing displacement is restricted below 4cm, being influenced by the energy dissipation of the viscous damper.

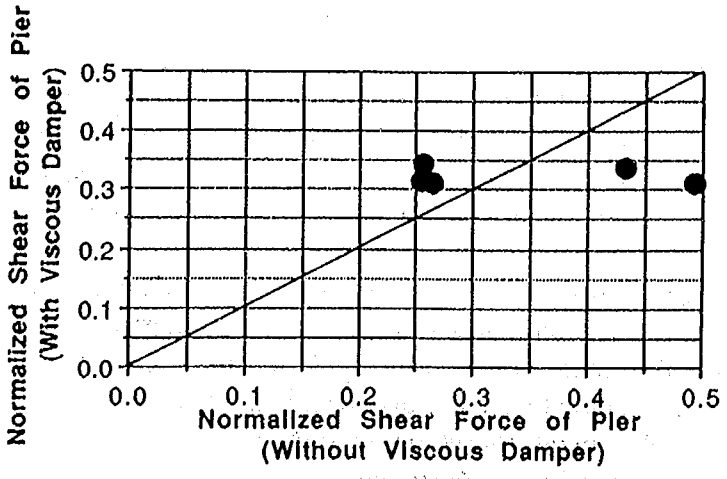


Fig.21 Comparison of Normalized Shear Force of Pier (With and Without Viscous Damper)

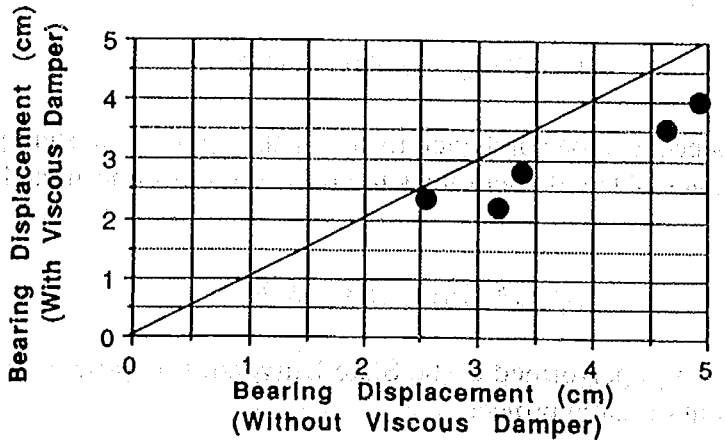


Fig.22 Comparison of Bearing Displacement (With and Without Viscous Damper)

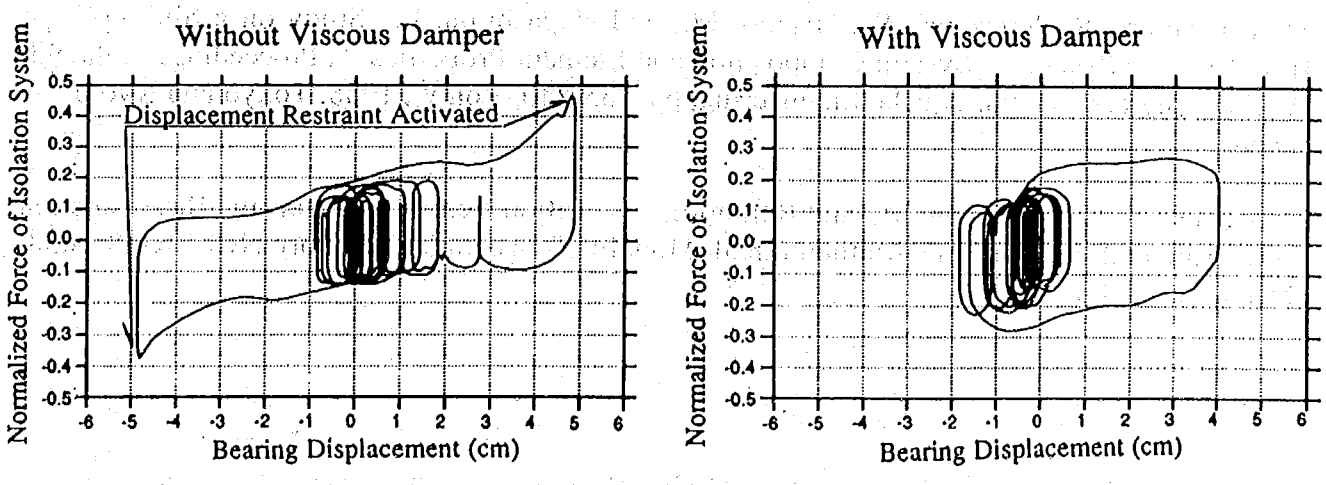


Fig.23 Relationship between Normalized Force of Isolation System and Bearing Displacement (Under Level 2 Motion, Rock Site, With and Without Viscous Damper)

CONCLUSIONS

The sliding type seismic isolation system composed of a sliding bearing and a rubber restoring force device is proposed. The shake table test of the model bridge using the system was conducted and is described in this paper. As a result of these tests, following remarkable characteristics of the system and noticeable points needed in the design of the system are clarified.

1) Isolation effect of the proposed system was confirmed by the shake table test.
2) When the device acts as a displacement restrainer, responses increase quickly. So in the design of the system, relative displacement between the deck and the pier must be designed below the displacement where the device starts to act as a displacement restrainer.
3) To restrict the relative displacement, following three methods are effective.
   a) To use a teflon with large friction coefficient.
   b) To use the rubber restoring force device with large stiffness.
   c) To add a viscous damper.

FUTURE DIRECTIONS

A dynamic analysis needs to be conducted to clarify the optimum system properties in design of different types of bridges. Also element tests to confirm the long term stability of the system will be performed.

ACKNOWLEDGEMENT

The shake table test was performed at the State University of New York at Buffalo, as one part of Taisei-NCEER joint research project.

REFERENCES

1) Kawamura, S., Kitazawa, K., Hisano, M., and Nagashima, I., "Study on a Sliding-Type Base Isolation System - System Composition and Element Properties -", Proceedings of the 9th World Conference on Earthquake Engineering, pp. 735-740, Vol. V, 1988, Tokyo and Kyoto, Japan.

2) Mokha, A., Constantinou, M., and Reinhorn, A., "Teflon Bearing In Aseismic Base Isolation : Experimental Studies and Mathematical Modeling", Technical Report NCEER-88-0038, December 5,1988.

Session-3

Testing of Seismic Isolation Hardware-3

J-5) Evaluation of Shear Modulus of High Damping Rubber Bearings and Lead Rubber Bearing during Low-Rate Load Reversals
(Kawashima, K., Koshitoge, M., Sudo, C., Makiguchi, Y. and Endo, K.)

J-6) Loading Facilities for Menshin Devices
(Makiguchi, Y., Endo, K., Kawai, N., Suizu, Y. and Nishikawa, I.)

J-7) Temperature-Dependency of Base-Isolated Bearings
(Nakano, O., Nishi, H., Shirono, T. and Kumagai, K.)

J-8) Load Durability Test for Highway Bridge Rubber Bearing Pads
(Matsuda, T., Maeda, Y. and Murayama, A.)

EVALUATION OF SHEAR MODULUS OF HIGH DAMPING RUBBER BEARINGS AND LEAD RUBBER BEARING DURING LOW-RATE LOAD REVERSALS

Kazuhiko KAWASHIMA[1], Masahiro KOSHITOGE[2], Chiaki SUDO[3], Yutaka MAKIGUCHI[4] and Kazuo ENDO[5]

1) Head, Earthquake Engineering Division, Public Works Research Institute, Ministry of Construction, Tsukuba Science City, Japan
2) Engineer, Testing Division, MB Material Development Department, The Yokohama Rubber Co., Ltd, Hiratsuka City, Kanagawa-ken, Japan
3) Chief Engineer, New Products Department (Seismic Isolation), Bridgestone Corporation, Yokohama City, Kanagawa-ken, Japan
4) Staff Manager, Second Technical Development Department, Oiles Corporation, Fujisawa City, Kanagawa-ken, Japan
5) Chief Engineer, Technical Development Division, The Yokohama Rubber Co., Ltd, Hiratsuka City, Kanagawa-ken, Japan

ABSTRACT

Presented are two loading schemes proposed for evaluating the equivalent stiffness of Menshin devices against low rate loading developed due to the elongation and shrinkage of a bridge deck associated with the daily change of temperature. Although it is important for properly designing the Menshin devices against such deformation, it is generally difficult to evaluate it because the test requires a special loading facility which can produce the loading with extremely low frequency. Therefore the Extrapolation Method and the Relaxation Method are proposed for such purpose. The validity of the two methods is examined through the tests to two high damping rubber bearings and a lead rubber bearing.

INTRODUCTION

Menshin devices are subjected to various loadings developed by not only seismic effects but creep, shrinkage and temperature change effect. It is one of the main feature in bridge application that the elongation and shrinkage of a deck becomes important as the total deck length becomes long. Menshin devices are designed so that the lateral force developed in the devices by not only seismic effects but such temperature change, creep and shrinkage be properly distributed to as many piers as possible. For distributing the lateral force to piers, it is important to correctly evaluate the equivalent stiffness of the devices.

Some Menshin devices have the loading rate dependence of their equivalent stiffness. For example, some high damping rubber bearings (HDR) have lower equivalent stiffness against low rate loading such as the one developed due to the daily temperature change than the equivalent stiffness against seismic loading. Such characteristics are favorable for constructing super multi-span continuous bridge with the deck length over 1 km, because the

lateral force developed due to shrinkage and elongation of the deck associated with temperature change becomes quite large in such bridge. Therefore, if the equivalent stiffness against the low rate loading is small, it is favorable to reduce the lateral force caused by the deformation of the deck associated with temperature change.

For studying the equivalent stiffness against the low rate loading, a special loading facility which can produce the loading with extremely low frequency is required. However because the loading rate required is very low, it is not always easy to produce such low rate loading. Therefore special loading procedures are required for studying the equivalent stiffness against the low rate loading.

Two methods are proposed for such purpose in this paper. The validity of the procedures is presented through the implementation of the methods to two high damping rubber bearings and a lead rubber bearings.

EVALUATION METHOD OF SHEAR MODULUS AGAINST LOW RATE LOADING

Low Loading Rate Expected due to Daily Temperature Change

Associated with the deck elongation and shrinkage due to the daily temperature change, the Menshin devices are subjected to cyclic loading reversals with very low loading rate. The deck elongation and shrinkage is evaluated as

$$\triangle L = \varepsilon \cdot \triangle t \cdot L \qquad (1)$$

where,

$\triangle L$: elongation and shrinkage of deck (m)

ε : coefficient of elongation per unit length and unit temperature (1/m/℃)

$\triangle t$: increase of temperature (℃)

L : effective length of deck (m) against temperature change

The coefficient ε of elongation per unit length and unit temperature is 1.0×10^{-5} in concrete.

It is required to design the devices against such temperature change effect as[1]

$$u_D \leqq \gamma_{DA} \cdot \Sigma t_e \qquad (2)$$

$$u_B \leqq \gamma_{BA} \cdot \Sigma t_e \qquad (3)$$

where,

u_D : design displacement of Menshin device against normal load such as creep, shrinkage and temperature change effect (cm)

γ_{DA} : allowable shear strain of rubber against normal load (= 0.7)

u_B : design displacement of Menshin device against normal load and seismic effects

γ_{BA} : allowable shear strain of rubber against normal load and seismic

effects, and shall be 1.5 in the Seismic Coefficient Method and 2.5 in the Bearing Capacity Method

Σt_e : total thickness of rubber (cm)

Because the Menshin devices are designed so that Eqs. (2) and (3) are satisfied, it can be considered that the shear strain induced in the Menshin devices due to the temperature change effect should be less than γ_{dd}, i.e., 70 %. There are other contribution by the creep and shrinkage in concrete bridges. Therefore the shear strain induced in the Menshin devices against the temperature change effect may be between 50 % and 70 %.

Assuming that the daily temperature changes in a harmonic way as shown in Fig. 1 with the period of 24 hours, the averaged shear strain rate may be approximated as

$$\dot{\gamma} = \frac{\gamma}{t^*} = \frac{50\% \sim 70\%}{6 \text{ hours}} = 2.3 \times 10^{-5}/\text{sec} \sim 3.2 \times 10^{-5}/\text{sec} \quad (4)$$

in which γ and $\dot{\gamma}$ represent the shear strain and shear strain rate, and t^* represents a quarter of a day (6hours).

It should be noted that the shear strain rate during an earthquake is much larger than those values. Because the Menshin devices are designed against normal load and seismic load so that Eq. (3) be satisfied, one can consider that the shear strain developed in the Menshin device during an earthquake is at maximum 150 % in the Seismic Coefficient Method. Therefore assuming that the first natural period of the bridge is 2 second, the shear strain rate during an earthquake may be estimated as

$$\dot{\gamma} = \frac{\gamma}{t^*} = \frac{150\ \%}{1/4 \text{ second}} = 3 /\text{sec} \quad (5)$$

Extrapolation Method

If the loading rate vs. the equivalent stiffness of the Menshin devices can be evaluated for a set of loading rates which can be produced by the testing machine available, the equivalent stiffness for the desired loading rate may be estimated by extrapolating the relation. This method is not special but may be used for most type of Menshin devices.

In the Manual for the Menshin Design of Highway Bridges, it is recommended to conduct the test for loading rate of 0.002 cm/sec, 0.005 cm/sec, 0.01 cm/sec, 0.05 cm/sec, 0.1 cm/sec, 0.5 cm/sec, 1.0 cm/sec and 5.0 cm/sec. The Menshin devices are subjected to a harmonic excitation with either strain amplitude of $\pm$ 50% or displacement amplitude of $\pm$ 7.5 cm under the vertical load equivalent to the dead weight of superstructure and at the temperature of 20°C.

Relaxation Method

Although the mechanism causing the loading rate dependence of the shear modulus of rubber (high damping rubber) is not well known, it may be related to the relaxation of the rubber. Therefore the loading rate dependence of the shear modulus of rubber may be evaluated by the relaxation method.

When a rubber specimen is subjected to a constant shear strain for a certain period, the stress induced in the specimen decreases as shown in Fig. 2 (a) and (b). Because shear modulus of the rubber is defined as

$$G_S = \frac{\tau}{\gamma} \tag{6}$$

where,

G_S : shear modulus of rubber (kgf/cm^2)
τ : shear stress (kgf/cm^2)
γ : shear strain

shear modulus G_S vs. period of relaxation t^* relation can be written as shown in Fig. 2(c). The averaged shear strain rate for a period of relaxation t^* may be evaluated from Eq. (4) as

$$\dot{\gamma} = \frac{\gamma}{t^*} \tag{7}$$

Therefore, the shear modulus G_S vs. shear strain rate $\dot{\gamma}$ relation may be written as shown in Fig. 2(d). It should be noted that this relation is similar in nature with the loading frequency dependence of the shear modulus of rubber subjected to a harmonic excitation. Therefore, by specifying an appropriate shear strain rate $\dot{\gamma}$, one can estimate the shear modulus for $\dot{\gamma}$. It should be noted that the equivalent stiffness of the Menshin devices can be obtained from the shear modulus of the rubber as

$$K_B = \frac{A_R \cdot G_S}{\Sigma t_e} \tag{8}$$

where,

K_B : Equivalent Stiffness of Menshin device (kgf/cm)
A_R : Sectional area of Menshin device (cm^2)
G_S : Shear modulus of rubber (kgf/cm^2)
Σt_e: Total thickness of rubber (cm)

This method is proposed hereinafter as the "Relaxation Method".

However various consideration has to be made for applying the Relaxation Method for evaluating the equivalent stiffness of the Menshin devices subjected to the daily temperature change, because the shear strain developed in the Menshin devices by the daily temperature effect changes with time as shown in Fig. 1.

As the first approximation for such change, a constant strain may be applied to the devices as shown in Fig. 3(a). But more accurate result may be obtained by applying the strain in several steps as shown in Fig. 3 (b) and (c). It is expected that the accuracy would be improved by increasing the number of load step.

In such a stepwise loading, the load need to be applied as follows. Consider the case where the shear strain is applied to the devices in three steps. The shear strain for which the low loading rate stiffness is required (target shear strain γ_T) is divided into three steps as shown in Fig. 4(a). The load needs to be applied to the specimen until the shear strain induced in the specimen reaches to 1/3 of the target shear strain. Then hold this shear strain for two hours so that relaxation be developed. The stress of the specimen decreases as shown in Fig. 4(b) due to relaxation. Then, apply the load until the shear strain induced in the specimen reaches to 2/3 of the target shear strain and hold it for two hours. Finally the same procedure needs to be repeated for the target shear strain. The stress developed in the specimen after the relaxation for two hours at this shear strain level is the shear stress required. This approximates the shear strain developed against a quarter cycle of harmonic loading with the period of 24 hours. Because actuator can be held for two hours after each stepwise loading, a special loading facility which is capable to produce the extremely low frequency loading is not required.

The shear stress vs. shear strain relation of Fig. 4 (a) and (b) can be obtained as shown in Fig. 4(c).

Although it was proposed to apply the shear strain as shown in Fig. 4 (a), it may be applied as shown in Fig. 5 (Loading Scheme B) as an alternative scheme. The Loading Scheme A which was proposed in Fig. 4 (a) would give higher equivalent stiffness than the Loading Scheme B, because relaxation time at the target shear strain is longer. Loading scheme for approximating the actual change of the daily temperature needs to be carefully set.

TEST MODELS

Three types of test specimens as shown in Table 1 were used to evaluate the stiffness of the devices against low strain rate load reversals. The HDR-A and LRB are specimens fabricated for this test. The HDR-B is the specimen with the same size and characteristics with the one adopted for the Yama-age Bridge[2]. Figs. 6,7 and 8 as well as photos 1, 2 and 3 show the specimens.

LOW LOADING RATE SHEAR MODULUS OF HDR-A

Extrapolation Method

In the Extrapolation Method, the HDR-A was subjected to a harmonic loading with the displacement amplitude equivalent to 50% shear strain of the rubber. The loading frequency was varied as 0.05 Hz, 0.1 Hz, 0.05 Hz, 0.01 Hz,

0.005 Hz, 0.001 Hz and 0.00025 Hz. Because the strain rate may be evaluated as

$$\dot{\gamma} \fallingdotseq 4 \cdot \gamma \cdot f \qquad (9)$$

where,

$\dot{\gamma}$: strain rate (1/sec)

γ : shear strain

f : frequency (Hz = 1/sec)

the strain rate in the tests was from 1/sec to 0.00041/sec.

The vertical load of 14.7 tf, which corresponds to the vertical stress of 60 kgf/cm^2, was applied to the specimen for representing the dead weight of the deck. A special loading facility at the Yokohama Rubber Co. was used for the test.

Fig. 9 shows the hysteresis of shear strain vs. shear stress relation for the shear strain rate of 1/sec, 0.021/sec and 0.00041 /sec. It is apparent that the equivalent stiffness decreases as the shear strain rate decreases. Fig. 10 and Table 2 show how the equivalent stiffness in terms of shear modulus decreases as the shear strain rate decreases.. Because the test results for various strain rates are consistent, they may be approximated as

$$G_S = 5.83 \dot{\gamma}^{0.204} + 7.0 \qquad (10)$$

where,

G_S : shear modulus of HDR-A (kgf/cm^2)

$\dot{\gamma}$: shear strain rate (1/sec)

By substituting γ = 2.3 x 10^{-5}/sec from Eq. (4), one can estimates the shear modulus of 7.7 kgf/cm^2. Because the shear strain during an earthquake is about 3/sec by Eq. (5), the shear modulus at the shear strain rate of 3/sec is evaluated by Eq. (10) as 14.3. The 7.7 kgf/cm^2 is about 46 % smaller than 14.3.

Relaxation Method

After the Extrapolation Method was made, the same specimen was used for the Relaxation Method. In the Relaxation Method, the target shear strain of 50 % was applied in the period of 6 hours. The loading step was set as 1, 2 and 4. In case of loading step of 1, the specimen was subjected to a load with the loading rate of 1 mm/sec (shear strain rate of 2.1 x 10^{-2}/sec) until 50 % shear strain. Then holding of the shear strain was made for 6 hours to have the relaxation. In the case of loading step of 4, the specimen was firstly loaded until 12.5 % shear strain, and the the shear strain was kept constant for 1.5 hour. The load was then increased so that 25% shear strain was developed, and the holding of the shear strain was made for 1.5 hour. Similarly, the load was stepwisely increased until the shear strain reached to 50%. It should be noted that because the shear strain was increased from 0 to 50% for 6 hours, the shear strain rate is 2.3 x 10^{-5}/sec for all the three tests.

Fig. 11(a) shows the shear strain vs. relaxation time relation thus used for the three types of loading steps. The relaxation of shear force of the specimen was developed as shown in Fig. 11(b). It is seen that the shear force at the shear strain of 50% slightly increases as the number of load step increases from 1 to 4. It is expected that the case of 4 loading step would give more accurate result. Fig. 11 (c) shows the shear force vs. shear strain relation.

From those results, the shear modulus of the HDR-A was evaluated as shown in Table 3. The shear modulus was 7.0 kgf/cm^2 in case of 4 load step. Reminding that for the shear strain rate of 2.3 x 10^{-5}/sec the shear modulus of the HDR-A evaluated by the Extrapolation Method was 7.7 kgf/cm^2, the shear modulus evaluated by the Relaxation Method is very close with that evaluated by the Extrapolation Method.

LOW LOADING RATE SHEAR MODULUS OF LRB

Extrapolation Method

The specimen was subjected to a harmonic loading with the displacement amplitude equivalent to 70% shear strain of the rubber. The loading frequency was varied as 1 Hz, 0.023 Hz, 0.0023 Hz, 0.00023 Hz and 0.000012 Hz. Because a specially designed facility which is capable for evaluating the low rate loading at Oiles Corporation was used, loading test could be made for the target shear strain (70 % / 6 hours = 3.2 x 10^{-5}/sec). The shear strain rate by Eq. (9) is from 4.4/sec to 0.00005/sec in this series of tests. The vertical load of 30.2 tf, which corresponds to the vertical stress of 60 kgf/cm^2, was applied to the specimen.

Fig. 12 shows the hysteresis of shear strain vs. shear force relation for the shear strain rate of 4.4/sec, 0.01/sec and 0.0002/sec. From these results, shear strain rate dependence of the shear modulus was obtained as shown in Fig. 13 and Table 4. The shear modulus G_S vs. shear strain rate $\dot{\gamma}$ relation may be approximated as

$$G_S = 12.1\,\dot{\gamma}^{0.0406} \qquad (11)$$

From Eq. (11) the shear modulus for the shear strain rate of 3.2 x 10^{-5} /sec is estimated as 7.9 kgf/cm^2. On the other hand, the shear strain rate developed during an earthquake is estimated by Eq. (5) as 3/sec. The shear modulus corresponding to this shear strain rate is evaluated by Eq. (11) as 12.7 kgf/cm^2. Therefore the above shear modulus for the daily temperature change is approximately 38 % smaller than the one developed during an earthquake.

Relaxation Method

The same specimen was used for the Relaxation Method. The target shear

strain was assumed as 70 %, and the number of load step was 1. Therefore the load was increased until the shear strain of the specimen reached 70 %, and then holding of this shear strain was made for 6 hours.

Fig. 14 shows the decrease of stress developed in the specimen and the shear force vs. shear strain relation. From these results, the shear modulus of the specimen was obtained as 7.7 kgf/cm^2 for the loading rate of 3.2 x 10^{-5}/sec. Because the shear modulus evaluated from the Extrapolation Method is 7.9 kgf/cm^2, this value is quite close with the one evaluated by the Extrapolation Method.

LOW LOADING RATE SHEAR MODULUS OF HDR-B

Only Extrapolation Method was applied to the HDR-B. The specimen was subjected to a harmonic loading with the displacement amplitude of 70 % of the shear strain of the rubber. The loading frequency was varied as 0.005 Hz, 0.0011 Hz, 0.00011 Hz and 0.000012 Hz. The vertical load of 238 tf, which corresponds to the vertical stress of 40 kgf/cm^2, was applied to the specimen beside the lateral loading.

Fig. 15 shows the hysteresis of shear force vs. shear strain. From these results, the shear strain rate dependence of the shear modulus was evaluated as shown in Fig. 16 and Table 5. This can be approximated as

$$G_S = 11.1 \cdot \dot{\gamma}^{0.0418} \qquad (12)$$

Based on Eq. (12), the shear modulus corresponding to the shear strain rate of 3.2 x 10^{-5}/sec and 3/sec is evaluated as 7.2 kgf/cm^2 and 11.6 kgf/cm^2. Therefore, the shear modulus developed during the daily temperature change is 38 % smaller than that developed during an earthquake.

CONCLUSIONS

For evaluating the equivalent stiffness of the Menshin devices subjected to low shear strain rate loading, two methods were proposed. In both the Extrapolation Method and the Relaxation Method, the test can be made even if a loading facility which is capable for producing extremely low frequency loading is not available. A series of loading tests were made for verifying the test methods proposed with use of two high damping rubber bearings and a lead rubber bearing. From the results presented in, the following conclusions may be deduced :

1) The shear modulus of HDR-A evaluated by the Extrapolation Method for the shear strain rate of 2.3 x 10^{-5}/sec (= 50 % / 6 hours) is 7.7 kgf/cm^2, while the value evaluated by the Relaxation Method is 7.0 kgf/cm^2.

2) The shear modulus of LRB evaluated by the Extrapolation Method for the shear strain rate of 3.2 x 10^{-5}/sec (= 70 % / 6 hours) is 7.9 kgf/cm^2, while the value evaluated by the Relaxation Method is 7.7 kgf/cm^2.

3) Based on 1) and 2), it can be said that the Relaxation Method gives the close shear modulus by the Extrapolation Method. Therefore, the Relaxation Method can be used as well as the Extrapolation Method for estimating the equivalent stiffness of Menshin devices for low rate loading developed by the temperature change.

4) Based on the Extrapolation Method, the shear strain rate dependence of the shear modulus is given by Eq. (10) for HDR-A and by Eq. (11) for LRB.

5) Assuming that the shear strain rate developed during an earthquake is 3/sec and that the shear strain rate due to the daily temperature change is 2.3×10^{-5} for HDR-A and 3.2×10^{-5} for LRB and HDR-B, the shear modulus against the daily temperature change is 46 % (HDR-A), 38 % (HDR-B) and 38 % (LRB) smaller that the one developed during an earthquake.

REFERENCES

1) Public Works research Institute and 28 Private Firms : Manual for Menshin Design of Highway Bridges, Bulletin of PWRI, Vol. 59, Public Works research Institute, March 1992
2) Ikeda, T., Kumakura, K, Oozeki, K. and Abe, N. : Design of Karasuyama (Yama-Age), Bridge, Bridges and Foundation, Vol. 91-6, 1991

Table 1 Specimens Used for Loading Tests

Specimen	Natural Period in Design (sec)	Dead Weight with Live Load		Design Displacement of Menshin Device (cm)
		Vertical Load (tf)	Vertical Stress (kgf/cm^2)	
HDR-A	1.2	15	60	7
HDR-B	1.4	328	56	33
LRB	0.9	30	60	6

Table 2 Shear Strain Rate Dependence of Shear Modulus of HDR-A evaluated by Relaxation Method

Frequency Hz	Strain Rate (1/sec)	Shear Modulus (kgf/cm^2)
2.5×10^{-4}	4.1×10^{-4}	8.3
1.0×10^{-3}	2.1×10^{-3}	8.5
5.0×10^{-3}	1.1×10^{-2}	9.3
1.0×10^{-2}	2.1×10^{-2}	9.7
5.0×10^{-2}	1.1×10^{-1}	10.6
1.0×10^{-1}	2.1×10^{-1}	11.2
5.0×10^{-1}	1.0	12.9

Table 3 Effect of Number of Load Step by Relaxation Method (HDR-A)

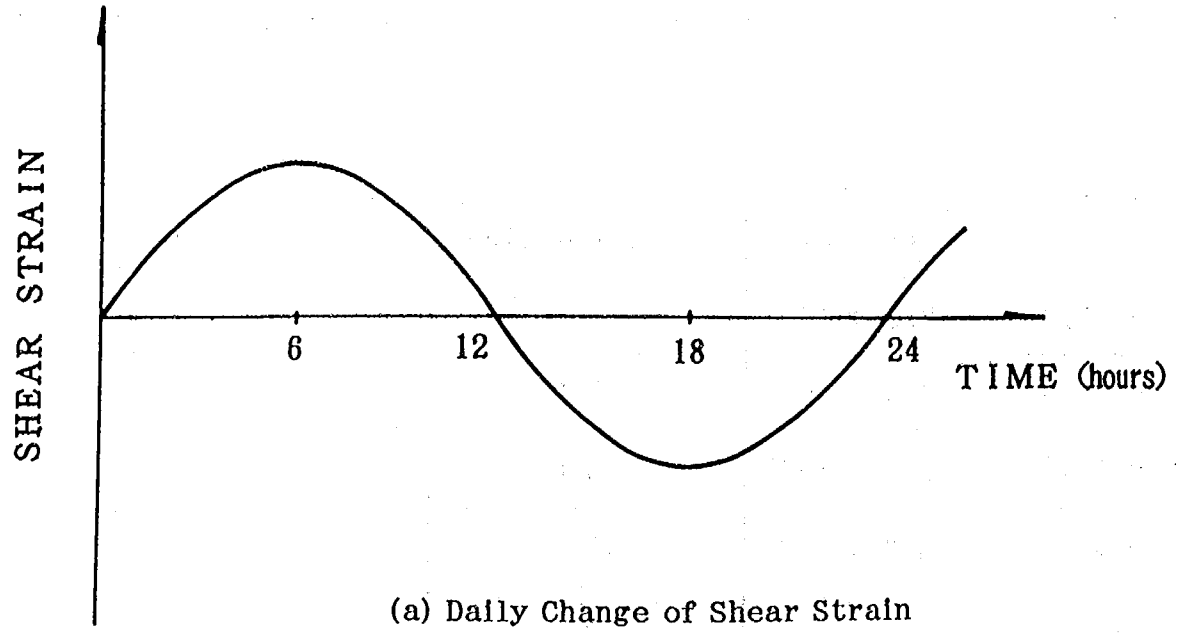
Number of Load Step	Shear Modulus G_s (kgf/cm^2)
1	6.1
2	6.5
4	7.0

Table 4 Shear Strain Dependence of Shear Modulus of LRB by Extrapolation Method

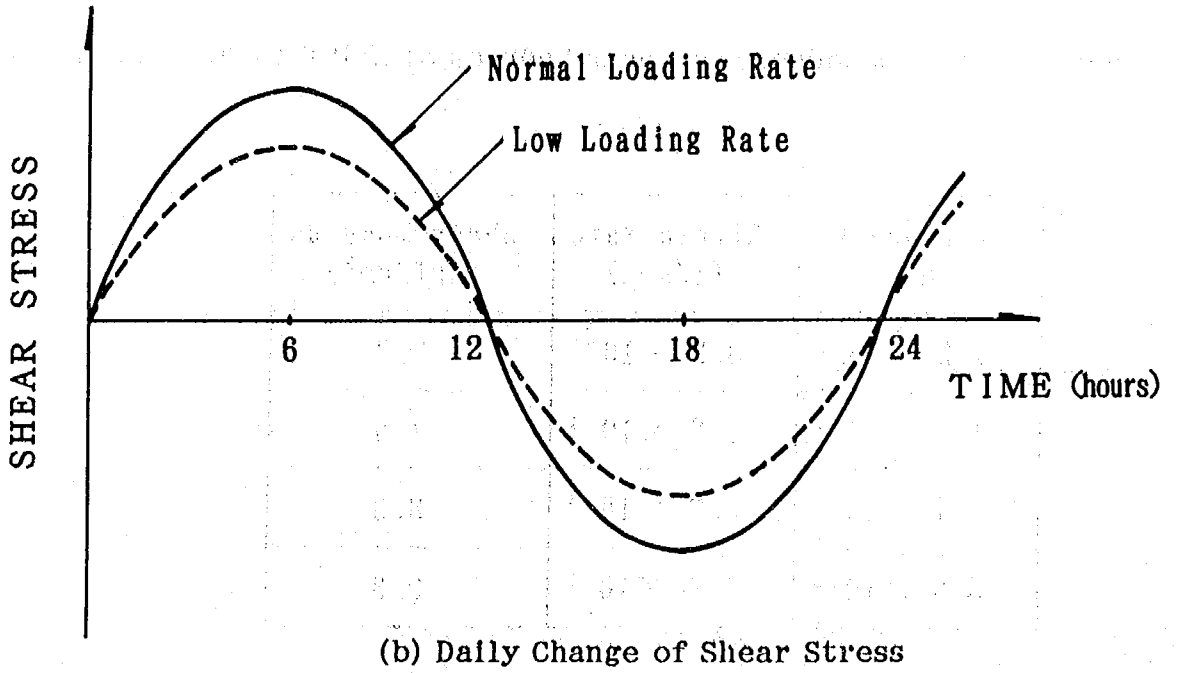
Frequency Hz	Strain Rate (1/sec)	Shear Modulus (kgf/cm^2) No.1 Facilities	No.2 Facilities
4.6×10^{-5}	2.0×10^{-4}	–	8.7
2.0×10^{-4}	8.8×10^{-4}	9.0	9.2
2.0×10^{-3}	8.8×10^{-3}	9.8	10.1
2.0×10^{-2}	8.8×10^{-2}	10.7	–
1.0	4.4	13.1	–

Table 5 Shear Strain Dependence of Shear Modulus of HDR-B by Extrapolation Method

Frequency Hz	Strain Rate (1/sec)	Shear Modulus (kgf/cm^2)
1.2×10^{-5}	3.3×10^{-5}	7.2
1.1×10^{-4}	3.2×10^{-4}	7.9
1.1×10^{-3}	3.2×10^{-3}	8.8
5.0×10^{-3}	1.4×10^{-2}	9.3

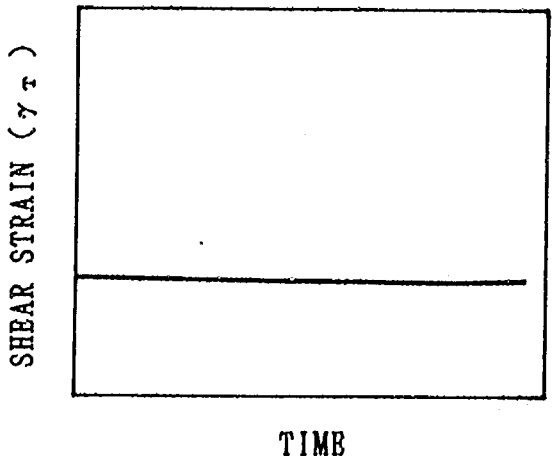


(a) Daily Change of Shear Strain

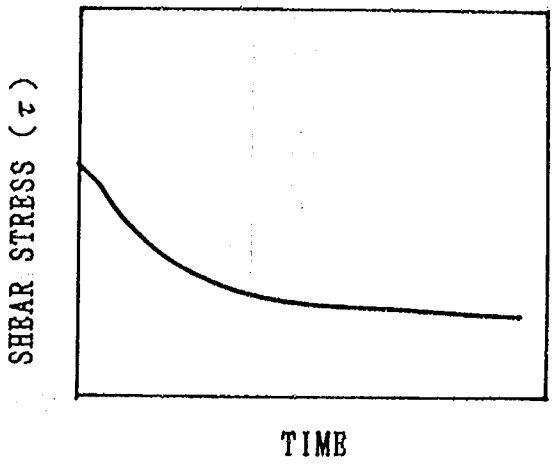


(b) Daily Change of Shear Stress

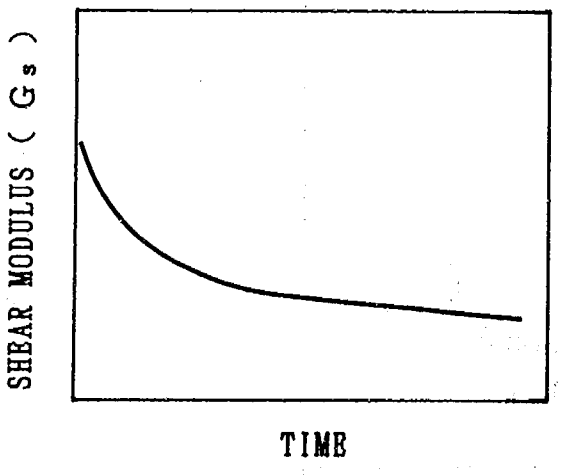
Fig. 1 Change of Shear Stress Shear Strain Induced in Menshin devices by Daily Change of Temperature



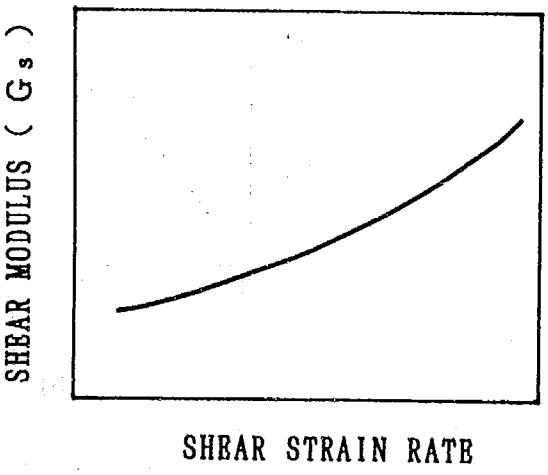
(a) Constant Strain Applied to Specimen



(b) Relaxation of Stress

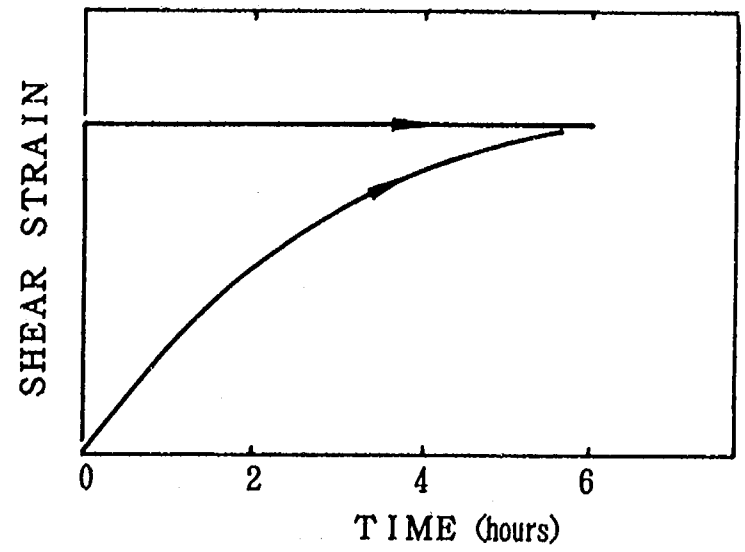


(c) Relaxation of Shear Modulus

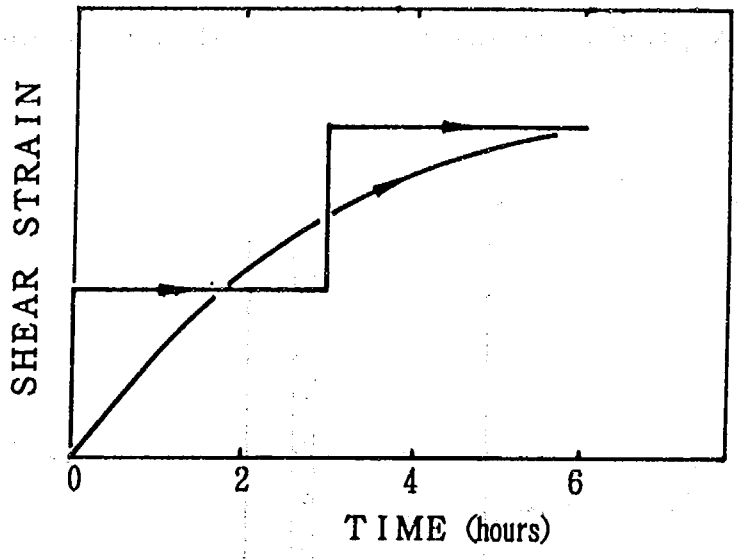


(d) Shear Modulus vs. Shear Strain Rate

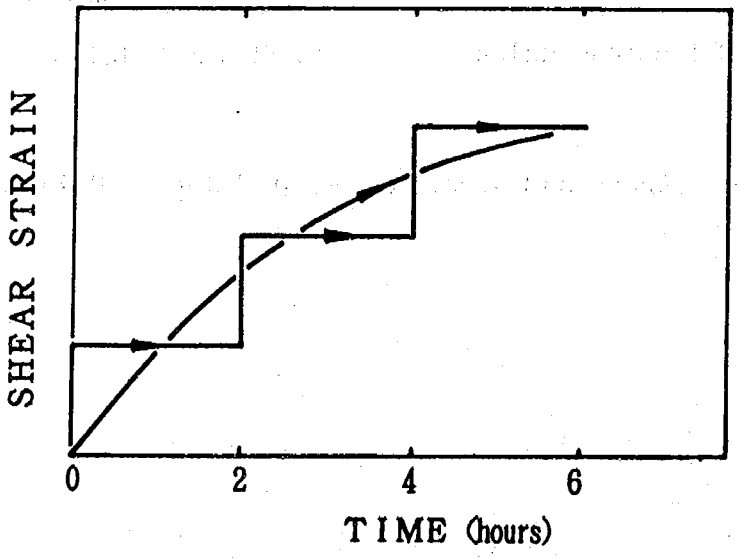
Fig. 2 Stress and Strain developed due to Relaxation



(a) 1 Step Loading

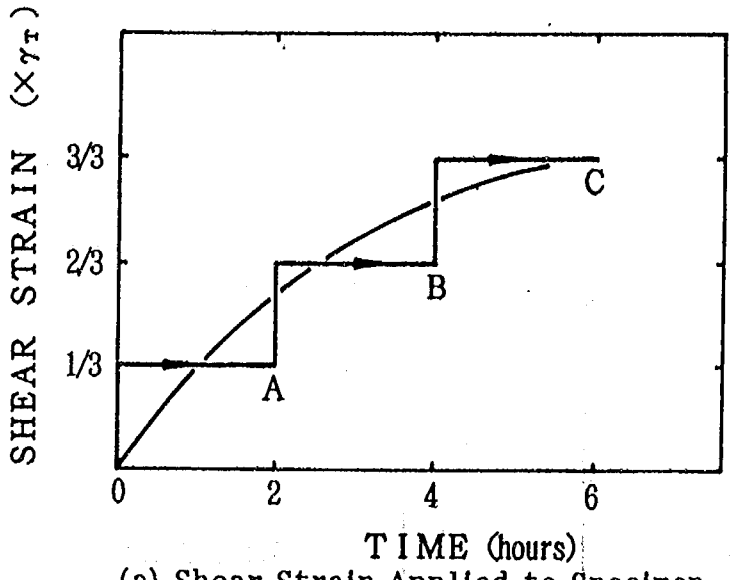


(b) 2 Step Loading

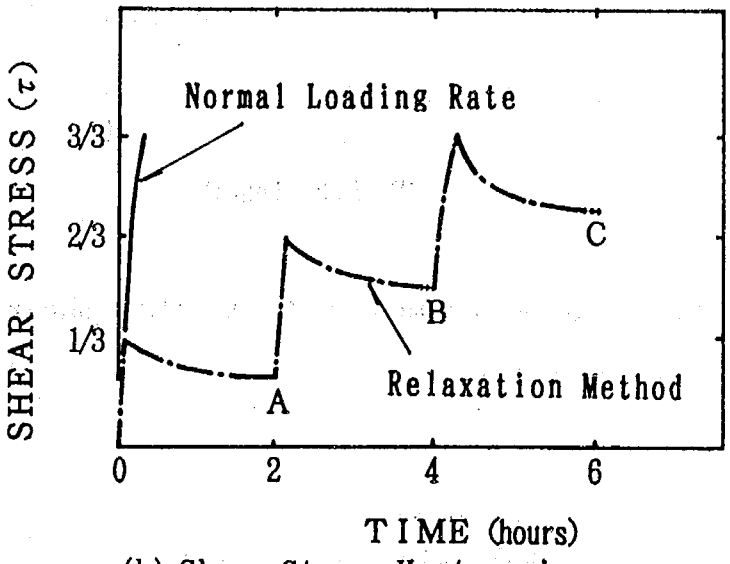


(c) 3 Step Loading

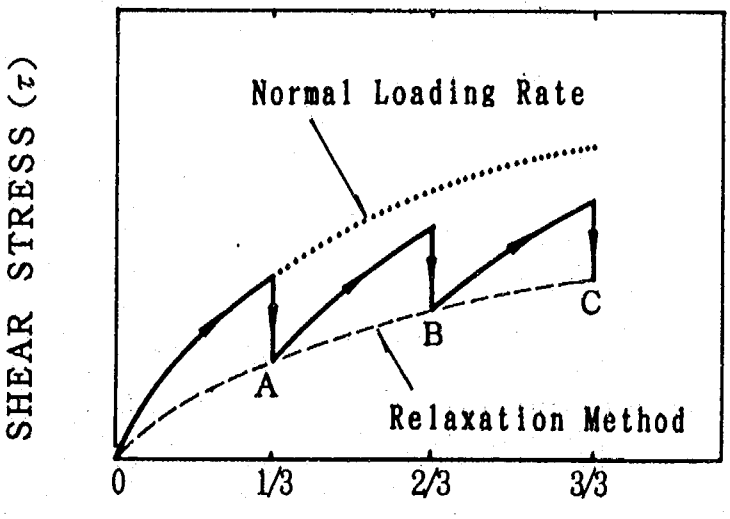
Fig. 3 Approximation by Stepwise Loading in Relaxation Method



(a) Shear Strain Applied to Specimen



(b) Shear Stress Hysteresis



(c) Shear Stress vs. Shear Strain Rate Relation

Fig. 4 Relaxation of Shear Stress vs. Shear Strain Rate in Relaxation Method for 3 Step Loading

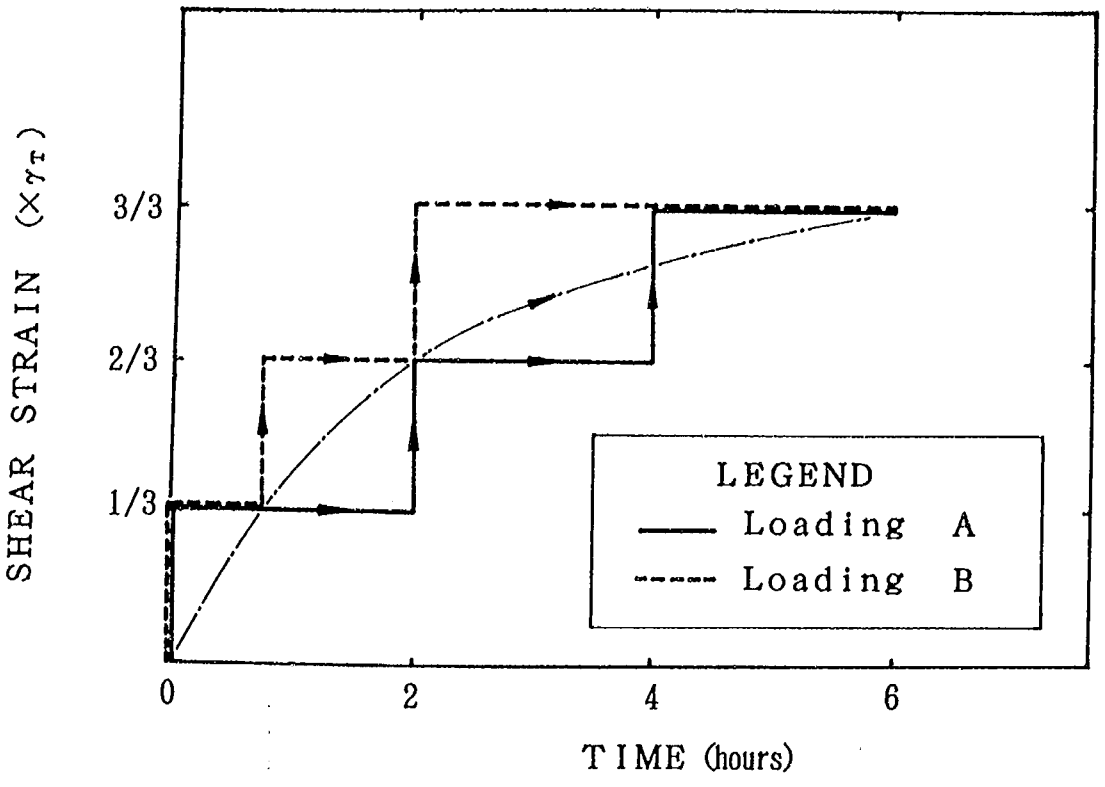
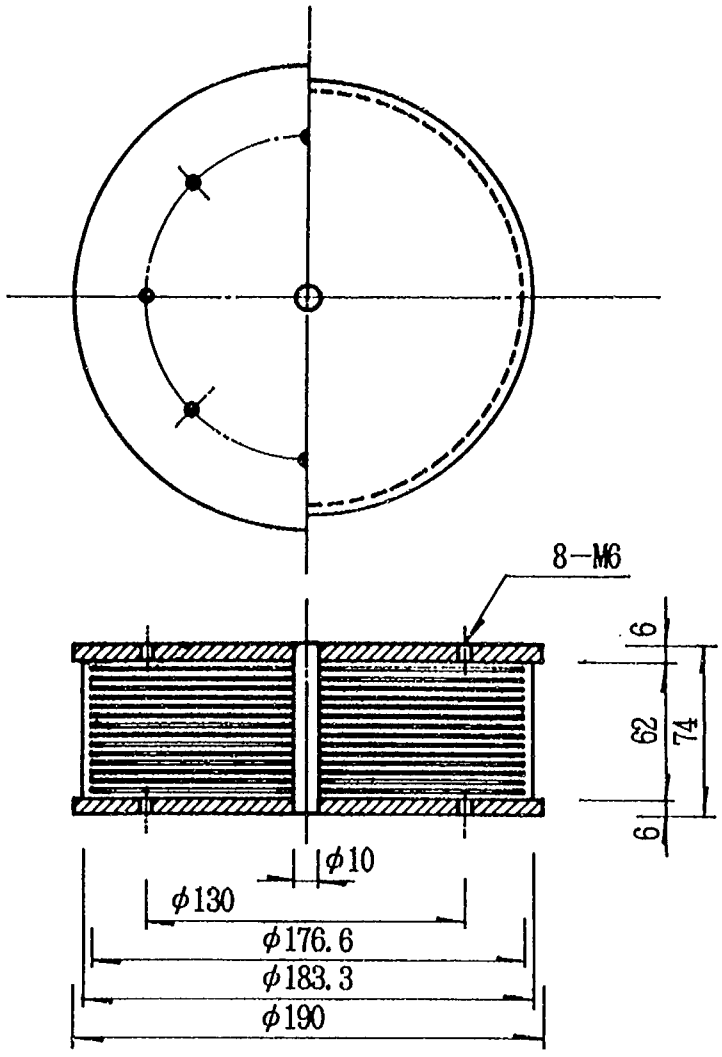


Fig. 5 Two Loading Schemes for Controlling Shear Strain



Rubber Layer 3.17mm×15=47.5mm

Steel Plate 1.0 mm×14=14.0mm

Fig. 6 Test Specimen of HDR-A

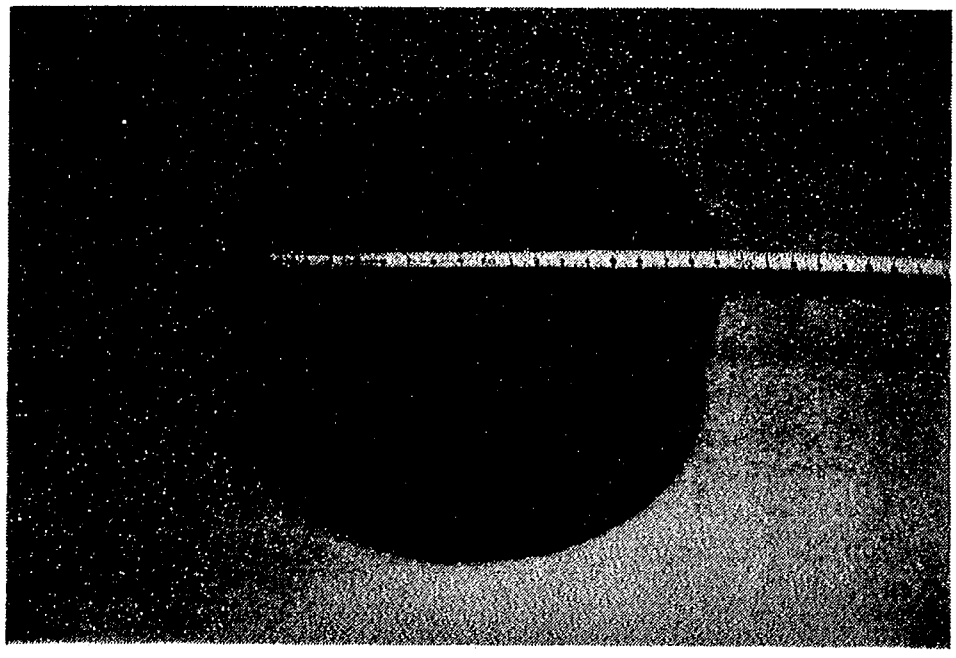
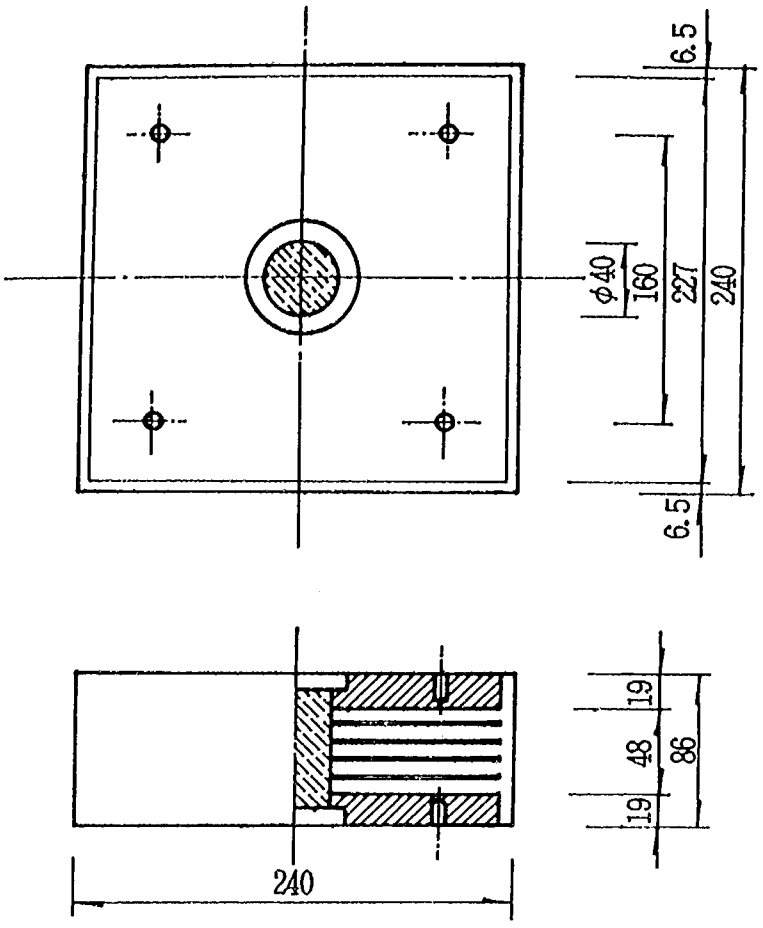


Photo 1 Test Specimen of HDR-A



Rubber Layer 8.0mm × 5=40.0mm
Steel Plate 2.0mm × 4= 8.0mm
Fig. 7 Test Specimen of LRB

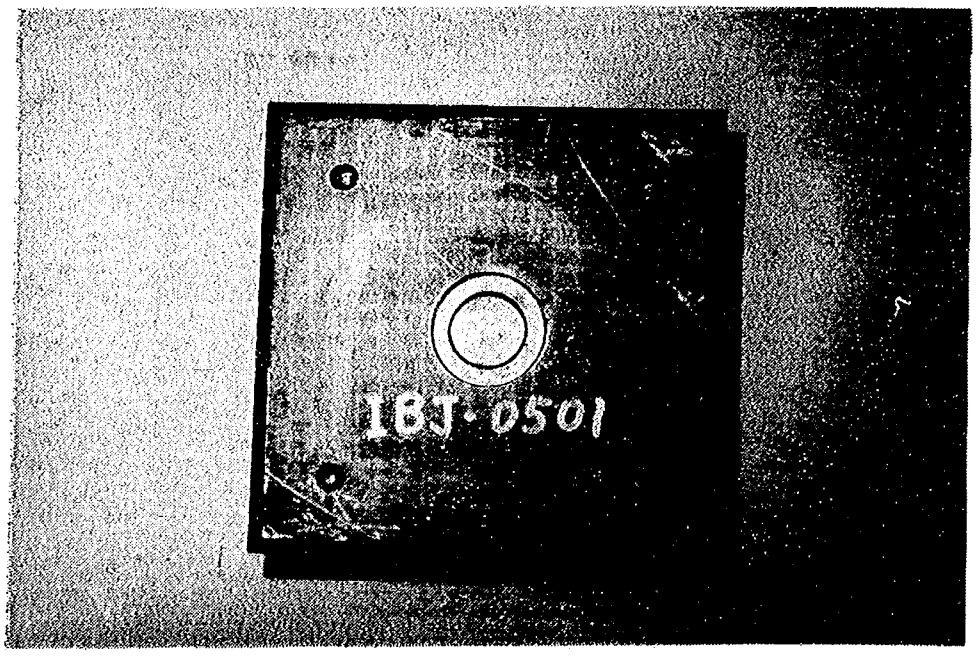
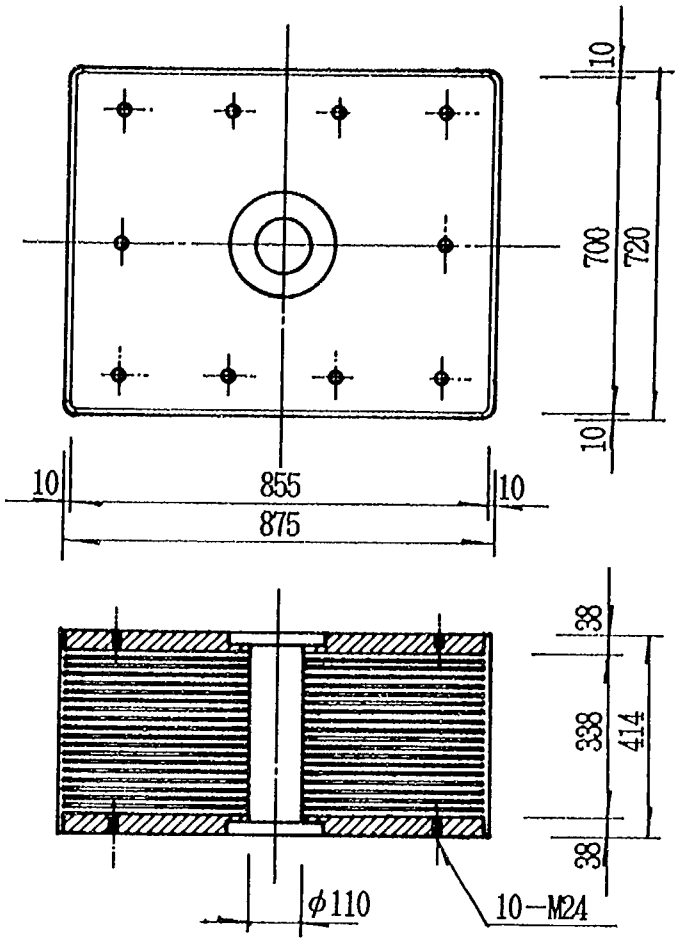


Photo 2 Test Specimen of LRB



Rubber Layer 13.8mm ×19=262.2mm

Steel Plate 4.2mm ×18= 75.6mm

Fig. 8 Test Specimen of HDR-B

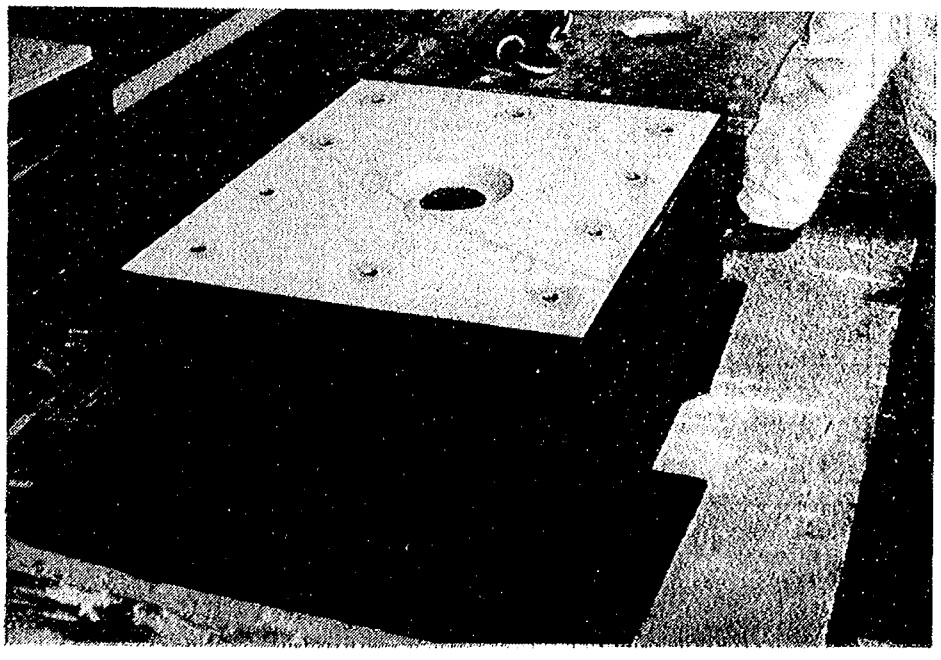


Photo 3 Test Specimen of HDR-B

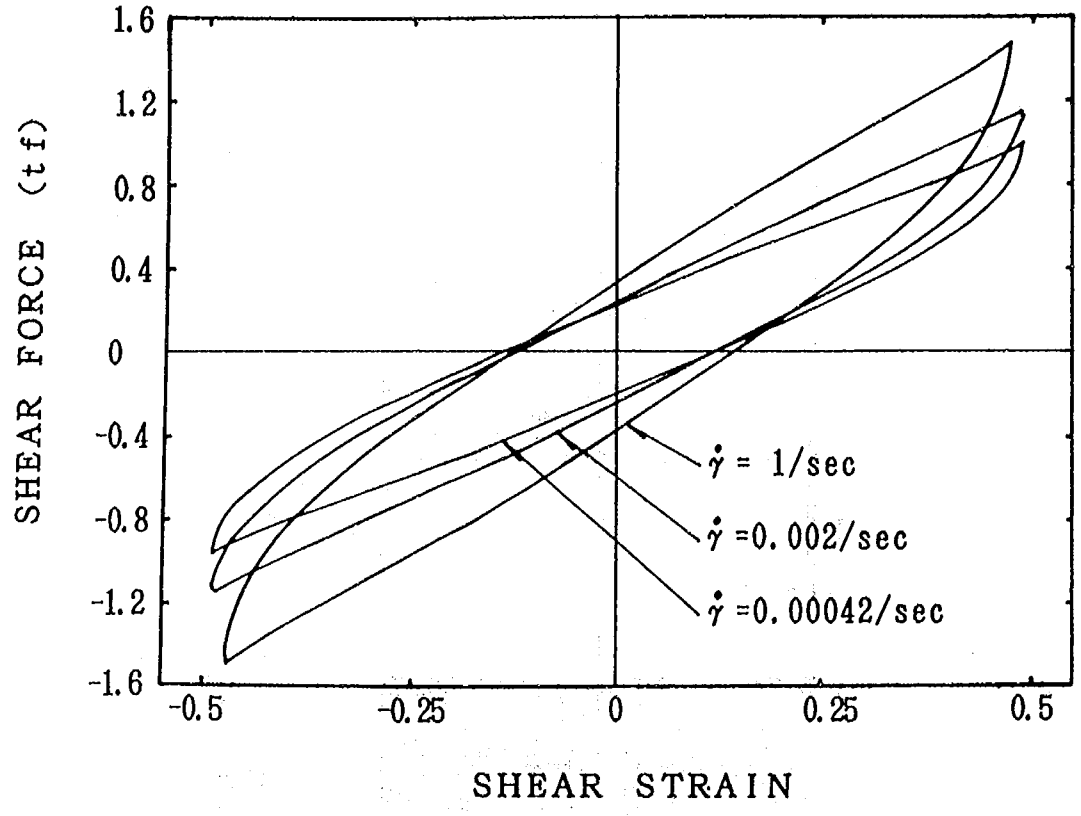


Fig. 9 Hysteresis Loops of HDR-A Subjected to a Harmonic Excitation with Displacement Amplitude of 50% Shear Strain of Rubber

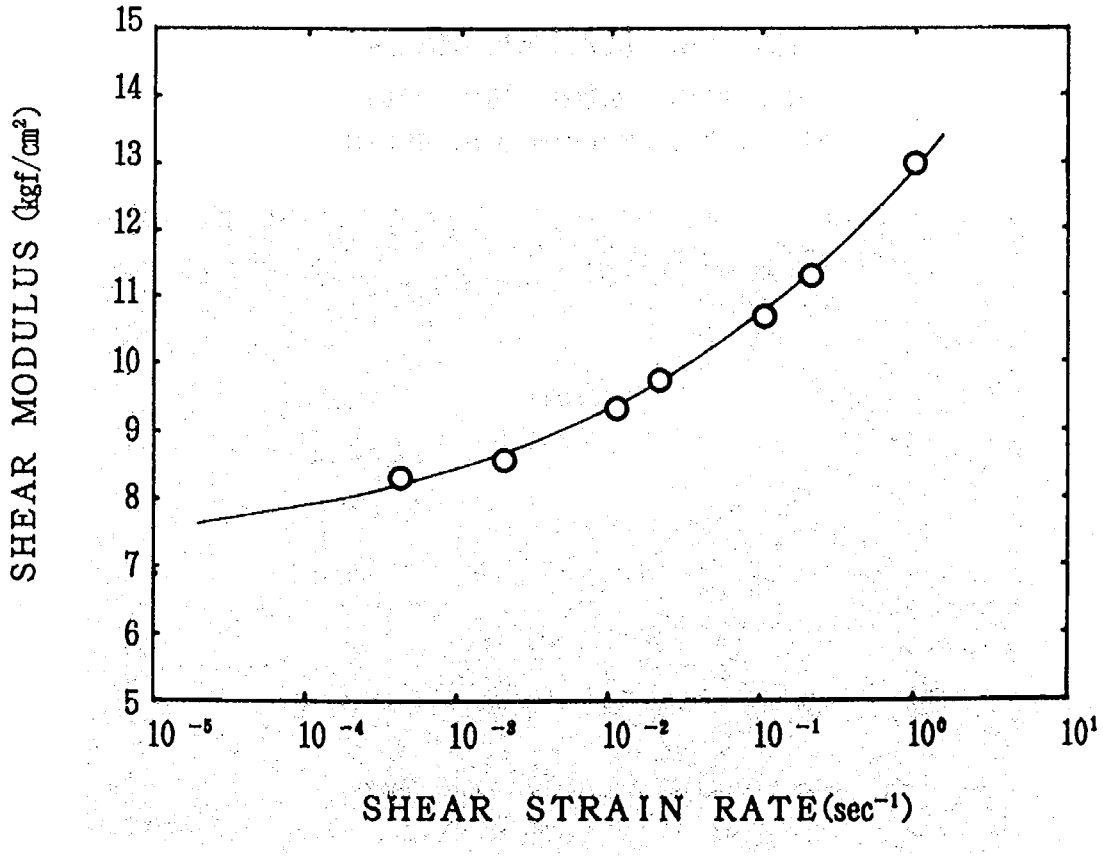
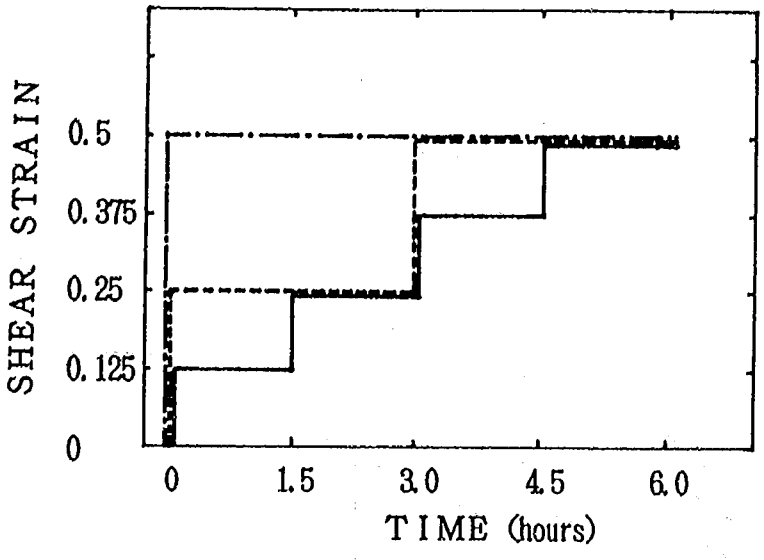
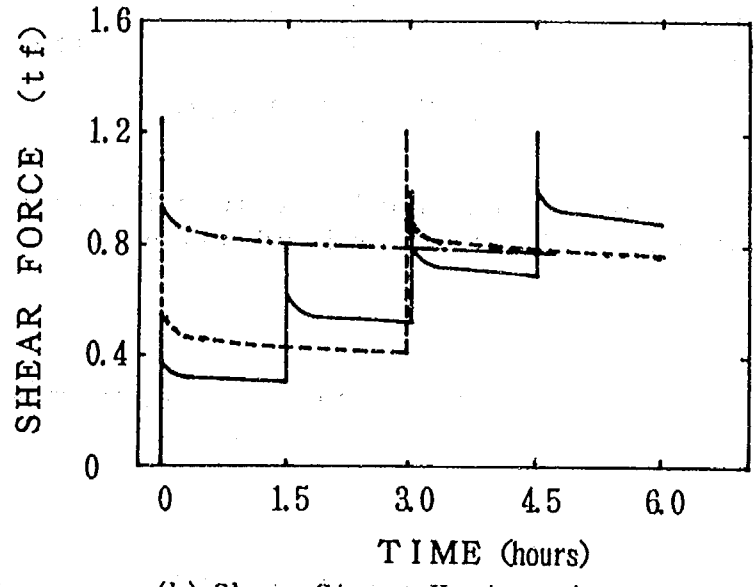


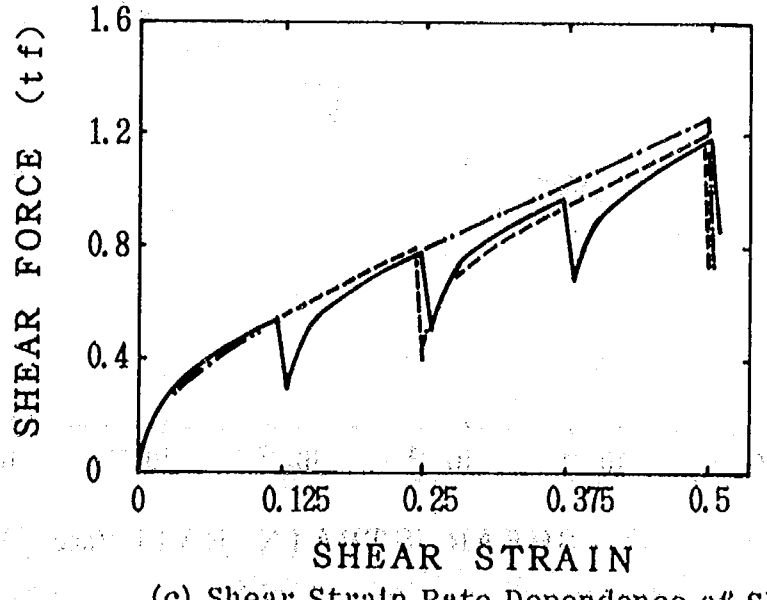
Fig. 10 Shear Strain Dependence of Shear Modulus of HDR-A Evaluated by Extrapolation Method



(a) Shear Strain Applied to Specimen



(b) Shear Stress Hysteresis



(c) Shear Strain Rate Dependence of Shear Strain

Fig. 11 Relaxation Method for HDR-A

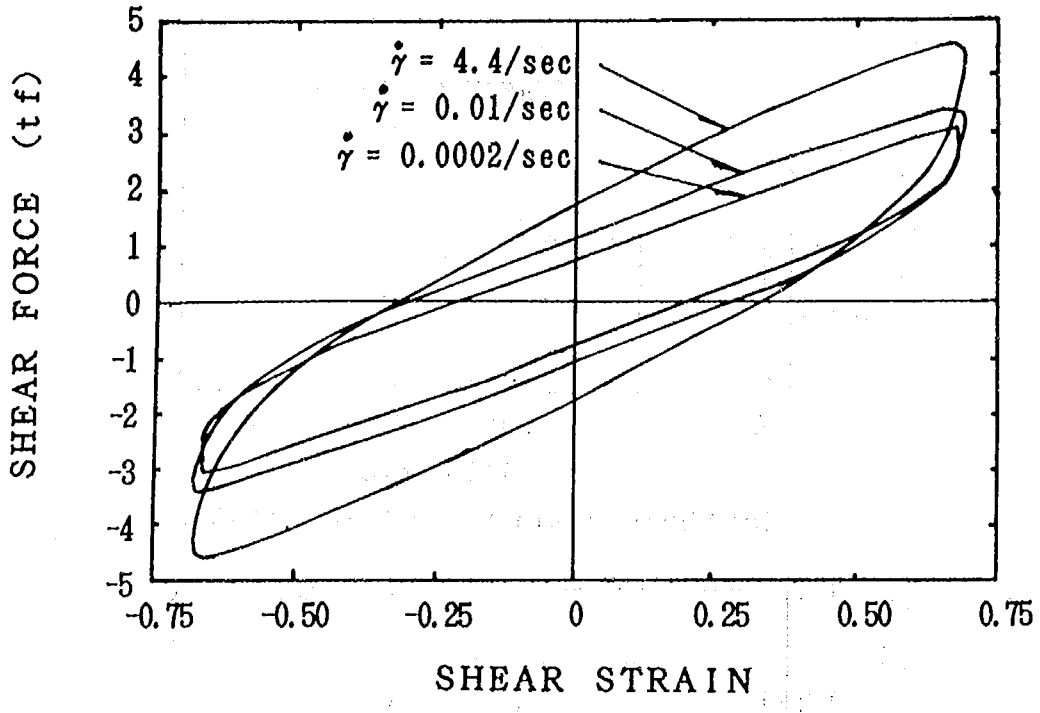


Fig. 12 Hysteresis Loops of LRB Subjected to a Harmonic Excitation with Displacement Amplitude of 50% Shear Strain of Rubber

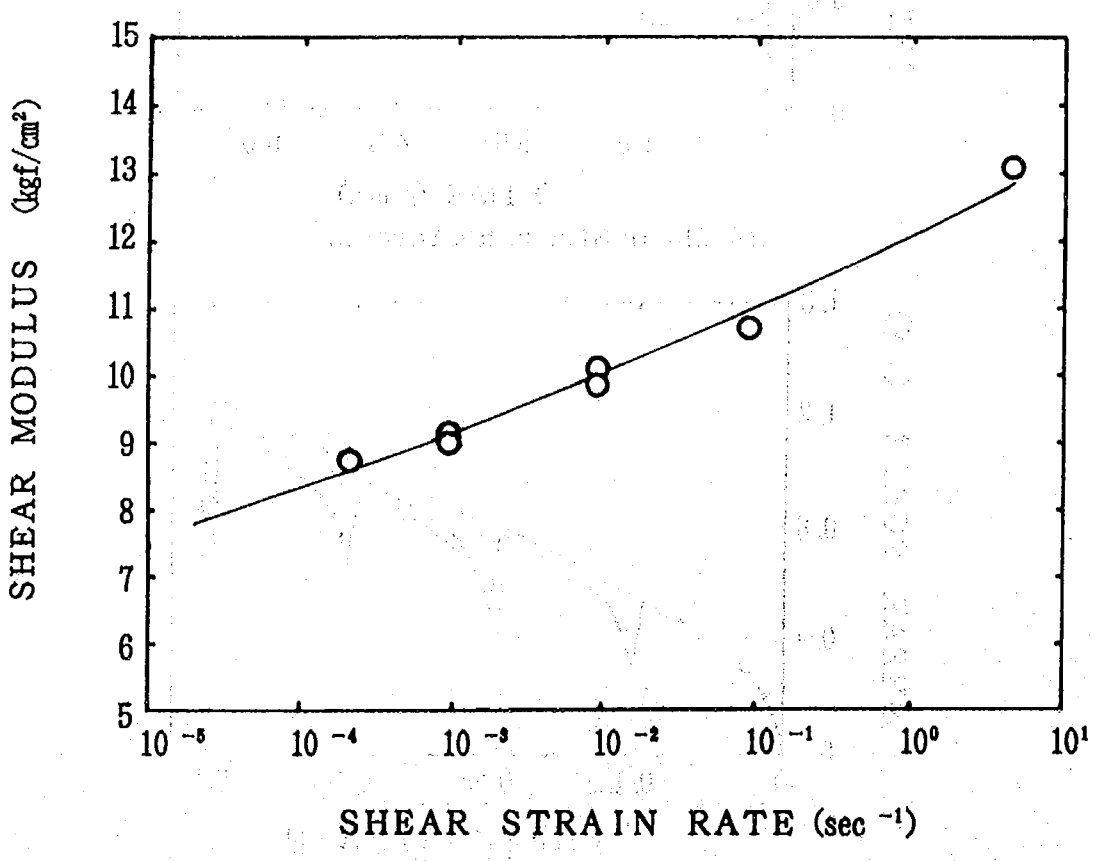
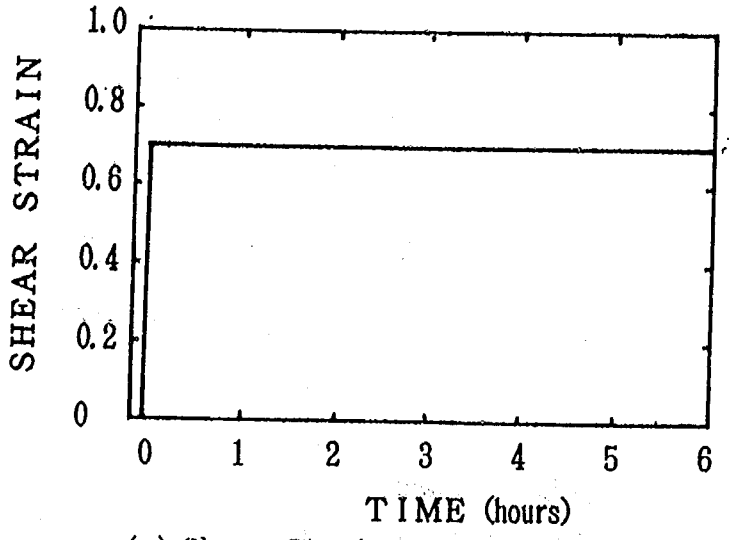
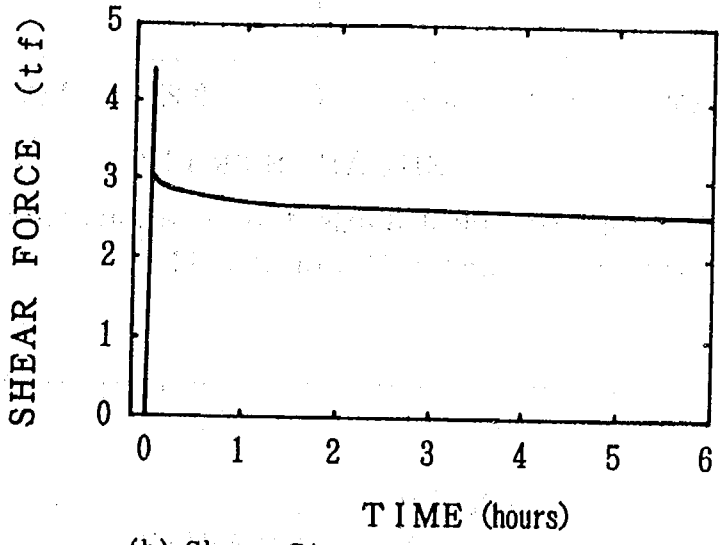


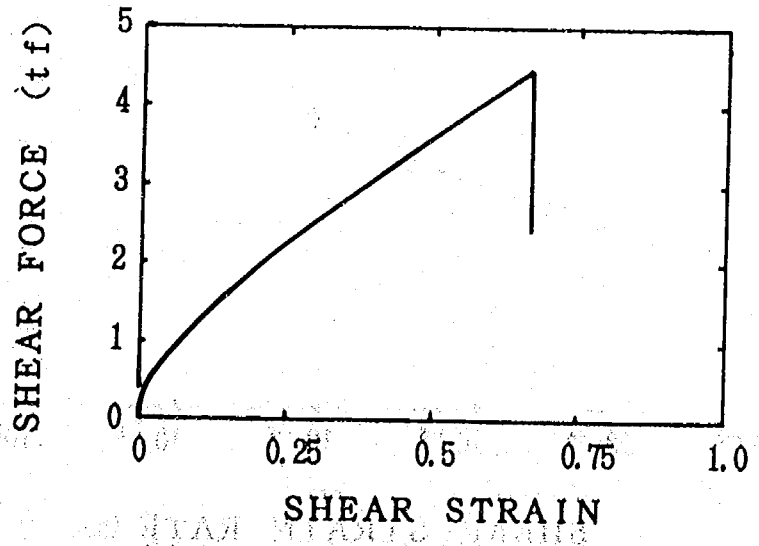
Fig. 13 Shear Strain Dependence of Shear Modulus of LRB Evaluated by Extrapolation Method



(a) Shear Strain Applied to Specimen



(b) Shear Stress Hysteresis



(c) Shear Strain Rate Dependence of Shear Strain

Fig. 14 Relaxation Method for LRB

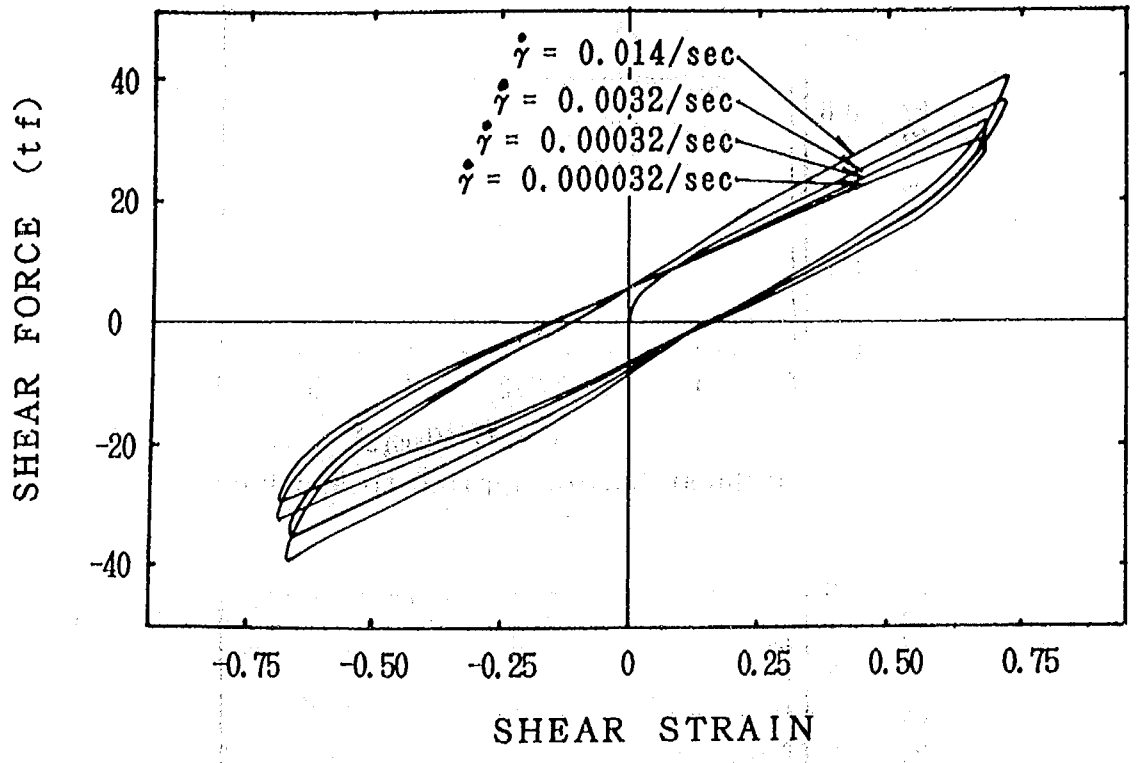


Fig. 15 Hysteresis Loops of HDR-B Subjected to a Harmonic Excitation with Displacement Amplitude of 50% Shear Strain of Rubber

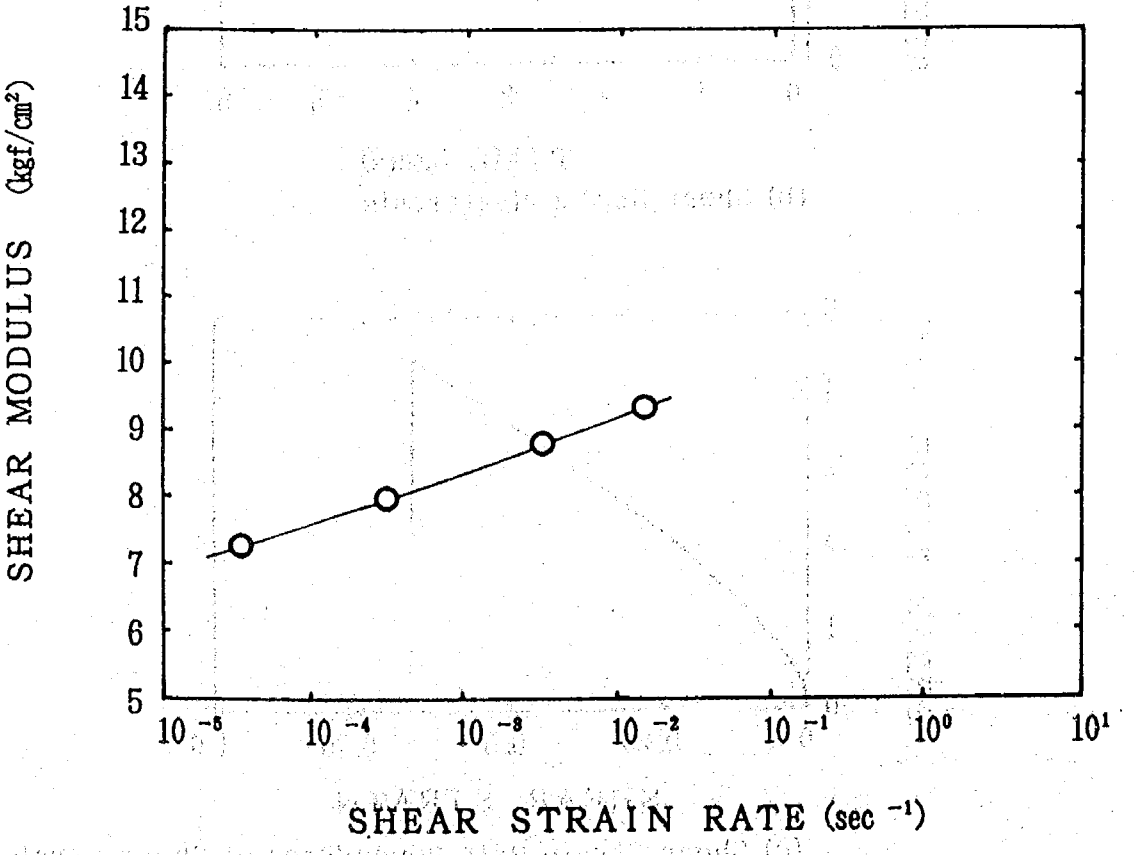


Fig. 16 Shear Strain Dependence of Shear Modulus of HDR-B Evaluated by Extrapolation Method

LOADING FACILITIES FOR MENSHIN DEVICES

Yutaka MAKIGUCHI[1], Kazuo ENDO[2], Norio KAWAI[3], Yoji SUIZU[4] and Ichiro NISHIKAWA[5]
1) Oiles Corporation
2) The Yokohama Rubber Co., Ltd.
3) Toyo Tire & Rubber Co., Ltd.
4) Bridgestone Corporation
5) Showa Electric Wire & Cable Co., Ltd.

SUMMARY

This paper presents loading facilities for Menshin devices, which are owned by five corporations involved in the Joint Research Program between the Public Works Research Institute and 28 private corporations on the "Development of Menshin systems of Highway Bridges."

INTRODUCTION

Various loading facilities are being used to study static and dynamic properties of Menshin devices. The purpose of the test is as

1) Bearing capacity for vertical loading
2) Lateral restoring force
3) Energy absorption and damping ratio
4) Stability of restoring and damping characteristics against load reversals
5) Failure mechanism and failure pattern

The important characteristics for representing the capability of the loading facilities include loading frequency and amplitude, loading rate, vertical loading, and temperature of the testing space. This paper briefly introduces the characters of major loading facilities owned by the five corporations (Oiles Corporation, The Yokohama Rubber Co., Ltd., Toyo Tire & Rubber Co. Ltd., Bridgestone Corporation, Showa Electric Wire & Cable Co., Ltd.) which were involved in the Joint Research Program between the Public Works Research Institute and 28 Corporations on the "Development of Menshin system of Highway Bridges."

TESTING MACHINES

Large Type Dual-Axis Load Testing Machine (Oiles Corporation)

The testing machine can be used for deformation test at the speed of 3.2 cm/sec for full-scale model. The machine can be also used to perform the shear fracture test for small-size model.

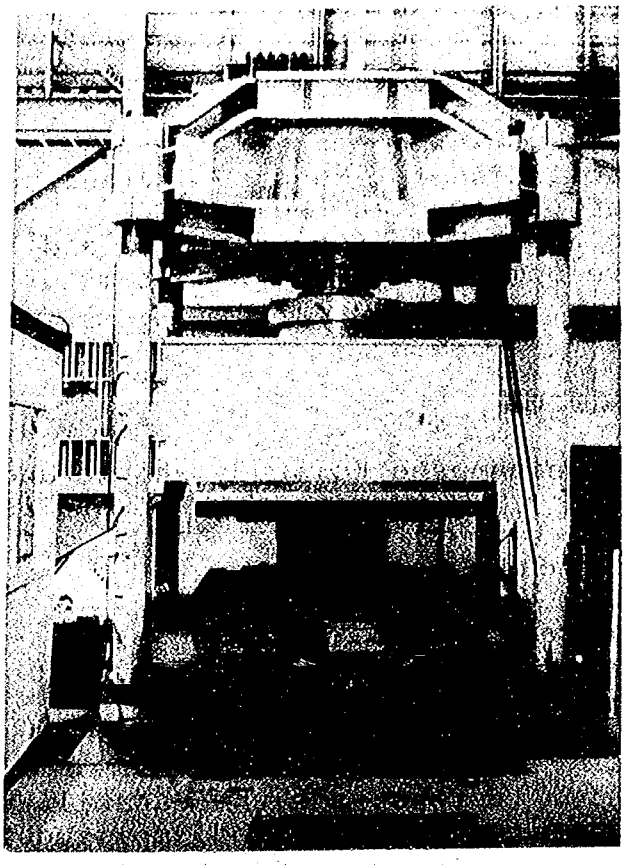


Photo 1 Overall View

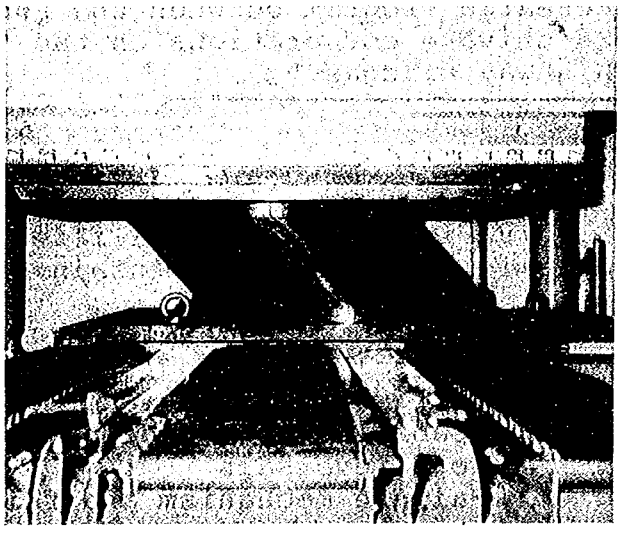


Photo 2 Testing View

Table-1 Characteristics of testing machine

Characteristics	Horizontal direction	Vertical direction
Maximum excitation force [tf]	±300	Compression: 1500 Tension : 0
Maximum displacement [mm]	±500	500 peak to peak
Maximum speed [mm/sec.]	±32.0	3.5 (1000 tf or less) 0.6 (1500 tf or less)
Dimension [mm] of device to mount	□2000 x (285 ~ 780)H	
Maximum dimension [mm] of specimen	□ 170 x 600H	

Medium Type Dual Axis Load Testing Machine (Oiles corporation)

The testing machine can be used for deformation test for reduced-scale model of medium-size at the speed 40 cm/sec.

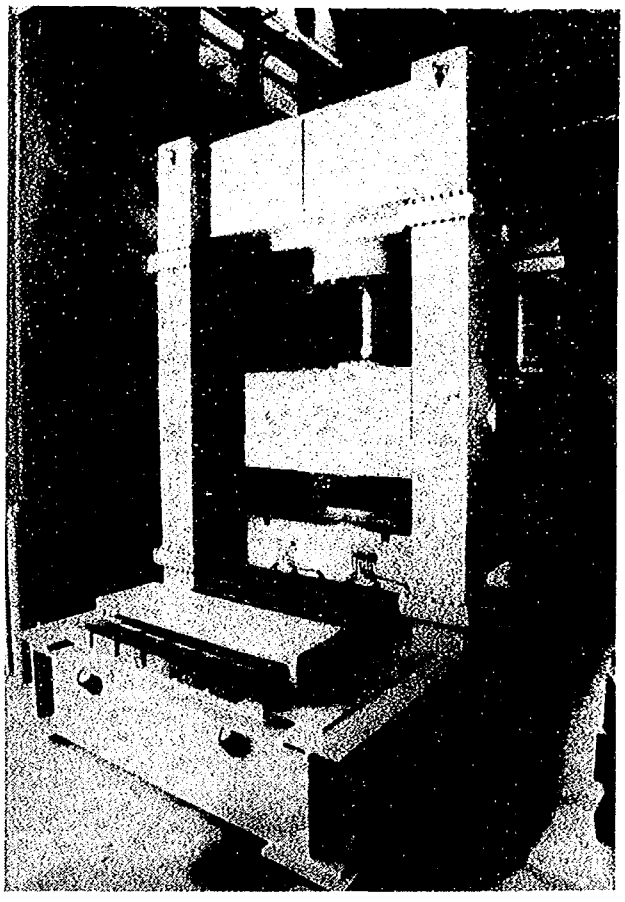


Photo 3 Overall View

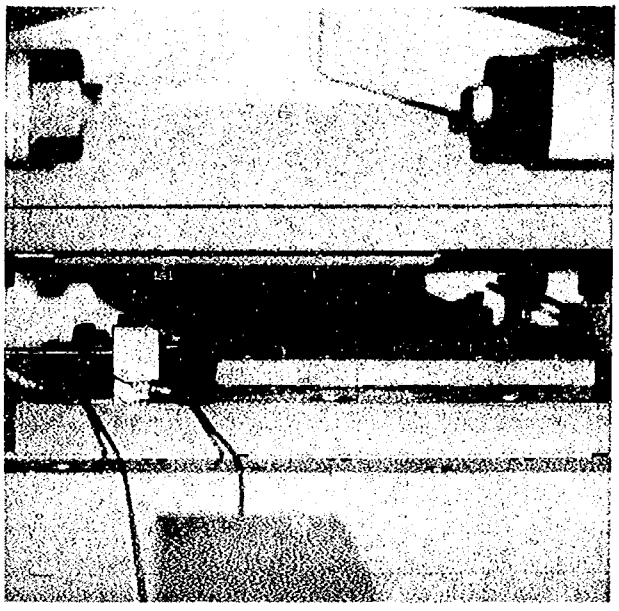


Photo 4 Testing View

Table-2 Characteristics of testing machine

Characteristics	Horizontal direction	Vertical direction
Maximum excitation force [tf]	±30	Compression: 300 Tension : 100
Maximum displacement [mm]	±550	500 peak to peak
Maximum speed [mm/sec.]	±400.0	15.0
Dimension [mm] of device to mount	□1250 x (450 ~ 950)H	
Maximum dimension [mm] of specimen	□1000 x 800H	

Medium Type Dual Axis Load Testing Machine (The Yokohama Rubber Co., Ltd.)

The testing machine can be used for deformation test for full-scale model of medium-size under static loading condition.

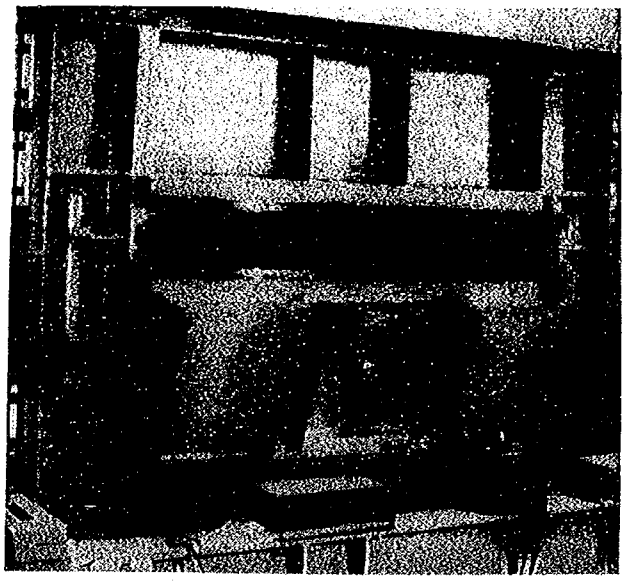


Photo 5 Overall View

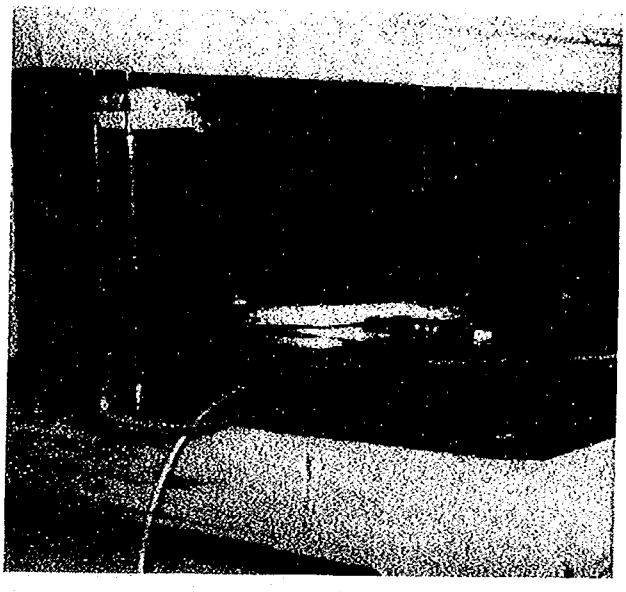


Photo 6 Testing View

Table-3 Characteristics of testing machine

Characteristics	Horizontal direction	Vertical direction
Maximum excitation force [tf]	±100	Compression: 500 Tension : 0
Maximum displacement [mm]	±300 (0~600)	400 peak to peak
Maximum speed [mm/sec.]	static	static
Dimension [mm] of device to mount	□1600 x 500H	
Maximum dimension [mm] of specimen	□1500 x 500H	

Small Type Dual-Axis Load Testing Machine (The Yokohama Rubber Co., Led.)

The testing machine can be used for deformation test for reduced-scale model of small-size at the loading speed of 33 cm/sec.

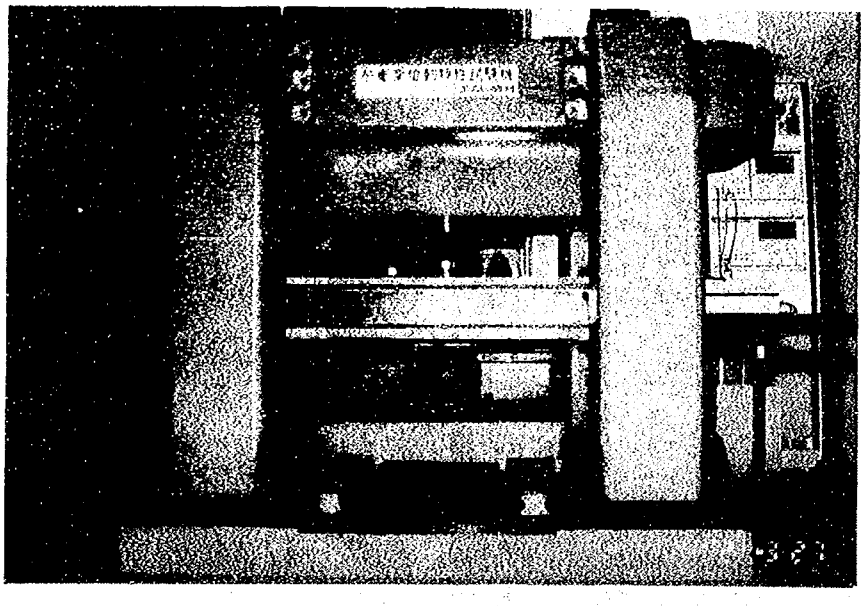


Photo 7 Overall View & Testing View

Table-4 Characteristics of testing machine

Characteristics	Horizontal direction	Vertical direction
Maximum excitation force [tf]	±10	Compression: 30 Tension : 10
Maximum displacement [mm]	±100	60 peak to peak
Maximum speed [mm/sec.]	330	35
Dimension [mm] of device to mount	□ 800 x 600H	
Maximum dimension [mm] of specimen	□ 700 x 600H	

Large Type Dual-Axis Load Testing Machine (Toyo Tire & Rubber Co., Ltd.)

This is the newest type of testing machine with a very large capacity in both vertical and horizontal directions.
It is installed in a very spacious work space which allows efficient setting of large specimens.

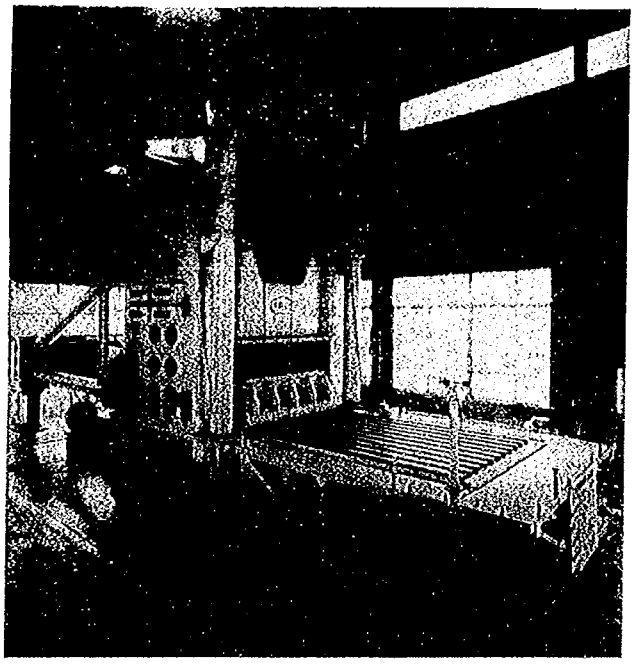


Photo 8 Overall View

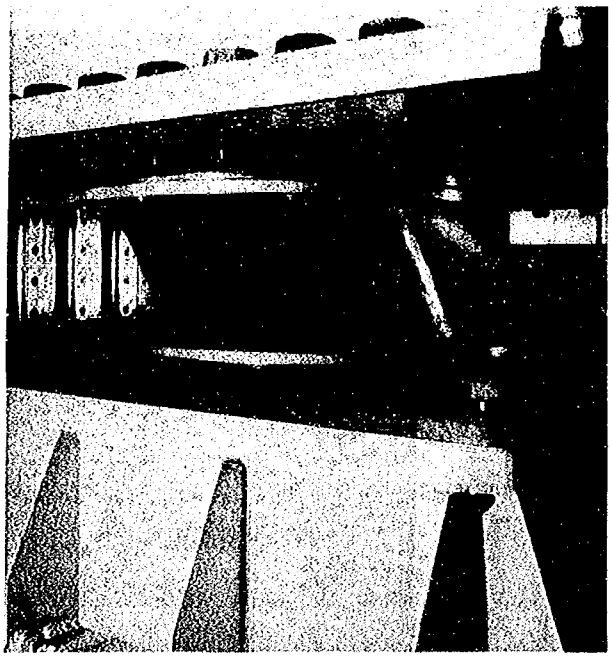


Photo 9 Testing View

Table-5 Characteristics of testing machine

Characteristics	Horizontal direction	Vertical direction
Maximum excitation force [tf]	±400	Compression: 2000 Tension : 200
Maximum displacement [mm]	±500 (0~1000)	500 peak to peak
Maximum speed [mm/sec.]	±3.7	2.5 (299 tf or less) 0.4 (2000 tf or less)
Dimension [mm] of device to mount	□ 2000 x (200~700)H	
Maximum dimension [mm] of specimen	□ 1700 x 600H	

Small Type Dual-Axis Load Testing Machine (Toyo Tire & Rubber Co., Ltd.)

The testing machine makes it possible to perform the deformation test for the reduced-scale model of small-size at higher speed.

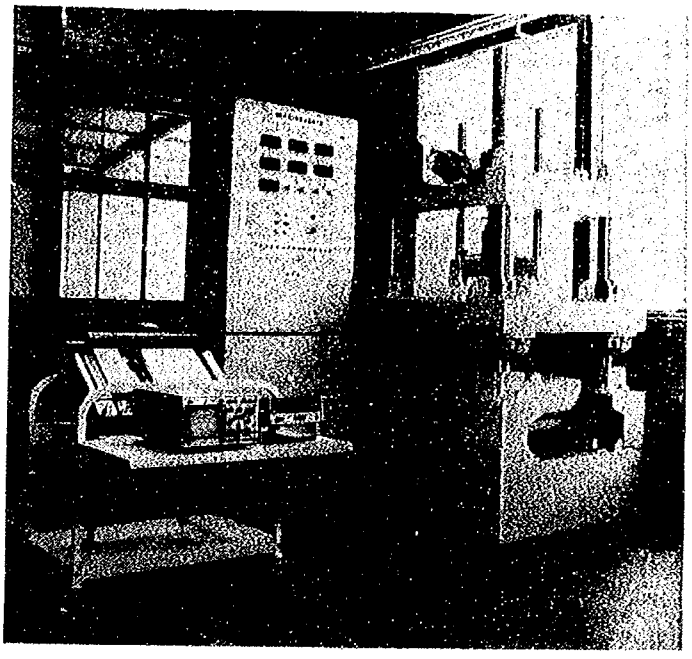


Photo 10 Overall View

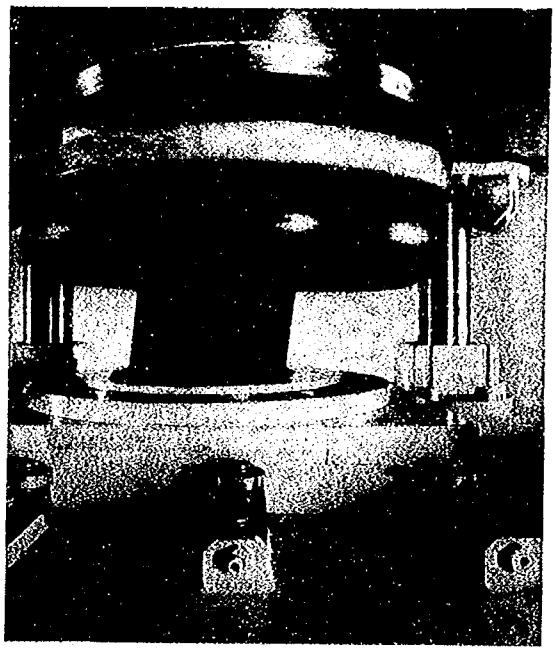


Photo 11 Testing View

Table-6 Characteristics of testing machine

Characteristics	Horizontal direction	Vertical direction
Maximum excitation force [tf]	±5	Compression: 20 Tension : 5
Maximum displacement [mm]	±200	250 peak to peak
Maximum speed [mm/sec.]	80	75
Dimension [mm] of device to mount	ø 600 x 400H	
Maximum dimension [mm] of specimen	ø 500 x 350H	

Large Type Dual-Axis Load Testing Machine (Bridgestone Corporation)

The testing machine is provided with world greatest scale load capacity both to horizontal direction and vertical direction. The static measurement is executable to range from small-size model having vertical reaction force of 50 tonf upto large-size model having that of 2,000 tonf.

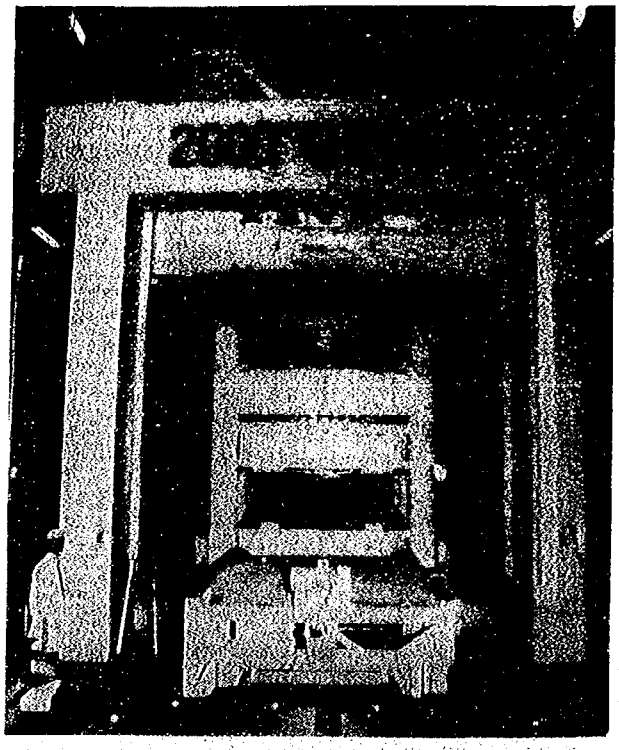


Photo 12 Overall View

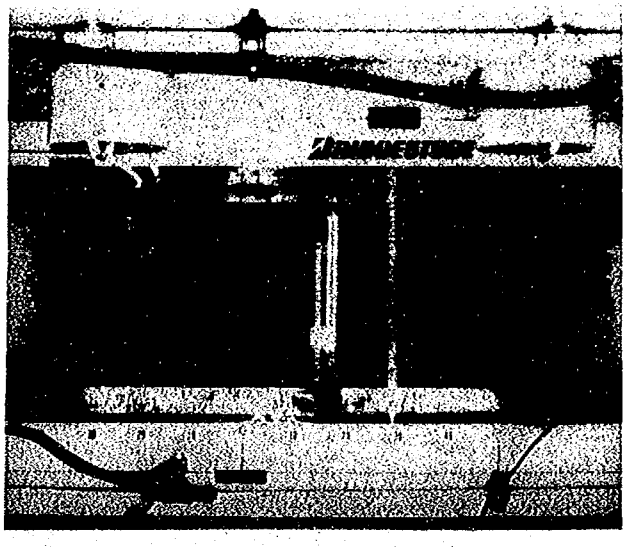


Photo 13 Testing View

Table-7 Characteristics of testing machine

Characteristics	Horizontal direction	Vertical direction
Maximum excitation force [tf]	±500	Compression: 2000
Maximum displacement [mm]	±500	-
Maximum speed [mm/sec.]	5.0	-
Dimension [mm] of device to mount	□ 2500 x 900H	
Maximum dimension [mm] of specimen	□ 2000 x 800H	

Medium Type Compression-Shear Double Axis Testing Machine (Showa Electric Wire & Cable Co., Ltd.)

The testing machine makes it possible to perform the deformation test at the static speed by setting the vertical load and horizontal displacement optionally.

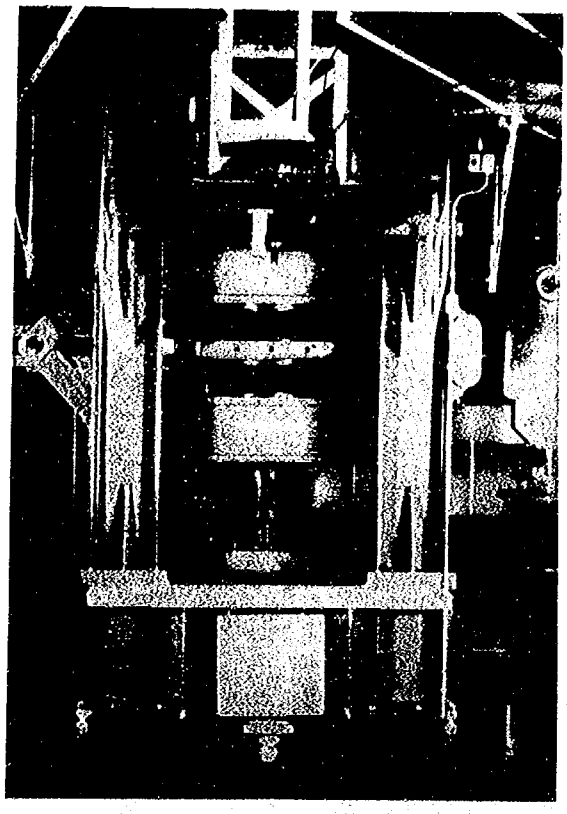


Photo 14 Overall View

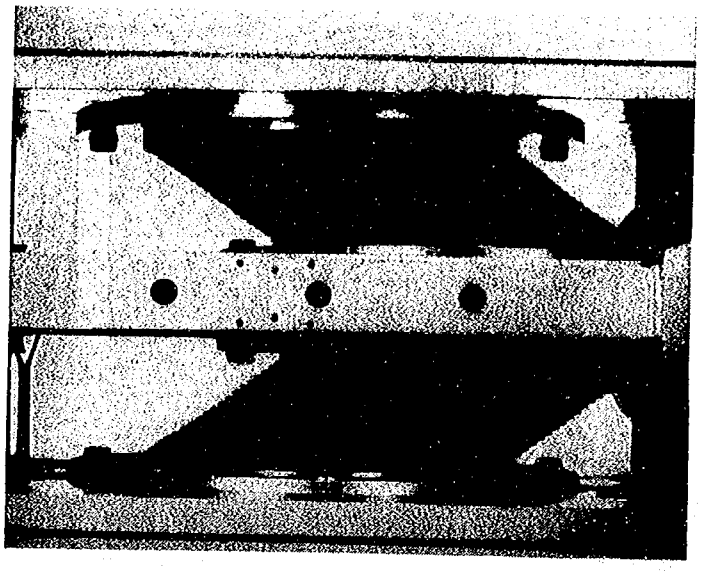


Photo 15 Testing View

Table-8 Characteristics of testing machine

Characteristics	Horizontal direction	Vertical direction
Maximum excitation force [tf]	PS(*): 300 PL(*): 400	Compression: 500 Tension : 0
Maximum displacement [mm]	±400	500 peak to peak
Maximum speed [mm/sec.]	PS(*): 1 PL(*): 2	High-pressure: 0.18 Low-pressure: 0.6
Dimension [mm] of device to mount	□ 1350 x 350H (2 stages)	
Maximum dimension [mm] of sample	ø 300 ~ ø 1000	

Note: PS: Push direction
PL: Pull direction

Small Type Dynamic Shear Loading Testing Machine (Showa Electric Wire & Cable Co., Ltd.)

The testing machine make it possible to perform the deformation test for reduced-scale model of small-size at the dynamic speed.

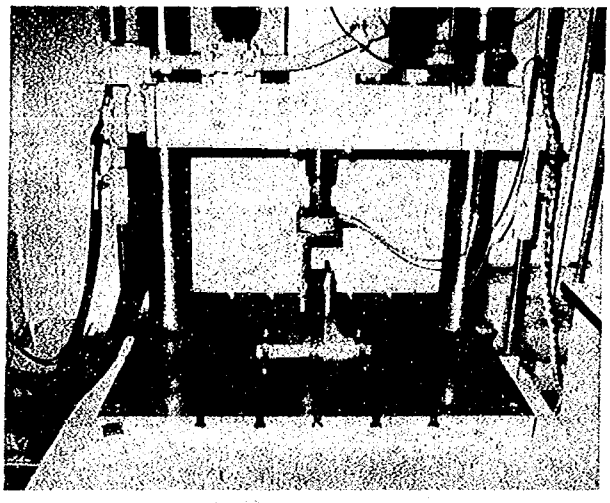


Photo 16 Overall View

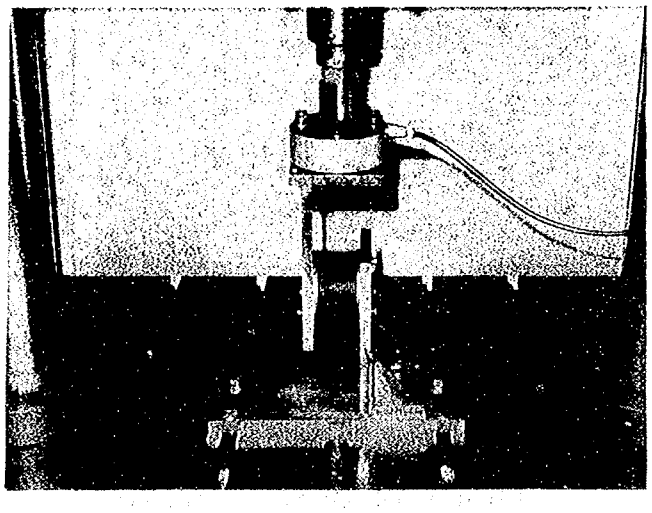


Photo 17 Testing View

Table-9 Characteristics of testing machine

Characteristics	Horizontal direction
Maximum excitation force [tf]	±5
Maximum displacement [mm]	±100
Maximum speed [mm/sec.]	200
Maximum dimension [mm] of sample	ø 200

Creep Testing Machine (Showa Electric Wire & cable Co., Ltd.)

The testing machine makes it possible to measure the vertical creep at the accuracy of 0.01mm. It is possible to make the evaluation at an optional temperature by putting the machine in constant temperature chamber.

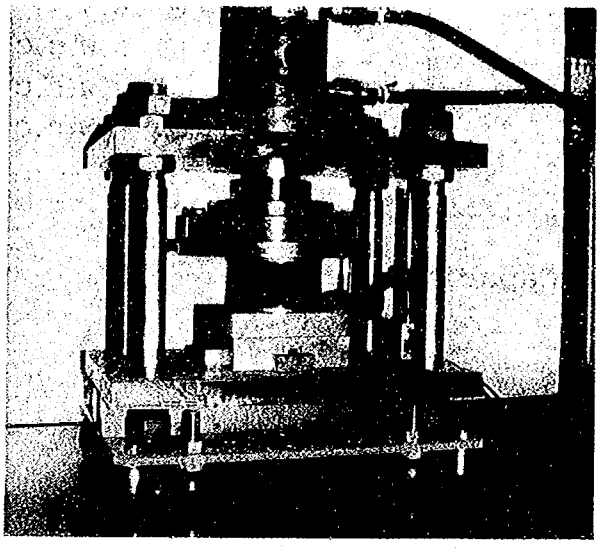


Photo 18 Overall View

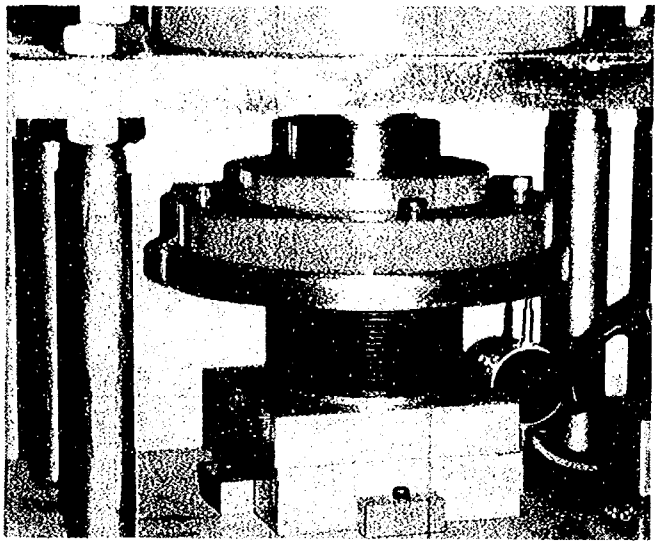
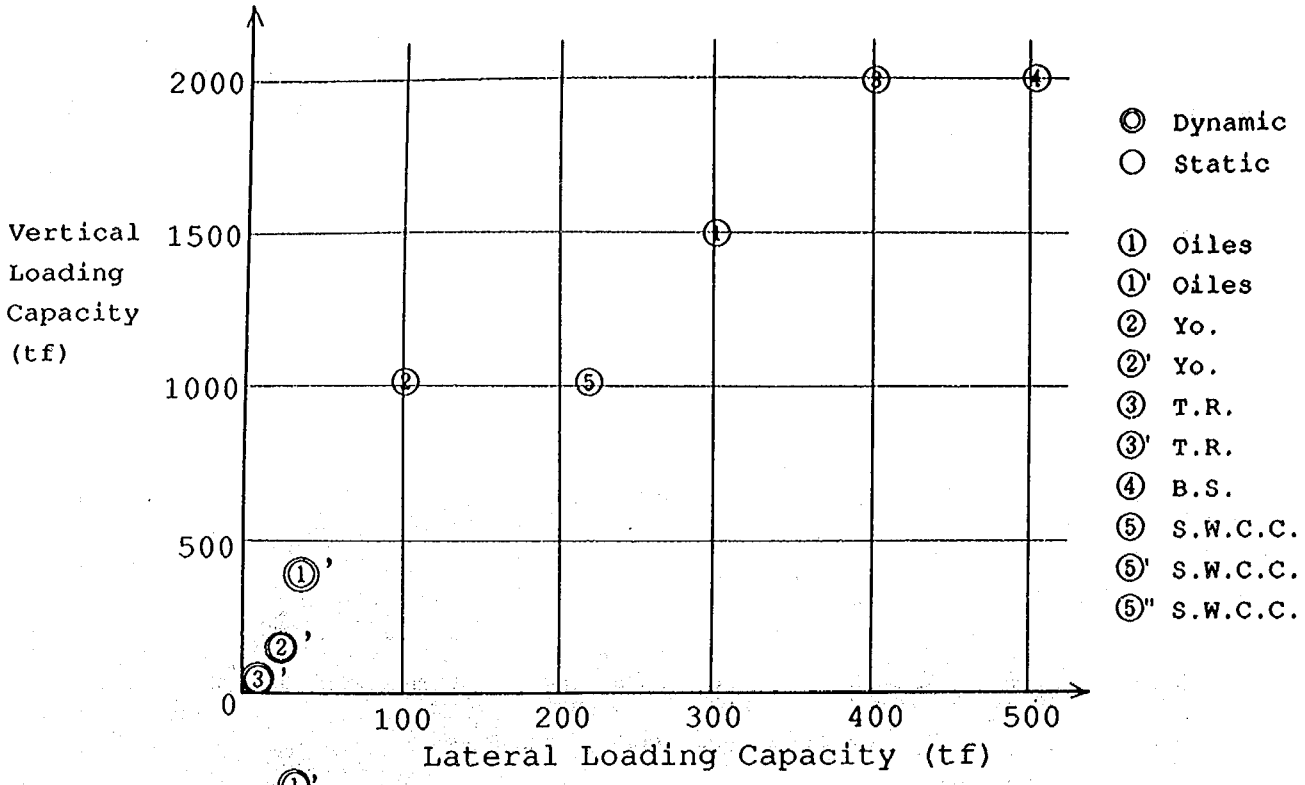
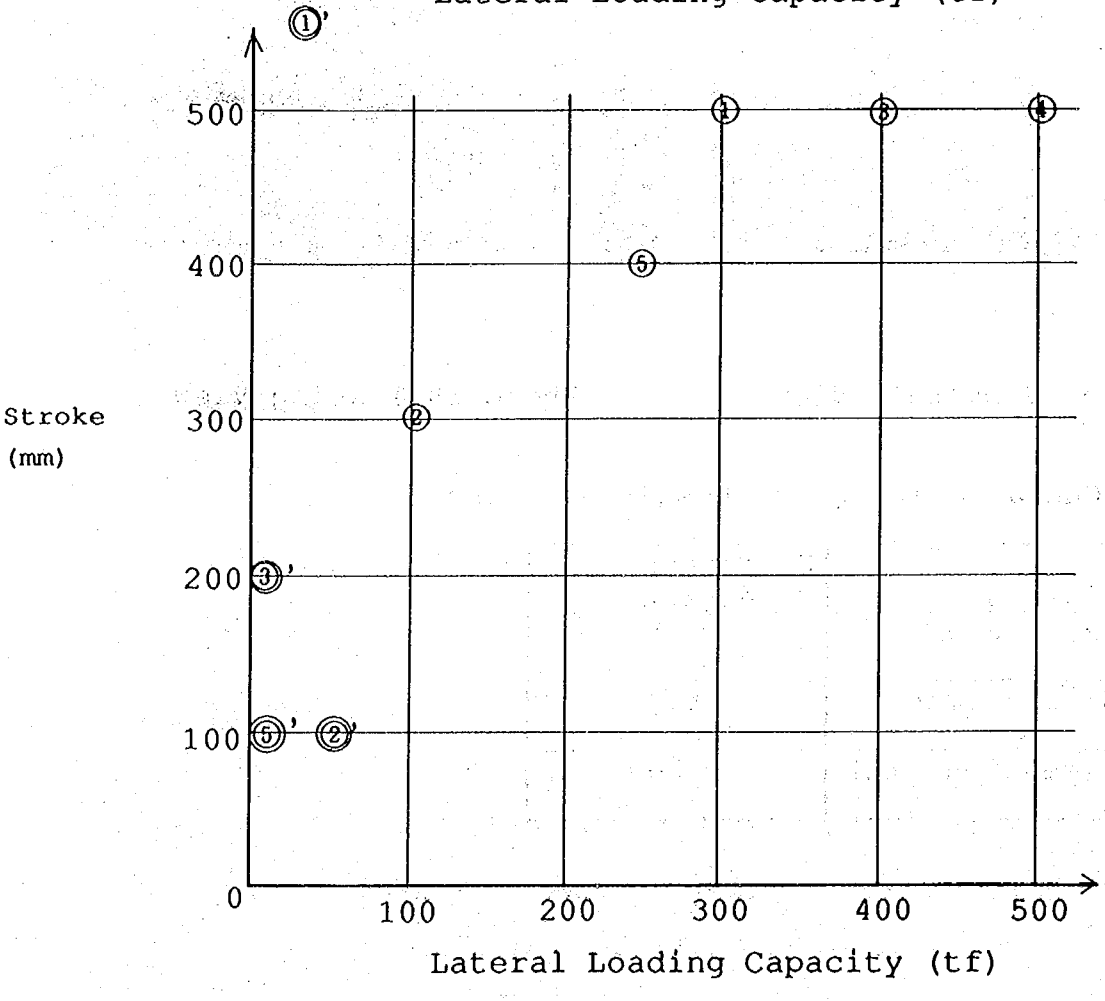


Photo 19 Testing View

Table-10 Characteristics of testing machine

Characteristics	Horizontal direction
Maximum excitation force [tf]	±15
Maximum displacement [mm]	±50
Maximum dimension [mm] of sample	ø 200


Vertical Loading Capacity (tf)
2000
1500
1000
500
0
100
200
300
400
500
Lateral Loading Capacity (tf)
◎ Dynamic
○ Static
① Oiles
①' Oiles
② Yo.
②' Yo.
③ T.R.
③' T.R.
④ B.S.
⑤ S.W.C.C.
⑤' S.W.C.C.
⑤" S.W.C.C.


Stroke (mm)
500
400
300
200
100
0
100
200
300
400
500
Lateral Loading Capacity (tf)

TEMPERATURE-DEPENDENCY OF BASE-ISOLATED BEARINGS

by

Osamu Nakano[1], Hiroaki Nishi[2], Tadayuki Shirono[2] and Katuhiro Kumagai[3]

ABSTRACT

It was revealed in the past study that the lead rubber bearings (called LRB hereinafter) and the high damping rubber bearings (called HDR hereinafter) possessed the strong temperature-dependency on their equivalent shear stiffness.

The following issues, however, still remain unsolved.

1 Elevation of temperature on the bearings during the 50-cycle shear test

2 Recrystallization of the lead plug

3 Thermo-traceability of the bearings

This paper describes the related tests on the LRB and the HDR, the properties of the bearings together with its behavior on various conditions and the results.

1. INTRODUCTION

Generally, the base-isolated bridge is so designed as to decrease the seismic force by elongating the natural period of the entire bridge with a special device called a base-isolated bearing, which provides the combined features of vertical load support, horizontal flexibility and energy absorbing capacity in a single unit.

The Onnetoh-Oohashi Bridge with the length of 456m is now under construction on National Trunk Road 44 in Nemuro by the Hokkaido Development Bureau, in which side-span on the Kushiro side was picked up as the above-mentioned structure.

As concern about the performance of base-isolated bearings in winter season was raised by a regional construction office, that meant the effectiveness might be changed in cryogenic environment, indoor experiments in terms of stiffness and damping factor of rubber material properties have been performed for the past three years, which include 50-cycle shear tests, shear tests and shear history tests etc. on on various temperatures.

Two types of full-scale models of the LRB (Photo.1) and the HDR (Photo.2) are used in the experiments. The models were designed and produced in accordance with the basic design[1)] of base-isolated bearings on the Onnetoh-Oohashi Bridge.

As the result[2)], it was proved that the base-isolated bearing itself had the strong dependency on temperature with regard to the stiffness, which was not expected before the tests.

---

1 Head, Structures Division, Civil Engineering Research Institute

2 Research Engineer, Structures Division, Civil Engineering Research Institute

3 Director, Road Construction Divison, Hokkaido Development Bureau

In this connection, additional experiments have been made in which focal points were placed on the elevation of temperature on the bearings during the 50-cycle shear test, recrystallization of the lead plug and thermo-traceability of the bearings.

2. OUTLINE OF THE EXPERIMENTS

2.1 Purpose of the experiments

In the application of base-isolated bearings in the cold region such as Hokkaido, the most critical factor is the influence upon the dynamic behavior at low temperature. Table 1 represents the mean temperature of some cities in Hokkaido in the past 30 years and the lowest temparature in the past.

The main subject of the experiments is to examine the effectiveness of the bearings under cryogenic environment.

Therefore, tests were made to watch the behavior carefully at low temperatures.

2.2 Tested specimens

A total of eight specimens were tested with four for each of the two models, with two specimens for each model having thermistors (T type) inserted in the center (Fig.1), to measure the temperature of a specimen at the beginning of each test, and the change of temperature during the tests.

The basic design conditions of the base-isolated bearings on the planned bridge were: maximum vertical reaction 135tons, dead-load reaction 92tons, design displacement u_B approx.15cm[3)] by the check of ultimate bearing capacity of reinforced concrete piers for lateral force (ground group II). The characteristic design conditions of the two kinds of specimens are shown in Table 2, and the test results of material properties of rubber in Table 3.

2.3 Testing equipment and procedures

The testing equipment consists of an actuator (maximum load 50tons, maximum amplitude $\pm$300mm) and a hydraulic servo-tester at the vertical-load (maximum load 150tons) (Photo.3), and the temperature of the specimens was controlled by surrounding the instrument with a huge refrigerator. For each specimens, tests were conducted for the items listed in Table 4. The procedures of each test are as follows.

2.3.1. Shear test

To determine the force-displacement hysteresis loops of each bearings, the experiments on 3-cycle shear test were performed under a vertical load of 92tons, which is equal to the dead-load reaction, in line with the following procedures.

As the design horizontal displacement u_B is 15cm, first of all, the test on $1/10*u_B$(1.5cm) was carried out, secondly, the case of $1/5*$ u_B(3cm), thirdly, the test on $1/2*u_B$(7.5cm), finally, the specimen was deformed toward u_B.

In this study, data on the third cycle are adopted as representing the experimental value in case of no explanation.

After the above-mentioned test using a virgin specimen at room temperature (15-20° C) and the successive shear history test mentioned below, the same procedure has been taken on different temperature levels between -20° C and +30° C.

During the shear tests, the displacement given at a uniform speed due to the characteristics of the actuator was controlled by a personal computer.

2.3.2. Shear history test

Immediately after a shear test (Phase 1) at room temperature for collecting basic data, the consecutive shear test (Phase 2) was carried out to observe the influence of the history which means that the equivalent stiffness might depend on an experienced displacement.

2.3.3. 50-cycle shear test

The shear test was performed for 50 cycles with horizontal displacement adjusted to the design displacement u_B, and the specimen temperature at -20° C, in order to observe how the number of cycle influences the equivalent shear stiffness and the equivalent viscosity-damping factor, while the change in specimen temperature was recorded.

Also, prior to each test, friction force was measured on the sliding part of the test instrument, confirming that a friction force of approx. 0.48tons was generated under a vertical load of 92 tons. It is considered, however, that this friction force has little influence on the test results, and therefore the test data are not corrected in terms of friction.

2.3.4. Special shear test

Shear test was done to check the influences upon the equivalent shear stiffness and the equivalent viscosity-damping factor after keeping the temperature of the specimen -10° C for 20days.

2.3.5. Test on the recrystallization of the lead

As the lead plug adds a large damping ratio to the laminated rubber bearing, it plays important roles in base-isolated structures. In general, the lead is said to recover the initial stiffness due to its recrystallization at normal temperature even if it experienced the plastic zone by a large shear displacement. But, there is a possibility that the damping capacity is decreaded under the condition of keeping the temperature of the bearings below zero.

To confirm the influence of recrystallization of lead, the shear test was conducted with the specimens at -20° C, and it was repeated two days later, one week later and also after being left at room temperature for a week.

The procedure is as follows:

1) The three-cycle shear test is performed first on that day
2) The above-mentioned test is repeated as the second test immediately after.

2.3.6. Test on the temperature-dependent thermal property of base-isolated bearings

Measurment was conducted to clarify the relationships between the ambient temperature and the temperature of the base-isolated bearing.

3. TEST RESULTS

3.1 Changes in equivalent shear stiffness due to shear history

Table 5 represents the equivalent stiffness of virgin specimens at the third cycle, after the first and successive second stages of shear tests at room temperature. It can be seen from the table that both LRB and HDR indicate lower stiffnesses in the second stage than in the first, and they reach very similar stiffnesses in both stages with the maximum displacement u_B. In other words, the difference of the equivalent stiffness between the first and the second decreases with increasing the shear displacement.

This means that the equivalent stiffness of a specimen with a given shear displacement is influenced by whether or not the specimen has been subjected to larger displacements than the given. Specimens of the former case have smaller stiffnesses than those of the latter.

3.2 50-cycle shear test

Figure 2,3 and 4 illustrate the changes in specimen temperature, equivalent stiffness and equivalent viscosity-damping factor obtained from the 50-cycle shear test, respectively. The equivalent stiffnesses of both the LRB and the HDR decrease to 64% and 59% of the initial values after the 50-cycle shear test. This may be due to the temperatures of the LRB and the HDR specimens rising by as much as 25° C from the start of the test. The final temperatures of the specimens are approximately 5° C after 50 cycles,and the stiffness is lower than that estimated from the shear test mentioned in 2.3.1. at that temperature. This implies an influence of the shear cycles in addition to the increase in temperature. The viscosity-damping factor becomes stable after around the 10th cycle, and is little affected by further shear cycles.

Figure 5 and 6 show the hysteresis loops of the LRB and the HDR at 10th cycle intervals, and the ratio of the equivalent shear stiffness at every 10th cycle (Ki) to that at the first (K1).

The Guidlines[3] provide for the 50-cycle shear test where a period in the shear test corresponds to the natural period of the base-isolated bearings. The period in this experiment is about 40 seconds, not equal to the natural period of the base-isolated bearings. As the equivalent stiffness of both the LRB and the HDR decreases to less than 70%, this provision could not be satisfied.

3.3 Shear Tests After Long Term Maintenance Below 0° C

The equivalent shear stiffness at -10° C obtained in the section of 3.1 and those measured in shear tests after specimens have been maintained at -10° C for 20 days are compared in Table 6. The LRB1 and HDR1 specimens are used in this experiment. As can be understood easily, both the LRD and the HDR show a lower stiffness after the 20 days than in the initial stage. An increase in the shear stiffness due to crystallization presents no problem. Additional tests will be carried out to determine why the equivalent stiffness dose not completely return to the initial state despite being left for 20 days.

3.4 Test on recrystallization of lead

Table 7 compares the equivalent shear stiffness and the equivalent viscosity-damping factor obtained in this manner. The upper data indicates results of the first shear test at different times, and the lower for the immediately following second test. The test results show that the second set of values are somewhat smaller than the first, and that the specimens return to the initial condition in two days. There is little change in the equivalent shear stiffness between that in the test after maintenance at room temperature and that in the three-cycle tests before that. The equivalent viscosity-damping factor is almost unchanged. This indicates that recrystallization dose not play a role. Figure 7 shows the hysteresis loops from the first-round tests.

3.5 Test on the temperature-dependent thermal property of base-isolated bearings

Observations were made of how the specimen temperature followed variations in the ambient temperature. During the course of experiment, the air temperature of the refrigerator was set up to be varied between 0° C to -30° C as shown in Table 8. The actual air temperature was, however, decreased from -2.0° C to -28.5° C. Enter Fig.8 with time on the abscissa and temperature on the ordinate. Changes in the refrigerated and specimen temperatures are displayed in this figure. As is evident from the figure, the specimen temperature becomes approximate to the refrigerated air one after 18 hours by the recovery of the 17.5° C difference, and that once the specimen temperature reached a steady-state value of the ambient temperature, the former follows slightly later after the latter. This event appears to imply that the lowest temperature of the base-isolated could be predicted if historical data on temperature at the construction site were available.

4. CONCLUSIONS

To investigate the behavior of base-isolated bearings of bridges at low temperatures, indoor tests were conducted with two kinds of full-scale laminated rubber bearings. The most important points pertaining to the stated objectives are summarized as follows.

1. The equivalent shear stiffness at a given shear displacement depends on whether the specimen has been subjected to large displacements or not. Specimens which have been subjected to such loads may show smaller stiffnesses. This indicates the need for bearing manufacturers to conduct shear tests up to the maximum possible displacement before shipment to confirm design values of base-isolated bearings.
2. The 50-cycle shear test decreased the equivalent shear stiffness of LRB and HDR to 64% and 69% of the initial values. This may be due to temperature rises and also the repeated shear cycles. The stipulations in the Guidelines may be impossible to satisfy. The 50-cycle shear test increased specimen temperatures by as much as about 25° C.
3. Long term specimen maintenance at low temperatures influences the equivalent shear stiffness and equivalent viscosity-damping factor little.
4. Specimens which have been subjected to successive shear loads at low temperatures may be little different from specimens subjected to one shear load in equivalent shear stiffness and equivalent viscosity-damping.
5. The specimen temperature follows slightly later after an ambient temperature if the former reached a steady-state value of the latter.
6. The lowest temperature of the bearings can be predicted if air-temperature records are available.

FERERENCES

1) Heizyurou Ikeda, Naoki Matsumoto and Kouichi Fukuda : The design planning of the Onnetoh-Oohasi Bridge (in Japanese), Bridge and Foundation, May, 1990
2) Osamu Nakano, Hisashi Konno, Hideyuki Taniguchi and Yuji Ono : On the behavior of base-isolated bearings at low temperature, 7th U.S.-Japan Bridge Workshop, May, 1991
3) Japan Instutute of Construction Engineering : Guidelines for the base-isolated bearing design method for road bridges (draft), March 14, 1989 (in Japanese)

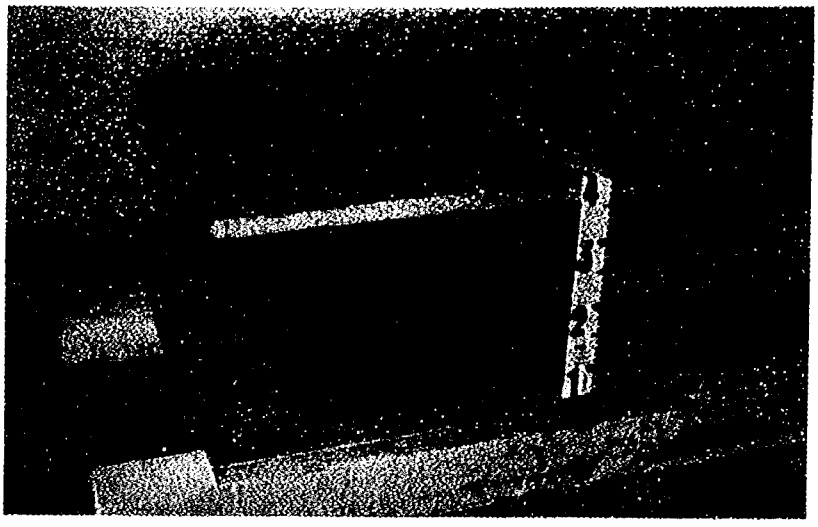


Photo 1 Specimen (LRB)



Photo 2 Specimen (HDR)

Table 1 Temperature of Some City in Hokkaido

Location	Mean Monthly Temperature(℃)		Lowest Temperature (℃)
	Maximum	Minimum	
Sapporo	25.9	−8.9	−23.9
Asahikawa	25.8	−13.4	−41.0
Nemuro	20.5	−9.1	−22.9

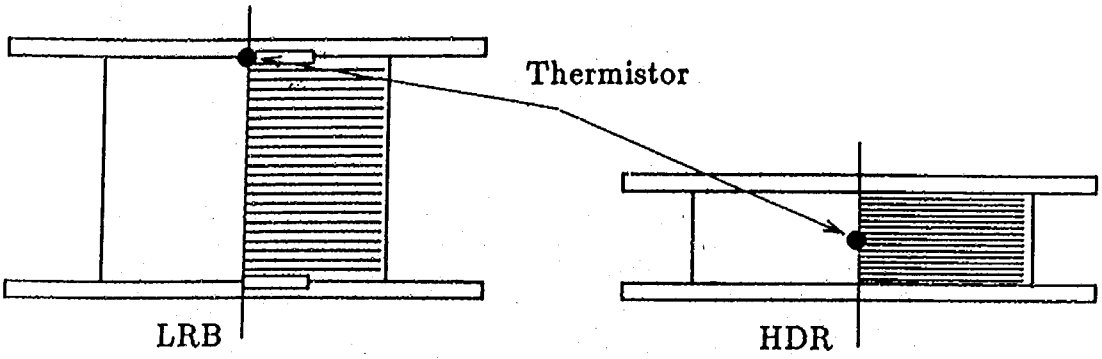


Figure 1 Thermistor

Table 2 Characteristic Design Condition of Specimen

	LRB	HDR
Maximum Vertical Reaction R(ton)	135	
Dead-Load Reaction W(ton)	92	
Live-Load Reaction W(ton)	43	
Design Displacement u_B(cm)	15	
Equivalent Shear Stiffness K_B(kg/cm)	2280	
Equivalent Viscosity-Damping Factor h_{eq}(%)	21	14

Table 3 Test Results of Material Properties of Rubber

LRB

Rubber(Natural Rubber) Material Properties			
Test Item		Standard Value	Measured Value
Static Shear Modulus (kgf/cm^2)		8 ± 1.0	8.4
Tensile Strength (kgf/cm^2)		over 150	229
Elongation (%)		over 450	628
Aging Test	Rate of Stress-Change at 25% Elongation (%)	$-10 \sim +30$	17.1
	Rate of Elongation -Change (%)	over -25	-15.1
Rate of Parmanent Compressive Strain (%)		under 25	22
Ozone Resistance		No Cracking	No Cracking
Adhesion Test		Rubber Rupture	18.1(R100)

• The above result is an average value from 4 specimens
• Test Method by JIS K 6301

HDR

Inner Rubber(KL401) Material Properties		
Test Item	Standard Value at B Company	Measured Value
300% Modulus (kgf/cm^2)	37 ± 6	34
Tensile Strength (kgf/cm^2)	over 90	104
Elongation at Rupture (%)	over 650	755

Coating-Rubber

Coating-Rubber(AN920) Material Properties		
Test Item	Standard Value at B Company	Measured Value
Tensile Strength (kgf/cm^2)	over 125	147
Elongation at Rupture (%)	over 650	838

• Test Method by JIS K 6301



Photo 3 Test Instument

Table 4 Content of Test for Each Specimen

Specimen	Temperature	Content of Test
LRB1* , HDR1*	+30℃	Compression Test,Shear Test
	Room Temperature	Compression Test,Shear Test
LRB2* , HDR2*	0℃	Compression Test,Shear Test
	−10℃	Compression Test,Shear Test
	−20℃	Compression Test,Shear Test
LRB2* , HDR2*	−20℃	50-Cycle Shear Test
LRB3 , HDR3	Room Temperature	Compression Test,Shear History Test
LRB4 , HDR4	Room Temperature	Compression Test,Shear Test

* Specimen with Thermistor

Table 5 Shear History Test Result

Specimen	Phase	Equivalent Shear Stiffness after the Third Cycle K_e(kg/cm)			
		$1/10\times U_B$	$1/5\times U_B$	$1/2\times U_B$	U_B
LRB3	1	7753	5429	2943	1558
	2	6151	4689	2701	1543
HDR3	1	9180	5680	2985	2082
	2	4301	3413	2201	1920

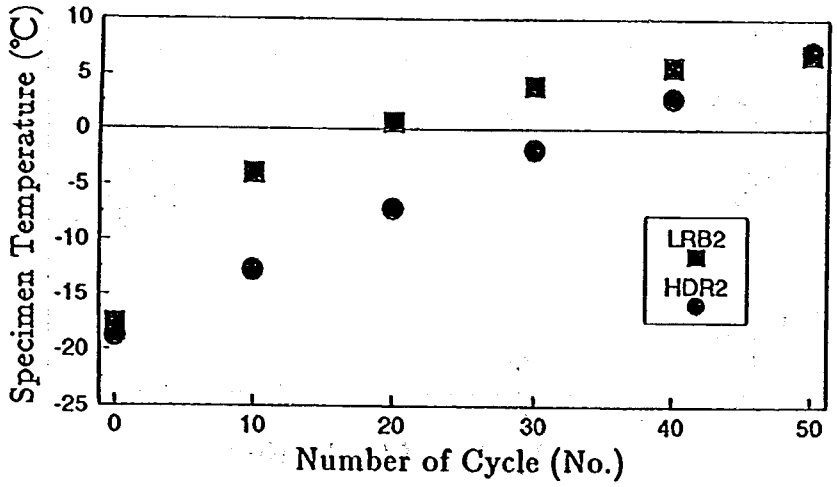


Figure 2 Specimen Temperature during 50-Cycle Shear Test

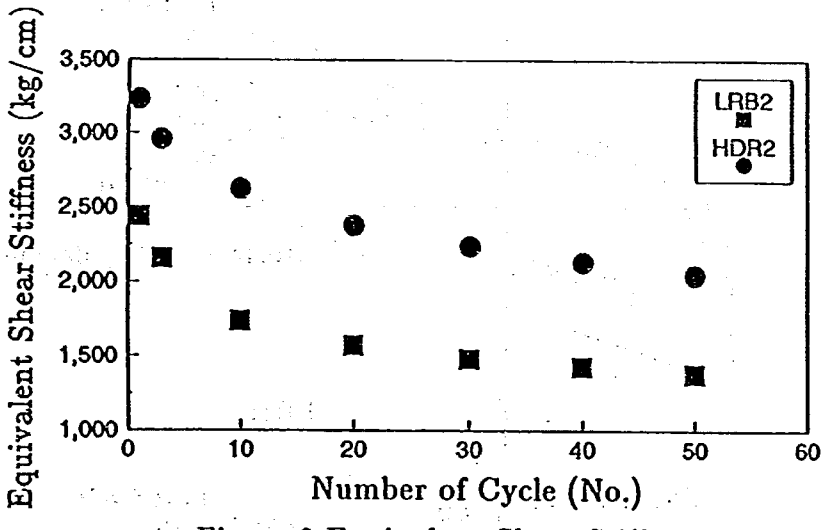


Figure 3 Equivalent Shear Stiffness during 50-Cycle Shear Test

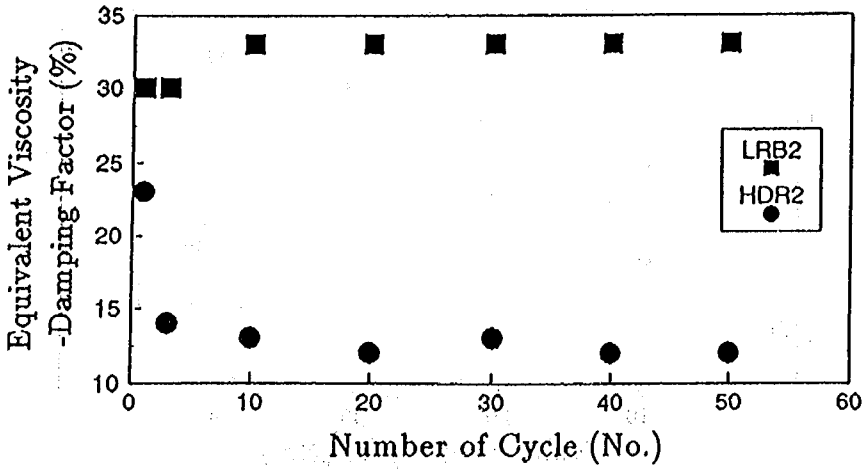


Figure 4 Equivalent Viscosity-Damping Factor during 50-Cycle Shear Test

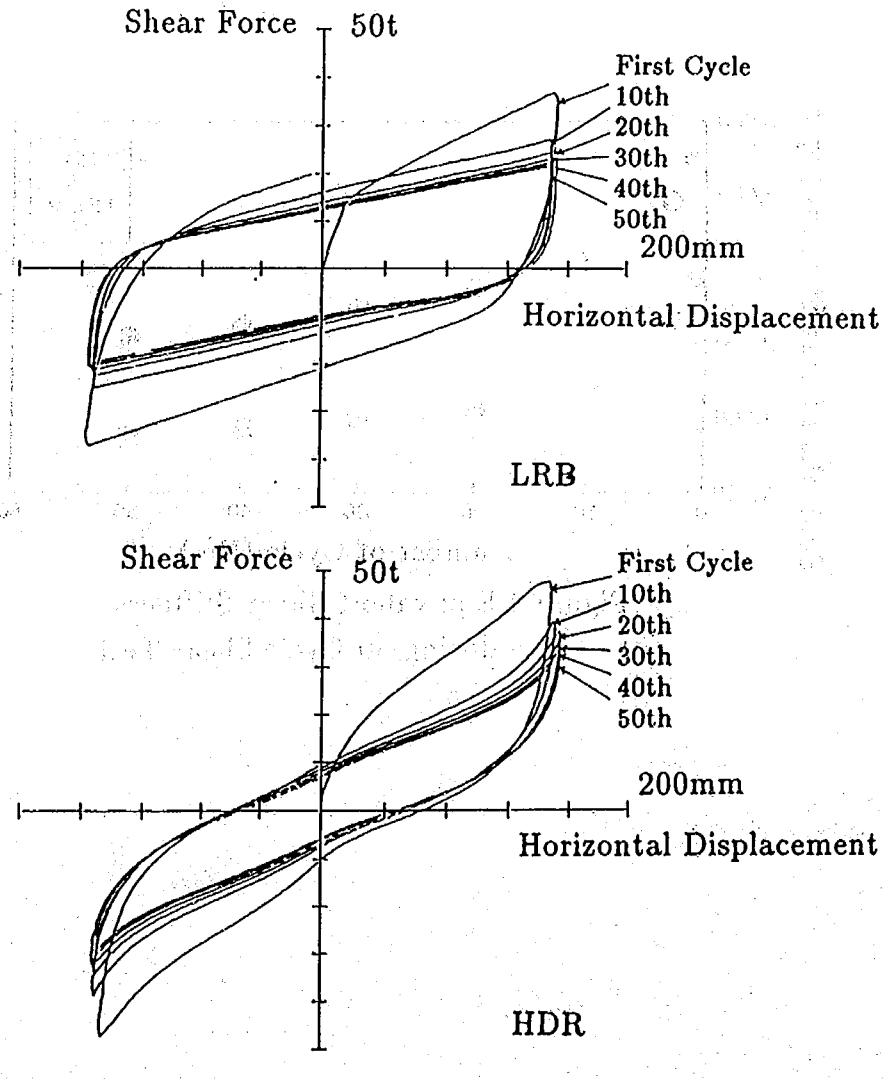


Figure 5 Hysteresis Loops during 50-Cycle Shear Test

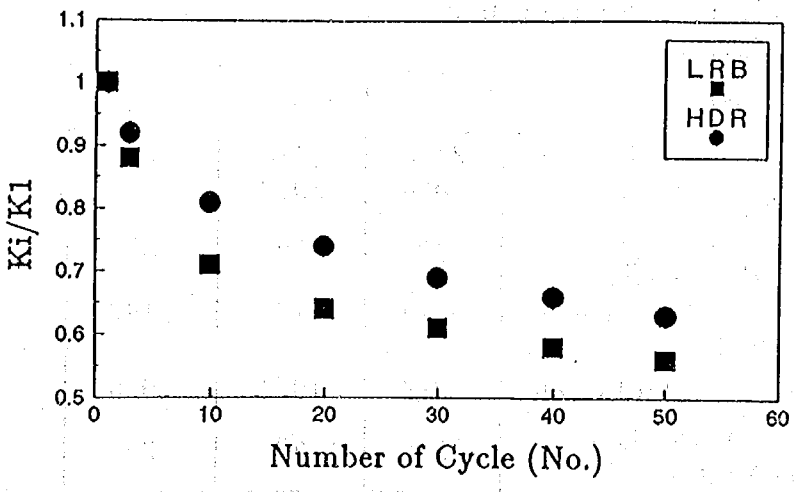


Figure 6 Ratio of Ki to K1

Table 6 Equivalent Shear Stiffness after Long Term Maintenance Below 0℃

	LRB		HDR	
	Initial Stage	After 20 Days	Initial Stage	After 20 Days
First Cycle	2309	1940	2965	2730
Third Cycle	2072	1686	2586	2370

Table 7 Test Result on Recrystallization of Lead

			Initial Stage	After 2 Days	After 7 Days	After Maintenance at Room Temperature
1	Equivalent Shear Stiffness (kg/cm)	First Cycle	2313	2418	2326	2397
		Third Cycle	2016	2079	2027	2058
	Equivalent Viscosity -Damping Factor (%)		32	32	32	32
2	Equivalent Shear Stiffness (kg/cm)	First Cycle	2073	2194	2147	2229
		Third Cycle	1874	1974	1935	2036
	Equivalent Viscosity -Damping Factor (%)		34	33	32	33

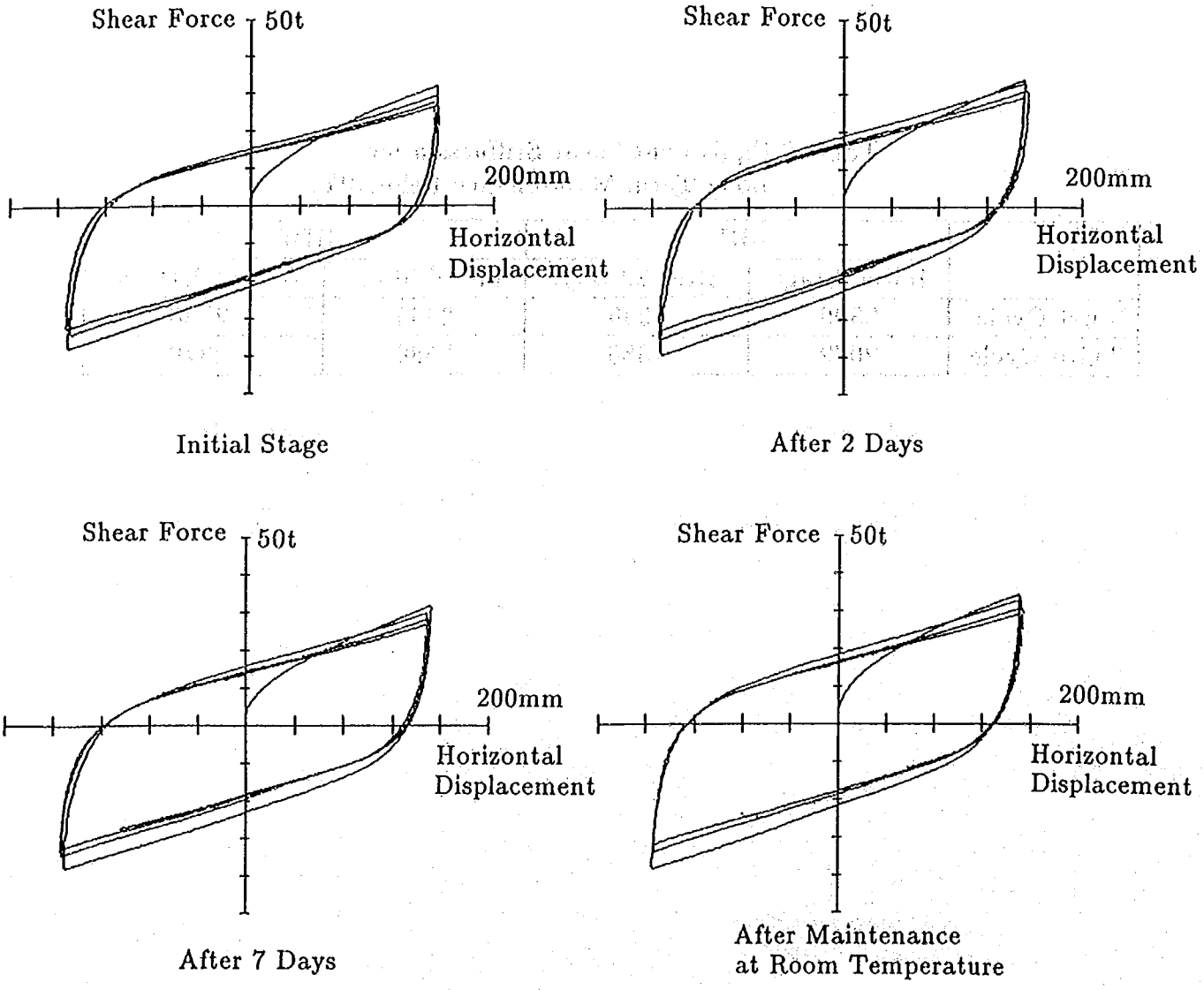


Figure 7 Hysteresis Loops

table 8 Established Temperaure of Refrigerator

Refrigerated Air Temperature (℃)	Time (hr)	Cumulative Time (hr)
−20	32	32
−20 → −30	6	38
−30	12	50
−30 → −20	6	56
−20	12	68
−20 → 0	6	74
0	12	86
0 → −30	6	92
−30	12	104
−30 → 0	6	110
0	3	113

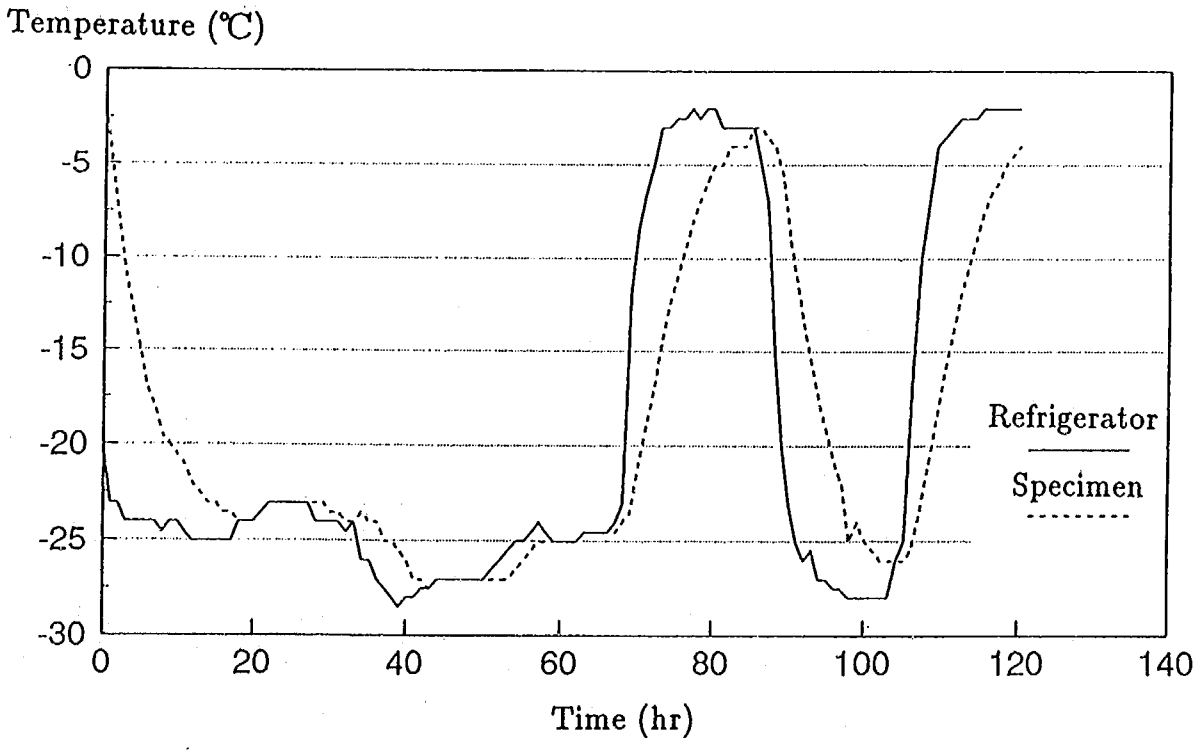


Figure 8 Change in Refrigerator and Specimen Temperature

LOAD DURABILITY TEST FOR HIGHWAY BRIDGE RUBBER BEARING PADS

Tetsuo Matsuda (I)
Yoshifumi Maeda (II)
Akira Murayama (III)
(Presenting Author : Akira Murayama)

SUMMARY

Rubber bearing pads are more economical and require less maintenance than metal bearings do. However, their use in highway bridges is limited. A physical property test, a compression test and a fatigue test were carried out for rubber bearing pads over 7 and 10 years usage periods, and in order to promote the usage of rubber bearing pads.

The results of the load tests are as follows.

(1) Rubber bearing pads maintain their good physical properties.

(2) The durability of the bearing pads sufficiently satisfies bridge design codes and enable significant changes to be made to these codes.

INTRODUCTION

In Japan Highway Public Corporation (JHPC), the use of rubber bearing pads was started from early 1960's when Meishin Expressway was constructed. However, for worrying about the durability of rubber bearing pads, its use was limited in single bridge and slab bridge with span length less than 15 m.

To the end of 1991, the total length of highway in operation was 5047 km. 14% of that, 714 km, was the total length of 6036 bridges. The number of total bearing pads were 325,944 with average 54 per bridge, in which the ratio of rubber bearing pads were about 20.6% (except the Mesnager hinge bearings).

According to the investigation held in 1982 on the damages of bearings in Tomei and Meishin expressways, the ratio of damage of metal bearings was much higher than that of rubber bearing pads. Especially in case of the superstructure is made of concrete, 80 % of metal bearings were damaged. This result indicates that rubber bearing pads not only are more economical but also require less maintenance than metal bearings do.

In order to enlarge the use of rubber bearing pads, intensive studies have been done on used and new rubber bearing. This includes three types of samples: used rubber bearing that was obtained from Tomei Expressway and Higashimeihan Expressway where the old rubber bearing has been replaced by new one, new rubber bearing that is of the same model as the used one and new rubber bearing obtained from construction site. For the first two samples, compression test on prototype sample, compression shear test on prototype sample, chemical component analysis and physical property test were carried out. For the third sample, fatigue test was performed as well as the tests for the first two samples. On the basis

(I) Head, Bridge Section
Research Institute of Japan Highway Public Corporation (JHPC)
(II) Deputy Head, Bridge Section (JHPC)
(III) Engineer, Bridge Section (JHPC)

of the investigation on chemical and physical properties, the durability of rubber bearing has been examined.

LOADING TEST

Samples and Tests

The shape of the old and new rubber bearing is illustrated in Tables 1 and 2, respectively. Table 3 shows the tests for each sample. For the old bearing, there were residual compressional and shear strain. This might be the reason of the settlement and the lateral flow of the abutments.

Table 1 Shape and apperancea of old bearing pads

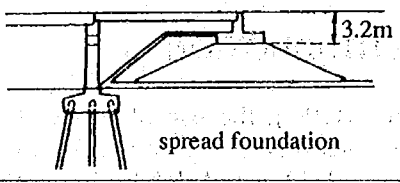
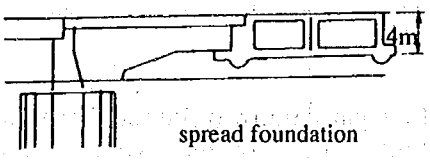
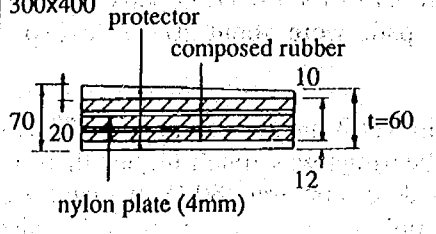
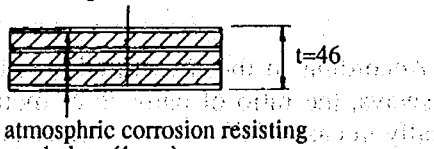
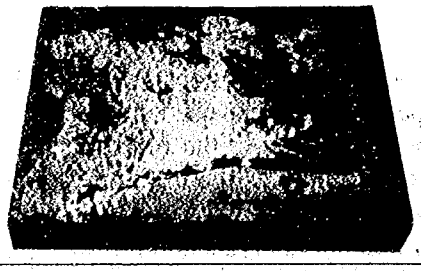
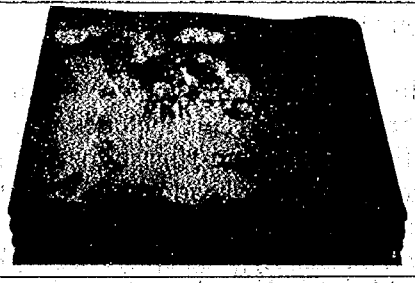
Expressway name	Tomei Expressway	Higashi meihan Expressway
Bridge name	Nagamachi Bridge	Chikura Viaduct
Commencement of service	March 1969	October 1975
Daily average traffic volume	60,845 (1981)	18,138 (1981)
Abutment type	 spread foundation	 spread foundation
Type of bearing pads	Type A used for 10 years	Type B used for 7 years
Shape	3 layers 300x400 	3 layers 300x400 
Appearance		
Residual compression strain in rubber layer	6%	7%
Residual shear strain in rubber layer	4%	68%

Table 2 Shape and appearance of new bearing pads

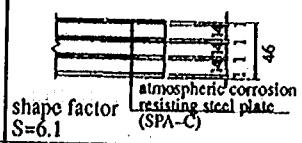
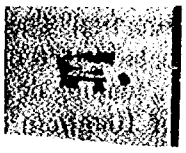
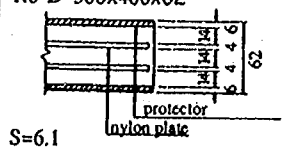
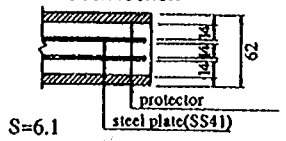
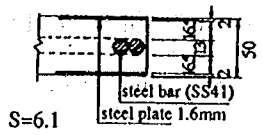
			Shape of samples	Appearance	Notes on structure
Composed rubber	Type B	60tf shoe	Rb•F 300x400x46  shape factor S=6.1		Atmosphric corrosion resisting steel plates were stuck on both the surfaces of composed rubber by a vulcanize adhesive. The surface of the plate was protected by resinous paint that is of high adhesive force and high friction coefficient.
	Type A	60tf shoe	Rb•D 300x400x62  S=6.1		As DSF pads were protected by hard rubber (the hardness is 95°), the contact between bearing pad and structure was quite good. The friction resistance also increased. (Nowadays, almost no nylon type bearing pads are produced again.)
	Type A	60tf shoe	Rb•D 300x400x62  S=6.1		As DSF pads were protected by hard rubber (the hardness is 95°), the contact between bearing pad and structure was quite good. The friction resistance also increased. (Nowadays, almost no nylon type bearing pads are produced again.)
Natural rubber	Type C	60tf shoe	400ø x50  S=6.1		The top and bottom surfaces were protected by steel plates. Ring mesh made of steel bar was embedded in the middle of rubber to prevent the swelling deformation in free lateral surface.

Table 3 Samples and corresponding tests

Group	Samples	Compression test				Compressional shear test				Compressional fatigue test under constant shear
		Compression test			Ultimate compression test	Compression test			Ultimate compression test	
		gradual	cyclic	continuous		N	S	E		
1	Type B 400x300x46 Old bearing pads	○	○	○		○	○	○		
	Type B 400x300x46 New bearing pads	○	○	○	◎	○		○	◎	◎
2	Type A nylon plate 400x300x60(70) Old bearing pads	○	○	○		○	○	○		
	Type A nylon plate 400x300x62 New bearing pads	○	○	○	◎	○		○	◎	◎
	Type A steel plate 400x300x62 New bearing pads				◎				◎	◎
3	Type C 400ø New bearing pads				◎				◎	◎

notes : The tests of ○ mark and ◎ were carried out in 1982 and in 1983 respectively.
N, S, AND E of compressional shear test mean the direction of horizontal load shown figure 4.

Experimental Method

(1) Compression test

Sample was loaded in vertical direction. The deformation was measured at each loading step. The compression spring constant was computed based on the relationship of vertical load and deformation. In compression test on prototype sample, a loading device of capacity 200 tf was used. After the sample was loaded for two cycles at initial load of 10kgf/cm^2, loading followed three patterns (Figure 1), gradual increase, cyclic gradual increase and gradual increase and continued, until 150kgf/cm^2. For limit compression test, prototype samples were loaded until failure. The compression strains have been compared. A loading device of capacity 1000 tf was used. The sample was loaded, as initially loaded to 50kgf/cm^2 (corresponding to 60 tf for rectangular bearing and 63 tf for circular bearing), following the gradual increase loading path as shown in Figure 1. The other two loading path did not use on the basis of the test results in 1982.

The layout of compression test is illustrated in Figure 2.

(2) Compressional shear test

Prototype sample was first loaded by a press machine for two cycles under a pressure 10kgf/cm^2. Then, it was further loaded to a vertical pressure of 50kgf/cm^2. Shear was applied by use of jack under this constant vertical load. The capacity of jack was 10 tf. A shear force of 5 ~ 6 tf was applied finally.

The static shear modulus was calculated based on the measured shear force and shear deformation.

For the ultimate compressional shear test, an initial shear was applied under a vertical load of 50kgf/cm^2 to a shear deformation of 50 % for one cycle. Then, shear force was increased till the shear deformation of 200 %. In order to make the experimental status more similar to that in a real bridge, concrete loading plates were put in the top and bottom of sample respectively.

The layout of compressional shear test is shown in Figure 3 and 4.

(3) Compressional fatigue test under a certain shear

In this test, sample was first sheared to a shear strain 50 %. Then, a cyclic vertical load with amplitude of 15 ~ 35 kgf/cm^2 (corresponding to 18 ~ 42 tf for rectangular bearing and 18.8 ~ 44 tf for circular bearing) and frequency of 5 Hz was applied for 2,000,000 cycles. The temperature change and cracking were measured. It was intended to applied the vertical load to a maximum amplitude of 50kgf/cm^2. However, for the limitation of the capacity of the fatigue test machine, vertical load was applied to a maximum amplitude of 35kgf/cm^2.

The layout of the test is given in Figure 5.

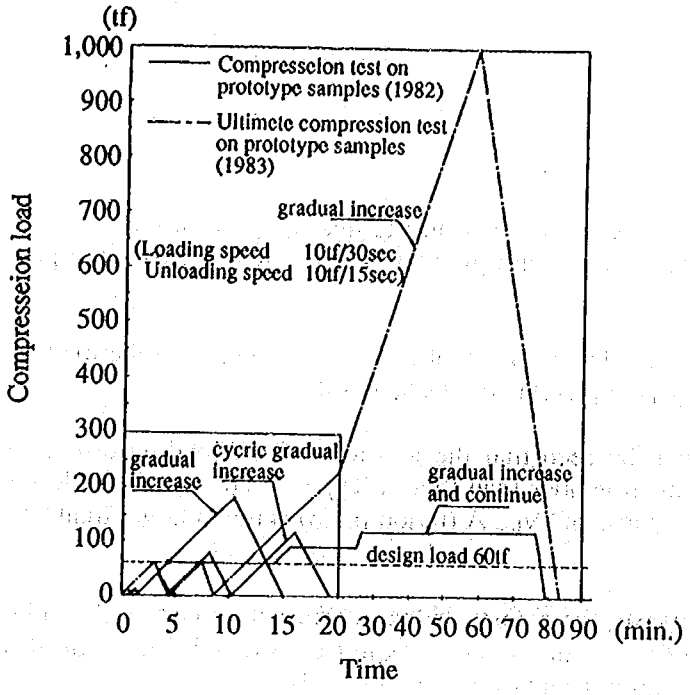


Fig. 1 Loading pattern of compression test

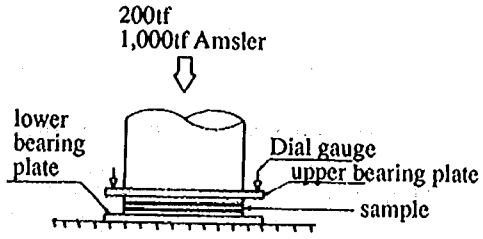


Fig. 2 Compression test

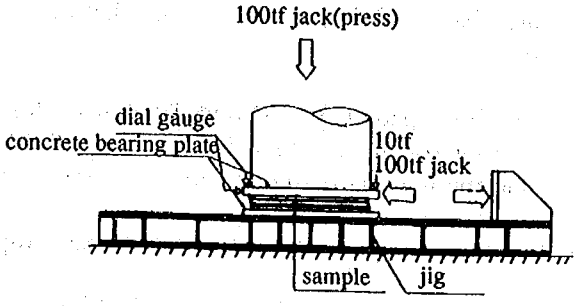


Fig. 3 Compressional shear test

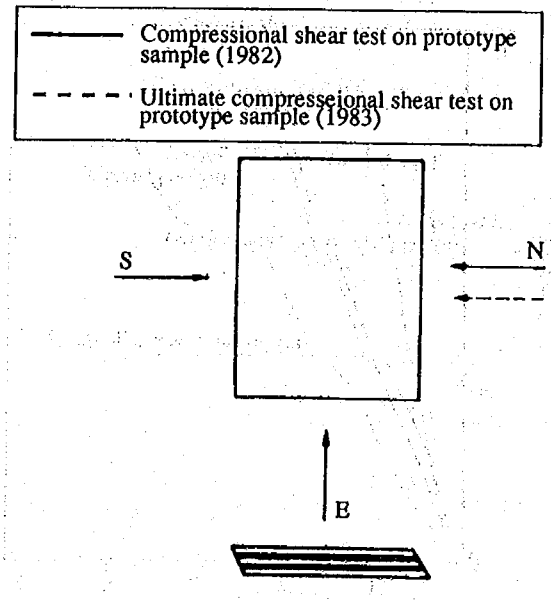


Fig. 4 Direction of horizontal load

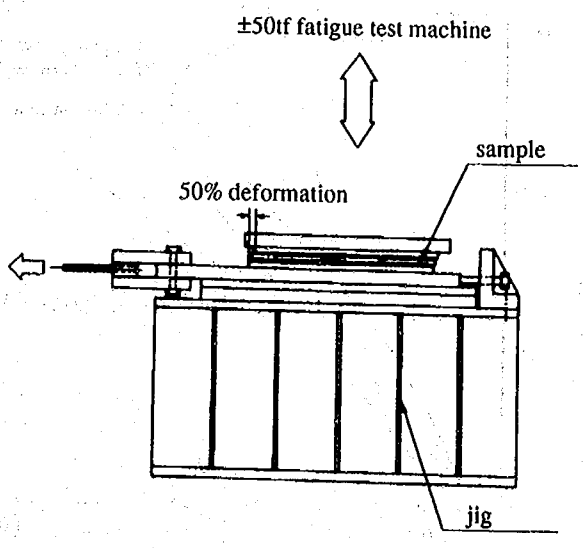


Fig. 5 Compressional fatigue test

Test Results

1. Compression test

(1) Compression test on prototype sample

The load-deformation curves for each loading path are given in Figures 6, 7 and 8, respectively. The load-deformation relationships of old bearings under cyclic gradual increase loading path are presented in Figures 9 and 10.

a) For Type B, the spring constant of old bearing was larger than that of new bearing for all the loading paths. The opposite was obtained for Type A (nylon plate) (Figures 6, 7 and 8).

b) Comparison of Figure 9 and Figure 10, it can be seen that the gradient of the load-deformation curves of Type A (nylon plate, Fig. 10) are much gentler than that of Type B. The hysteresis loops are also much larger. This means that the energy loss of Type A (nylon plate) is much larger than that of Type B.

c) For both pads (Type B and Type A (nylon plate)), the shapes of load-deformation curves are quite similar for all the three loading path if the effect of initial part does not considered. This indicates that the loading path does not affect the deformation behavior of bearing pads.

(2) Ultimate compression test on prototype sample

The relationship between vertical load and strain is illustrated in Fig. 11. Comparison of compression spring constants is given in Table 4.

a) For both layered rubber bearing and Type C, failure occurs in the middle reinforcing material.

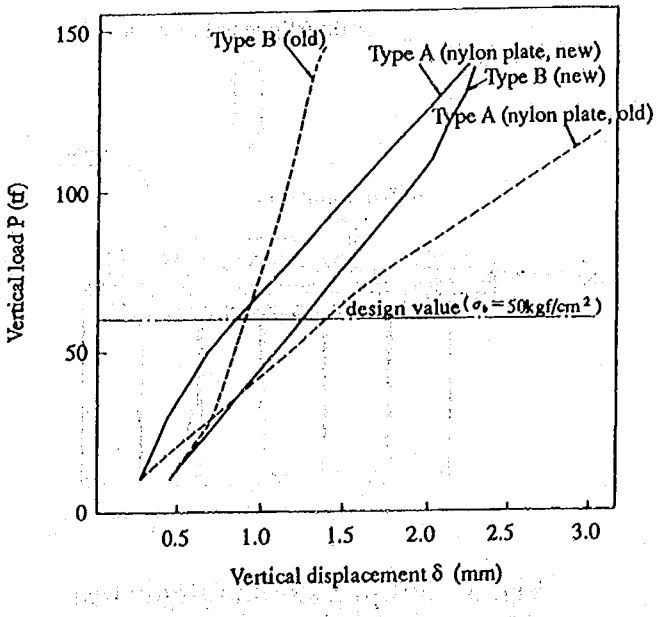


Fig. 6 Load-displacement curves (gradual increase)

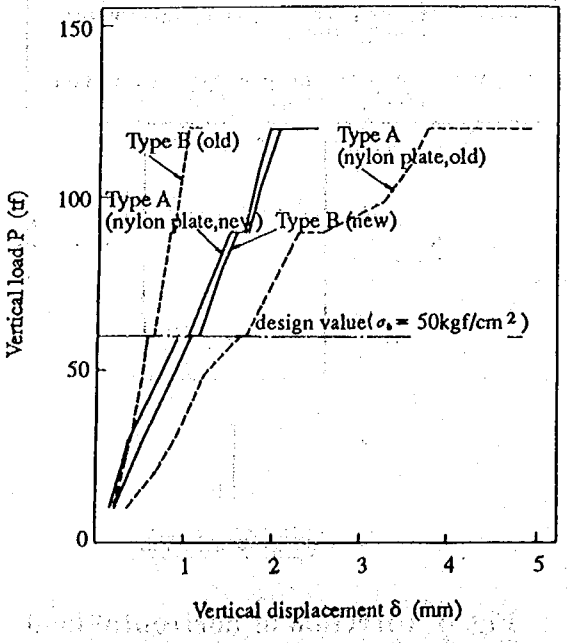


Fig. 8 Load-displacement curves (gradual increase and continue)

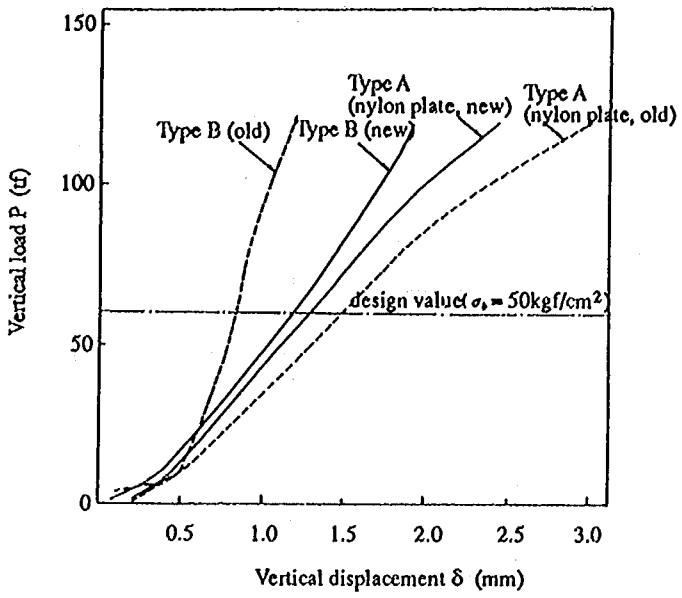


Fig. 7 Load-displacement curves (cyclic gradual increase)

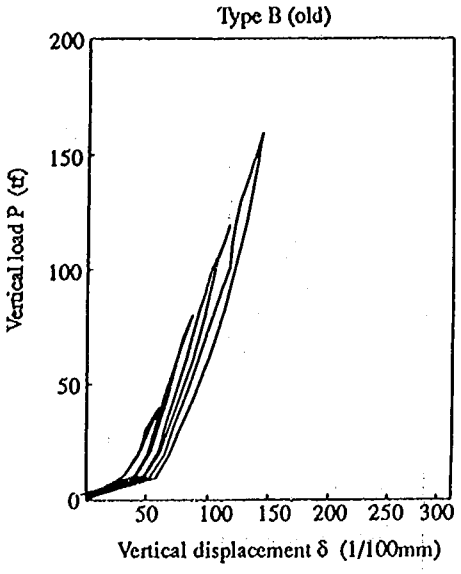


Fig. 9 Load-displacement curve (cyclic gradual increase)

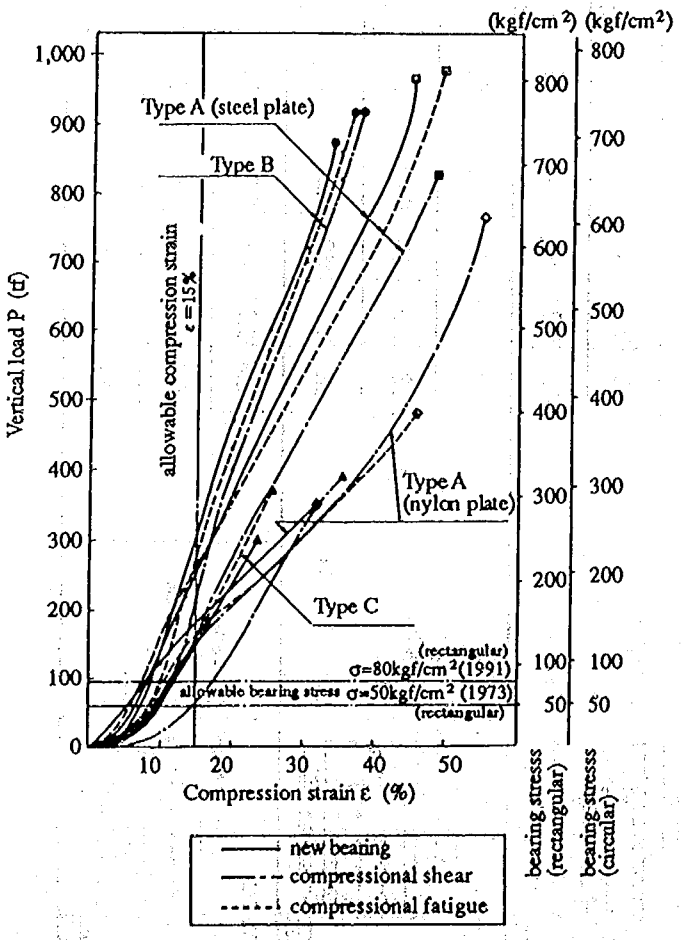


Fig. 11 Vertical load-compression strain curves

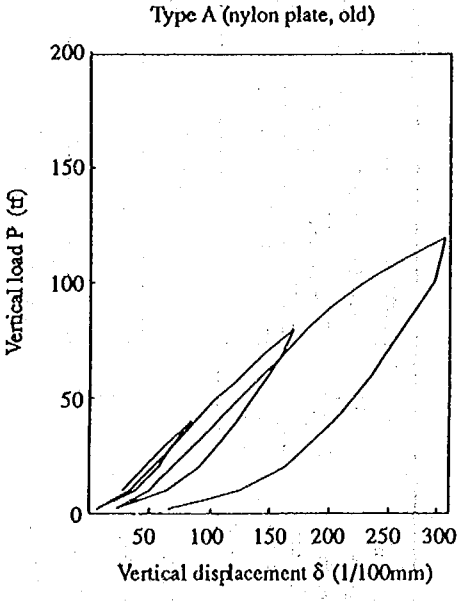
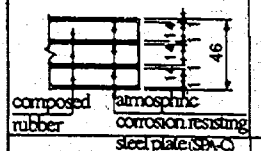
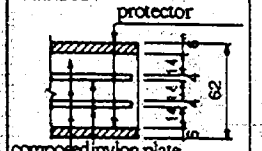
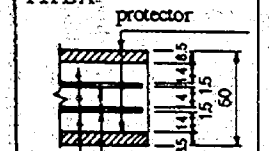
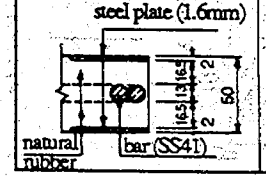


Fig. 10 Load-displacement curve (cyclic gradual increase)

Table 4 Comparison of compression spring constant

Samples (cross section)	Bearing size a : length b : width D : diameter te : thickness of a rubber layer Σte : total thickness	Shape factor • rectangular $S=\frac{a\times b}{2\times(a+b)te}$ • circular $S=\frac{D}{4te}$	measured spring constant (σ_c=15～ 50kgf/cm²) top : new bearing middle : compressional shear bottom : compressional fatigue					Computed spring constant		Reference values			
			compression stress σ_c=15kgf/cm²		compression stress σ_c= 50kgf/cm²		$Kc=\frac{Pc_2-Pc_1}{\delta_2-\delta_1}$	theoretical elastic shear modulus G	rectangular $Kc_1=G(3+6.58S^2)\frac{a\times b}{\Sigma te}$ circular $Kc_1=G(3+4.935S^2)\frac{A}{nte}$	Physical test		Compressional shear test	
			Vertical load Pc_1	Vertical displacement δ_1	Vertical load Pc_2	Vertical displacement δ_2				G	Kc_2	G	Kc_2
TYPE B  composed rubber / atmospheric corrosion resisting steel plate (SPA-C)	a =30cm b =40cm te=1.4cm Σte=3×1.4=4.2cm	6.1	tf 18	cm 0.19	tf 60	cm 0.29	tf/cm 420 ratio for Kc1=0.74	kgf/cm² 8	tf/cm	kgf/cm² 7.4	tf/cm	kgf/cm² 7.8	tf/cm
			18	0.31	60	0.42	382 0.67	tf/cm² (0.008)	566	tf/cm² (0.0074)	524	tf/cm² (0.0078)	552
			18	0.24	60	0.35	382 0.67						
TYPE A  protector composed rubber / nylon plate	a =30cm b =40cm te=1.4cm Σte=3×1.4=4.2cm	6.1	18	0.19	60	0.27	525 0.74	10	708	10	708	12.2	863
			18	0.27	60	0.40	323 0.46	(0.01)		(0.01)		(0.0122)	
			18	0.24	60	0.34	420 0.59						
TYPE A  protector composed rubber / steel plate (SS41)	a =30cm b =40cm te=1.4cm Σte=3×1.4=4.2cm	6.1	18	0.21	60	0.29	525 0.74	10	708	10	708	12.0	850
			18	0.39	60	0.47	525 0.74	(0.01)		(0.01)		(0.012)	
			18	0.17	60	0.24	600 0.85						
TYPE C  steel plate (1.6mm) natural rubber / bar (SS41)	D =40cm te=1.65cm nte=2×1.65=3.3cm	6.1	18.8	0.21	63	0.34	340 0.35	13.5	959	14.3	1,016	11.0	782
			18.8	0.31	63	0.48	260 0.27	(0.0135)		(0.0143)		(0.011)	
			18.8	0.19	63	0.31	368 0.38						

b) The ultimate loads of new bearings are: Type B, 876 tf (730kgf/cm^2); Type A (nylon plate), 351 tf (293kgf/cm^2); Type A (steel plate), 964 tf (803kgf/cm^2) and Type C 300 tf (239kgf/cm^2). (Fig. 11)

c) The ultimate loads of samples that were subjected to compressional shear test (shown in experimental method (2)) are: Type B, 918 tf (765kgf/cm^2); Type A (nylon plate), 765 tf (638kgf/cm^2); Type A (steel plate), 825 tf (688kgf/cm^2) and Type C 389 tf (310kgf/cm^2). (Fig. 11)

d) The ultimate loads of samples that were subjected to compressional fatigue test (shown in experimental method (3)) are: Type B, 918 tf (765kgf/cm^2); Type A (nylon plate), 480 tf (400kgf/cm^2); Type A (steel plate), 975 tf (813kgf/cm^2) and Type C 373 tf (297kgf/cm^2). (Fig. 11)

e) The measured spring constants are small than that calculated (Table 4).

2. Compressional shear test

(1) Compressional shear test on prototype sample

The shear force-shear strain relationship of the samples loaded in N direction is given in Fig. 12.

a) For all the samples (both new and old), no residual shear strain occurs in N, S and E directions in a shear strain range of 35 ~ 50%.

b) The elastic shear moduli are ranged in 12 ~ 14 kgf/cm^2 for all the bearings (old Type B, old and new Type A) except new Type B which has the value of 7.0 ~ 7.7 kgf/cm^2 (Fig. 12).

(2) Ultimate compressional shear test on prototype sample

Fig. 13 shows the relationship of shear force and shear strain. Shear moduli at shear strain 50% and 70% are listed in Table 5.

a) For Type B, the shear deformation is as much as 84 mm (200%) at a shear load of 22 tf. Residual deformation occurred in the middle reinforcing material after unloading.

b) The final shear deformation of Type A (nylon plate) is 81.4 mm (194%) corresponding to a shear force of 19.1 tf. Sample comes into contact with concrete plate. Type A (steel plate) also has shear deformation of 84.2 mm (200%) at a load of 19.3 tf. Similarly, sample gets in touch with concrete plate. For both the samples, no residual deformation can be seen in outside. Because sample is covered with rubber, it is uncertain whether there is residual deformation in reinforcing material. (Fig. 13)

c) The shear deformation of Type C is 87.1 mm (189%) at a load of 198.4 tf. Sliding occurred at this deformation. Cracking occurred in 0.44 mm thick covering rubber after unloading. In design, there should have a ring mesh (steel bar) in the middle of rubber bearing. For this ring mesh had not been set in the middle, the deformation is unusual (Fig. 13 and 14).

d) From Table 5, it can be seen that the value of elastic shear modulus of Type B from test is about the same as theoretical value G_0=8kgf/cm^2. For Type A, the theoretical value is G_0=10kgf/cm^2. While the test results show that at γ =50%, G=12.0 ~ 12.2kgf/cm^2, and at γ =70%, G=11.1 ~ 11.2kgf/cm^2. On the other hand, the theoretical value of Type C is G_0=13.5kgf/cm^2. The test results are at γ =50%, G=11.0kgf/cm^2, and at γ =70%, G=10.8kgf/cm^2.

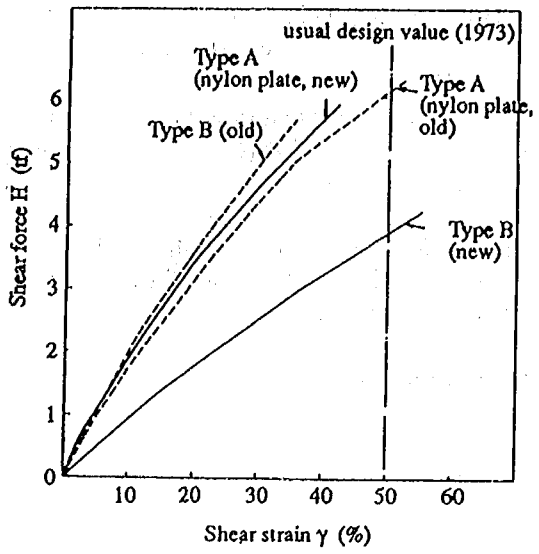


Fig. 12 Shear force-strain curves

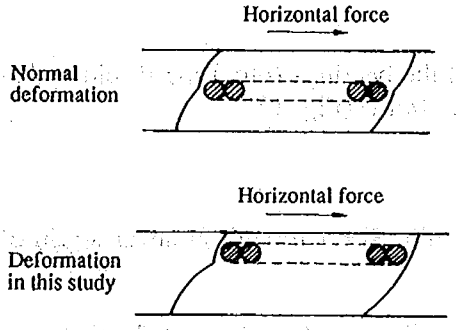


Fig. 14 Deformation of Ring Shoe

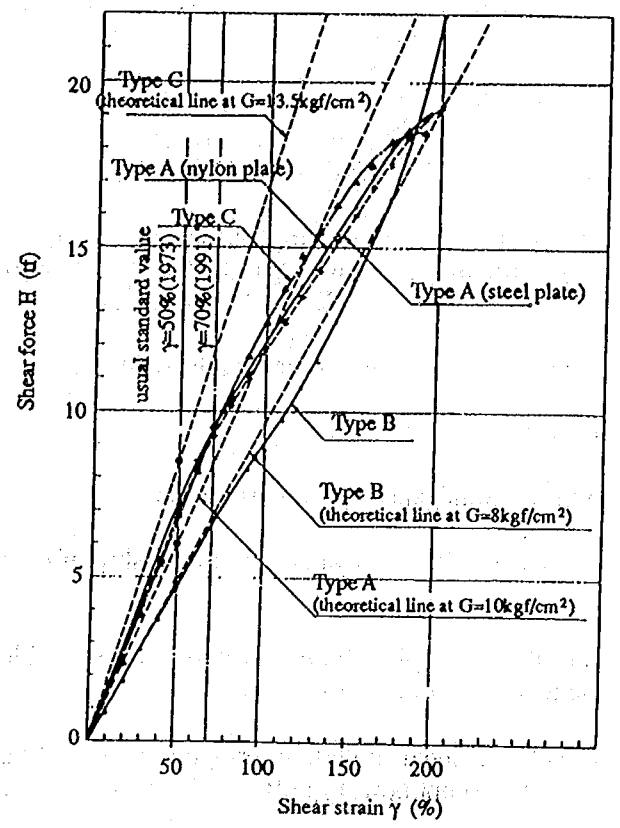


Fig. 13 Shear force-strain curves

Table 5 Elastic shean module

Samples theoretical G0	Shape of bearings	Bearing area A_{cm}^2	Total thickness Σt_e cm	Shear strain $\gamma=50\%$			Shear strain $\gamma=70\%$		
				Horizontal force H kgf	Horizontal displacement Δcm	Elastic shear modulus $G=\frac{H_{50}\cdot\Sigma t_e}{A\cdot\Delta_{50}}$ (kgf/cm²)	Horizontal force H kgf	Horizontal displacement Δcm	Elastic shear modulus $G=\frac{H_{70}\cdot\Sigma t_e}{A\cdot\Delta_{70}}$ (kgf/cm²)
Type B $G_0=8$ kgf/cm²	300×400×46	1,200	3×1.4 =4.2	4,700	2.1	7.8	6,700	2.9	8.0
Type A (nylon plate) $G_0=10$ kgf/cm²	300×400×62	1,200	3×1.4 =4.2	7,300	2.1	12.2	9,400	2.9	11.2
Type A (steel plate) $G_0=10$ kgf/cm²	300×400×62	1,200	3×1.4 =4.2	7,200	2.1	12.0	9,300	2.9	11.1
Type C $G_0=13.5$ kgf/cm²	400φ×50	1,257	5.0−0.4 =4.6	6,900	2.3	11.0	9,500	3.2	10.8

3. Compressional fatigue test under a certain shear load

The results of compressional fatigue test under a certain shear load are listed in Table 6.

a) On the basis of the examination on the outside of samples after unloading, there is a 5 mm residual deformation in Type B and 8 mm in Type A (steel plate). No separating in contact part and cracking in rubber was found for the four kind of samples.

b) The variation of temperature in sample surface ranged from 5 to 12 °C. Temperature change in Type C is the largest. Temperature increased till 25 °C.

TEST ON CHEMICAL AND PHYSICAL PROPERTIES

Test Materials

Materials used in chemical component analysis and physical experiment are shown in Table 7. For old bearing, sample for physical test was sampled from the middle of bearing for considering the environmental effect. As for chemical component test, samples were sampled from both near surface and in middle for comparison. For new bearings, samples were sampled from middle of bearing for both chemical and physical tests.

Test Method

(1) Chemical component analysis

Seven chemical components have been analyzed based on JIS K 6350 (Method of Analysis for Rubber Goods) and JIS K 6388 (Testing Methods for Synthetic Rubber CR).

(2) Physical test

Physical tests were performed based on JIS K 6301 (Physical Testing Methods for Vulcanized Rubber), JIS K 6386 (Rubber materials for Vibration Isolators) and JIS K 6854 (Testing Method for Peel Strength of Adhesive).

Table 6 Compressional fatigue test under constant shear

Samples (size)	Amplitude vertical force	Vertical displacement	Temperature change				Residual deformation δ / sample	Remarks
			Sample		Laboratory			
			highest	lowest	highest	lowest		
Type B (300×400×46)	18~42 tf (15~35kgf/cm²)	0.4mm	21°C	16°C	11°C	7°C	5 mm	
Type A (nylon plate) (300×400×62)	18~42 tf (15~35kgf/cm²)	0.8mm	17°C	10°C	8°C	4.5°C	—	
Type A (steel plate) (300×400×62)	18~42 tf (15~35kgf/cm²)	0.8~0.9mm	23°C	18°C	8°C	6°C	8 mm	
Type C (400φ×50)	18.8~44 tf (15~35kgf/cm²)	13.4mm	25°C	13°C	9°C	4°C	—	Large value of vertical displacement was caused by the miss placed steel bar.

Table 7 Table materials

Type	Group	Samples	Chemical component analysis		Physical test	Stripping test
			Middle	Near surface		
Composed rubber	1	Type B old bearing pads	○	○	○	
		Type B new bearing pads	◎		◎	◎
	2	Type A (nylon plate) old bearing pads	○	○	○	
		Type A (nylon plate) new bearing pads				◎
		Type A (steel plate) new bearing pads	◎		◎	◎
Natural rubber	3	Type C new bearing pads	◎		◎	◎

(notes) Near surface is about 1mm from surface
○ and ◎ mark were carried out in 1982 and 1983 respectively

Test Results

(1) Chemical component analysis

The results of chemical component analysis are presented in Table 8. The followings are cleared.

a) For old bearing, the quantity of rubber in near surface is more than that in middle. On the other hand, the quantity of ethyl ether in near surface is less than that in middle. As for sulphur and ash content, almost no change occurs.

b) There is a little difference in the quantity of carbon black between old and new bearings.

c) For new Type B and new Type C, the combination of each component is in balance in total.

d) In new Type A, synthetic rubber is blended with natural rubber.

(2) Physical experiment

Test results together with standard values are given in Table 9. The followings are cleared based on test results.

a) The elastic shear modulus of old bearing is larger than that of new one.

b) The temperature of impact brittleness of new Type A is –51 °C that is lower than the Japanese National Railways standard value of –40 °C. This is because of the blending effect. However, for durability to oil, there is as much as 148% volumetric swelling deformation. The permanent compressional strain is also as high as 77%. These values being higher than JHPC standard values mean that it is necessary to make lower the quantity of mixed natural rubber.

c) The bear-ability to ozone of new Type C that is made of natural rubber is said not good enough. In this test, nothing was observed unusual. However, the ratio of volumetric change that represents to oil is as large as 180%.

d) For Type A (nylon plate), the stripping strength between rubber and nylon plate is relatively low.

e) Other items approximately satisfy standard values although some differences exist between old and new bearings.

Table 8 Chemical component analysis

Item \ Sample		Type B			Type A			Type C
		New	Old		New	Old		New
			Middle	Surface		Middle	Surface	
1 Polymer qualitative		CR	CR	CR	CR-NR	CR	CR	NR
2 Total amount of rubber	%	50.8	50.5	51.8	56.2	48.2	51.4	65.6
3 Amount of CR	%	50.8	50.5	51.8	36.5	48.2	51.4	—
4 Amount of NR	%	—	—	—	19.7	—	—	65.6
5 Amount of Carbon black	%	26.5	22.0	22.7	19.4	26.5	25.1	22.8
6 Amount of ethyl ether	%	17.6	14.9	12.8	13.6	11.3	9.3	7.0
7 Total amount of sulphar	%	0.9	0.7	0.6	1.9	2.0	2.0	1.8
8 Amount of ash	%	4.2	12.7	12.7	8.9	13.2	13.3	2.8
9 SiO_2	%	—	4.1	5.3	3.2	4.5	4.5	—
2+5+6+7+8		100.0	100.8	100.6	100.0	101.2	101.1	100.0

Table 9 Physical properties of rubber (standard values and test results)

Items		Unit	Test method	Standard value			Type B		Type A			Type C
				A		Type C	Old	New	Nyon plate		Steel plate	
				Type A	Type B				Old	New	New	
Static shear modulus		kgf/cm^2	JIS K 6386/6.1	8±1.0	10±1.0	13.5±1.0	9.4	7.4	14.8	10.0		14.3
Hardness			JIS K 6301/5.2	50±5	60±5	60±5	52	52	63	56		60
Tension (minimum)		%	JIS K 6301/3	400	350	400	540	480	380	580		480
Durability to oil (ratio of volumetric change) (maximum)		%	JIS K 6301/12	+120		—	+71.6	+58.1	+65	+148		+180
Aging test	Stress change ratio of 25% tension	%	JIS K 6386/6.3 100°C x 70h	−10~+100		−10~+30	+34.8	+46.7	+42.9	+49.2		+3.4
	Tensile change ratio	%		−50 and more		−50 and more	2.7	−7.9	−8.8	-32.2		−26.2
Permanent compressional strain		%	JIS K 6301/10 100°C x 70h	45 and less		50 and less	28	24	44	77		36
Durability to ozone		—	JIS K 6301/16 50±5pphm20% 40°C x 96h	Non crack and Non remarkble change		Same as the left	Non crack Non change	No problem	Non crack Non change	No problem		No problem
Durability to water (weight change ratio)		%	JIS K 6911/5.26 (Water absorption ratio) Temperature of disfilled water 50±2°C x 72h	10 and less		—	+4.3	+2.2	+4.8	+2.3		+1.8
Low temperature impact brittleness		°C	JIS K 6301/14	—		—	−37	−42	−36	−51		−65
Low temperature torsional shear test	Apparent stiffness ratio	kgf/cm^2	JIS K 6301/19	—		—	—	10.8	—	—	14.7	15.8
	T_2	°C		—		—	—	−28	—	—	−24	−51
	T_5			—		—	—	−36	—	—	−33	−56
	T_{10}			—		—	—	−38	—	—	−35	−57
	T_{100}			—		—	—	−42	—	—	−41	−64
Stripping strength	steel / rubber	kgf/25mm	JIS K 6854 (180°stripping)	—		—	—	34.8*	—	—	10.2	100 and more
	felt / rubber			—		—	—	—	—		—	—
	nylon / rubber			—		—	—	—	—		—	—
remarks		Standard values of type A are based on JHPC(1988). Standard values of Type C are reference value. T2, T5, T10, T100 : The temperature at which the stiffness 2, 5, 10 or 100 times harder than that in laboratory. * : 49.0 ~ 6.5 variations										

CONCLUSIONS

Aging Effect on Rubber

It used to worried about the dimensional change and strength reduction caused by physical change such as creep and fatigue and chemical change such as acidolysis because of aging. However, test results on both Type B and Type A showed that no significant changes, whether physical or chemical, were observed. Rubber bearing pads maintain good physical and chemical properties as time going on.

Failure strength and bearing stress

It is considered that the failure strength of rubber bearing pads depends on the strength of reinforcing materials. Because the tensile strength of nylon plate is less than that of steel plate, ultimate load is small. However, the vertical load at allowable compressional strain of ε=15% is more than 150 tf (125kgf/cm^2). This quite satisfies the allowable bearing stress of σ = 50kgf/cm^2. (Fig. 11)

Fatigue resistance

Results of ultimate compression test show that for all the four bearing pads, there is no big difference between load and deformation relationship before and after fatigue test. It is considered that the durability is good enough after loaded for 2,000,000 cycles.

Shear resistance

It is considered the shear stiffness will be the same for either longitudinal direction or perpendicular direction to the bridge axis when the shear strain is in the range of γ=50% in usual loading condition. The results of Ultimate compressional shear test show that the allowable shear strain under earthquake is less than γ=175%. This satisfies the value of 200%. However, for ability of shear deformation, state at shear strain of 200% is ultimate state.

Problems in future

1) Properties of rubber materials

The low temperature properties of the mixture of composed rubber and natural rubber is better than that of single composed rubber. However, the problem that the standard value of physical properties doesn't satisfy is caused by the consequence of blending. Therefore, either composed rubber or natural rubber should be used as the material of rubber bearing. It is prohibitive to blend the two.

2) Management of rubber properties

In the present, physical property tests are conducted on samples that are made in plant, not on prototype bearing pads. The vulcanized state and time are different between rubber samples and real rubber bearing pads, it is impossible that the test results from rubber samples completely represent the physical properties of real bearing pads. Therefore, it is necessary to perform physical property tests on samples obtained from real rubber bearing pads.

REMARKS

Both static and dynamic properties of rubber bearing pads have been widely investigated in laboratory for the purpose of enlarging the use of rubber bearings. However, comparison studies on used bearing pads from real bridges and commercial available new bearing pads are quit rare. Therefore, this study is significant.

Results from this study showed that it is not necessary to worry about the durability of rubber bearing pads and the aging effect on their physical properties. This has advantages in maintenance of rubber bearings. It will be expected, at the same time to improve the quality of rubber bearing, to revise the design conditions and to use rubber bearing positively.

REFERENCES

1) Nagoya Construction Bureau, JHPC, (1983), Analysis of factors resulting damages of bearing pads in Tome and Meshin expressway, Report in 1982.

2) Japan Road Association, (1973), Handbook of bearings in road bridges.

Session–4

Seismic Isolation Design–1

NZ–1) Seismic Isolation of Bridges in New Zealand
(Robinson, W. H.)

J–9) Manual for Menshin Design of Highway Bridges
(Kawashima, K.)

U–3) Application of AASHTO Seismic Isolation Design and Analysis Requirements to Bridges
(Mayes, R. L.)

SEISMIC ISOLATION OF BRIDGES IN NEW ZEALAND

W. H. Robinson

New Zealand Institute for Industrial Research and Development,
P O Box 31 310 , Lower Hutt, New Zealand.

ABSTRACT

Since starting our studies of seismic isolation in 1968 we have seen the field mature to the stage where, in New Zealand, it is standard practice for the seismic isolation option to be considered for both new and retrofitted bridges, and to a lesser extent, specialist structures and buildings. In this paper we describe two devices invented and developed in our laboratory, namely the lead-extrusion damper (LED) and the lead-rubber bearing (LRB). We list the bridges isolated in New Zealand to date, and describe some of the bridges in more detail.

INTRODUCTION

Our research team has been studying seismic isolation since 1968, initially as part of the Department of Scientific and Industrial Research (DSIR) and now within the new Research Institute structure.

The topic is of interest because of the seismic nature of the country. Our laboratory, and many of the structures with which we have been involved, are sited close to the Wellington fault, in New Zealand's most active seismic region, which is thought to be capable of generating $M_S = 7.5$ events at average intervals of 500-600 years. Various isolation and damping devices have been invented, tested and applied, including steel dampers, lead extrusion dampers (LEDs) and lead-rubber bearings (LRBs)[1,2].

The research has had three main components: experiments, theoretical work and application of the devices to real situations. Our 25 years of experience are summarised in a book "An Introduction to Seismic Isolation", by RI Skinner, WH Robinson and GH McVerry, to be published by Wileys early in 1993 [3]. The present paper is intended as a companion to the paper presented at the International Workshop on Recent Developments in Base Isolation Techniques for Buildings, Tokyo, April 1992 [4].

Our approach has changed over the years, evolving from one where we were attempting to produce devices which would withstand thousands of cycles to economic devices which would withstand less than 100 major cycles. This solution is closer to the requirements of seismic isolation of real structures, since all that is required is three to five major cycles during each significant earthquake. We have found that the level of protection afforded by seismic isolation is greater than can be provided by conventional strength measures, and a significant cost saving is often realised, amounting to 5 to 10 percent of the total cost of the structure in many cases.

The designs are all 'passive', requiring virtually zero maintenance. It is vital in all cases that the 'seismic gap', which allows the structure freedom to move during an earthquake, is kept secure at all times.

Technology transfer, both within New Zealand and in Japan and the USA, has been remarkably rapid. Technology transfer in Japan was initiated by Oiles Corporation.

In New Zealand we have interacted most successfully with the (then) Ministry of Works and Development (MWD), as well as with local consultants and the manufacturers. This interaction has both guided us and stimulated further research. For example, although the LED had only been invented in 1970, it was installed in two bridges (bridges 3 and 4 in Table 1) by 1974. Similarly, almost immediately after the invention in 1976 of the LRB, design proposals were produced to instal this method of seismic isolation in a new building (the William Clayton Building) and in the Toetoe Bridge. Independent design calculations for both the building and the bridge resulted in much the same values for the yield force-to-weight ratio and for the design displacement. These values were 0.07 and $\pm$100 mm respectively. These values are more or less typical for a wide range of bridges.

Table 1 shows the bridges seisimically isolated in New Zealand to date. In this table the abbreviations PSC (pre-stressed concrete) and UB (U-beam) have been used. It is seen that, to date, 49 bridges in New Zealand have been fitted or retrofitted with seismic isolation. Virtually all bridges suitable for retrofit have now been isolated. The option of seismic isolation for bridges is now routinely considered by engineers and their clients.

Several of the bridges shown in Table 1 are worthy of comment. Bridge (2) is a rail bridge with the superstructure supported on rocking piers , the damping being provided by steel torsional dampers. Bridges (21 to 24) and (32 to 35) have been retrofitted with sesimic isolation at the dates specified.

DEVICES AND THEIR APPLICATIONS

Steel dampers

Initial experiments involved the design and testing of various steel devices, both models and full-size devices. The major problem encountered was brittle failure at the welds. Nevertheless, with care successful designs were achieved, notably the cantilever design incorporated in the retrofit of seismic isolation at a major power substation at Haywards, near Wellington, and the 'E-type' damper used in the Rangitikei stepping bridge (See Table 1)

Lead-extrusion dampers (LEDs)

The LED, shown schematically in Figure 1, was developed [1] as the result of investigations into the possibility of using the plasticity of lead for energy absorption. The advantage of lead is that it does not fatigue at room temperature. Instead, a process of recovery, recrystallisation and grain growth occurs. The biggest problems encountered here were lubrication for the LED and containment of the lead for the various lead shear devices. Nevertheless, LEDs have been successfully developed, manufactured and installed, for example in the recently completed Wellington Central Police Station. Their first successful application in bridges was in two steeply sloping bridges over the Wellington motorway (Bridges 3 and 4 in Table 1) one of which is discussed in more detail below.

A complete discussion of the extrusion of lead and the principles of the LED is given in our book [3].

Lead-rubber bearings (LRBs)

Many of the problems associated with lead shear devices were solved by the development of the LRB [2]. The LRB in its simplest form comprises an elastomeric bearing, made of laminated layers of steel and rubber, with a lead insert in its centre. LRBs have been

installed in a variety of buildings all over the world and have proved particularly useful in the seismic isolation of new and existing bridges. Retrofit is particularly straightforward because the bridges are often already mounted on elastomeric bearings to accommodate thermal expansion and dimension changes due to curing of the concrete. Addition of a lead insert, together with establishment of a seismic gap, effectively incorporates seismic isolation.

LRBs are by far the most common form of isolation system for bridges. They are usually installed between the bridge superstructure and the supporting piers. One of the reasons for the popularity of this mode of seismic isolation is the fact that it combines the functions of isolation and hysteretic damping in a single compact unit, whilst supporting the weight of the superstructure and providing an elastic restoring force. The unit also allows for any differential movement and locks the structure in place during wind and traffic loading.

Figure 2 is a schematic drawing of the lead-rubber bearing. Figure 3 illustrates a typical force-displacement hysteresis loop. A complete discussion of the principles of the LRB is given in our book [3].

SEISMIC DESIGN OF BRIDGES

When detailing a bridge with a seismically isolated superstructure, care should be taken to give as much continuity as possible. Buffers and links should be provided to limit the maximum relative displacements between the superstructure and its supports, and between sections of the superstructure if it is not continuous over its whole length. With such precautions some damage may occur in the event of an extreme earthquake, but there should be no danger of collapse.

Care must be taken in detailing road surface links across seismic gaps. These must be designed to minimise the likelihood of the seismic gap becoming blocked and exerting forces which may seriously degrade the aseismic performance of the isolation system. As with isolated buildings, bridge builders must be clearly instructed on the aims and requirements of the isolation system, and bridge controllers must be clearly instructed on the maintenance which is required to ensure that the seismic isolation system may operate as intended.

Designs for seismically isolated New Zealand bridges were generally undertaken or reviewed by the Ministry of Works (MWD). Research and development work for the seismic design of New Zealand bridges, nonisolated and isolated, has been strongly supported by the National Roads Board with important results published in Road Research Unit (RRU) Bulletins and in various papers and reports. For example, RRU Bulletins 41 to 44 review work undertaken from 1975 to 1978 [5].

An approach to the seismic isolation of the superstructures of simple bridges was outlined by Blakeley [6], supported by charts giving maximum seismic responses of simple bridge models for a range of earthquake accelerations. Design requirements particular to bridges include the substantial non-seismic lateral displacements and loads to which the bridge may be subjected.

A procedure for the design of Japanese highway bridges with seismically isolated superstructures, referred to as the Menshin design method, is outlined by Matsuo and Hara [7].

EXAMPLES OF BRIDGES

Since 1973 49 road and rail bridges in New Zealand have been seismically isolated, as shown in Table 1. Most bridges suitable for the retrofitting of seismic isolation have now been fitted with this option. Further information on the seismic isolation of road bridges in New Zealand, including case studies and design procedures, is given by Blakeley [6], Billings and Kirkcaldie [8], and Turkington [9].

The first bridge to be seismically isolated in New Zealand was the Motu Bridge, built in 1973. The light-weight replacement superstructure was a 170m steel truss supported by the existing reinforced-concrete slab-wall piers. The superstructure was isolated using sliding bearings with the damping provided by vertical-cantilever structural-type steel columns.

A good example of the use of LRBs in bridges is illustrated in Figure 4, which shows the Moonshine Bridge, a 168 m prestressed concrete, curving bridge on a motorway in the Hutt area, New Zealand. In this case all of the bearings supporting the bridge deck contain lead inserts. Since the piles are circular in cross-section, these bearings operate in both the longitudinal and transverse directions.

Figure 5 shows a bridge over the Wellington Motorway which is fitted with LEDs at the lower abutment. It is one of a pair of sloping bridges which were seismically isolated by being mounted on glide bearings, the restoring force being provided by steel columns. The advantage of the extrusion dampers is that they lock the bridges in place during the braking of vehicles travelling downhill, yet at earthquake loads allow the bridges to move. Thermal expansion forces can be released by the creep of the extrusion dampers. After a large earthquake it is expected that the bridges will no longer have the seismic gaps ideally positioned. If necessary the bridges can then be jacked to the ideal position or allowed to creep back with the flexible columns providing the restoring force.

Examples of superstructure isolation systems in New Zealand which include longitudinal dampers to protect tall slab-wall piers founded in moderate-strength ground, are the Bannockburn bridge (Figure 6) and the Cromwell bridge, in Central Otago [12]. These bridges have partly submerged piers about 33mm high. The Bannockburn bridge has both abutments founded on ground of moderate strength. Each abutment is provided with three longitudinal lead-extrusion dampers, and hence they share the seismically-induced damping forces.The hysteretic dampers provide yield forces of 20 percent of the superstructure weight longitudinally and 10 percent transversely. The maximum displacements at the abutment-deck joints and of the bearings is limited to less than 100 mm. With the avoidance of yielding, limited ductility design procedures were adopted for the design of the piers. Moreover, inspection of the dampers indicates that lower-force creep displacements, arising from slow changes in superstructure length, are shared by the dampers at each abutment. In the case of the Cromwell bridge, one abutment has moderate strength, while the other abutment is founded on rock and is considerably stronger. For this bridge, a set of 6 U-type flexural steel-beam dampers, for longitudinal operation, was provided at the rock-based abutment.

PERFORMANCE OF SEISMICALLY ISOLATED BRIDGES

Of the buildings and bridges seismically isolated in New Zealand to date, only one, the Te-Teko bridge over the Rangitaiki River, has suffered the effects of a large earthquake. This was the Edgecumbe earthquake in March 1987, Richter magnitude 6.3, MM9, epicentre 9km north of the bridge. A strong-motion accelerograph located 11km south of the bridge recorded a peak horizontal ground acceleration of 0.33g. This bridge "provides an example of good performance of modern earthquake resistance technology, i.e., base isolation using

lead-rubber bearings"[10]. However, one of the standard elastomeric bearings elsewhere on the bridge was not properly restrained against sliding, and was thrown out of position, so that it ceased supporting the deck [11]. The behaviour of the bridge was, therefore, not perfect.

CONCLUSIONS

1. Of the 49 seismically isolated bridges in New Zealand, 40 use the lead-rubber bearing, 2 use lead extrusion dampers, one uses a combination of these and 6 use steel dampers.

2. The reason for the popularity of the LRB is that it combines, in a single unit, the functions of

    •decoupling the bridge deck from the piers
    •providing hysteretic damping
    •supporting the weight of the superstructure
    •locking the structure in place against wind and traffic loading.

3: In all cases it is vital that the seismic gap be kept secure

REFERENCES

1. W. H Robinson . & L.R. Greenbank, 1976. "An extrusion energy absorber suitable for the protection of structures during an earthquake", *Earthquake Engineering and Structural Dynamics* 4(3): 251-259.

2. W. H. Robinson, W.H., 1982. "Lead-rubber hysteretic bearings suitable for protecting structures during earthquakes", *Earthquake Engineering and Structural Dynamics* 10(4):593-604.

3. Skinner, R.I., W.H. Robinson and G.H. McVerry, "An Introduction to Seismic Isolation", Wileys, to be published 1993.

4. W. H. Robinson 1992, "Recent Developments in Seismic Isolation in New Zealand", International workshop on recent developments in base isolation techniques for buildings, Tokyo, April 1992. Companion paper

5. Road research bulletins:

• Road Research Unit, National Roads Board, Wellington, NZ, *Bulls. 41-44, 1979.*

• R. Park and R.W.G. Blakeley (1979), "Seismic Design of Bridges", *Road Research Unit, National Roads Board, NewZealand, Bull. 43*, 101-105.
• R.W.G. Blakeley (1979b), "Parameter Studies for (Bridge) Design", Road Research Unit, National Roads Board, NZ, Bulletin 43, 117-42

6. R.W.G. Blakeley (1987), "Analysis and Design of Bridges Incorporating Mechanical Energy Dissipating Devices for Earthquake Resistance", *Proc. NZ-Japan Workshop on Base Isolation of Highway Bridges, Technology Research Center for National Land Development, Japan,* New Zealand, November 1987.

7. Yoshiro Matsuo and Koji Hara (1991), "Design and Construction of Miyagawa Bridge (First Menshin Bridge in Japan)", *1st US-Japan Workshop on Earthquake Protective Systems for Bridges,* Buffalo, Sept. 1991.

8. I.J. Billings and D.K. Kirkcaldie (1985), "Base isolation of bridges in New Zealand". *Proc. Second Joint US-NewZealand Workshop on Seismic Resist. Highway Bridges ATC-12-1, May 1985,* Applied Technology Council, California, USA.

9.D.H. Turkington (1987), "Seismic Design of Bridges on Lead-rubber Bearings", *Research Report 87/2 Department of Civil Engineering, University of Canterbury, NZ, Feb. 1987,* 172 pages.

10. D.J. Dowrick (1987), "Edgecumbe Earthquake of March 2, 1987", *NZ Engineering*, 7-9.

11. R.I. Skinner and H.E. Chapman (1987), "Edgecumbe Earthquake Reconnaisance Report", M.J. Pender and T.W. Robertson eds., *Bull. NZ Nat. Soc. for Earthq. Eng.*, Vol. 20, No. 3, 239-240.

12. G.R. McKay, H. E. Chapman and D. K. Kirkcaldie (1990), "Seismic Isolation: New-Zealand Applications", *Earthquake Spectra*, Vol. 6, No. 2, 203-222.

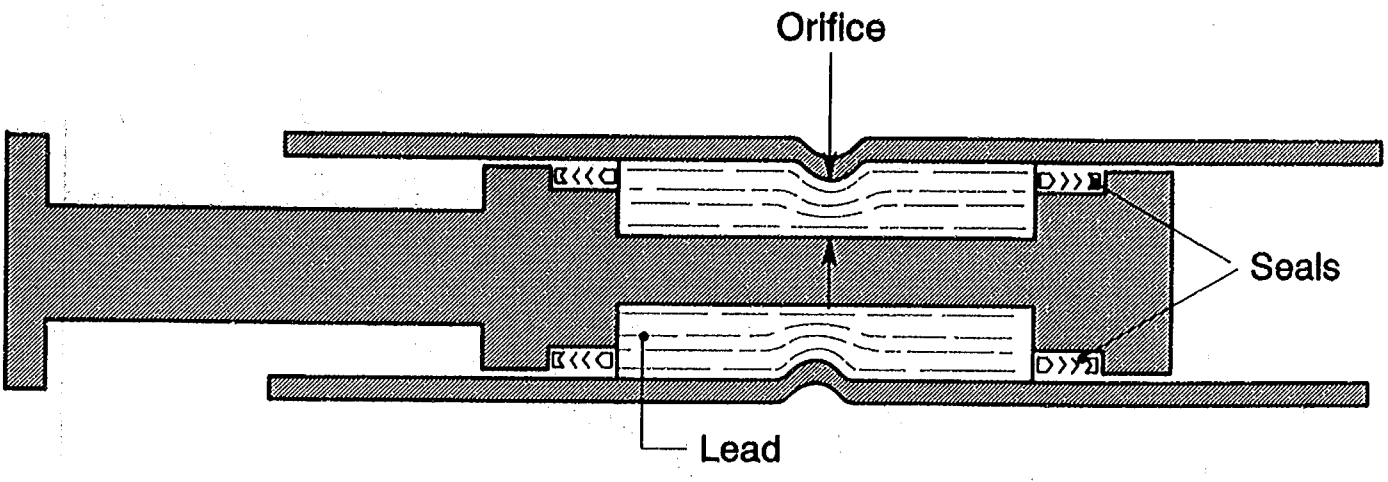


Figure 1: The lead-extrusion damper illustrating schematically the pistons, the tie rod joining them, the orifice and the seals containing the lubricant.

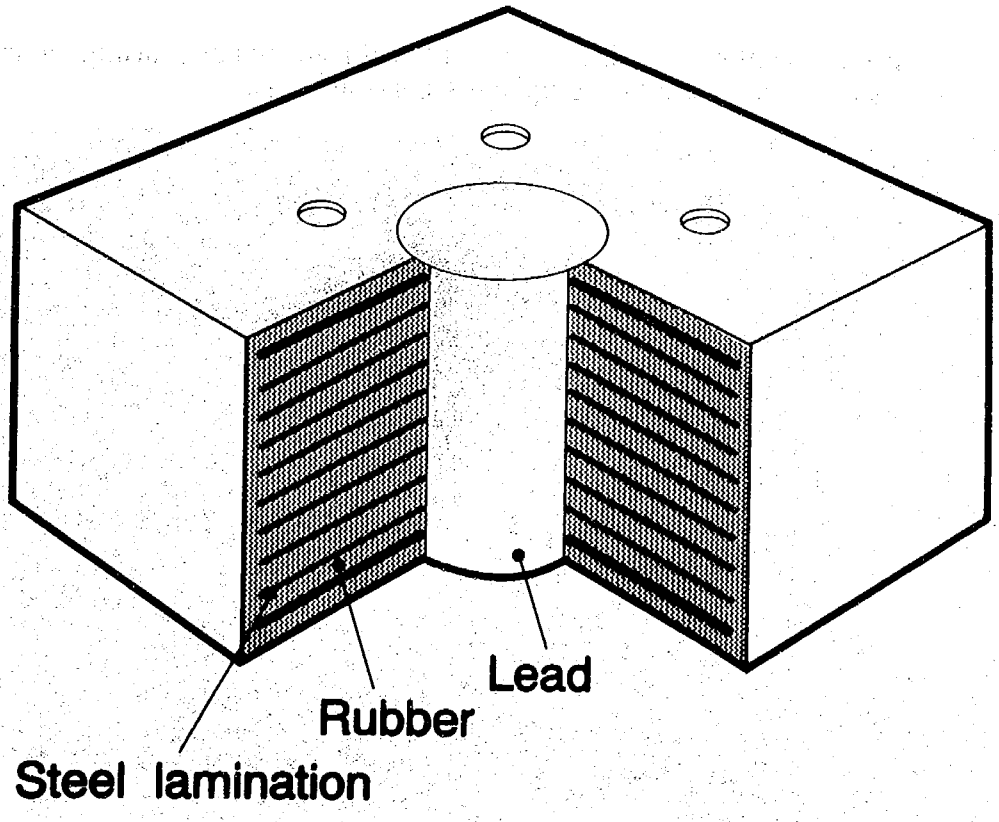


Figure 2: The lead-rubber bearing showing the lead insert, rubber and steel laminations.

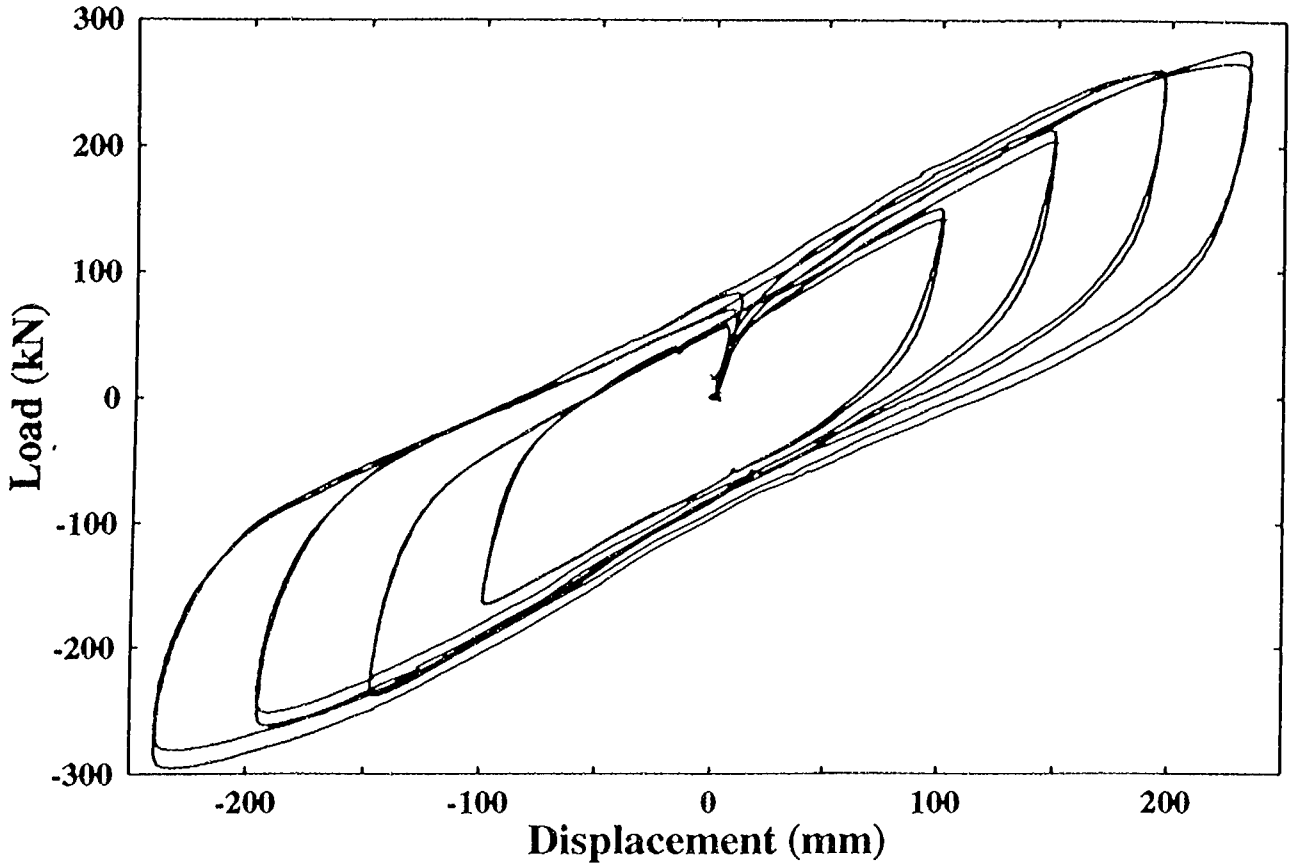


Figure 3: Force-displacement hysteresis loop for a typical lead-rubber bearing. Note the relatively high initial stiffness followed by a more compliant second stiffness.

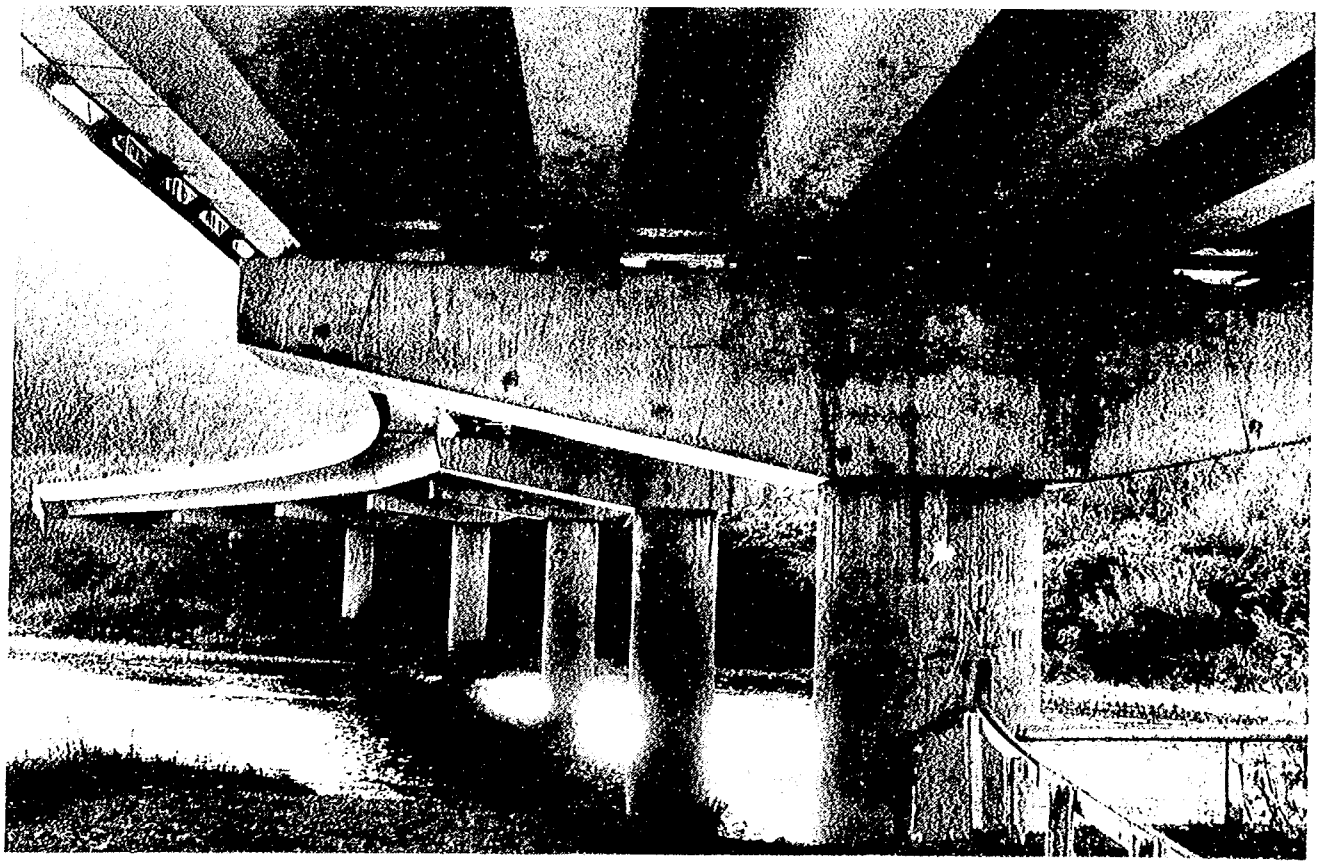


Figure 4: Moonshine Bridge over the Hutt River, Wellington, mounted on lead-rubber bearings.

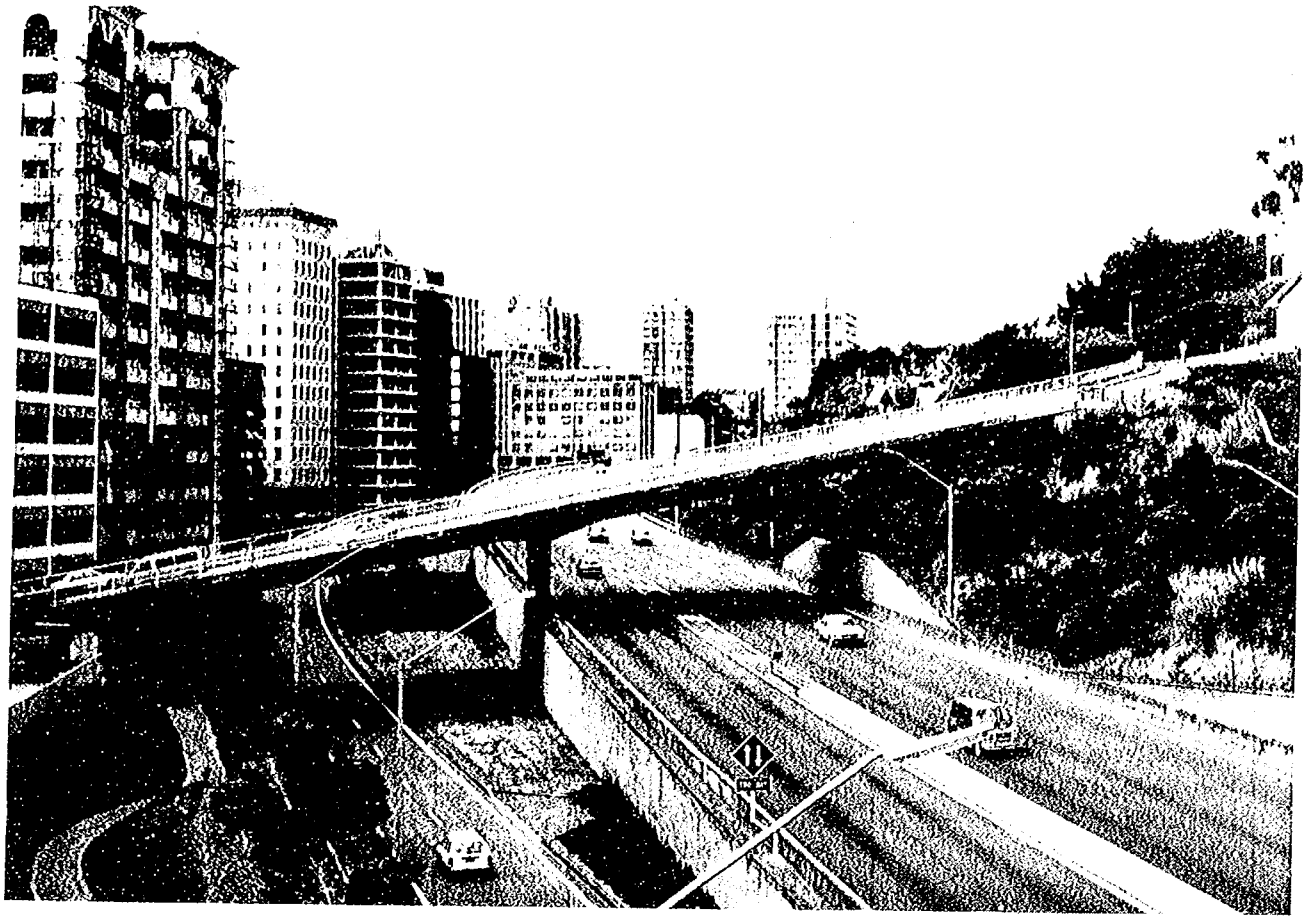


Figure 5:Aurora Terrace overpass, Wellington

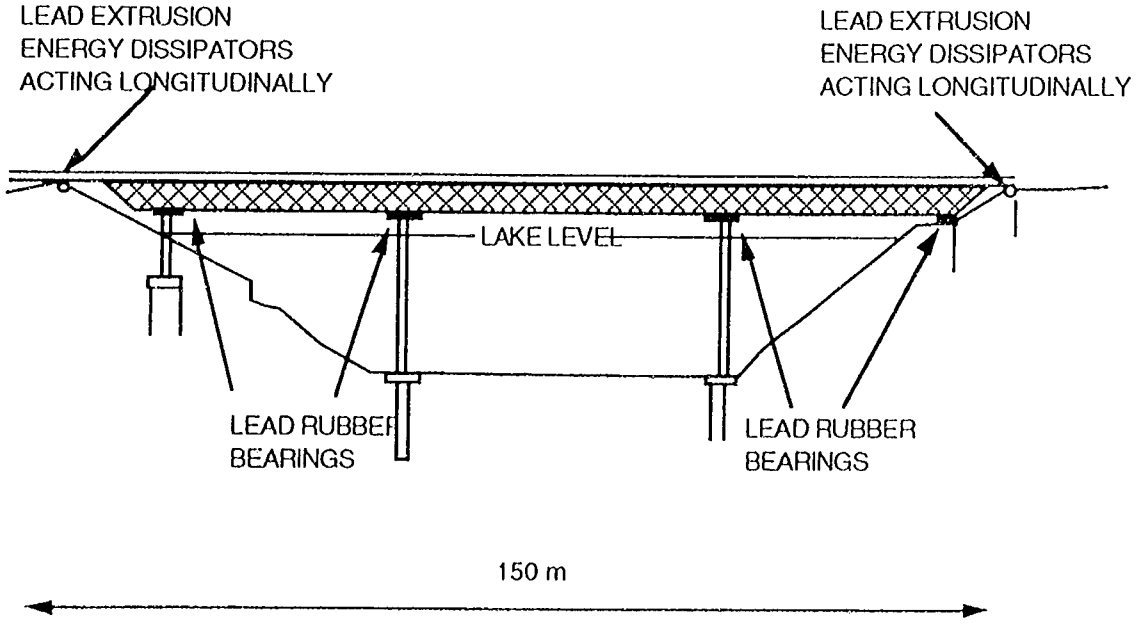


Figure 6: Schematic diagram of Bannockburn Bridge, Otago, New Zealand.

TABLE 1
Seismically Isolated Bridges in New Zealand

	Bridge Name	Superstructure Type	Length (m)	Isolation System	Date Built
1	Motu	Steel Truss	170	Steel UBs in flexture	1973
2	South Rangitikei viaduct	PSC Box	315	Steel torsion bar/rocking piers	1974
3	Bolton Street	Steel I Beam	71	Lead extrusion	1974
4	Aurora Terrace	Steel I Beam	61	Lead extrusion	1974
5	Toetoe	Steel Truss	72	Lead/rubber	1978
6	King Edward Street	PSC Box	52	Steel Cantilever	1979
7	Cromwell	Steel Truss	272	Steel flexural beam	1979
8	Clyde	PSC U-Beam	57	Lead/rubber	1981
9	Waiotukupuna	Steel Truss	44	Lead/rubber	1981
10	Ohaaki	PSC U-Beam	83	Lead/rubber	1981
11	Maungatapu	PSC Slab	46	Lead/rubber	1981
12	Scamperdown	Steel Box	85	Lead/rubber	1982
13	Gulliver	Steel Truss	36	Lead/rubber	1983
14	Donne	Steel Truss	36	Lead/rubber	1983
15	Whangaparoa	PSC I-Beam	125	Lead/rubber	1983
16	Karakatuwhero	PSC I-Beam	105	Lead/rubber	1983
17	Devils Creek	PSC U-Beam	26	Lead/rubber	1983
18	Upper Aorere	Steel Truss	64	Lead/rubber	1983
19	Rangitaiki (Te Teko)	PSC U-Beam	103	Lead/rubber	1983
20	Ngaparika	Steel Truss	76	Lead/rubber	1983
21-24	Hikuwai No. 1-4 (retrofit)	Steel Plate Girder	74-92	Lead/rubber	1983-4
25	Oreti	PSC I-Beam	220	Lead/rubber	1984
26	Rapids	PSC I & U-Beam	68	Lead/rubber	1984
27	Tamaki	PSC I-Beam	40	Lead/rubber	1985
28	Deep Gorge	Steel Truss	72	Lead/rubber	1984
29	Twin Tunnels	PSC I-Beam	90	Lead/rubber	1985
30	Tarawera	PSC I-Beam	63	Lead/rubber	1985
31	Moonshine	PSC U-Beam	168	Lead/rubber	1985
32	Makarika No. 2 (retrofit)	Steel Plate Girder	47	Steel Cantilever	1985
33	Makatote (retrofit)	Steel Plate Girder	87	Lead/rubber	1986
34,35	Kopuaroa No. 1 & 4 (retrofit)	Steel Plate Girder	25 & 55	Steel Cantilever	1986-7
36,37	Glen Motorway & Railway	PSC T-Beam	60	Lead/rubber	1987
38	Grafton No. 4	PSC T-Beam	50	Lead/rubber	1987
39	Grafton No. 5	PSC I-Beam	80	Lead/rubber	1987
40	Northern Wairoa	PSC I-Beam	492	Lead/rubber	1987
41	Ruamahanga at Te Ore Ore	PSC U-Beam	116	Lead/rubber	1987
42	Maitai (Nelson)	PSC I-Beam	93	Lead/rubber	1987
43	Bannockburn	Steel Truss	147	Lead/rubber & Lead extrusion	1988
44	Hairini	PSC Slab	62	Lead/rubber	
45	Limeworks	Steel Truss	72	Lead/rubber	1989
46	Waingawa	PSC U-Beam	135	Lead/rubber	1990
47	Mangaone	Steel Truss	52	Lead/rubber	1990
48	Porirua State Highway	PSC T-Beam	38	Lead/rubber	1992
49	Porirua Stream	PSC U-Beam	84	Lead/rubber	1992

MANUAL FOR MENSHIN DESIGN OF HIGHWAY BRIDGES

Kazuhiko KAWASHIMA

Head, Earthquake Engineering Division, Eartrhquake Disaster Prevention Department, Public Works Research Institute, Ministry of Construction, Tsukuba Science City, Japan

ABSTRACT

A three-year research program on "Development of Menshin Design of Highway Bridges" was made from April 1989 to March 1992. Concentrated efforts were paid to develop energy dissipating devices and falling-off prevention devices for bridges. An appropriate design method of highway bridges with energy dissipating devices and favorable application of the menshin design to highway bridges were studied. Final accomplishment of the three-year research was compiled in the form of "Manual for Menshin Design of Highway Bridges" in March 1992. This paper outlines the Manuals.

INTRODUCTION

A three-year Joint Research Program between the Public Works Research Institute and 26 groups consisting of 28 private firms on "Development of Menshin Design of Highway Bridges" was made from April 1989 to March 1992. This program intended to develop a rational seismic design method of highway bridges with energy dissipating devices. The highway bridges with span length from 20 m to 100 m were considered as the major target for this Joint Research Program.

As will be discussed later, "menshin" means "reduction of response" in Japanese. Although the menshin design is close with the base-isolation, natural period of bridge is not forcibly elongated in the menshin design, because there are various restrictions for increasing the natural period. Instead of elongating the natural period, emphasis is placed in the menshin design for increasing energy dissipating capability and distribution of lateral force to as many substructures as possible for decreasing lateral force for design of substructures.

As shown in **Table 1**, concentrated efforts were paid to 1) development of

menshin (energy dissipating) devices for highway bridges, 2) development of falling-off prevention devices and expansion joints appropriate for the menshin bridges, 3) development of rational and simple menshin design method and 4) favorable application of menshin design to highway bridges.

In the research project, four high damping rubber bearings, 2 sliding friction dampers, a steel damper, a roller menshin bearing a link bearing and a viscous damper were newly developed for bridges (refer to **Fig. 1**). The menshin devices for highway bridges have to be more compact and more weather-proof than the base-isolation devices for buildings since the menshin devices are installed at narrow and exposed crest of bridge columns.

The knock-off mechanism at an abutment to ease the impact force induced by the collision between the deck and the abutment (refer to **Photo 1**), and a finger type expansion joint (refer to **Photo 2**) which is distinguished from regular finger joints by the transverse movement as well as the longitudinal movement were also developed.

In the research project, a simple but rational menshin design method was developed. A series of shaking table tests were made to study the response of menshin bridges, and to provide realistic data of the seismic response of menshin bridges (refer to **Photo 3**). Analysis of strong motion records measured at a menshin bridge was also made.

From the study to investigate the favorable application of menshin design, it was found that the menshin design is effective for constructing super-multi-span continuous bridge with total deck length over 1 km. Application of the menshin design for seismic retrofit of exiting bridges and deck connection for making existing simply supported girder bridges continuous was also studied (refer to **Photo 4**).

The reports of the project were compiled and published by the Public Works Research Institute in the form of the Joint Research Report. As well as these reports, as the final accomplishment of the three-year research program, the Manual for Menshin Design of Highway Bridges was compiled.

This paper presents the outline of the Manual.

SCOPES AND CONTENTS OF THE MANUAL

The Manual presents the seismic design method of highway bridges including

design details when "the Structures Expecting Reduction of Inertia Force", which is specified in the "Part V Seismic Design" of the "Specifications of Design of Highway Bridges", is adopted. Application of the menshin design to seismic strengthening of substructures and connection of adjacent decks for making existing simply supported girder bridges continuous is also presented.

It should be noted that although the description of the Manual is given in the format of the specifications, it merely represents the accomplishments of the three-year research program, and it is not the mandate specifications.

The table of contents of the Manual is as follows:

1. General
   1.1 Scope of Application
   1.2 Definition of Terms
2. Basic Principle of Menshin Design
3. Menshin Design
   3.1 General
   3.2 Lateral Force Coefficient for Seismic Coefficient Method
   3.3 Lateral Force Coefficient and Equivalent Lateral Force Coefficient for Bearing Capacity Method
   3.4 Characteristics value for Menshin Devices
   3.5 Computation of Natural Period of Bridge
   3.6 Computation of Modal Damping Ratio of Bridges
4. Design of Menshin Devices
   4.1 Basic Principle for Design of Menshin Devices
   4.2 Design of Laminated Rubber Bearings
   4.3 Design of Lead Rubber Bearings
   4.4 Design of High Damping Rubber Bearings
   4.5 Design of Steel Dampers
   4.6 Design of Friction Dampers
   4.7 Design of Viscous Dampers
   4.8 Design of Roller Dampers
5. Dynamic Response Analysis
   5.1 General
   5.2 Dynamic Response Analysis Method
   5.3 Analytical Models
   5.4 Design Seismic Forces

5.5 Check of Safety
6. Design Details
6.1 General
6.2 Gap between Structures
6.3 Falling-off Prevention Devices
6.4 Knock-off Devices
6.5 Details of Expansion Joints
7. Approving Tests of Menshin Devices
7.1 General
7.2 Approving Tests for Confirming Requirements for Dynamic Loads
7.3 Approving Tests for Confirming Requirements for Static Loads
8. Seismic Retrofit of Existing Bridges with Use of Menshin Design
9. Application of Menshin Design for Making Existing Simply Supported Girder Bridges Continuous

Appendices
1. Procedure of Menshin Design
2. Menshin Devices for Highway Bridges
3. References for Dynamic Response Analysis
4. Expansion Joints and Falling-off Prevention Devices for Highway Bridges
5. Design Example of Prestressed Concrete Bridges
6. Design Examples of Steel Girder Bridges
7. Design Examples of Super-multi-span Continuous Bridges
8. Design Examples for Seismic Retrofit
9. Design Examples for Making Existing Simply Supported Girders Continuous
10. Standard Acceleration Ground Motions Recommended for Dynamic Response Analysis

BASIC PRINCIPLE OF MENSHIN DESIGN

Whether the menshin design should be adopted or not has to be decided based on the advantages of increasing energy dissipating capability from not only seismic safety but function at normal time.

In general, menshin design can be adopted with advantage for the following conditions:

1) bridges on stiff and stable soils
2) bridges with stiff substructures with short natural period

It is recommended that the natural period of the bridge designed by the menshin design is at least 1.5 times longer than that of the bridge without menshin devices. Such elongation of the natural period of the menshin bridge makes the coupling vibration so small that the deformation of the bridge be concentrated at the menshin devices.

The most important decision of the menshin design is how much increase of the natural period be made. In Japan soils are generally very weak at the bridge construction sites. Significant earthquakes with magnitude over 8, which produce long period ground motions, occur at shorter recurrence period than other countries. Taking account such evidences into account, the design seismic force level is take very high for design of highway bridges in Japan in comparison with the seismic force level adopted in U.S.A., New Zealand and Italy. The natural period at which the design acceleration decrease with increasing the natural period is taken longer, i.e., 1.1 second for type I soils (stiff site), 1.3 second for type II soils (medium site) and 1.5 second for type III soils (soft soils). Therefore, the advantage for reducing deck response can be realized only by elongating the natural period longer than 1.1 $\sim$ 1.5 second.

However elongation of the natural period brings the increase of the deck response displacement, and this requires the adoption of joints with long legs. This is, however, a crucial requirements difficult to adopt, in particular, for overcrossing in city area because it causes noise and vibration pollution, which is the most serious concern in city area. Furthermore it will have the disadvantage for maintenance because replacement of the damaged expansion joint due to traffic load as well as the pavement adjacent to the joint has to be frequently made.

Based on these reasons, it is not adopted to forcibly elongate the natural period in order to decrease the deck response acceleration. It is therefore more appropriate to adopt the concept of base isolation not for elongating the natural period but for increasing energy dissipating capability. Distribution of the inertia force to as many substructures as possible, which is the practice adopted in Japan for long time, is also significantly advantageous.

Therefore basic principle recommended for introducing the base isolation to highway bridges in Japan is as follows :

1) Distribute the inertia force to many substructures so intentionally that the inertia force be distributed equally by selecting the spring stiffness of the isolators. Simultaneously, reduce deck response by increasing energy dissipating capability by means of damper.

2) Do not forcible elongate the natural period, but select the natural period so that the resonance of the bridge with soils be avoided.

Such design criteria is no more the "isolation" of the "base". Therefore it is proposed to call the design concept as "menshin". The "menshin" means "reduction of seismic response" in Japanese.

In menshin design, bridges can be designed by following the standard static design method (static frame analysis). More precise approve of the seismic safety can be made by the dynamic response analysis, if required. In such analyses, the menshin devices (isolators and dampers) are idealized by as a set of equivalent linear springs. Equivalent stiffness and the equivalent damping ratio of the isolator and damper are the major parameters used in the analyses. In the static frame analysis, natural period of the bridge can be computed for each seismic design structural unit as :

$$T = 2.01\sqrt{\delta} \tag{1}$$

$$\delta = \frac{\int w_i \cdot u_i^2}{\int w_i \cdot u_i} \tag{2}$$

where

T :natural period (sec)

w_i :dead weight (tf/m) of the seismic design structural unit (super structure and substructure above the ground surface assumed in seismic design) at point "i"

u_i :lateral displacement (m) developed in the seismic design structural unit at point "i" when subjected to w_i in the direction considered in design

Damping ratio of the bridges is computed as

$$h = \frac{\Sigma K_{Bi} \cdot u_{Bi}^2 \cdot c_{hi}}{\Sigma K_{Bi} \cdot u_{Bi}^2 \cdot c_i} \tag{3}$$

$$c_{hi} = h_{Bi} + \frac{h_{Pi}}{K_{Pi}} + \frac{h_{Fui}}{K_{Fui}} + \frac{h_{F\theta i} \cdot H^2}{K_{F\theta i}}$$

$$c_i = 1 + \frac{K_{Bi}}{K_{Fi}} + \frac{K_{Bi}}{K_{Fui}} + \frac{K_{Bi} \cdot H^2}{K_{F\theta i}}$$

where

h :Modal damping ratio of bridge
h_{Bi} :Damping ratio of i-th damper
h_{Fi} :Damping ratio of i-th pier/abutment
h_{Fui} :Damping ratio of i-th foundation associated with translational movement
$h_{F\theta i}$:Damping ratio of i-th foundation associated with rotation
K_{Fi} :Equivalent stiffness of i-th pier/abutment
K_{Fui} :Translational stiffness of i-th foundation
$K_{F\theta i}$:Rotational stiffness of i-th foundation
u_{Bi} :Design displacement of i-th menshin device
H :Height from the bottom of pier to the gravity center of deck

Eq.(3) give the approximate estimation of the damping ratio of bridge assuming that translation and rotation of the foundation are developed only by the inertia force of the deck. When the effect of the inertia force of piers and abutments for evaluating the translation and rotation of the foundation can not be disregarded, it is appropriate to compute the modal damping ratio as

$$h = \frac{\sum_{j=1}^{n} \phi_{ij}^T \cdot h_j \cdot k_j \cdot \phi_{ij}}{\phi_i^T \cdot K \cdot \phi_i} \qquad (4)$$

where

ϕ_{ij} :Mode vector of j-th structural component for i-th mode
h_j :Damping ratio of j-th structural component
k_j :Stiffness matrix of j-th structural component
ϕ_i^T :Mode vector of bridge for i-th mode
K :Stiffness matrix of bridge

Table 2 shows the damping ratio recommended for structural components for Eqs.(3) and (4).

DESIGN FORCE FOR MENSHIN DESIGN

In menshin design, the menshin devices are designed by the Seismic Coefficient Method and the Bearing Capacity Method. In both method, the lateral force is

statically applied to the bridge, and the seismic safety is examined based on the allowable stress design approach in the Seismic Coefficient Method and bearing capacity basis considering ductility in the Bearing Capacity Method. Bridges are designed by the Seismic Coefficient Method, and then the ductility is checked for reinforced concrete piers by the Bearing Capacity Method.

In the Seismic Coefficient Method, the design lateral force coefficient k_h is given as

$$k_h = c_Z \cdot c_G \cdot c_I \cdot c_T \cdot c_E \cdot k_{h0} \geqq 0.1$$

where

$$c_T \cdot c_E \geqq 0.8 \qquad (5)$$

where

k_h :Lateral force coefficient
c_Z :Modification factor for zone (refer to **Fig. 2**)
c_G :Modification factor for ground condition (refer to **Table 3**)
c_I :Modification factor for importance (refer to **Table 4**)
c_T :Modification factor for structural response (refer to **Table 5**)
c_E :Modification factor for energy dissipation capability (refer to **Table 6**)
k_{h0} :Standard design horizontal seismic coefficient (= 0.2)

Those factors excluding c_E are the ones specified in the Specifications of Design of Highway Bridges. The modification coefficient c_E takes a value as shown in Table 6 depending on the first modal damping ratio of the bridge. Reduction of the design lateral force as large as 20 % is proposed in the Manual.

In the Bearing Capacity Method, the lateral force coefficient k_{ho} and the equivalent lateral force coefficient k_{he} are given as

$$k_{he} = \frac{k_{h0}}{\sqrt{(2\mu - 1)}} \geqq 0.3 \qquad (6)$$

$$k_{ho} = c_Z \cdot c_I \cdot c_R \cdot c_E \cdot k_{h0} \qquad (7)$$

where

k_{he} :Equivalent lateral force coefficient for Bearing Capacity Method
k_{ho} :Lateral force coefficient for Bearing Capacity Method

c_z :Modification factor for zone (refer to **Fig. 2**)

c_I :Modification factor for importance (refer to **Table 4**)

c_R :Modification factor for structural response (refer to **Table 7**)

c_E :Modification factor for energy dissipation capability

k_{hc0} :Standard lateral force coefficient for Bearing Capacity Method (=1.0)

μ :Allowable ductility factor of reinforced concrete piers

The modification factors excluding c_E are the ones specified in the Specifications of Design of Highway Bridges. The modification factor c_E depends on the modal damping ratio of the bridge, and takes a value of **Table 8.** Reduction of the design force as large as 30 % is proposed.

DESIGN OF MENSHIN DEVICES

Characteristics Value of Menshin Devices

In the menshin design, the displacement assumed in design for the devices u_B (design displacement of menshin device), the equivalent stiffness K_B and the equivalent damping ratio h_B of the menshin device are the key factors. They are evaluated as:

(1) Design Displacement of Menshin Device

The design displacement of menshin device is evaluated as

$$u_B = \frac{k_h \cdot W_u}{K_B} \quad \text{(S. C. Method)} \tag{8}$$

$$u_B = \frac{k_{hc} \cdot W_u}{K_B} \quad \text{(B. C. Method)} \tag{9}$$

where

u_B :Design displacement (m) of menshin device

k_h :Lateral force coefficient by Eq.(5) for Seismic Coefficient Method

k_{hc} :Lateral force coefficient by Eq.(6) for Bearing Capacity Method

K_B :Equivalent stiffness (tf/m) of menshin device

W_u :Weight of superstructure (tf) supported by the menshin device

(2) Equivalent Stiffness and Equivalent Damping Ratio

The equivalent stiffness and the equivalent damping ratio of menshin device are evaluated from the hysteresis loops as

$$K_B = \frac{F(u_{BE}) - F(-u_{BE})}{2u_{BE}} \quad (10)$$

$$h_B = \frac{\Delta W}{2\pi W} \quad (11)$$

where

K_B :Equivalent stiffness (tf/m) of menshin device

h_B :Equivalent damping ratio of menshin device

u_{BE} :Effective design displacement (m) of menshin device, and is given as

$$u_{BE} = c_B \cdot u_B \quad (12)$$

u_B :Design displacement (m) of menshin device

c_B :Modification coefficient for evaluating the effective design displacement (=0.7)

$F(u)$:Lateral force required to produce u for the menshin device

W :Strain energy induced in menshin device associated with c_{BE} displacement (refer to **Fig. 3**)

ΔW :Energy dissipated in menshin device per cycle (refer to **Fig. 3**)

Requirements for Dynamic Load

(1) Menshin devices have to be designed and fabricated so that their equivalent stiffness K_B and equivalent damping ratio h_B be within $\pm$ 20 % of the design values. The equivalent stiffness K_B and equivalent damping ratio h_B for this requirement have to be evaluated by Eqs. (10) and (11), and they shall be the ones averaged over K_B and h_B from 4th to 10th loading hysteresis among 10 cyclic loading reversals with harmonic displacement of c_{BE}. This is because deck acceleration and displacement are within tolerable range when the scatter of equivalent stiffness and the equivalent damping ratio are within $\pm$ 20 % of the design values. However, the devices which produce unstable hysteretic behavior should not be adopted.

(2) Menshin devices have to be stable against 50 cycles of harmonic loading with displacement of u_B. The number of 50 was determined from the fact that number of load reversals developed during a major earthquake may be about 30. About 50 % tolerance was included in 50.

(3) Deck should return to the rest position even after it was subjected to a large earthquake. Therefore the residual displacement developed in menshin

devices after smoothly releasing from the deformed displacement of u_B by Eq. (9) has to satisfy

$$u_{BR} \leqq 0.1 \cdot u_B \qquad (13)$$

where

u_{BR} :Residual displacement (cm)

u_B :Design displacement(cm) of menshin device by Eq. (9)

(4) The equivalent stiffness and the equivalent damping ratio of menshin devices have to be stable against the change of load condition at normal time, change of natural environment such as the temperature change and cyclic loading developed by an earthquake. Stability has to be examined against the following requirements:

1) cyclic loading due to elongation and shrinkage of deck due to the temperature change and the active load
2) effect of loading hysteresis
3) variation of vertical loading
4) effect of loading rate
5) effect of pre-deformation due to creep and shrinkage
6) direction of excitation
7) change of the equivalent stiffness and the equivalent damping ratio depending on the temperature change

Requirements for Static Load

(1) Materials and mechanism of menshin devices have to give credit to long term use. They have to be stable against cyclic elongation and shrinkage of deck due to temperature change.

(2) Menshin devices have to be stable against local shear strain. Check of the local shear strain has to be made in accordance of "3.6 Design of Rubber Bearings" of the "Design Guidelines of Bearings".

(3) For rubber-type menshin devices, the creep of rubber in vertical direction due to dead weight of superstructure shall not exceed 5 % of total thickness of the rubber.

(4) The equivalent stiffness of menshin device at -10 ℃ normalized by the equivalent stiffness at 40 ℃ shall not exceed 1.5. Because the temperatures of -10 ℃ and 40 ℃ is for moderate climate area, at cold area they have to be

decided based on the appropriate site condition.

(5) Menshin devices have to have appropriate initial stiffness so that harmful displacement of deck due to non-seismic lateral force such as wind effects be avoided.

APPROVING TESTS OF MENSHIN DEVICES

General

Because the menshin device is one of the the important structural components of menshin bridges, their requirements have to be well approved by the tests. There are various types of menshin devices for use of bridges. Based on the mechanism for producing the energy dissipation, the devices may be classified into three groups as

(a) displacement dependent type,
(b) friction force type, and
(c) velocity dependent (viscous) type.

The approving tests for the menshin devices are presented in the Manual for each of the three types.

Approving Tests for Dynamic Loads

For approving the requirements for dynamic loads presented in **5.2**, the following approving tests are provided in the Manual.

(1) Approving test for confirming the equivalent stiffness and the equivalent damping ratio

(2) Approving test for confirming stableness against 50 cycles harmonic load reversals with u_B displacement

(3) Approving test for confirming residual displacement requirement

(4) Approving tests for confirming stableness against variation of load condition at normal time, change of natural environment such as the temperature change and cyclic loading developed by an earthquake. These tests include :

(a) Stableness against Cyclic Load Reversals

Some menshin devices have the dependence of the equivalent stiffness and the

equivalent damping ratio on number of cyclic loading. Because considerable change of these parameters during an earthquake produces bridge response significantly different from the one assumed in design, it is not desirable.

(b) Stableness against Load Hysteresis

In some menshin devices, the equivalent stiffness and the equivalent damping ratio depend on the past experience, in particular, the largest deformation ever experienced. Such dependence of K_B and h_B on the hysteresis ever experienced is significant, it produces different bridge response during an earthquake. Therefore, effect of load hysteresis has to be examined.

(c) Stableness against Change of Compression Force

Compression force applied to the menshin device due to dead weight of superstructure may change associated with the error involved in construction stage and settlement of substructure. If the menshin device shows significantly different stiffness and damping properties due to such change of compression force, it brings different structural response . Therefore, stableness of the equivalent stiffness and the equivalent damping ratio of menshin devices have to be checked.

(d) Stableness against Change of Loading Rate

Because loading rate to the menshin devices is not the same during excitation, dependence of the equivalent stiffness and the equivalent damping ratio on the loading rate has to be examined.

(e) Stableness against Pre-deformation

Menshin devices often start to deform from the displacement drifted to the rest point. This is actually developed if an earthquake occurs when the menshin devices deform due to the deck elongation associated with temperature change and shrinkage of concrete. Because the equivalent stiffness and the equivalent damping ratio depend on the amount of such pre-deformation, their properties have to be checked.

(f) Stableness against Temperature Change

Menshin device have to be stable against daily and yearly change of temperature.

Approving Tests for Static Loads

For approving the requirements for static loads presented in 5-3, the following tests are required.

(1) Approving test for confirming durability and stableness against cyclic loading associated with the daily and yearly elongation and shrinkage of deck.

(2) Test for evaluating the stiffness of menshin devices subjected to extremely low-rate deformation such as the one encountered due to yearly temperature change and concrete creep. The stiffness of the menshin device during such low-rate deformation is quite important in static design for computing the lateral force developed in substructures due to the temperature change and shrinkage of concrete.

(3) Approving test for confirming the dependence of the equivalent stiffness of menshin device on temperature.

Two examples of the Approving Test

Approving test methods presented in **6.2** and **6.3** are precisely described in the Manual for each of the displacement dependent type devices, friction force type devices and the velocity dependent type devices. As the example of such approving tests, the test method for confirming stableness against cyclic loading and the test method for confirming the effect of loading rate are briefly described for the displacement dependent type devices in the following.

(1) Approving Test for Confirming Stableness against Cyclic Loads

At the room temperature of 20 ℃ apply 10 cycles of harmonic lateral load to the menshin device with loading displacement of u_B computed by Eq. (9) or smaller and with the frequency of 0.5 Hz. The vertical load equivalent to the design dead load shall be simultaneously applied. The equivalent stiffness and the equivalent damping ratio from the test have to satisfy Eqs. (14) and (15).

$$R_{KC} = \frac{|K_{BJ} - K_{Bm}|}{K_{Bm}} \begin{cases} \leqq 0.3 \quad (j=1,2,3) \\ \leqq 0.1 \quad (j=4,5\cdots10) \end{cases} \tag{14}$$

$$R_{hC} = \frac{|h_{BJ} - h_{Bm}|}{h_{Bm}} \begin{cases} \leqq 0.3 \quad (j=1,2,3) \\ \leqq 0.1 \quad (j=4,5\cdots10) \end{cases} \tag{15}$$

where

R_{KC} :Variation ratio of equivalent stiffness

R_{hC} :Variation ratio of equivalent damping ratio

K_{Bj} :Equivalent stiffness at j-th load reversal(tf/m)

K_{Bm} :Averaged equivalent stiffness by Eq. (16)

h_{Bj} :Equivalent damping ratio at j-th load reversal

h_{Bm} :Averaged damping ratio by Eq. (17)

$$K_{Bm} = \frac{1}{7} \sum_{j=4}^{10} K_{Bj} \tag{16}$$

$$h_{Bm} = \frac{1}{7} \sum_{j=4}^{10} h_{Bj} \tag{17}$$

Being different with Eqs. (10) and (11), the equivalent stiffness and the equivalent damping ratio for the approving tests are defined as

$$K_B = \frac{F(u_B) - F(-u_B)}{2u_B} \tag{18}$$

$$h_B = \frac{\Delta W}{2\pi W} \tag{19}$$

where

K_B :Equivalent stiffness (tf/m) of menshin device

h_B :Equivalent damping ratio of menshin device

u_B :Design displacement (m) of menshin device

$F(u)$ Lateral force (tf) required to produce u displacement for the menshin device

W :Strain energy (tfm) induced in menshin device associated with u_B displacement (refer to Fig. 4)

ΔW :energy dissipated in menshin device per cycle (refer to Fig. 4)

(2) Approving Test for Confirming the Stableness against Loading Rate

At the temperature of 20 ℃ apply 10 cycles of harmonic load with the displacement equivalent to either 100 % of the total thickness of rubber or ± 15 cm. Frequency of the load reversal shall be 0.1 Hz, 0.5 Hz and 1.0 Hz. The equivalent stiffness and the equivalent damping ratio have to satisfy Eqs. (20) and (21).

$$R_{Kf} = \frac{|K_{Bmj} - K_{Bm1}|}{K_{Bm1}} \leqq 0.2 \quad (j=1,2) \tag{20}$$

$$R_{hf} = \frac{| h_{Bm1} - h_{Bmj} |}{h_{Bm1}} \leqq 0.2 \quad (j=1,2) \qquad (21)$$

where

R_{Kf} :Variation ratio of equivalent stiffness

R_{hf} :Variation ratio of equivalent damping ratio

K_{Bm1}, K_{Bm2}, K_{Bm3}:Equivalent stiffness by Eq. (16) at frequency of 0.5 Hz, 0.1 Hz and 1.0 Hz, respectively

h_{Bm1}, h_{Bm2}, h_{Bm3}:Equivalent damping ratio by Eq. (17) at frequency of 0.5 Hz, 0.1 Hz and 1.0 Hz, respectively

CONCLUDING REMARKS

Excluding specially long-span bridges, it is not easily adopted for highway bridges to reduce the lateral force by forcibly elongating the natural period, because seismic force level is very high even at long natural period, and because the increase of deck response displacement brings various problems such as environmental pollution. Therefore the menshin design, which places emphasis not on the forcible elongation of the natural period but on the increase of energy dissipating capability and distribution of inertia force of superstructure to as many substructures as possible, is proposed. By the menshin design, it is proposed to decrease the lateral force as large as 20 % for the Seismic Coefficient Method and 30 % for the Bearing Capacity Method.

ACKNOWLEDGEMENTS

For executing the three-year joint research project, various supports and encouragement were obtained from many organizations including the Head-quarters of the Ministry of Construction. Without endeavour of more than 130 participants from the Public Works research Institute and 28 private firms, this project could not be successfully made. The author expresses his sincere thanks for all who participated in this Joint Research Program.

REFERENCES

1) Public Works Research Institute and 28 Private Firms : Report of the Joint Research on Menshin Systems for Highway Bridges, No. 1, July 1990, No. 2,

July 1991 and No. 3, March 1992, Joint Research Report, No. 44, No. 60 and No. 75, Public Works Research Institute (in Japanese)
2) Public Works Research Institute and 28 Private Firms : Manual for Menshin Design of Highway Bridges (Draft), March 1992, Joint Research Report, Public Works Research Institute (in Japanese)
3) Japan Road Association : Part V Seismic Design of the Specifications of the Design of Highway Bridges, February 1990 (in Japanese)
4) Technology Research Center for National Land Development : Guidelines for Base Isolation of Highway Bridges, March 1989 (in Japanese)
5) Japan Road Association : Guide-Specifications of Design of Bearings, July 1991 (in Japanese)
6) Buckle, I. G. and Mayes, R. L. : Seismic Isolation : History, Application and Performance - A World View, Earthquake Spectra, Vol. 6, No. 2, May 1990
7) AASHTO : Guide Specifications for Seismic Isolation Design, June 1991
8) McKay, G. R., Chapman, H. E. and Kirkcaldie, D. K. : Seismic isolation : New Zealand Application, Earthquake Spectra, Vol. 6, No. 2, May 1990
9) Guidelines for Seismic Design of Bridges with Isolation/Dissipator Devices, Antiseismic Protection of Structures on the Autostrade S.p.A/ Network, October 1991
10) Kawashima, K., Hasegawa, K. and Nagashima, H. : A Perspective of Menshin Design for Highway Bridges in Japan, Proc. 1st U.S.-Japan Workshop on Earthquake Protective Systems of Highway Bridges, National Center for Earthquake Engineering Research, Buffalo, N.Y., U.S.A., September 1991
11) Kawashima, K., Hasegawa, K. and Nagashima, H. : Experiment and Analysis on Seismic Response of Menshin Bridges, Proc. 1st U.S.-Japan Workshop on Earthquake Protective Systems of Highway Bridges, National Center for Earthquake Engineering Research, Buffalo, N.Y., U.S.A., September 1991

Table 1 Research Theme and Organizations of Joint Research Program between the Public Works Research Institute and 28 Private Firms for Developing Menshin Design Method of Highway Bridges

Research Theme	P	Ka	Si	Ob	Ku	Tn	H	Ni	Su	M	G	Ok	Ti	I	Nk	Ko	Ns	Ot	Y	To	Bs	Bb	Se	Sh	Pc	J	N	Chief	Sub-Chief
1. Development of Device for Isolation																													
1.1 High Energy Absorbing Rubber Bearing								○											○	⊙	○			○					
1.2 Friction Damper													○									○	○						
1.3 Steel Damper								○							○													Ol	Bs
1.4 Link Bearing Develop of																	○												
1.5 Viscous Damper																		○											
1.6 Test Method	○							○							○		○	◎	○	○	○	○	○	○					
2. Development of Expansion Joint and Falling-off Prevention Device for Isolated Bridge																													
2.1 Expansion Joint				○									○															Tc	—
2.2 Falling-off Prevention Device	○												○					○											
3. Development of Design Method for Isolated Bridge																													
3.1 Design Philosophy	◎	○	○	○		○						○	◎					○							○	○	○		
3.2 Dynamic Responce Analysis Method	○		○		○	◎		○			○			○														Ka	Pc
3.3 Design Method of Device for Isolation	○						○	○				◎	○		○		○	○	○	○	○	○	○	○					
3.4 Simplified Design Method	○	○	◎		○	⊙					○	○																	
3.5 Design Method of Expansion Joint and Falling-off Prevention Device	○			○			○								○			○							◎				
4. Application of Base Isolation to Bridge																													
4.1 Application to Prestressed Concrete Bridge	○	◎							○	○			○														○		
4.2 Application to Steel Bridge	○													⊙	○	○											◎	Ob	J
4.3 Application to Multiple Super-long Bridge	○			◎					○							○									○	○	○		
4.4 Application to Seismic Retrofit	○									○				○				○								◎			

P: Public Works Research Institute, Ka: Kajima, Si: Shimizu, Ob: Ohbayashi, Ku: Kumagai, Tn: Takenaka Doboku + Takenaka, H: Hazama, Ni: Nishimatsu, Su: Sumitomo, M: Mitsui, G: Goyoh, Ok: Okumura, Ti: Taisei + Tokyo Fablic + Nippon Chuzo, I: Ishikawajima Harima, Nk: NKK + Nippon Chuzo, Ko: Kobe Steel, Ns: Nippon Seiko, Oe: Oiles, Y: Yokohama Rubber, To: Toyo Rubber, Bs: Bridgestone, Bb: BBM, Se: Seibu Polymer, Sh: Showa Densen, Pc: Pacific Consultants, J: Japan Engineering Consultant, N: New Structural Engineering Consultants.

Table 2 Damping Ratio Recommended for Structural Components

Structural Components	Steel	Concrete
Superstructures	0.02～0.03	0.03～0.05
Menshin Device	Damping Ratio by Eq.(11)	
Pier/Columns	0.03～0.05	0.05～0.1
Footing	0.1～0.3	

Table 3 Modification Factor for Ground Condition c_G

Ground Group	I	II	III
c_G	0.8	1.0	1.2

Table 4 Modification Factor for Importance c_I

Group	c_I	Definition
1st class	1.0	Bridges on expressway (limited access highways), general national road and principal prefectural road. Important bridges on general prefectural road and municipal road.
2nd class	0.8	Other than the above

Table 5 Modification Factor for Structural Response c_T

Ground Group	Structural Response Coefficient c_T		
Group I	$T < 0.1$ $c_T = 2.69T^{1/3} \geqq 1.00$	$0.1 \leqq T \leqq 1.1$ $c_T = 1.25$	$1.1 < T$ $c_T = 1.33T^{-2/3}$
Group II	$T < 0.2$ $c_T = 2.15T^{1/3} \geqq 1.00$	$0.2 \leqq T \leqq 1.3$ $c_T = 1.25$	$1.3 < T$ $c_T = 1.49T^{-2/3}$
Group III	$T < 0.34$ $c_T = 1.80T^{1/3} \geqq 1.00$	$0.34 \leqq T \leqq 1.5$ $c_T = 1.25$	$1.5 < T$ $c_T = 1.64T^{-2/3}$

Table 6 Modification Factor for Energy Dissipation Capability c_E

Damping Ratio h	Modification Factor c_E
$h < 0.1$	1.0
$h \geqq 0.1$	0.9

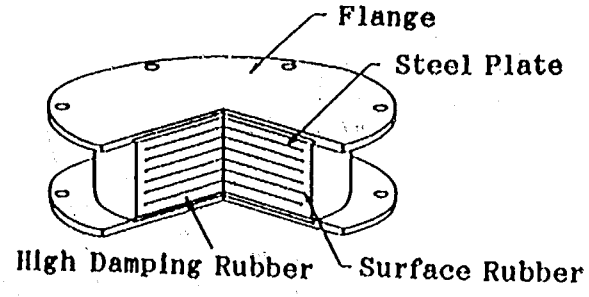
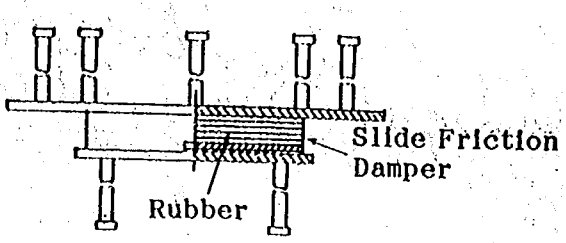
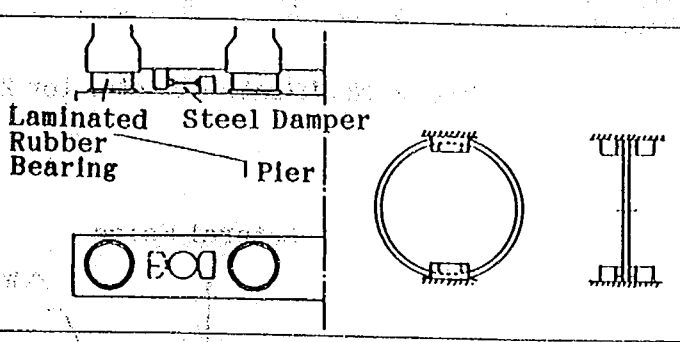
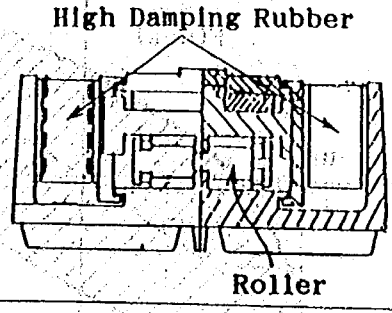
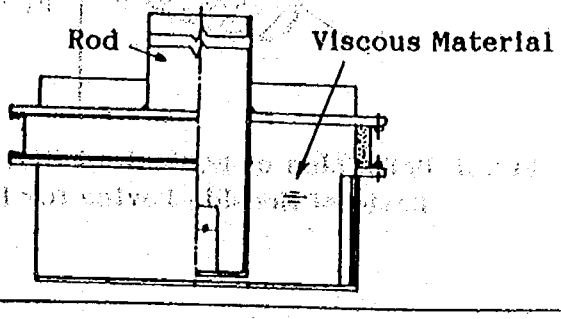
Table 7 Modification factor for Structural Response c_R

Ground Group	Structural Response Coefficient c_R		
Group I	$T_{EQ} \leqq 1.4$ $c_R = 0.7$		$1.4 < T_{EQ}$ $c_R = 0.876T_{EQ}^{-2/3}$
Group II	$T_{EQ} < 0.18$ $c_R = 1.51\ T_{EQ}^{1/3} \geqq 0.7$	$0.18 \leqq T_{EQ} \leqq 1.6$ $c_R = 0.85$	$1.6 < T_{EQ}$ $c_R = 1.16T_{EQ}^{-2/3}$
Group III	$T_{EQ} < 0.29$ $c_R = 1.51T_{EQ}^{1/3} \geqq 0.7$	$0.29 \leqq T_{EQ} \leqq 2.0$ $c_R = 1.0$	$2.0 < T_{EQ}$ $c_R = 1.59T_{EQ}^{-2/3}$

Table 8 Modification Factor for Energy Dissipating Capability

Damping Ratio h	Modification Factor c_E
$h < 0.1$	1.0
$0.1 \leqq h < 0.12$	0.9
$0.12 \leqq h < 0.15$	0.8
$0.15 \leqq h$	0.7

Fig. 1 Menshin Devices Developed

TYPE	OUTLINE OF MENSHIN DEVICE
HIGH DAMPING RUBBER BEARING	
SLIDE FRICTION -RUBBER BEARING	
STEEL DAMPER	
ROLLER MENSHIN BEARING	
VISCOUS	

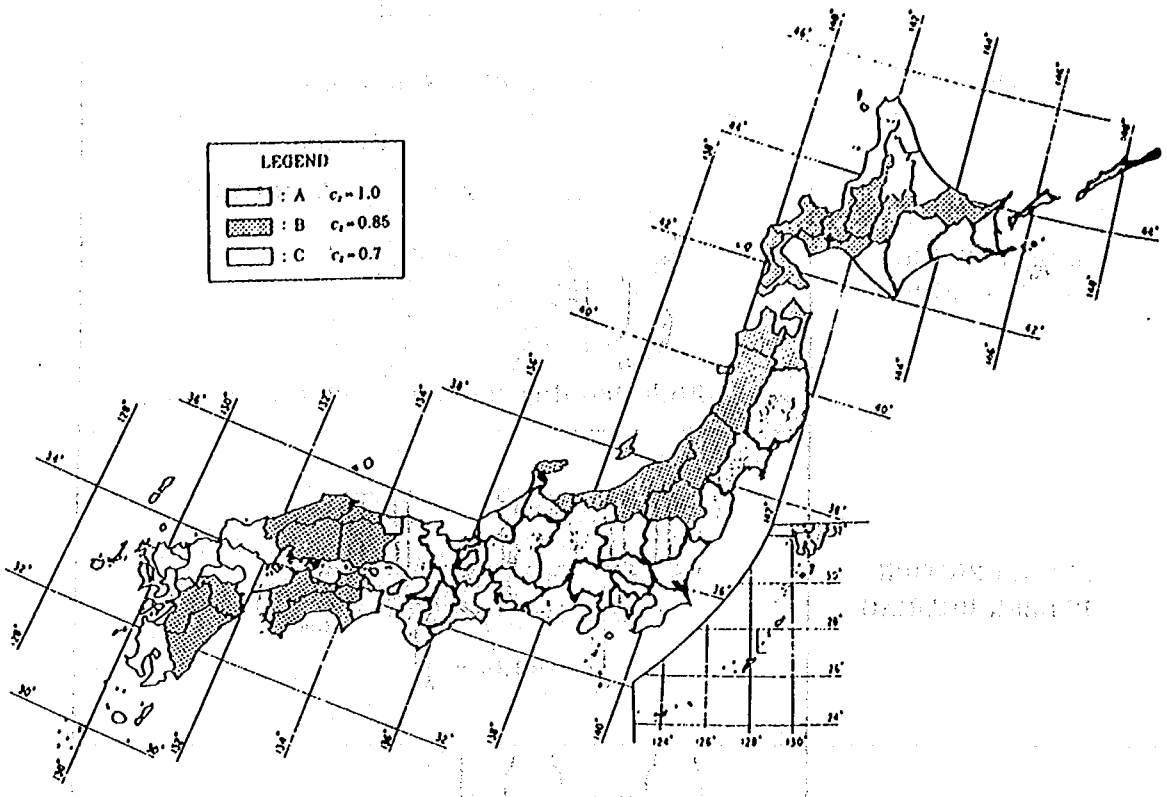


Fig. 2 Modification Factor for Zone c_z

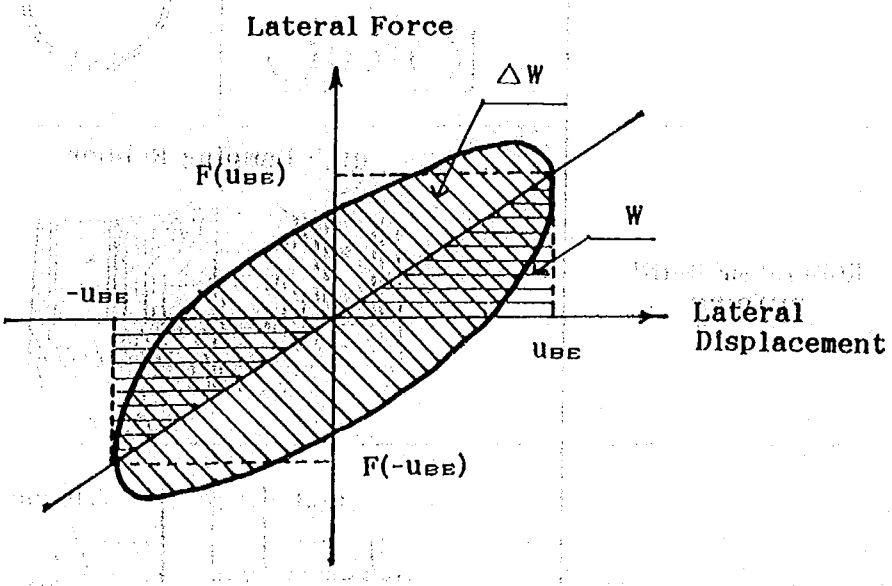


Fig. 3 Definition of Equivalent Stiffness and Equivalent Damping Ratio of Menshin Device for Design of Menshin Device

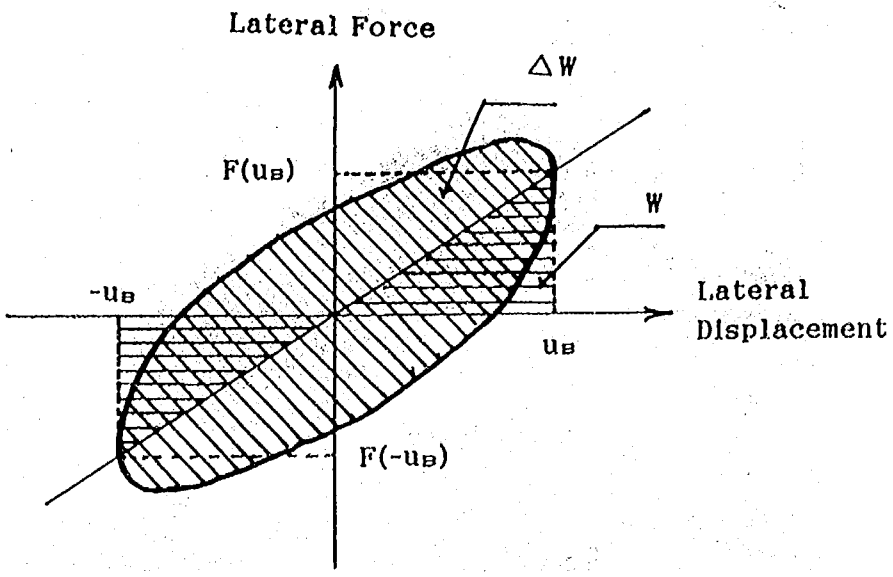


Fig. 4 Definition of Equivalent Stiffness and Equivalent Damping Ratio of Menshin Device for Approving Tests

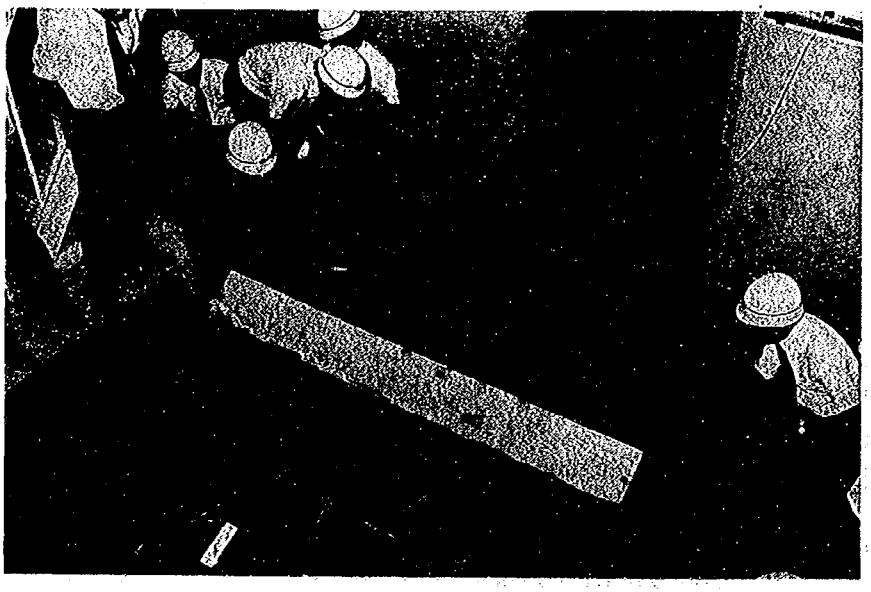


Photo 1 Knock-off Abutment

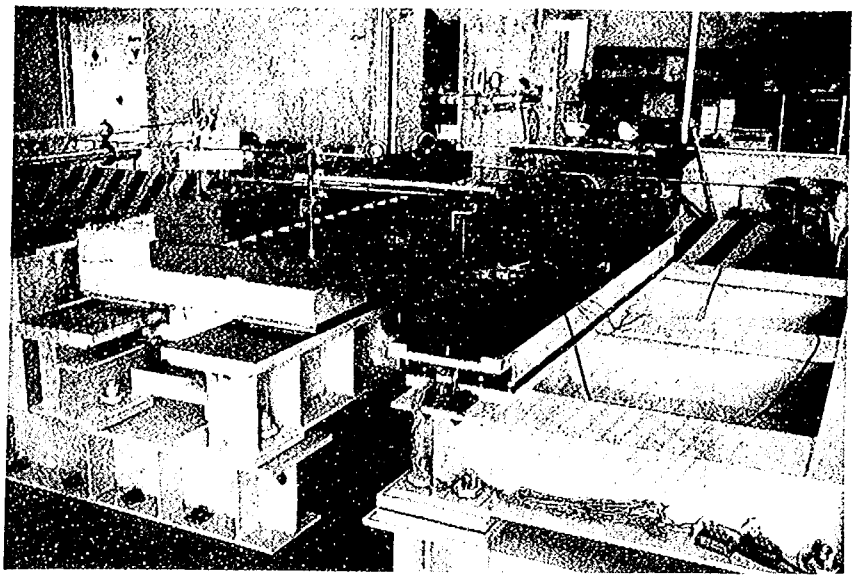


Photo 2 Expansion Joint Movable in Longitudinal and Transverse Directions

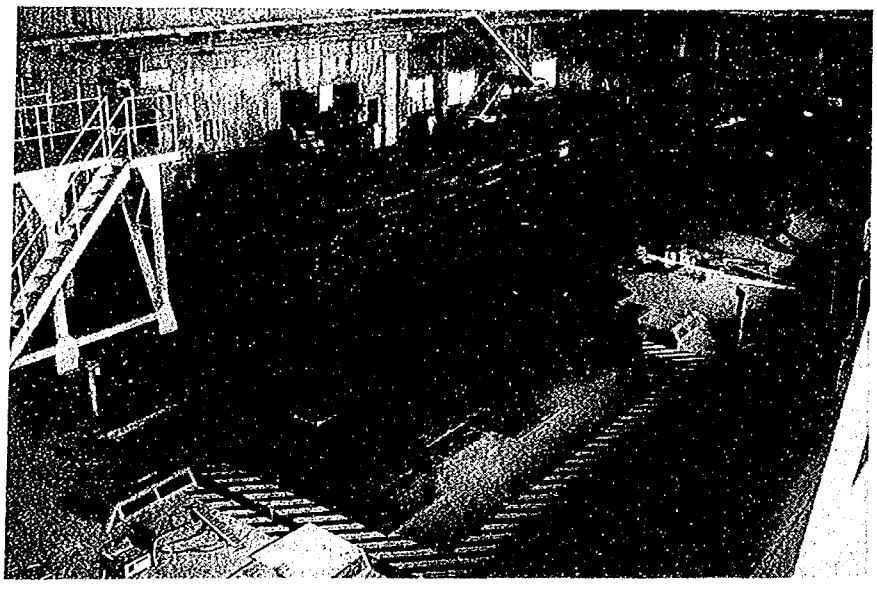
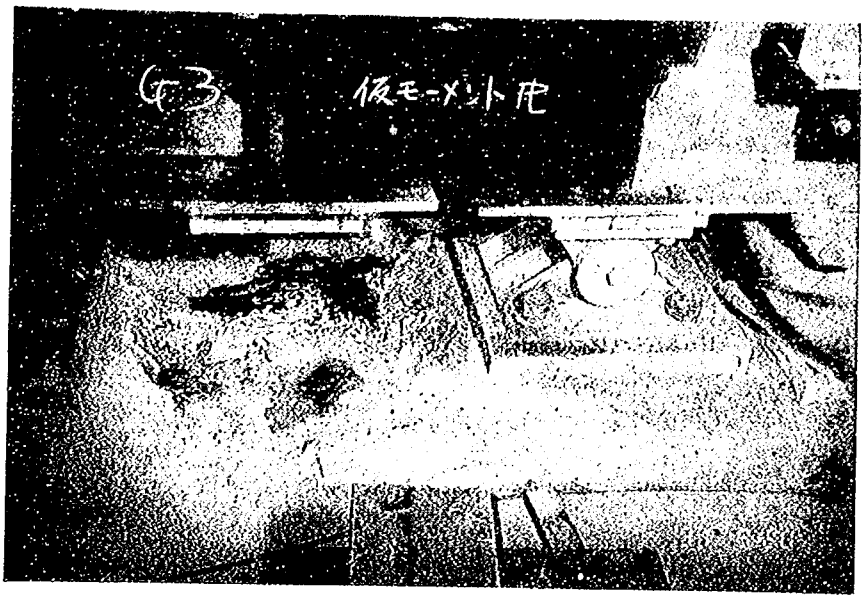


Photo 3 Shaking Table Tests for Studying Structural Response of Menshin Bridges



(a) Replacement of Existing Steel Bearings



(b) Setting of Menshin Bridges

Photo 4 Deck Connection of Existing Bridge with use of Menshin Bridges

APPLICATION OF AASHTO SEISMIC ISOLATION DESIGN AND ANALYSIS REQUIREMENTS

Ronald L. Mayes

Dynamic Isolation Systems, Inc.
Berkeley, CA 94705

ABSTRACT

In October 1990, the American Association of State Highway Transportation Officials (AASHTO) adopted Guide Specifications for the Seismic Isolation Design of Highway Bridges. This paper will overview the objectives and philosophy of the provisions, summarize the design requirements of elastomeric based systems, and use a 4-span bridge as an example to compare the three different methods of analysis permitted by the provisions.

INTRODUCTION

In the past 15 years, a relatively new technology called "seismic isolation" has emerged as a practical and economic alternative to conventional design. This concept has received increasing academic and professional attention (ASCE, 1989; Applied Technology Council, 1986; EERI 1990) and is being applied to a wide range of civil engineering structures. To date there are several hundred bridges in New Zealand, Japan, Italy, Iceland and the United States which use seismic isolation principles and technology for their seismic design. The basic intent of seismic isolation is to increase the fundamental period of vibration such that the structure is subjected to significantly lower earthquake forces.

One of the major impediments to the implementation of seismic isolation has been the lack of code requirements (Mayes, 1990). With liability issues being a major concern to design professionals in today's litigious society, many firms have been unwilling to use the technology without the protection of professionally acceptable code provisions. Thus the October, 1990 adoption of Seismic Isolation Design Requirements by AASHTO (AASHTO, 1991; Mayes, 1992) is a key step forward in the more widespread use of seismic isolation. This paper summarizes the AASHTO Guide Specifications for Seismic Isolation Bridge Design and provides a comparison of design forces with those obtained with conventional design requirements.

The design of a seismic isolation system for bridges consists of two interrelated parts. First, the isolation system must be designed for all non-seismic load cases using AASHTO group load factors. The second step involves the determination of the seismic design forces and displacements. The paper will summarize both parts of the procedure as it relates to elastomeric based isolation systems. Once a preliminary design of the system is completed, the bridge must be analyzed to determine the forces and displacement of the columns, foundations and

abutments. There are three methods of analysis permitted by the AASHTO seismic isolation design requirements: a single-mode method, an equivalent linear multi-mode method of analysis, and a nonlinear time history method of analysis. The paper will provide a comparison between the results of the three methods of analysis for a 4-span bridge.

OBJECTIVES OF THE PROVISIONS

In the development of the seismic isolation design requirements for bridges there were three basic objectives as follows:

- To be as consistent as possible with the recently adopted AASHTO Standard Specifications for conventional seismic design.
- To be as consistent as possible with the recently adopted Uniform Building Code provisions for seismically isolated buildings.
- To be applicable to a wide range of possible seismic isolation systems.

The first objective necessitated that the requirements fit within the Seismic Performance Category (SPC) concept of the new seismic design provisions. This concept provides a gradation of requirements from minimal requirements for the lowest category SPC-A with an acceleration coefficient less than 0.10, to the most stringent requirements for the highest category SPC-D with an acceleration coefficient greater than 0.29. The second objective formed the primary basis for the isolation design requirements. Some modifications were required due to the differences between building and bridge structural form and design loads. Others were required to provide consistency with the first objective. The third objective necessitated that the requirements remain general and as such rely on mandatory testing of isolation system hardware to confirm the engineering parameters used in the design and to verify the overall adequacy of the isolation system.

Both static and dynamic analysis procedures are included (depending on the SPC) and are based on the same level of seismic input and require the same level of performance from the bridge. The design basis earthquake load corresponds to a level of ground motion that has a 10 percent probability of being exceeded in a 50 year time period, i.e. 475 year return period.

PHILOSOPHY OF THE PROVISIONS

Seismic isolation provides a significant reduction in the elastic seismic forces the bridge must resist when compared to conventional fixed base design (Buckle et al., 1986, 1989, 1990). As a consequence, there are two possible design philosophies that can be used and both are included in the AASHTO Seismic Isolation Guide Specifications (AASHTO, 1991; Mayes, 1992). The first is to take advantage of the reduced forces and provide the most economical bridge design. This option utilizes the same Response Modification Factors (R-Factors) as the recently adopted AASHTO Standard Specifications and thus provides the same level of

seismic safety. The advantage of this design option is that if seismic forces are governing the design of the bridge, cost savings up to approximately 10% of the total bridge cost can be realized (Billings, 1985; Thorkildsen, 1991; O'Conner and Mayes, 1992).

The second design option is to provide a bridge with much better seismic performance characteristics than that of a conventional design using the AASHTO Standard Specifications. The intent of this design option is to eliminate or significantly reduce damage (inelastic deformation) to the substructure and abutments. In this case an R-Factor of 1 to 1.5 will ensure essentially elastic response by eliminating the ductility demand on the substructure. In bridges this design option can generally be achieved for similar or less cost than a conventional design. Furthermore, it provides protection for earthquakes that may exceed the 475 year design event.

DESIGN FORCES FOR SEISMIC PERFORMANCE - CATEGORY A

The AASHTO Standard Specification (AASHTO, 1991) for conventional design has only two requirements for SPC-A. All bearing and column connections are required to be designed for 0.2 times the dead load and the minimum support length requirements need to be met. In the isolation design requirements the isolation bearing connections are required to be designed for

$$F = K_{eff}D$$

where

K_{eff} = Effective linear stiffness of the isolation bearing
D = Displacement of the isolated superstructure using a minimum acceleration coefficient, A, of 0.10.

This permits utilization of the real elastic force reduction provided by seismic isolation and will result in a lower connection design force than conventional design.

DESIGN FORCES FOR SPC B, C, AND D

Design forces for a seismically isolated bridge in SPC B, C and D are obtained using the same load combinations as for a conventionally designed bridge. The two design philosophies discussed previously are incorporated in the determination of the design forces. The provisions permit the use of the same R-factors as conventional design with a lower limit on the design forces being the yield level of the isolation system. This option permits a more economic design with the same performance level as conventional design. If a higher level of performance is desired it is recommended that an R-factor of 1.0 to 1.5 is used to ensure essentially elastic response.

A comparison of the design forces for a conventional and an isolated design can be obtained from the lateral force design equations (AASHTO, 1991; Mayes, 1992). The lateral force (V) is the uniform load applied in a manner similar to wind loads and calculated as follows:

$$V = C_s W \tag{1}$$

Conventional

$$C_s = \frac{1.2AS}{T^{2/3}} \tag{2}$$

Isolation

$$C_s = \frac{AS_i}{T_i B} \tag{3}$$

where

A = Acceleration coefficient obtained from the seismic risk map. A varies from 0.4 for SPC D to 0.1 for SPC B. A is less than 0.1 for SPC A.
S = Soil Coefficient (1.0, 1.2 and 1.5 for Soil Types I, II and III, respectively).
S_i = Soil Coefficient (1.0, 1.5 and 2.0 for Soil Types I, II and III, respectively).
T = Period, seconds
T_i = Isolated period seconds
B = Damping Coefficient of the isolation system (1.0 for 5%, 1.2 for 10% and 1.7 for 30%).

For most conventional bridges with column heights less than 30 feet the fundamental period calculated for use in the above equation will be less than 0.6 seconds resulting in C_s attaining it's maximum value of 2.5A. A comparison of the elastic design forces resulting from Equations 1, 2 and 3 is given in Table 1, together with the ratio of the conventional to isolated (V_C/V_I) base shear value. It will be noted that seismic isolation provides a factor of 3 to 8 reduction in the elastic forces. In order to compare column, foundation and connection design forces, a factor of 5 reduction will be assumed in the value of elastic base shear (V) for the isolation design. The actual reduction in elastic forces will vary between 3 and 8, and depends on several factors including; the isolation period which generally varies between 1.5 and 2.5 seconds; the soil type, with stiffer soils producing higher factors of reduction; and the damping of the isolation system, with higher damping values producing higher factors of reduction.

Table 2 presents a comparison of the design forces for 3 cases. A conventional design where the elastic force $C_s W$ is obtained, assuming the period of the bridge is less than 0.6 seconds resulting in an elastic force of 2.5AW. For SPC B where A may be as low as 0.1, this results in a lateral force of 0.25W. The two isolation design cases are based on the assumption that there is a factor of 5 reduction in the elastic force with V = 0.5AW. The two columns of results presented for an isolation design are the two design alternates permitted by the AASHTO Guide Specifications. The first uses the same R-Factors as conventional design, whereas the second uses an R-Factor of 1. The second design alternate will result in an elastic design with no damage, whereas the use of the same R-Factors will produce the same performance as a conventional design.

It will be noted from Table 2 that when the same R-Factors are used for a conventional and isolation design the reduction in design forces for the isolation design are the same as the elastic force reduction, which in this example is a factor of 5. For the no damage isolated design option (R=1) a column design force reduction is only obtained for single columns. However, for the foundations, a factor of 2 to 3 reduction is obtained, and the factor of 5 elastic force reduction is also obtained in the connection design forces.

Table 1: Comparison of Elastic Forces
(T_{conv} < 0.6 secs, B = 1.7)

Isolation Period T_I	Soil Type I			Soil Type II			Soil Type III		
	V_{conv}	V_{isol}	V_D/V_I	V_{conv}	V_{isol}	V_D/V_I	V_{conv}	V_{isol}	V_D/V_I
1.5 secs.	2.5AW	0.4AW	6.3	2.5AW	0.59AW	4.2	2.5AW	0.78AW	3.2
2.0 secs.	2.5AW	0.3AW	8.3	2.5AW	0.44AW	5.7	2.5AW	0.59AW	4.2

Table 2: Comparison of Design Forces

	Conventional Code R-Factors	Isolation Code R-Factors	Isolation No Damage, R=1
Elastic Forces - C_sW	2.5A[1]W	0.5AW	0.5AW
Column Design Forces R = 3 R = 5	C_sW/R[2] 0.8AW 0.5AW	C_sW/R[4] 0.2AW 0.1AW	C_sW 0.5AW 0.5AW
Foundation Design Forces[3] R = 3 R = 5	$2C_sW/R$ 1.7AW 1.0AW	$2C_sW/R$[4] 0.3AW 0.2AW	C_sW 0.5AW 0.5AW
Connection Design Forces R = 0.8 R = 1.0	C_sW/R 3.0AW 2.5AW	C_sW/R 0.6AW 0.5AW	C_sW 0.5AW 0.5AW

Notes:

1. A = Acceleration coefficient from seismic risk map and varies from 0.1 for SPC B to 0.4 for SPC D.
2. R = Reduction factor. It varies by component and is 3 for a single column, 5 for a multi-column bent, and between 0.8 and 1.0 for all connections.
3. For the purpose of this tabulation, SPC B foundation design forces are used. They are double the column design force. Other values are permitted for SPC C and D.
4. The lower limits on these values are based on the yield level of the isolation system, and these may govern for some Acceleration Coefficients.

DESIGN ISSUES FOR ISOLATION SYSTEMS

The global design issues for the isolation system involve the desired isolation period, the base shear, the damping of the system and the required margins of safety for the system. There are many interrelated variables involved in an isolation system design and to provide an overview of how these variables impact the structural design process the new AASHTO seismic isolation design requirements are used.

The displacement across the isolators (D), the elastic base shear (V) and the isolation period (T) are given by the following formulas:

$$D = \frac{10AS_1T_1}{B} \tag{4}$$

$$T_1 = 2\pi\sqrt{\frac{W}{K \cdot g}} \tag{5}$$

$$V = KD = \frac{AS_1}{T_1B} \cdot W \tag{6}$$

where

D	=	Isolator Displacement, Inches
K	=	Overall Isolator Stiffness (GA/Tr for plain reinforced elastomeric isolators where Tr is the total elastomer height).
V	=	Elastic Base Shear, Kips
W	=	Structure Weights, Kips
G	=	Shear Modulus of Elastomer, Kips/Inch.
Tr	=	Total Elastomer Heights, Inches

The important design variables are impacted by the isolation system properties as follows:

DISPLACEMENT - The isolator displacement is given by equation 4 and the two isolation system properties that impact isolator displacements, D, are the isolated period T and damping coefficient B. D increases as the isolation period T increases and decreases as the damping coefficient B increases.

BASE SHEAR - The base shear, V, is given by Equation 6 and is inversely proportional to the isolation system period T and damping coefficient B. That is V decreases as both the isolation period T and damping coefficient B increase.

ELASTOMERIC BEARING DESIGN REQUIREMENTS

Elastomeric bearings which are used for seismic isolation will be subjected to earthquake induced displacements and must therefore be designed to safely carry the vertical loads at these displacements. Since earthquakes are infrequently occurring events, the factors of safety required under these circumstances will be different from those required for more frequently occurring loads. Since the primary design parameter for earthquake loading is the displacement of the bearing, the design procedures must be capable of incorporating this displacement in a logical, consistent manner. The requirements of Section 14.2 of the AASHTO *Standard Specifications* limit vertical loads by use of a limiting compressive stress and therefore do not have a mechanism for including the simultaneous effects of seismic displacements. The British Specifications BE 1/76 and BS 5400 recognize that shear strains are induced in reinforced bearings by both compression and shear deformation. In these codes, the sum of these shear strains is limited to a proportion of the elongation-at-break of the rubber. The proportion (½ or ⅓ for service load combinations and ¾ for seismic load combinations) is a function of the loading type.

Since the approach used in BE 1/76 and BS 5400 incorporates shear deformation as part of the criteria, it can be readily modified for seismic isolation bearings. The design requirements given in the seismic isolation code provisions are based on the appropriate modifications to BE 1/76 and BS 5400.

The more conservative aspects of BE 1/76 and BS 5400 have been used in AASHTO. For example, BS 5400 requires the summation of compression, thermal and rotational shear strains and requires this to be less than 5.0. BE 1/76 requires the summation of only the compression and thermal shear strains and requires this to be less than $\epsilon_u/2$, where ϵ_u is the ultimate elongation at break of the elastomer. The AASHTO requirements limit the summation of the three different shear strains (compression, thermal, rotational) to $\epsilon_u/2$.

Elastomeric isolators are also checked for the following limit states:

- axial load capacity
- critical (buckling) load
- stability (rollover)

The axial load capacity of the elastomeric isolator to withstand vertical load is based on the limiting strain criterion given in the AASHTO Specification. The sum of the shear strains in the elastomer due to the combination of vertical load, rotation and horizontal deflection is expressed as a fraction of the ultimate elongation-at-break of the elastomer ϵ_u. The reciprocal of this fraction is defined as the factor of safety for load capacity. This can be expressed as follows:

$$FS = \epsilon_u/(\epsilon_{sc} + \epsilon_{sr} + \gamma)$$

where

ϵ_μ = ultimate elongation-at-break

ϵ_{sc} = shear strain due to vertical load, adjusted to allow for the reduction in foot print area of the bearing as it is deflected horizontally

= $6\ SP/[K_{vi} \cdot t_i \cdot (1-\Delta/B)]$

ϵ_{sr} = shear strain due to rotation

= $B^2\ \theta/(2\ t_i\ T_r)$

γ = shear strain due to horizontal deflection

= Δ/T_r

P = vertical load on bearing, kips

Δ = horizontal deflection of bearings, inches

S = layer shape factor

B = width of bearing in direction of Δ, inches

K_{vi} = vertical stiffness of typical rubber layer, i, kips/inch

t_i = thickness of rubber layer, i, inches

T_r = total rubber thickness, inches

θ = rotation, radians

Using these requirements, the design procedure for nonseismic loads is as follows:

- The minimum plan size is governed by the dead and live load requirements. The rated load method (discussed above) is used to determine the minimum values of the plan size. These are shown in Table 3 for square bearings.
- The thickness of the internal rubber layers is determined by the vertical load, vertical stiffness, and rotational capacity requirements. Table 3 shows increasing vertical load capacity with decreasing internal rubber layer thickness.
- The total rubber thickness in the bearing (and hence the number of layers) is generally governed by thermal loads and the desired earthquake force reduction and distribution (Mayes et al., 1991). The minimum height of the elastomer is twice the R + S + T displacements.
- In a lead-rubber system, the sizes of the lead cores are based on ultimate strength design procedures using AASHTO's group load factors (Dynamic Isolation Systems, Inc., 1992). The minimum diameter of the lead core is determined by the requirement to maintain elastic response under AASHTO prescribed combinations of wind, braking and centrifugal loads. For a given bearing, the diameter of the lead core should be between ⅓ and 1/6 of the minimum plan dimension. The distribution of the lead cores throughout a continuous segment of the superstructure can be used to control the force levels transmitted to various substructures (Mayes, 1991). The lead core is designed to remain elastic and thus provide the necessary initial stiffness for Groups II, III and IV.

Table 3: Square Bearings - Total Dead Plus Live Load Capacity In Kips

Plan Size		Bonded Area	Rubber Layer Thickness			
W	B	(sq. ins.)	1/4"	3/8"	1/2"	3/4"
9	9	64	53	36	28	19
10	10	81	76	51	39	27
11	11	100	104	70	53	37
12	12	121	138	93	70	48
13	13	144	179	120	91	62
14	14	169	227	152	115	79
15	15	196	284	190	144	98
16	16	225	349	234	176	119
17	17	256	423	283	214	144
18	18	289	507	339	256	173
19	19	324	602	403	303	205
20	20	361	708	473	356	240
21	21	400	826	552	415	279
22	22	441	956	639	480	323
23	23	484	1099	734	552	371
24	24	529	1255	838	630	423
25	25	576	1426	952	716	480
26	26	625	1612	1076	809	542
27	27	676	1813	1210	909	610
28	28	729	2030	1355	1018	682
29	29	784	2264	1511	1135	760
30	30	841	2515	1678	1261	844
31	31	900	2784	1858	1395	934
32	32	961	3071	2050	1539	1030
33	33	1024	3378	2254	1693	1133
34	34	1089	3705	2472	1856	1242
35	35	1156	4052	2703	2030	1358
36	36	1225	4420	2949	2214	1481

METHODS OF ANALYSIS

The basic premise of the seismic isolation equivalent linear analysis design provisions (consistent with those for buildings and hospitals) is twofold. First, the energy dissipation of the isolation system can be expressed in terms of equivalent viscous damping and, second, the stiffness of the isolation system can be expressed as an effective linear stiffness. These two basic assumptions permit both the single and multimodal methods of analysis to be used for seismic isolation design.

For sliding systems without a self-centering mechanism, for highly nonlinear systems or pure elasto-plastic isolation systems the equivalent viscous damping concept is no longer valid. The equivalent viscous damping formula produces a value that is independent of the coefficient of friction for sliding systems or the yield point for elasto-plastic systems. Furthermore, because these systems lack a restoring force, the Total Design Displacement may be underestimated. Consequently, it is necessary to perform a nonlinear time history analysis for all seismic isolation systems that have no self-centering mechanism.

The above AASHTO Guide Specifications specify two analysis procedures and the applicable procedure for a given type of bridge depends on the number of spans, the geometric complexity and the Seismic Performance Category, as given in Table 4, below. A more rigorous, generally accepted procedure may be used in lieu of the recommended minimum and a nonlinear analysis is required for some isolation systems. Procedure 1 is the single-mode method of analysis and Procedure 2 is the multi-mode method of analysis – both are discussed in more depth.

Table 4: AASHTO Required Analysis Procedure

Seismic Performance Category	Regular [1] Bridges with 2 or More Spans	Irregular [2] Bridges with 2 or More Spans
A	–	–
B	1	1
C	1	2
D	1	2

[1] A "regular" bridge has no abrupt or unusual changes in mass, stiffness, or geometry along its span, and has no large differences in these parameters between adjacent supports (abutments excluded). For example, a bridge may be considered regular if it is straight, or describes a sector of an arc not exceeding 90°, and has adjacent columns or piers that do not differ in stiffness by more than 25%. (Percentage difference is to be based on the lesser of two adjacent quantities as the reference.)

[2] An "irregular" bridge is any bridge that does not satisfy the definition of a regular bridge.

Single Mode Spectral Analysis

The single mode method of analysis given in Section 5.3 of the AASHTO *Standard Seismic Specifications* is also appropriate for seismic isolation design. In fact, use of the method is simplified with seismic isolation. Steps 1, 2 and 3 of the procedure are not necessary since the use of an isolation system will ensure a simple rigid body deformation pattern of the superstructure.

In Step 4 of the procedure, the value of $p_e(x)$, the intensity of the equivalent static seismic loading, is determined as

$$p_e(x)=w(x)\cdot C_s \tag{11}$$

where C_s is calculated by Equation 9 and w(x) is the dead load per unit length of the bridge superstructure. In Step 5 of the procedure, the loading $p_e(x)$ is applied to the superstructure to determine the resulting member forces and displacements.

Multimode Spectral Analysis

The guidelines given in Section 5.4 of the AASHTO *Standard Seismic Specifications* are also appropriate for the response spectrum analysis of an isolated structure with the following modifications:

a. The isolation bearings are modelled by use of their effective stiffness properties determined at the design displacement D (Δ_m in Figure 1).
b. The ground response spectrum is modified to incorporate the damping of the isolation system (Figure 2).

The response spectrum required for the analysis needs to be modified to incorporate the higher damping value of the isolation system. This modified portion of the response spectrum should only be used for the isolated modes of the bridge and will then have the form shown in Figure 2.

Time History Analysis

When a time history analysis is required for systems with a non-centering capability, it is necessary for the time histories to be frequency scaled so they closely match the appropriate ground response spectra for the site. In addition, the analytical model should incorporate the nonlinear deformational characteristics of the isolation system.

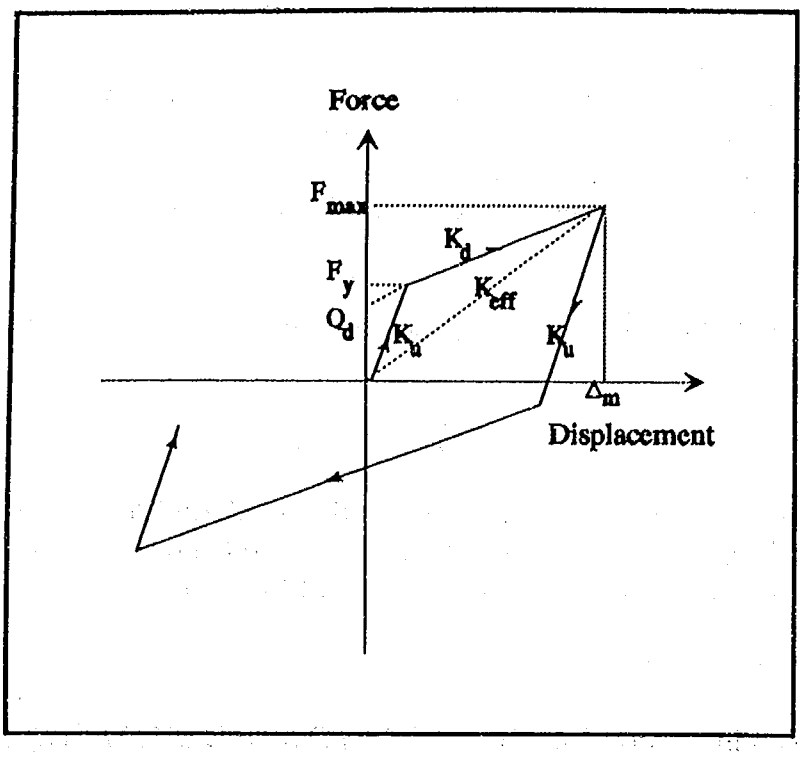


Figure 1: Characteristics of Bilinear Isolation Bearings

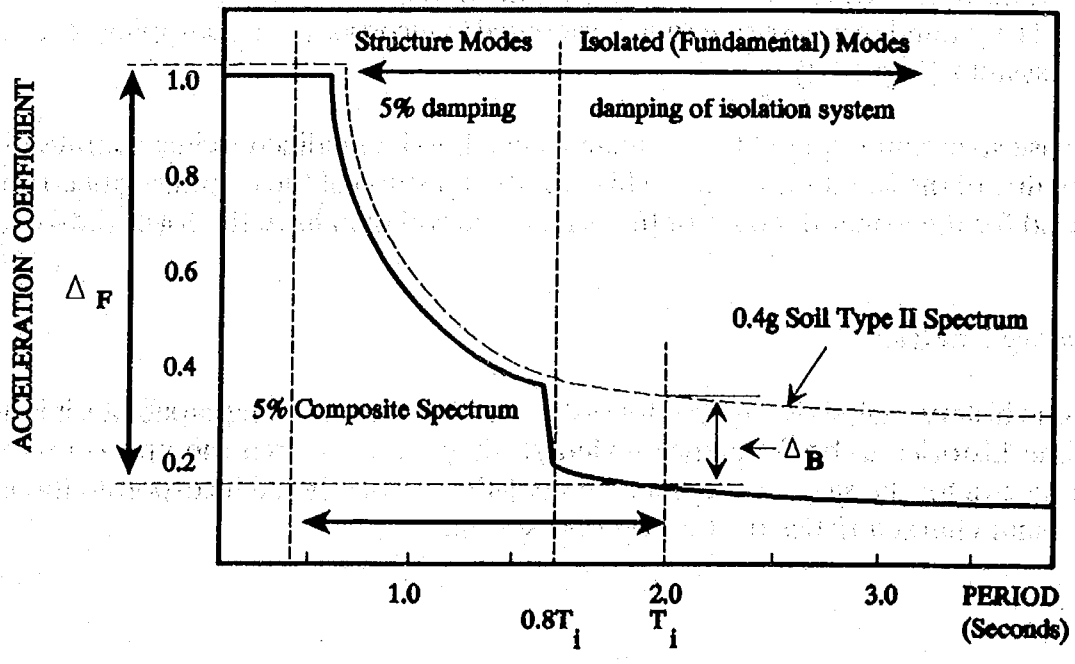


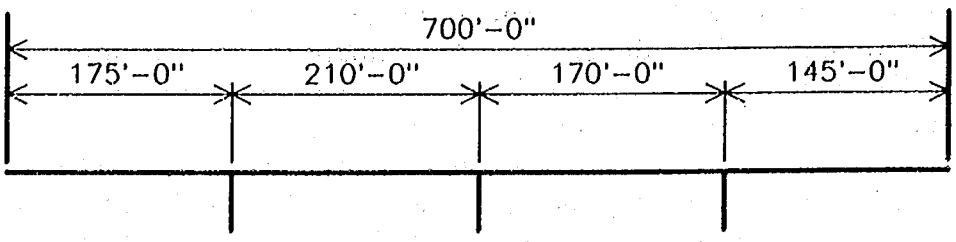
Figure 2: Development of Modified Response Spectrum

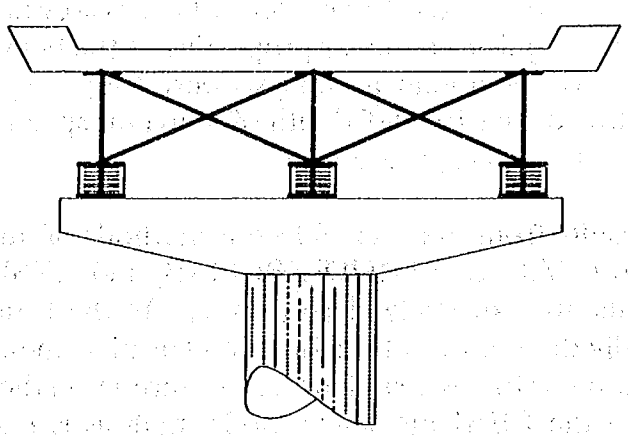
COMPARISON OF ANALYTICAL METHODS

A 4-span continuous bridge with 3 steel plate girders and spans of 175', 210', 170', and 145', as shown in Figure 3, is used for the example to compare the analytical methods permitted by AASHTO. The bents are each single columns, 7' in diameter with a 39' clear height. Each bent has 3 bearings, one under each girder, with bearing dead loads ranging from 150 kips at the abutments to 600 kips at Pier 2. A schematic of the layout and all the loads are given in Figure 3. The lead-rubber bearings designed, using the AASHTO requirements discussed previously, are also given in Figure 3 and were used for the analysis. The design and analysis of the system was performed for a Caltrans 0.6g spectrum with 10'–80' depth of alluvium.

The analyses performed were the single mode method of analysis using the program PC-LEADeR (Dynamic Isolation Systems, Inc., 1992); the multimode method of analysis using the computer programs STRUDL and SEISAB; and a 3-D nonlinear time history analysis using the computer program ANSR, where the explicit nonlinear properties of the bearings were included. The seven time histories used for the nonlinear analysis were frequency scaled so that they were compatible with the Caltrans 0.6g 10'–80' depth of alluvium spectrum. The average results of these seven time histories are reported herein.

A comparison of the results from the four different methods of analysis are given in Table 5. A comparison of the LEADeR, STRUDL, SEISAB, and ANSR results for longitudinal forces and displacements are extremely close (±5%). In the transverse direction there is more variation in the individual substructure forces and displacements, although the total sum of column and abutment shear forces is similar. The difference in the individual column forces and displacements from the LEADeR single mode analysis is because there are two key parameters missing: (1) the transverse deformation of the deck, which in this example is significant; and (2) the rotation of the deck due to unequal span lengths.





BEARING LOCATION	No. of Brcs.	DL	LL	W	WL	CF	LF	R+S+T	BEARING
Abutment 1									
Bearings	3	150	90						S23-10-5.50
SUB-TOTAL:	3	480	270	37.1	0.0	15.3	4.5	1.64	
Bent 2									
Bearings	3	600	200						S27-10-5.50
SUB-TOTAL:	3	1800	600	82.1	0.0	34.0	10.0	0.87	
Bent 3									
Bearings	3	500	200						S27-10-5.50
SUB-TOTAL:	3	1500	600	86.6	0.0	34.0	10.0	0.07	
Bent 4									
Bearings	3	500	200						S27-10-5.50
SUB-TOTAL:	3	1500	600	75.4	0.0	34.0	10.0	0.94	
Abutment 2									
Bearings	3	160	80						S23-10-5.50
SUB-TOTAL:	3	480	240	33.8	0.0	13.6	4.0	1.64	
SEGMENT TOTAL	15	5760	2310	315.0	0.0	130.9	38.5	1.64	

Figure 3: Bridge Example - Single Column Bent

Table 5: Comparison of Analytical Results

	DISPLACEMENT (ft.)				FORCE (kips)			
	LEADeR	STRUDL	SEISAB	ANSR	LEADeR	STRUDL	SEISAB	ANSR
LONGITUDINAL								
Abutment 1	0.74	0.78	.76	0.80	286	272	294	284
Pier 2 Deck	0.74	0.78	.76	0.80	325	337	322	344
Pier	0.12	0.12		0.13				
Pier 3 Deck	0.74	0.78	.76	0.80	325	337	322	341
Pier	0.12	0.12		0.13				
Pier 4 Deck	0.74	0.78	.75	0.80	325	336	322	348
Pier	0.12	0.12		0.13				
Abutment 2	0.74	0.78	.75	0.80	286	269	292	288
Total Force					1547	1551	1552	1605
TRANSVERSE								
Abutment 1	0.74	0.68	.64	0.67	286	228	243	229
Pier 2 Deck	0.74	0.89	.85	0.98	325	362	359	397
Pier	0.12	0.14		0.15				
Pier 3 Deck	0.74	1.01	.95	1.12	325	411	440	445
Pier	0.12	0.16		0.17				
Pier 4 Deck	0.74	0.75	.69	0.95	325	304	306	380
Pier	0.12	0.11		0.14				
Abutment 2	0.74	0.55	.58	0.48	286	192	214	171
Total Force					1547	1497	1562	1622

SUMMARY

Seismic isolation offers particular advantages to bridge structures. Reductions in earthquake loads can be significant and savings can be achieved in the foundations of new designs along with improved seismic performance (elastic response). Isolation also offers an elegant solution to many of the common retrofit problems encountered in existing bridges. Limited experience to date has shown that isolation can be adapted and implemented to meet a wide variety of different site and bridge conditions.

The adoption of the seismic isolation code requirements discussed herein is a key step in the implementation of any new technology and these code requirements should significantly increase the implementation phase of the technology. They provide engineers with professionally

acceptable procedures without which, liability issues dominate decision making. The lack of code provisions to date has been an impediment to the more widespread use of the technology and thus these new code requirements are a key step forward in the application of this beneficial technology.

REFERENCES

1. AASHTO (1991), "Standard Specifications for Highway Bridges," American Association for State Highway and Transportation Officials (AASHTO), 15th Edition, 1989 and Interim Specifications 1990, 1991.

2. ASCE (1989), "Seismic Engineering: Research and Practice," Proceedings ASCE Structures Congress, May 1989.

3. Applied Technology Council (1986), "Proceedings of a Seminar and Workshop on Base Isolation and Passive Energy Dissipation," ATC Report No. 17, Palo Alto, CA, 1986.

4. Billings, I.J. and Kirkcaldie, D.K. (1985), "Base Isolation of Bridges in New Zealand," Proceedings US-NZ Workshop on Seismic Resistance of Highway Bridges, Report No. 12-1, Applied Technology Council, May 1985.

5. Buckle, I.G., Mayes, R.L. and Button, M.R. (1986), "Seismic Design and Retrofit Manual for Highway Bridges," Computech Engineering Services, Berkeley, CA. Also Published by Federal Highway Administration as Report FHWA/RD-86/006, 1987.

6. Buckle, I.G. and Mayes, R.L. (1987), "The Application of Seismic Isolation to Bridges," Proceedings ASCE Structures Congress: Seismic Engineering - Research and Practice, pp 633-642, May 1990.

7. Buckle, I.G. and Mayes, R.L. (1990), "Seismic Isolation: History, Application and Performance - A World View," Earthquake Spectra, EERI, Vol.6, No.2, May 1990.

8. Dynamic Isolation Systems, Inc. (1992), "AASHTO Design Procedures for Seismically Isolated Bridges," Seminar Notes, March 1992.

9. Earthquake Engineering Research Institute (1990), "Seismic Isolation: From Idea to Reality," Earthquake Spectra Journal, Vol. 6, No. 2, May 1990.

10. Mayes, R.L., Jones, L.R., and Buckle, I.G., (1990), "Impediments to the Implementation of Seismic Isolation," Earthquake Spectra Journal, Theme Issue: Seismic Isolation, EERI, May 1990.

11. Mayes, R.L., Jones, D., Kelly, T.E., and Knight, R.P. (1991), "An Alternate Approach to the Distribution of Lateral Loads in Bridges," Proceedings, ACI 3rd World Congress on Joints and Bearings, October 1991.

12. Mayes, R.L., Buckle, I.G., Kelly, T.E., and Jones, L.R. (1992), "AASHTO Seismic Isolation Design Requirements for Highway Bridges," ASCE Journal of Structural Engineering, Vol. 118, No. 1, January 1992.

13. O'Conner, T.F. and Mayes, R.L. (1992), "Controlling Lateral Load Distribution in Bridges to Achieve Overall Economy," Proceedings, 9th International Bridge Conference, june 1992.

14. Thorkildsen, E. (1991), "The Use and Subsequent Reuse of Seismic Isolation Bearings on a California Interchange," Proceedings, 8th International Bridge Conference, June 1991.

Session-5

Seismic Isolation Design-2

U-4) Stability of Elastomeric Base Isolators
(Buckle, I. G. and Liu, H.)

J-10) Development of Expansion Joint, Stopper and Knock-off Abutment for Menshin Bridges
(Goto, Y., Kikuchi, T., Kimishima, T., Matsumoto, F., Ozaki, D. and Tsukamoto, A.)

U-5) Development and Application of Simple Analytical Models of Lead Rubber Base Isolated Bridges
(Maragakis, E. and Saiidi, M.)

J-11) Design of 9-span Continuous Prestressed Concrete Girder Bridge with Base Isolation
(Kubota, N., Shikauchi, S., Osaki, H., Mitake, Y. and Arai, H.)

STABILITY OF ELASTOMERIC BASE ISOLATORS

Ian G. BUCKLE and He LIU
Department of Civil Engineering
State University of New York at Buffalo
Buffalo, New York 14261

ABSTRACT

Most isolation systems in use today are based on elastomeric bearings. The combination of rubber layers and reinforcing steel gives an isolator which is stiff axially but soft laterally. Flexibility may be introduced and large period shifts achieved with these bearings simply by increasing the number and thickness of the rubber layers.

Of particular interest to the design engineer is the failure mode or limit state of a system of these isolators. This is currently determined by examining the limit state of the single most heavily loaded bearing in the case of buckling and the bearing with the lightest load, in the case of rollover. However, instability in a single bearing does not necessarily mean that the system as a whole is unstable. Since the axial load varies throughout a bridge or building structure, it follows that not all isolators are of the same size or carry the same axial load. Therefore, while one isolator may have reached its limit state, others may not be critical or even close to a critical state and these neighboring isolators may act to restrain the unstable isolator from failure. Accordingly, the system factor of safety is more accurately calculated if all of the isolators in the system are included in the analysis rather than focusing on the state of a single bearing.

This paper describes a numerical study of the system factor of safety taking into account variations in axial load (including those due to overturning moments) and variations in shear stiffness between groups of isolators of different physical size. It is shown that system stability is not only a function of the properties of individual bearings but is also determined by the distribution of these properties between bearings, their axial loads and the shear displacement.

INTRODUCTION

Recent surveys of seismic isolation systems around the world (Reference 1) indicate that the majority of these systems use elastomeric bearings as the element of flexibility. These bearings may be of natural or synthetic rubber and maybe specially compounded to enhance their hysteretic damping. Alternatively the bearings may be structurally modified to include a damping element, such as the inclusion of a lead or granular core on the vertical axis of the bearing.

In a typical building, isolators are located under each column, usually in a sub-basement. In a bridge they are usually placed under each girder at the abutment seats and between the column capbeam and the superstructure. There may be from 40 to 400 bearings in such a structure depending on its size and weight. The individual bearings which make up the isolation system are frequently interconnected by a diaphragm which is rigid in its own plane and which enforces displacement compatibility amongst the various isolators.

Of particular interest to the design engineer is the failure mode or limit state of the system. This is currently done by examining three separate limit states for each individual bearing; these are the maximum shear strain in the elastomer, the displacement at which rollover commences and the load at which buckling may occur. The shear strain in the elastomer is used as a measure of load capacity since it compares the total strain from all sources (compression, shear and rotation) against the elongation-at-break for the elastomer. The other two limit states are measures of bearing stability. System stability is currently estimated by examining the bearing with the lightest axial load, in the case of rollover, and the greatest axial load, in the case of buckling.

However, instability in a single bearing does not necessarily mean that the system as a whole is unstable. Since the axial load varies throughout the structure, it follows that not all isolators are of the same size and stiffness or carry the same axial load. Therefore, while one isolator may reach a limit state, others may not be critical or even close to a critical state and these other isolators may act to restrain the unstable isolator from failure. It follows that system factors of safety related to stability which are based on individual bearing limit states, may be unduly conservative.

SYSTEM STABILITY

To gain insight into system stability, it is useful to assume that the load - displacement behavior for the system can be represented by a single curve. Such a relationship is shown in Figure 1, in which the total shear force is plotted against shear displacement for the structure. Under the above assumption, this structure displacement is the same as the displacement for each individual bearing. Characterizing the displacement by a single value is valid provided a rigid diaphragm interconnects all the isolators and torsion about a vertical axis may be neglected. It follows that the system load-displacement curve is the sum of the individual bearing load-displacement curves.

Three regions of system stability can be defined by reference to Figure 1. They are:

a. stable equilibrium, where the force-displacement curve has positive slope i.e. when the system has positive stiffness.
b. unstable equilibrium, where the force-displacement curve has negative slope i.e. when the system has negative stiffness.
c. neutral equilibrium, where the force-displacement curve has zero slope i.e. when the system has zero stiffness.

The displacement at which the system passes from stable to unstable equilibrium (i.e. through the neutral point) is called the critical displacement for the system. The corresponding shear force is clearly the maximum force that the system can sustain.

A system factor of safety can be calculated using either the critical displacement or the maximum force. If the system is linear, as assumed in Figure 1, both methods will give the same result. Ideally, this is the factor that should be used to estimate system stability, rather than using worst case scenarios from individual bearings.

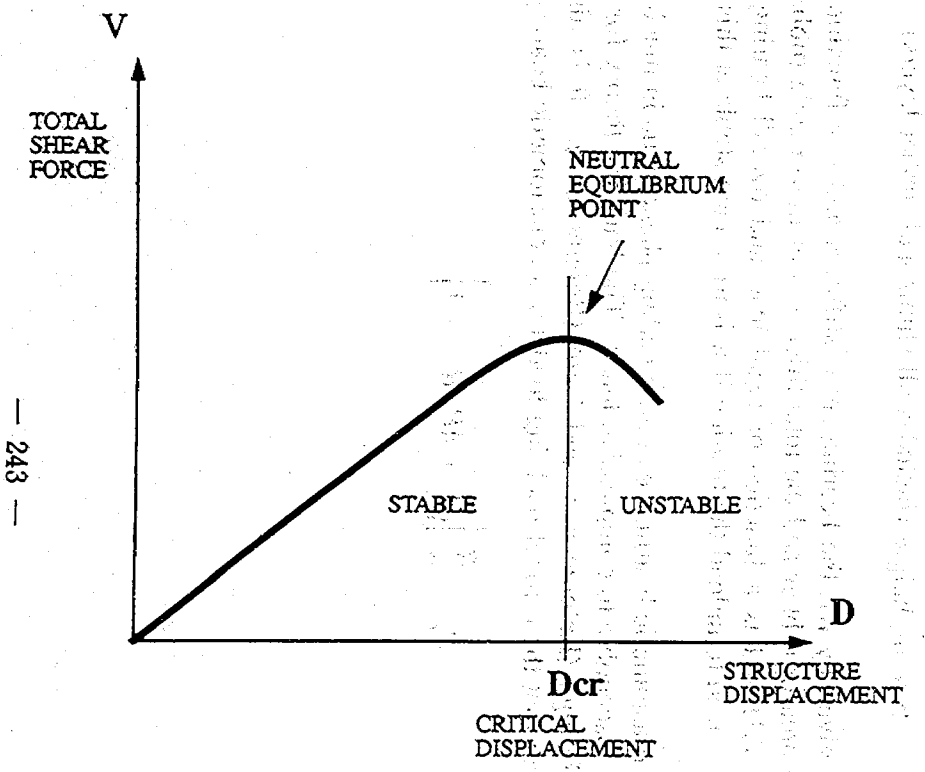


Fig. 1 SYSTEM STABILITY

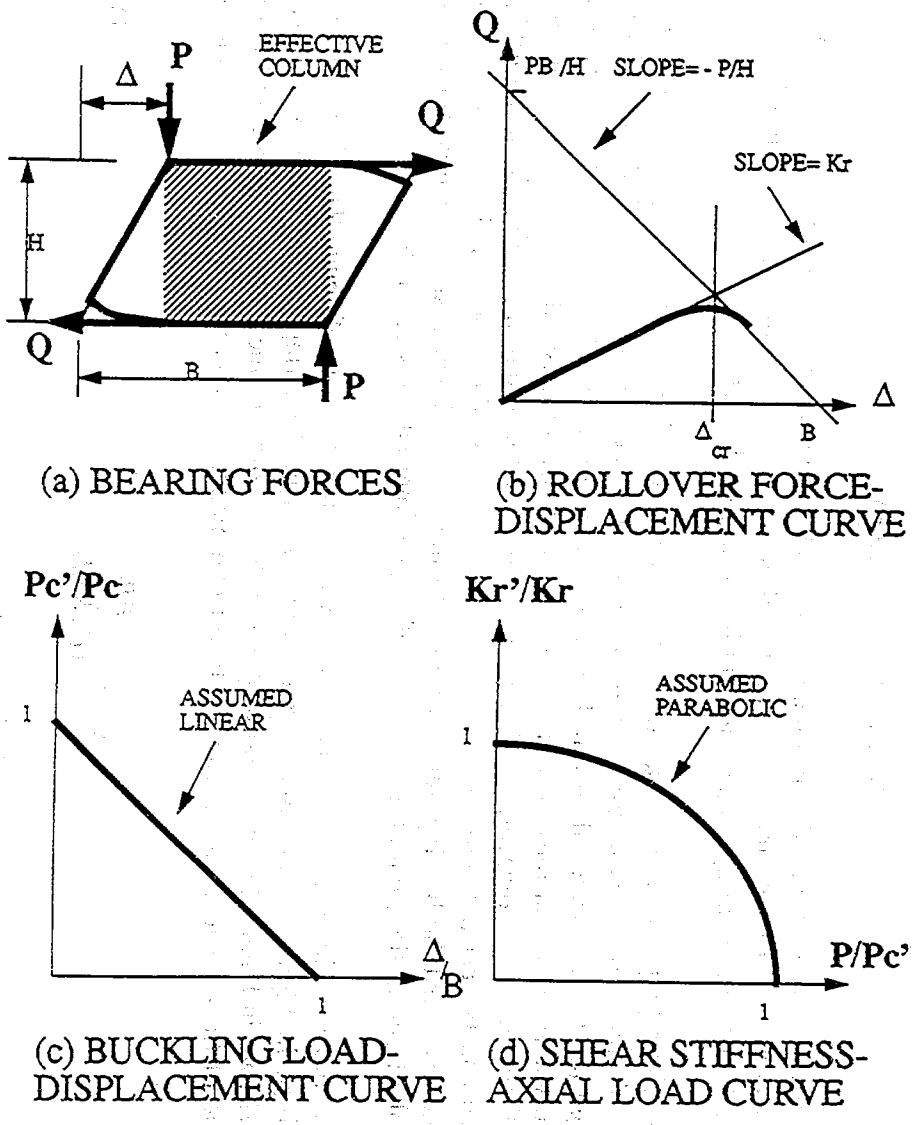


Fig. 2 ROLLOVER AND BUCKLING LIMIT STATES FOR AN ELASTOMERIC BEARING

BEARING STABILITY

To construct a system load-displacement curve such as that shown in Figure 1, the individual bearing limit states must first be modelled. As noted above, the two limit states affecting bearing stability are rollover and buckling. These are further described below.

The Rollover Limit State Rollover may occur in bearings which are fastened by dowels to the masonry and sole plates of the structure. These shear-only connections do not permit the transfer of tension through the bearing which therefore limit tensile stresses in the elastomer to acceptably low levels. Conservative limits on these stresses have been imposed because of the uncertain behavior of rubber in direct tension. However, the absence of a tension connection means that the overturning moment which can be resisted across the upper and lower faces of the bearing is limited to a finite value and once exceeded the bearing must overturn. Rollover at high shear strains can be prevented by using a bolted connection, but at the expense of higher internal stresses in the bearing.

The theory describing rollover has been previously presented (Reference 2). The essential results are given in Figure 2 and summarized below. A typical bearing on the point of rollover instability is shown in Figure 2a and the corresponding force - displacement curve is given in Figure 2b. The value of the displacement at which rollover commences, unless the shear force is reduced, is given by:

$$\Delta_{ro} = \frac{PB}{(P+Kr.H)} \qquad (1)$$

where:

Δ_{ro}	=	rollover displacement
P	=	axial (compressive) load on bearing
B	=	bearing width (shim width)
Kr	=	bearing shear stiffness
H	=	bearing height (includes all shims and rubber layers)

The initial slope is given by Kr, the bearing shear stiffness and is a function of the rubber shear modulus, the bonded area of rubber and the total thickness of deformable rubber layers. The second slope is given by -P/H and is a function of axial load and overall bearing height. It is negative which indicates the need to unload the bearing if it is to remain stable at this displacement.

The Buckling Limit State Elastomeric bearings exhibit buckling phenomena in much the same way that structural columns are susceptible to compressive loads. The buckling theory for these bearings has been developed by Haringx (Reference 3) and Gent (Reference 4). It is also reported in Reference 2. It will be seen that the critical buckling load for an elastomeric bearing is given by:

$$P_c = \frac{R}{2}\left[\sqrt{1 + 4P_E/R} - 1\right] \qquad (2)$$

where:

P_E	=	$\pi^2 T/H^2$
T	=	tilting (bending) stiffness for bearing of unit total height
	=	$(E_b I)\ (H/T_r)$
R	=	shear stiffness for bearing of unit total height
	=	$K_r H$
K_r	=	shear stiffness ignoring axial load effects
	=	GA/T_r
G	=	shear modulus of rubber
A	=	bonded area of rubber
T_r	=	total thickness of rubber (excludes shims)
H	=	effective height of bearing (includes shims)
E_b	=	bending modulus
	=	$E_o\ (1 + f_b.S^2)$
E_o	=	elastic modulus of rubber
f_b	=	bending constant
S	=	layer shape factor
I	=	moment of inertia of bearing about axis of bending

However this expression neglects the effect of large shear deformation on the properties of the elastomeric "column". One way to account for these reduced section properties is to use an effective column as shown in Figure 2a. This approximate method simply scales the critical load given by Equation 2, by the ratio of the areas of the effective and actual "columns". The result, for rectangular bearings, is then as follows:

$$P_c' = P_c\left(1 - \frac{\Delta}{B}\right) \tag{3}$$

where:

P_c'	=	modified buckling load
P_c	=	classical buckling load given by Equation (2)
Δ	=	shear displacement

This relationship is illustrated in Figure 2c.

Associated with the buckling phenomenon is the corresponding dependence of shear stiffness (Kr) on axial load (a sudden decrease in stiffness may be used to indicate the onset of buckling). This dependence has also been rigorously established [Reference 4] and approximate formulations developed which are slightly easier to use. For the purpose of this study the following approximation is used [Reference 2]:

$$Kr' = Kr\left(1 - \left(\frac{P}{Pc'}\right)^2\right) \tag{4}$$

where:

Kr'	=	modified shear stiffness

This relationship is illustrated in Figure 2d. It will be seen that when the axial load is small compared to the buckling load ($P < 0.3Pc'$), there is less than a 10% reduction in stiffness and in these cases this effect can be neglected. Since most elastomeric bearings have squat aspect ratios, their buckling loads are inherently high at small shear displacements. But, at higher displacements and for bearings with more slender geometries, this reduction in stiffness will be important.

NUMERICAL CASE STUDIES OF AN ELASTOMERIC SYSTEM

To investigate system stability and its relationship to individual bearing stability, a number of simple case studies have been completed (Reference 5). The method of analysis was to impose a monotonically increasing shear displacement to the system and back-calculate the resulting forces using a step-by-step procedure. The following assumptions were made:

a. the isolated structures are rigid masses.
b. the elastomeric bearings have linear properties, and
c. the bearing displacements are small compared to the dimensions of the structure so that the equations of equilibrium can be written in the undeformed state.

Instabilities due to rollover and buckling were studied. The influence of variable axial loads (due to overturning effects in the superstructure), and the stabilizing effect of bearings of different stiffnesses and in less critical states were examined (Reference 5).

In this paper the earlier studies relating to buckling are re-examined. Two cases are examined in which three bearings support a rigid superstructure. In the first case all of bearings are identical in size even though they carry different axial loads. In the second case the middle bearing is twice the size of the two outer bearings. These details are summarized in Table 1.

TABLE 1

BEARING PROPERTIES FOR BUCKLING STUDY

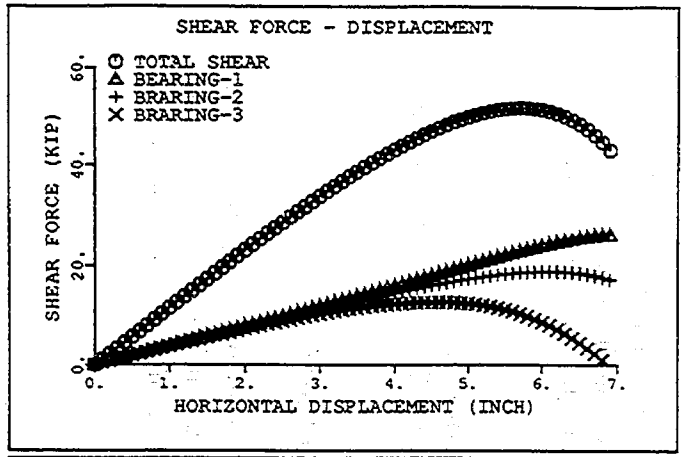
CASE	NUMBER OF BEARINGS	BEARING PROPERTIES						TOTAL STRUCTURE WEIGHT W
		BEARING NO. 1		BEARING NO. 2		BEARING NO. 3		
		K_1	B_1xH_1	K_2	B_2xH_2	K_3	B_3xH_3	
1	3	4.12	10x3	4.12	10x3	4.12	10x3	181.2
2	3	4.12	10x3	16.48	20x3	4.12	20x3	

Notes: K_i = Shear stiffness of bearing i
B_i = Width of bearing i
H_i = Height of bearing i
All dimensions in inches
All weights and forces in Kips

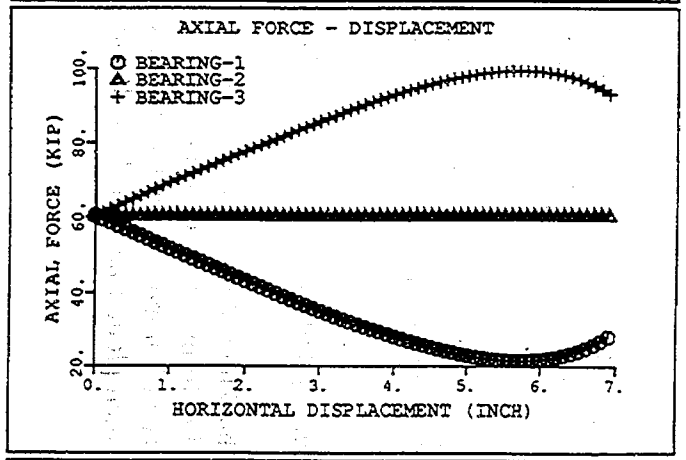
System Stability During Buckling As noted above, this study on buckling involved a 3-bearing system. In the first instance the three bearings were identical and had a classical buckling load (Pc) of 302 Kips each. The total weight of the structure was set at 20% of the total buckling load. In the second case, bearing 2 was replaced with one twice the size which had a buckling load (Pc) of 4795 Kips. In this case the weight of the structure was increased to about 30% of the new total buckling load.

The results of the analyses are shown in Figures 3 and 4. Both figures show the dependence of shear force, bearing axial force and bearing stiffness on shear displacement. The variation in axial force (Figures 3b and 4b) arises from overturning effects in the superstructure and the consequential

(a)



(b)



(c)

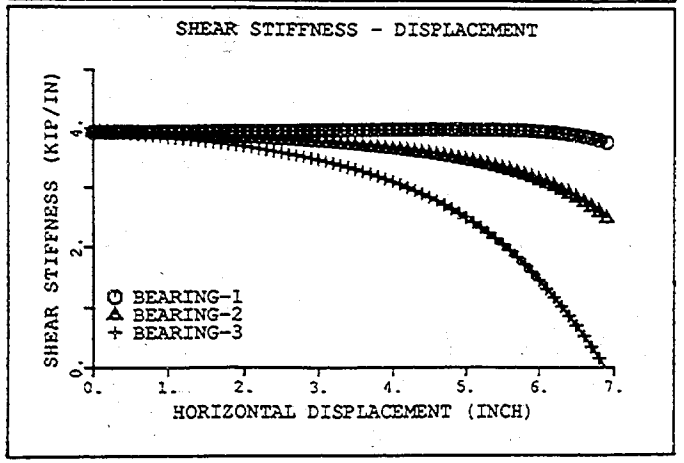
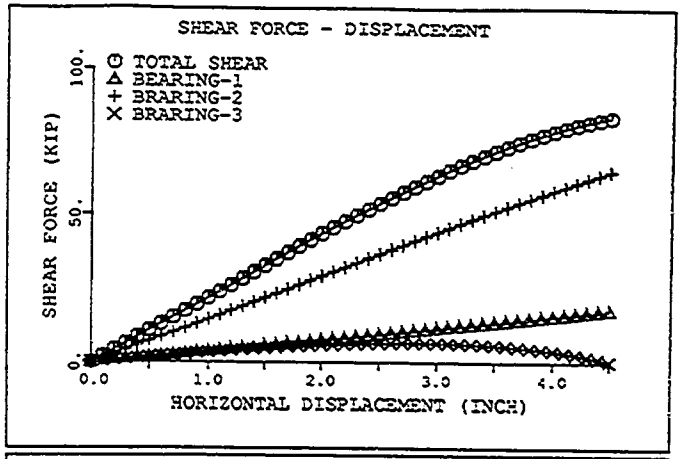
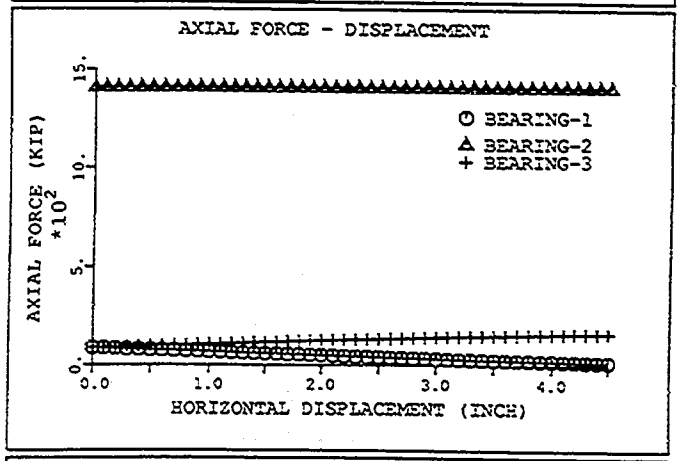


Fig.3 BUCKLING BEHAVIOR IN A 3-BEARING SYSTEM WITH EQUAL PROPERTIES

(a)



(b)



(c)

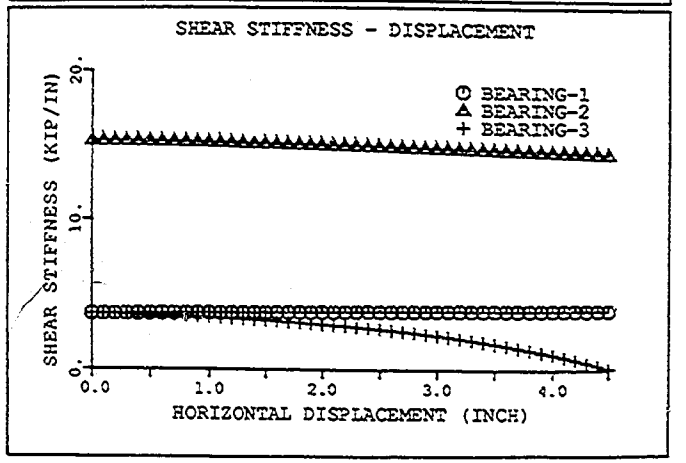


Fig. 4 BUCKLING BEHAVIOR IN A 3-BEARING SYSTEM WITH UNEQUAL PROPERTIES

changes needed in the reactions to counter this effect. As noted above in Equations 3 and 4, both the axial force and shear displacement affect the shear stiffness. Note also that Kr' in Equation (4) is a secant stiffness, and is not a measure of the tangential slope of the load - displacement curve.

Examination of Figure 3c shows that bearing 3, which carries the greatest axial load, softens under the combined effect of increasing axial load and decreasing buckling load until it has zero stiffness at approximately 6.8 inches. (The buckling load decreases because of the increasing shear displacement and the corresponding reduction in effective column area.) At this point, bearing 3 has reached its buckling limit state. The other two bearings are also softening due to similar effects but not to the same extent as bearing 3. The combined effect for the system of three bearings is a load-displacement curve shown in Figure 3a. It is seen that the positive (tangential) stiffnesses of bearings 1 and 2 are not sufficient to counter the destabilizing influence of bearing 3 and the whole system passes from stable to unstable equilibrium at about 5.7 inches.

It follows that if the combined stiffnesses of bearings 1 and 2 were larger, the system could remain stable despite the unstable state of bearing 3. This is demonstrated in Figure 4. Here bearing 2 has been doubled in size and to keep the result meaningful the total structure weight has also been increased in proportion to the increased bearing capacity. The same trends are seen in Figure 4 as in Figure 3 but the system does indeed remain stable despite the instability of bearing 3. Figure 4c shows the secant shear stiffness of bearing 3 decreasing steadily until it is zero at 4.5 inches of displacement. At this point the bearing has reached its buckling limit state but cannot fail while it is restrained by the other bearings in the system. Figure 4b shows the variation in axial load with shear. The large load attracted to the bearing 2 is due to its much larger axial (compressive) stiffness and because of its symmetrical location, its share of the total axial load does not change with increasing shear. As a consequence this bearing has a strong stabilizing influence on the system as a whole, which is seen in Figure 4a. Despite the condition of bearing 3 at 4.5 inches, the system shear force - displacement curve continues to have positive stiffness and the system critical displacement (its neutral point) is in excess of 4.5 inches.

The instability of bearing 3 in both of the previous cases is of also particular interest. It arises (theoretically) because the apparent critical load P_c' reduces dramatically with increasing deflection (Δ), in accordance with Equation (3). This reduction in P_c' in turn affects the apparent stiffness K_r' as given by Equation (4).

Since Equation (3) is an empirical expression and in view of its profound effect on the results, it was decided to investigate the validity of this relationship more carefully. This is described in the following sections.

CRITICAL (BUCKLING) LOADS AT HIGH SHEAR STRAIN FOR SINGLE BEARINGS

The approach used for this buckling study was to analyze a series of single elastomeric bearings of varying shape factors and deformed to increasing shear strains, using a nonlinear finite element methodology. Critical loads at each imposed shear strain were determined using a Southwell Plot procedure and these loads were then plotted against the Δ/B ratio.

Finite Element Solution

The ADINA [6] computer program was used for this analysis. ADINA permits the geometrical and material nonlinear analysis of both compressible and almost incompressible solids. Incremental analysis, using contact boundary elements as necessary, is performed using a displacement - pressure finite element formulation. The Mooney-Rivlin material model was used to characterize the elastomer at high strains and large deformations. A hydrostatic work term was added to the energy function to permit the inclusion of compressibility in the elastomer (although very small).

In order to reduce the computational effort a plane strain restriction was imposed so that 2-dimensional analyses could be performed. This assumption is valid for strip bearings, and care must be taken when applying these results to square or rectangular bearings. For this reason the ratio of the critical loads at different Δ is considered to be more reliable than the absolute value of the critical load.

Bearings Analyzed

Table 2 summarizes the six bearings analyzed thus far. These are seen to comprise 3, 5" wide bearings with internal layers of 1/4, 1/2 and 3/4 inch and 3, 10" wide bearings with the same range of layer thicknesses. The shape factors range from 3.3 to 20. The number of layers also varies so that the total height remains virtually constant (which is important in a comparative study of buckling loads).

TABLE 2

BEARING PROPERTIES FOR FINITE ELEMENT STUDY

No.	Bearing Size	Number of Layers	Thickness of Steel (in)	Shape Factor	Critical Loads at Zero Shear		
					Gent [4] Pcr (kip)	ADINA Pmax (kip)	ADINA Southwell (kip)
1	5x4.375	3	0.75	3.33	4.467	5.586	5.749
3	5x4.375	4	0.50	5.0	6.961	9.078	9.22
4	5x4.385	8	0.25	10.0	13.304	15.16	15.352
5	10x4.375	3	0.75	6.67	32.783	35.28	33.36
7	10x4.375	4	0.50	10.0	54.01	61.09	57.282
8	10x4.385	8	0.25	20.0	106.771	109.69	102.050

Analysis Procedure

Each bearing was first deformed in shear to a predetermined lateral displacement (Δ) and then additional lateral displacements (δ) were monitored as the axial load (P) was montonically increased. The ratio P/δ was plotted against P, as in the Southwell procedure, and a straight line fitted to the calculated responses. The intercept of this line with the horizontal axis is an indicator of the critical load at this displacement (Δ). Δ was then increased, and the procedure repeated to find a new critical load corresponding to this new displacement. Figure 5 shows the Southwell plot for a 10" bearing, that has 8, 1/4 inch rubber layers, a shape factor of 20, and an initial shear displacement (Δ) of 2.9 inches. The apparent critical load is 51 kips. This value is compared to the value at zero shear displacement (which was 102.5 kip) and the ratio (0.5) then plotted against Δ/B (0.29), as shown in Figure 6. Also shown in this plot are the results for all six bearings in Table 2 and for comparative purposes, the expression given by Equation (3) is included.

Discussion

It is seen in Figure 6 that whereas the trend of the ADINA results is similar to Equation (3) at small shear displacements, they differ significantly when $\Delta/B \geq 0.5$. The limiting value of $P_c' = 0$ when $\Delta = B$ is not substantiated by the ADINA/Southwell Plot data.

It appears that as the initial shear displacement (Δ) is increased, the elastomeric column changes its characteristic properties. The effective moment of inertia (I) appears to decrease with increasing Δ whereas the effective shear area appears to remain constant. Therefore, one theoretical approximation might be to calculate I based on a width (b) which reduces with increasing Δ while keeping the shear area constant.

Two such solutions are shown in Figure 7 where they are compared to the ADINA solution for a 5 inch bearing with 3, 3/4 inch layers and the straight line prediction by Equation (3).

One of these approximate solutions is labelled Case 1 in Figure 7 and is based on b = width of the equivalent column shown in Figure 2a. This value for b vanishes when $\Delta = B$. The other is labelled Case 2 and is based on b = the shortest distance between the two inclined faces of the bearing. This value for b does not vanish when $\Delta = B$, and only becomes negligibly small at extremely high values of shear strain. It is interesting to note that the ADINA result falls in between these two approximate solutions except when $\Delta/B > 0.5$. At small Δ, the Case 1 model is a good predictor of the ADINA results but as Δ increases, the Case 2 model is the better fit.

CONCLUSIONS

Many seismic isolation systems in use today, involve the use of multiple sets of elastomeric bearings of different sizes and stiffnesses. The stability of any one bearing at high shear strain is governed by rollover and buckling considerations but the stability of the complete bearing system is a function of total system stiffness. As a consequence, instability in one bearing does not necessarily mean that the system as a whole is unstable.

Instabilities which arise from the loss of lateral stiffness due to buckling effects, can be determined by maintaining a real-time summation of the instantaneous (tangential) bearing stiffnesses. A change in the sign of this summation is indicative of the system passing from stable to unstable equilibrium. The displacement at which this occurs can be used to calculate a system factor of safety against buckling once the system displacement has been calculated for the design earthquake. It is

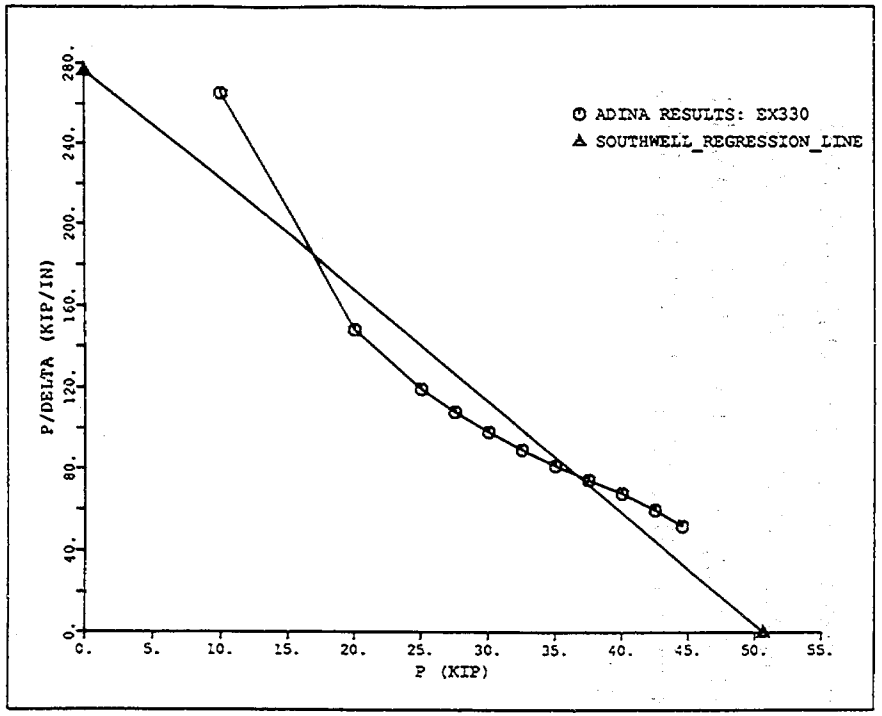


Fig.5 SOUTHWELL PLOT FOR A 10 INCH ELASTOMERIC BEARING AT 2.9 INCH INITIAL SHEAR DISPLACEMENT

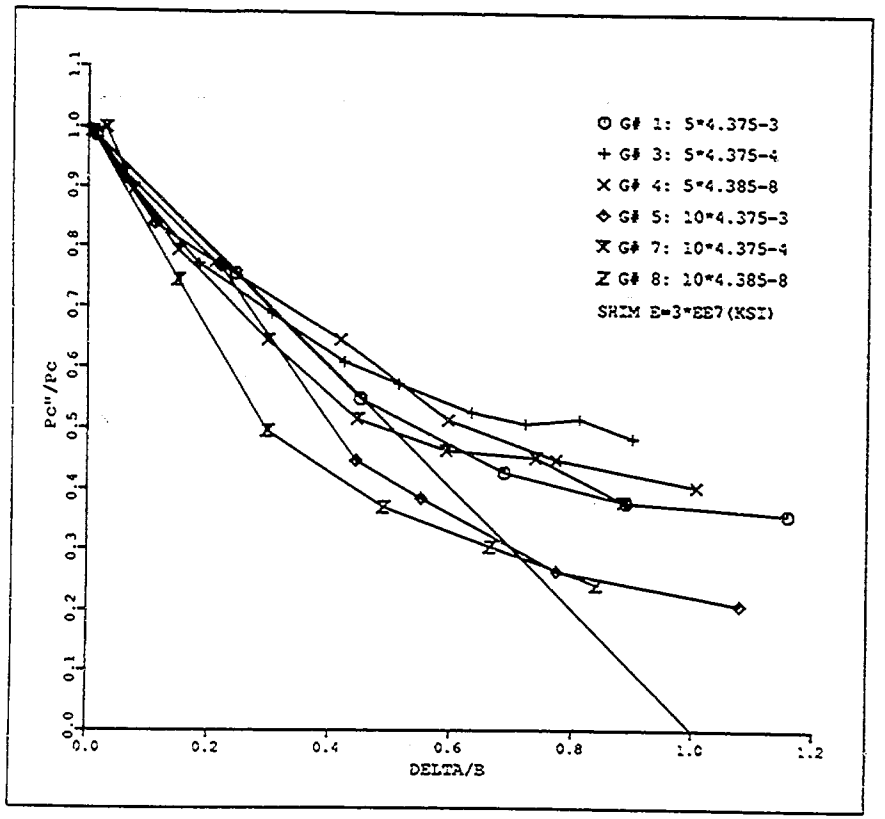


Fig.6 EFFECT OF SHEAR DISPLACEMENT ON THE CRITICAL LOADS OF VARIOUS ELASTOMERIC BEARINGS

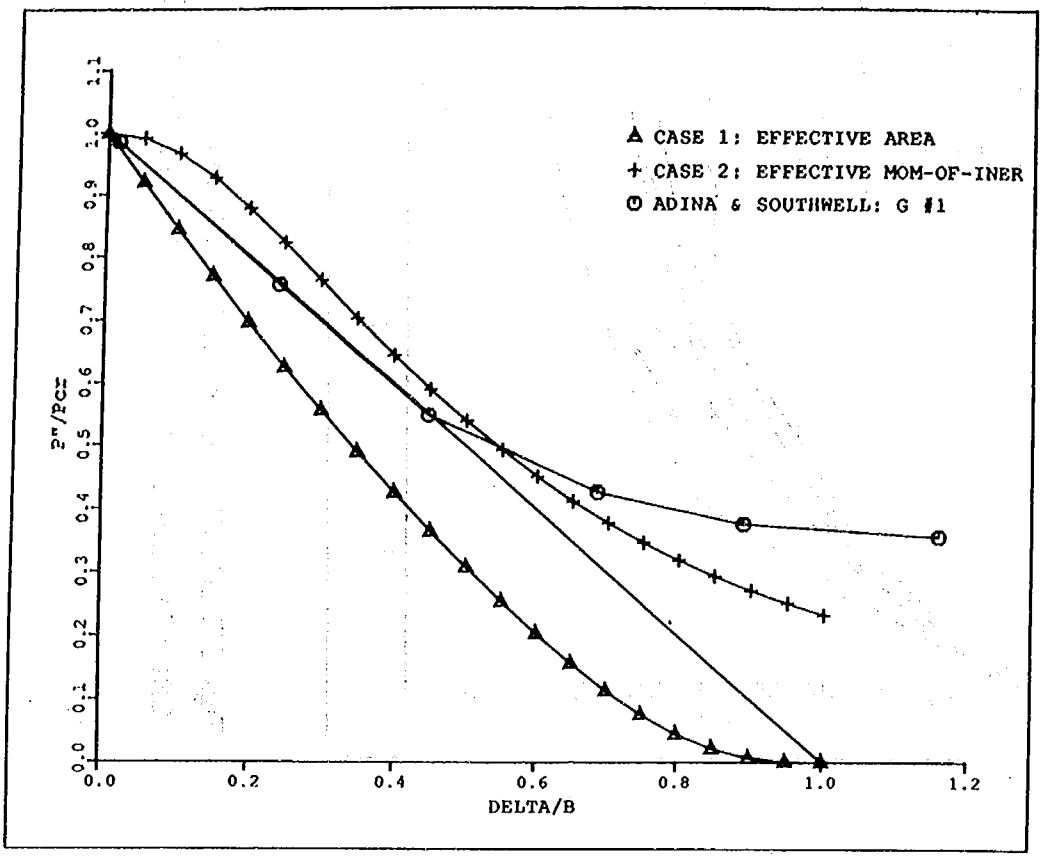


Fig.7 COMPARISON OF TWO APPROXIMATE METHODS, THE ADINA SOLUTION AND THE AREA REDUCTION FORMULA FOR THE ESTIMATION OF CRITICAL LOADS OF A 5 INCH ELASTOMERIC BEARING AT INCREASING SHEAR DISPLACEMENT

noted however that the calculation of the instantaneous stiffnesses is not a trivial exercise, and further work is required here to develop a practical procedure for the calculation of the factor of safety.

It is also concluded that the reduction in critical buckling load due to the effect of high shear strain is conservatively estimated by the area reduction formula especially at high shear displacements. It appears from a limited set of ADINA finite element analyses that a substantial reserve of vertical load capacity exists even when the shear displacement is equal to the width of the bearing.

ACKNOWLEDGEMENT

The work described in this paper was funded by the National Science Foundation through the National Center for Earthquake Engineering Research under Projects 89-2105 and 89-2106. These Projects are part of a larger coordinated study on the mechanics of elastomeric isolation bearings at high shear strain which involves researchers at the State University of New York at Buffalo, the University of California at Irvine and the University of Washington. The contributions of these researchers to this study is hereby acknowledged.

REFERENCES

1. Buckle, I.G. and Mayes, R.L., "Seismic Isolation: History, Application and Performance -- A World View," Earthquake SPECTRA, Vol. 6, No. 2, May 1990, pp. 161-201.

2. Buckle, I.G. and Kelly, J.M., "Properties of Slender Elastomeric Isolation Bearings During Shake Table Studies of a Large Scale Model Bridge Deck," Proc. Second World Congress on Joints and Bearings, San Antonio, 1986, also in Special Publication on Joint Sealing and Bearing Systems for Concrete Structures, American Concrete Institute, SP-94, Detroit, 1986, pp. 247-269.

3. Haringx, J.A., "On Highly Compressible Helical Springs and Rubber Rods and Their Application for Vibration-Free Mountings, II," Philips Research Report, Vol. 4, No. 49, 1949.

4. Gent, A.N., "Elastic Stability of Rubber Compression Springs," J1. Mechanical Engineering Science, Vol. 6, No. 4, 1964, pp. 318-326.

5. Buckle, I.G. and Liu, He, "Stability of Elastomeric Isolation Systems for Buildings", Proc. Intl. Workshop Recent Developments in Base-Isolation Techniques, Architectural Institute of Japan, Tokyo, 1992.

6. Bathe, K.J., "Nonlinear Finite Element Analysis and ADINA", Proc. Sixth ADINA Conference, Massachusetts Institute of Technology, Cambridge, 1987.

DEVELOPMENT OF EXPANSION JOINT, STOPPER AND KNOCK-OFF ABUTMENT FOR MENSHIN BRIDGES

Yozo GOTO[1], Toshio KIKUCHI[2], Teruo KIMISHIMA[3],
Fumio MATSUMOTO[4], Daisuke OZAKI [5], Atsuyuki TSUKAMOTO[6]

[1] Technical Research Institute, Obayashi Corporation, Kiyose-shi, Tokyo, Japan
[2] Technical Research Institute, Obayashi Corporation, Kiyose-shi, Tokyo, Japan
[3] Engineering Department, Nippon Chuzo Co.,Ltd., Kawasaki, Kanagawa, Japan
[4] Technical Department, Tokyo Fabric Industry Co., Shinjuku-ku, Tokyo, Japan
[5] Technology Research Center, Taisei Corporation, Yokohama, Kanagawa, Japan
[6] Civil Engineering Division, Taisei Corporation, Shinjuku-ku, Tokyo, Japan

SUMMARY

This report deals with the development of expansion joint, stopper and knock-off abutment for Menshin bridges. Together with Menshin devices, these ancillary facilities are also important for Menshin bridges. The basic characteristics of these devices have been understood to a certain extend, as reported in the U.S.-Japan Workshop last year[5), 6), 7)]. This paper elaborates on the main points of design method for each device, and the possibility to design each device through test design is mentioned.

INTRODUCTION

Menshin design is a design method capable of dispersing the inertia force of superstructure. In addition to this, by extending the seismic period and improving the damping performance, the inertia force during earthquakes can be reduced. However, relative displacement between super and substructure tends to become larger even though the inertia force decreases. In order to avoid great gap at the location of abutment due to this large displacement, knock-off abutment is necessary. Generally, Menshin design is done in longitudinal direction. If this is also to be applied to transverse direction, relative displacement between super and substructure in this direction occurs. Therefore, expansion joint is required to be fixed in transverse direction at the meeting point of deck and abutment. Moreover, it is necessary to restrain the relative displacement at stopper to ensure no detriment to Menshin devices, besides preventing the worst situation: falling-off caused by displacement between super and substructure which exceeds the value stated in design. If stopper operates in a sudden, intensed impact happens, to alleviate this, development of stopper equipped with shock absorber is necessary.

From the points stated above, it is obvious that new technical development for expansion joint, stopper etc. is required for Menshin bridges, apart from Menshin devices. This paper reports on 3 unique ancillary facilities used in Menshin bridges : all direction expansion joint, stopper with shock absorber and knock-off abutment which were developed in the effort to solve the above technical problems.

EXPANSION JOINT

Basic Structure In the case of applying Menshin design to both longitudinal and transverse directions, expension joint movable in two horizontal directions is required.

With this in mind, expension joint used for Menshin bridges, movable in two horizontal directions without hindering the movement of deck during earthquakes was developed.

Basic structural outline is shown in Fig.1 and Fig.2. The sliding surface in transverse direction consists of a teflon plate and a stainless plate. The movement of bridge deck in transverse direction is absorbed when the substructure finger plate is moved by the comb shaped superstructure finger plate. On the other hand, the movement of bridge deck in longitudinal direction is absorbed by the combed shape part of superstructure finger plate placed on substructure finger plate.

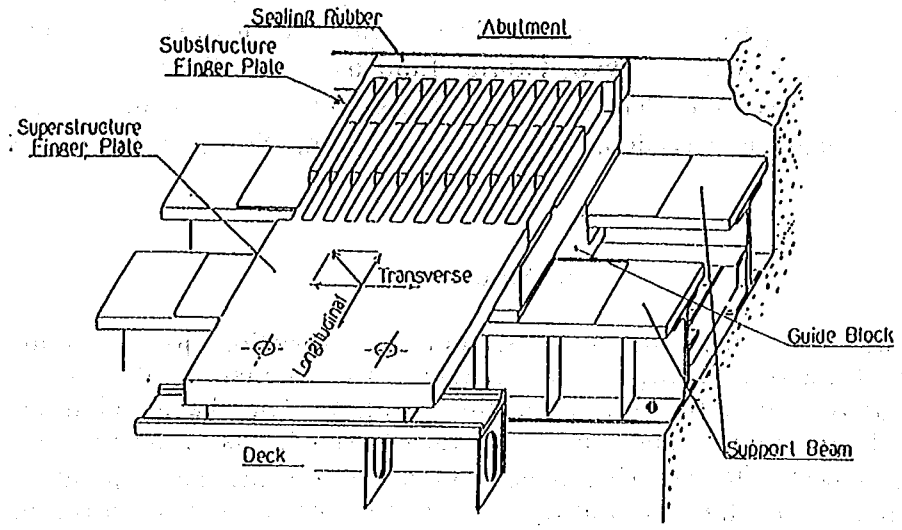


Fig. 1 Structural Outline (Showing 1 Block of Finger Plate)

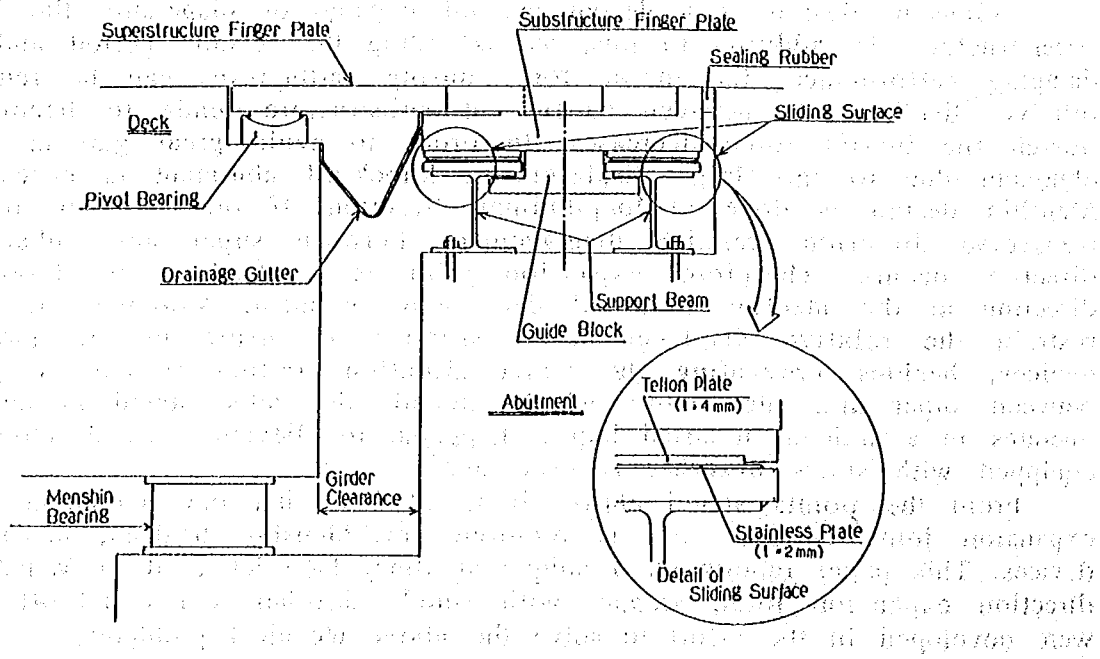


Fig.2 Cross-Section

Substantiated Experiment Excitation test on shaking table as shown in Photo 1 was conducted to confirm the ability of relative displacement absorption in both longitudinal and transverse directions simultaneously as well as to confirm that the

resistant force was small. In this experiment, besides sinusoidal excitation, wave model of deck vibration was applied in three directions i.e., longitudinal direction, transverse direction and direction at 45 degree from longitudinal direction.

Through this subtantiated experiment, the ability of the expansion joint developed in this research to cope with the vibration of bridge deck in various directions of horizontal surface was verified[5]. It was also clarified that the effect of resistant force of expansion joint on the inertia force of Menshin bridges was small[5].

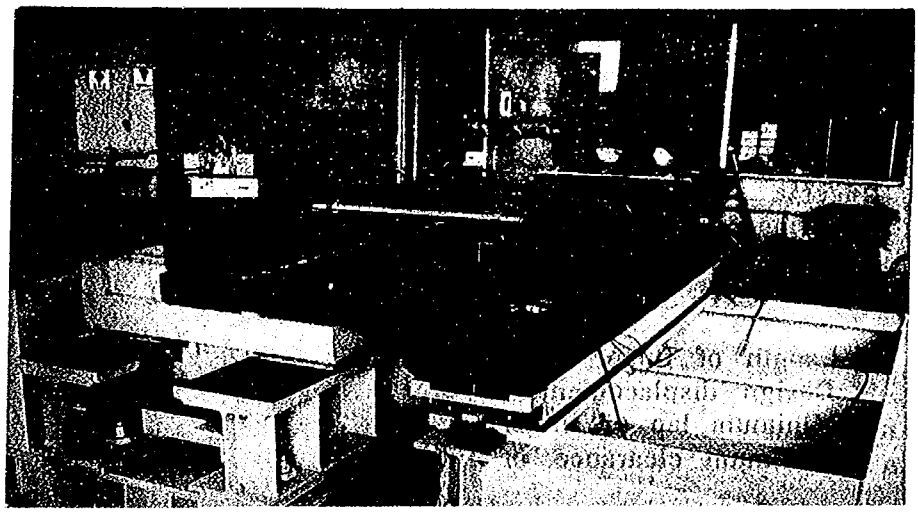
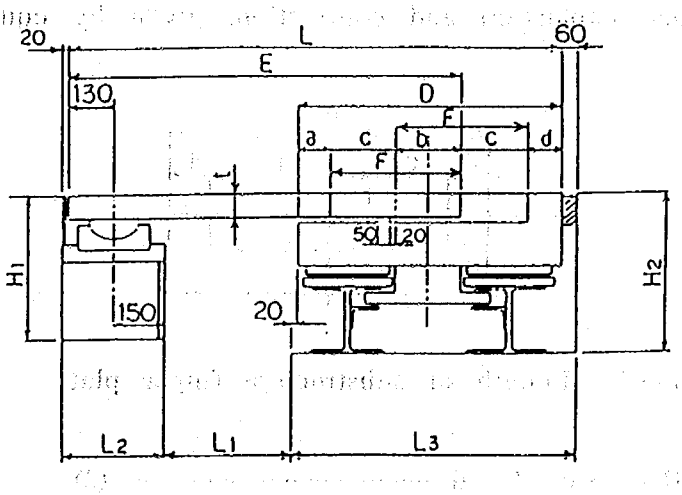


Photo 1 Substantiated Experiment of all direction expansion joint

Design Method

(a) Sphere of Application This device allows movement of bridge deck in all horizontal directions i.e. in both longitudinal and transverse directions. Possible maximum designed movement of this expansion joint is about 300 mm. The applicability of this expansion joint to bridge with large longitudinal gradient is limited, the maximum longitudinal gradient allowed is about 7%.

(b)Basic Dimensions The basic dimensions of this device are shown in Fig.3.



a : Lap length of plate (at standard temperature)
b : Lap length of finger (at standard temperature)
c : Clearance of finger (at standard temperature)
d : Length of plain part of substructure finger plate
F : Length of finger

E : Length of superstructure finger plate
L : Total length (at standard temperature)
L_1 : Gap of deck (at standard temperature)
L_2 : Length of cut of superstructure
L_3 : Length of cut of substructure

Fig.3 Basic Dimensions

i) Minimum lap length and clearance of finger

Minumum lap length and clearence of finger are as given below.

Minimum lap length of finger b_{min} = 20 mm
Minimum clearence of finger c_{min} = 15 mm

ii) Length of finger

The length of finger shown in Fig.4 is calculated by equation (1).

$$F = \Delta L + b_{min} + c_{min} \quad \cdots\cdots (1)$$

where,

F : Length of finger
ΔL : Design displacement
b_{min} : Minimum lap of finger
c_{min} : Minimum clearance of finger

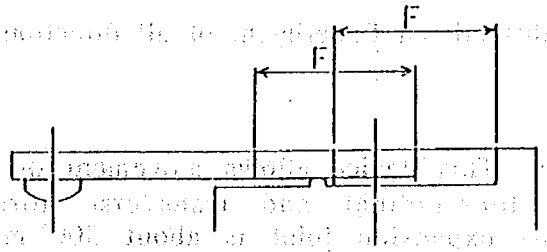


Fig.4 Length of finger

iii) Length of substructure finger plate

The length of substructure finger plate shown in Fig.5 is determined so that the comb shaped part of superstructure finger plate will not split from the substructure finger plate due to thermal expansion and contraction, given by equation (2)~(5).

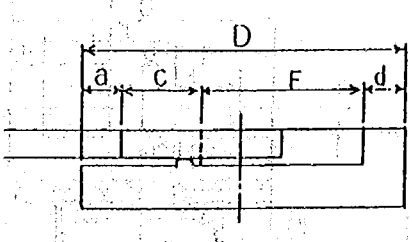


Fig.5 Length of substructure finger plate

$$D = a + c + F + d \quad \cdots\cdots (2)$$
$$a = \Delta l_t + b_{min} + \alpha \quad \cdots\cdots (3)$$
$$c = MAX(\Delta l_t, \Delta l_c) + \Delta l_c + c_{min} \quad \cdots\cdots (4)$$
$$d = a \quad \cdots\cdots (5)$$

where,

D : Length of substructure finger plate
a : Lap length of plate (at standard temperature)

c : Clearance of finger (at standard temperature)
F : Length of finger
d : Length of plain part of substructure finger plate
Δl_t : Expansive and contractive displacement of deck from standard temperature (including displacement of deck due to rotation and other alowances)
Δl_e : Displacement of deck caused by level 1 earthquake
Δl_c : Contractive displacement due to creep and shrinkage
b_{min} : Minimum lap length of finger
c_{min} : Minimum clearance of finger
α : Adjustment value of substructure finger plate

iv) Shape of finger plate

To ensure that the substructure finger plate moves smoothly in transverse direction, shape of finger plate shown in Fig.6 was chosen and it is irrelevent of length of finger plate.

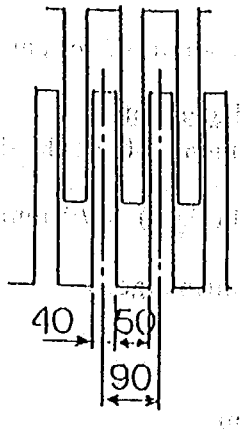


Fig.6 Shape of finger plate

v) Form of sliding surface in transverse direction

Taking into consideration the smooth sliding performance against friction and weather proof characteristic, the sliding surface in transverse direction is formed by a teflon plate and a stainless plate. The size of skid bearing's teflon plate is determined as a size adequate to stand the rear wheel load taking into account coefficient of impact for one skid bearing. The form of stainless plate is given by equation (6)~(7).

$$A = a + \alpha \quad \cdots\cdots (6)$$

$$B = b + \Delta L + \alpha \quad \cdots\cdots (7)$$

where,

A : Length of stainless plate
B : Width of stainless plate
a : Length of teflon plate
b : Width of teflon plate
ΔL : Design displacement
α : Allowance (minimum value is 20 mm)

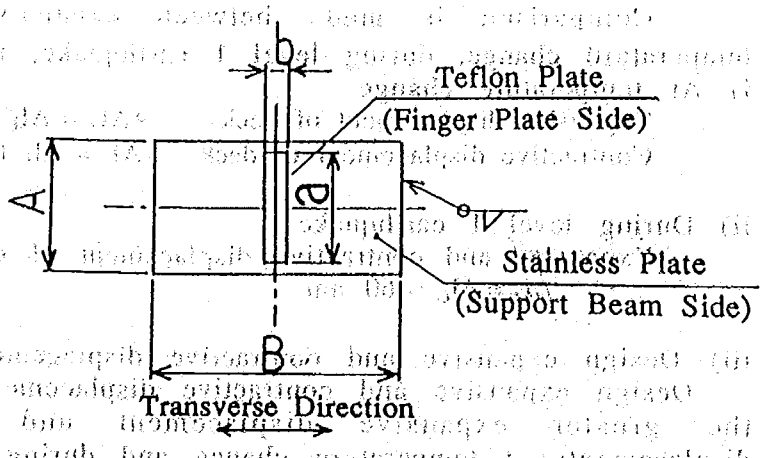


Fig.7 Form of sliding surface in transverse direction

Test Design Design of expansion joint at the location where decks of two bridges meet as shown in Fig.8 is done. Each bridge is a 5-span continuous Menshin bridge with equal span length (prestressed concrete bridge, bridge length=197.5 m).

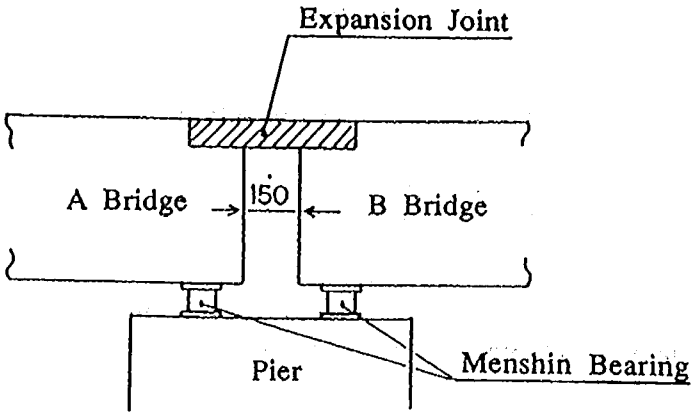


Fig.8 Location of Expansion Joint

(a) Expansive and Contractive Displacement

i) Expansive and contractive displacement of deck due to temperature change (-5 ~ +35°C)

ΔL_t = 0.4 x 197.5 / 2 x 2 (for 2 bridges) = 79 mm

ii) Displacement due to creep and shrinkage

Δl_c = 80 mm

iii) Allowance

$\Delta L_s \doteq (79 + 80) \times 0.2 + 10 = 42$ mm

iv) Expansive and contractive displacement from standard temperature(+15°C) (including allowance)

$\Delta l_t = (\Delta L_t + \Delta L_s) / 2 = 61\text{mm} \rightarrow 65$ mm

v) Expansive and contractive displacement caused by level 1 earthquake

$\Delta l_{eA} = \pm 44$ mm for Bridge A, $\Delta l_{eB} = \pm 36$ mm for Bridge B

Therefore, displacement at the meeting point of two bridges is as follow.

$$\Delta l_e = \sqrt{\Delta l_{eA}^2 + \Delta l_{eB}^2} = \sqrt{44^2 + 36^2} = 57 \text{ mm} \rightarrow 60 \text{ mm}$$

(b) Design Expansive and Contractive Displacement

Comparison is made between expansive and contractive displacement at temperature change, during level 1 earthquake, and at standard temperature (+15°C).

i) At temperature change

Expansive displacement of deck $+\Delta L = \Delta l_t = 65$ mm

Contractive displacement of deck $-\Delta L = \Delta l_t + \Delta l_c = 65 + 80 = 145$ mm

ii) During level 1 earthquake

Expansive and contractive displacement of deck is :

$\Delta L = \Delta l_e = 60$ mm

iii) Design expansive and contractive displacement

Design expansive and contractive displacement is determined as the summation of the greater expansive displacement and contractive displacement between displacements at temperature change and during level 1 earthquake.

Design expansive and contractive displacement $\Delta L = (+\Delta L_{max}) + (-\Delta L_{min})$

$= 65 + 145 = 210$ mm

(c) Structural Design The condition of expansion joint at standard temperature after creep and shrinkage is shown in Fig.9. Test design according to design method stated above was conducted.

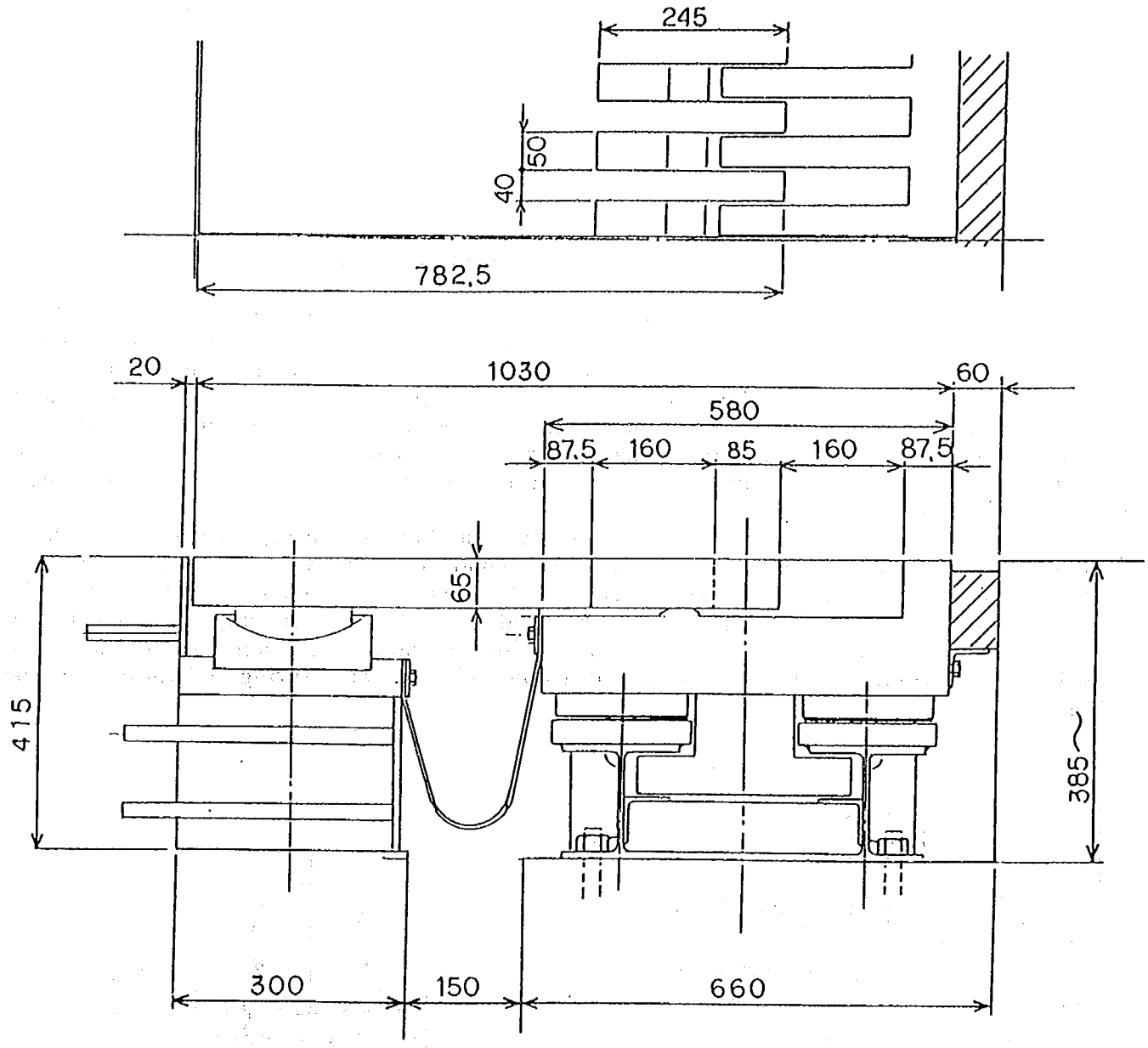
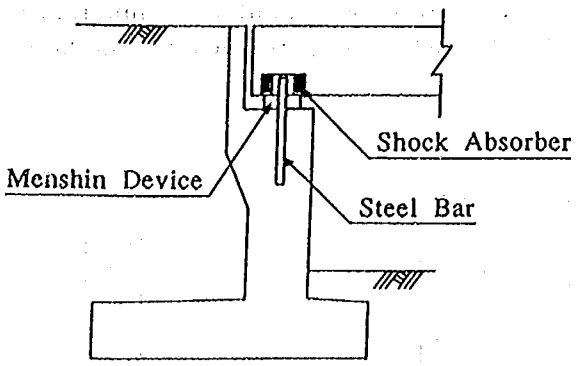


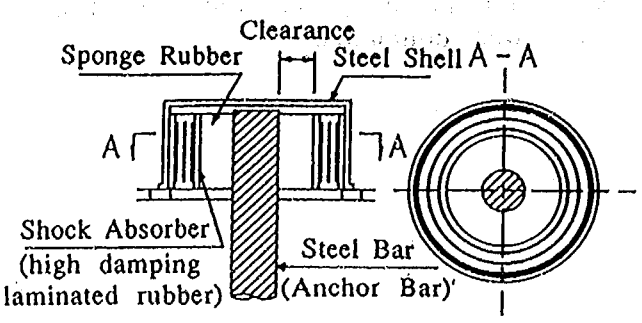
Fig.9 Example of Test Design (at standard templature, after creep and shrinkage)

STOPPER

Basic Structure Stopper equipped with shock absorber is effective in restraining the relative displacement occurred during severe earthquakes, flexibly and compulsively. With the existance of shock absorber, the intensed lateral force caused by collision between deck and abutment or pier can be softened.

By using high damping rubber as shock absorber, damping performance is increased. On the other hand, stiffness can be controlled and durability improved if high damping laminated rubber is used. Based on these factors, stopper made of high damping laminated rubber and steel bar was developed. Basic structural drawing of stopper is shown in Fig.10.





(a) Location of Stopper (b) Structural Outline

Fig. 10 Stopper with shock absorber

Equation of Spring Stiffness In order to clarify the force-deformation characteristics due to partial contact between high damping laminated rubber and steel bar, static loading test shown in Fig.11 was conducted. When the high damping laminated rubber is subject to compressive loading from steel bar as illustrated in Fig.12, contact area increases due to deformation of rubber. Since the rubber is laminated, analitical estimation of the force-deformation characteristics is difficult. Thus, experiment was carried out and empirical equations representing the force-deformation characteristics were established.

An example of the test results is shown in Fig.13. Spring stiffness of shock absorber increases slowly until one point, and beyond this, the value is almost constant. Compressive deformation of rubber varies with number of rubber layer before the spring stiffness becomes constant. From the results of this experiment, it is clear that even in the case of local loading on laminated rubber through steel bar, like considering distribution of reaction as isotropic distribution, spring stiffness can be calculated.

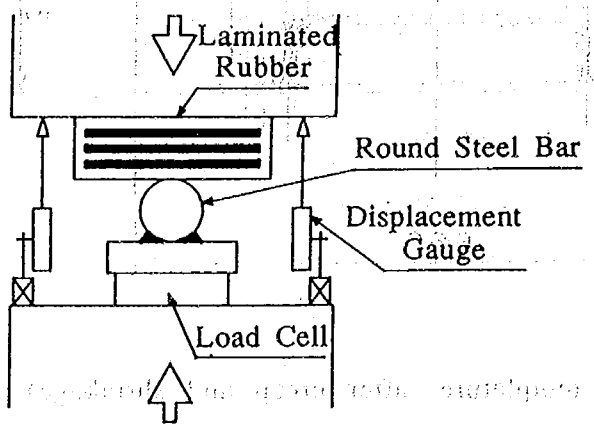


Fig.11 Compressive Deformation Test - local compression imposed by steel bar on shock absorber

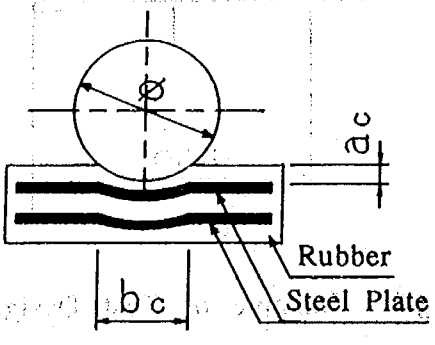


Fig.12 Contact area of shock absorber and steel bar

$$K_c = T_f \cdot G_o \cdot A_c / a_c \quad \cdots\cdots (8)$$

$$A_c = b_c \cdot L \quad \cdots\cdots (9)$$

$$a_c = (\phi - \sqrt{\phi^2 - b_c^2}) / 2 \quad \cdots\cdots (10)$$

$$b_c = b_{co} + b_{cm} n \quad \cdots\cdots (11)$$

where,

K_c : Spring stiffness of shock absortion rubber (kgf/cm)

T_f : Coeffifient obtained from experiment, equals to 212.0
G_o : Shearing modulus of laminated rubber (kgf/cm^2)
A_c : Compressive loading area of rubber and steel bar (cm^2), given by equation (9)
a_c : Caving deformation of rubber (cm) (refer to Fig.12), given by equation (10)
b_c : Compressive loading width between rubber and steel bar (cm), given by equation (11)
b_{co} : Standard value of bc for two layer of laminated rubber (cm), given in Table 1
b_{cm}: Modification value corresponding to the number of layer of laminated rubber (cm), given in Table 2
L : Length of shock absorber (cm)
ϕ : Diameter of steel bar (cm)

Table 1 Standard value b_{co} of rubber with compressive loading width b_c (two layer of laminated rubber)

Thickness of one Layer of Laminated Rubber	Diameter of Steel Bar (mm)		
	ϕ =100	ϕ =150	ϕ =200
t =12mm	5.5 cm	6.5 cm	7.5 cm
t =16mm	6.5 cm	7.5 cm	9.0 cm
t =20mm	7.5 cm	9.0 cm	11.0 cm

Table 2 Modification value b_{cm} of rubber with compressive loading width b_c (Modification value is added for each additional layer)

Thickness of one Layer of Laminated Rubber	Diameter of Steel Bar (mm)		
	ϕ =100	ϕ =150	ϕ =200
t =12mm	0.5 cm	0.5 cm	0.5 cm
t =16mm	0.5 cm	1.0 cm	1.0 cm
t =20mm	0.5 cm	1.0 cm	1.0 cm

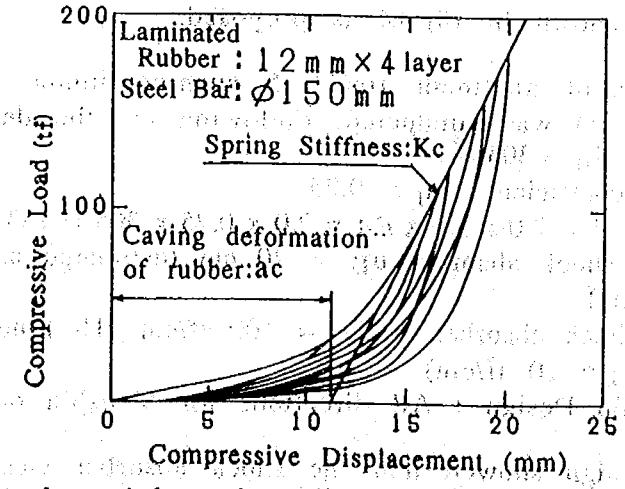


Fig. 13 Compressive force-deformation characteristics of shock absorber - an example

Spring stiffness K_c, calculated by equation (8) and deformation of shock absorber until spring stiffness becomes linear a_c, calculated by equation (10), are compared with test results in Table 3. The calculated values represent well the test results.

Table 3 Comparison of calculated values and test results for spring stiffness of shock absorber

(a) Spring stiffness of shock absorber : K_c

Unit:tf/cm

Test Case	Test Results			Calculated Values		
	Diameter of Steel Bar			Diameter of Steel Bar		
	φ100	φ150	φ200	φ100	φ150	φ200
12mm×2layers	218	321	367	226	298	349
12mm×3layers	231	300	321	204	274	325
12mm×4layers	191	212	269	184	253	304
16mm×2layers	202	273	295	184	253	285
16mm×3layers	162	205	228	166	218	253
16mm×4layers	142	164	191	150	190	226
20mm×2layers	173	214	231	150	204	226
20mm×3layers	149	180	207	136	178	204
20mm×4layers	129	137	171	122	155	184

(b) Caving deformation until spring stiffness becomes liner : a_c

Unit:mm

Test Case	Test Results			Calculated Values		
	Diameter of Steel Bar			Diameter of Steel Bar		
	φ100	φ150	φ200	φ100	φ150	φ200
12mm×2layers	7.2	7.4	7.2	8.2	7.4	7.3
12mm×3layers	9.9	8.9	9.3	10.0	8.7	8.3
12mm×4layers	11.9	10.9	10.6	12.0	10.0	9.5
16mm×2layers	11.4	11.1	10.5	12.0	10.0	10.7
16mm×3layers	14.9	14.4	13.3	14.3	13.2	13.4
16mm×4layers	17.5	16.6	16.3	16.9	17.0	16.5
20mm×2layers	16.5	17.6	16.0	16.9	15.0	16.5
20mm×3layers	21.1	20.2	19.3	20.0	19.1	20.0
20mm×4layers	25.3	23.9	23.0	23.7	24.0	24.0

Design Procedure Spring stiffness of shock absorber, K_c and deformation of shock absorber until spring stiffness becomes linear, a_c can be calculated correctly as mentioned above. After obtaining these informations, design procedure of diameter, length and number of steel bar, thickness and width of high damping laminated rubber which impose design terms such as dead load reaction and design lateral force coefficient on substructure, shown in Fig.14 is proposed.

Test Design Test design of abutment for a 5 span-continuous prestressed concrete bridge (bridge length=197.5 m) was conducted. Following are the design terms.

1 Dead load rection R_d = 305 tf
2 Design lateral force coefficient k_h = 0.25
3 Design lateral reaction H = 2.0 x k_h x R_d = 2.0 x 0.25 x 305 = 153 tf
4 Design clearence of shock absorber u_B = 20 cm (estimated as design displacement of Menshin device u_B)
5 Spring stiffness of shock absorber K_c = 100 tf/cm (10 times secondary stiffness of Menshin device K_{B2}=10 tf/cm)
6 Direction for Menshin Design : All directions for Menshin design

Results of the test design showed that the shock absorber was 20 mm x 7 layers (total thickness 185 mm) and height 170 mm, the diameter of anchor bar was φ = 180 mm and length 2425 mm. The layout and dimensions of stopper are shown in Fig.15.

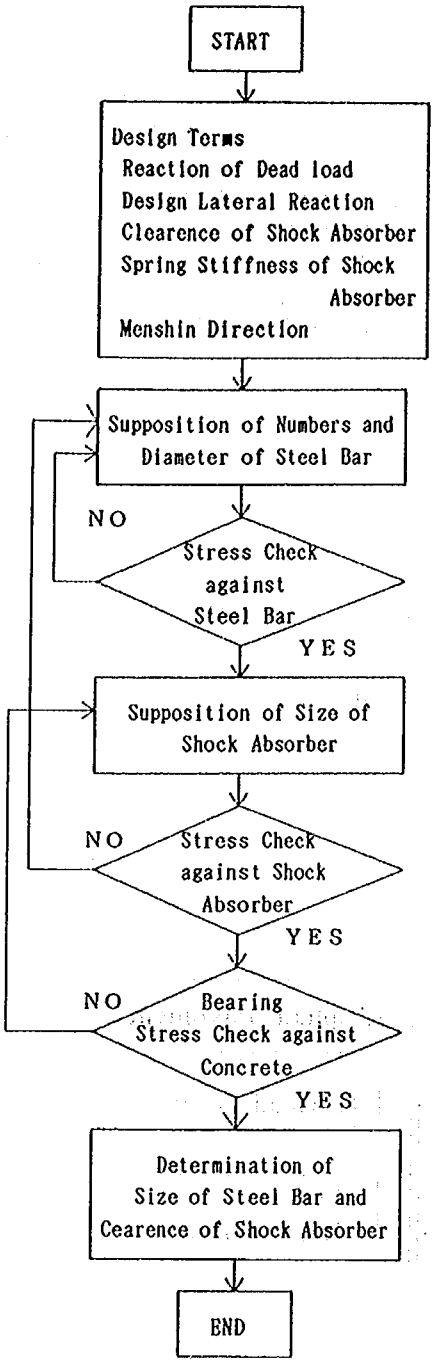


Fig. 14 Design Procedure of Stopper

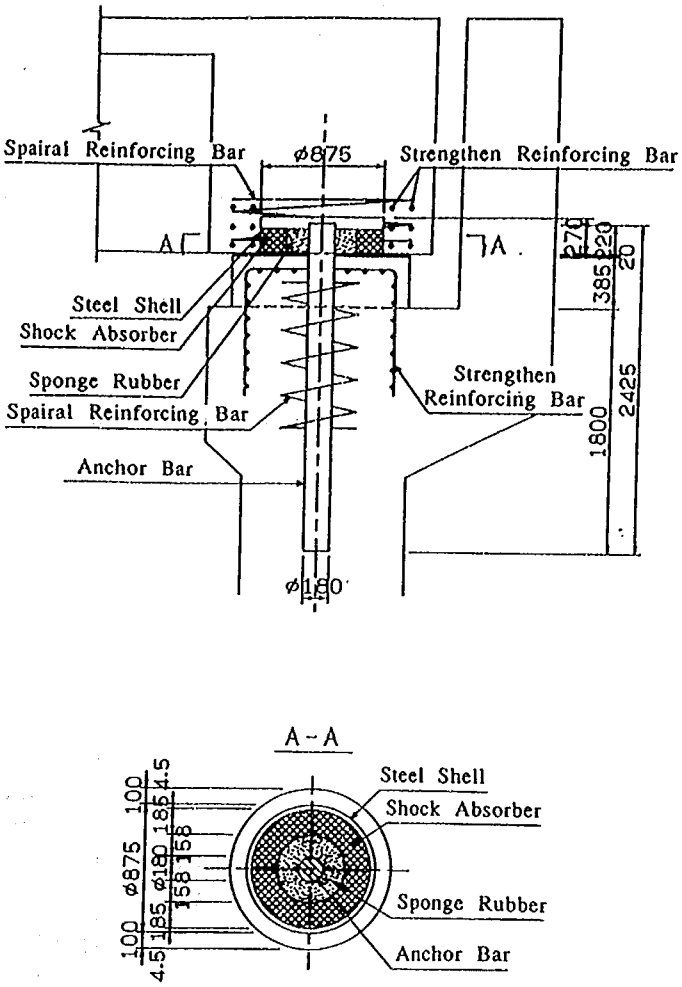
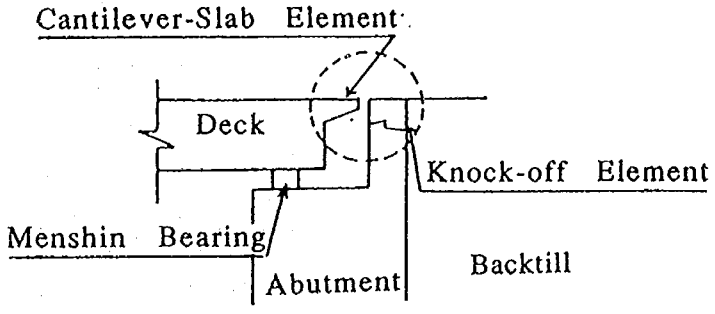


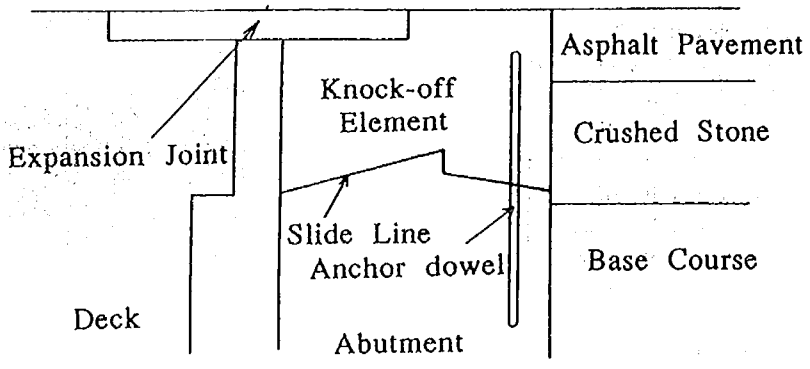
Fig.15 Layout and Dimensions of Stopper (Example of Test Design)

KNOCK-OFF ABUTMENT

Basic Structure Knock-off abutment shown in Fig.16, is already in practical use in New Zealand as one of the efforts to decrease the gap between deck and abutment of Menshin bridges. Knock-off abutment is an abutment which upper and lower parts of parapet are split in advance (the upper side is called knock-off element). In case of severe earthquake, deck vibrates strongly and collision with abutment occurs, this knock-off element is made moving toward the direction of backfill. As a result, damage to the whole parapet of abutment is avoided. Moreover, the vibration energy of deck is absorbed through the collision of deck and knock-off element, movement of knock-off element toward backfill earth and the subsequent backfill deformation.



(a) General view

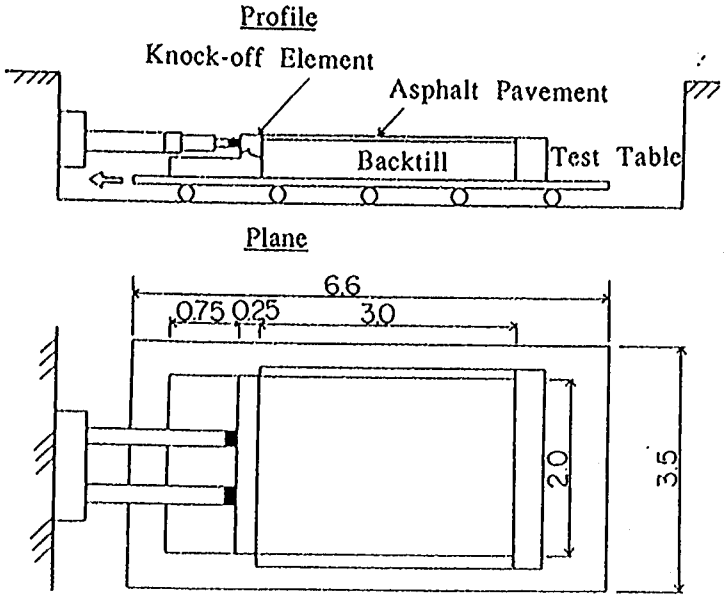


(b)Detail

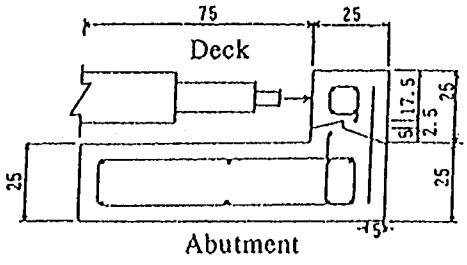
Fig. 16 Structural Outline of Knock-off Abutment

Model Experiment Damages of abutment's parapets due to collision with decks occur frequently in Japan. Though these kind of ideas were proposed and suggested, no practical effort has been done. Therefore, relevent design method has to be established.

In order to clarify the basic characteristics of knock-off abutment, model experiment shown in Fig.17 was conducted. In this experiment, parameters such as backfill (including asphalt pavement) and cases with or without anchor dowel used for resisting wheel load were studied. Through this experiment, it was understood that the resistant force was almost totally composed of passive earth pressure and deformation of asphalt pavement. Moreover, the resistant force was dependence of velocity; the larger the loading velocity, the larger the resistant force was. Also, the behavior of knock-off element was different with the existance of anchor dowel, the resistant force increased.



(a) Model drawing (unit : m)



(b) Model of knock-off abutment (unit : cm)

Fig. 17 Model of Knock-off Abutment

Calculation Method of Resistant Force The resisting elements to the sliding of knock-off element are friction force of slide surface, anchor dowel pullout resistant force, passive earth pressure of backfill and deformation resistant of asphalt pavement. Thus, these four resistant forces shown in Fig.18 are calculated and the summation of these forces is taken as the resistant load during sliding. The flow of design method is shown below.

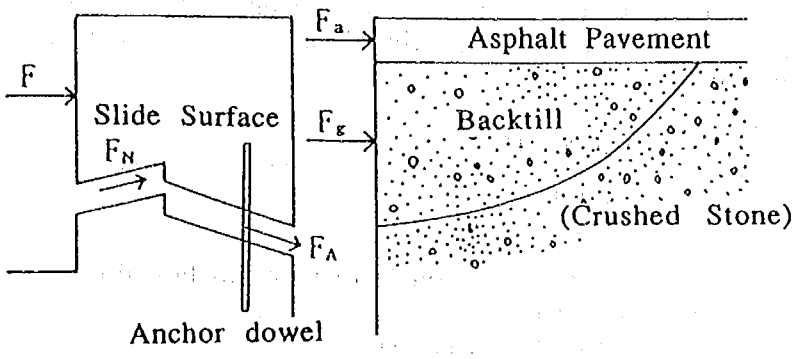


Fig. 18 Failure zone of Knock-off Abutment Backfill

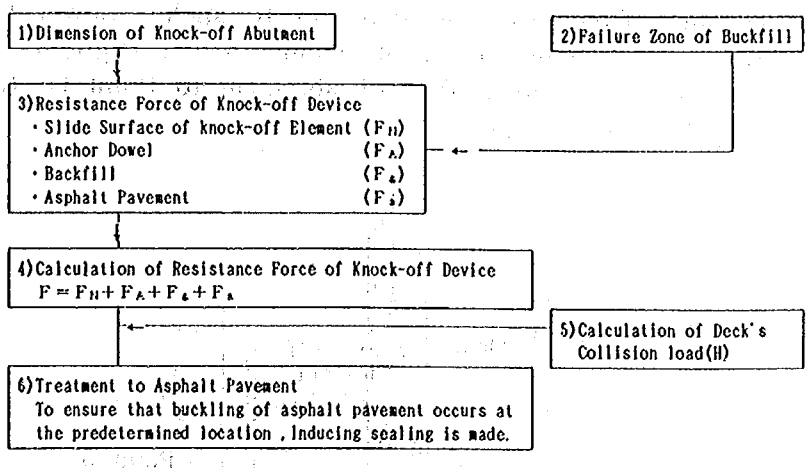


Fig. 19 Design Flow of Knock-off Abutment

(a) Resistant Force of Slide Surface Resistant force (F_N) obatined by equilibrium of forces during sliding of knock-off element shown in Fig.20 is given by the following equation.

$$F_N = \frac{W_n\ (\sin\theta_n + \mu_3 \cos\theta_n)}{\cos\theta_n - \mu_3 \sin\theta_n} \times B \quad \cdots\cdots\cdots(12)$$

where,

W_n : Weight of knock-off element
μ_3 : Coefficient of friction of concrete (from experiment, μ_3=0.2)
θ_n : Gradient of slide surface
B : Width of abutment (m)

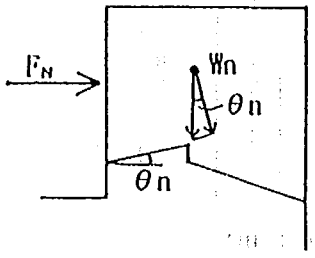


Fig.20 Force equilibrium diagram of slide Surface

(b) Resistant Force of Anchor Dowel

i) Calculation of required cross sectional area of anchor dowel

The abutment and knock-off element is connected by anchor dowel. Anchor dowel is designed against the pullout force occurred when wheel load and brake load act on the expansion joint.

Taking into consideration the rotation around Point O` in front of the abutment shown in Fig.21, required cross sectional area of anchor dowel is calculated by the following equation.

$$A_{sn} = \frac{P \cdot \ell + H \cdot e}{d \cdot \sigma_{sa}} \quad \cdots\cdots\cdots\cdots\cdots\cdots(13)$$

where,

A_{sn} : Required cross sectional area of anchor dowel (cm^2)
P : Wheel load (tf)
H : Brake load [= P x 0.1] (tf)
l : Distance from front of abutment to the location where wheel load acts (cm)
d : Distance from front of abutment to anchor dowel (cm)
σ_{sa} : Allowable tensile stress of anchor dowel (kgf/cm^2)
e : Distance from top surface of abutment to Point O` (cm)

l, d and e are as shown in Fig.21.

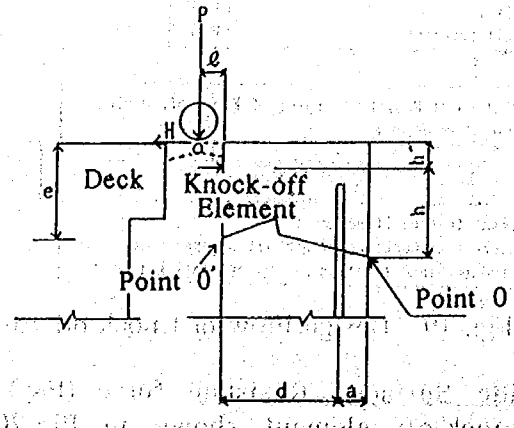


Fig.21 The actions of wheel load and brake load

ii) Required cross sectional area of anchor dowel

The following equation must be satisfied for the required cross sectional area per unit length of anchor dowel.

$$A_s \geq A_{sn} \,/\, (\text{Width of wheel load} + \text{Width of load distribution}) \quad \cdots\cdots\cdots (14)$$

iii) Resistant force of anchor dowel

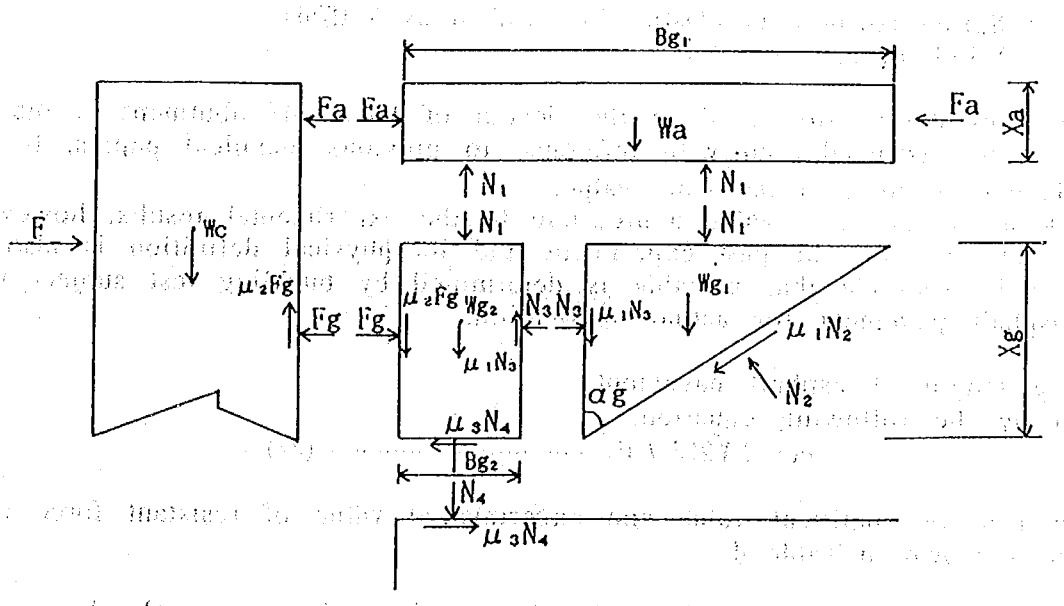
Based on the rotation around Point O, resistant force of anchor dowel (F_A) is given by the following equation.

$$F_A = \frac{A_s \cdot \sigma_{sy} \cdot a}{h} \times B \quad \cdots\cdots\cdots\cdots\cdots (15)$$

where,

A_S : Cross sectional area per m of anchor dowel (cm^2)
σ_{Sy} : Yield stress of anchor dowel (cm^2)
a : Distance from back of abutment to anchor dowel (cm)
h : Distance from Point O to the point where resistant load acts (cm)
B : Width of abutment (m)

(c) Resistant Force of Backfill Resistant force of backfill is calculated from the sub-blocks of knock-off part, asphalt pavement and crushed stone block shown in Fig.22. From the equilibrium of forces for each block, equation (17)~(19) are obtained, further, resistant force (F_g) can be calculated by equation (16).



Legend	
W_n:Weight of Knock-off Element	E_a:Modulus of Deformation of Asphalt Pavement
W_a:Weight of Asphalt Pavement	E_s:Modulus of Deformation of Crushed Stone
W_{s1}, W_{s2}:Weight of Crushed Stone	μ_1:Friction Coefficient between Crushed Stone and Crushed Stone
γ_a:Density of Asphalt Pavement	μ_2:Friction Coefficient between Crushed Stone and Concrete
γ_s:Density of Crushed Stone	
ϕ :Friction Angle of Crushed Stone	
α_s:Sliding Angle of Crushed Stone	

Fig.22 Force Equilibrium Diagram of Knock-off, Asphalt Pavement and Crushed Stone

$$F_s = \frac{N_3 + \mu_1 w_{s2}}{1 - \mu_1 \mu_2} \quad \cdots\cdots (16)$$

$$N_3 = \frac{-(N_1 + w_{s1})}{K} \quad \cdots\cdots (17)$$

$$K = \frac{\mu_1 \cos \alpha_s - \sin \alpha_s}{\mu_1 \sin \alpha_s + \cos \alpha_s} \quad \cdots\cdots (18)$$

$$N_1 = \frac{B_{s1}}{2} w_a \times \frac{3}{B_{s1} - 2 B_{s2}} \quad \cdots\cdots (19)$$

(d)Resistant Force of Asphalt Pavement

i) Calculation of resistant force of asphalt pavement

Based on buckling theory of beam on elastic floor, resistant force of asphalt pavement is calculated by the following equation.

$$F_a = 2\sqrt{E \cdot I \cdot k \times B} \quad \cdots\cdots (20)$$

where,

E : Modulus of deformation of asphalt pavement (kgf/cm^2)
I : Asphalt pavement's moment of inertia of area (cm^4)
k : Spring stiffness of elastic floor (taken as 5 tf/m)
B : Width of abutment (m)

Modulus of deformation used in the design of knock-off abutment is the possible and largest value assumed, and with reference to previous technical papers, E = 28000 kgf/cm^2 is considered as a resonable value.

This k is chosen as a value appropriate to the experimental results, however, there were very few examples of past experiment and its physical definition is also unclear. Therefore, it is desirable that k value is determined by buckling test subject to lateral force of asphalt pavement for actual application.

ii) Buckling length of asphalt pavement

Given by the following equation.

$$l_B = 2\sqrt{2EI / F_a} \quad \cdots\cdots (21)$$

Comparison of analitical value and experimental value of resistant force of knock-off element is shown in Table 4

Table 4 Comparison of analitical value and experimental value of resistant force of knock-off abutment

Unit:tf

Experimental Value	Analitical Value				
	Sliding Surface	Anchor Dowel	Backfill	Asphalt Pavement	Total
38.5	0.1 (1%)	4.9 (12%)	1.8 (5%)	32.5 (82%)	39.3 (100%)

Test Design

(a) Dimensions of Device and Failure Zone of Backfill Dimensions of knock-off abutment and assumed failure zone of backfill are shown in Fig.23 and Fig.24, respectively. Width of abutment (B) is taken as 10.7 m.

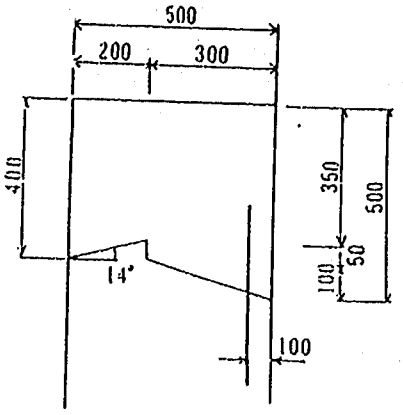


Fig. 23 Dimensions of knock-off abutment

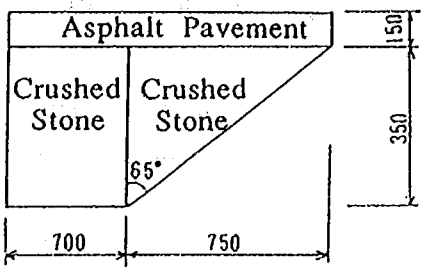


Fig.24 Failure Zone of Backfill

(b) Resistance Force of Knock-off Abutment

i) Resistant Force of Slide Surface

Resistant force of slide surface is given by equation (12),

$$F_N = \frac{0.5(\sin 14^\circ + 0.2 \times \cos 14^\circ)}{\cos 14^\circ - 0.2 \times \sin 14^\circ} \times B = \frac{0.5 \times 0.390}{0.922} \times 10.7 = 2.25\,tf$$

ii) Resistant Force of Anchor Dowel

- Required cross sectional area of anchor dowel is given by equation (13),

$$A_{Sn} = \frac{16000 \times 10 + 800 \times 40}{40 \times 1400} = 3.43\,cm^2$$

- Taking into consideration the width of wheel load and distribution of wheel load up to the location of anchor dowel, arrangement of anchor dowel is ϕ13 @250 within the region of D = 0.5 +2 x 0.5 = 1.5 m

thus, the cross sectional area of anchor dowel is 7.60 cm^2 and is satisfactory.

$A_S = 1.267 \times 150 / 25 = 7.60\ cm^2 > A_{Sn}$

- Resistant force of anchor dowel is given by equation (25),

$$F_A = \frac{7.60 \times 3700 \times 10}{40} \times 10.7 = 75.2\,tf$$

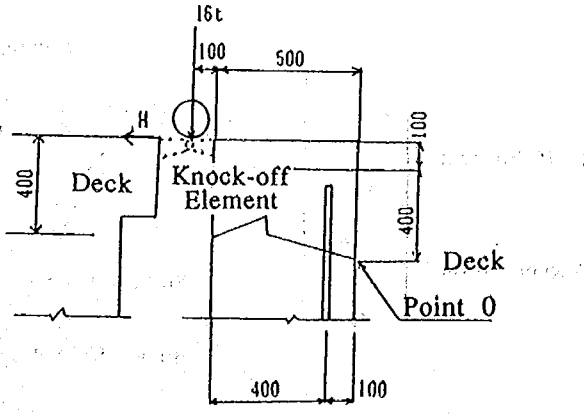


Fig.25 The actions of wheel load and brake load

iii) Resistant Force of Backfill

With reference to Fig.24, the weight of asphalt pavement (W_a) and crushed stone (W_{g1}, W_{g2}) are calculated. The values are W_a = 2.50 tf/m, W_{g1} =5.66 tf/m and W_{g2} = 3.03 tf/m. Beside these, μ_1 = 0.839, μ_2 = 0.364 and α = 65 . Resistant force is calculated by substituting constants of crushed stone and asphalt obtained from physical experiments or previous technical papers.

$$K = \frac{0.839\times\cos 65^\circ - \sin 65^\circ}{0.839\times\sin 65^\circ + \cos 65^\circ} = -0.466$$

$$N_1 = \frac{145}{2} \times 2.5 \times \frac{3}{145+2\times 70} = 1.908 \text{ tf}$$

$$N_3 = \frac{-(1.908 + 5.66)}{-0.466} = 16.24 \text{ tf}$$

$$F_s = \frac{16.24 + 0.839\times 3.03}{1-0.839\times 0.364} = 27.04 \text{ tf}$$

iv) Resistant Force of Asphalt Pavement

Resistant force of pavement is given by equation (20),

$$F_a = 2\sqrt{28000 kg/cm2 \times 28125 cm4 \times 0.5 kgf/cm2} \times 10.7 m$$

$$= 2 \times 19.8 tf \times 10.7 m$$

$$= 424 \text{ tf}$$

v) Resistant Force of Knock-off Abutment

Resistant force of knock-off abutment is as given below.

F = 2.3 + 75.2 + 27.0 + 424 = 529 tf

(1%) (14%) (5%) (80%)

vi) Calculation of deck's Collision Load (H)

The bridge under study is a 2-span continuous prestressed concrete deck bridge, with bridge length 76.95 m and width 10.7 m. The weight of deck is 1780 tf and resistant force of knock-off abutment is about 30% of this value.

vii) Treatment to Asphalt Pavement

To ensure that buckling of asphalt pavement occurs at the predetermined location, cut(binder course) is made as shown in Fig.26.

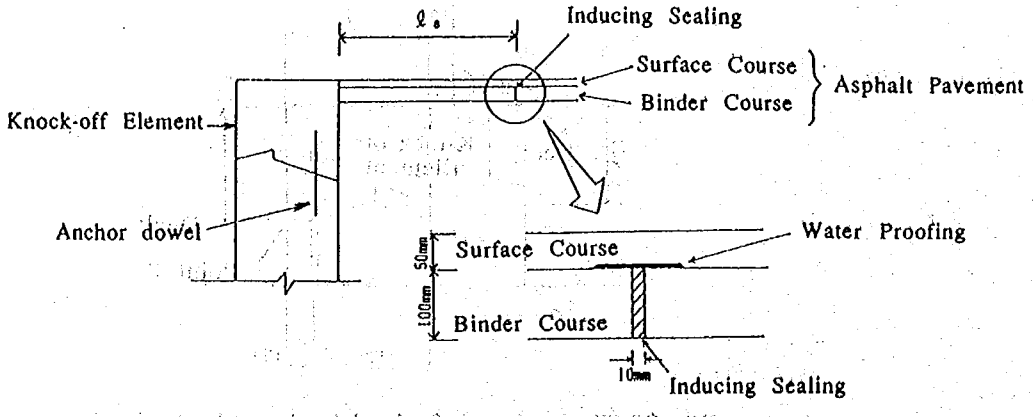


Fig.26 Sealing of Asphalt Pavement

8. Ozaki,D.,Tsukamoto,A.,Matsumoto,F. : "Development of Falling-off Prevention Devices for Menshin Bridges",Proceeding of The 21 Earthquake Engineering Conferrence of The Japan society of civil Engineers, July 1991 (in Japanese)
9. Kikuchi,T.,Goto,Y.,Kuroiwa,I. : "Model experiment for Abutment with knock-off facaluty",Proceeding of The 21 Earthquake Engineering Conferrence of The Japan society of civil Engineers, July 1991 (in Japanese)
10. Ozaki,D.,Tsukamoto,A.,Matsumoto,F. : "Development of Falling-off Prevention Devices for Menshin Bridges",Proceeding of The 46 Annual Conferrence of The Japan society of civil Engineers, September 1991 (in Japanese)
11. Kikuchi,T.,Goto,Y.,Kuroiwa,I. : "Model experiment for Abutment with knock-off facaluty",Proceeding of The 46 Annual Conferrence of The Japan society of civil Engineers, September 1991 (in Japanese)
12. Ozaki,D.,Tsukamoto,A.,Kimishima,T.,Harada,T. : "Development of Finger Joint Movable in Transverse Direction for Menshin Bridges",Proceeding of The 47 Annual Conferrence of The Japan society of civil Engineers, September 1992 (in Japanese)
13. Higuchi,S.,Kikuchi,T.,Goto,Y.,Kuroiwa,I. : "Numerical analysis for backfill resistant force of knock-off device "Proceeding of The 47 Annual Conferrence of The Japan society of civil Engineers, September 1992 (in Japanese)

CONCLUSIONS

The characteristics of each device have been clarified and are given below.

(a) Expansion Joint

i) Substantiated experiment was conducted, smooth movement and small resistant force were verified and is applicable to actual bridge.

(b) Stopper

i) Linear spring stiffness can be determined from the Force-deformation characteristics of shock absorber and steel bar.

(c) Knock-off Abutment

i) Resistant force of asphalt pavement is dominant among other components of resistant force, therefore, determination of asphalt's stiffness is impotent. The largest stiffness possible in design is used.

ii) The resistant force of knock-off abutment can be set to a predetermined value by providing cut to the asphalt pavement.

Design methods taking into consideration of the characteristics mentioned above were established and rational design was proved to be possible.

ACKNOWLEDGEMENT

The studies reported here were conducted as a part of the joint research project on "Development of Menshin Systems of Highway Bridges" between the Public Works Research Institute (PWRI) of the Ministry of Construction and 28 private firms in Japan. The authors would like to acknowledge their debt to Dr.K.Kawashima, Mr.K.Hasegawa, Mr.S.Unjo and Mr.H.Nagashima of the PWRI for their advice concerning the basic principles behind these devices and the direction of the development.

REFERENCES

1. PWRI and 28 Private Firms : " Manual on the Design of Menshin Highway Bridges (Draft)", March 1992 (in Japanese)
2. PWRI and 29 Private Firms : " Development of Menshin Systems of Highway Bridges - Report N0.1-", PWRI Joint Research Reports No. 44, March 1990 (in Japanese)
3. PWRI and 28 Private Firms : " Development of Menshin Systems of Highway Bridges - Report N0.2-", PWRI Joint Research Reports No. 60, July 1991 (in Japanese)
4. PWRI and 28 Private Firms : " Development of Menshin Systems of Highway Bridges - Report N0.3-", PWRI Joint Research Reports No. 44, March 1992 (in Japanese)
5. Ozaki,D.,Kimishima,T.,and Harada,T. : "Development of Finger Joint Movable in Transverse Direction for Menshin Bridges", Proc. U.S.-Japan Workshop on Earthquake, Peoteccive Systems of Highway Bridges, National Center for Earthquake Engineering Research,Buffalo,New York,September 1991
6. Ozaki,D.,Matsumoto,F. : "Development of Falling-off Prevention Devices for Menshin Bridges",Proc. U.S.-Japan Workshop on Earthquake Peoteccive Systems of Highway Bridges, National Center for Earthquake Engineering Research,Buffalo,New York, September 1991
7. Kikuchi,T.,Goto,Y. : "Lateral Loading Tests of Knock-off Mechanism for Menshin Bridges",Proc. U.S.-Japan Workshop on Earthquake Peoteccive Systems of Highway Bridges, National Center for Earthquake Engineering Research,Buffalo,New York, September 1991

DEVELOPMENT AND APPLICATION OF SIMPLE ANALYTICAL MODELS OF LEAD-RUBBER BASE ISOLATED BRIDGES

Emmanuel "Manos" Maragakis and Mehdi Saiidi
Civil Engineering Department
University of Nevada, Reno

ABSTRACT

Four linear unidirectional analytical models of base isolated bridges are compared. The results are used for the development of simplified linear models for these structures. These models are the basis for the development of a three-dimensional nonlinear model for base isolated bridges, which is then used for the evaluation of the effects of base isolation on pier ductility demand.

INTRODUCTION

Seismic isolation is a technique which has been used in both buildings and bridges to decouple these structures from the damaging components of earthquake induced vibrations (Ref. 1). In the case of bridges, seismic isolation can be applied to both the design of new structures and the retrofitting of existing structures. In the case of new structures, the primary objective is to reduce the column forces and, therefore, remove the requirement for an expensive ductile detailing of the joints. When used as a retrofitting method, seismic isolation can be an effective solution for many common deficiencies exhibited during recent earthquakes by bridges built before the mid 1970's. The increase in the period of vibration due to the incorporation of isolators generally results in lower shear forces. Elastomeric bearings with a lead core are known to exhibit the initial stiffness and energy absorption characteristics which are necessary for earthquakes with different intensities.

One of the potential benefits of using isolators in bridges is to reduce pier ductility demand. The purpose of this paper is to describe the development of a series of simple analytical models which were finally used to evaluate the effect of base isolation on the pier ductility demand. Initially, elastic unidirectional models were developed and their validity was tested by comparing them to more detailed models of isolated bridges. These models were then expanded to nonlinear unidirectional models; and, finally, a more general nonlinear three-dimensional model was developed. This model was used to demonstrate the effectiveness of isolators in reducing the ductility demand in a typical two-span highway bridge supported on single column piers.

DESCRIPTION OF THE UNIDIRECTIONAL LINEAR MODELS

The four models initially considered are described below.

Model 1: In this model, the flexibility of the deck is neglected and the isolators are assumed to be located at the connections between the deck and the bents and between the deck and the abutments. Therefore, the deck is represented by a rigid mass connected to the piers and the abutments through isolator springs. The lumped method is used to represent the piers. All of the piers are modeled by a single "equivalent" pier. This pier is represented by a mass equal to half of the total pier mass and connected to the deck and the ground by a spring representing the total resistance of all of the piers. All of the springs are assumed to be elastic at this point. The connections of the pier and the isolator springs to the ground are assumed to be rigid. A picture of this model is shown in Fig. 1.

Model 2: The difference between this model and Model 1 is that the pier isolators are located at the bottom of the pier. Therefore, the deck and the pier are represented by one rigid mass, which is connected to the abutments through isolator springs and to the ground through a series of an isolator and a pier spring. All of the other assumptions are the same as the assumptions for Model 1. A picture of the model is shown in Fig. 1.

Model 3: In this model, the bridge deck and the columns are represented by bending beam elements. The isolators are located at the connections between the bridge deck and the columns and between the deck and the abutments. The connections of the abutments and columns to the ground are assumed to be rigid. Each isolator is modeled by a longitudinal and a vertical linear spring. These springs are connected to either the beam elements of the deck and the column or to the deck and the abutment through rigid elements. Pictures of the model and the base isolator details are shown in Fig. 1.

Model 4: This model is similar to Model 3 except that the base isolators are placed at the bottom of the columns. A picture of the model is show in Fig. 1.

All of the models described above were subjected to earthquake excitation in the longitudinal (the deck axis) direction. The computer program IMAGES 3D was used to evaluate the response of these models (Ref. 2); this is a three-dimensional linear structural analysis program which can be used to evaluate the static, modal, and dynamic responses of structural systems.

PARAMETRIC STUDIES

A variety of parametric studies were performed to identify the differences in the response of the various models. The primary goals of these studies were:

(i) To compare Models 1 and 3 and Models 2 and 4 in order to assess the importance of including the flexibility of the deck when studying the base isolation effects on the response of bridges and

(ii) To compare Models 1 and 2 in order to identify the effects of the placement of the pier isolators on the response of bridges.

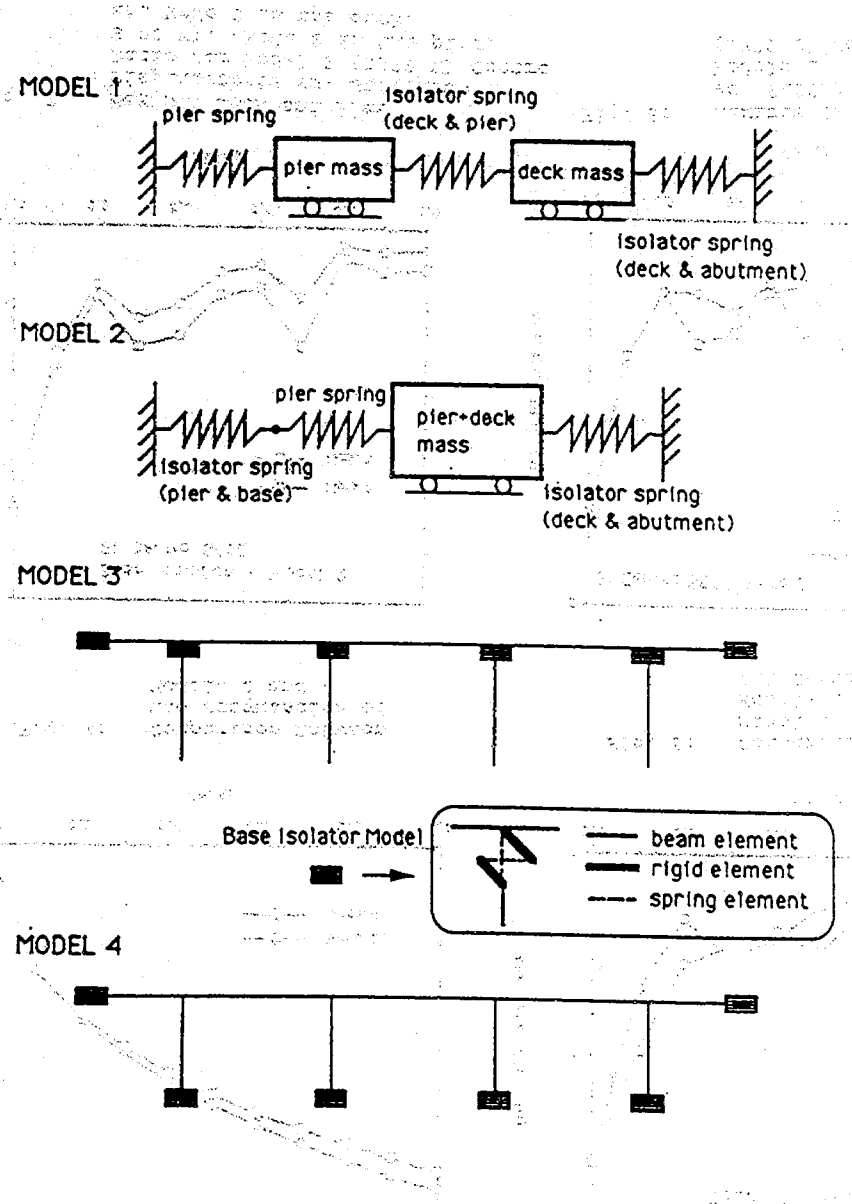


Fig. 1: Base Isolation Linear Unidirectional Bridge Models

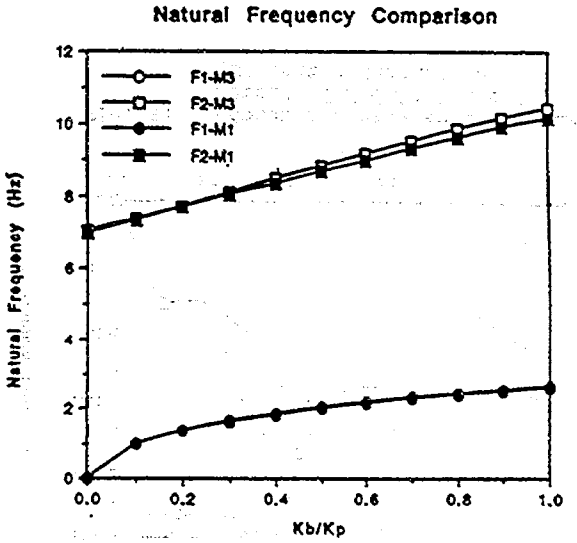


Fig. 2: Comparison Between the Frequencies of Models 1 and 3

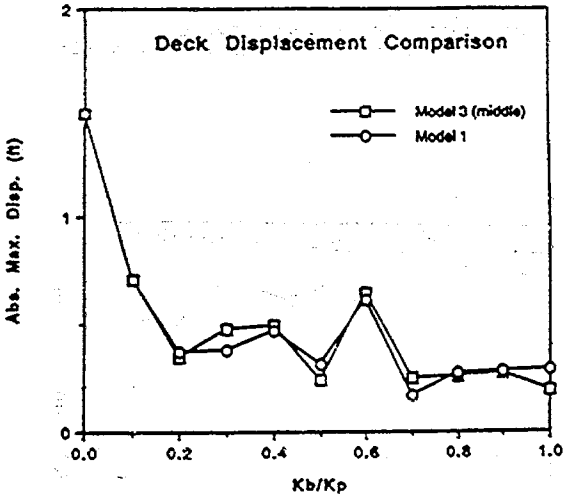


Fig. 3: Comparison Between the Displacements of Models 1 and 3 (El Centro Earthquake)

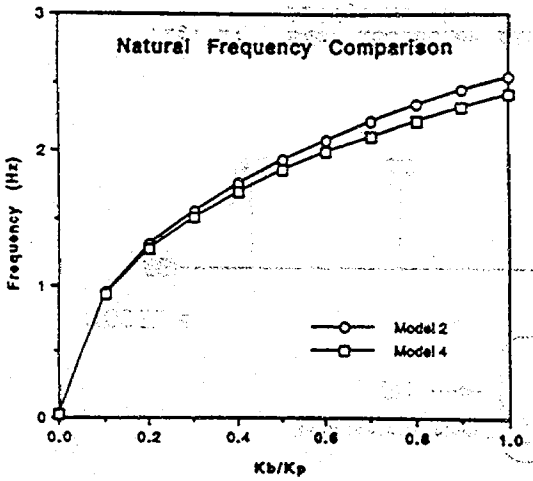


Fig. 4: Comparison Between the Frequencies of Models 2 and 4

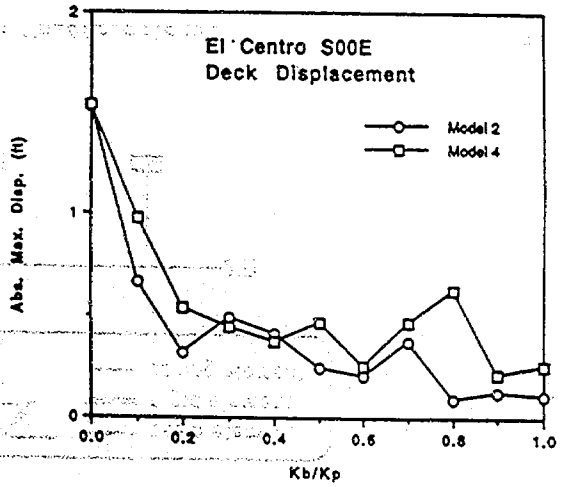


Fig. 5: Comparison Between the Displacements of Models 2 and 4 (El Centro Earthquake)

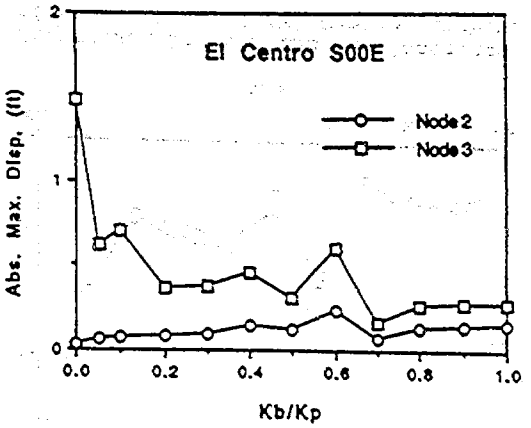


Fig. 6: Maximum Deck and Pier Displacements vs. Stiffness Ratio for Model 1 (1979 El Centro S 00 E). Node 2 is the pier, and Node 3 is the deck.

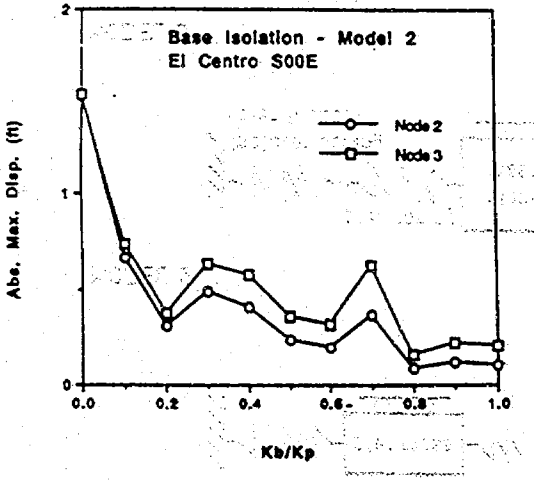


Fig. 7: Maximum Deck and Pier Displacements vs. Stiffness Ratio for Model 2 (1979 El Centro S 00 E). Node 2 is the pier, and Node 3 is the deck.

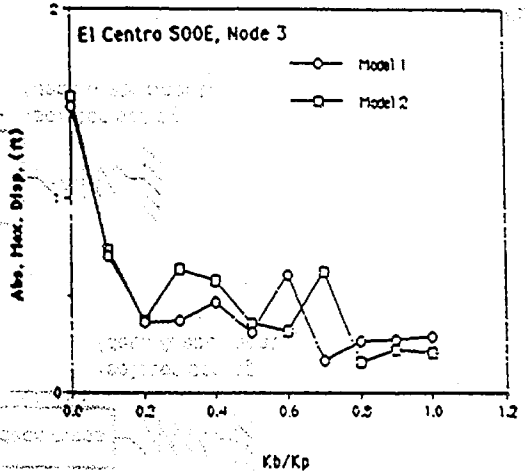


Fig. 8: Maximum Deck Displacement vs. Stiffness Ratio for Models 1 and 2 (1979 El Centro S 00 E).

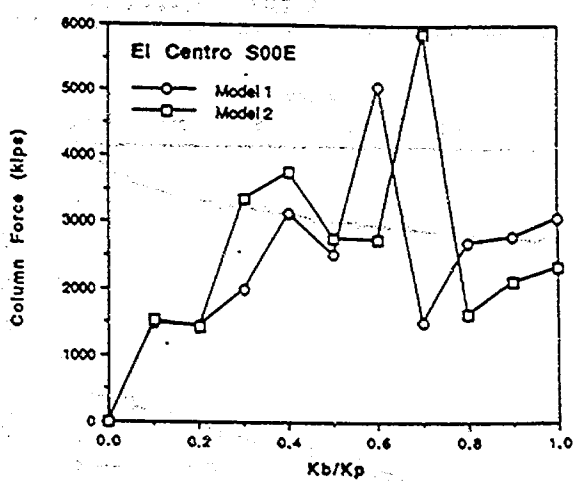


Fig. 9: Comparison Between the Column Forces of Models 1 and 2 (El Centro Earthquake)

Figure 2 shows comparisons between the variation of the first two natural frequencies of Models 1 and 3 as a function of the ratio between the base isolation and the bridge pier stiffnesses. Figure 3 shows a similar comparison of the maximum deck displacements predicted between the two models. One can see that, in both cases, there were no major differences between the two models. Similar studies were performed comparing the pier displacements and the column forces between the two models. In all cases, it was found that both models produced very similar results. Figures 4 and 5 show similar comparisons between Models 2 and 4. The differences in the responses were not significant. Details of all of the parametric studies are given in Ref. 3. Based on the results of these comparisons, it can be concluded that the flexibility of the deck does not play a major role when modeling the effects of the base isolation of the bridge response. Therefore, the deck can be considered rigid, which simplifies the analytical models significantly. Consequently, Models 1 and 2 were used as a modeling basis for the rest of this study.

Then, the response of Models 1 and 2 were compared in order to identify the importance of the pier isolator's location. Representative results from the series of the comparison studies are shown in Figs. 6, 7, and 8. Figure 6 shows the effect of the isolator in the dynamic system, showing both pier (Node 2) and deck (Node 3) maximum displacements for Model 1. The large differences in displacement at low ratios of Kb/Kp indicate that the isolator is undergoing large displacements as the pier and deck masses respond separately. The same comparison for Model 2 shows markedly different performance. The pier and deck masses are both atop the isolator; and, therefore, the displacements are much closer and follow the same pattern. However, the displacement which the isolator actually undergoes is about the same. The isolator in Model 1 experiences the difference of the deck and pier displacements, in this case, approximately 1.5 ft. at Kb/Kp of zero and 0.35 ft. up to a Kb/Kp ratio of 4. Model 2's isolator undergoes the displacement associated with Node 2 on the plot because it is fixed at one end. Model 2's isolator experiences nearly the same displacement maximum as Model 1. Therefore, although the plots appear different, the results for the isolator are approximately the same. Furthermore, the deck displacements are very similar for both models as shown in Fig. 8.

Figure 9 shows a comparison between the maximum column forces for Models 1 and 2. Although there are some differences, the results are close together and exhibit a similar trend and response maximums.

Based on the results of these comparisons, it can be concluded that the top mounted isolator (Model 1) and the bottom mounted isolator (Model 2) both produce similar deck displacements and pier forces. Therefore, the location of the pier isolators makers no significant difference in the overall bridge response. More details and results of the parametric studies are provided in Ref. 3.

NONLINEAR MODELS

The unidirectional models, 1 and 2, described above were used as a basis for the development of unidirectional and three-dimensional models for base isolated

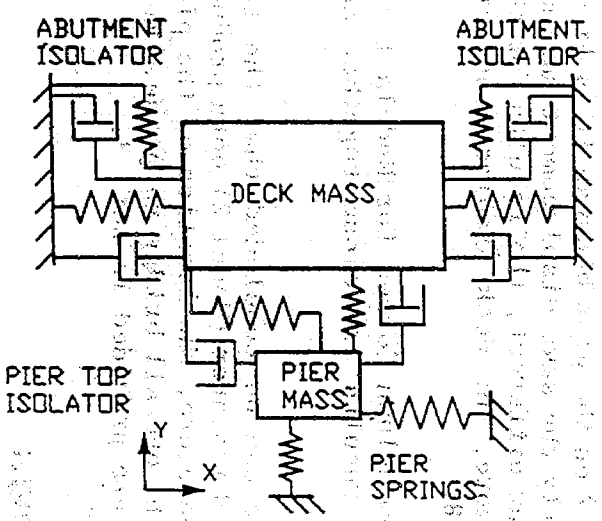


Fig. 10: Plan View of the Three-Dimensional Nonlinear Analytical Model

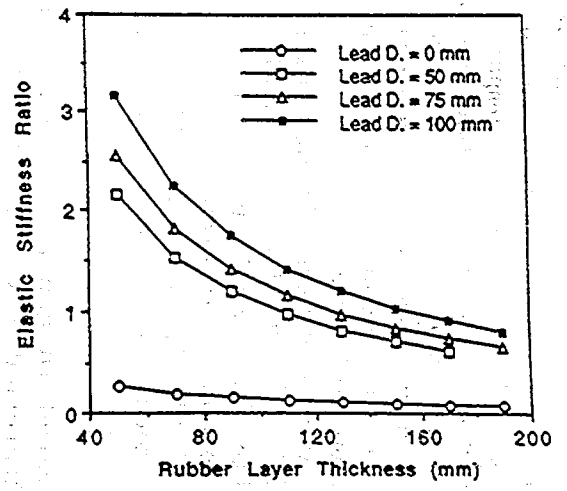


Fig. 11: Elastic Stiffness Ratio vs. Rubber-Layer Thickness for the Rose Creek Bridge

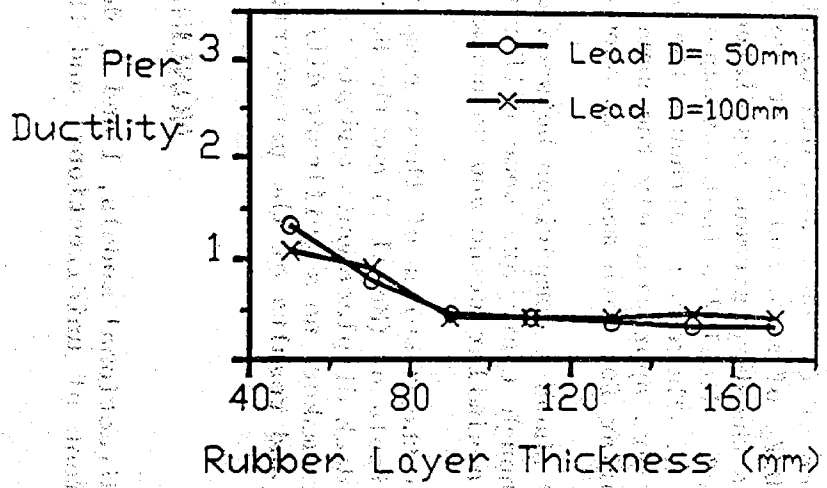


Fig. 12: Ductility in the X Direction (Model A)

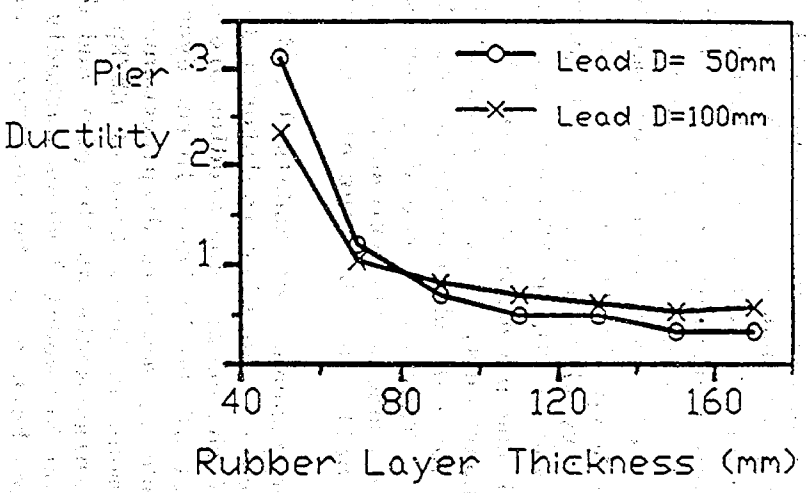


Fig. 13: Ductility in the Y Direction (Model A)

bridges. In this paper, only the three-dimensional model is discussed. Details about the unidirectional nonlinear models are given in Ref. 3.

The plan-view of the three-dimensional nonlinear model is shown in Fig. 10. The deck was modeled as a rigid mass supported on isolators at abutments and at the pier. The pier mass is one-half of the total mass of the pier. The isolators at each abutment and the pier were modeled by two uncoupled nonlinear springs and dash pots. The springs were assumed to be uncoupled due to a lack of sufficient data for biaxial response of lead-rubber isolators.

The hysteretic response of the isolator springs in each direction was modeled by a bilinear model. Comparisons with test data indicate that the bilinear hysteresis model represents the actual response with reasonable accuracy (Ref. 4). The flexibility of the pier is accounted for by a four-spring nonlinear element at the base of the pier (Ref. 5). The model is relatively simple and allows for stiffness degradation of the column. The pier springs in Fig. 10 incorporate the stiffness of the four-spring element. The pier base and the abutment isolators are assumed to be fixed to the ground. The dynamic equilibrium equation is formed for small time intervals and is solved using Newmark's β method.

NONLINEAR ANALYTICAL STUDIES AND RESULTS

The model was used to study the influence of different base isolators on pier ductility demand and displacement response of the superstructure in a typical two-span bridge. The properties of the model were calculated based on the geometry of the Meloland Road Overcrossing. Two parameters were considered in these studies: the rubber layer thickness of the isolator and the diameter of the lead core. Figure 11 presents the elastic stiffness ratio (the stiffness between the isolator stiffness and the pier stiffness) as a function of rubber-layer thickness in the isolators. Note that, as rubber-layer thickness decreases, stiffness ratio increases. Stiffness ratio also increases as the size of the lead core increases. The pier stiffness used in Fig. 11 was based on the properties of the Rose Creek Bridge. Seven different isolators and two different lead core diameters were used in the study. Two models of the bridge, one with isolators at abutments and the pier top (Model A) and the other with isolators at the abutments only (Model B), were studied. The horizontal acceleration components of the 1940 El Centro earthquake were used, with a peak of 0.7g. The isolator properties were obtained from Ref. 6.

Results for Model A An increase in rubber thickness indicates a reduction in the effective stiffness of the isolator. An increase in the lead core diameter corresponds to a larger effective stiffness. It can be seen in Figs. 12 and 13 that, for a rubber thickness of 70 mm and higher, the yielding of the column can be avoided. Figures 14 and 15 show that, with a lead core of 50 mm, it is possible to develop large deck displacements. However, the maximum displacement is insensitive to the isolator thickness when the core diameter is raised to 100 mm.

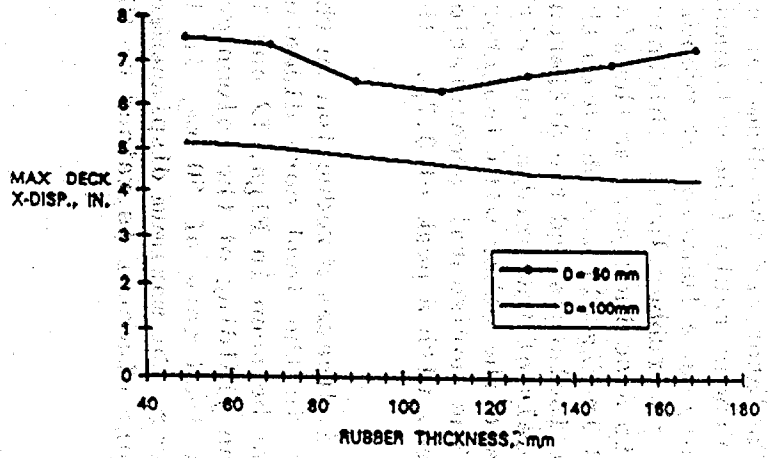


Fig. 14: Maximum Deck Displacement in the X Direction (Model A)

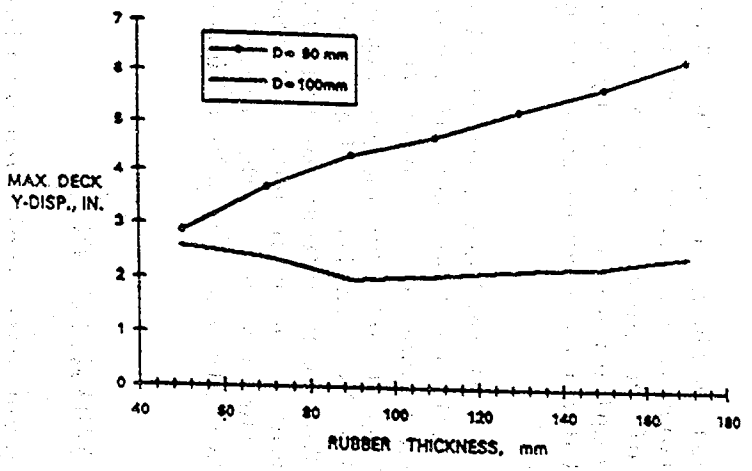


Fig. 15: Maximum Deck Displacement in the Y Direction (Model A)

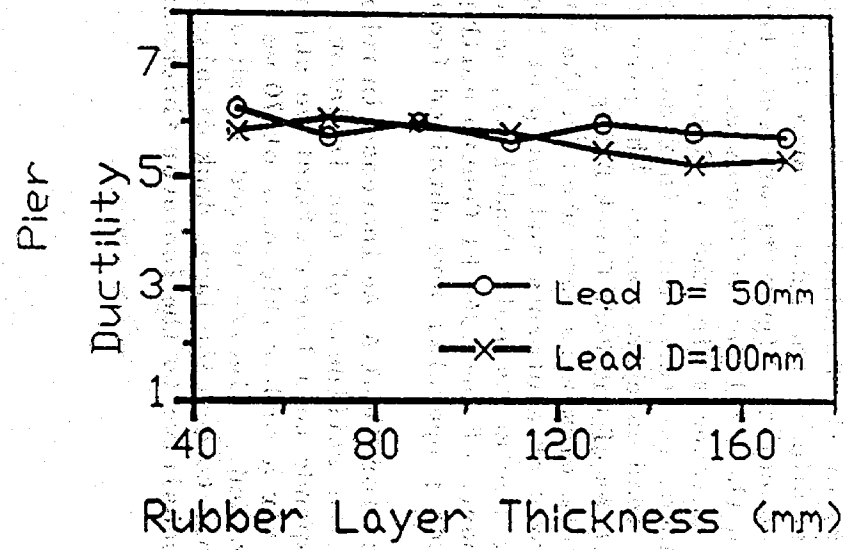


Fig. 16: Ductility in the X Direction (Model B)

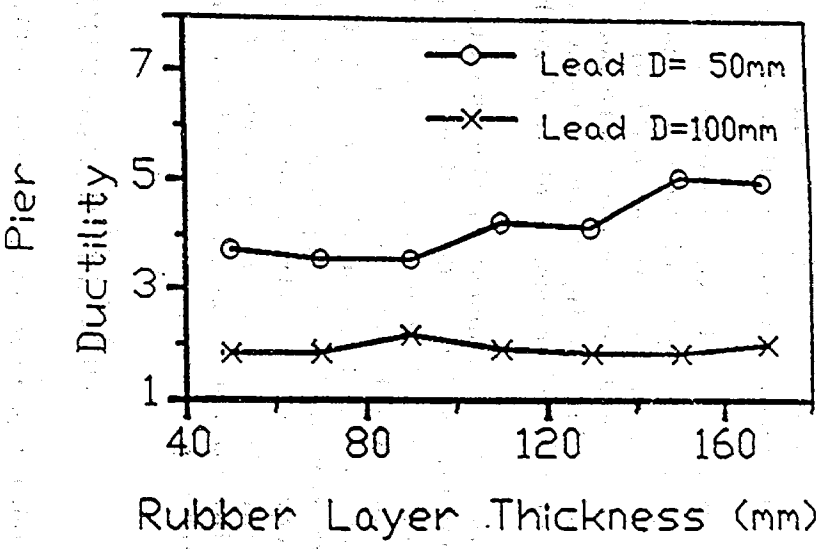


Fig. 17: Ductility in the Y Direction (Model B)

Results for Model B In many cases, base isolation is used as a seismic retrofit measure. A possible approach may be to install isolators only at the abutments, with the expectation that the absorbed energy will be sufficient to avoid yielding of the pier. Model B represented such a bridge. The results of the analysis are shown in Figs. 16 and 17. It can be seen that the ductility demand can remain high even when relatively thick isolators are used.

SUMMARY AND CONCLUSIONS

A brief description of a study to compare four analytical models that can be used for the analysis of lead rubber base isolated bridges has been presented in this paper. These models were used as a basis for the development of a three-dimensional nonlinear base isolated bridge model, which was used for the study of the effects of base isolation on the pier ductility demand. Based on the results of this study, the following conclusions can be derived.

a. Models 1 and 3 and Models 2 and 4 produce similar results. Therefore, the flexibility of the deck can be neglected for the study of the effects of base isolation. Consequently, simpler modeling techniques (Models 1 and 2) can be used and produce reasonably accurate results.

b. Models 1 and 2 produced similar deck displacements and column forces. Therefore, the results were insensitive to the location of the base isolation.

c. With appropriate designed isolators installed at the abutments and the pier, it may be possible to reduce the ductility demand in the pier and avoid the yielding of the columns. For many of the existing bridges which were designed prior to the development of modern seismic codes, this means that the insufficient anchorage length for column steel bars and the lack of concrete confinement in the pier may be less of a concern if base isolation is used.

d. Base isolation may be ineffective unless it is applied at piers as well as to the abutments.

ACKNOWLEDGEMENT

The study presented in this article was funded by the Department of Energy through the Center for Infrastructure Studies at the University of Nevada, Reno.

REFERENCES

1. Buckle, I.G. and Mayes, R.L., "The Application of Seismic Isolation to Bridges," *Seismic Engineering: Research and Practice, Proceedings of Structures Congress 1989*, pp. 633-642.

2. *Images 3D, A Computer Program for Three Dimensional Analysis of Structures (Manual)*, Celestial Software, Berkeley, California, 1985.

3. Maragakis, E.A., Saiidi, M., Hwang, E.S., and Ghusn, G., "Placement of Seismic Isolators in Bridges," Report No. CIS-91-26, College of Engineering, University of Nevada, Reno.

4. Blakeley, R.W.G., "Application of Base Isolation to Seismic Resistant Bridges," *Comparison of United States and New Zealand Practices for Highway Bridges*, Applied Technology Council, ATC-12, August 1982, pp. 77-82.

5. Jiang, Y. and M. Saiidi, "4-Spring Element for Cyclic Response of R/C Columns," *Journal of Structural Engineering*, ASCE, Vol. 116, No. 4, April 1990, pp. 1018-1029.

6. Turkington, D.H., "Seismic Design of Bridges on Lead-Rubber Bearings," Report 87/2, Department of Civil Engineering, University of Canterbury, Christchurch, New Zealand, February 1987.

Design of 9-span Continuous Prestressed Concrete Girder Bridge with Base Isolation

Nobuo Kubota[1], Shigemi Shikauchi[1], Hiroshi Osaki[1], Yuzuru Mitake[1] and Hideo Arai[2]

1) Metropolitan Expressway Public Corporation
2) Sumitomo Construction Co. Ltd.

Summary

The Higashi-Ohgishima Viaduct of the Metropolitan Expressway Bay-Shore Route (4th phase) is a 9-span continuous prestressed concrete box girder bridge using base-isolators.

In order to improve seismic resistance, a reaction distributed method using rubber bearing supports was adopted for the bridge. In addition, menshin design was carried out so that the piers, bearing supports and main girders would not be damaged even by an earthquake of the magnitude of the Great Tokyo Earthquake of 1923.

The paper describes the menshin design technique, bearing support performance tests and dynamic analysis.

Introduction

The Higashi-Ohgishima viaduct (construction area BK452) of the Expressway Bay-Shore Route, which forms part of the Tokyo Bay Ring Road, is situated in the Higashi-Ohgishima district of Kawasaki City, Kanagawa Prefecture.

This viaduct crosses national Route 132 and a local road of Kawasaki City, and has a total length of 417.6m. The bridge is a 9-span continuous prestressed concrete box girder bridge (standard span 45m, deck width 14.25m). The construction method used was basically on-site post-tensioning using timbering, but cantilevering using a pylon was adopted for the span crossing national route 132.

Since the Metropolitan Expressway Bay-Shore Route is an arterial road for the Tokyo region, it was felt necessary, in addition to adopting the distributed method system using rubber bearings, to apply seismic isolation to the design, in accordance with the "Manual of Menshin Design for Highway Bridges" (PWRI, et al.). Menshin design is applied in the superstructure (including bearings) because the

reaction distributed system includes uncertainty by reference to ultimate level earthquakes. However, since no previous examples exist of the application of this system to substructures, normal seismic design is applied to the substructure.

Laminated rubber bearings with lead plugs (LRBs) (size 1800 x 1230 x 180mm) were used as base isolators. This bridge is one of the largest prestressed concrete bridges using Menshin design in the world, and therefore bearing support performance tests, vibration tests on the bridge itself, and observations of seismic shocks are carried out.

Outline of the viaduct

A general view is shown in figure 1. The superstructure consists of a 9-span continuous prestressed concrete box girder bridge, with standard span length of 45m. The substructure consists of two box-type abutments and eight wall-type piers, with pile foundations. The specifications of the viaduct are as follows:

Road category: Type 2, class 1
Bridge category: 1st class
Bridge length: 417.6m
Width of carriageway: 2 × 14.25m
Design load: TL-20, TT-43
Ground classification: Type III (classification for seismic design)
Design seismic coefficient: Kh = 0.33

The girder A_1 to P_8 could be constructed by timbering, but between P_8 and A_2, it is necessary to adopt the cantilever method in order not to interrupt traffic on Route 132. As is shown in figure 2, work is started from span P_4-P_5, and proceeds by stages towards A_1 and A_2. In order to ensure the stability of the structure in case of an earthquake occurring while the work is in progress, the super- and substructures are fixed temporarily as required by the progress of the work.

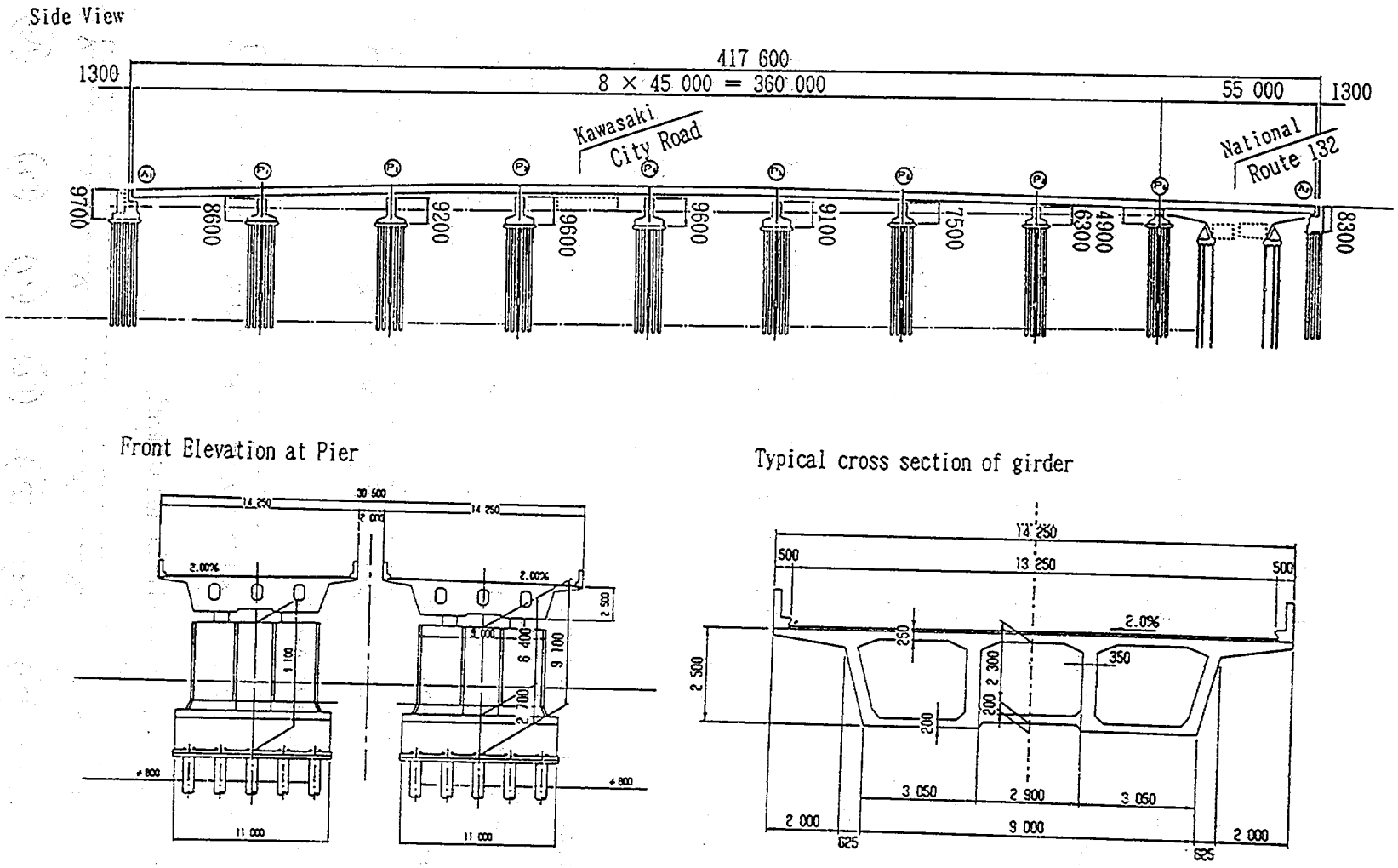


Fig. 1 General view

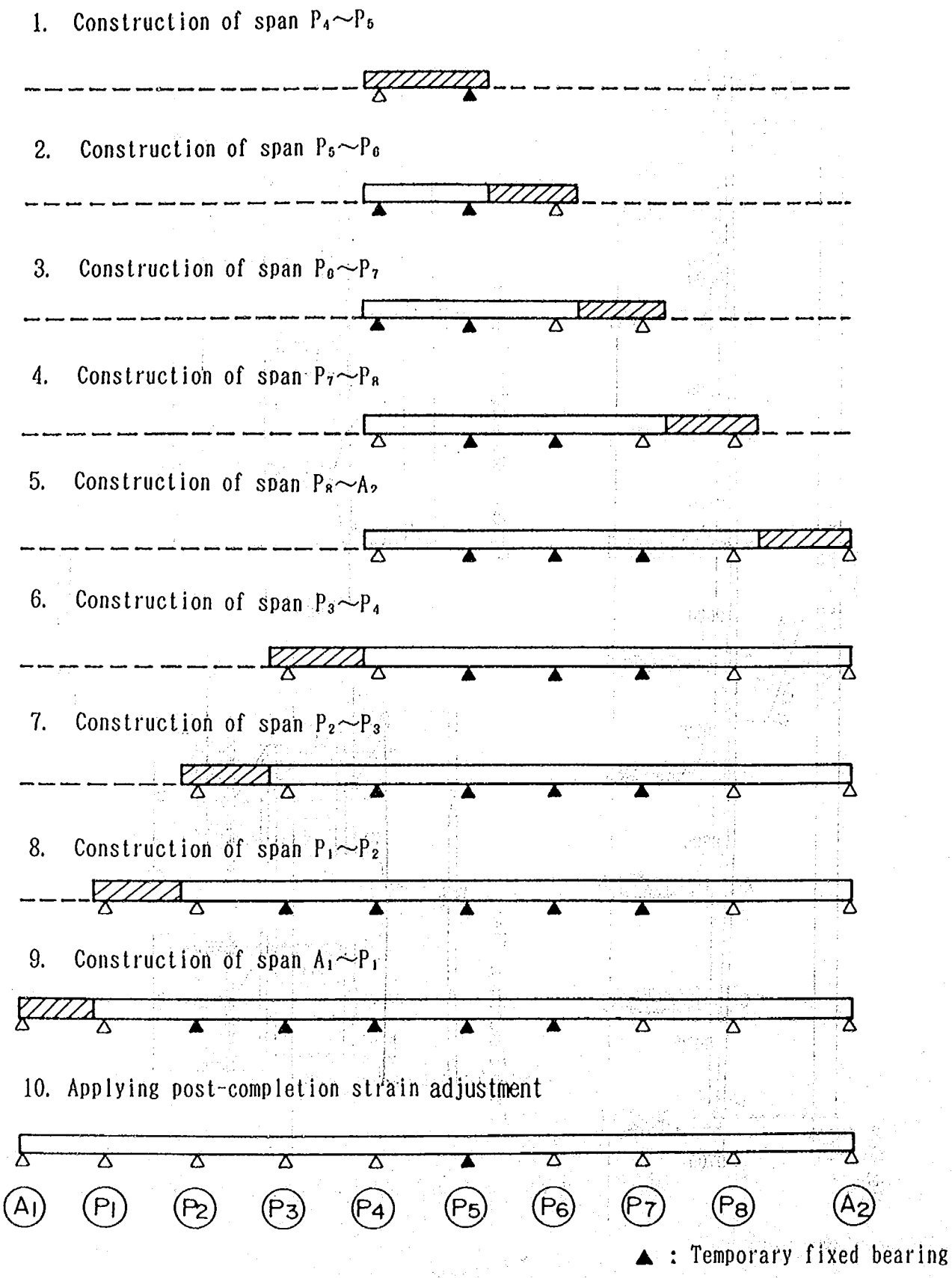


Fig. 2 Sequence of construction

Menshin design

1) Basic policy

Seismic isolation design is a form of aseismic design which aims to reduce inertia force by lengthening the natural period of a bridge at the same time as increasing its damping abilities. In this case, however, since the ground at the location of the bridge is poor, including layers of land-fill (known as type III ground), it would have been necessary to lengthen the natural period a great deal in order effectively to reduce the inertia force. In this case, the displacement of the superstructure would have increased, and the size of the bearings implied in this design would have been uneconomical. The decision was therefore taken not to attempt to lengthen the natural period of the bridge more than was economical, but rather to reduce the inertia force by adding to the damping.

For the seismic isolation bearings, laminated rubber bearings with lead plugs are used. This device has a simple structure and clear dynamic behaviour, shown in figure 3.

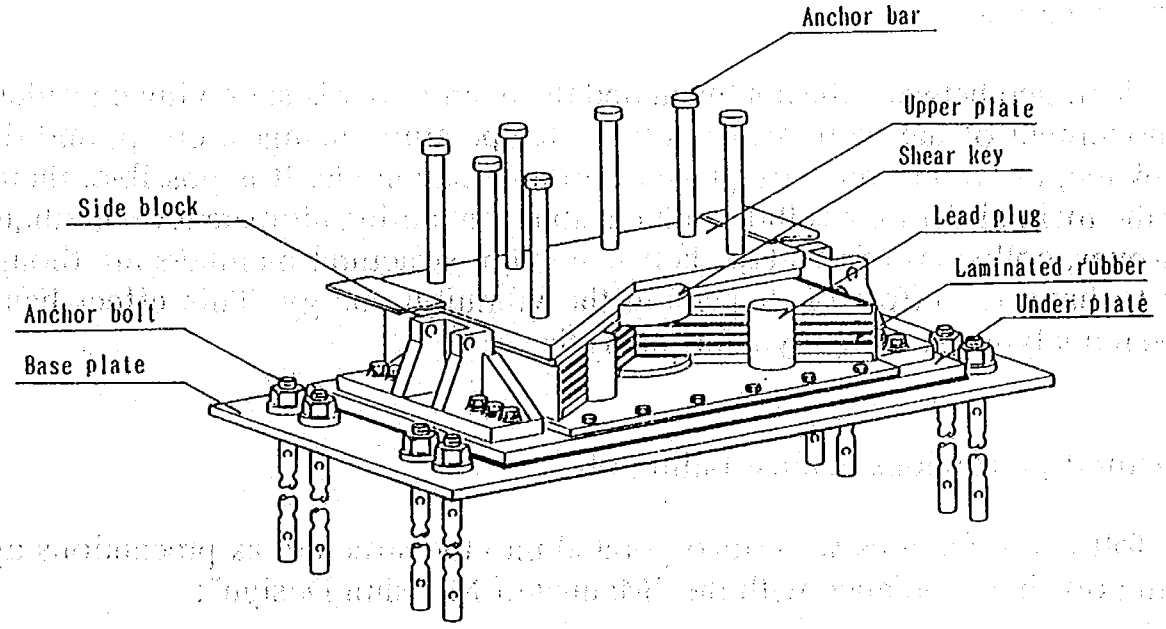


Fig. 3 Structuture of LRB

Direction of seismic isolation

Bearings are isolated in the longitudinal direction for earthquakes of normal magnitude, and fixed in the transverse direction using a restrainer. This decision is taken in consideration of the fact that the piers are of the reinforced concrete wall type, and also of the fact that earthquakes of normal magnitude cause almost no damage to the piers, as well as of the difficulty of adapting expansion devices to movement of the main girder in the transverse direction.

On the other hand, with regard to ultimate level earthquakes (level of checking bearing capacity for lateral force), seismic isolation was introduced in both directions, in consideration of the low probability of earthquakes of this magnitude occurring, and of the principle of seismic design that the function of the bridge should be maintained even after a major earthquake.

In order to give the bridge this kind of function, steel side-blocks were fitted to the bearings on the side in the transverse direction, with a design strength so as to support the bearings during normal magnitude earthquakes, but break during ultimate level earthquakes.

Girder clearance

The clearance between the abutment and the main girder is set giving consideration to movement of the main girders due to temperature changes, creep, and drying shrinkage, as well as an earthquake of normal magnitude. It is possible, therefore, that the main girder may collide with the abutment during ultimate level earthquakes. However, collisions of this type between major structural members are thought in fact to have the effect of dispersing the vibration energy. This effect has been proven analytically using dynamic analysis.

Structural precautions against falling off

The following features were incorporated into the structure as precautions against falling off, in accordance with the "Manual of Menshin Design":

(1) Restrainers were not included, since the seismic isolation bearings are designed to offer steady resistance even to ultimate level earthquakes.

(2) Length from the girder above the abutment is made greater than the standard length.

(3) At the girder ends, a restrainer connecting the girder with the abutment is

installed as prestressing cables.

Table 1 presents a summary of the menshin design policy described above, while Table 2 presents the limited states applied.

Table 1 Summary of seismic isolation design policy

Item \ Earthquake level	Normal magnitude earthquakes	Ultimate-level earthquakes
·Design lateral magnitude	$K_h = C_Z \cdot C_G \cdot C_I \cdot C_T \cdot C_E \cdot K_{h0}$ $=1.0 \times 1.2 \times 1.1 \times 1.25 \times 0.9(1.0) \times 0.2$ $=0.30$ (0.33 = for substructure design) Here: C_E = coefficient corrected for energy absorption characteristics	$K_h = C_Z \cdot C_I \cdot C_R \cdot C_E \cdot K_{he0}$ $=1.0 \times 1.1 \times 1.0 \times 0.7(1.0) \times 1.0$ $=0.77$ (1.1 = for substructure design
·Level of damage to bridge	·No damage, functions of bridge preserved	·Partial damage, but no major destruction ·Bridge functions preserved without destruction or collapse
·Seismic isolation direction	·Longitudinal direction: Seismic isolation ·Transverse direction: Fixed	·Longitudinal direction: Seismic isolation ·Transverse direction: Seismic isolation

Table 2 Limited State

Limit State		
Superstructure	Elastic behaviour, below allwable stress limit	Range elasticity ~ yield strength
Substructure	Elastic behaviour, below allwable stress limit	Range elasticity ~ level of checking bearing capacity for lateral force
Isolators (LRB)	·Rubber deformation within safety limits ·Steel parts below allwable stress limit	·Rubber deformation within guaranteed performance ·Steel parts below ultimate strength
Expansion gap	·Movement due to creep, drying shrinkage, temperature change + movement during earthquakes	As left (possibility of collisions between main girders and abutments)
Restrainer	·Longituclinal direction none ·Transvers direction fitted	·Longituclinal direction none ·Transvers direction none
Seat length	$S_E = 70 + 0.5l$ or above where l = span length	$S_E = 70 + 0.5l$ or above, and movement during earthquake is $> U_B$
Falling-off prevention device	Not triggered	Triggered: $H = 2.0 \cdot K_h \cdot R_d$

Design of the seismic isolation bearings

Laminated rubber bearings with lead plugs inserted are used in the seismic isolation bearings of this bridge. The various specifications of the bridge as regards the design of the bearings were determined as follows, in order to obtain the menshin effect previously described.

1) The natural period is set at around T= 1.55s, taking account of the value (T_g) expressing the ground characteristics, the need to avoid coupled vibration, the need to raise the natural period to a level at least 1.5 times that calculated for the bridge without seismic isolation (0.4s), and the need to reduce the size of the bearings as much as possible. Figure 5 shows the relationship between the volume of the bearing rubber and the natural period.

2) The Menshin Manual states that the design seismic inertia force can be reduced in proportion to the damping coefficient (h) of the bridge, based on the energy absorption characteristics of the seismic isolation device. In order to make full use of this damping effect in this bridge, efforts were made to ensure a value of at least $h>0.1$ during earthquakes of normal magnitude, and of at least $h>0.15$ during ultimate level earthquakes.

3) Since this bridge is quite long, at 417.6m, significant movements due to main girder creep and drying shrinkage are calculated, and the amount of movement differs at different locations on the sub-structure. When this fact is considered in relation to bearing design, it implies bearings with large dimensions, and uneven distribution of horizontal forces acting on the substructure. Therefore, deformation equivalent to the movement due to creep and drying shrinkage of the main girder is applied to the bearings in the form of shear deformation, in order to eliminate the effect. This measure allows reduction and uniformity in the size of the bearings, and a rational distribution of lateral forces on each part of the substructure. The method adopted of applying shear deformation was not the existing method of application in the factory, but a new method of application on site. This method consisted of fixing the bearings temporarily during construction of the main girders, fixing the bearings permanently after completion of the main girder after applying a relative displacement between the lower plate and the base plate of the bearing. This method offers more accurate setting of the quantity and direction of the pre-applied shear deformation than is possible using the existing method. Figure 6 shows the post-strain adjustment method.

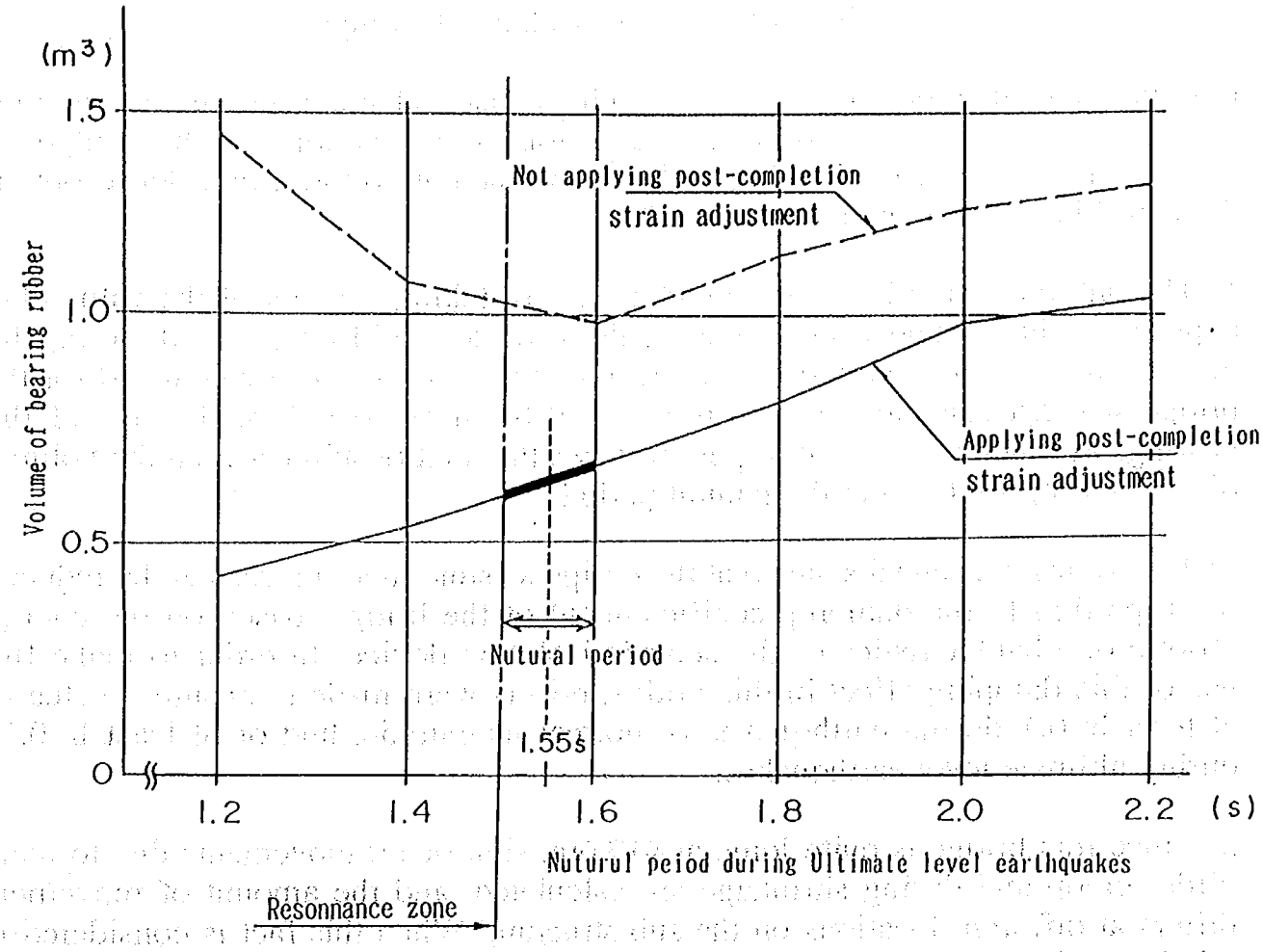


Fig. 4 Relationship between volume of bearing rubber and natural period

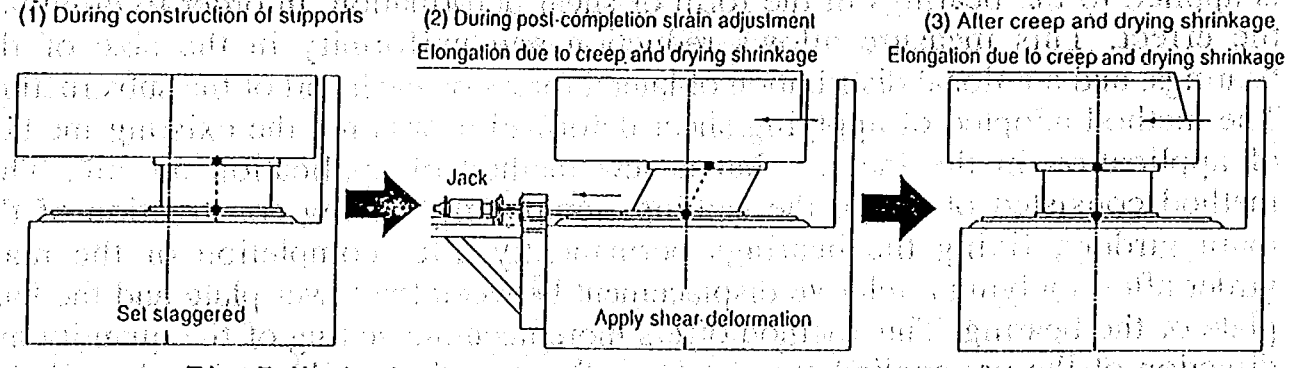


Fig. 5 Method of applying post-completion strain adjustment

2) Design of the LRB

Design criteria and specifications for the LRB units are shown in Table 3, and design results in Table 4. Specifications for the LRBs were made uniform throughout the substructure, achieving even distribution of lateral forces during earthquakes.

Table 3 Design criteria and specifcations for LRB

		A_1, A_2	P_1	$P_2 \sim P_7$	P_8
Vertical reaction (t)	Dead load reaction	418.4	800.4	771.3	953.3
	Dezign reaction	585.3	1075.5	1045.5	1252.5
Displacement (mm)	Creep・shrinkage	111	82	71	71
	Temperature (±20℃)	41	30	21	30
Size of LRB (cm)		1 2 3 × 1 8 0			
Shear modulus of Rubber G (kg/cm²)		G = 1 0			
Thick of rubber (cm)		3.6 × 5 = 1 8. 0			
Area of load plug A_P (cm²)		φ 2 0 × 4 A_P = 1 257			
Bearing prestressed area of rubber A_R (cm²)		A_R = 20 883			
Shape factor S		S = 9.57			
Axial stiffness of Rubber K_V (tf/m)		K_V = 7 030.1			
Lateral stiffness of Rubber K_R (tf/m)		K_R = 1 160.2			
Characteristic shear strength load Q_d (tf)		Q_d = 106.8			

Table 4 Design results for LRB

Item		Earthquake level	Nommal level	Ultimate level
Weight of superstructure		W(tf)	14 035	14 035
Design lateral force coefficient		K_h	0.30	0.77
Stiffness of substructure		K_P (tf/m)	423 406	401 596
Dynamic properties of LRB (one pier)	Post-yield stiffness	K_2 (tf/m)	3 669	1 953
	Initial stiffness	K_1 (tf/m)	23 845	12 691
	Effective stiffness	K_B (tf/m)	7 525	2 436
	Damping ratio	h(%)	27.6	16.1
properties of bridge	Effective stiffness of bridge	K_T (tf/m)	63 895	22 945
	Natural period	T(sec)	0.941	1.57
	Damping ratio of bridge	h_T (%)	23.5	15.4
Displacement of supersturucture		U_T (mm)	65	471
Strength of LRB	Design displacement of bearing	U_B (mm)	55	444
	Shear strain due to lateral force	γ_1 (%)	30.6 < 150	246.7 < 250
	Shear strain	γ (%)	94.9 < 277	346.0 < 417

Design of piers

Design of the substructure was carried out as prescribed in the Highway Specifications, comparing design according to the seismic level and the retained lateral strength during earthquakes of the reinforced concrete piers.

Figure 8 shows the bending moment working on the bottom of the piers. It can be seen from the diagram that the bending moment due to earthquakes is significantly better than the bending moment due to temperature changes, and the specifications of the substructure were determined according to the bending moment during earthquakes.

Next, the relationship between lateral force and deformation of the piers is shown in figure 9 .

The figure shows the results of menshin design, and the elasticity ratio of the piers during ultimate level earthquakes. As can be seen from the diagram, when seismic isolation is performed, the ductility ratio is u = 1.57, and even during large earthquakes only minor damage is sustained.

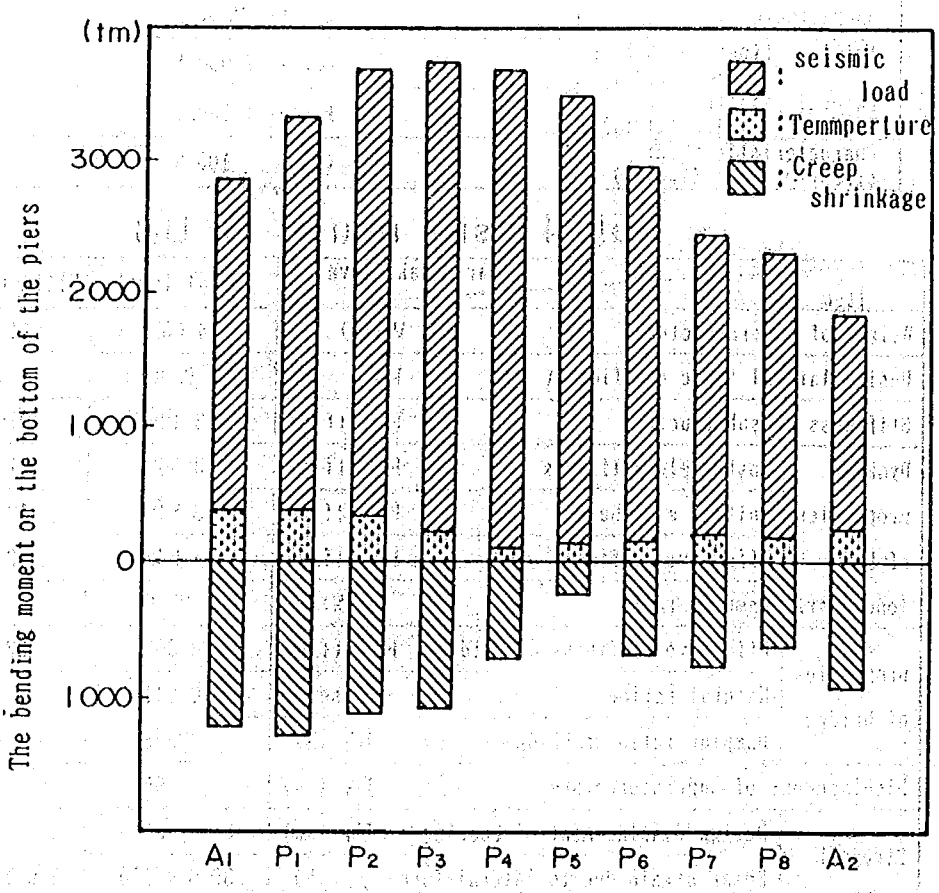


Fig. 8 The bending moment on the bottom of the piers

3) Design of steel parts

Limit states are set as follows for the steel parts of the bearings for normal magnitude earthquakes and ultimate level earthquakes, and specifications for the steel parts determined.

Table 5: Limited state of steel parts

Table 5 Limited state of steel parts

Earthquake level	Damage Level	Limited state
Nommal level	No damage, funcion of bearing maintained	Blastic behaviour, within allowable stress
Ultimate level	Localised damage without collapse, minimum functioning of bearings maintained	Blasticity-ultimate strength limit

The ultimate strength of steel members referred to in the table was determined by applying the following safety coefficients to the tensile strength of the steel members:

*Bending/ shear/ tensile stress

Material factor: $\gamma_s = 1.05$
Member factor: $\gamma_b = 1.15$
Safety factor: $\gamma = 1.05 \times 1.15 = \underline{1.2}$

*Bearing stress

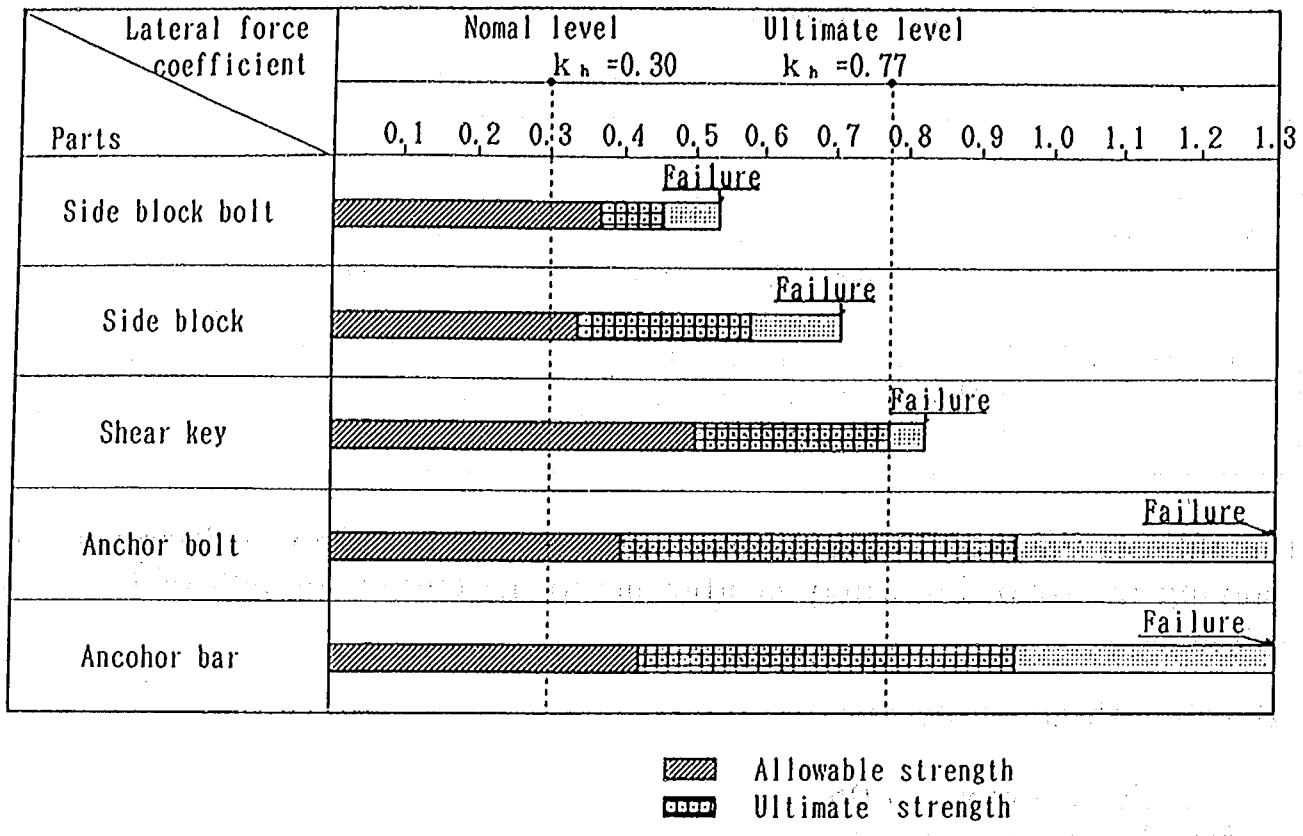
$\gamma_s = 1.05$
$\gamma = \underline{1.05}$

However, the shear strength of the anchor bolts is set at a member factor of $\gamma_b = 1.33$, in consideration of the uncertainties accompanying construction work, the high probability of forces being encountered which were not allowed for in the calculations, and the lack of uniformity of the shear forces exerted on a number of bolts. This figure also takes into consideration the permitted reducing ratio ($\alpha = 800/600 = 1.33$) of the shear stress of anchor bolts during normal magnitude earthquakes.

*Anchor bolt safety factor $\gamma = 1.05 \times 1.33 = 1.4$

Table 6 shows the relationship between earthquake levels and the limit state of steel parts.

Table 6 The limited state of steel



4) Bearing performance confirmation tests

The relationship between the shear force of the LRB and its deformation is almost bilinear, and as is shown in figure 6, can be modelled as an idealised hysteresis loop. In seismic isolation design, design is carried out by changing this into effective lateral strength and effective damping ratio.

In order to prove the appropriateness of these models on this bridge, performance tests were carried out on full-size models of the bearings. Figure 7 shows one example of results of a lateral strength test on a bearing. ⅓ reduced scale model tests will be carried out to confirm behaviour in larger strain. Table 7 shows a comparison of the effective lateral strength obtained from the results of this test, and the design values.

Also, the permitted discrepancy between measured and calculated values was set at ±20%, and it was confirmed that even if such a discrepancy arose, no problems

would be encountered in the bearings, substructure or superstructure.

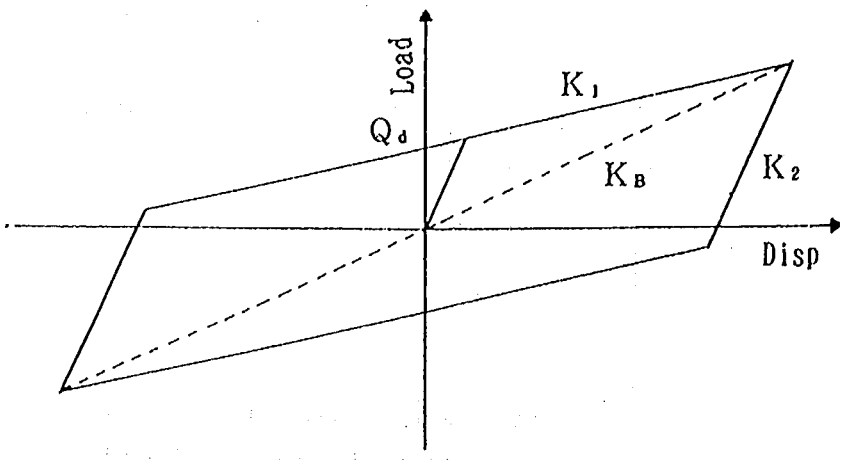


Fig. 6 Idealized hysteresisloop of LRB

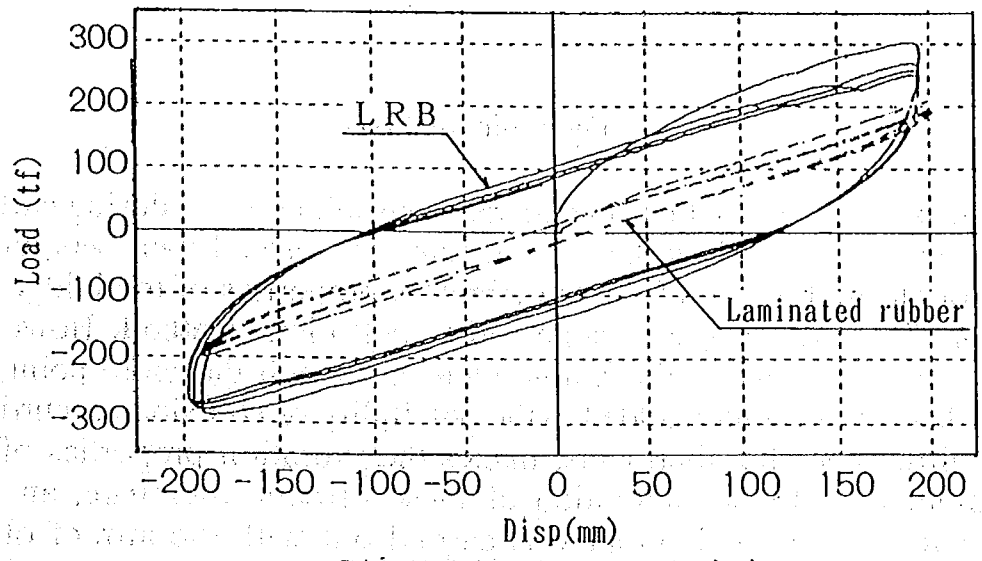


Fig. 7 Actual hysteresisloop

Table 7 The results of bearing performance tests

		Design values	Model-1		Model-2		Model-3		Model-4		Average	
			R_{max}	R_{min}	R_{max}	R_{min}	R_{max}	R_{min}	R_{max}	R_{min}	R_{max}	R_{min}
Effective stiffness K_B (tf/m)	70%	2029	1708 (0.84)	1796 (0.89)	1799 (0.89)	1984 (0.98)	1797 (0.89)	1873 (0.92)	1782 (0.88)	1905 (0.94)	1772 (0.87)	1890 (0.93)
	109%	1522	1379 (0.91)	1430 (0.94)	1412 (0.93)	1428 (0.94)	1386 (0.91)	1382 (0.91)	1354 (0.89)	1367 (0.90)	1383 (0.91)	1402 (0.92)
Effective damping ratio h (%)	70%	23.1	28.1 (1.22)	24.7 (1.07)	27.4 (1.19)	22.3 (0.97)	28.5 (1.23)	25.1 (1.09)	27.5 (1.19)	22.1 (0.96)	27.9 (1.21)	23.6 (1.02)
	109%	20.4	23.8 (1.17)	22.8 (1.12)	22.7 (1.11)	21.5 (1.05)	22.5 (1.10)	21.8 (1.07)	21.5 (1.05)	20.4 (1.00)	22.6 (1.11)	21.6 (1.06)

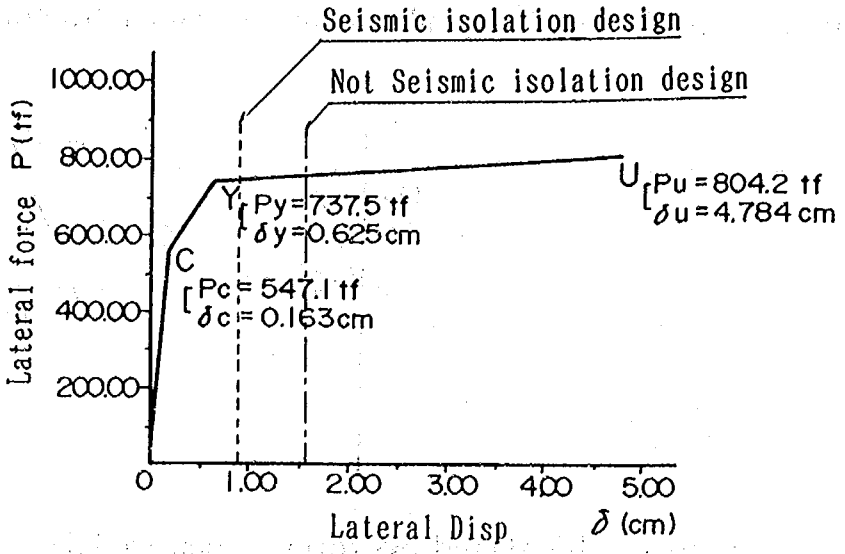


Fig. 9 Relationship between the lateral forces and deformation of the piers

Dynamic analysis

This bridge is designed so that no damage is sustained even during earthquakes of normal magnitude, including the substructure, because all members remain within the range of elasticity. Therefore, the vibration properties of the bridge correspond to those predicted using the seismic force coefficient method. However, during ultimate level earthquakes, the bridge members reach the yield point, exhibiting non-linear behaviour, which added to the possibility of collisions occurring between the main girder and the abutments, makes the vibration properties of the bridge quite complicated. In consideration of these effects, therefore, an analysis of elasto-plastic dynamic behaviour was carried out with the aim of obtaining the vibration properties of the bridge during ultimate level earthquakes, and of confirming seismic safety.

1) Analysis method and model

The method used for dynamic analysis is elasto-plastic dynamic analysis, taking into consideration the non-linearity of the bearings and the piers. The analysis model, as shown in figure 10, is a lumped mass system. Further, gap elements are included in abutments A_1 and A_2, to allow for collisions between the main girder and the abutments. A gap element is an element which has no effect up to a certain level of displacement, but takes effect suddenly when that level is passed.

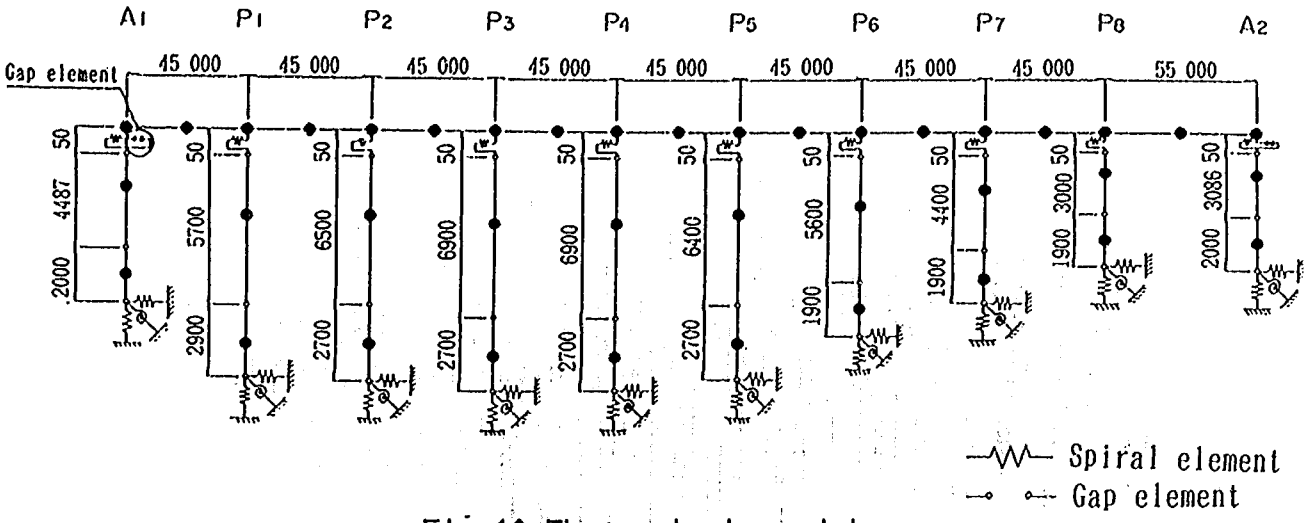


Fig. 10 The analysis model

The LRBs have bilinear type hysteresis properties, and further, characteristic shear strength (Q_d) of the lead and post-yield stiffness (K_2), which determines this hysteresis curve, has strain-dependent properties. The LRB model, in consideration of this, is made a modified bilinear hysteresis.

The seismic wave data input is shown in figure 13. The basis for this data is the revised seismic wave for the earthquake off Tsugaru, issued by the Public Works Research Institute of the Ministry of Construction, multiplied by a structure importance coefficient of 1.1, to account for the type-III ground.

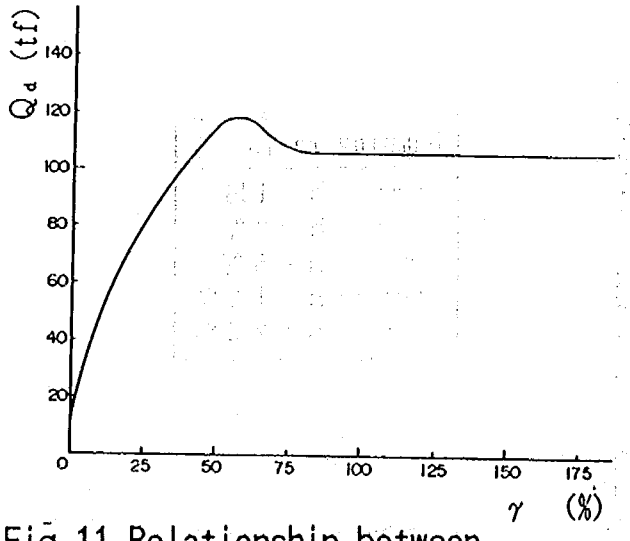


Fig. 11 Relationship between the characteristic shear strenfth and shear strain

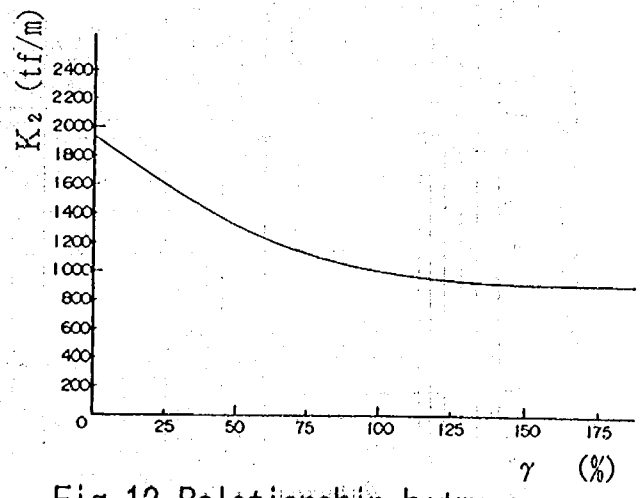
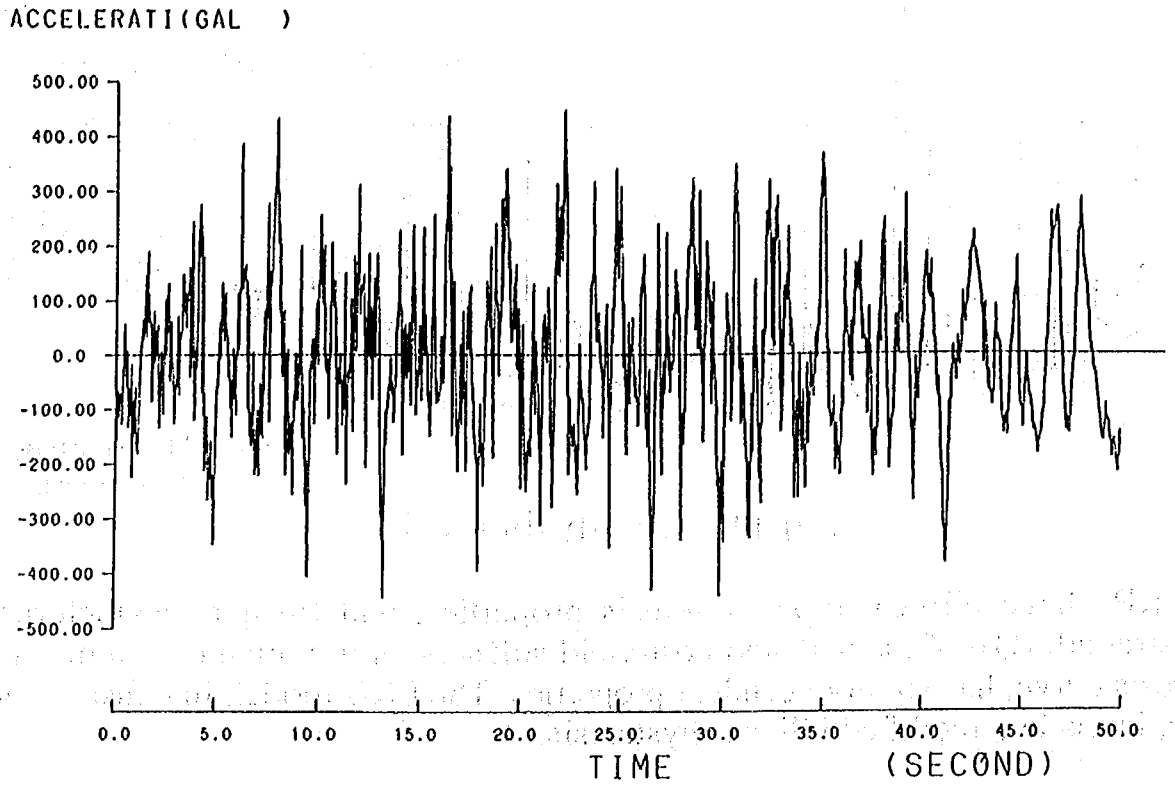


Fig. 12 Relationship between the post-yield stiffness and shear strain



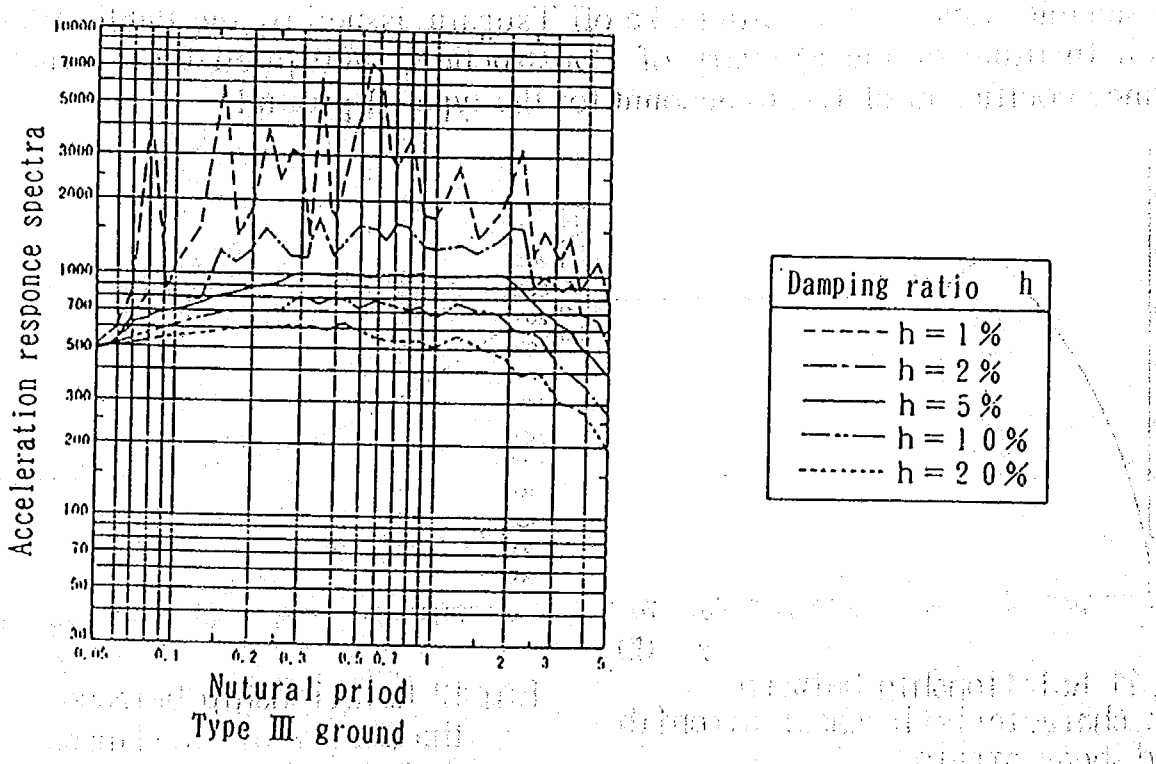


Fig. 13 Input Acceleration

2) Analysis results

First, we give the analysis results for the case where no collision occurs between the main girder and the abutments (without gap elements). Analysis results are shown in figures 14-17.

In Table 8 are compared the static analysis with the dynamic analysis values during ultimate level earthquakes. According to the table, the response values obtained from dynamic analysis are lower than the static analysis results, and thus the safety of the static design is confirmed.

According to the analysis results, the displacement of the main girder is around 235mm, and since the clearance between the main girder and the abutment is less than 300 mm, no collision occurs. However, this clearance may fall below 300 mm due to displacement due to creep and drying shrinkage over the years, and to displacement due to temperature changes. Taking this into account, similar dynamic analyses were performed with various clearances. The analysis results are shown in figure 18-20.

Also, figure 21 shows the relationship between the clearance and the lateral forces working on the abutment. As can be seen from this diagram, with narrower clearances, the lateral forces grow larger, and when the clearance is less than 160mm, these forces become larger than the lateral resistance of the abutment. However, according to this analysis, when creep and drying shrinkage are completed, the clearance will be at least 260mm, the main girder and the abutment will not collide, and the bridge will be functioning as a whole after an ultimate level earthquake.

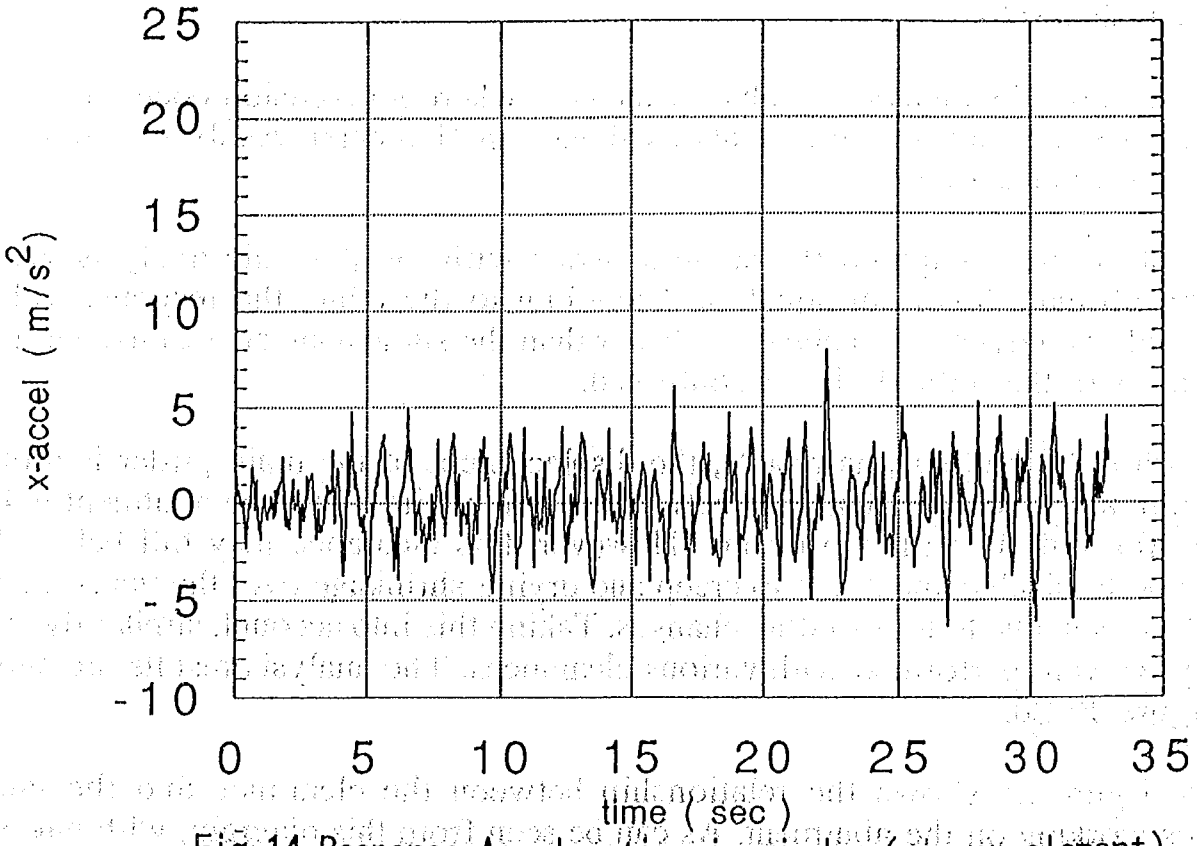


Fig. 14 Responce Acceleration in girder (no gap element)

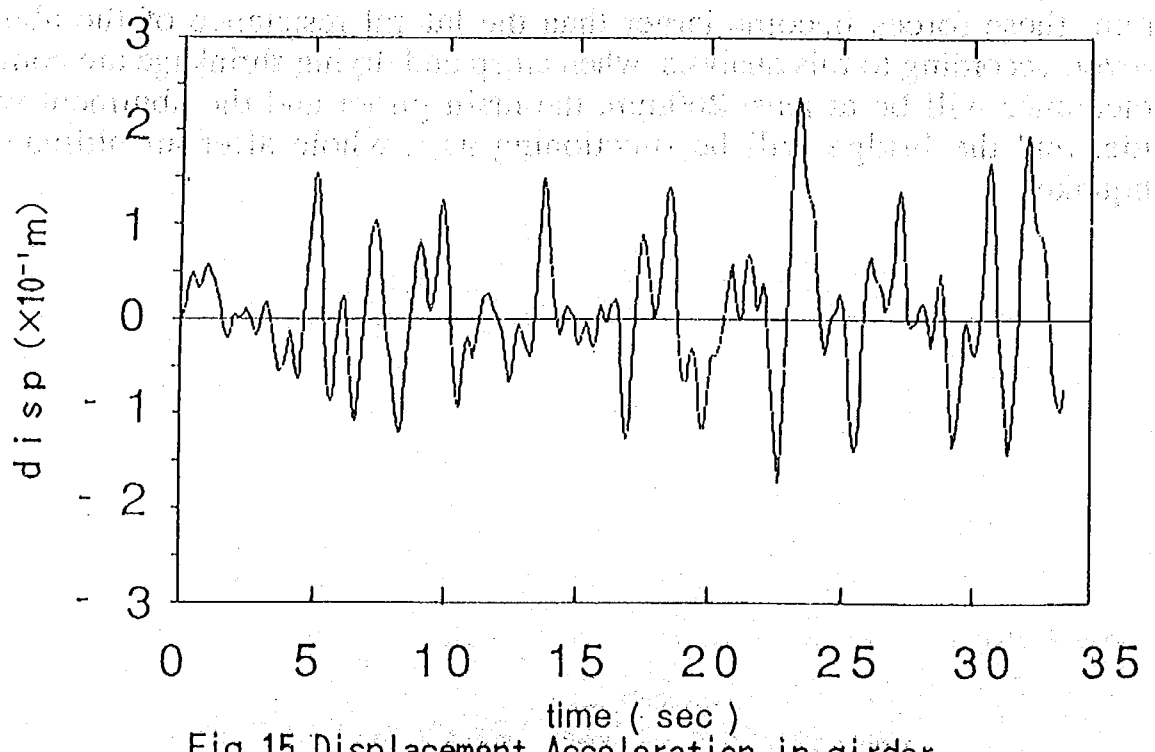


Fig. 15 Displacement Acceleration in girder

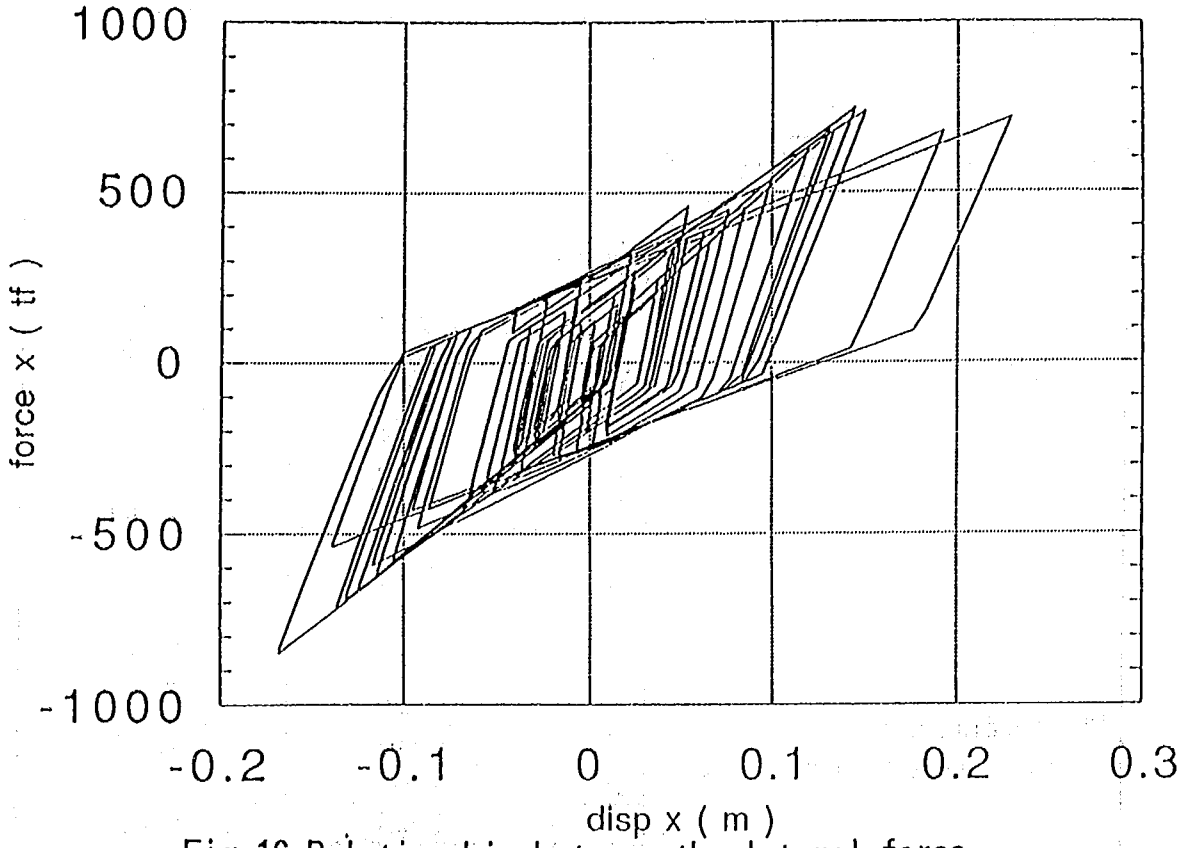


Fig. 16 Relationship between the lateral force and the lateral displacement in the bearing

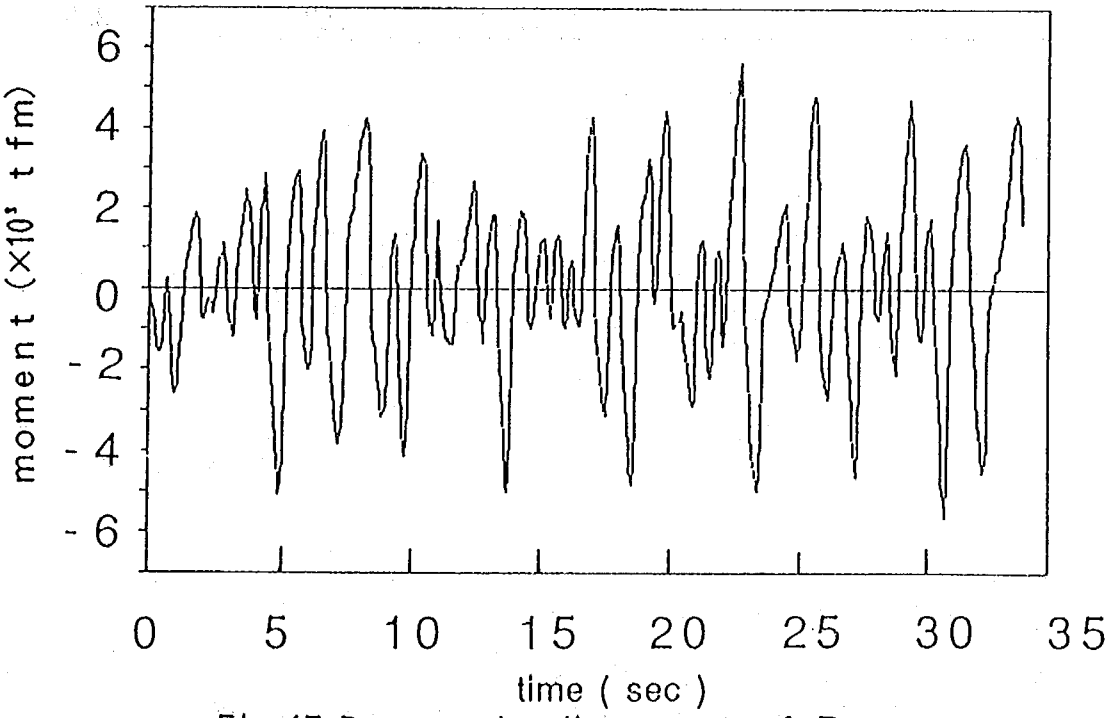


Fig. 17 Responce bending moment of P_4

Table 8 Dynamic analysis values and Static analysis values

Item		The dynamic Anarysis values	The static Anarysis values
Displacement of superstructure (mm)		235	471
Lateral forces (tf)	A_1	841	1,080
	P_1	825	1,080
	P_2	822	1,080
	P_3	823	1,080
	P_4	824	1,080
	P_5	829	1,080
	P_6	822	1,080
	P_7	830	1,080
	P_8	825	1,080
	A_2	827	1,080
The bending moment on the bottom of piers (tfm)	A_1	3,738	4,846
	P_1	4,658	6,156
	P_2	5,315	7,020
	P_3	5,659	7,452
	P_4	5,668	7,452
	P_5	5,277	6,912
	P_6	4,561	6,048
	P_7	3,598	4,752
	P_8	2,471	3,240
	A_2	2,553	3,333

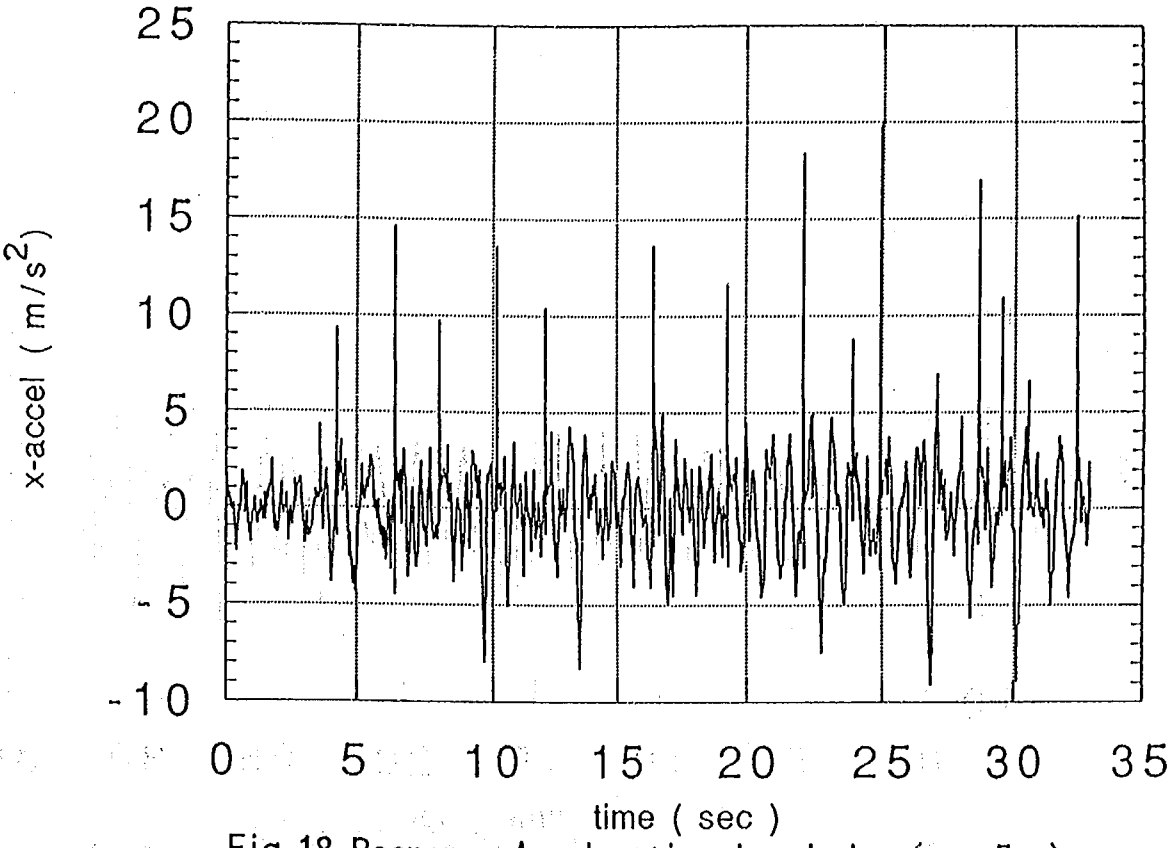


Fig. 18 Responce Acceleration in girder (gap 5cm)

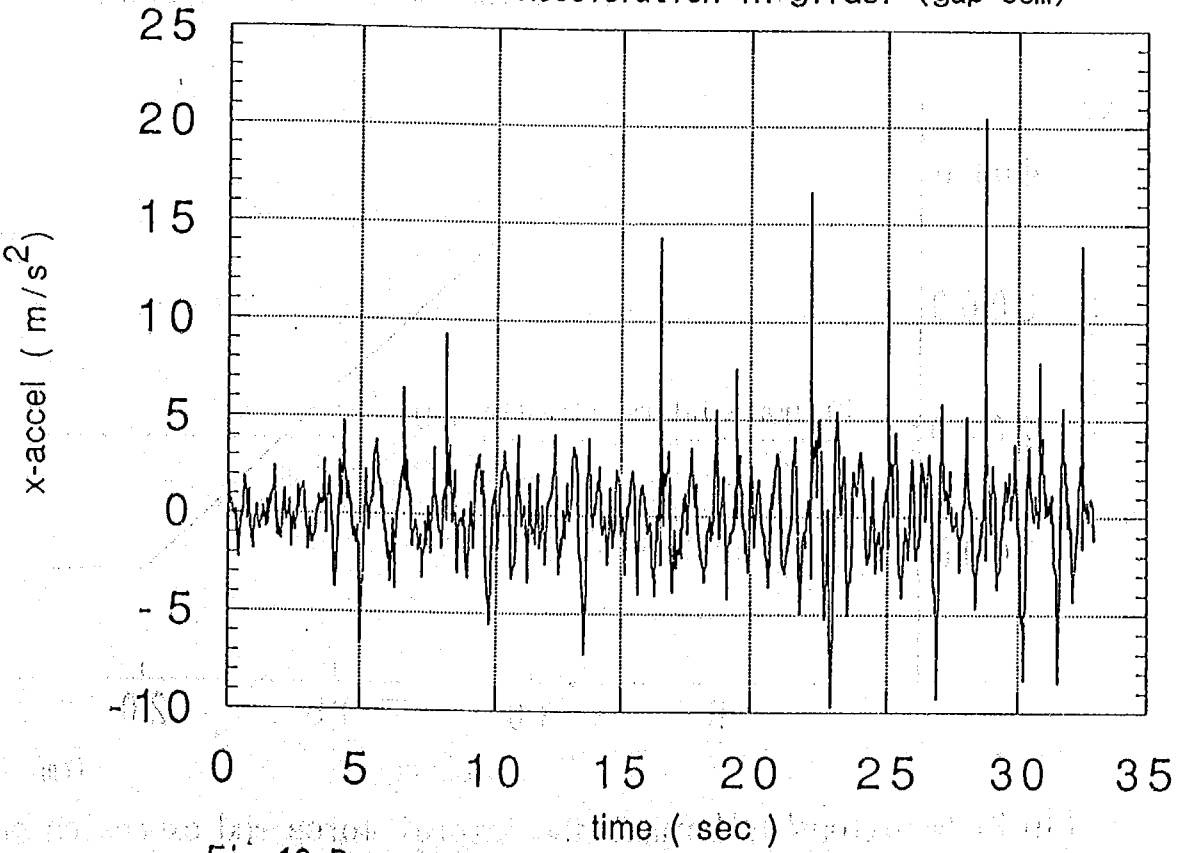


Fig. 19 Responce Acceleration in girder (gap 10cm)

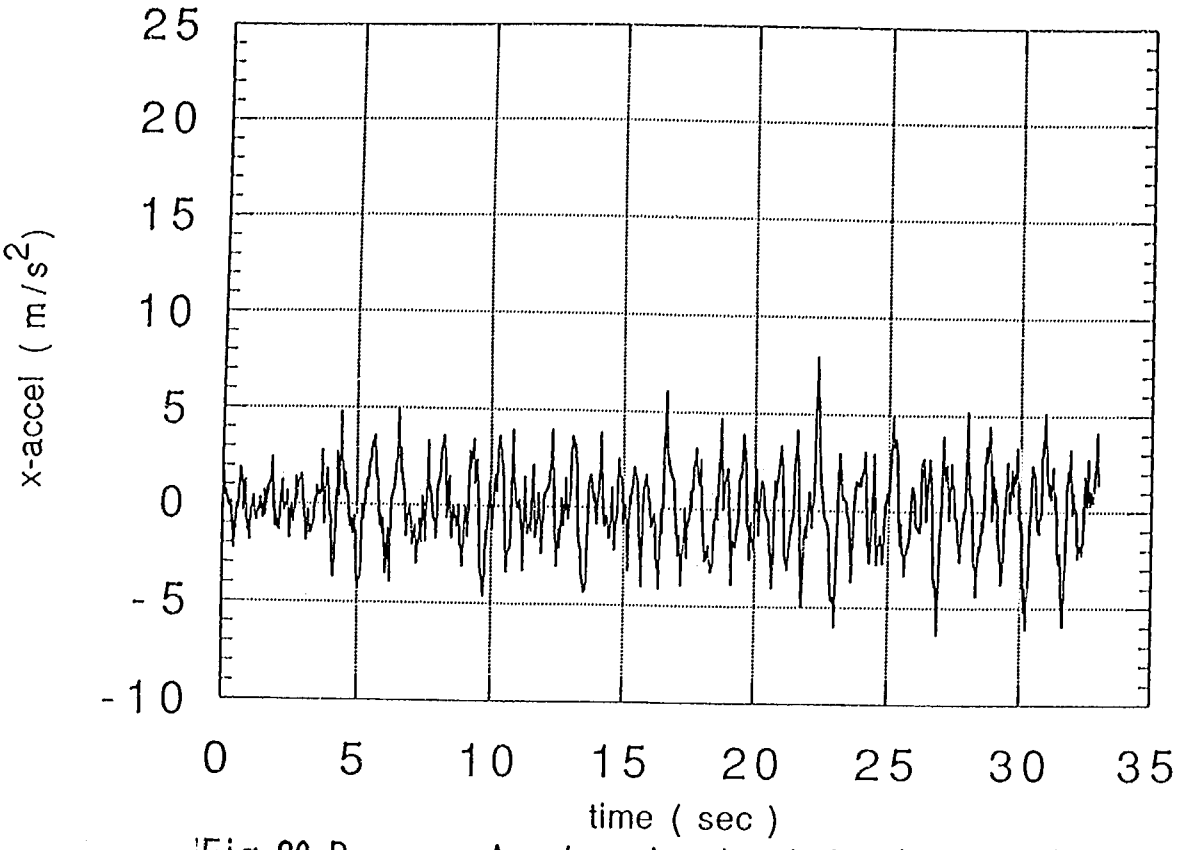


Fig. 20 Responce Acceleration in girder (gap 20cm)

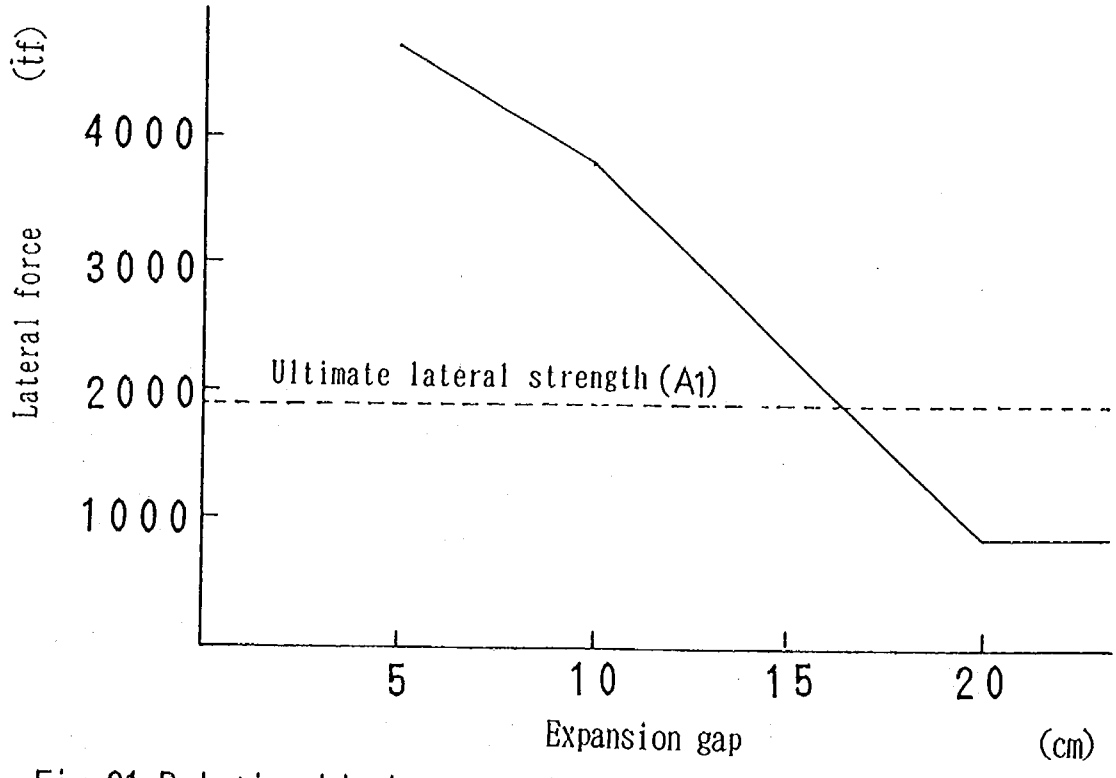


Fig. 21 Relationship between the lateral force and expansion gap

Session-6

Design Applications-1

U-6) A Simplified Preliminary Design Approach for Base Isolated Bridges
(Mahin, S. A.)

J-12) Preliminary Analysis of the Effects of Spatially Correlated Input Motions on the Response of Multiple-Span Continuous Bridges
(Tokida, K., Tamura, K. and Fukada, H.)

U-7) Recent Developments in Seismic Isolation at CALTRANS
(Yashinsky, M.)

J-13) Seismic Design of the Trans-Tokyo Bay Highway Bridges
(Shioi, Y., Yoshida, O. and Homma, M.)

A SIMPLIFIED PRELIMINARY DESIGN APPROACH FOR BASE ISOLATED BRIDGES

Stephen A. Mahin
Nishkian Professor of Structural Engineering
Earthquake Engineering Research Center
University of California at Berkeley
Berkeley, California 94720

ABSTRACT

A preliminary seismic design method is postulated for simple base isolated bridges based on conservation of displacement and energy for the long and short period ranges of structural response, respectively. The approach focuses on estimation of overall displacements of the deck level of the bridge. Simple, physically based equations are presented which allow displacements and design forces in the supporting columns to be determined. Application is demonstrated for friction sliding systems. A special non-dimensionalized form of the equations of motion for simple bridge structures is introduced to assess the adequacy of this design approach and to identify through a parametric investigation the variation of response indices with changes in ground motion, isolator and structure characteristics.

INTRODUCTION

Base isolation is often cited as being effective in reducing seismic design forces because the flexibility of elastomeric isolators shifts the effective period of the overall structural system to a less damaging frequency range and because energy dissipation in the isolators increases the effective viscous damping for the entire system. Based on this concept, U.S. practice for the design of base isolated structures typically utilizes an equivalent elastic analysis model . In such models, structural elements are represented by their elastic stiffness, but the stiffness of the isolator is reduced considering its secant stiffness under the design displacement. The structure is then analyzed considering an design response spectrum based on an amplified viscous damping coefficient.

This equivalent linearization or "substitute" structure approach is conceptually appealing and facilitates analysis. However, it has several limitations related to determining appropriate stiffness and damping values as a function of the hysteretic characteristics of the structural/isolation system and of the temporal variation of frequency content in the ground motion. Nonlinear analyses also indicate that the equivalent linear approach may not work satisfactorily for systems with high equivalent viscous damping values. Thus, U.S. practice mandates the use of nonlinear analysis for structures with high equivalent damping values.

This approach loses its conceptual appeal for some types of base isolation systems. For example, friction systems do not reduce the initial stiffness of the structure, but still achieve isolation. They respond more like a conventional inelastic system. These systems also generally result in high equivalent viscous damping values, requiring explicit nonlinear analysis in order to validate the design.

A series of analytical studies have been carried out to determine if there are alternate means for carrying out the preliminary design of base isolated structures that can overcome the limitations of the equivalent linear idealization and to more explicitly

acknowledge the nonlinear inelastic behavior present in friction based systems. In these studies, an attempt is made to use the un-modified elastic properties of the bridge system, and to use simple methods to predict the deck level displacements in simple bridges. these are then interpreted to estimate design displacements and forces in the structure and isolator. The non-dimensionalized form of the response spectra developed facilitates identification of the factors that influence the behavior of the isolated system.

At the moment, these studies have been limited to simple systems that can be idealized as single degree of freedom systems. This characterization may be appropriate for a broad class of bridge structures; e.g., over-crossings and viaducts. The results suggest that the use of nonlinear response spectra can be a powerful tool in design of simple base isolated structures of all types, and significantly, shifts attention from force, to displacement.

STRUCTURAL IDEALIZATION

These studies were carried out as a part of a more comprehensive study [1] of the feasibility of improving the seismic performance of structures using the Friction Pendulum System (FPS). The FPS connections are fabricated from steel and consist of an articulated low friction slider supported on a spherical concave surface (Fig. 1). This arrangement is similar to typical pot bearings used in bridges for many years, except that the size of the articulated slider in FPS connections is much smaller than the spherical support to accommodate the potentially large lateral displacements associated with seismic isolation.

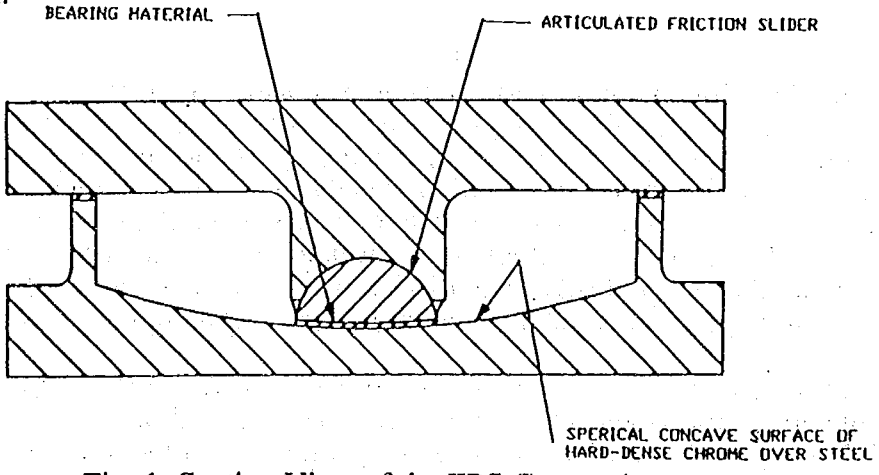


Fig. 1 Section View of the FPS Connection

Such devices have the advantages of a proven track record in bridge applications, the ability to resist large loads in a small space, full three-dimensional action, stable isolator behavior even under large lateral displacements (regardless of the load), compact size and simple mechanical behavior. Other advantages of this system is its benign response characteristics under large mass and stiffness eccentricities.[1].

In addition, the ability of FPS connections to rotate accommodates accidental deformations that may occur in a bridge structure due to foundation settlement and environmental actions (temperature, creep and shrinkage). Moreover, the ability of the connections to rotate as well as slide allows for relatively versatile installation. For example, typical installations for isolation devices would place the isolators between relatively rigid bent caps and the superstructure as shown in the two sketches on the left hand side of Fig. 2. While such installations are possible with FPS connections, the pin

action permits use of the simpler and less expensive arrangements on the right hand side of the figure.

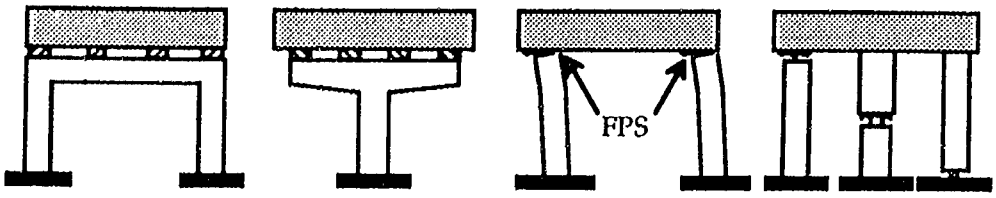


Fig. 2 Some Installation Arrangements for Isolated Bridges

Friction connections will be activated only if the earthquake induced forces exceed the frictional threshold that can be developed by the connections. Once the threshold is exceeded, the structure's response is governed by that of the connection. The hysteretic characteristics for sliding connections are essentially rigid-plastic with the initial strength governed by the friction coefficient ν. The resulting hysteretic loops are bilinear, but the nonlinearity is not due to yielding of structural members, but rather to sliding of the friction device.

Numerous studies have shown the need for deformation hardening once sliding commences. Deformation hardening (K_C) during sliding may be provided by supplementary elastomeric or metallic springs, or in the case of FPS connections by the curvature of the sliding surface. As the FPS slider moves along the spherical surface, the structure is lifted through an arc like that of a pendulum. This motion develops an additional restoring force Wu_{sl}/R, where W is the weight supported by the connection, R is the radius of curvature of the sliding surface and u_{sl} is the amount of sliding measured from the origin.

The resistance of the friction connections is given by:

$$V \approx \nu W \frac{\dot{u}_{sl}}{|\dot{u}_{sl}|} + K_c u_{sl} = \nu W \frac{\dot{u}_{sl}}{|\dot{u}_{sl}|} + \frac{W}{R} u_{sl} \qquad (1)$$

where the first equation corresponds the general case and the second relates to the FPS connections.

We now consider the case of a simple bridge structure where the bridge deck is supported on multiple columns, like those situations illustrated on the right hand side of Fig. 2. Initially the structure remains elastic with a lateral stiffness K and the isolator is not activated. Once the connection begins to slide, the effective lateral stiffness of the combined system reduces to $K_e = KK_C/(K+K_C)$. Thus, Ke and ν, along with K and W/g, fully characterize the mechanical properties of the system. This relation can be simplified further in terms of ν, the period of the supported structure (T), and the ratio $s = K_e/K$. It can be shown that:

$$s = \frac{K_c}{K + K_c} = \frac{1}{1 + \left(T_c/T\right)^2} \qquad (2)$$

where $T_c = 2\pi\sqrt{M/K_c}$ is the period of a sliding connection supporting a perfectly rigid structure. For the FPS connection, $T_c = 2\pi\sqrt{R/g}$ where g is the acceleration of gravity. Thus, T, Tc and ν become convenient parameters to characterize fully the properties of the system.

NORMALIZED EQUATIONS OF MOTION

It is possible to normalize the equations of motion in order to generalize the results of any analyses of this system. In this case the equations will be normalized in terms of the peak ground acceleration ($\ddot{u}_{g_{max}}$). Normalized response parameters of interest become:

$\lambda(t) = u(t) / \ddot{u}_{g\,max}(t)$ — the normalized total displacement at the deck level;

$\eta_{sl} = \nu W / M\ddot{u}_{g_{max}}$ — the normalized sliding strength coefficient (initial sliding); and

$\rho(t) = V(t) / V_{sl}$ — the normalized restoring force (base shear) in the supporting columns, where $V_{sl} = \nu W$.

The normalized equation of motion for the equivalent system can then be written as:

$$\ddot{\lambda}(t) + 2\omega\xi\dot{\lambda}(t) + \eta_{sl}\rho(t) = -\ddot{u}_g(t) / \ddot{u}_{g_{max}} \qquad (3)$$

This equation can be solved numerically for λ(t) given an earthquake record, damping ratio (ξ), natural circular frequency (w) and η_{sl}. Peak values of λ can be plotted in the form of spectra for different values of η_{sl} (Fig. 3). The non-dimensional nature of the plots allows one plot to be interpreted for several different combinations of parameters. For example, η_{sl} corresponds to a ν value of 0.04 for a peak ground acceleration of 40% g as well as to 0.06 for 60% g. The minimum normalized strength coefficient (base shear coefficient divided by the peak ground acceleration expressed as a fraction of gravity) required for the structure's columns to remain elastic $\eta_{st} = V_{max} / M\ddot{u}_{g_{max}} = Cg / \ddot{u}_{g_{max}}$ can be related by the geometry of the hysteretic loop of the equivalent single degree of freedom system to the maximum deck level displacement as [1]:

$$\eta_{st} = \frac{4\pi^2\lambda_{max} + \eta_{sl}T_c^2}{T^2 + T_c^2} \qquad (4)$$

Thus, once the peak deck level displacement is known, Eq. 4 can be used to design the column. Similarly, the maximum normalized column displacement can be related to the maximum deck displacement as:

$$\lambda_{st_{max}} = \frac{\lambda_{max} + \eta_{sl} T_c / (4\pi^2)}{1 + [T_c/T]^2} \tag{5}$$

The maximum displacement in the isolator is determined by subtracting the maximum column displacement from the maximum deck level displacement.

These expressions permit some general observation to be developed regarding the behavior of this simple bridge system. For example, Newmark and Hall [2] note that, with the exception of short period structures, the maximum lateral displacements of elastic and inelastic systems are similar and tend to increase with increasing structural period. If this observation is accepted, Eq. 4 indicates that for a system with a given connection period, period of the structure and damping coefficient, the minimum strength coefficient required for the structure to remain elastic will be reduced if the sliding strength coefficient decreases. Similarly, from Eq. 5, it can be observed that, if the period of the connection is increased, the displacements in the supporting columns will usually be reduced. Other trends can also be identified from these equations.

PARAMETRIC INVESTIGATION

A wide variety of statistically based parametric studies have been performed [1] top assess the response of this simple system and to evaluate various preliminary design methods. Elastic structures with periods ranging between 0.1 and 2.0 seconds were considered. Mass proportional viscous damping equal to 5% of critical and connection periods of 2 and 3 seconds were assumed in the studies. Ten different ground motion records, representing moderate earthquake motions on firm ground, were utilized.

Maximum Total Displacements. -- The peak total deck level displacement, regardless of isolator strength, tends to approximate the maximum displacement response for a similar elastic system, provided the period of the structure is relatively long. This tendency is observed in Fig. 3a for the north-south component of the 1940 El Centro record for structures with periods in excess of 0.5 seconds (the solid lines in the plots correspond to elastic response). In general, the total displacement increases with period of the structure. If only periods greater than about 0.5 seconds are considered, the sliding strength coefficient does not influence maximum system displacements too much (Fig. 3b). It is also observed (see Ref. 1) that the influence of deformation hardening (or the period of the connection) is not a significant variable, at least over the range studied.

In the short period range it is significant to note that the maximum bridge deck displacements are larger than corresponding elastic response values. In this region, if the sliding strength coefficient is reduced, total deck level displacements are increased. This trend is consistent with observations by Newmark and Hall [2] that inelastic and elastic systems tend to absorb the same amount of energy in this range. In this region, the maximum total displacement can be estimated using conservation of energy principles whereby one solves:

$$s u_{max}^2 + 2(1-s) u_{sl} u_{max} + u_{el}^2 + (1-2s) u_{sl}^2 = 0 \tag{6}$$

where u_{sl} is the deck level displacement at first sliding.

Data presented in Ref. 1 indicates that this general approach can be successfully used to predict total deck level displacements based on an elastic response spectrum. Equations 4 and 5 can then be used to estimate column strength requirements and displacements.

Maximum Column Displacements. -- The maximum column displacements tend to vary as a parabolic function of structural period (Fig. 4). In general, the shape of the plot is smooth and similar for the different earthquake motions considered. For short period structures, the displacements in the supporting columns are very small. The maximum structural displacement for a structure supported on sliding connections is always smaller than the structural displacement for a similar structure constructed with out sliding connections.

If the sliding strength coefficient is reduced (by reducing the friction coefficient or increasing the intensity of the ground motion) the maximum structural displacement is reduced. If the period of the connection is increased, structural displacements are always decreased.

Ratio of Column to Deck Displacements. -- The ratio of column to deck level displacements indicates how much of the total displacements are sustained by the columns, and how much is absorbed by the isolator. The smaller the value of this ratio, the more effective the friction isolator is in protecting the structure from earthquakes.

This ratio tends to vary like an increasing linear function of the structural period (Fig. 5). For short period structures, the deck displacement is mainly due to the sliding displacements. If the sliding strength coefficient reduced, this ratio is reduced and its shape becomes smoother. If the period of the connection is increased, the ratio is always reduced.

Residual Displacements. -- The residual displacement of a friction base isolation system is an important parameter governing post earthquake functionality of the bridge. In the analyses, the columns are assumed to remain elastic so that all residual displacements for the system considered are due to the friction isolator.

From Fig. 6 it can be observed that the residual displacements are small. The residual displacement is an irregular function of the structural period. It also varies considerably from one earthquake record to another. If no deformation hardening is provided, large residual displacements are possible [1] (averaging on the order of half of the maximum displacements developed). If the period of the connection is reduced, residual displacements are usually reduced.

Maximum Total Acceleration. -- The total acceleration is an important parameter as it is an indication of the inertial forces developed in the bridge deck. The maximum total acceleration tends to be a smooth decreasing function of the structural period (Fig. 7). For structural periods greater than about 0.6 seconds, maximum total accelerations are nearly constant. It is important to observe that the maximum total acceleration for structures supported on sliding connections is considerably reduced compared to the total acceleration for similar elastic structures without isolation. If the sliding strength coefficient is reduced or if the period of the connection is increased, the maximum total acceleration is always reduced.

Structural Strength Coefficient. -- The structural strength coefficient indicates the design forces required for the columns to remain elastic (expressed as a percentage of the weight of the structure). This coefficient initially increases with structural period, but subsequently remains mainly constant with period (Fig. 8). This trend is opposite those in most codes for non-isolated structures where required design forces decrease with increasing period. However, in this case the forces shown are those needed to prevent any damage to the structure, where as code forces generally permit significant amounts of structural damage. Friction isolators were shown to be most effective in protecting short period structures, and thus, significant savings may be recognized in short period structures over those designed according to typical codes. Design forces required may be higher than those required for conventional designs in the long period range, however, no damage will be experienced in such isolated structures. Like trends identified for total acceleration, increasing the period of the connection, or reducing the sliding strength coefficient always reduces the required structural strength coefficient.

CONCLUDING OBSERVATIONS

It appears that a preliminary design approach like that suggested by Newmark and Hall may be promising for simple base isolated bridges. In this case, the system may be modeled as an equivalent elastic single degree of freedom system. Maximum displacements at the deck level may be estimated directly from elastic response spectrum (for normal amounts of damping; i.e., 5%) outside the short period range. For short period structures, simple conservation of energy principles may be used to estimate amplified displacement. Once the displacements are determined, simple equations developed from the mechanical properties of the structure and isolators allows determination of the base shear coefficient required to keep the supporting columns elastic and estimation of the displacements in the columns and isolators. The normalized form of the equations of motion presented also permit development of site specific nonlinear response spectrum that can be conveniently used in design. Additional research is needed to more fully validate the effectiveness and practicality of this design approach.

ACKNOWLEDGMENTS

The research reported herein was funded by a grant from the National Science Foundation to Earthquake Protection Systems (EPS), San Francisco, through the Small Business Innovative Research awards program. Dr. S. C. Liu of NSF and Dr. Victor Zayas of EPS are gratefully acknowledged for their support of this research. Special thanks is given to Luis Bozzo, graduate student who carried out the analytical studies reported in this paper. The findings and conclusions made in this paper are those of the author alone, and are not necessarily those of the sponsors or other contributors.

REFERENCES

1. Zayas, V. et al, "Feasibility and Performance Studies on Improving the Earthquake Resistance of new and Existing Buildings using the Friction Pendulum System," Report No. UCB/EERC-89/09, Earthquake Engineering Research Center, University of California, Berkeley, September 1989.

2 Newmark, N. and Hall, W., "Earthquake Spectra and Design," EERI, Engineering Monographs on Earthquake Criteria, Structural Design and Strong Motion Records, EERI, Vol. 3, 1982.

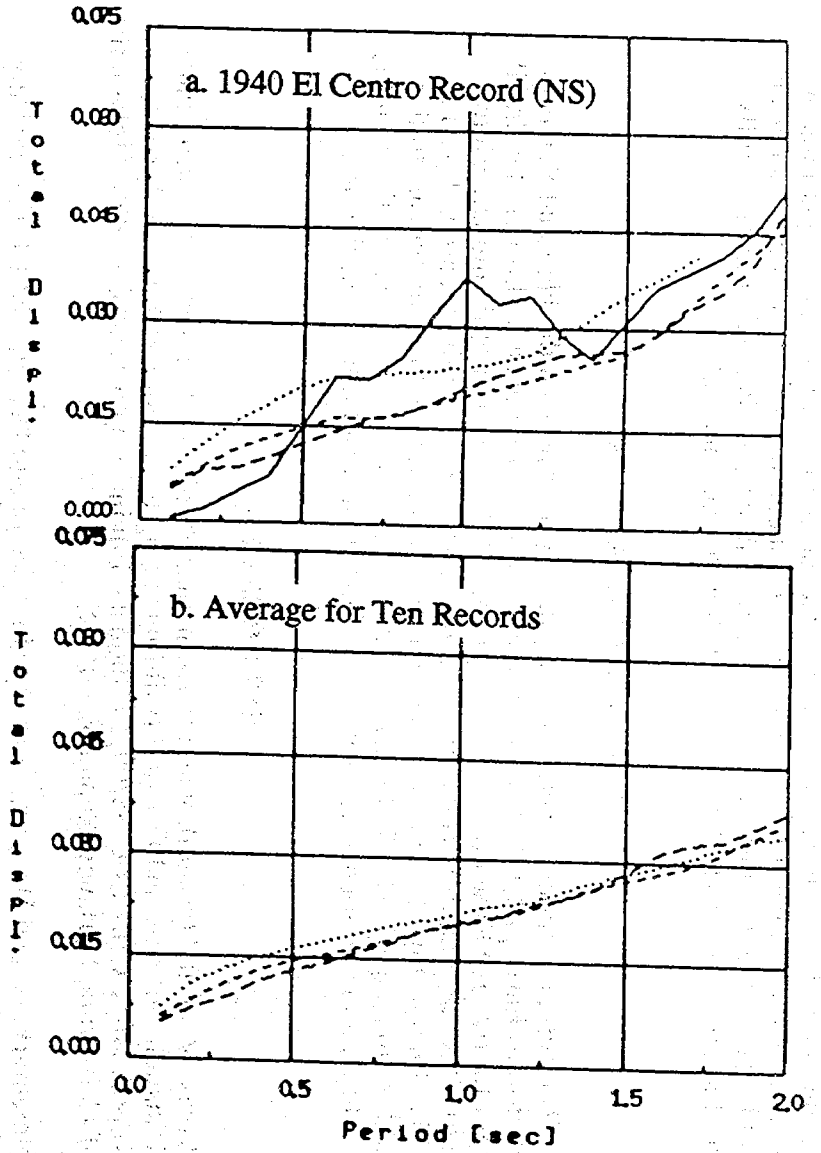


Fig. 3 Maximum Normalized Deck Displacement [sec^2]

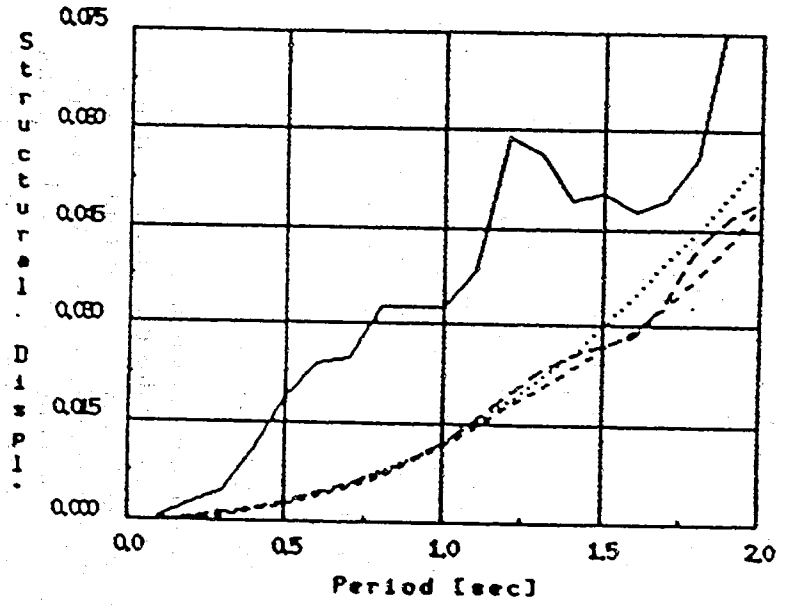


Fig. 4 Normalized Column Displacement [sec^2] for 1940 El Centro Record (NS)

$\cdots\eta_{sl} = 0.1$ $---\eta_{sl} = 0.2$ $--\eta_{sl} = 0.3$

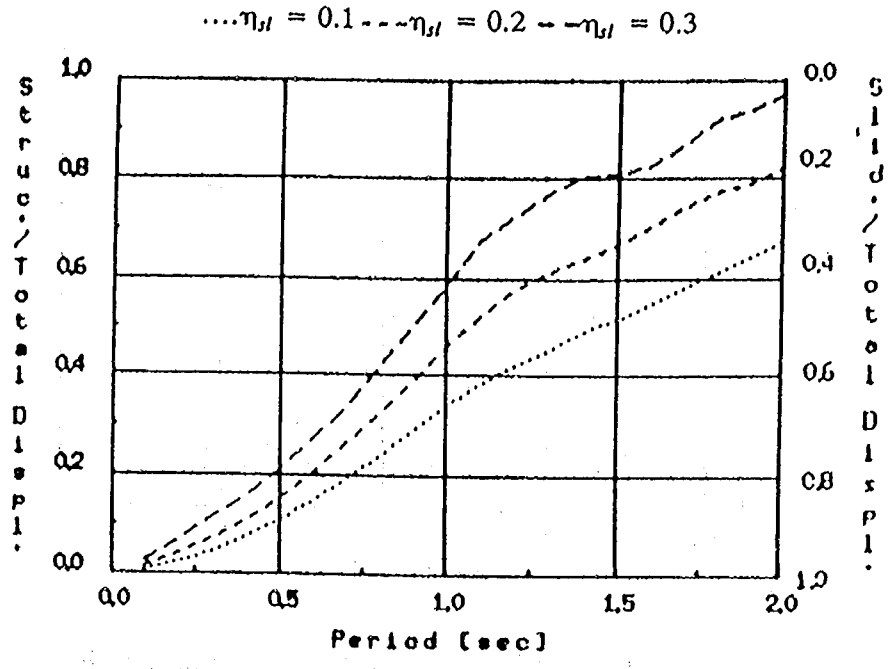


Fig. 5 Ratio of Column to Deck Displacement -- Average for Ten Records

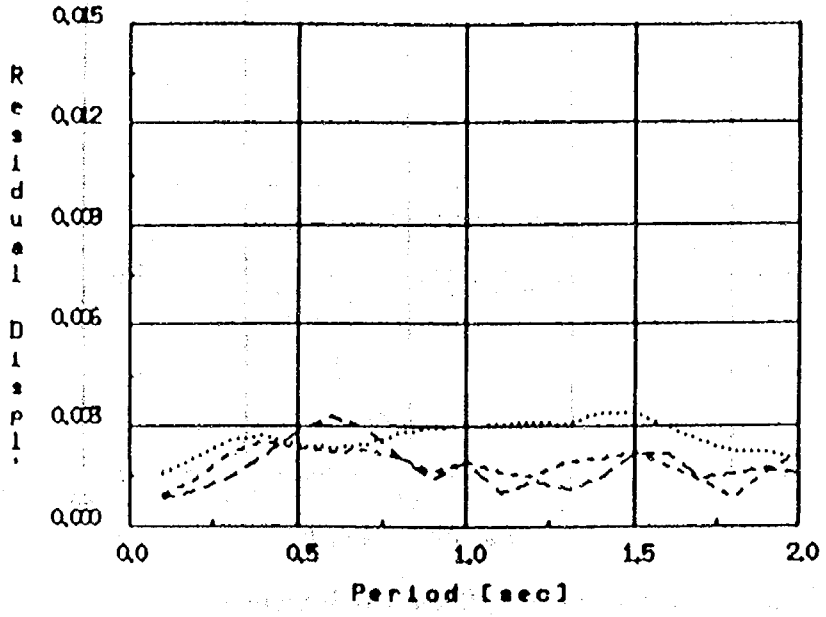


Fig. 6 Normalized Residual Displacements in Isolators -- Average for Ten Records

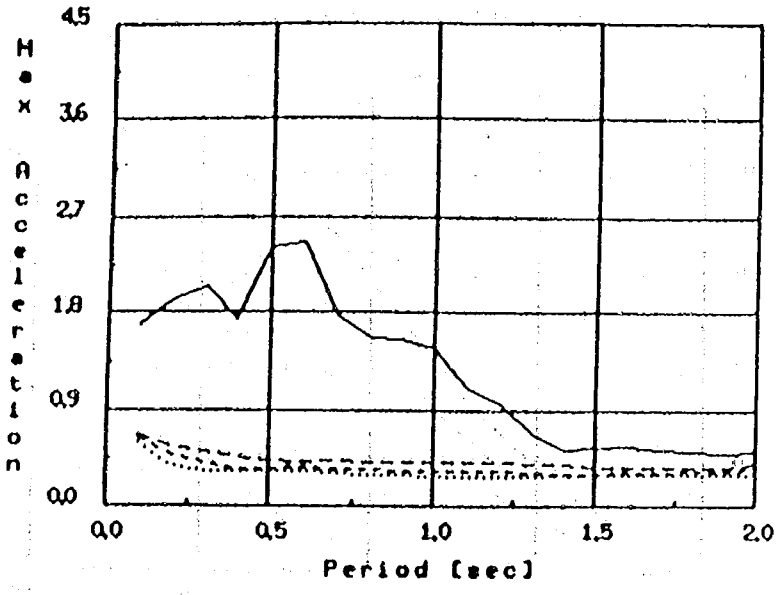


Fig. 7 Normalized Maximum Deck Total Acceleration -- 1940 El Centro Record (NS)

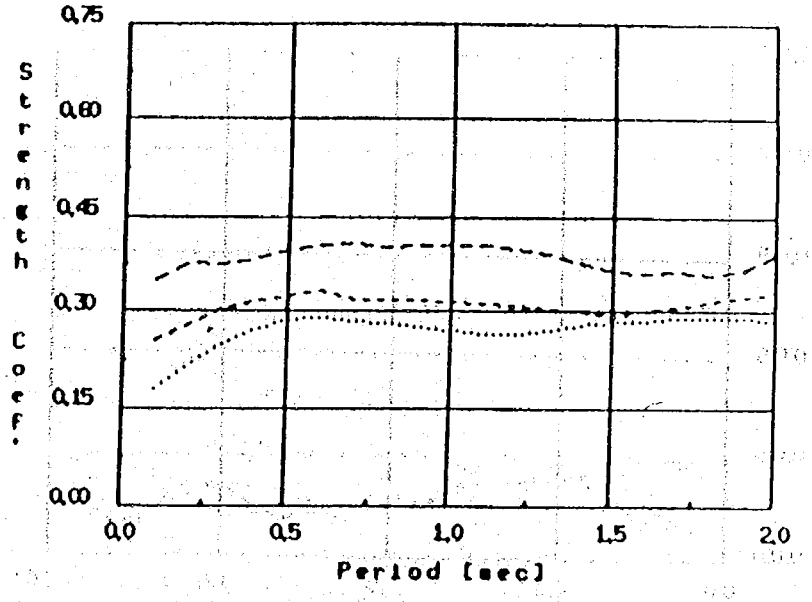


Fig. 8 Normalized Base Shear Coefficient -- 1940 El Centro Record (NS)

PRELIMINARY ANALYSIS OF THE EFFECTS OF SPATIALLY CORRELATED INPUT MOTIONS ON THE RESPONSE OF MULTIPLE-SPAN CONTINUOUS BRIDGES

Ken-ichi Tokida[1], Keiichi Tamura[2] and Hidemi Fukada[3]

ABSTRACT

Considering the spatial variation of ground motion, a simple method is proposed to establish the spatially correlated input ground motions, and the seismic response of 5 to 20-span continuous bridges to this spatially correlated motions is studied by dynamic response analysis. The results are compared to the response estimated for the uniform input motions, and the time-lagged input motions that consider the apparent propagation of seismic waves.

INTRODUCTION

Numerous studies on the spatial variation of ground motion have been performed with the recent development of closely spaced arrays of accelerographs (e.g., Bolt et al., 1982; Abrahamson et al., 1987). Particularly, a number of studies focus on the differential ground motion characteristics, which may have significant influence on the dynamic behavior of buried lifeline facilities, multiple-span bridges, widely spread tanks, and so on.

The number of multiple-span continuous bridges has been recently increased in Japan, with the demand of decreasing the number of expansion joints that make annoying vibration and noise, and are vulnerable to traffic load. Since the seismic lateral force acting on a multiple-span continuous bridge in longitudinal direction becomes large as the number of spans increases, distributing this lateral force to substructures is one of the major design problems of multiple-span

[1]Head, Ground Vibration Division, Public Works Research Institute, Ministry of Construction
1 Asahi, Tsukuba-shi, Ibaraki-ken 305 Japan
[2]Senior Research Engineer, Ground Vibration Division, ditto
[3]Ground Vibration Division, ditto

continuous bridges. The use of rubber bearings is effective in distributing the lateral force, and a number of multiple-span continuous bridges have been constructed with rubber bearings. When the bridge length is long, the ground motion along the structure may be different from point to point, and each substructure may be subjected to different seismic effect, however this effect has not been sufficiently studied.

Considering the background mentioned above, a simple method is proposed to establish the spatially correlated input ground motions for the seismic design of multiple-span continuous bridges. The spatial variation characteristics of ground motion is taken here into account. The effects of the spatially correlated input motions on the response of multiple-span continuous bridges are studied by dynamic response analyses, and the results are compared to the response estimated for the ordinal uniform input motions, and the time-lagged input motions that consider the propagation of seismic wave.

SPATIAL CORRELATION OF GROUND MOTION

Based on strong motion array records, several models of the spatial correlation function of ground motion have been proposed (Harada, 1984; Loh and Yeh, 1988; Tamura et al., 1990, 1991). Among them, Tamura et al. (1990) introduced the following spatial correlation function and calibrated it from the measured array data:

$$\rho_S(\eta)=\{1-(\eta/\xi_0)^2\}\exp\{-(\eta/\xi_0)^2\} \quad (1)$$

where η is the separation distance between two points, and ξ_0 represents the distance at which the spatial correlation is 0. Fig.1 shows an example of the spatial correlation coefficients calculated from the measured data and the least squares fit correlation function. The magnitude and epicentral distance of the analyzed event are 6.0 and 96 km, respectively. According to the analysis of eight small to medium events, ξ_0 varies from 300 m to 1000 m, and the mean value is approximately 500 m (Tamura et al., 1992).

SPATIALLY CORRELATED INPUT GROUND MOTIONS

Assuming that ground motions at two points have the spatial correlation given by Eq.(1) according to the separation distance, and each ground motion has the same power spectral density

function, a set of spatially correlated ground motions is estimated. This assumption corresponds essentially to the case in which the infinite propagation velocity of seismic waves is assumed in the general spectral ground motion model. The procedure to establish the spatially correlated ground motions is as follows:

The standard ground motion is at first selected, and the target spatial correlation is calculated according to the distance from this standard motion. Then, preserving the Fourier amplitude of the standard ground motion, a ground motion is synthesized to have the target correlation with the standard motion by adjusting the phase of the Fourier transform.

The acceleration time history shown at the top of Fig.2 is selected as the standard ground motion. This time history is the design input motion of time history analysis for alluvial and diluvial sites, prescribed in the design specifications for the highway bridges in Japan (Japan Road Association, 1990). Fig.2 shows a set of synthesized spatially correlated ground motions using Eq.(1) as a spatial correlation function, in which ξ_0 is taken as 500 m.

DYNAMIC RESPONSE ANALYSIS

Analytical Model

The prototype bridges considered in this study are multiple-span continuous steel girder bridges. An example of analyzed bridges is illustrated in Fig.3. The wall type pier and pile foundation are adopted. The height of pier is 15 m. The number of spans is changed as 5, 10, 15 and 20, where the each span length is fixed as 50 m. Consequently, the total span length is changed from 250 to 1000 m. Dimensions of the superstructure and the substructure are fixed in every case to enable easy comparison of response analysis results. Aiming to distribute lateral force to substructures, the girder is supported by fixed bearings except at the both end piers where it is supported by movable bearings.

The bridges are modeled as two dimensional frames in both longitudinal and transverse directions for time history analyses. Fig.4 shows an example of analytical models. The piles are replaced by equivalent horizontal and rotational springs. The damping ratio to the critical is assumed to be 0.05.

Method to Apply Input Motions

The following three methods are employed to apply input motions to a bridge:

1) Uniform input motions

The standard ground motion shown at the top of Fig.2 is applied to every substructure.

2) Spatially correlated input motions

The acceleration time histories shown in Fig.2 are applied to piers according to the distance from one end of a bridge: P_2 and P_1 in longitudinal and transverse directions, respectively, shown in Fig.4.

3) Time-lagged input motions

Considering the apparent propagation of seismic wave, a time lag is added according to the distance from one end of a bridge and the apparent propagation velocity, where the propagation velocity is assumed to be 500 m/s.

RESPONSE CHARACTERISTICS TO VARIOUS INPUT MOTIONS

Longitudinal Direction

Figs.5, 6 and 7 show the distribution of the maximum acceleration and displacement on a pier top, and the maximum bending moment at a pier base, respectively, for the 10-span continuous bridge. The spatially correlated and the uniform input motions yield the similar level of response with regard to the maximum acceleration, displacement and bending moment, respectively. The maximum response values for the time-lagged input motions are smaller than those for the uniform input motions and the spatially correlated input motions. The variations of the maximum acceleration, displacement and bending moment among piers are not large for each input motion applying method.

Fig.8 shows the maximum axial force of the superstructure of the 10-span continuous bridge. The distribution of the maximum axial force shows a concave shape for the uniform input motion, whereas it shows a convex shape for the spatially correlated and the time-lagged input motions. The largest axial force arises near the center of the bridge in case of the spatially correlated input motions, however note that the stress of the superstructure due to this axial force is not critical from a design point of view.

Figs.9 through 12 show the maximum response values among all piers of each span bridge, where the number of spans is changed from 5 to 20. As for acceleration response on a pier top, the maximum values against the uniform and the spatially correlated input motions are almost equal for each case of the number of spans. The maximum acceleration value for the time-lagged input motions is smaller than those for the uniform and the spatially correlated input motions.

The changes of the maximum displacement on a pier top and the maximum bending moment at a pier base show similar trend. The maximum displacement and bending moment for the spatially correlated input motions are almost equal to those for the uniform input motions, in case of the 5 and 10-span bridges. However, the spatially correlated input motions yield smaller response than the uniform input motions, when the number of spans is 15 or 20. The time-lagged input motions cause the smallest response among the three input formulae, in general.

The difference of response characteristics of the maximum acceleration and displacement on a pier top, and the maximum bending moment at a pier base for the spatially correlated input motions may be interpreted as follows:

The acceleration response of a span of a bridge is mainly affected by the input motions acting on that span, whereas the displacement and bending moment response is principally governed by the relative movement of substructures.

In the spatially correlated input motions, the ground motion acting on each substructure is different in detail, however the difference of ground motions at adjacent substructures is not large, and the structural acceleration response induced by each motion is almost equivalent independent of location. Therefore, the acceleration response to the spatially correlated input motions is not remarkably changed from that to the uniform input motions even if the number of spans is large.

Relative movement of substructures is determined not only by the ground motions acting on that portion, but also by ground motions acting on distant portions through the superstructure. Accordingly, the displacement and bending moment response of a substructure is subjected to a mixture of various input motions, as bridge length becomes long. This may be the reason why the displacement and bending moment response to the spatially correlated input motions is different from that to the uniform input motions, when the number of spans is large.

The maximum axial force of the superstructure is small for the uniform input motions, as compared to the cases of the spatially correlated and the time-lagged input motions. The spatially

correlated input motions cause the largest axial force when the number of spans is 10 or greater. However, the stress resulting from this axial force does not exceed the allowable stress of steel even for the case of the 20-span continuous bridge.

Transverse Direction

Since a wall type pier is employed in the present study and the rigidity of this type pier is considerably larger in transverse direction as compared to the longitudinal direction, an attention is focused on the bending moment of the superstructure due to seismic load.

Fig.13 shows the distribution of the maximum bending moment of the superstructure for the 10-span continuous bridge. The bending moments for the uniform input motions are 0 for all piers. Note that large bending moment is induced by the time-lagged input motions.

Fig.14 shows the maximum bending moment of the superstructure among all piers of each bridge. The bending moment for the time-lagged input motions is considerably larger than that for the spatially correlated input motions. The bending moments for the 10 to 20-span bridges do not vary very much in case of either the spatially correlated or the time-lagged input motions, and they show a little higher value than the case of the 5-span continuous bridge.

CONCLUSIONS

A simple method to establish the spatially correlated input ground motions for the seismic design of multiple-span continuous bridges is proposed. The response characteristics of 5 to 20-span continuous bridges are studied against the spatially correlated, the uniform and the time-lagged input motions, and the results are compared. The following conclusions may be deduced from the present study:

1) The spatially correlated and the uniform input motions have similar seismic effects on the response of a multiple-span continuous bridge, when the number of spans is 10 or fewer. However, the spatially correlated input motions cause different seismic response from the uniform input motions, when the number of spans is 15 or greater.

2) The spatially correlated input motions cause the axial force of the superstructure, however the stress level resulting from this axial force may not be a serious concern in design practice.

3) The time-lagged input motions may cause different seismic effects to a multiple-span continuous bridge, comparing to the case of the uniform input motions. Close attention should be paid to the results, when the time-lagged input motions are employed in analysis.

REFERENCES

Abrahamson, N. A., Bolt, B. A., Darragh, M., Penzien, J. and Tsai, Y. B. (1987). "The SMART-1 Accelerograph Array (1980-1987): A Review", *Earthquake Spectra*, Vol.3, No.2.

Bolt, B. A., Loh, C. H., Penzien, J. and Tsai, Y. B. (1982). "Preliminary Report on the SMART-1 Array in Taiwan", *Earthquake Engineering Research Center Report*, No.UCB/EERC-82/13, University of California, Berkeley.

Harada, T. (1984). "Probabilistic Modeling of Spatial Variation of Strong Earthquake Ground Displacements", *Proc. of 8th World Conference on Earthquake Engineering*.

Japan Road Association (1990). *Design Specifications for Highway Bridges, Part V Seismic Design* (in Japanese).

Loh, C. H. and Yeh, Y. T. (1988). "Spatial Variation and Stochastic Modelling of Seismic Differential Ground Movement", *Earthquake Engineering and Structural Dynamics*, Vol.16, No.4.

Tamura, K., Winterstein, S. R. and Shah, H. C. (1990). "Random Field Models of Spatially Varying Ground Motions", *John A. Blume Earthquake Engineering Center Report*, No.92, Stanford University.

Tamura, K., Winterstein, S. R. and Shah, H. C. (1991). "Spatially Varying Ground Motion Models and Their Application to the Estimation of Differential Ground Motion", *Proc. of Japan Society of Civil Engineers*, No.437/I-17.

Tamura, K. and Aizawa, K. (1992). "Differential Ground Motion Estimation Using a Time-Space Stochastic Process Model", *Proc. of Japan Society of Civil Engineers*, No.441/I-18.

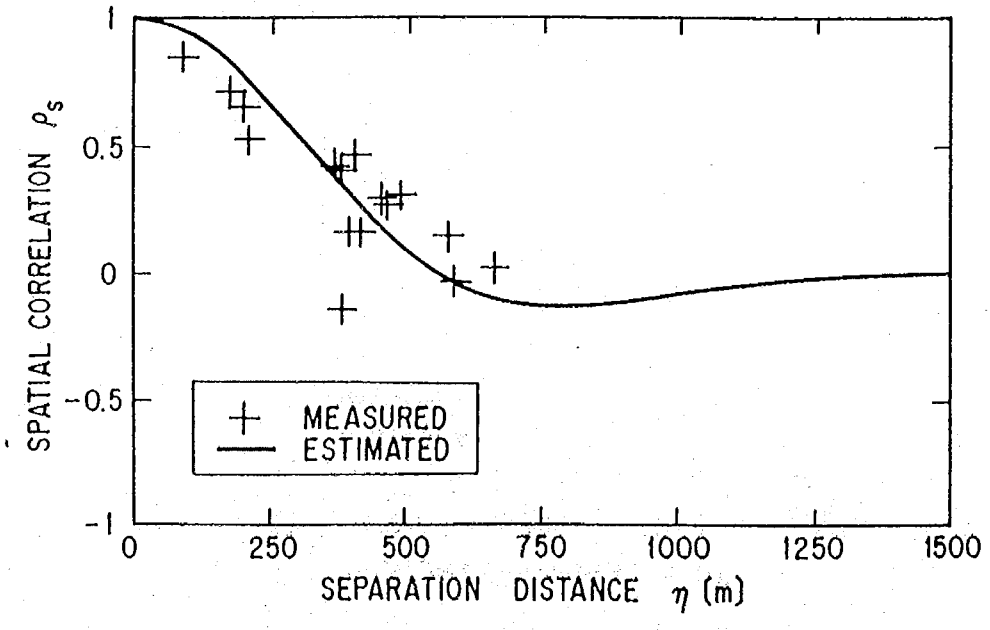


Fig.1 Spatial Correlation Function of Ground Motion

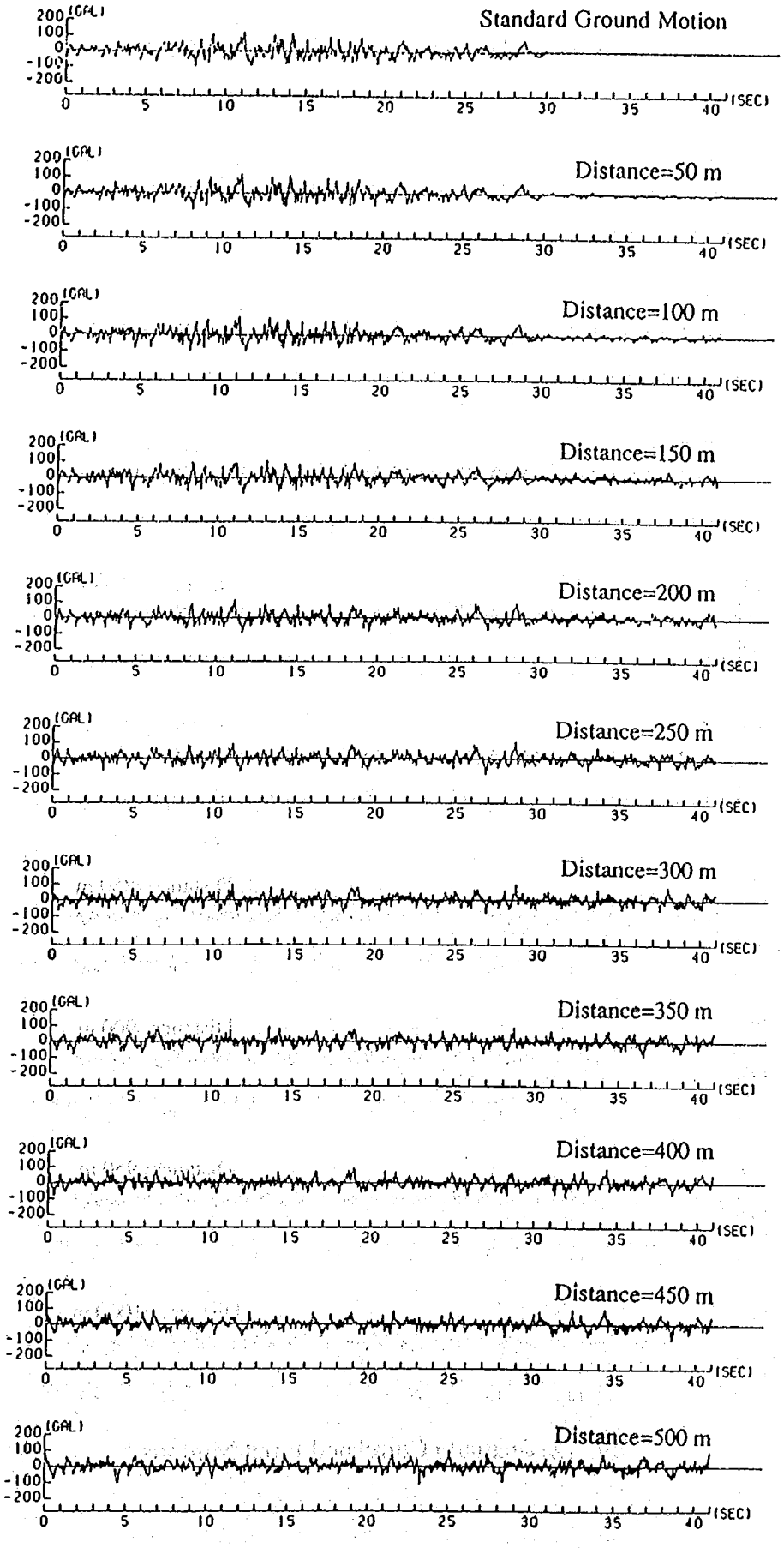


Fig.2(1) Spatially Correlated Input Motions

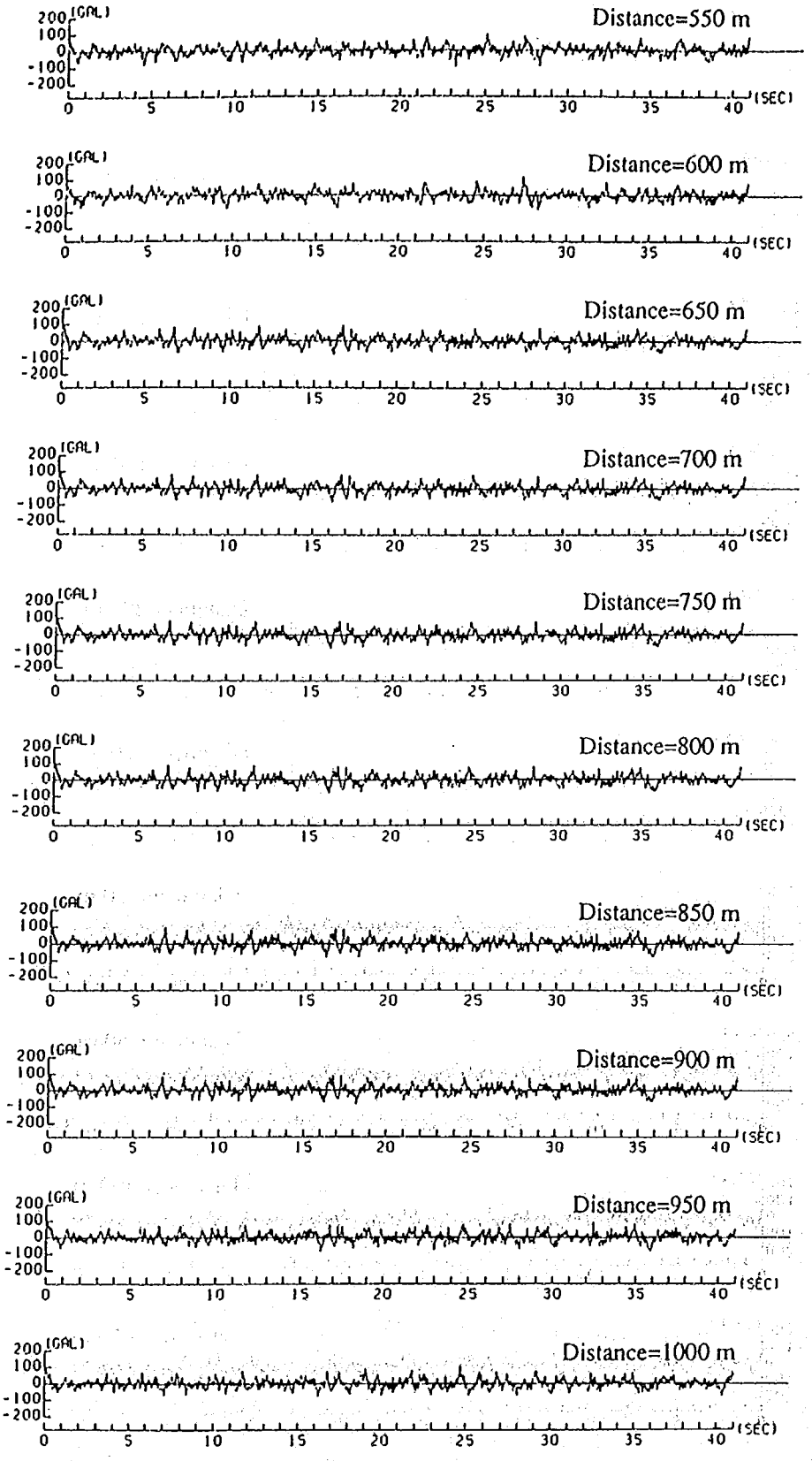


Fig.2(2) Spatially Correlated Input Motions

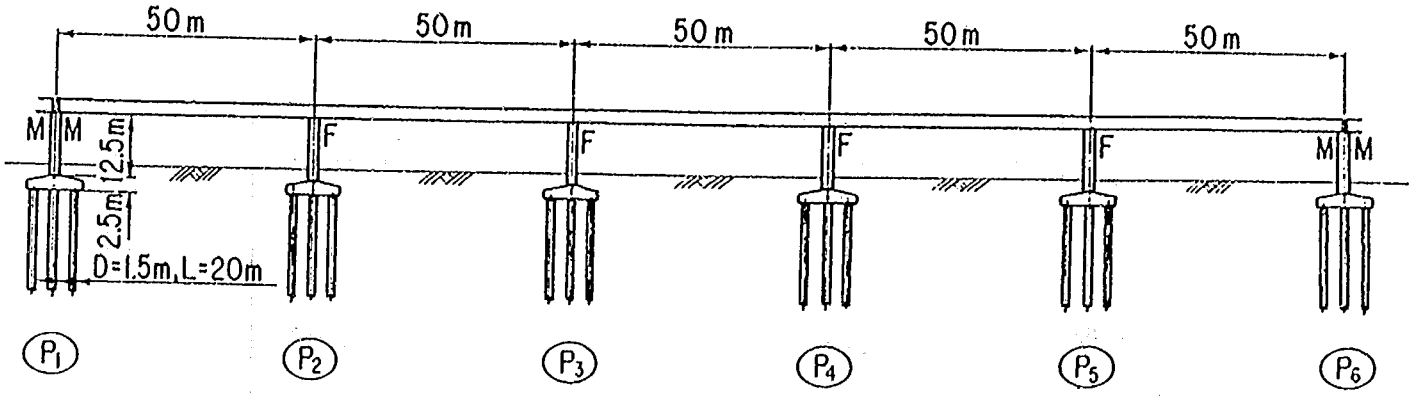
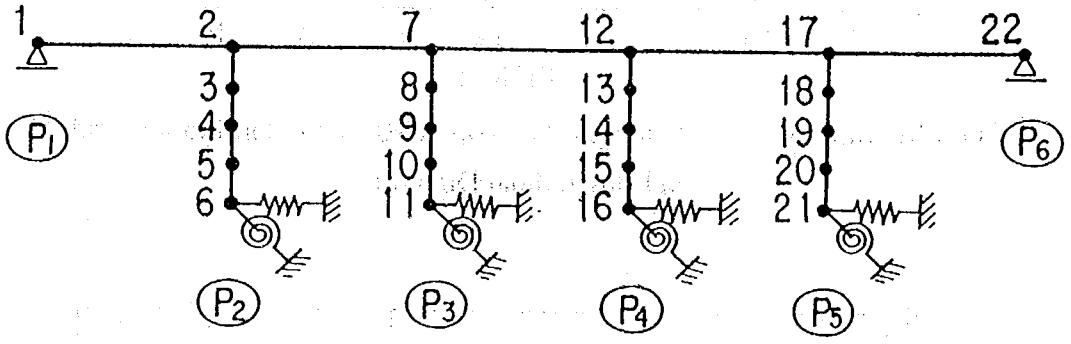
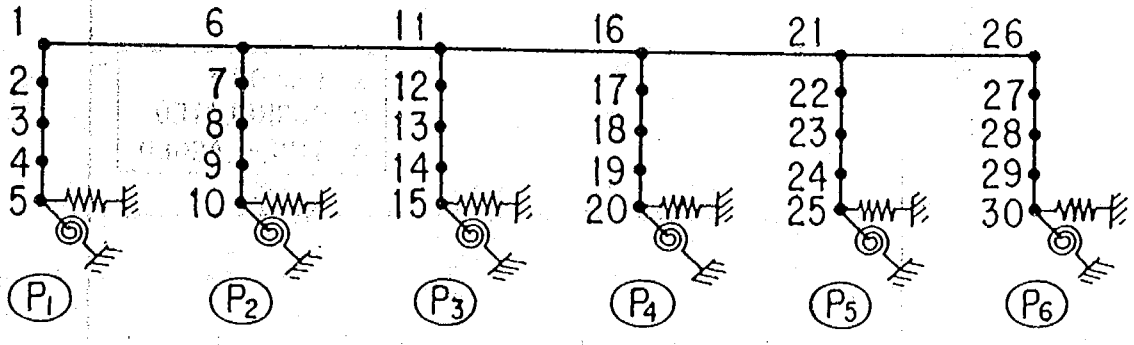


Fig.3 General View of 5-Span Continuous Bridge



(a) Longitudinal Direction



(b) Transverse Direction

Fig.4 Analytical Model of 5-Span Continuous Bridge

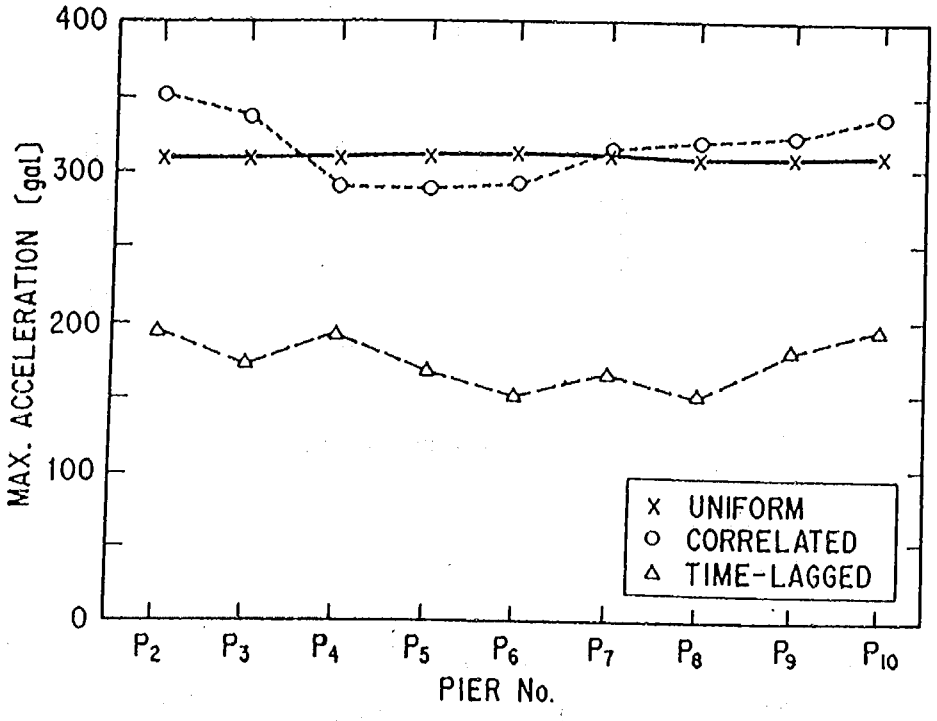


Fig.5 Maximum Acceleration on Pier Top of 10-Span Continuous Bridge in Longitudinal Direction

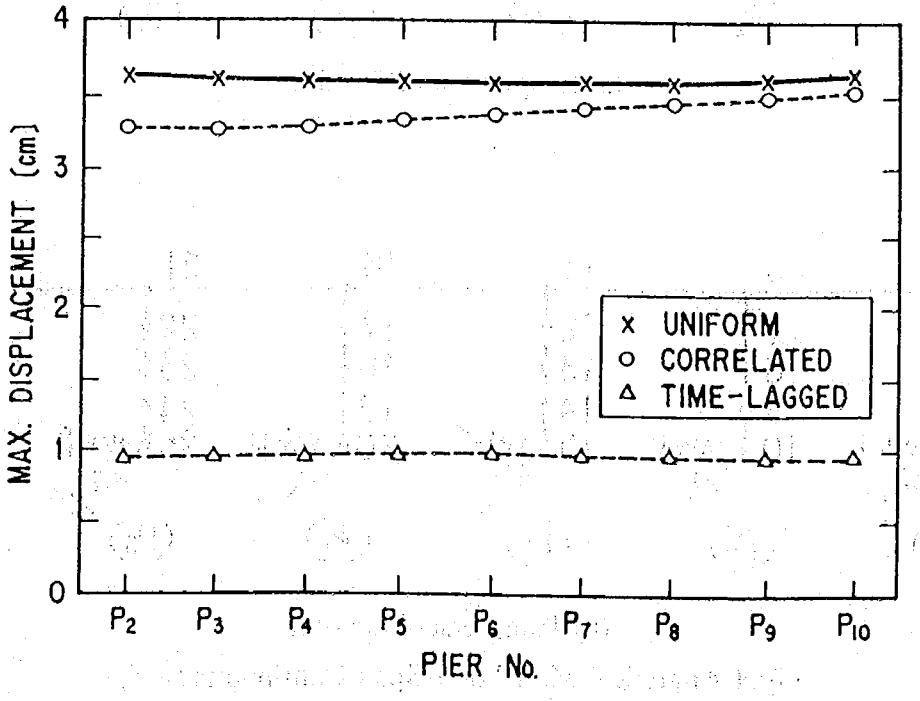


Fig.6 Maximum Displacement on Pier Top of 10-Span Continuous Bridge in Longitudinal Direction

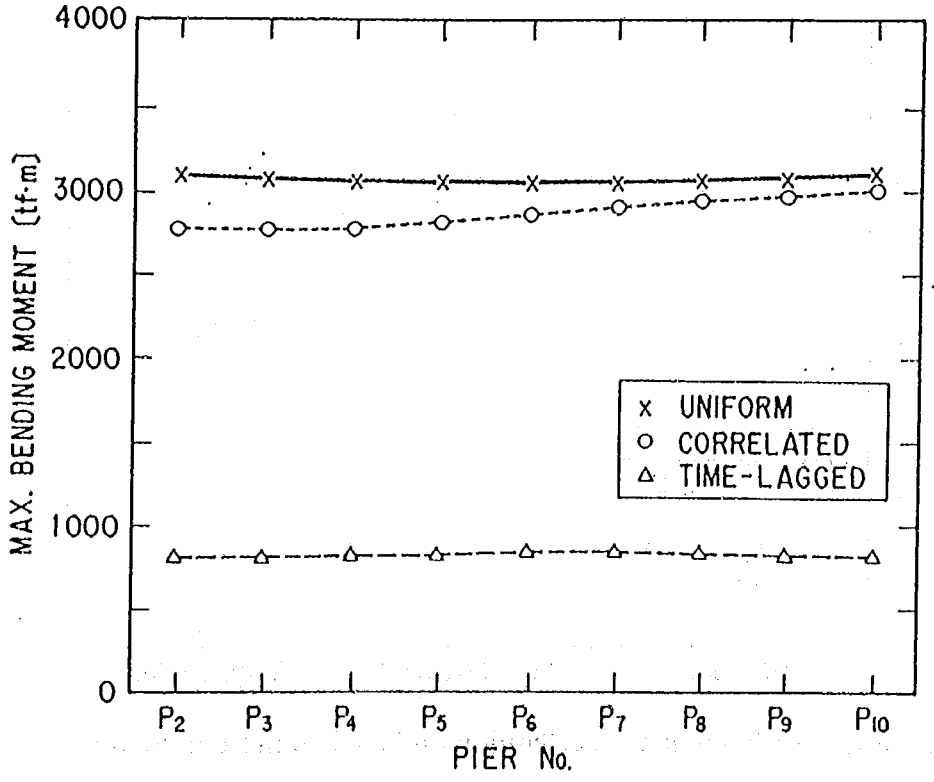


Fig.7 Maximum Bending Moment at Pier Base of 10-Span Continuous Bridge in Longitudinal Direction

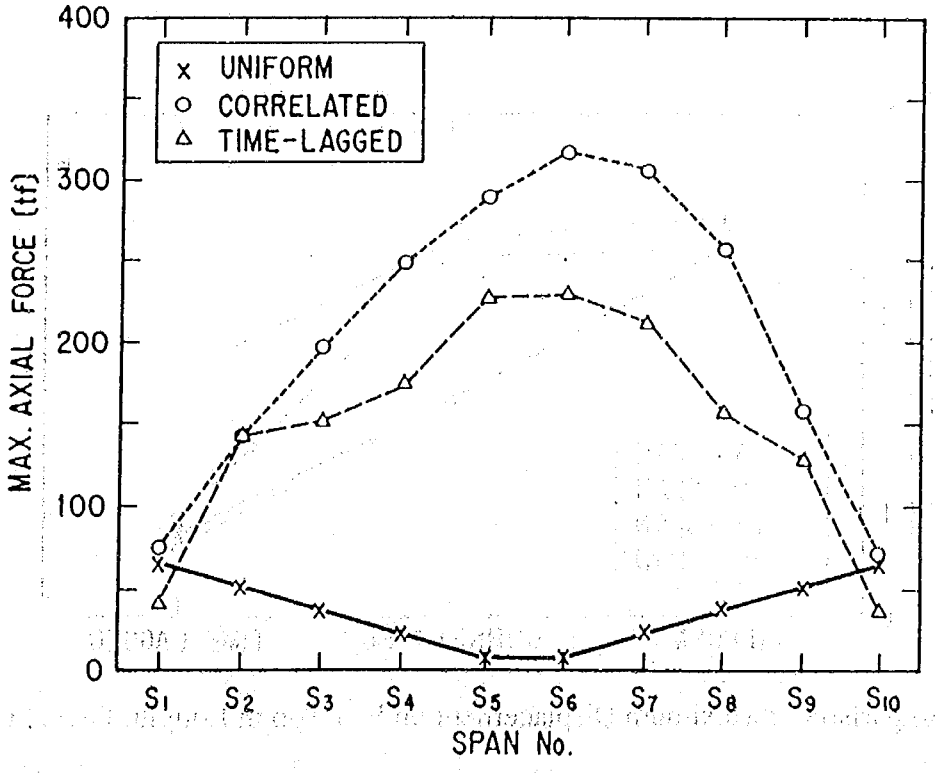


Fig.8 Maximum Axial Force of Superstructure of 10-Span Continuous Bridge in Longitudinal Direction

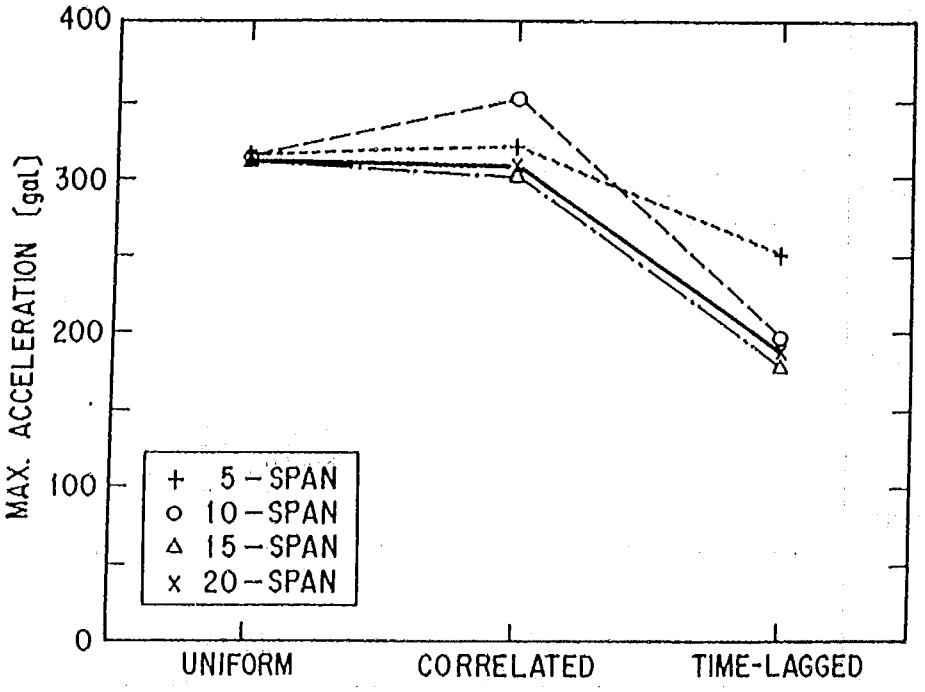


Fig.9 Comparison of Maximum Acceleration on Pier Top in Longitudinal Direction

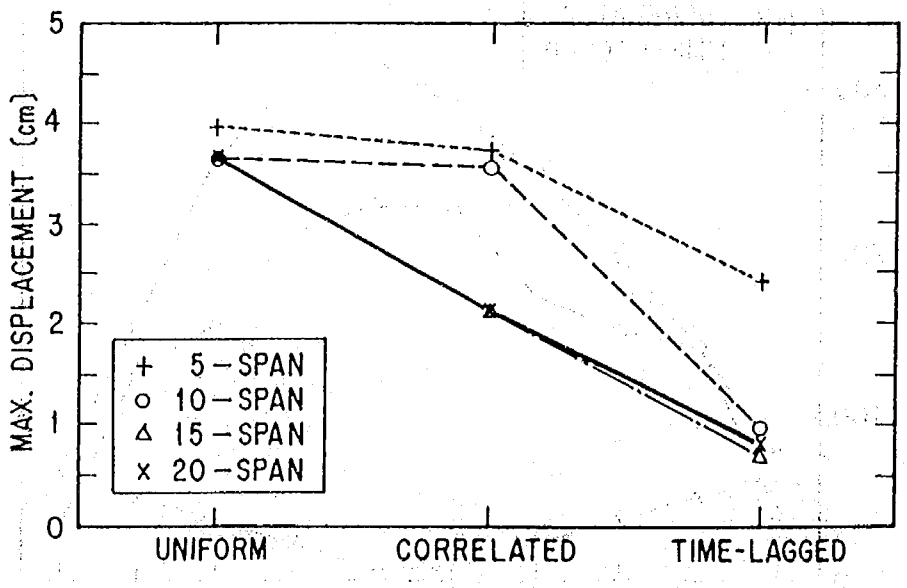


Fig.10 Comparison of Maximum Displacement on Pier Top in Longitudinal Direction

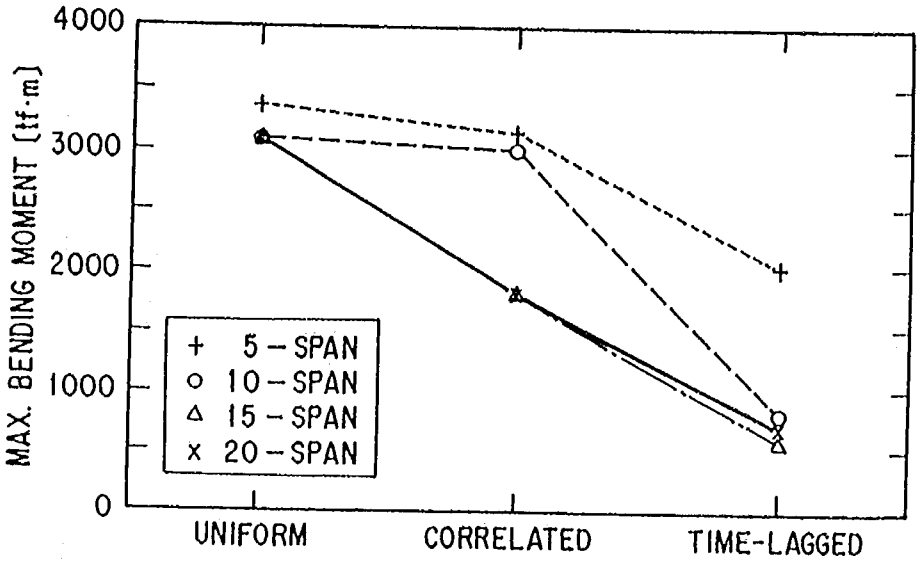


Fig.11 Comparison of Maximum Bending Moment at Pier Base in Longitudinal Direction

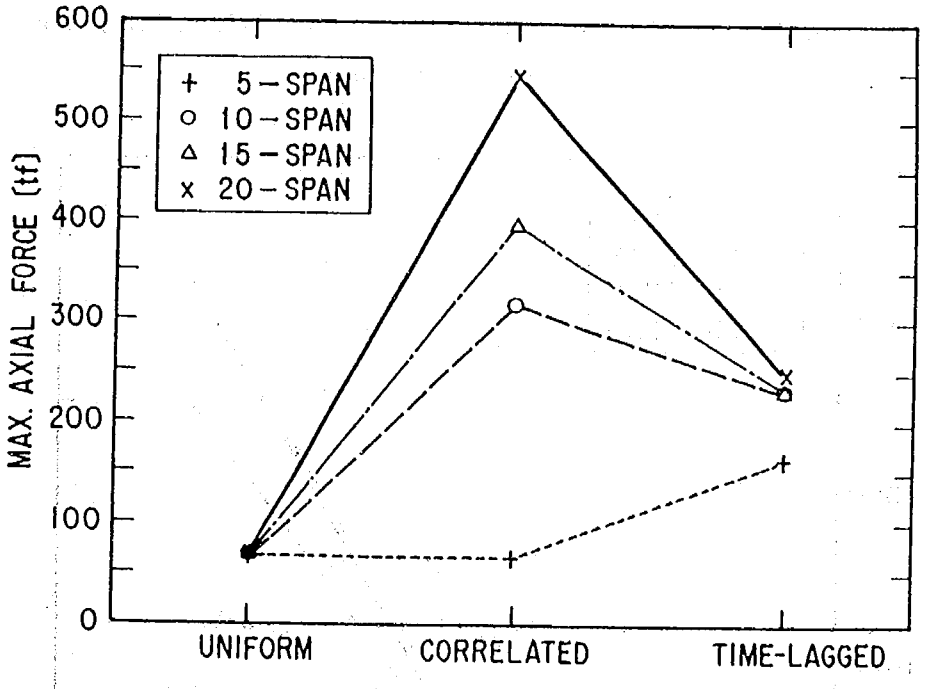


Fig.12 Comparison of Maximum Axial Force of Superstructure in Longitudinal Direction

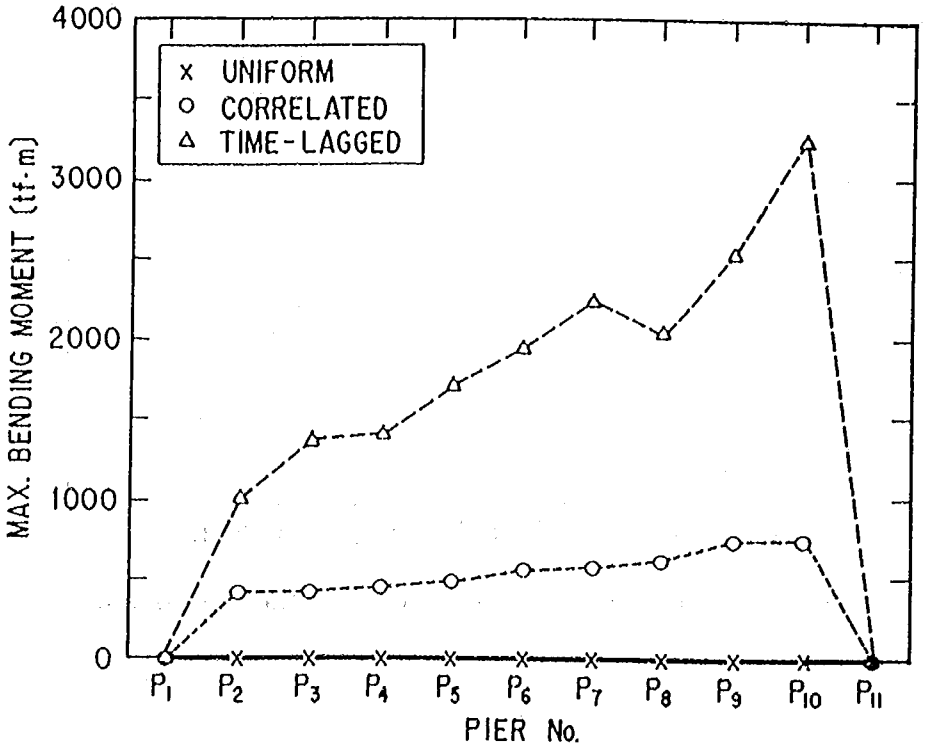


Fig.13 Maximum Bending Moment of Superstructure of 10-Span Continuous Bridge in Transverse Direction

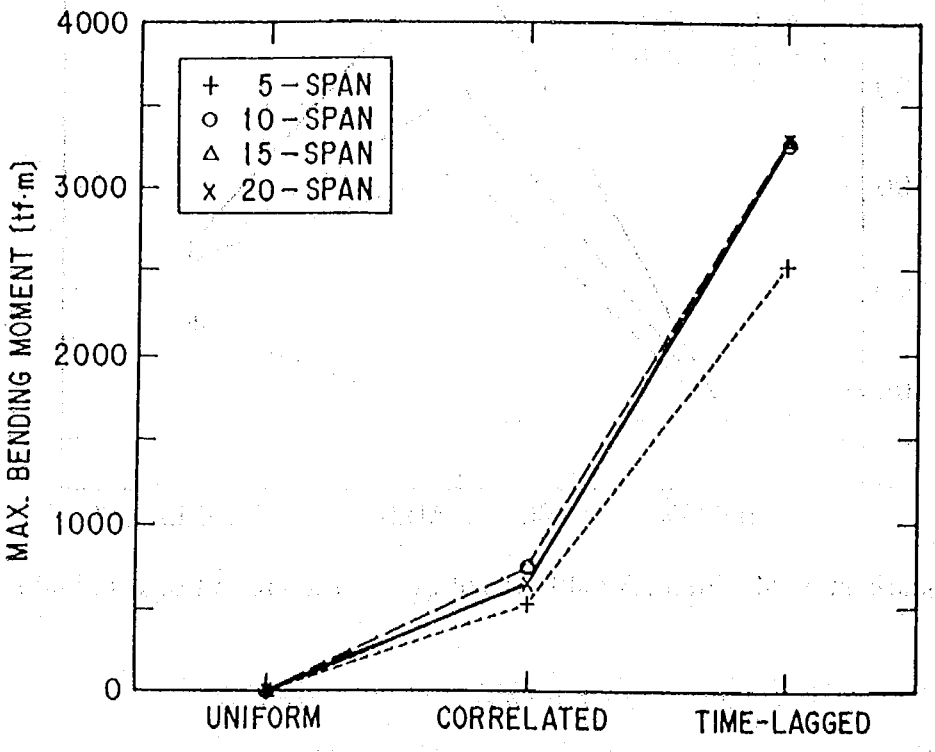


Fig.14 Comparison of Maximum Bending Moment of Superstructure in Transverse Direction

RECENT DEVELOPMENTS IN SEISMIC ISOLATION AT CALTRANS

Mark Yashinsky

California Department of Transportation
Office of Earthquake Engineering
P. O. Box 942874
Sacramento, CA 94274-0001

ABSTRACT

The California Department of Transportation (Caltrans) was the first U. S. Agency to use seismic isolation on a bridge at the Sierra Point Overcrossing in 1985. However, Caltrans' usual policy has been to protect bridges from seismic forces by using ductility rather than isolation. Events since the Loma Prieta Earthquake have increased Caltrans' involvement with seismic isolation. This paper relates what's new in seismic isolation at Caltrans.

INTRODUCTION

Caltrans has now completed a review of its large bridge inventory for seismic vulnerability. The process of designing and building seismic retrofits for those bridges considered most vulnerable has begun. Several of these retrofits include the use of seismic isolation devices.

New seismic performance criteria have been developed with input from the Seismic Advisory Board headed by George Housner. The new criteria requires minimal damage on important bridges for smaller earthquakes with more frequent return periods. This could result in Caltrans using more seismic control devices in the future.

Caltrans has written a performance specification that will allow different types of seismic isolation and energy dissipating devices to bid on the same job.

1992 has been a year of intense seismic activity for California. Currently, three Caltrans' bridges have been retrofit with seismic isolation. One of these bridges, the Eel River Bridge in Humboldt County, experienced a large earthquake this year.

Caltrans has recently created the Office of Earthquake Engineering to develop policy and procedures related to bridges and earthquakes. Among the many subjects being studied are tools and procedures for analyzing bridges that have isolation devices. Two of these studies are presented in this paper.

Caltrans current policy regarding seismic isolation and control is one of caution with an attempt to better understand its uses and limits. The activities described in the following pages shows how Caltrans is attempting to learn about the behavior of seismic devices for bridges.

CALTRANS' NEW BRIDGE RETROFITS USING SEISMIC ISOLATION

Route 280/101 Interchange (Alemany Interchange) Bridge #34-70 P.M. 1.8 in S.F.

The Alemany Interchange is a double deck connector in San Francisco. The retrofit contract for this bridge was awarded to Parsons Brinkerhoff Quade and Douglas, Inc. with Super Computer Solutions doing a nonlinear analysis of the existing bridge and the retrofitted structure.

This is the first use by Caltrans of seismic isolation for a retrofit of a reinforced concrete box girder bridge. Moreover, this unique retrofit uses seismic isolation only at 2 sensitive portions of the bridge.

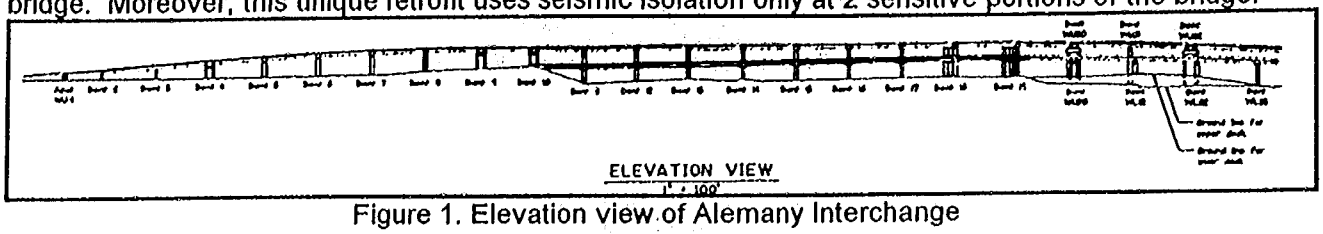


Figure 1. Elevation view of Alemany Interchange

At the south end of the bridge, the lower deck is at grade and, at the north end, both decks are fairly high (see figure 1). Therefore, Bents 2 and 3 have shorter, stiffer columns that could not be made to handle the large displacements. Moreover, the existing Abutment had a small seat. To protect Bents 1 and 2 and to handle the large displacements, the existing columns at Bents 2 and 3 were cut at the soffit and drop bent caps were built under the superstructure to support the bridge. Seismic isolation bearings connect the superstructure to the new bent cap, providing stiffness for service loads and the required displacement for the maximum credible earthquake (see figure 2). At the abutment, an additional support with seismic isolation is provided in case the superstructure should become unseated (see figure 3). The lateral force of the superstructure is still resisted at the existing abutment and at Bent 4, but now the large displacements will not create damaging shear forces at Bents 2 and 3 or drop the superstructure.

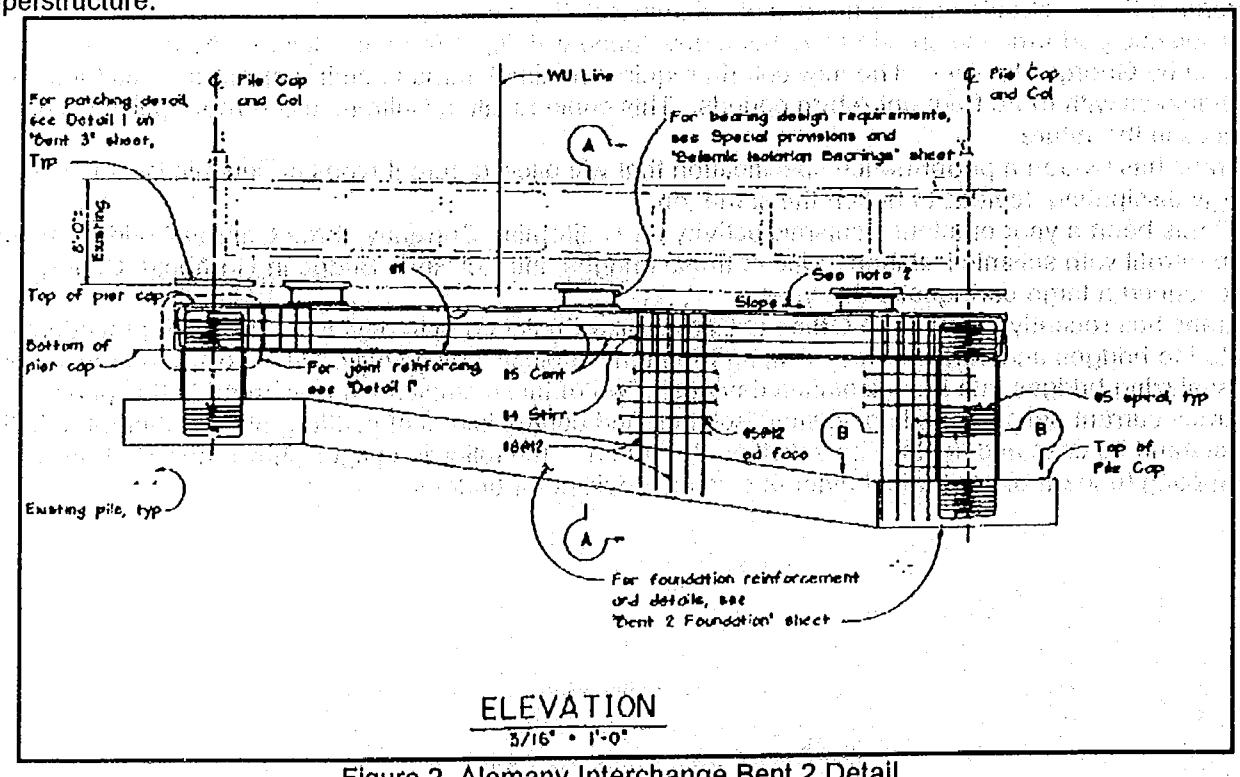


Figure 2. Alemany Interchange Bent 2 Detail.

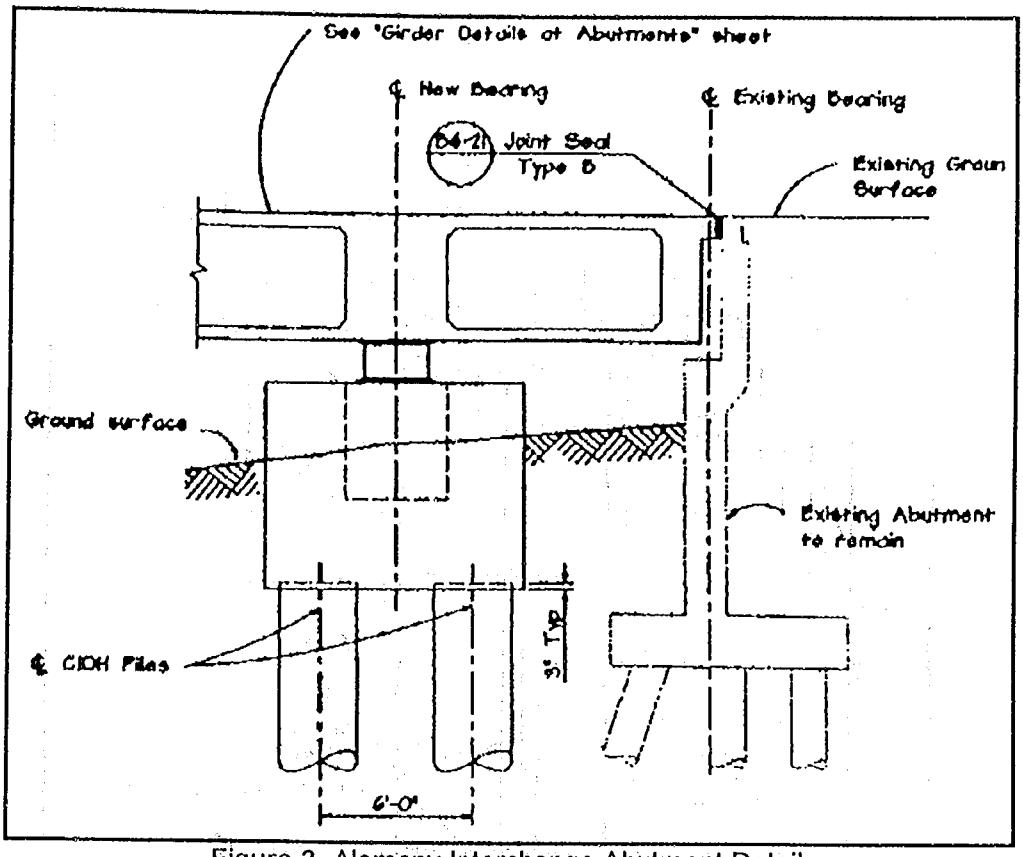


Figure 3. Alemany Interchange Abutment Detail.

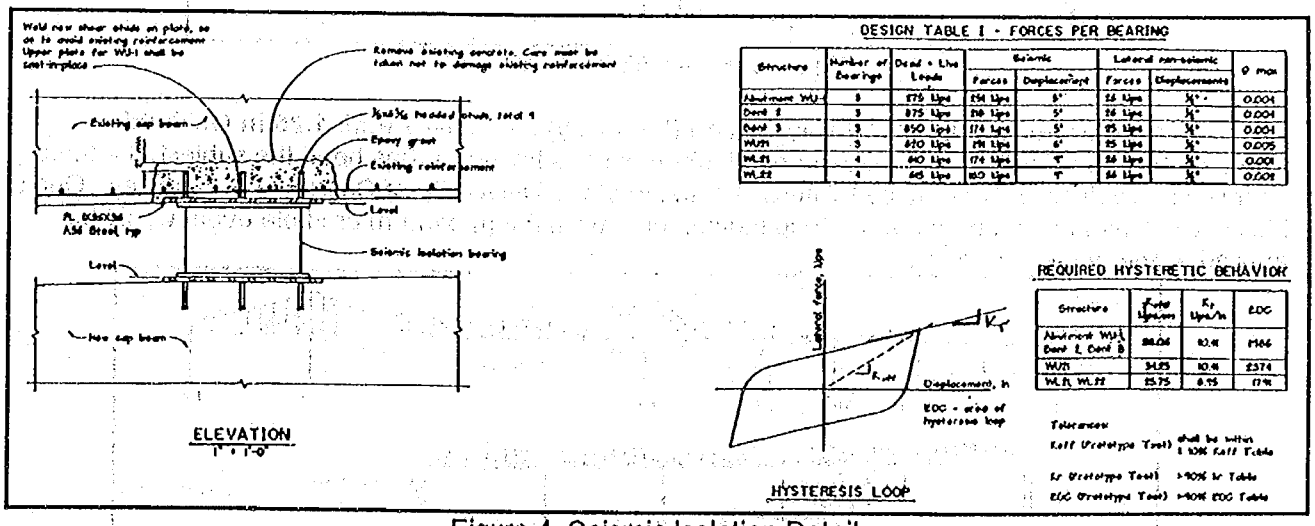


Figure 4. Seismic Isolation Detail

Figure 4 shows seismic isolation details for this project as well as the required effective stiffness, post-yield stiffness, design displacement, and energy dissipation capacity of these devices.

The north end of the bridge requires isolation for a different reason. The existing columns are large and have an enormous plastic moment that could not be resisted by the bent cap, the superstructure, or the footing. The seismic isolation acts as a load limiting device to protect these members from the large moments the column could generate (see figure 5) . These isolators were sized to match the displacement of the other columns in the frame.

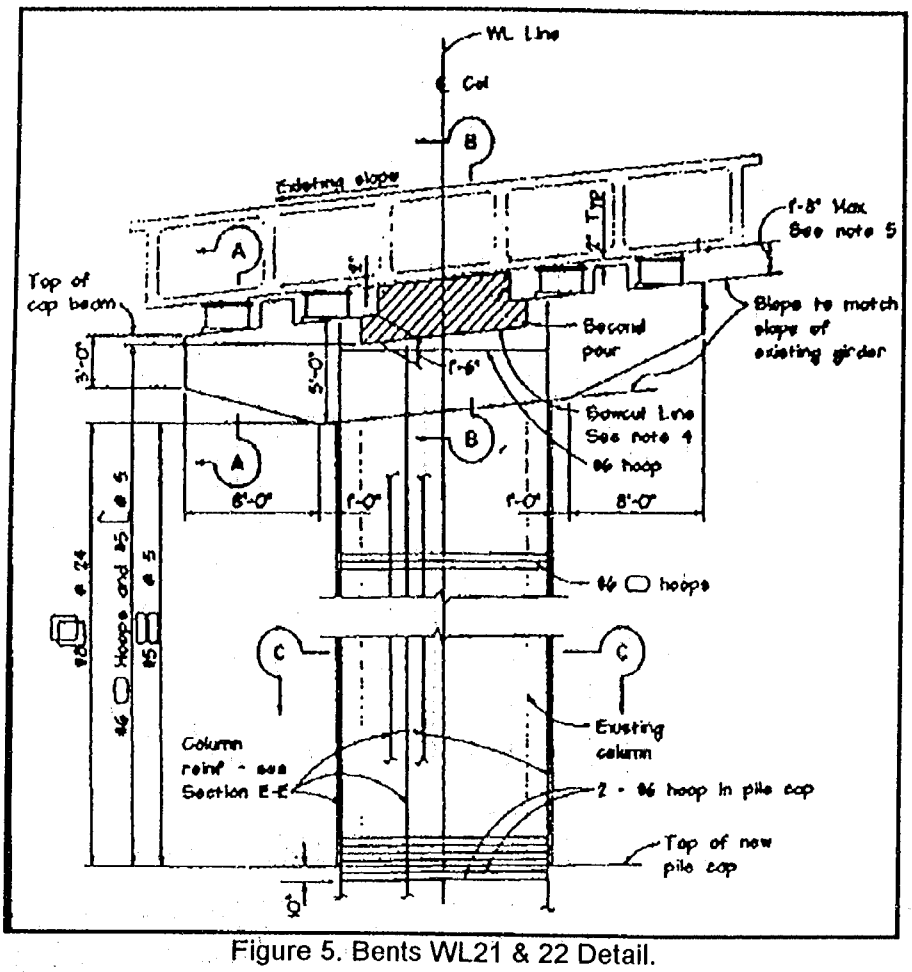


Figure 5. Bents WL21 & 22 Detail.

San Francisco-Oakland Bay Bridge (East Bay) Br. #33-25 P.M. 1.25 in Oakland

The East Bay Crossing is a two mile double deck steel truss bridge. It has been the subject of a three year seismic vulnerability study by Professor Astaneh of the University of California at Berkeley. One of his conclusions was that much of the longitudinal force from the maximum credible event would be applied at Pier 9 (see figure 6).

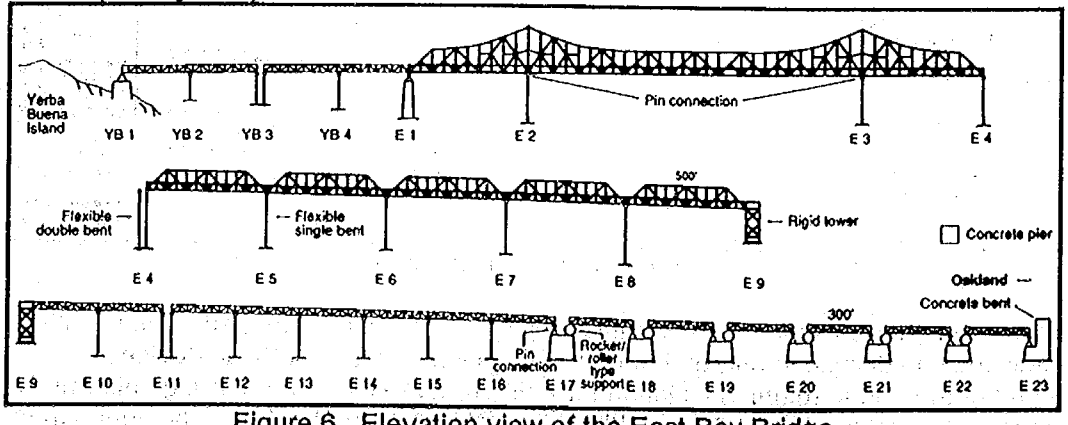


Figure 6. Elevation view of the East Bay Bridge

Any attempt to strengthen Pier 9 to handle this force would result in 0.6g to 0.7g of force at that location. To reduce this force level, Professor Astaneh is recommending the use of Semi-rigid Devices (see figures 7 & 8).

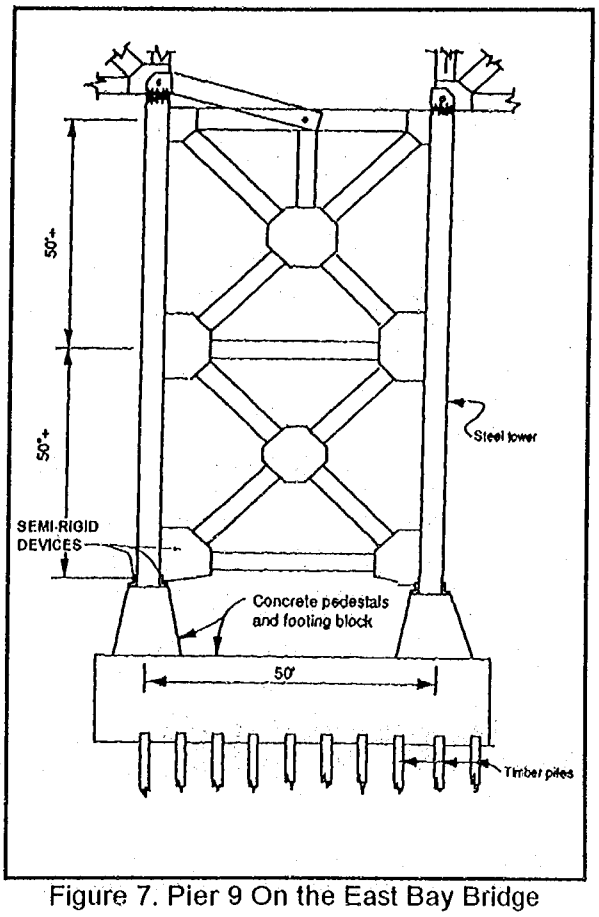


Figure 7. Pier 9 On the East Bay Bridge

These devices would be carefully designed angles connecting the pier legs to the concrete pedestals. If the pier develops an overturning moment during the earthquake, the angles on the compression legs would act rigidly while the devices on the tension legs would have an initial stiffness equal to the flexural stiffness of the bottom legs. If overturning continues, the stiffness would degrade as plastic hinges form in the angles. This perfectly plastic behavior would continue until the angle deforms from a bending device into a tension device. Then a final stiffness change would occur equal to the angles tensile stiffness (see figure 8).

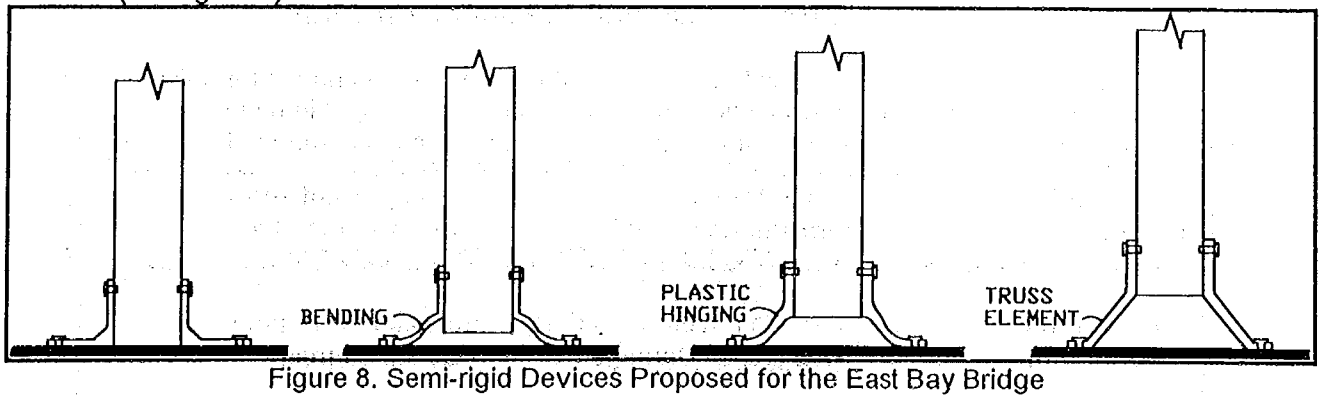


Figure 8. Semi-rigid Devices Proposed for the East Bay Bridge

These devices would reduce the forces at Pier 9 to below 0.4g by lengthening the fundamental period for the pier. Figure 9 shows the force-displacement diagram for the semi-rigid devices at Pier 9.

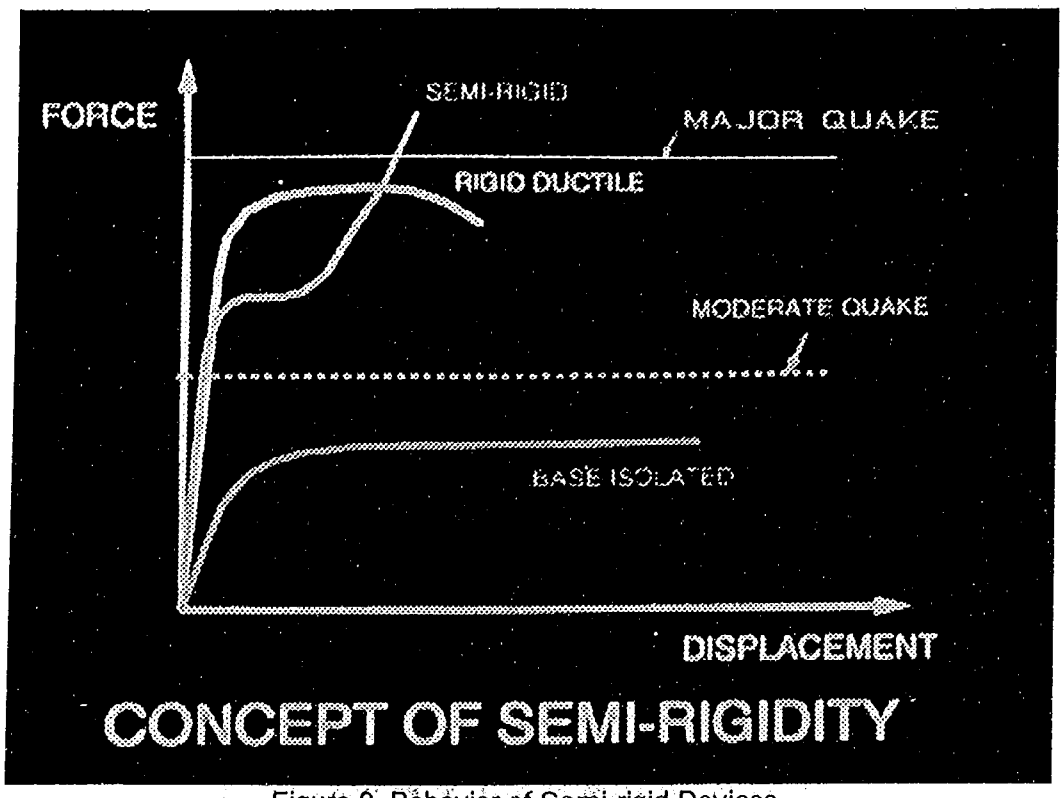


Figure 9. Behavior of Semi-rigid Devices.

One can see the effectiveness of these devices in absorbing energy, in reducing the amount of displacement required, and in providing a final stiffness to protect the structure.

Route 680/24 Interchange Br. #28-312K P.M. 9.13 Walnut Creek (Contra Costa)

This bridge was the subject of Eric Thorkildsen's presentation at last year's First US-Japan Workshop on Earthquake Protective Systems. Among its interesting features was the fact that the isolation system would first be used on a temporary structure before being reused on a final permanent portion of the interchange. This interchange is a five year project and, thus far, none of the isolated portions have been constructed. For more information see Eric's report from last year's workshop.

CALTRANS' NEW SEISMIC PERFORMANCE CRITERIA

In the past, Caltrans' design philosophy has been to prevent the collapse of bridges for seismic loads. This meant that considerable damage would be accepted as long as it resulted in no loss of life. Recently, more elaborate criteria has been developed. These criteria are summarized in figure 10.

Ground Motion at Site	Minimum Performance Level	Important Bridge Performance Level
Functional Evaluation	Service Level-Immediate 'Repairable' Damage	Service Level-Immediate 'Minimal' Damage
Safety Evaluation	Service Level-Limited 'Significant' Damage	Service Level-Immediate 'Repairable' Damage

Figure 10. New Performance Criteria

The new criteria requires that important bridges must be analyzed for two seismic events: A maximum credible time history, for which only immediately repairable damage may result; and a probabilistic response spectrum with a reasonable chance of occurring during the structure's life for which essentially no damage should result. The definitions of important structures and reasonable return periods still needs to be developed. However, this is a significant departure from Caltrans previous policy of no collapse. Moreover, the list of important bridges may include many bay and river crossings as well as some vital city interchanges. Substructure retrofits that maintain elastic behavior during large earthquakes may be too expensive or impossible at some locations. Therefore, more use of seismic isolation or even hybrid control systems may be a possible outcome of these criteria.
Since the minimum performance level for other bridges requires immediately repairable damage for the short return period event, isolation may be the only alternative. However, Caltrans' policy for these criteria has yet to be established.

CALTRANS' NEW PERFORMANCE SPECIFICATIONS FOR SEISMIC ISOLATION

Caltrans has a new performance specification for evaluating energy dissipating and isolating devices. This specification will allow any device that has been in use for over a year and that can meet the design requirements in the plans to be used by contractors on Caltrans' bridges. So far, Caltrans has included rubber-lead core devices and rubber energy dissipating devices in our specifications. We are working on including friction-pendulum devices in the near future. A unique feature of this specification is that it requires the units to be tested at a specific frequency as shown on the plans. This is to check the damping characteristics of the rubber devices which are frequency dependent.
The specifications require that all devices are to be wider than they are tall and 1.5 times wider than their maximum displacement. This is to maintain stability of the bearings.
Two full size specimens must be provided for testing. These tests include:

1) Twenty full cycles of the non-seismic forces.
2) Three full cycles of the seismic displacement at the increments 0.25, 0.5, 0.75, 1.0, & 1.1.
3) Ten full cycles of the seismic displacement.
4) Three full cycles at the seismic displacement times 1.25 and 1.5.

These tests will be considered successful if:

1) The load-displacement plots have a positive stiffness.
2) The change of stiffness after each three cycle increment for test 2 is under 10% of the average stiffness.
3) The effective stiffness of each test specimen will not change by over 15% for test 3.
4) The energy dissipated per cycle for test 3 shall be within 10% of that shown in the plans.
5) The tests must be performed at the period of vibration shown on the plans.
6) The specimens shall remain in good shape through all the tests.

Also each seismic isolation bearing must be proof tested in the presence of the engineer before installation. For a list of these tests and all other requirements of Caltrans' Performance Specification contact the Caltrans Specifications Unit.

PERFORMANCE OF THE EEL RIVER BRIDGE DURING THE CAPE MENDOCINO EARTHQUAKE

The State of California has been very seismically active in 1992. Four of the largest earthquakes in California's history occurred this year.

List of Major Earthquakes in California in 1992		
1) Joshua Tree	M_l = 6.1	April 22, 1992
2) Cape Mendocino	M_l = 6.4	April 25 & 26,1992
3) Landers	M_l = 7.4	June 28, 1992
4) Big Bear	M_l = 6.5	June 28, 1992

The Joshua Tree and Landers earthquakes represent a new fault system that is extending northward from the San Andreas. The San Andreas goes through a bend at this location. These earthquakes were due to the large forces locked up by the bend. Long surface ruptures and considerable movement

accompanied the Landers quake. Many moderate earthquakes have been continuing on this new fault. Whether the pressure in this area can be relieved by the new fault system or will inevitably be released as a large earthquake on the San Andreas affecting the Los Angeles area remains to be seen.
The Big Bear Earthquake occurred a few hours after the Landers event on a nearby fault. It resulted in many rock slides on the mountain roads in this area. Several smaller earthquakes have occurred at this previously unidentified fault during the Fall of 1992.
The Cape Mendocino Earthquakes were three events that occurred during two days in the Pacific off the coast of Cape Mendocino. All three events were very strong and caused considerable damage to the small towns in the area. These events caused some of the largest accelerations ever recorded during an earthquake.
None of these earthquakes resulted in any significant bridge damage. This was due to the remote location of all these earthquakes and to what we hope is the effectiveness of our seismic retrofit program. However, an isolated bridge did suffer minor damage from the Cape Mendocino Earthquakes. This is the Eel River Bridge (Bridge # 04-16R). This bridge was rebuilt several times due to damage from large floods (see figure 12).

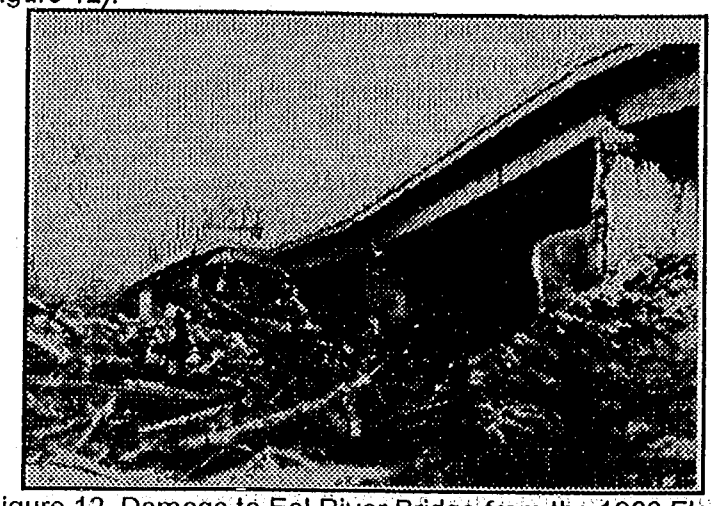


Figure 12. Damage to Eel River Bridge from the 1986 Flood



Figure 13. Original Eel River Bridge

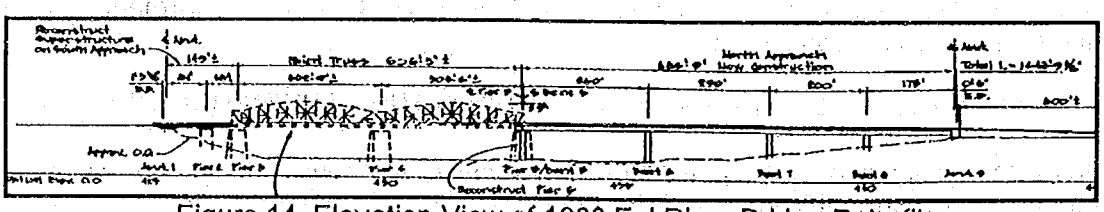


Figure 14. Elevation View of 1988 Eel River Bridge Retrofit

The Eel River Bridge is located in Humboldt County on Highway 101 at post mile R54.0. Its main spans are steel trusses with approach spans that were rebuilt after each flood (see figures 13 &14). Part of the 1988 retrofit was to raise the steel trusses to match a new 12 foot box girder approach span (see figure 14). Another part of the contract was to retrofit the existing bearings with seismic isolation bearings to protect the Piers from large seismic forces. The existing roller bearings were kept but locked with gusset plates and the isolation bearings placed below them (see figure 15). The existing expansion joints were retained at Piers 3 and 4. These were sliding plate joints with a movement of about three inches. A new

joint was placed at Pier 5 with a four inch movement. The isolation bearings were designed for a 12-inch maximum movement.

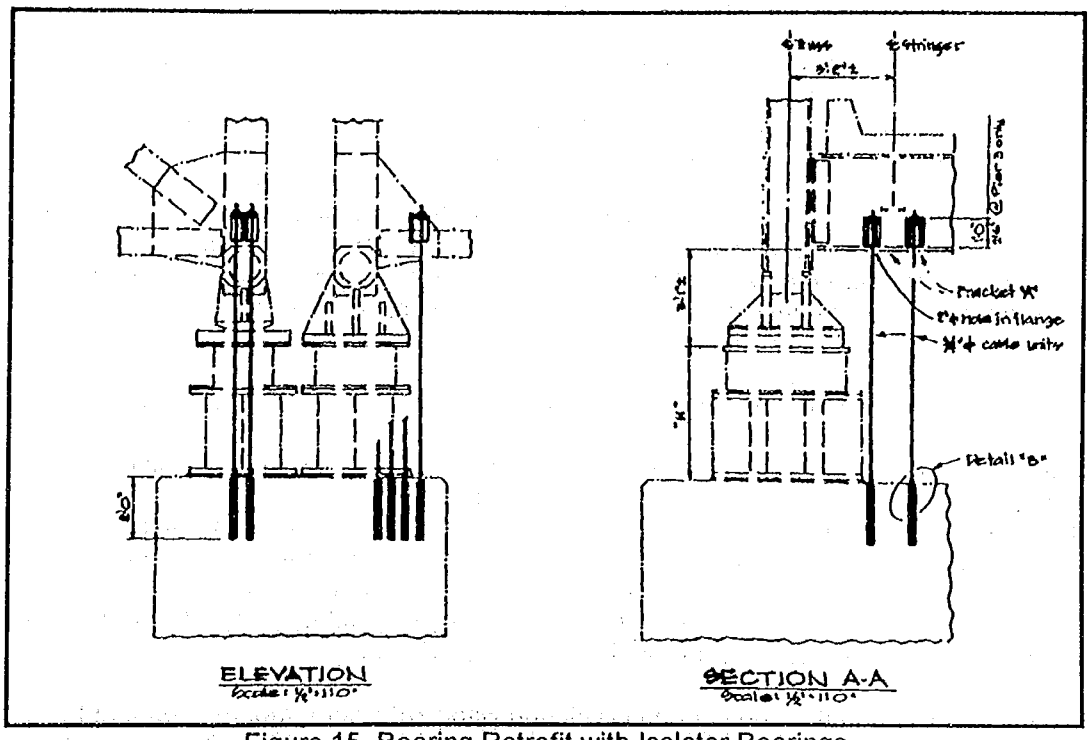


Figure 15. Bearing Retrofit with Isolator Bearings

The Eel River Bridge was about 20 miles from the epicenters of the Cape Mendocino Earthquakes. The Painter Street Bridge, one mile away, was fully instrumented. Accelerations on the ground measured 0.34g to the west and 0.43g to the north for the main shock.

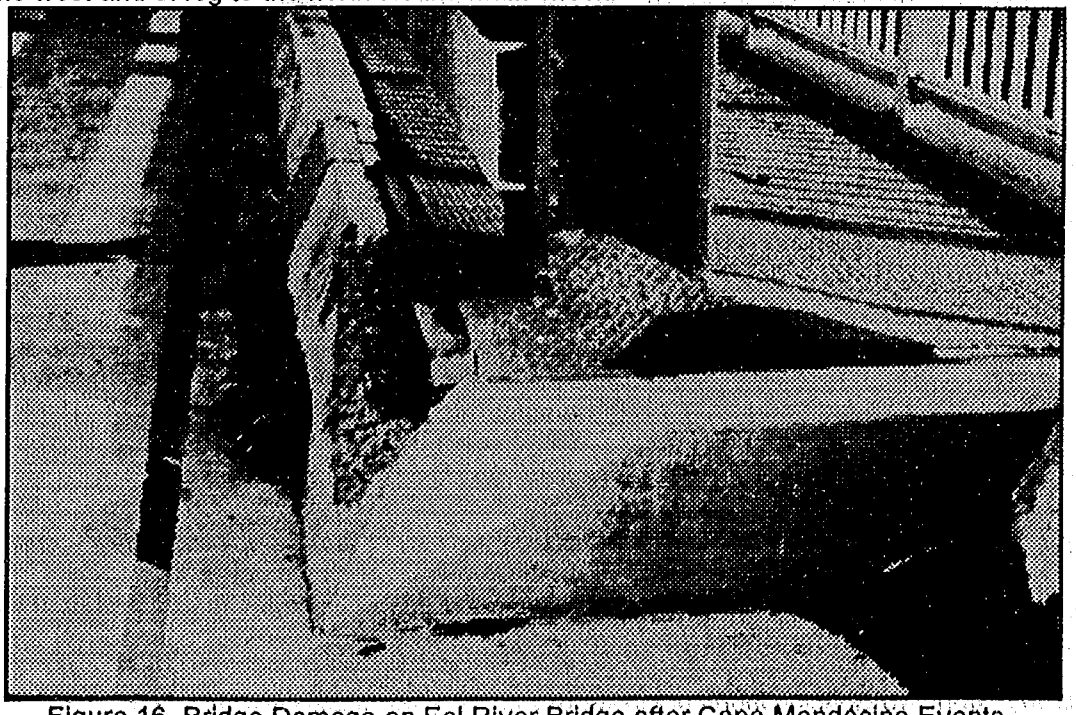


Figure 16. Bridge Damage on Eel River Bridge after Cape Mendocino Events

A steel diamond plate walkway that was attached to the truss spans banged against the concrete barrier attached to the approach spans, causing damage near Piers 3 & 5 (see figure 16). There was no damage near the expansion joint at Pier 4. A scrape mark on the east side of the expansion joint at Pier 3 showed the truss spans moved 9 inches during the main shock. The Post Earthquake Investigation Team (PEQIT) reported that the north abutment came to rest 3 inches to the south of its former location. The approach span settled about 1 inch at the north abutment and the abutment banged against a retaining wall. There was no damage to any of the Piers below the isolators. Bridge Maintenance estimated that damage to this bridge will cost about $15,000 to repair.

The isolated bridge carries northbound traffic on highway 101. A southbound structure is a cast-in-place continuous box girder bridge with well-confined ductile single column bents. During the Cape Mendocino Earthquakes there was damage to the shear blocks at the hinges of the southbound structure. Also there was some damage to the expansion joint at Pier 6 and to railing sleeves at both abutments. The total cost of repairs to this bridge was under $20,000.

CURRENT RESEARCH IN BASE ISOLATION AT CALTRANS

Among the many areas of research by the Office of Earthquake Engineering is a study of the AASHTO method of analyzing isolated bridges by Dr. Jenn-Shin Hwang and Li-Hong Sheng. This study has resulted in a new empirical method for calculating the period shift and damping ratio. Using these values, a new analysis procedure has been developed for calculating the maximum responses for any earthquake. The results of this analysis have been compared to an inelastic analysis with excellent results. A paper describing this method will be presented by the authors at the ATC-17-1 Seminar on Seismic Isolation on March 11, 1993, in San Francisco, California.

Also, the Office of Earthquake Engineering is working with Professor Graham Powell at the University of California at Berkeley to create nonlinear bridge elements for use in DRAIN3DX and ANSR. One of these elements is a generic expansion joint that includes subelements for simple bearing, a shear key, a gap-impact subelement, a cable restrainer, a back wall, a friction bearing, and an energy absorbing bearing (base isolation device). It is hoped that this generic element will allow us to capture the nonlinear behavior of bridges that use various passive control devices.

CONCLUSION

This paper briefly describes some of Caltrans' current work involving seismic isolation devices. It is the Department's belief that sharing our experiences with scientists and engineers will result in bridges that perform better during earthquakes. Jim Roberts, Chief of Caltrans' Structures Division has proposed spending 1% of Caltrans' annual construction budget (about $5,000,000) on bridge research. Caltran's encourages research proposals that will help in this task.

REFERENCES

1. Hwang J.S., Sheng L.H. *Equivalent Elastic Seismic Analysis of Base-Isolated Bridges with Lead-Rubber Bearings* Submitted to ATC-17-1 Seminar on Seismic Isolation, March 11, 1993

2. AASHTO, *Guide Specifications for Seismic Isolation Design* June 1991

3. *CSMIP Strong Motion Records From The Petrolia, California Earthquakes of April 25-26, 1992*

4. Thorkildsen E, *Caltrans Seismic Isolation Design and Future Concepts* First U.S.-Japan Conference on Protective Systems for Bridges September 1991

5. *Caltrans' Standard Specifications* (Proposed)

SEISMIC DESIGN OF THE TRANS-TOKYO BAY HIGHWAY BRIDGES

Y. Shioi[1], O. Yoshida[2], M. Homma[3]

Outline

The seismic design for the Trans Tokyo Bay Highway bridges is based on the Design standard for the Trans-Tokyo Bay Highway (draft) and on the Design Specifications for Highway Bridges (referred to as the "Design Specifications" hereafter). Based on a static design made by the seismic coefficient method, investigations were made using a seismic response analysis.

In the present report a summary of studies is presented both into the seismic response of the bridges and liquefaction.

Outline of ground conditions

As shown in Figure 1, for the bridge section of this project there is generally a mix of relatively good diluvial sand strata together with clayey layers at comparatively shallow depth below the sea bed. However, there are areas where soft waste-filled valley also exists. In consideration of the ground composition, the site has been divided into five sections as shown in the figure.

The base stratum considered to govern seismic design is the D5 layer having a shear wave velocity of over 400m/s. Since this is a deep layer 50–90m below the sea bed, the ground characteristic value To (natural period) will be long at about one second, and hence for seismic design the ground conditions have been classified as type III. Accordingly, the ground is classed as soft from the viewpoint of seismic design, and therefore needs to be handled with caution.

In addition, a layer of loose alluvial sand deposits prone to liquefaction exists in the offshore section close to the sea bed.

Outline of bridge structure

As shown in Figure 1 the bridge can be separated into an offshore section in water depths of 20–10m, and a shallow section with water depths 8–0m.

By employing a continuous multiple-span superstructure it was planned to improve ride quality, reduce maintenance costs, and improve seismic performance. For the offshore section, 3 and 10 span continuous steel box girders were used, and for the shallow section 11, 10 and 9 span continuous steel box girders with rubber bearings at intermediate supports. For the substructures, Y-form steel supports with steel tubular piles were used for the offshore section, and Y-form reinforced concrete supports on steel tubular sheet piles for the shallow section.

Figure 2 shows a standard section of superstructure.

---

1): General Manager of Design Department, Trans-Tokyo Bay Highway Corporation
2): Manager of Bridge Design Division
3): Chief of Bridge Design Division

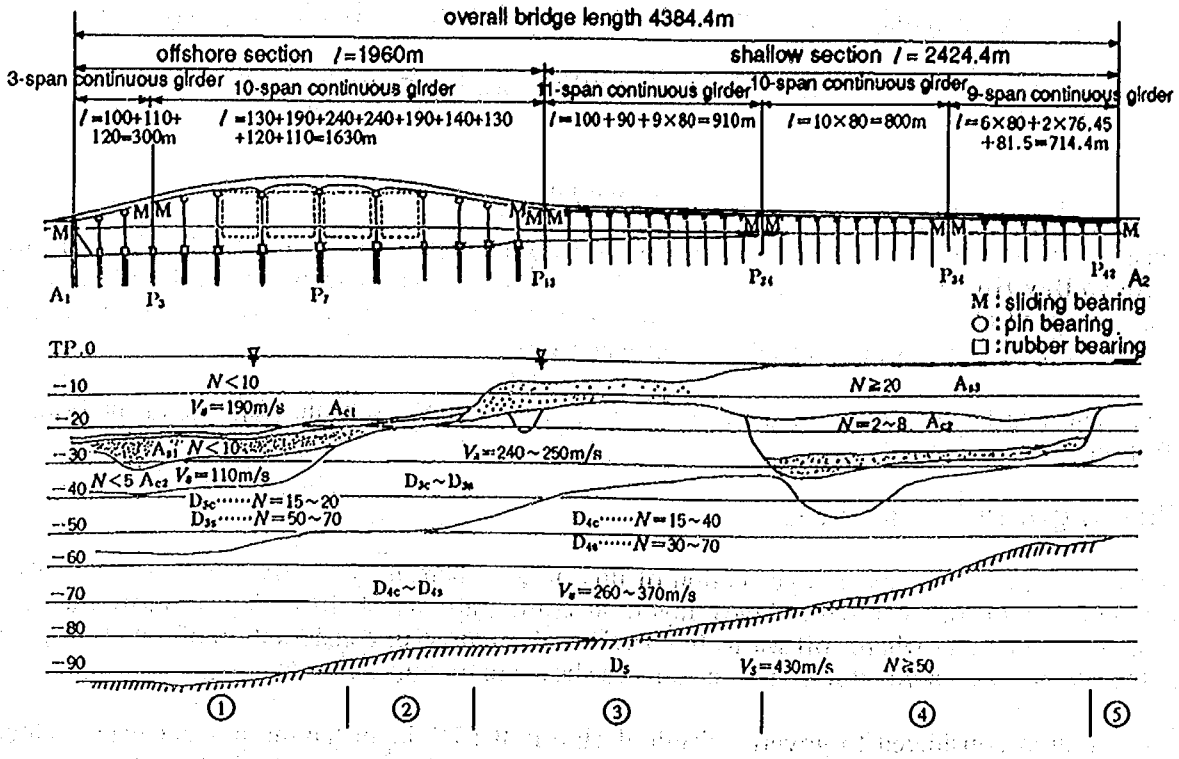


Figure 1 Ground conditions of vertical section and outline of bridges

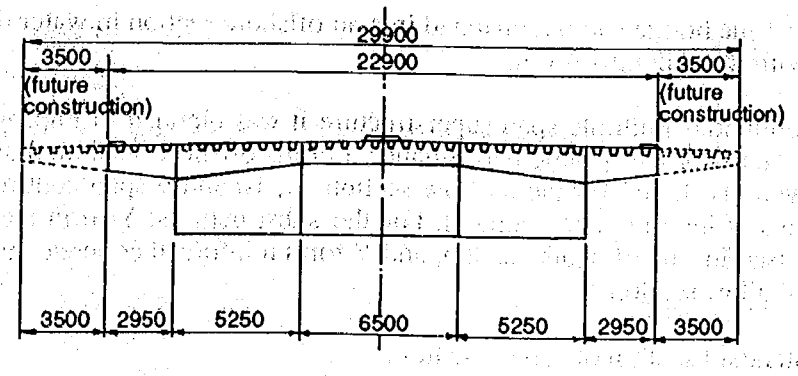


Figure 2 Standard section of superstructure

Design conditions

Design seismic coefficient

The seismic coefficient for static design was evaluated in accordance with the Design Specifications. The results are given in Table 1.

Here,

ground type correction coefficient	$Cg = 1.2$
ground type classification	type III
ground characteristic value	$Tg = 0.7$ — 1.2 seconds
regional correction coefficient	$Cz = 1.0$
importance correction coefficient	$Cz = 1.0$
standard design seismic coefficient	$Kho = 0.2$

In addition, the natural period of 1.75 seconds for the shallow section in the bridge axis direction is a period reduced for safety. Whilst the design natural period for the rubber bearings was 2.0 seconds, in consideration of possible variations in the shear modulus, the period was reduced as shown in Figure 3.

Table 1 Design horizontal seismic coefficient

	eathquake direction	natural period (sec)	correction factor C_T	horizontal seismic coefficient kh
offshore	bridge axis	1.46	1.25	0.30
	perpendicular to bridge axis	1.59	1.20	0.29
shallows/tidal	bridge axis	1.75	1.13	0.27
	perpendicular to bridge axis	0.6 ~ 0.3	1.25	0.30

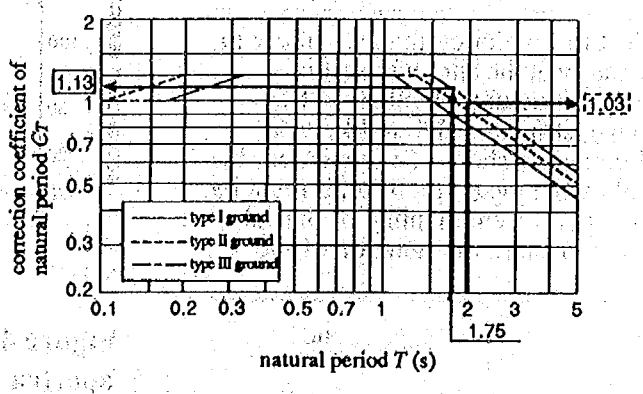


Figure 3 Correction coefficient of Natural period

Level of investigations

Two levels of seismic performance were studied in this investigation as shown in Table 2. The seismic force relevant to each target level was set, and the seismic performance investigated under these loads.

Input earthquake motions for the earthquake response analysis

The earthquake input motions used were formed in order to be appropriate for all the various structures in the Trans Tokyo Bay Highway. For the L-1 input motion the record obtained during the 1978 Miyagi-ken-Oki Earthquake on a rock bedding adjacent to Kaihoku Bridge located 100km from the epicenter is taken as the basis, with adjustments made to the amplitude to achieve agreement with the acceleration response spectrum shown in Figure 4. Figure 5 shows the acceleration wave form of L-1.

Input earthquake motion for L-2 is obtained by doubling the amplitude for the L-1 input.

The bedding plain for seismic design was taken as the D5 layer, and for analysis the interval of 15 seconds (Δt = 0.01 sec.) of main motion was used.

Ground constant

The ground constant was determined from the "Trans Tokyo Bay Highway bridge section ground investigation report, parts 1 and 2". As an example, the ground constants for section ① are shown in Table 3.

Table 2 Investigation levels for seismic design

level	contents of investigation level
L - 1	The structure should not suffer damage likely to impair primary function when subject to earthquake motion likely to occur during its life span. In addition, the structure should be easily repairable following the earthquake so that the full function before the earthquake can be quickly recovered.
L - 2	When subject to a major earthquake likely to occur only rarely at the site, whilst it is acceptable that structural members suffer heavy damage, structural failure likely to endanger human life should be prevented. In addition, following the earthquake, it must be possible by repair, strengthening, or partial replacement, to restore the function of the structure.

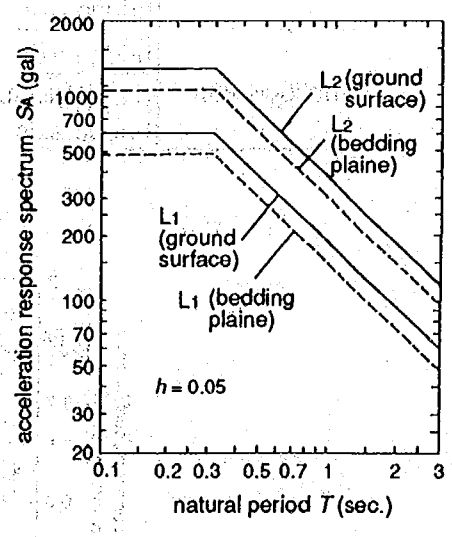


Figure 4 Acceleration response spectra curve of L-1, L-2 input

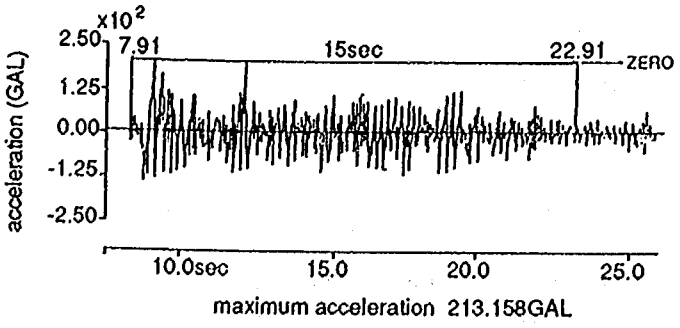


Figure 5 Acceleration wave form of L-1

Table 3 Ground parameters (ground section ①)

depth (TP–)	stratum name	stratum thickness	sub-division of stratum thickness	stratum number	unit density γt	shear wave velocity Vs	initial shear modulus G_0	damping constant (%)	Poisson's ratio ν
22.25									
23.45	AC1	1.20	1.20	1	1.65	100	1630	2	0.49
29.25	AS1	5.80	2.90 2.90	2 3	1.85	190	6810	2	0.49
40.25	AC2	11.0	2.20 2.20 2.20 2.20 2.20	4 5 6 7 8	1.56	110	1930	2	0.49
41.15	D3C	0.90	0.09	9	1.77	240	10400	2	0.49
42.85	D3S	1.70	1.70	10	1.93	250	12310	2	0.49
44.65	D3C	1.80	1.80	11	1.77	240	10400	2	0.49
55.55	D3S	10.9	5.45 5.45	12 13	1.93	250	12310	2	0.49
75.25	D4CU	19.7	4.93 4.93 4.93 4.93	14 15 16 17	1.69	260	11660	2	0.49
80.55	D4S	5.30	5.30	18	1.86	370	25980	2	0.48
89.75	D4CD	9.20	4.60 4.60	19 20	1.69	340	19940	2	0.47
94.05	D4S	4.30	4.30	21	1.86	370	25980	2	0.48
	D5			22	1.90	430	35850	2	0.46

Seismic response analysis

Remarks on the analysis method

(1) Offshore section

For the offshore section steel bell-type foundation with piles as shown in Figure 6 were used.

The conventional method for earthquake response analysis has been to use the lumped mass model (LMM). In this method caution is required in the determination of the spring and damping constants used to model the interaction between the foundation and ground. Results of recent research [1),2),3)] have shown that results of 2-dimensional FEM analysis give good agreement with strong earthquake motion records and experimental results from exciter tests.

The scale of the present bridge meant that it was not realistic to perform a 2-dimensional FEM analysis for the response of the whole system. For this reason an LMM model was used, but in order to achieve a better assessment of dynamic foundation-ground interaction, the spring and damping constants between the piles and ground used in the LMM analysis were investigated by comparison with the results of a 2-dimensional FEM analysis on a single pier model.

Figure 7 shows the analysis results of the LMM analysis with varying pile-ground damping constant and pile group efficiency, and the results of the FEM analysis. Figure 8 shows the both models used in the analysis.

From the results of the LMM analysis as shown in Figure 7 it is not possible to gain an adequate estimate of the dissipation damping between the piles and ground. For this reason it was necessary to set the damping constant at a level of about 3 times the SHAKE convergence value. Also, by setting the pile group efficiency at between 0.1-0.2, the peak frequency of the transfer function became nearly equal, and clarity was achieved by making the results of the LMM and FEM analyses agree in terms of the values of constants.

As a result of these studies, an analysis procedure as shown in Table 4 was adopted.

(2) Shallow section

The piers in the shallow section use steel tubular sheet pile foundations, as shown in Figure 9.

Using the same method as for the offshore section, an earthquake response analysis for the whole system was made using an LMM model.

To gain a reasonable assessment of the dynamic ground-foundation interaction, a frequency response analysis was made using an axially symmetric FEM analysis to evaluate the damping constant. The analysis model is shown in Figure 10, and an example of the damping constant frequency response in Figure 11.

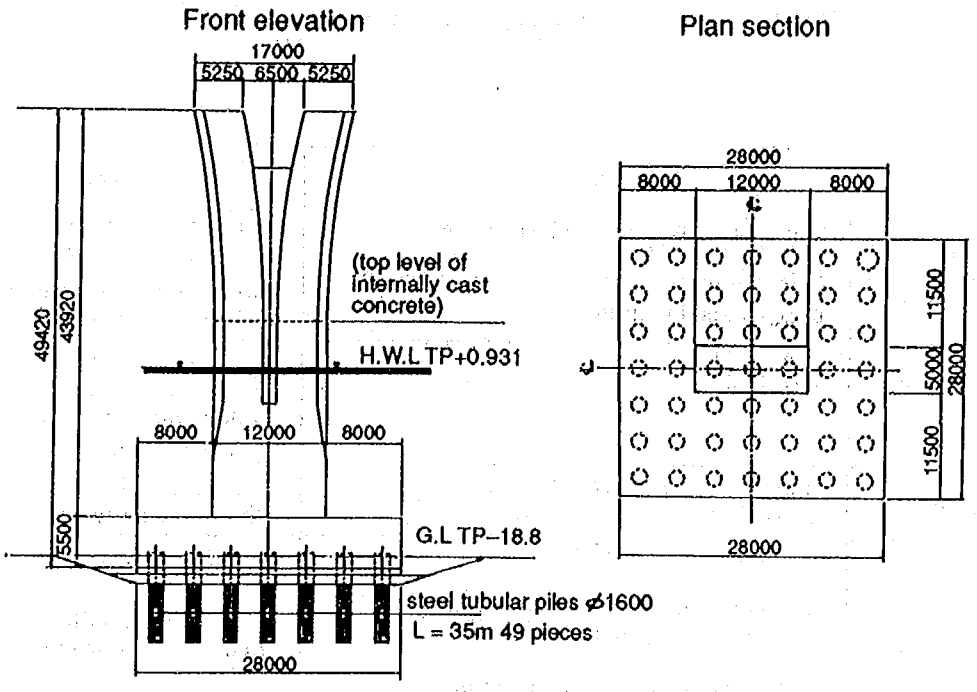
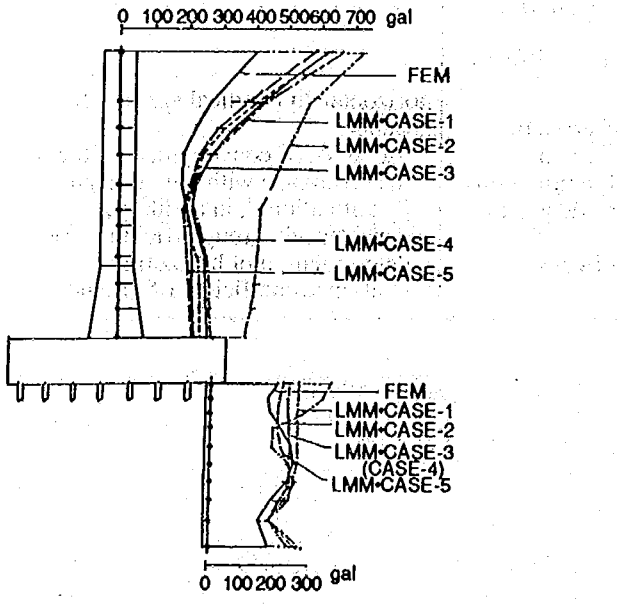


Figure 6 Steel bell type foundation (P_7)



case no. / parameter	1	2	3	4	5
pile group efficiency	0.2	1.0	0.2	0.16	0.16
damping constant	convergence	convergence	convergence x 2	convergence	convergence x 4

Figure 7 Results comparison of LMM and FEM analyses

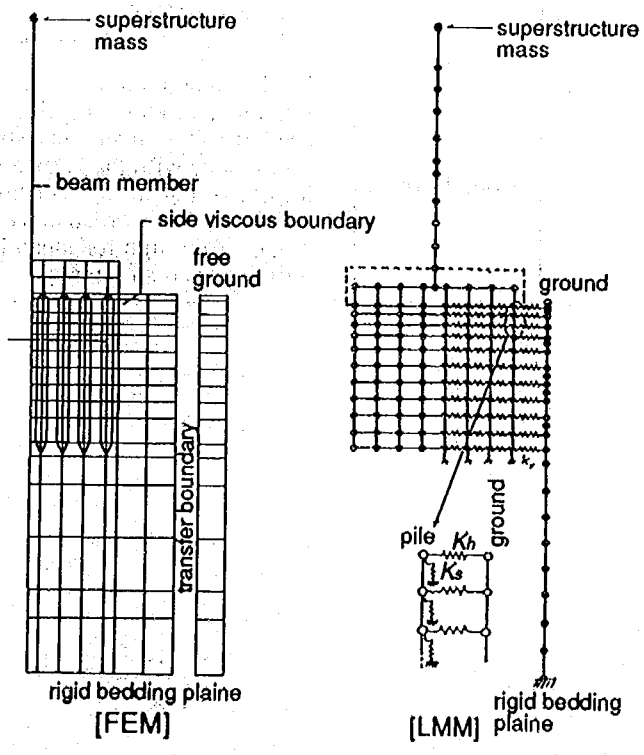


Figure 8 Analysis model

Table 4 Earthquake response analysis method

		single pier	whole system
analysis method		time history response anlysis using complex analysis	time history response analysis using modal analysis
direction of seismic force		bridge axis direction	bridge axis, perpendicular to bridge axis directions
input earthquake motion		L-1, L-2	use L-1 and L-2 as bedding plaine waves, find response of footing position using ground response analysis
damping constant		appraise as complex stiffness, refer to Table 5	modal damping proportional to strain energy
analysis model	substructure	beam and mass model superstructure mass weight borne by substructure applied to upper edge L-2 analysis: stiffness reduced in accordance with P-δ curve	beam and mass model L-2 analysis: stiffness reduced in accordance with P-δ curve
	ground	shear beam model beam cross-sectional area: in order to avoid the influence from piles take $A = 10^7 m^2$ stiffness: use SHAKE convergence stiffness	
	ground - piles	piles: beam and mass horizontal and vertical springs of ground: use SHAKE convergence stiffness in accordance with the "Design Specifications"; for horizontal springs consider pile group efficiency in accordance with "Standard design for Japan Railways buildings and structures"	horizontal and vertical springs of ground: use SHAKE convergence stiffness in accordance with the "Design Specifications", in addition, consider pile group efficiency for determination of horizontal resistance coefficient of ground

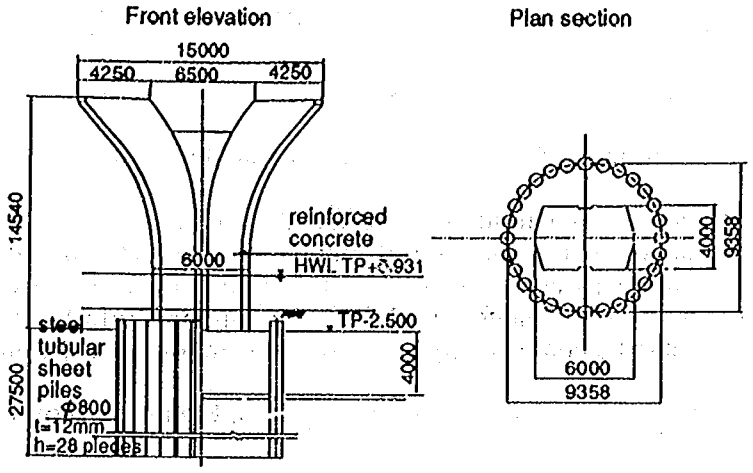


Figure 9 Steel tubular sheet pile foundation (P_{30})

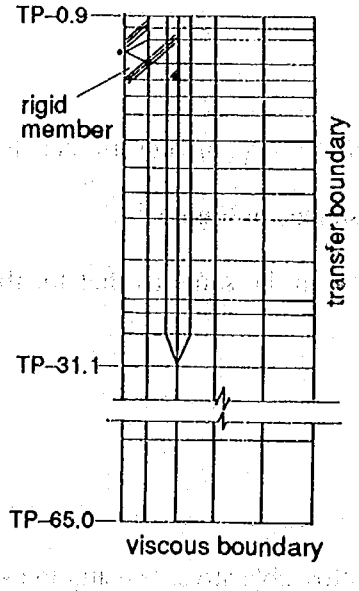


Figure 10 Axially symmetric FEM analysis model

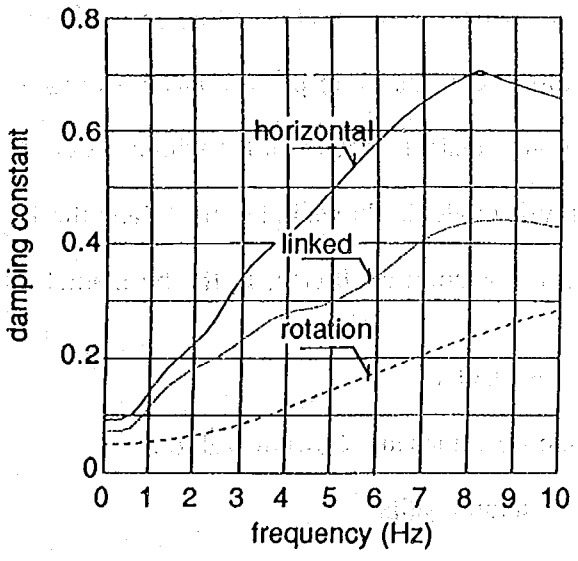


Figure 11 Dependence of damping constant on frequency

Results of earthquake response analysis for offshore section.

(1) Results of earthquake response analysis of single pier

The results of the earthquake response analysis of pier P_7 as a single pier shown below.

Regarding the ground reaction coefficient in the horizontal direction, as a result of the liquefaction investigations described later leading to the adoption of ground improvement by sand compaction (termed SCP hereafter), no liquefaction was assumed to occur at L-1, and a coefficient taken as a conservative estimate of the actual ground value without consideration of improved effect. For L-2 liquefaction does occur, but this is assumed not to be complete liquefaction, and therefore a reduction of 1/3 was made.

The analysis model was an LMM model as shown in Figure 8. Figure 12 shows the 1st and 2nd mode shapes.

a. Analysis results

Table 6 shows the response values

b. Investigation results

In this single pier analysis the pile foundations were investigated. For L-1 the results are below the static design values. For L-2 stress levels exceed yield values for the material properties used in the static design, and therefore a change in materials is required. However, on determining the value of Broms's ultimate horizontal resistance with consideration of the strength of the dense sand at liquefaction after improvement [4], it was found that this resistance was greater than the dynamic response of shear force, and so no changes in material properties were made.

(2) Results of earthquake response analysis of whole system

The response analysis results for the whole system of 10 spans between P_3–P_{13} are described below.

The analysis model is shown in Figure 13 and the 1st and 2nd mode shapes in Figure 14.

The ground reaction coefficient in the horizontal direction was taken as the same as that for the single pier.

a. Analysis results

The response values are shown in Table 7.

b. Investigation results

- Pier columns: For L-1 the stresses in the pier columns are below allowable stresses using the steel section only. For L-2, if the concrete inside the columns is considered to act compositely with the steel, then stresses remain below yield values.
- Footings: For L-1, stresses in the footing section are below allowable values considering the steel section only. For L-2, if the footing concrete is considered as a reinforced concrete beam, then stresses in the steel remain below yield, and those in the concrete below 0.85 σck.

Table 6 Dynamic response values (single pier)

			L-1	L-2	static analysis (seismic coefficient method)
natural period (Hz)	1st	pier top edge	0.537	0.448	for design 0.685 (T=1.459sec)
	2nd	ground, piles	0.749	0.658	
	3rd	ground, piles	1.575	1.383	
acceleration (gal)		pier top	215	263	design horizontal seismic coefficient kh=0.30
		middle of pier	347	436	
		footing	336	452	
		pile head	323	447	
		ground	183	300	
displacement (mm)		pier top	163	326	
		middle of pier	67	172	
		footing	65	174	
		pile head	64	172	
		ground	63	154	
moment (tf•m)		bottom of column	67650	86680	72980
		pile head (pile stress) kgf/cm^2	321 (1670)	735 (2653)	388 (1834)

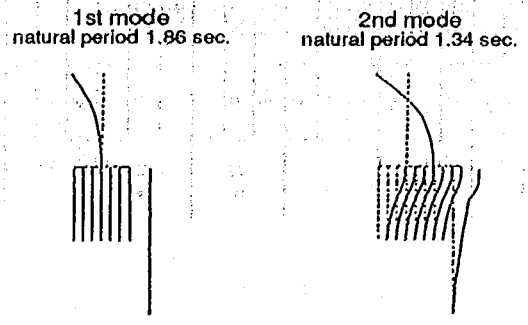


Figure 12 Mode diagram (single pier L-1)

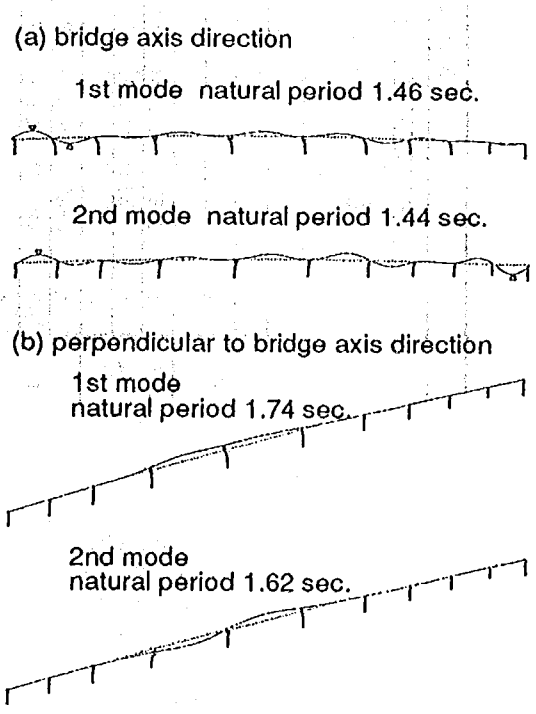


Figure 14 Mode diagram (offshore section whole system)

Figure 7 Comparison of results of LMM and FEM analyses

		bridge axis direction						perpendicular to bridge axis direction					
		bending moment (tf·m)			shear force (tf)			bending moment (tf·m)			shear force (tf)		
		static design value	dynamic response value		static design value	dynamic response value		static design value	dynamic response value		static design value	dynamic response value	
			L-1	L-2		L-1	L-2		L-1	L-2		L-1	L-2
P 3	a							32831	33742	63118	1647	1557	2594
	b							10166	13019	20442	651	817	1537
	c										372	686	1192
P 4	a	98871	97986	115827	3731	3166	4711	69477	80071	144949	2499	2729	4313
	b	46535	41362	49960	2228	2366	2754	33824	36920	68639	1494	1912	3472
	c				1890	2219	2708				1167	1826	3395
P 5	a	88203	74494	93875	3486	2565	3336	80129	84136	143851	2777	2325	4348
	b	42164	36619	47142	1764	1593	2148	41682	41581	67696	1544	1749	2991
	c				1422	1576	2017				1212	1600	2522
P 6	a	88494	78577	95163	3191	2534	3703	123243	100614	173998	3233	2425	3742
	b	42599	36511	48552	1832	1777	2049	71904	53539	97858	2297	1942	3203
	c				1488	1655	2183				1965	1715	3321
P 7	a	72980	69467	93049	2756	2383	4454	130677	99063	182134	3359	2246	4852
	b	38280	34066	53036	1599	1630	2117	72727	55623	105398	2558	2035	3773
	c				1257	1455	2311				2106	1893	2213
P 8	a	83900	73044	99458	3045	2842	4110	111563	68160	110166	3030	1743	3080
	b	46881	37919	48749	1673	1827	2435	71921	36621	65840	2294	1586	2338
	c				1650	1723	2223				1965	1309	2213
P 9	a	71069	59200	89850	2948	2837	3642	70617	57974	100501	2504	1849	3599
	b	39656	31068	48576	1670	1495	2291	42453	28480	53763	1574	1474	2523
	c				1326	1366	2087				1244	1226	2355
P 10	a	89366	76729	118072	3548	2692	4449	52509	40454	74760	2225	1674	3402
	b	50795	40266	55752	2393	2087	3387	29756	26303	40372	1322	1168	2133
	c				2070	2171	2995				1007	1179	2071
P 11	a	118538	112761	143557	4701	4221	4992	42612	44976	80701	1898	1784	3267
	b	68084	56625	67488	3641	3642	4708	25119	24534	37707	1298	151	2756
	c				3513	3803	4503				993	1353	2174
P 12	a							32313	36160	60675	1623	1440	2437
	b							19484	18900	30415	1178	1172	1927
	c										909	955	1619

Here, a : column bottom, b : top of internally cast concrete, c : bearing

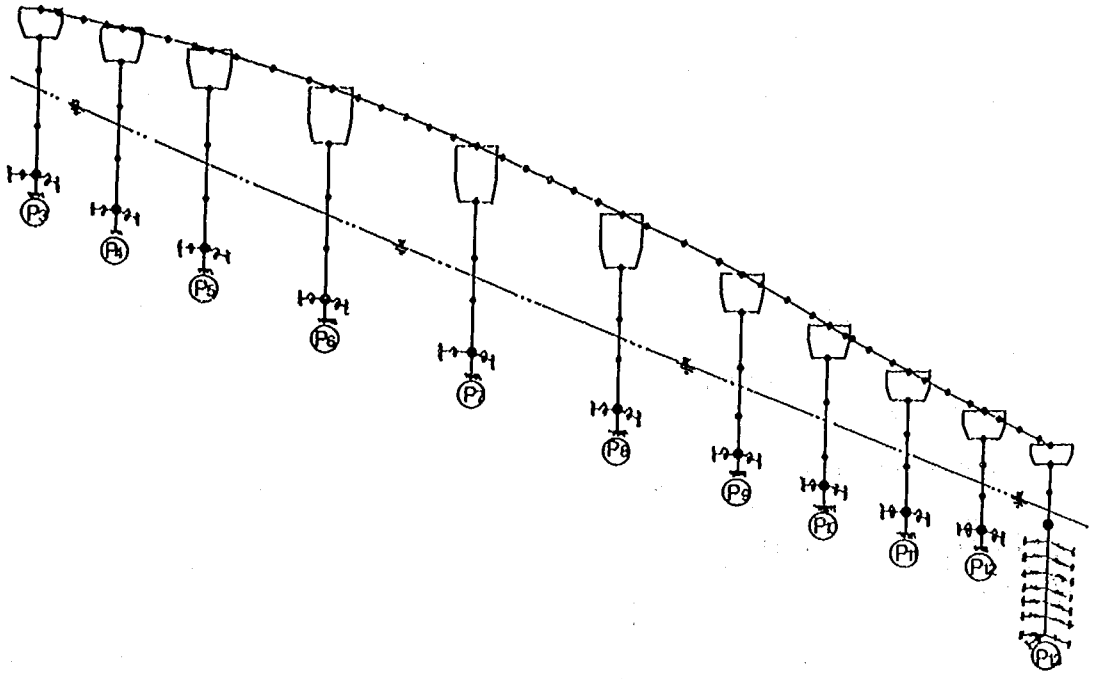


Figure 13 Analysis model for whole system (offshore section)

Results of earthquake response analysis for shallow section

The response analysis results of the 10 span continuous section between P_{24}–P_{34} are described below.

The analysis model type is the same as that of the offshore section. Figure 15 shows the models of the bearings and foundations. The bearings restraint conditions are shown in Table 8.

Figure 16 shows the shapes of the 1st and 2nd modes.

a. Analysis results

Table 9 shows the response values of sectional forces in the bottom of pier columns, and Table 10 response values for the bearings.

b. Investigation results

- Bearings: For L-1 the dynamic response of displacement and horizontal force are below the values from the static design. For L-2 the displacements are slightly larger than the static values. However, since there is ample distance between the end of the girder and edge of the bridge pier, there is no danger of a girder falling. In addition, the rubber bearings posses a large in-built deformation capacity which will not cause problems, and the stresses developed in the movement restraint devices are also for the most part below yield stress.

- Substructure: For L-1 the dynamic response of sectional forces are below those of the static analysis. For L-2, referring to the ultimate resistance assessment given in the "Design Specifications", for both the ultimate horizontal resistance and shear resistance, the response values were less than the resistance values.

- Foundations: (steel tubular sheet piles) At L-1 level the response of sectional forces are below those of the static design. For L-2, the response of sectional forces give the reaction forces of steel sheet piles below the allowable pile capacity, and the stresses in the steel sheet piles are below the yield value.

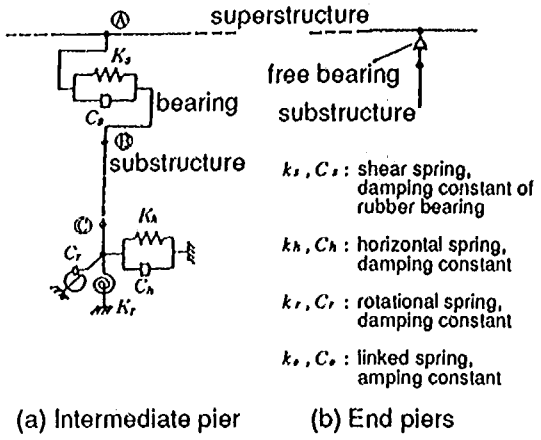


Figure 15 Models for bearings and foundations

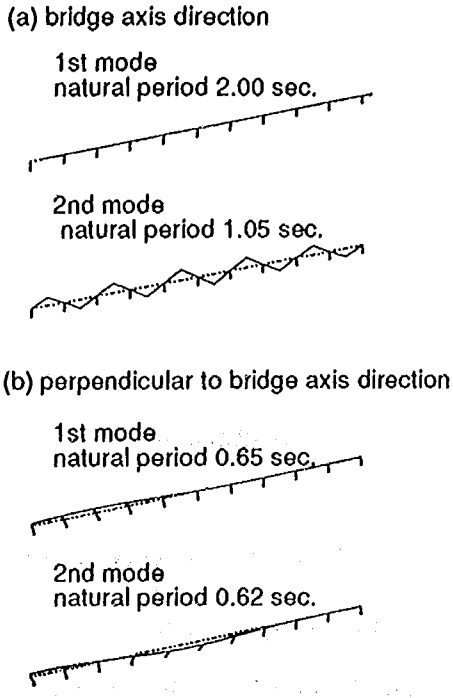


Figure 16 Mode diagram (shallows/tidal section whole system)

Table 8 Bearing resfraint conditions

	bridge axis direction	perpendicular to bridge axis direction	vertical axis direction	rotation around bridge axis	rotation around axis perpendicular to bridge axis	rotation around vertical axis
G	shear spring	fixed	fixed	fixed	fixed	rotational spring
M	free	fixed	fixed	fixed	free	free

note- G: rubber bearing M: free bearing

Table 9 Response value of sectional forces (column bottom)

	bridge axis direction						perpendicular to bridge axis direction					
	bending moment (tf·m)			shear force (tf)			bending moment (tf·m)			shear force (tf)		
	static design value	dynamic response value		static design value	dynamic response value		static design value	dynamic response value		static design value	dynamic response value	
		L-1	L-2		L-1	L-2		L-1	L-2		L-1	L-2
P 24	7021	5549	7651	602	473	658	11777	6162	14801	809	432	976
P 25	11466	6329	11103	863	477	761	14025	7856	16806	924	575	1196
P 26	10731	6269	10881	825	485	771	12250	7957	17447	835	579	1234
P 27	10536	6199	10726	821	476	767	12484	7501	16603	855	552	1181
P 28	10341	6218	10597	818	484	762	12161	7173	15972	845	542	1156
P 29	10148	6461	10504	814	507	764	11999	6899	15780	843	529	1169
P 30	9955	6416	10399	810	499	756	11760	6637	15235	837	522	1148
P 31	9763	6229	10200	807	488	748	11676	6182	14805	839	497	1140
P 32	9169	5835	9570	793	485	722	10667	5907	14083	801	503	1173
P 33	9435	5834	10480	825	498	832	11846	6030	12466	882	512	1080

Table 10 Response value at bearing (bridge axis direction)

item			symbol	unit	24	25	26	27	28	29	30	31	32	33	34
rubber bearing specification	dimensions $a_0 * b_0$		a_0	mm		1550	1450	→				←	1450	1550	
			b_0	mm		1550	1450	→				←	1450	1550	
	rubber thickness		te	mm		228	200	→				←	200	228	
horizontal shear spring			k_s	t/cm		21.4	21.3	→				←	21.3	21.4	
girder displacement	normal	(temperature)	Δt	mm	168	134	101	67	34	0	34	67	101	134	168
	earthquake	(static)	Δte	mm	270	→								←	270
		(dynamic L 1)	Δte1	mm	153	153	152	152	151	151	151	152	152	153	153
		(dynamic L 2)	Δte2	mm	344	342	341	339	338	337	337	338	340	341	343
bearing deflection	normal	(temperature)	δ	mm		124	93	62	31	0	31	62	93	124	
	earthquake	(static)	δe	mm		248	→						←	248	
		(dynamic L 1)	δe1	mm	161	143	→			←	143	141	141	143	152
		(dynamic L 2)	δe2	mm	347	308	307	→		←	307	308	312	314	343
shear strain	normal	(temperature)	γ			0.54	0.46	0.31	0.16	0	0.16	0.31	0.46	0.54	
	earthquake	(static)	γe			1.09	1.24	→				←	1.24	1.09	
		(dynamic L 1)	γe1			0.63	0.72	→		←	0.72	0.71	0.71	0.63	
		(dynamic L 2)	γe2			1.35	1.54	→			←	1.54	1.56	1.38	
horizontal force (per unit)	normal	(temperature)	H	tf		123	99	66	33	0	33	66	99	123	
	earthquake	(static)	He	tf		266	264	→				←	264	266	
		(dynamic L 1)	He1	tf		155	154	154	155	157	157	157	158	160	
		(dynamic L 2)	He2	tf		331	328	328	329	330	331	333	336	345	

Study on liquefaction

Assessment of liquefaction

The surface stratum of the offshore section, A_{S1}, shown in Figure 1 has a small average N value of below 10, and consists of the saturated sandy soil having an average particle diameter D_{50} of 0.31mm, there is a possibility of liquefaction.

Regarding the assessment of liquefaction, results of liquefaction resistance ratio, F_L, in accordance with the Design Specifications are given in Table 11. According to this, the F_L value falls below 1 in the offshore section between P_2–P_9, and there is a possibility of liquefaction.

Also, based on a dynamic response analysis using the multi-reflection theory and the cumulative damage index method [5], it was possible to obtain the same results.

Investigation into the need for additional measures

Static design coefficients obtained by factoring the soil parameters given in the "Design Specifications" are given in Table 11. Where it is not possible to deal with problems through stiffness of piles (increasing wall thickness), it is necessary to apply the liquefaction countermeasures described below.

The results of this assessment are also given in the same table.

Investigation into liquefaction countermeasures

(1) Selection of countermeasure

A comparison of liquefaction countermeasures is given in Table 12.

From the same table an overall assessment was made of the effectiveness, past experience, and economy, and the method for increasing dynamic shear strength by vibro-compaction known as sand compaction pile (SCP) was selected.

Table 11 Assessment of requirement for SCP liquefaction counter measures

pierpieces		symbol	unit	P1	P2	P3	P4	P5	P6	P7	P8	P9	P10	P11	P12
FL value				1.09	0.55	0.85	0.94	0.48	0.89	0.77	0.90	0.70	1.10	1.07	1.33
liquefaction anticipated occur : ●					●	●	●	●	●	●	●	●			
coefficient on soil parameter		D_E			0	2/3	2/3	0	2/3	1/3	2/3	1/3			
specification	material				SKK490	SKK490	SKK490	SKK490	SKK490	SKK400	SKK400	SKK400			
	thickness	t	mm		25	19	20	25	19	25	21	20			
pile head displacement		δ	cm			13.9	15.8		13.8		8.0	6.0			
stress developed		σ	kg/cm²		2457	2198	2274	2522	2276	1831	2080	2087			
allowable stress		σ_a	kg/cm²		2850	2850	2850	2850	2276	2100	2100	2100			
requirement for SCP improvement					needed			needed		needed					

notes 1) pile diameter ϕ = 1600mm
2) allowable displacement δ_a = 16mm
3) maximum wall thickness of piles t_{max} = 25mm (from Design Specifications)

Table 12 Comparison of measures against liquefaction

countermeasure	deep mixing method (DMM)	gravel drains	sand compaction (SCP)	increasing number of piles	raked piles	concrete-filled piles
outline of method	liqefaction strata replaced by hardened zone by treatment with cement grout	liquefaction prevented by dissipation of excess pore water pressure	liquefaction prevented by increasing density by compaction	by increasing the number of piles the foundation stiffness is increased and displacement limited	the use of raked piles increases horizontal resistance and displacement is controlled	casting concrete inside the piles increases their stiffness and controls displacement
construction performance	plans for use in Ukishima Ramp and Kawasaki Man-made Island have revealed no problems, but compared with the SCP method actual implementation is less concern that it may not be possible to drive the piles to the solidified layer	little experience with use in open sea in locations of large water depth the error in drain position becomes large, and there is concern about trubble becoming an obstruction to pile driving	actual experience is great, no particular problems experienced	no particular problems	even with vertical piles the pile length is great, so that driving is very difficult the driving of raked piles is almost impossible the connection of the steel footing beam with raked piles is difficult	after driving, the interior of the pile would be excavated and concrete cast, but the cleaning of the pile interior is difficult because the pile length is long, driving is difficult
reliability of effectiveness, and stability considerations	long-term stability can be relied upon has ample resistance to flow of surrounding ground	few examples which actually prove effectiveness possibility of reduced efficiency through blockage of the drain, so there is no long-term guarantee of effectiveness	has ample resistance to flow of surrounding ground if the improved zone is considered as one structural body effectiveness in preventing liquefaction in previous earthquakes has been confirmed	even with an increased number of piles the allowable value of displacement of 16mm at the seismic design founding level cannot be satisfied	by raking the outer row of piles by 12 degrees the displacement at seismic design founding level can be limited to below the allowable 16mm the pile reaction force is large, and piles must be lengthened to 57m It is difficult oto drive raked piles because adjacent piles of the same type and diameter, have been driven	even by casting concrete within the piles the allowable displacement criteria at the seismic design foundation level cannot be met there is a problem with the bond between the pile and concrete, and concern that composite action may not be achieved the pile reaction is large, and pile length must be extended to 46m
environmental influences	depending on the pH value it may be necessary to consider environment effects	—	—	no particular problems	no particular problems	no particular problems
cost index	2.3	1.0	1.0	1.3	1.2	1.1
overall appraisal	x obstruction to pile driving study needed of environmental influences	x obstruction to pile driving no actual proof of effectiveness	o rational choice of cost and effectiveness	x cannot satisfy allowable displacement criteria worst on cost	x difficult to realize	x cannot satisfy allowable displacement criteria questionable effectiveness

a. Design of SCP method

• Level of improvement

The strength of soil after improvement by the SCP method is influenced by the following factors.

① N value of original ground (*No*)
② effective overburden pressure (σv)
③ proportion of fine particles (*Fc*)
④ proportion of sand pile improvement (*As*)
⑤ effectiveness of vibro-compaction

Several methods for assessing the level of improvement have been suggested. In this case the safest method using a formula based on the proportion of fine particles considering the increase in improvement was employed.

For the evaluation of liquefied strength, it was considered that the relative density after improvement would exceed 60%, and research results by Kokusho et al.[6] for dense sand were followed.

As a result, the proportion of sand pile improvement for pier P_7 was 27%, with a target N value of 18.

• Area of improvement

For consideration of the area of improvement, based on research by Tsuchida et al.[7], even where an improved area which adjoins a non-improved area failed actively, it was decided that this would not influence improved areas where passive resistance from piles could be expected.

b. Investigations of improvement effectiveness using earthquake response analysis

For piers P_5 and P_7, a 2-dimensional FEM model was made with the consideration of their foundations, piers, and the soil mass improved by the SCP method, and the improvement effectiveness was verified by the cumulative damage index method.

The analysis model was similar to the FEM model shown in Figure 8.

The physical properties of the improved ground were as follows.

$$Vs = (184 - 61.7 \cdot e_1)\sigma m^{0.25} \quad (1)$$

$$G = Vs^2 \cdot \rho / 9.8 \quad (2)$$

Vs : shear wave velocity (m/s)
G : shear modulus (t/m^2)
e_1 : improved ground void ratio
σm : average effective overburden pressure (t/m^2)
ρ : unit density (t/m^3)

The results of evaluation of the F_L value using the cumulative damage index method are shown in Figure 17. Table 13 shows average F_L values for elements in SCP-improved areas.

As seen in Table 13, after ground improvement the F_L values are greater than the F_L value given in the Design Specifications. For L-1 the F_L value becomes about 1.0, and it can be judged that liquefaction will not occur. For L-2 however, the F_L value is about 0.7, meaning that there will be liquefaction. However, because of the strength of dense sand at liquefaction, it is thought that complete liquefaction will not occur.

For the foundation piles at L-2 level, making a study similar to the LMM analysis in explained calier, the Broms's ultimate horizontal resistance considering the strength of liquefied dense sand is greater than the response shear force.

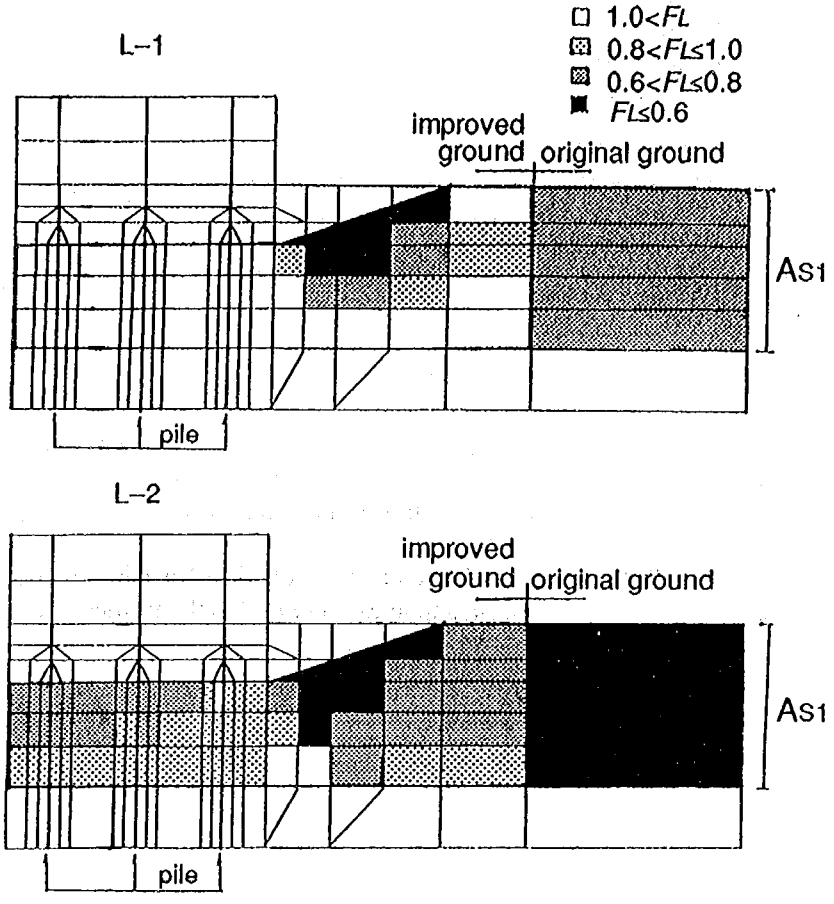


Figure 17 F_L value distribution diagram (P_5)

Table 13 Average F_L value

pier	L-1	L-2
P5	1.07	0.78
P7	0.96	0.67

References

1) Ohira, Tazoh, Nakahi, and Shimizu: "Observation and Analysis of Earthquake Response Behavior of Foundation Piles in Soft Soil Deposit," *Proceedings of JSCE*, No. 362/I-4, Japan Society of Civil Engineers, Oct., 1985.

2) Tazoh, Shimizu, Kikuchi, Sato, and Yashiromoto: "Seismic Response Analysis Method for Pile Foundation Structures considering Nonlinear Ground Vibration Characteristics," *Proceedings of the 20th JSCE Earthquake Engineering Symposium*, Japan Society of Civil Engineers, Jul., 1989.

3) Motoyama, Maruyama, Kikuchi, and Goto: "Excitation Experiment and Analysis on Access Bridge to Kansai International Airport," *Proceedings of the 20th JSCE Earthquake Engineering Symposium*, Japan Society of Civil Engineers, Jul., 1989.

4) Tatsuoka: "Cyclic Mobility," *Tsuchi-to-Kiso*, Japanese Society of Soil Mechanics and Foundation Engineering, Jun., 1980.

5) Yoshimi: "Liquefaction of Sandy Ground," Gihodo.

6) Kokusho, Yoshida, and Nagasaki: "Evaluation of Aseismic Strength of Dense Sand Layer due to SPT N-Value," *Proceedings of the 19th Japan National Conference on Soil Mechanics and Foundation Engineering*, Japanese Society of Soil Mechanics and Foundation Engineering, Jun., 1984.

7) Tsuchida and Iai: "Area of Improvement by Vibro-Compaction for Liquefaction," *Proceedings of the 14th Earthquake Engineering Symposium*, Japan Society of Civil Engineers, Jul., 1976.

Session-7

Design Applications-2

J-14) Menshin Design and Construction of Multi-Span Continuous Prestressed Concrete Bridge
(Uzuka, T., Kawakami, K., Kumakura, K. and Tani, H.)

U-8) Two Shake Table Experimental Studies of the Effectiveness of Damping-Augmentation Devices in Cable-Stayed Bridges
(Abdel-Ghaffar, A., Masri, S. F. and Ali, H.)

J-15) Improvement of Earthquake Resistance of Prestressed Concrete Cable-Stayed Bridges by Hysteresis Damper
(Ichinomiya, T., Takeda, T. and Kanda, K.)

J-16) Development of Jointless System with Menshin Bearing for Existing Simple-Spanned Steel Bridges
(Naganuma, T., Mizobuchi, S. and Uno, H)

MENSHIN DESIGN AND CONSTRUCTION OF MULTI-SPAN CONTINUOUS PRESTRESSED CONCRETE BRIDGE

Tsuneo UZUKA[1], Kazuhiko KAWAKAMI[2], Kazuomi KUMAKURA[3] and Hideo TANI[4]

1. Director, Road Construction Division, Department of Public Works, Tochigi Prefectural Government, Utsunomiya City, Tochigi, Japan

2. Section Chief, Ditto

3. Senior Officer, Ditto

4. Technical Staff, Ditto

SUMMARY

The purpose of this paper is to describe the Menshin Design that was applied the Yamaage Bridge. This design method for practical application was developed in New Zealand, U.S.A and other countries.

INTRODUCTION

Menshin Design, a design method to reduce seismic response of a bridge, has been developed under the concept of "releasing" and "not resisting" earthquake ground motion. The concept itself is quite old, and includes the following two main ideas; namely to isolate the structure from the base and to reduce the seismic response by extending the vibration period, taking note of the difference between the natural period of structures and the predominant period of seismic motion or natural period of ground motion. These ideas, though able to reduce the seismic forces, have difficulties in restoring structure due to excessive relative displacement during an earthquake, and thus have not been put into practical application with some exceptions.

Since 1970, several attempts have been made to develop devices that can absorb structural kinetic energy and realize the above-mentioned ideas. The most recent one is the so-called Menshin Design, and a rubber bearing for practical application was developed in New Zealand and other countries. In Japan, this modern bridge design method has been developed in consideration of the characteristics of Japanese earthquake condition, too. Other bridges of this kind in Japan are the Miyagawa Bridge of National Road Route 362 which was completed by the Shizuoka Prefectural Government in March of 1991 and the Nagakigawa bridge of National Road Route 7 which is at present under construction by the

Noshiro Construction Office, Tohoku Regional Construction Bureau, Ministry of Construction. It is noted, however, that Yamaage Bridge with a length of 246.3 meters is the first largest Menshin Design bridge in Japan.

OUTLINE OF YAMAAGE BRIDGE

The Yamaage Bridge was planned at the place on Bypath Highway of National Road Route 294 running through Karasuyama-cho in the northeast part of Tochigi Prefecture, to cope with the rapid growth of traffic. This area is notorious for frequent occurrence of earthquakes, represented by the Imaichi Great Earthquake in 1949. The ground condition consists of sand-gravel layers and slate formation. According to a standard penetration test, the N-value of the sand-gravel layers are 30 to 50, and that of the slate formation is over 50. The type of superstructure is prestressed concrete two-cell box-girder with width ranging from 6.5 meters (standard section) to 8.0 meters (wide section). Transverse tendons are provided in the slab. The abutment is an inverted T-type, while the pier is rectangular wall shaped. The location and structure of the Yamaage Bridge are shown in Figs. 1 to 4. The design condition of the bridge is shown in Table. 1.

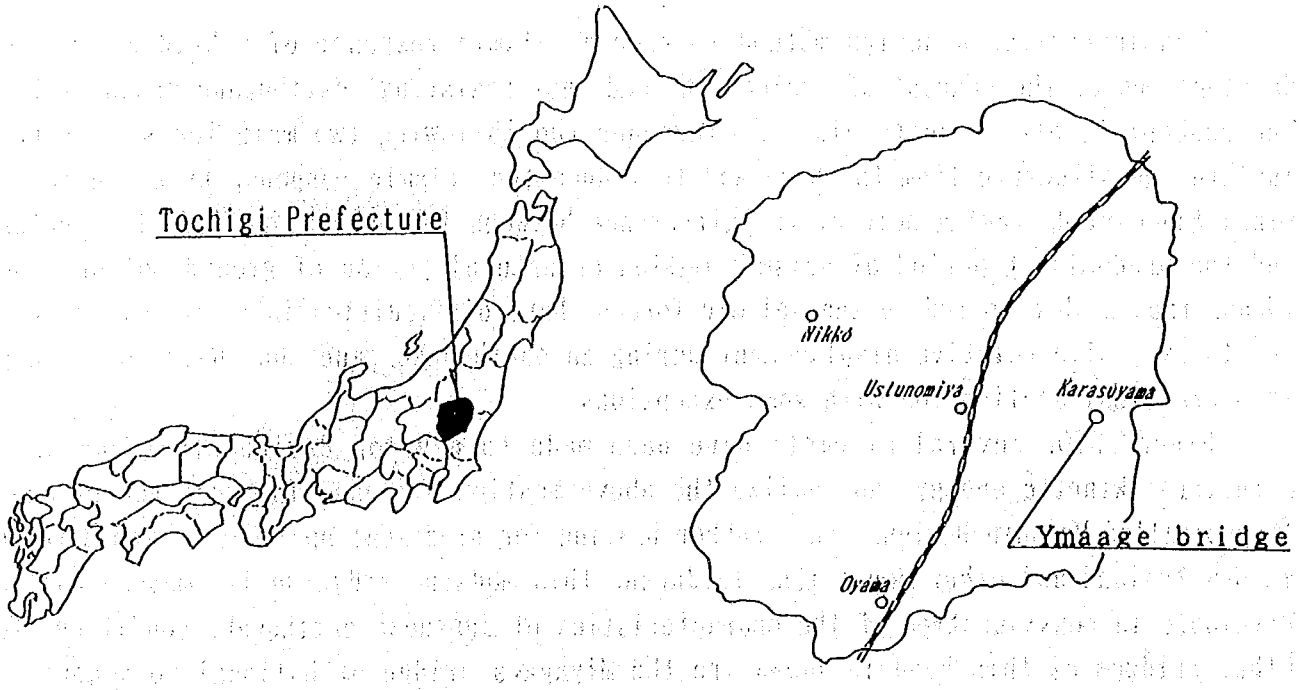


Fig. 1 Location of Yamaage Bridge

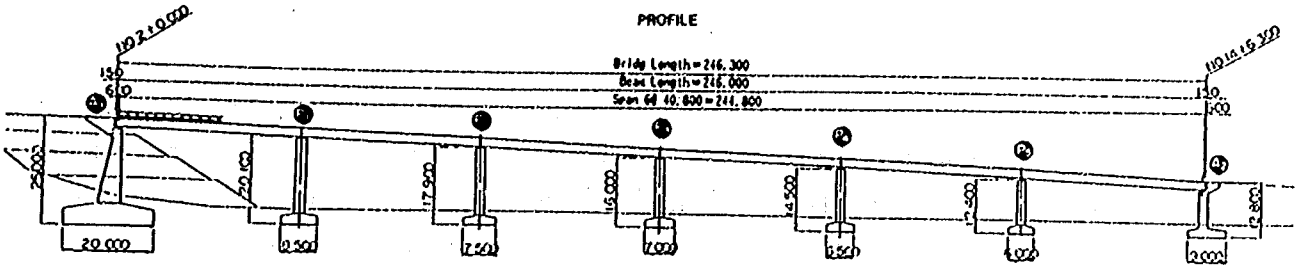


Fig. 2 Side View

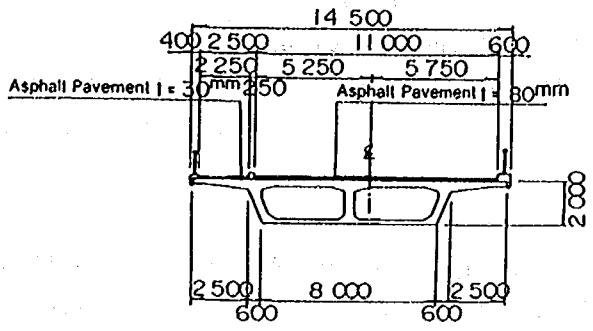


Fig. 3 Cross Section of Superstructure

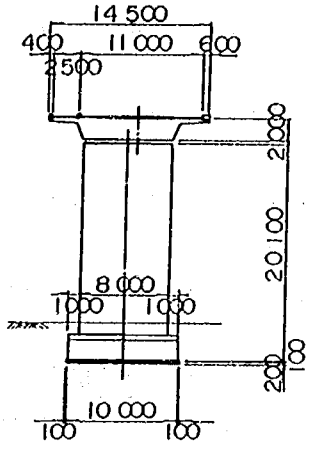


Fig. 4 Bridge Pier

Table. 1 Design Condition of the Bridge

Bridge Type	Prestressed concrete road bridge
Structure	PC post tensioning method, 6-span continuous box-girder
Road Class	Urban area, design car speed of 60km/h
Bridge Class	Class A
Bridge Length	246.3m
Span Length	6×40.8 = 244.8m
Bridge Width	Standard section; 8.0m(carriageway) + 2.5m(sidewalk) = 10.5m Widening section;11.0m(carriageway) + 2.5m(sidewalk) = 13.5m
Live Load	TL 20
Impact Coefficient	i = 10 / (20+L)
Alignment	R = ∞ ～ A = 240m
Vertical Grade	1.0% ～ VCL = 100 m , R = 2,500 m ～ 5.0%
Cross Slope	1.5%(carriageway), 2.0%(sidewalk)
Abutment Skew Angle	90° (A_1 side) , 90°-27′ 43″ (A_2 side)
Horizontal Design Seismic Coefficient	k_h = 0.16 (Longitudinal direction) k_h = 0.20 (Transverse direction)

MENSHIN DESIGN OF YAMAAGE BRIDGE

The Yamaage Bridge was designed in accordance with the regulations of the Design Specifications for Highway Bridges(Ref. 1). We also referred to some items on Menshin Design in "Guidelines for Design of Menshin Highway Bridges (Draft)" published by the Technology Research Center for National Land Development in March 1989(Ref. 2).

The most important factor in Menshin Design is the introduction of a Menshin device that can support the superstructure and simultaneously absorb the kinetic energy. The damper is able to disperse the horizontal seismic force and simultaneously reduce the seismic horizontal acceleration of superstructures, which can remarkably enhance the safety of substructures.

For this bridge, High Damping laminated Rubber Bearing (HDRB) is used as the Menshin device. The HDRB is composed of alternative lamination of specific compounds of rubber layers and steel plates. Also, because of the cold area where the Yamaage Bridge is located, the bearing has to have such features as a small residual deformation and a little temperature dependency.

Characteristic of the HDRB HDRB is characterized by its viscous damping capability and its hysteresis loop. The effective damping ratio is nearly a constant value of 15% in a wide range of amplitude. The equivalent stiffness depends on the amplitude in a non-linear manner that the stiffness decreases in contrast to the magnitude of displacement. HDRB has high initial stiffness against small vibration of the bridge caused by wind force, while it has low stiffness against large amplitude.

Further, the rubber presents a hardening phenomenon against excessive displacement (over the design value) to avoid the sliding-down of superstructure.

The Hysteresis Loop of HDRB is shown in Fig. 5.

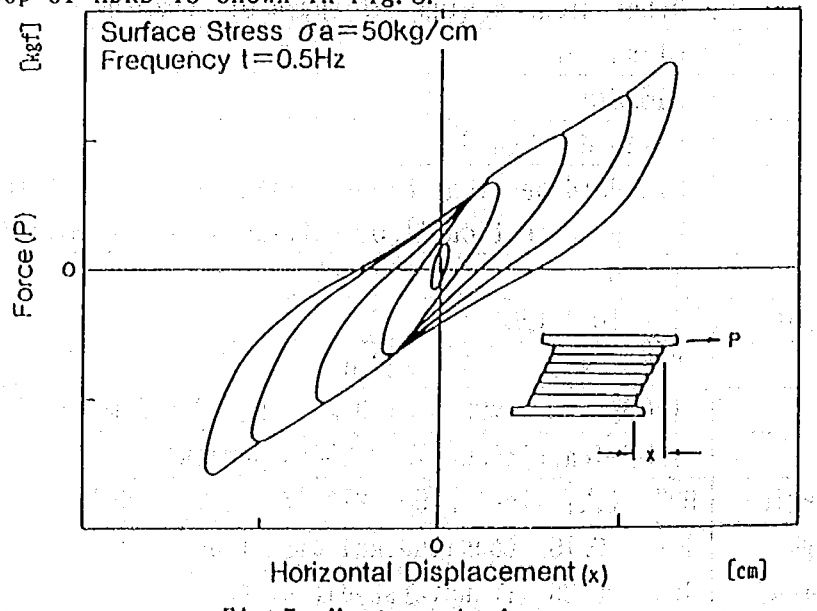


Fig. 5 Hysteresis Loop

The Structure of HDRB is shown in Fig. 6.

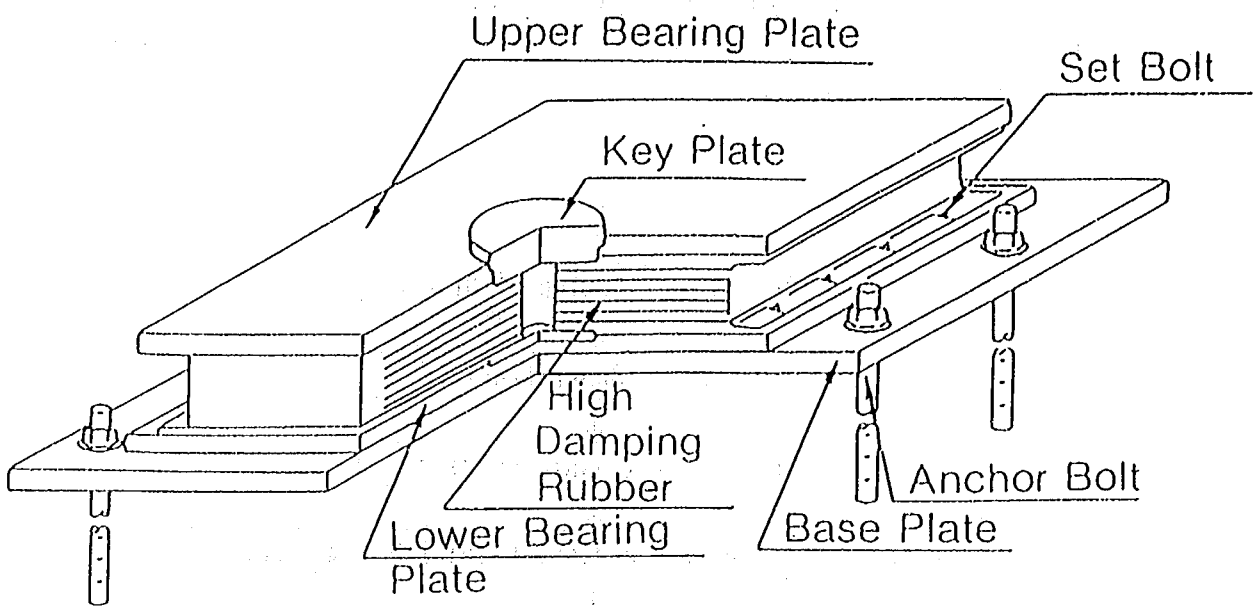


Fig. 6 Structure of HDRB

Main ideas for the design of Yamaage Bridge Main ideas, to apply the Menshin design to Yamaage Bridge, were decided as follows.

1) Menshin design is only applied for the longitudinal direction. Transverse direction of the bridge is restrained by stopper.

2) The displacement value of superstructure is determined to put it nearly with in the total value of drying shrinkage, creep, elastic deformation, and the deformation affected by temperature change.

3) The seismic coefficient applied for the check of bearing capacity for lateral force is obtained by the computation results of the whole structural analysis including the spring stiffness of the HDRB.

Flow chart of Menshin design Fig. 7 shows the flow chart of Menshin design used for the Yamaage Bridge in outline. According to the Specifications, two levels of seismic force shall be taken into consideration in the seismic design of highway bridges. The lower level, which is designated hereafter as Level 1, represents the effect of moderate earthquakes which are expected to take place with high possibility. The higher level, which is designated hereafter as Level 2, represents the effect of large earthquakes with the more rich scale than 8 which are supposed to take place very rarely, such as the

Kanto Earthquake (Magnitude 7.9) of 1923. For the Level 1, allowable stress method is adopted in the Specifications so that the stress developed due to the Level 1 seismic force be less than the seismic allowable stress which is almost equal to the yielding stress. For Level 2, the ductility of reinforced concrete piers shall be checked to avoid brittle failures during significant earthquakes.

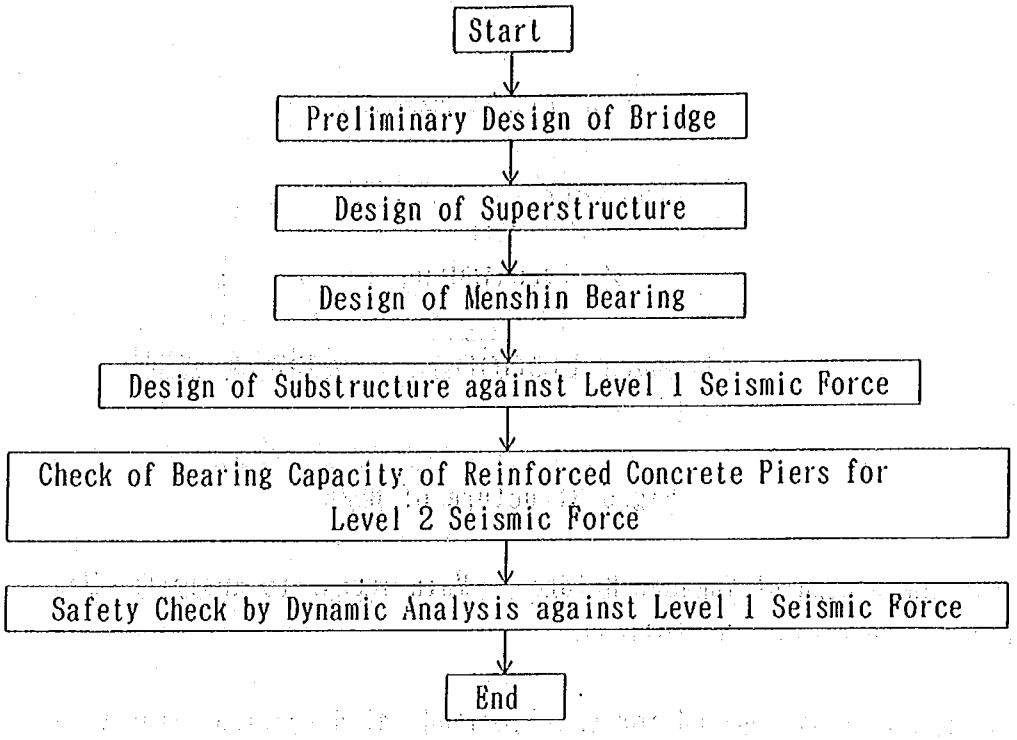


Fig.7 Flow Chart of Menshin Design

Design of Bearing The relation between shearing modulus of elasticity [$G(\gamma)$] and shearing strain [γ] on the High Damping Rubber is shown in Fig.8. The spring stiffness of this bearing's material depends on the amplitude in such a non-linear manner that the stiffness lessens in contrast to the strain. This is obtained by loading test, and represented the following formulas.

$$G(\gamma) = 26.3 - 46\gamma + 45.7\gamma^2 - 21.1\gamma^3 + 3.88\gamma^4 \qquad (0<\gamma<1.8)$$

$$G(\gamma) = 0.31 + 6.89\gamma - 1.08\gamma^2 \qquad (1.8<\gamma)$$

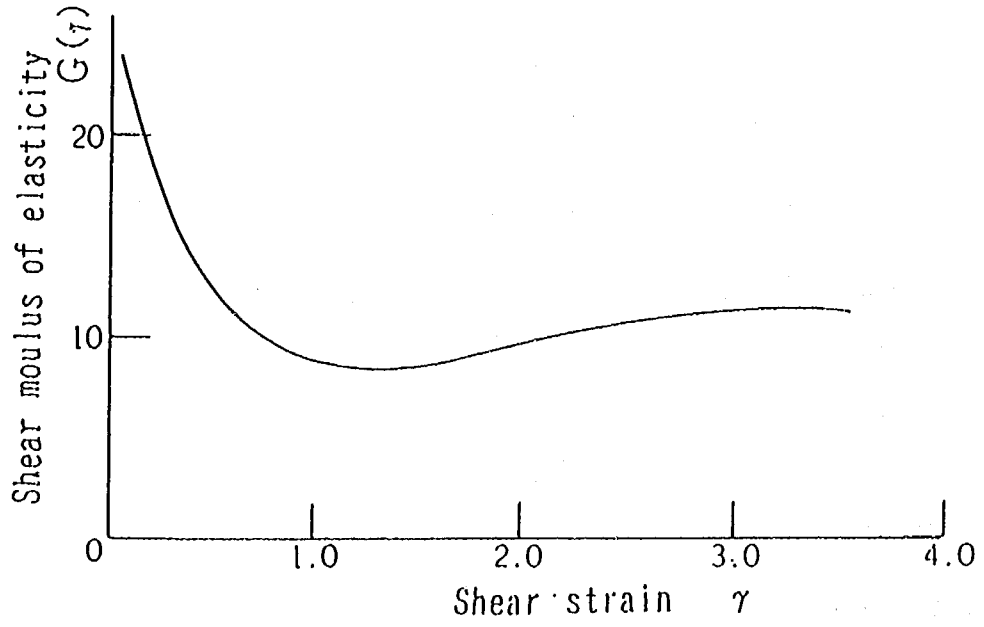


Fig.8 $G(\gamma)$ - γ Curve of High Damping Rubber

According to these formulas, the dimensions of the bearing were determined. Design process of HDRB was performed as follows;

1) Supposing the displacement value of HDRB against Level 1 and Level 2 seismic forces, and compute the shear strain .

$$\gamma = u_s' / H_R$$

γ : Shear strain
u_s' : Displacement of HDRB (supposed value) (cm)
H_R : Thickness of rubber bearing (cm)

2) Compute the shear modulus of elasticity and equivalent stiffness of HDRB.

$$G(\gamma) = 26.3 - 46\gamma + 45.7\gamma^2 - 21.1\gamma^3 + 3.88\gamma^4 \quad (0<\gamma<1.8)$$
$$G(\gamma) = 0.31 + 6.89\gamma - 1.08\gamma^2 \quad (1.8<\gamma)$$

$G(\gamma)$: Shear modulus of elasticity

$$K_B = A_0 \times G(\gamma) / H_R$$

K_B : Equivalent stiffness (kgf/cm)
A_0 : Area of the bearing that support the superstructure (cm^2)

3) Compute the natural period and horizontal design seismic coefficient that applying to the design of HDRB.

$$K_T = \Sigma K_B$$

$$T = 2 \times \pi \times R_d / \sqrt{(980 \times K_B)}$$

K_T : Sum of K_B on substructures

T : Natural period applied the design of HDRB (sec)

R_d : Dead road of the superstructure (kgf)

Calculation of horizontal design seismic coefficient is used properly for the formulas against Level 1 and Level 2 seismic forces.

【Against the Level 1】

$$k_h = c_z \times c_G \times c_I \times c_T \times k_{h0}$$

$$c_T = 1.33 \times T^{-2/3}$$

【Against the Level 2】

$$k_h = c_z \times c_I \times c_T \times k_{h0}$$

$$c_T = 0.876 \times T^{-2/3}$$

k_h : Horizontal design seismic coefficient applied for the design of HDRB (gal)

c_z : Modification factor for zone (Fig. 9)

c_G : Modification factor for ground condition (Table. 2)

c_I : Modification factor for importance (Table. 3)

c_T : Modification factor for structural response (Table. 4)

k_{h0} : Standard design horizontal seismic coefficient (Table. 5)

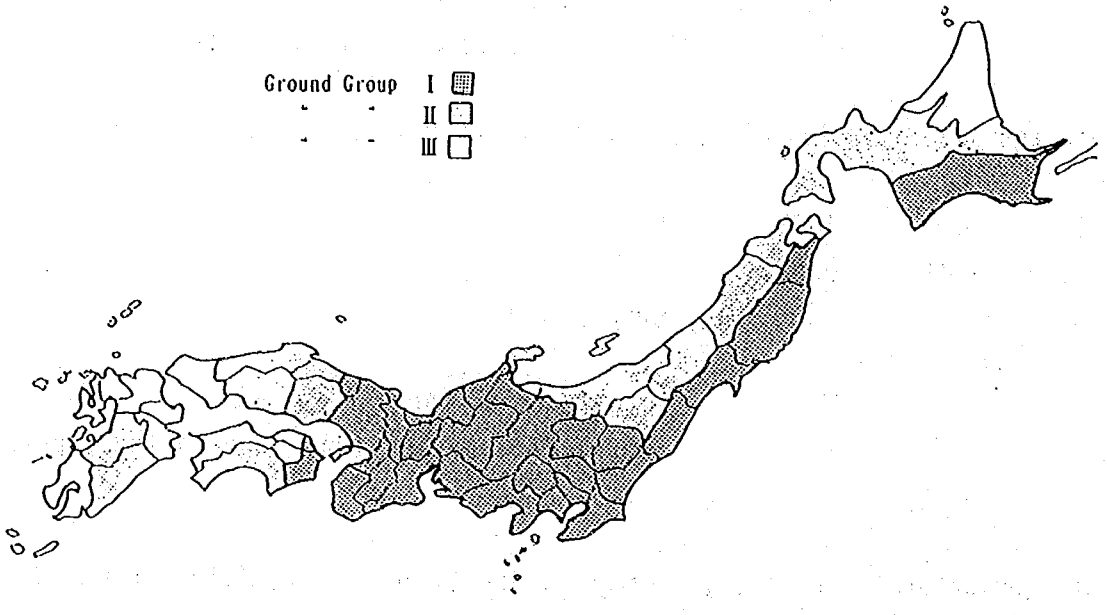


Fig. 9 Modification Factor for Zone

Table.2 Modification Factor for Ground Condition

Ground Group	I	II	III
c_G	0.8	1.0	1.2

Table.3 Modification Factor for Importance

Group	c_I	Definition
1st class	1.0	Bridges on expressway (limited access highways), general national road and principal prefectural road. important bridges on general prefectural road and municipal road.
2nd class	0.8	Other than the above

Table.4 Modification Factor for Structural Response

(For Level 1 seismic force)

Ground Group	Structural Response Coefficient		
Group I	$T < 0.1$ $C_T = 2.69T^{1/3} \geqq 1.00$	$0.1 \leqq T \leqq 1.1$ $C_T = 1.25$	$1.1 < T$ $C_T = 1.33T^{-2/3}$
Group II	$T < 0.2$ $C_T = 2.15T^{1/3} \geqq 1.00$	$0.2 \leqq T \leqq 1.3$ $C_T = 1.25$	$1.3 < T$ $C_T = 1.49T^{-2/3}$
Group III	$T < 0.34$ $C_T = 1.80T^{1/3} \geqq 1.00$	$0.34 \leqq T \leqq 1.5$ $C_T = 1.25$	$1.5 < T$ $C_T = 1.64T^{-2/3}$

(For Level 2 seismic force)

Ground Group	Structural Response Coefficient		
Group I	$T \leqq 1.4$ $C_T = 0.7$		$1.4 < T$ $C_T = 0.876T^{-2/3}$
Group II	$T < 0.18$ $C_T = 1.51T^{1/3} \geqq 0.70$	$0.18 \leqq T \leqq 1.6$ $C_T = 0.85$	$1.6 < T$ $C_T = 1.16T^{-2/3}$
Group III	$T < 0.29$ $C_T = 1.51T^{1/3} \geqq 0.70$	$0.29 \leqq T \leqq 2.0$ $C_T = 1.00$	$2.0 < T$ $C_T = 1.59T^{-2/3}$

Table.5 Standard Design Horizontal Seismic Coefficient

Seismic force Level	Level 1	Level 2
k_{h0}	0.2	1.0

4) Compute the displacement value of HDRB, and compare it with the supposed displacement.

$$u_s = R_d \times k_h / K_B$$

u_s : Displacement value of HDRB (cm)

$u_s \fallingdotseq u_s'$ ···· Ok

$u_s \neq u_s'$ ···· Do over again

Design results of HDRB are shown in Tables.6 to 8.

Table.6 Dimensions of HDRB (Unit : mm)

	A_1	P_1	P_2	P_3	P_4	P_5	A_2
Plane Dimensions	700x 855	950x1500	1030x1580	950x1500	950x1500	950x1500	700x 855
Thickness of Rubber Layers	14.7x14 =205.8	21.0x 6 =126.0	34.0x 3 =102.0	24.0x 5 =120.0	24.0x 6 =144.0	18.7x 8 =149.6	13.8x19 =262.2
Thickness of Insert Plates	4.2x13 = 54.6	4.2x 5 = 21.0	4.2x 2 = 8.4	4.2x 4 = 16.8	4.2x 5 = 21.0	4.2x 7 = 29.4	4.2x18 = 75.6
Height (except for Flanges)	260.4	147.0	110.4	136.8	165.0	179.0	337.8

Table.7 Design Results of HDRB Against Level 1

[]:Unit		A_1	P_1	P_2	P_3	P_4	P_5	A_2
Supposing Displacement Value	u_s' [cm]	7.784						
Thickness of Rubber Bearing	H_R [cm]	20.58	12.60	10.20	12.00	14.40	14.96	26.22
Shearing Strain	γ	0.378	0.618	0.763	0.649	0.541	0.520	0.297
Shearing Modulus of Elasticity	$G(\gamma)$	14.377	10.914	9.749	10.618	11.787	12.050	16.150
Area Support Superstructure	A_0 [cm²]	5872	14137	16161	14137	14137	14137	5872
Equivalent Stiffness	K_B [kg/cm²]	4102	12245	15446	12509	11571	11387	3617
Number of Shearing on Each		2						
Sum of K_B	K_T [kg/cm²]	141756						
Natural Period	T [sec]	1.337						
Dead load of Superstructure	R_d [kgf]	6294200						
Factor for Structural Response	c_T	1.096						
Design Seismic Coefficient	k_h	0.18						
Designing Displacement Value	u_s [cm]	7.770						

Table.8 Design Results of HDRB Against Level 2

[]:Unit	A_1	P_1	P_2	P_3	P_4	P_5	A_2
Supposing Displacement Value u_s [cm]	32.69						
Thickness of Rubber Bearing H_R [cm]	20.58	12.60	10.20	12.00	14.40	14.96	26.22
Shearing Strain γ	1.588	2.594	3.205	2.724	2.270	2.185	1.247
Shearing Modulus of Elasticity $G(\gamma)$	8.674	10.916	11.299	11.064	10.385	10.208	8.469
Area Support Superstructure A_0 [cm²]	5872	14137	16161	14137	14137	14137	5872
Equivalent Stiffness K_B [kg/cm²]	2475	12247	17902	13035	10195	9647	1896
Number of Shearing on Each	2						
Sum of K_B K_T [kg/cm²]	134794						
Natural Period T [sec]	1.372						
Dead load of Superstructure R_d [kgf]	6294200						
Factor for Structural Response c_T	0.700						
Design Seismic Coefficient k_h	0.70						
Designing Displacement Value u_s [cm]	32.69						

Horizontal Design Seismic Coefficient for the design of substructures Substructures were designed by the Seismic Coefficient Method. The theoretical model as shown in Fig.10, which replaced the bridge with elastic beams and included the springs of bearing and foundation ground, was used.

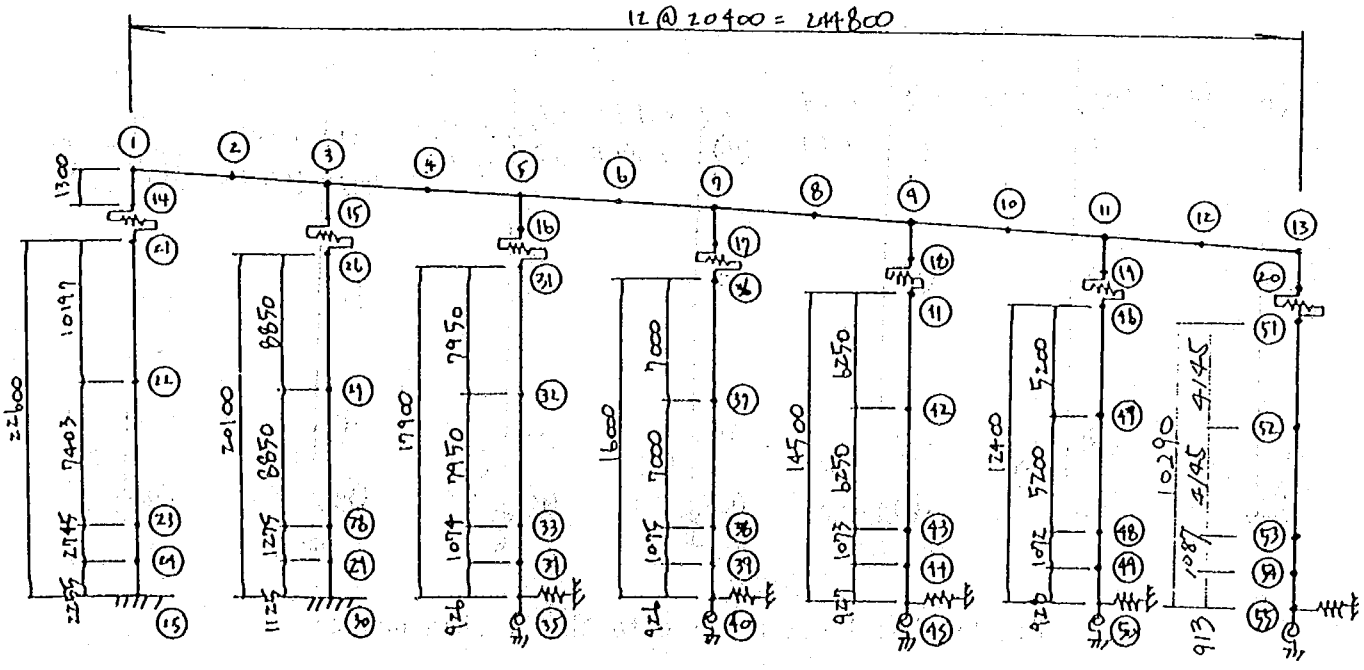


Fig.10 Theoretical Model

The natural period is computed by the following formula.

$$T = 2.01 \times \sqrt{\delta}$$

$$\delta = \frac{\int w(s)u(s)^2 ds}{\int w(s)u(s) ds}$$

T : Natural period of the seismic design structural unit (sec)
δ : Lateral displacement (m)
w(s) : Weight at position "s" of structures (tf/m)
u(s) : Displacement value at position "s" on occasion that horizontal force acts corresponding to the inertia force (m)
※ Consider the influence from transformation of foundation.

The natural period in the longitudinal direction is T=1.56sec, and that of the transverse direction is T=0.194sec. Supposing that not applied to Menshin design (Fig.11), the natural period of in the longitudinal direction is T=1.075sec.

Longitudinal direction: x
Transverse direction : y

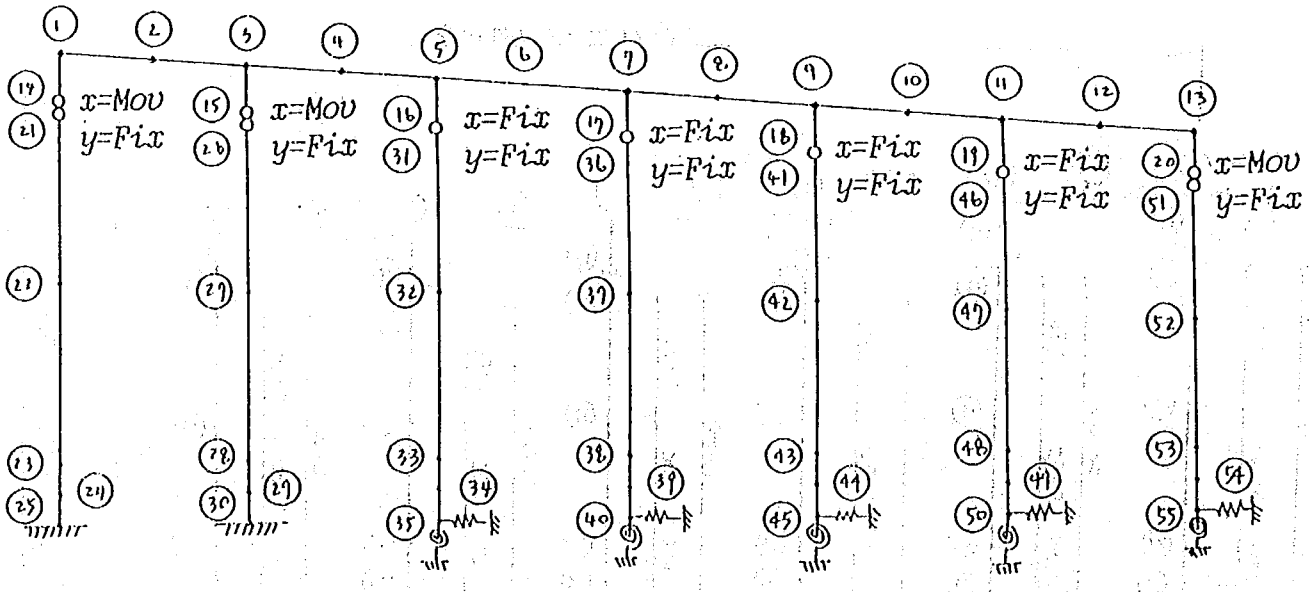


Fig.11 Model not applied to the Menshin Design

Table.9 shows the comparison of the horizontal design seismic coefficient of Menshin design with usual design. Table.9 shows that applying Menshin design is possible to be reduce seismic response from the superstructure, about 20%.

Table. 9 Comparison of The Horizontal Design Seismic Coefficient

	Menshin design	usual design
Modification factor for structural response c_T	0.991	1.25
Horizontal seismic design coefficient k_H	0.16	0.20

Relative displacement of bearing against Level 1 seismic force is shown in Table. 10. And we checked the safety of bearing when it strained so greatly.

Table. 10 Relative Displacement of Bearing Against Level 1 (Unit:cm)

	A_1	P_1	P_2	P_3	P_4	P_5	A_2
Relative displacement of bearings	10.04	8.31	5.65	6.33	6.62	7.22	9.75
Displacement value when designed bearings	7.77						

Table. 11 shows the comparison of the Bending Moment of Menshin design with that of not applied at bottom of piers.

Table. 11 Comparison of the Bending Moment (Unit:tm)

	P_1	P_2	P_3	P_4	P_5
Menshin design	4704.7	3677.2	2824.4	2345.0	2017.0
usual design	4793.2	5062.8	4760.8	4601.5	4578.2

Sectional form and reinforcement of piers were determined by Level 2 seismic force. The cross section of pier (P_1) is shown in Fig. 12.

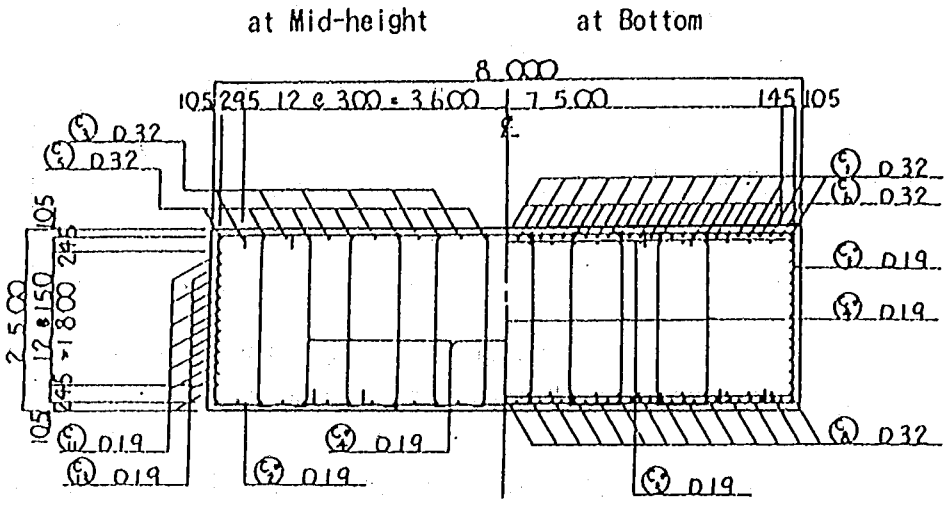


Fig. 12 Cross Section of Pier (P_1)

Check of Bearing Capacity for Lateral Force Bridges and other road facilities need to avoid brittle failures during significant earthquakes. The ductility of the reinforced concrete piers that designed by the Seismic Coefficient Method was checked against the Level 2 seismic force.

At the analysis, we used the theoretical model (Fig. 10) and took the energy dissipation effect of the HDRB in consideration. The horizontal seismic design coefficient against the Level 2 seismic force was computed K_{hc} = 0.60 with the natural period of T=1.77sec.

The flow chart applied the check of bearing capacity for lateral force is shown in Fig. 13.

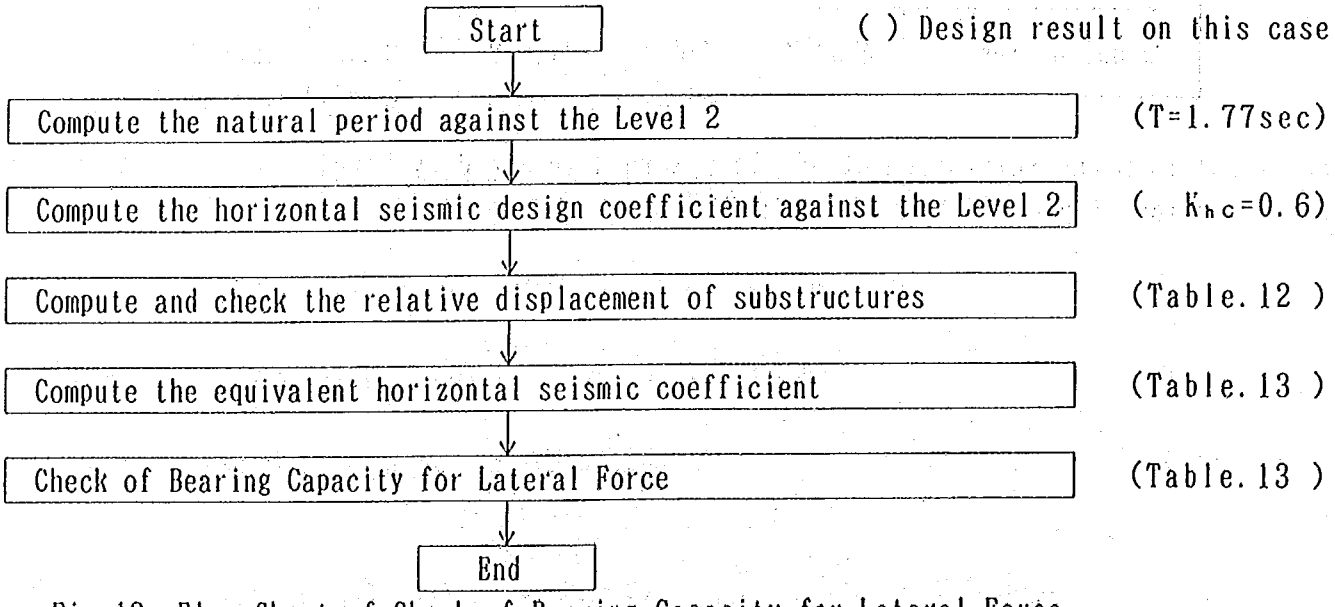


Fig. 13 Flow Chart of Check of Bearing Capacity for Lateral Force

Fig. 14 shows the relation between horizontal force [P] with horizontal displacement [δ] of the piers used for the investigation of this.

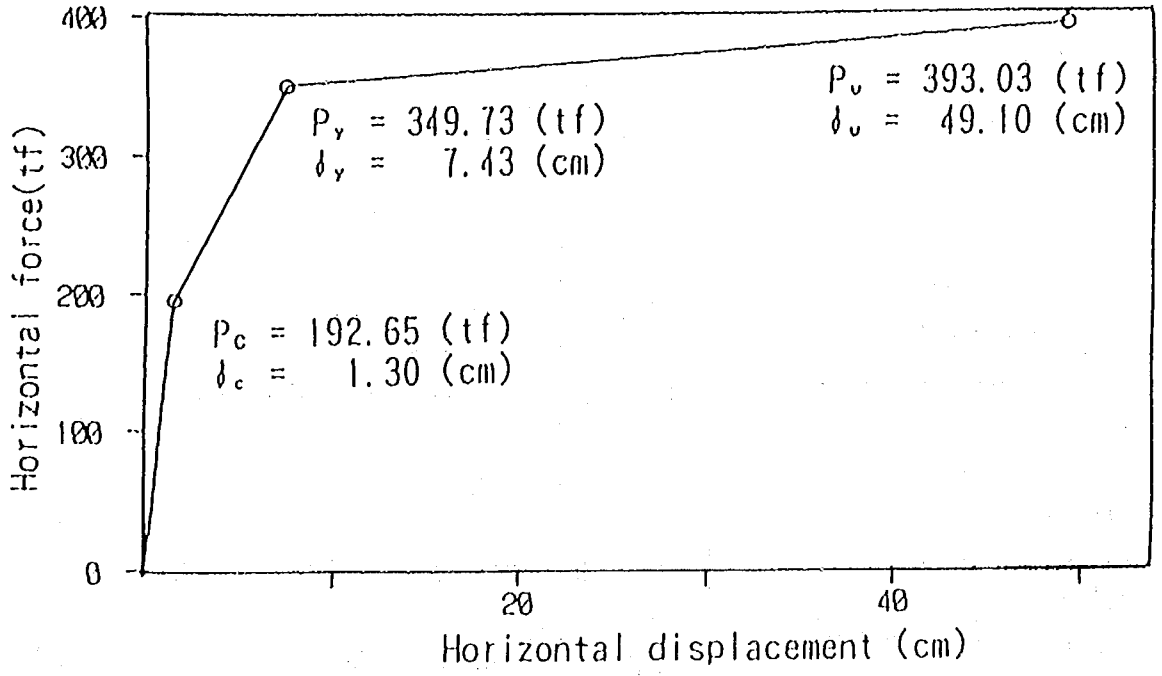


Fig. 14 P-δ curve of P_1 pier

Since the bearing capacity for flexral failure P_u is lower than that for shear failure P_s, the bearing capacity for lateral failure P_a is applied the P_u. The bearing capacity for lateral force P_a and the allowable ductility factor μ are obtained as:

$$P_a = P_y + (P_u - P_y) / \alpha$$
$$\mu = 1 + (\delta_u - \delta_y) / \alpha \delta_y$$

where P_y and δ_y are force and displacement when reinforcing steel is yielding, P_u and δ_u are ultimate force and ultimate displacement, and α is a safety factor over yielding to ultimate. The safety factor α is usually assumed as 1.5.

Table. 12 to 13 shows the results of analysis.

Table. 12 Relative Displacement of Bearing against Level 2 (Unit:cm)

	A_1	P_1	P_2	P_3	P_4	P_5	A_2
Relative displacement of bearings	48.86	30.50	20.08	24.85	28.51	34.06	48.11
Displacement value when designed bearings	32.69						

Table. 13 Results of Check of Bearing Capacity for Lateral Force

	Unit	P_1	P_2	P_3	P_4	P_5
Width of pier	m	8.00	8.00	6.50	6.50	6.50
Thickness of pier	m	2.50	2.20	2.20	2.00	2.00
Allowable Ductility Factor μ		4.739	3.683	5.393	4.991	4.984
Equivalent Horizontal Seismic Coefficient k_{he}		0.21	0.24	0.19	0.21	0.20
Bearing Capacity for Shear Failure P_s	tf	1385.95	1209.86	995.81	899.18	915.53
Bearing Capacity for Flexral Failure P_u	tf	378.60	347.17	285.88	278.04	269.70
Bearing Capacity for Lateral Force P_a	tf	378.60	347.17	285.88	278.04	269.70
Inertia Force for Level 2 $P = k_{he} \times w$	tf	348.20	346.58	239.58	245.54	250.82

From the results of investigation, we could confirm the piers has enough ductility against the Level 2 seismic force.

Dynamic analysis Dynamic Analysis of structures was made with a view to check the safety and movement of the Yamaage Bridge when an earthquake occurs. The analysis was made by both the Response Spectrum Analysis and the Time History Analysis.

The input seismic acceleration is shown in Fig. 15. And the damping ratio and equivalent stiffness of HDRB that applied the analysis is shown in Table. 14.

Table. 14 The Effective Damping Ratio of Bearing Applied for Dynamic Analysis

	[]:Unit	A_1	P_1	P_2	P_3	P_4	P_5	A_2
Designing Value	u [cm]	10.04	8.31	5.65	6.33	6.62	7.22	9.75
Area Support Superstructure	A [cm^2]	5872	14137	16161	14137	14137	14137	5872
Thickness of Rubber Bearing	H_R [cm]	20.58	12.60	10.20	12.00	14.40	14.96	26.22
Shear Strain	γ	0.488	0.660	0.554	0.528	0.460	0.483	0.372
Shear Modulus of Elasticity	G(γ)	12.505	10.512	11.621	11.955	12.934	12.583	14.503
Equivalent Stiffness	K_B [kg/cm^2]	3568	11805	18412	14084	12698	11890	3248
The Effective Damping Ratio	h_B	0.168	0.167	0.168	0.168	0.169	0.169	0.169

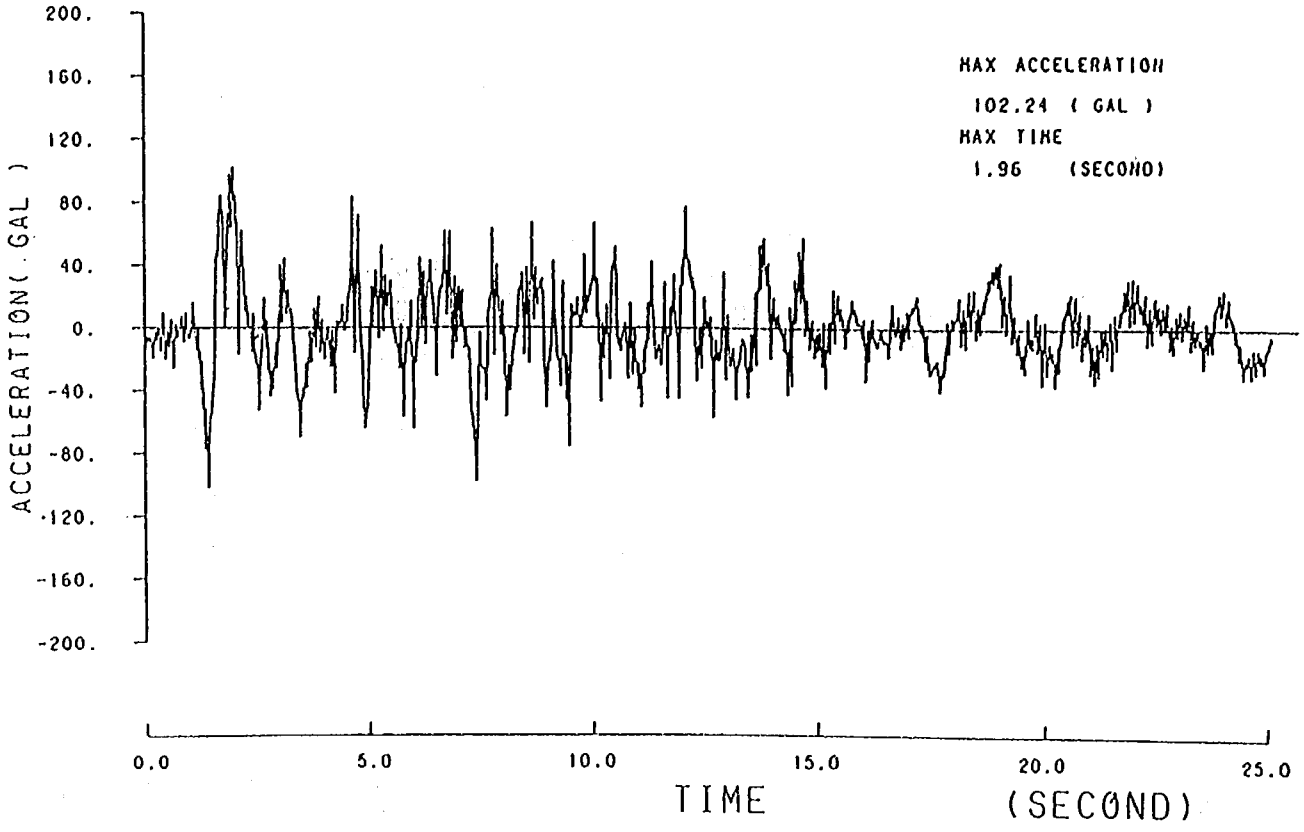


Fig. 15 Input Seismic Acceleration (The Record of Modify Kaihoku Bridge)

As the damping ratio changes the value which depends on the variation of displacement of bearing, the formula that was obtained by loading test was used.

$$h_B = 0.172 - 0.00693\gamma_s + 0.00276\gamma_s^2 - 0.00694\gamma_s^3$$

h_B : The effective damping ratio

γ_s : Shearing strain of bearing

And also we considered the damping ratio at the superstructure, substructure, and the foundation ground supposing that 3%, 5%, and 10% in accordance with the Specifications.

Table. 15 shows the natural period and the damping ratio of each vibration mode. The 1st to 3rd vibration modes are shown in Fig. 16.

Table. 15 The Natural Period and the Damping Ratio

Mode NO.	Natural period (sec)	Damping ratio
1	1.5464	0.1431
2	0.4510	0.0302
3	0.4192	0.0302
4	0.3567	0.0302
5	0.3023	0.0924
6	0.2986	0.0557
7	0.2733	0.1154
8	0.2590	0.0309
9	0.2526	0.1142
10	0.2355	0.0305

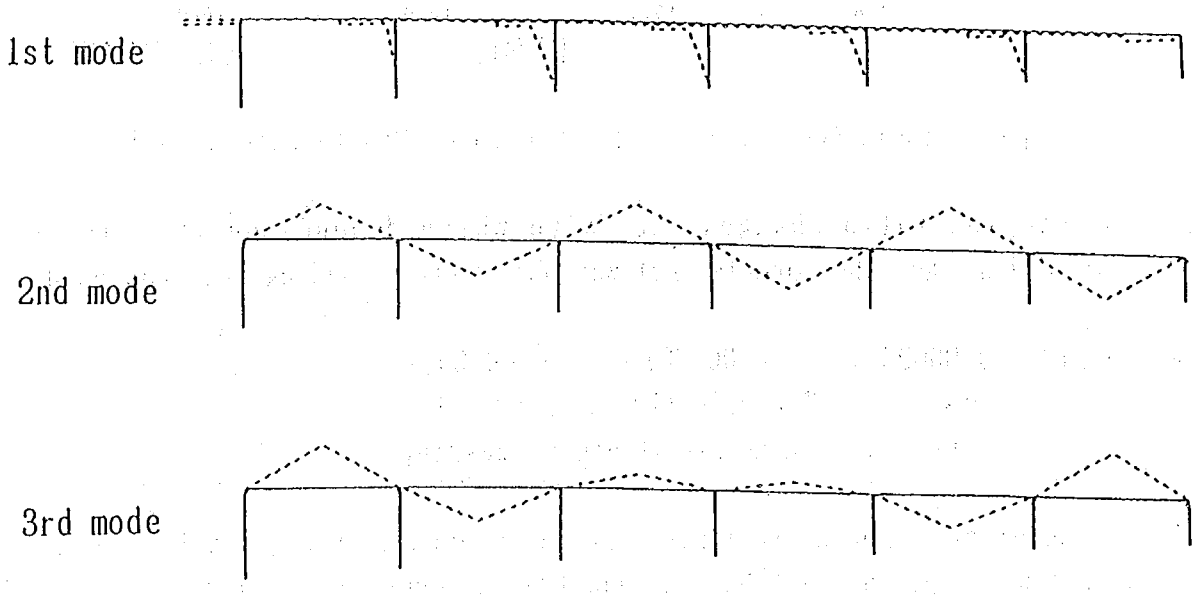


Fig. 16 Vibration Mode

Since the 1st is a only vibration mode that the superstructure is swaying with large shear displacement of the bearing and slight tenacious displacement of the substructures, we could confirm the damping ratio of 14.3% for the 1st vibration is predominated by the damping ratio of the bearing.

Tables. 16 to 17 shows the comparison the design results of seismic coefficient method with that of the dynamic analysis, on the displacement of bearing and the section force of piers at bottom.

Table. 16 Displacement of Bearing (Unit:mm)

	Design value	Dynamic Analysis	
		Response Spectrum Analysis	Time History Analysis
A_1	100.42	65.76	68.72
P_1	83.08	55.05	58.70
P_2	77.84	36.85	38.82
P_3	77.84	41.59	44.74
P_4	77.84	43.60	47.14
P_5	77.84	47.85	51.32
A_2	97.51	63.47	67.77

Table. 17 Section Forces of Piers at Bottom (Unit:tm)

		Design value	Dynamic analysis	
			Response Spectrum Analysis	Time History Analysis
Bending Moment (tfm)	A_1	3998.1	828.9	866.4
	P_1	4854.4	2665.1	2710.0
	P_2	3652.9	2325.6	2665.7
	P_3	2777.8	1754.7	1929.7
	P_4	2322.4	1464.7	1570.7
	P_5	1992.3	1234.7	1272.4
	A_2	900.7	514.4	533.4
Shearing stress (tf)	A_1	426.6	47.3	49.4
	P_1	345.1	200.0	186.2
	P_2	286.5	165.0	206.9
	P_3	238.5	140.8	162.6
	P_4	218.3	129.5	146.1
	P_5	218.6	128.2	138.2
	A_2	146.8	101.6	90.8

In all points, design results of the Seismic Coefficient Method are less than that of the Dynamic Analysis.

Fig. 17 shows the acceleration response at P_1 pier obtained through the Time History Analysis. From these results, we confirmed that the application of Menshin Design is able to distribute the horizontal seismic force and simultaneously reduce the seismic horizontal acceleration of superstructure, which can remarkably enhance the safety of structures.

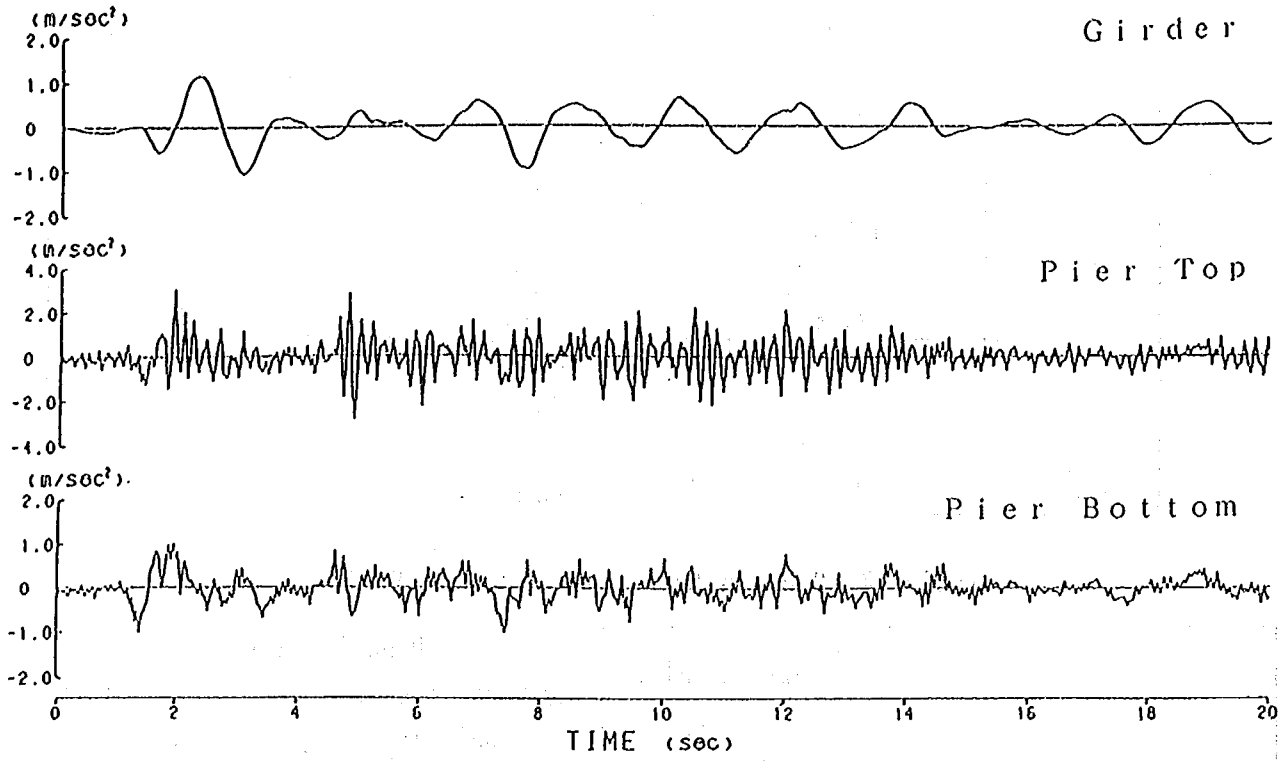


Fig. 17 Acceleration Response at P_1 pier

CONCLUDING REMARKS

A short report on the Menshin Design has been given in this paper. If this paper can help engineers, as a useful reference, in the planning for the application of the Menshin Design, which will become more common in the future, it would be our great pleasure. We have the plan of the vibration test on the actual bridge. We would like to report the result of the test, at next chance.

ACKNOWLEDGMENT

In conclusion, we would like to express our sincere gratitude to the many concerned staff members of the Public Works Research Institute, and to the Road Bureau in the Ministry of Construction including Dr. Kawashima K and Mr. Unjo S of the Public Works Research Institute of Ministry of Construction, who gave us a kind guidance and encouragement for the designing and construction of the Yamaage Bridge. We also hope that they will give us further assistance and guidance. We thank you very much for all of your help.

REFERENCES

1. Japan Road Association : Design Specifications for Highway Bridges, part I~V, February 1990 (in Japanese)
2. Technology Research Center for National Land Development : Guidelines for Base Isolation of Highway Bridges (Draft), March 1989 (in Japanese)
3. Ikeda T, Ozeki k, Kumakura K, Abe N : Design of the Karasuyama No.1 Bridge (Base Isolated Bridge), Bridge and Foundation Engineering, Vol.25, No.6, June 1991 (in Japanese)
4. Ikeda T, Kumakura K, Tani H, Abe N : Plan and Design of the Karasuyama No.1 Bridge, Bridge Engineering, Vol.27, No.6, June 1991 (in Japanese)
5. Matsuo Y, Hara K : Design and Construction of Miyagawa Bridge (First Menshin Bridge in Japan), The 1st U.S-Japan Workshop on Earthquake Protective Systems for Bridges, December 1991 (in U.S.A)

TWO SHAKE TABLES EXPERIMENTAL STUDIES OF THE EFFECTIVENESS OF DAMPING-AUGMENTATION DEVICES IN CABLE-STAYED BRIDGES

by

Ahmed M. Abdel-Ghaffar
Sami F. Masri, and
Hosam-Eddin Ali

Department of Civil Engineering
University of Southern California
Los Angeles, California 90089-2531
USA

ABSTRACT

In this study, the seismic response characteristics of a 1:100-scale model of a cable-stayed bridge (similar to the PC Yobuko cable-stayed bridge in Japan) with and without supplementary added hysteretic dampers are studied utilizing the USC dual shake tables and the model was subjected to uniform and non-uniform ground motion shakings in the transverse direction of the bridge. The experiment demonstrated the response improvements possible in earthquake-resistant bridges through the use of energy absorbers. Moreover, it is shown that an optimum model of the seismic performance of the bridges with these passive control devices can be obtained by balancing the reduction in forces along the bridge against tolerable displacements. Thus it is concluded that appropriate locations and hysteretic energy-dissipation properties of the devices can achieve significant reduction in seismic-induced forces and relatively better control of displacements. In addition, proper selection of the location of the control system can help redistribute forces along the structure which may provide solutions for retrofitting some existing bridges; however, caution should be exercised in simulating the device response for a reliable bridge structural performance.

INTRODUCTION

The increasing popularity the increase in span length of cable-stayed bridges, combined with the trend to more shallow or slender stiffening girders, has raised concern about their behavior under environmental dynamic loadings, such as traffic, wind, and earthquake loadings; thus it is essential to understand and realistically predict their structural response to these loadings.

The response of a cable-stayed bridge to applied loads is highly dependent on the manner in which the bridge deck is connected to the towers. If the deck is swinging freely at the towers, the induced seismic forces will be kept to minimum values, but the bridge may be very flexible under service loading conditions (i.e., dead loads and live loads). On the other hand, a rigid connection between the deck and the towers will result in reduced movements under service loading conditions but will attract much higher seismic forces during an earthquake. Therefore, it is important to provide special bearings or devices at the deck-tower connections to absorb the large seismic energy and reduce the response amplitudes. These devices should be dimensioned so that they provide an adequate stiffness high enough to produce acceptable performance under day-to-day service conditions, yet soft enough to prevent high seismic inertial forces from being transmitted to the towers from the deck. These devices, which can be used to retrofit existing structures, should also constitute a multi-defense line; that is, they should be composed of different tough structural sub systems which are interconnected by very tough structural elements. While there are many applications to tall buildings supplementary damping devices to reduce wind- and earthquake-induced vibrations, the possibility of using energy-dissipating devices to improve wind and earthquake resistance of bridges in general, and cable-supported bridges in particular, is a more recent development. The aim of including energy absorbers is to concentrate hysteretic behavior in especially designed and detailed zones of the structure and to avoid inelastic behavior in primary structural elements.

THE TEST FACILITY: DUAL SHAKE TABLE

The instrumented reduced-scale (1/100) model of the cable-stayed bridge was shaken by the newly acquired two USC shake tables (manufactured and constructed by MTS; see Figs. 1 and 2). Each Uni-directional table, which is 4 ft ˣ 4 ft (1.22 m ˣ 1.22 m) and separated by 12 ft. (3.70m) with synchronous or independent motions, is capable of moving with a maximum displacement strock of ± 2 inches (± 51 mm), a maximum velocity of ± 35 in/sec. (± 88.9 cm/s) and a maximum acceleration of 4g. The operating frequency is 0.0 to 50.0 Hz and the table mass is 800 lbs (363.20 kg); the maximum specimen mass is 450 lbs (204.30 kg). The maximum overturning moment (Max OTM) specification is 10,000 ft-lb. (13,563.60 m-N) which is sufficiently high so that the center of gravity of a 400 lb (182.60 kg.) specimen can be elevated 6 ft (182.88 cm) above the table surface and excited to 4 g. The two shake tables are constructed on a sufficiently large reaction mass to isolate the system loads from the rest of the building. The design foundation interface required a massive and heavily reinforced concrete foundation block of 10 ft. (3.0n) in depth and 10 (3.0m) ft. by 24 ft. (7.3m) in horizontal dimensions. Moreover, a large 2 inch thick steel base plate is placed under each table system to spread the load over a larger area and simplify the foundation interface design problem. In addition, USC has data reduction and instrumentation capabilities for rapid playback and evaluation of the 16-channel test data; data acquisition and processing capabilities provide complete post-test computer evaluation.

THE BRIDGE MODEL

It was considered desirable that the reduced (1/100 scale) bridge model simulate a typical contemporary cable-stayed bridge. The prototype bridge selected was the Yabuko Bridge (in Japan), which is a three-span continuous prestressed concrete bridge which has a 250m long main (center) span and has two 121.0m side spans with bridge width of 10.9m and pier height of 103.6m.

The length scale choice of 1/100 was determined from the total length of the prototype bridge and the available space of the shake tables. Not every detail of the bridge model can be reproduced from the prototype to the same scale. The fabrication of the model was made in house (at relatively smaller cost); suitable structural parts for the boundary conditions were commercially available and the connections were simple, albeit elaborate, to manufacture by the USC Machine Shop. The support details and the overall dimensions of the model are given in Figs. 2,3 and 3). The model is designed in such a way that the change of these various configurations can be made without affecting the basic structural system of stiffening beams and cables. A lumped mass system simulating the dynamic properties of the prototype structure was accomplished by adding steel blocks at discrete locations. There is one central spine that carries the vertical and lateral bending stiffness while the torsional stiffness is simulated by a C-shaped channel. The deck-tower and the deck-pier connections were designed to be either free (floating), hinged or fixed.

Piano wires with diameter of 0.50 mm were used as cables. Special mounting devices, as shown in Figs. 3, 6, 9 and 10, were used to anchor the cables at the tower in order to adjust cable tension. Several masses were attached at the different points of each cable to observe and capture local and nonlinear cable vibration. The cable tension due to dead-weight was calculated by an analytical model which provides valuable information regarding the natural frequencies of vibrating cable. The cable tension actually developed in the model was so adjusted to match with the computed values within the difference of ±10%.

For making the tower, two steel rods (with hollow box section) are rigidly fixed to a steel supporting plate, and two lateral members were attached to the top and at an intermediate height of the tower. The tower of gate type frame is very similar to the prototype. The position of holes for mounting the cables at the tower can be changed depending on the geometrical configuration of the cable system. For modeling the deck, an aluminum bar of one inch in width was used as shown in Figs. 2 and 3. Lateral members were attached at 10.5 inch intervals. Holes for attaching cables were provided in the shank of the screw connecting the lateral members and dead weights were placed (Figs. 2,6 and 7) to match the mass ratio.

The bridge model was installed on the two shake tables in such a way that the abutment-deck and the adjacent tower-deck connections are installed on one table. With this configuration, it was assured that any model vibrations were due to similar ground motion on one side of the bridge or different ground motion on the other side of the bridge.

TEST SETUP AND EXPERIMENTAL PROCEDURE

Figure 4 shows the locations of the proximity transducers with respect to the model. The transducers were arranged such that the sum of their outputs was proportional to the bending amplitude and the difference between their outputs was proportional to the torsion amplitude.

Rather than measuring the cable tensions directly, an alternate technique was employed. The desired values of model tension for each cable were known, and so the frequencies of each cable could be computed using vibrating string theory. Several methods were employed in the attempt to measure the natural frequencies of the cables. Cable tuning, which was done after each experimental run, was a time consuming iterative procedure since the deck/cable/tower system has strong interaction. During testing, the cable frequencies were checked occasionally, but no significant changes had occurred.

The analog outputs from the transducers were low pass filtered and fed to the data acquisition system. Data was acquired at 300 samples per second. A typical run consisted of sampling for one minute for the random excitation, 39 seconds for the 1979 earthquake, 54 seconds for the 1940 earthquake, 22, 24, and 48 seconds for the 3 level Japanese earthquakes. Relative displacement were recorded (with a very simple scale and pointer) between the moving deck and the tower or substructures.

DYNAMIC CHARACTERISTICS OF THE MODEL AND PROTOTYPE

Prior to the earthquake shaking, free vibration tests were carried out to identify the dynamic characteristics of the model with different support conditions. In the analysis, six different combinations of support schemes, as shown in Figs. 5 and 6, are considered. Shown in Figure 6 are the natural periods for 20 modes of the six cases. It can be noticed that allowing the deck to swing freely at the towers (case 5) adds more flexibility to the overall behavior than providing rollers at the abutments with a rigid deck-tower connections (cases 1 and 2). A significant change in dynamic properties is also clear in case 6 (Fig. 10). The calculated natural frequencies of case 5 (deck free at the tower and free at the abutment) match well with measured natural frequencies of the bridge model without the hysteretic dampers (Figs. 3 and 8. Moreover, the calculated natural frequencies of case 6 (deck and abutment with dampers) match well with measured natural frequencies of the bridge model having the hysteretic dampers installed at the deck-tower and the deck-abutment connections (see Fig. 9).

The dampers exhibit elliptical hysteresis loops (Fig. 9), typical of materials with velocity-dependent properties. The loops are regular in shape and show stable behavior. These dampers have no threshold or activation force level, and thus they dissipate energy at all levels of earthquake excitation.

TEMPORAL AND SPECTRAL ANALYSES OF THE RECORDED DATA

To assess the effects of uniform and nonuniform earthquake ground motions on the behavior of the bridge, the experiment was performed using the following earthquake simulations: (1) Random Excitation (Uniform Motion) (2) Imperial Valley Earthquake of 1979 (Nonuniform Motion) (3) El Centro Earthquake of 1940 (Uniform Motion) (4) Japanese Earthquake: Level 1 (Uniform Motion) (5) Japanese Earthquake: Level 2 (Uniform Motion) and (6) Japanese Earthquake: Level 3 (Uniform Motion)

The two configurations of the model structure (i.e. with and without the dampers) were also subjected to vibration (pull-back), tests.

CONCLUSIONS AND RECOMMENDATIONS

Experimentally, the seismic response characteristics of a 1:100-scale model of a cable-stayed bridge (similar to the PC Yobuko cable-stayed bridge in Japan) with and without supplementary hysteretic dampers are studied utilizing the "USC dual shake table system. Each side span (with the tower and anchor-pier) is supported on one table. The major emphasis of the experiments and measurements is placed on the effectiveness of these dampers. The shaking was in the lateral (transverse) direction, however large order of magnitudes of the longitudinal response were recorded.

From this experimental study, which has demonstrated the response improvements possible in earthquake-resistant cable-stayed bridges through the use of energy absorbers of the hysteretic type the following concluding remarks can be drawn:

1. In general the dynamic response of the bridge model is characterized by: the relatively (compared to the model dimensions) large displacements, the multi modal contributions (Fig.), the three dimensionality of the structure, and the cable vibration (both individually and dynamically coupled with the deck and tower).

2. Although the recorded (row) motions were acceleration and dynamic strain time histories it is extremely crucial that integrated velocity and displacement time histories or the computed input-output kinetic and strain energies should be utilized before any quantitative and precise analysis of the collected data. Because of the constraints of limited resources and strict time deadlines, such integration was not completely done for all records. Only a few cases were made to provide general conclusions addressing the effectiveness of the dampers in terms of reducing the earthquake-induced straining action and limiting the unacceptable displacements.

3. From the simple devices which were used at the tower-deck and the pier-deck connections to measure the maximum considerable reduction of the relative displacement of the two moving parts was obtained. Table 1 shows the approximate peak-response values provided by these simple devices (consists of scale, pointer).

4. It is shown that an optimum model of the seismic performance of the bridges with these passive control devices can be obtained by balancing the reduction in forces along the bridge against tolerable displacements. Thus it is concluded that appropriate locations and hysteretic energy-dissipation properties of the devices can achieve a significant reduction is seismic-induced forces, as compared to the case with no dampers added, and relatively better control displacements. In addition, proper selection of the location of the control system can help redistribute forces along the structure which may provide solutions for retrofitting some existing bridges. However, caution should be exercised in simulating the device response for a reliable bridge structural performance. Moreover, while seismic response of the bridge can be significantly improved with added dampers, their degree of effectiveness also depends on the energy absorption characteristics of the dampers.

ACKNOWLEDGMENT

This research was supported by a grant from CUREe (California Universities for Research in Earthquake Engineering) and Kajima Research Institute; this support is greatly acknowledged. The assistance provided by the USC lab technicians, staff, and graduate students are appreciated.

REFERENCES

1. Abdel-Ghaffar, A.M., Masri, S.F., and Ali, H.-E., "Passive Control of Highway Structures: Two Shake Tables Experimental Studies of the Effectiveness of Damping-Augmentation Devices in Cable-Stayed Bridges," a report to CUREe-Kajima Research Project, USC Dept. of Civil Eng., Aug. 1992.

2. Abdel-Ghaffar, Ahmed M. and Khalifa, Magdi A., "Importance of Cable-Vibration in Dynamics of Cable-Stayed Bridges," Journal of Engineering Mechanics, ASCE, Vol. 117, No. 11, November 1991, pp. 2571-2589.

3. Ali, Hosam-Eddin M., "Nonlinear Seismic Analysis of Cable-Stayed Bridges with Passive Energy Dissipation devices," Ph.D. Thesis, Department of Civil Engineering, Univ. of So. California May 1991.

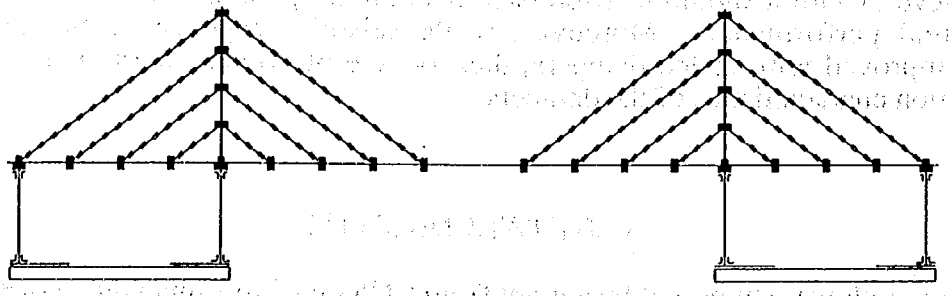
4. Abdel-Ghaffar, A.M. and Ali., H.M., "Energy Dissipation Devices for Cable Stayed Bridges", In the Second Workshop on Bridge Engineering Research in Progress, pages 221-224, Reno, Nevada, 1990.

5. Nazmy, A.S. and Abdel-Ghaffar, A.M., "Nonlinear Earthquake-Response Analysis of Long-Span Cable-Stayed Bridges", Theory. Earthquake Engineering and Structural Dynamics, 19:45-62, 1990.

6. Kajima Corp., "Earthquake Resistant Design Method of Prestressed Concrete Cable-Stayed Bridges in Japan", CUREe-Kajima Joint Project; C-1, Report by Kajima Corporation, May 1991.

7. Kawashima, K., Unjoh, S. and Tsunomoto, M., "Damping Characteristics of Cable-Stayed Bridges for Seismic Design," Report Published by Public Works Research Institute, Japan Ministry of Construction, Vol. 27, Journal of Research (PWRI), December 1991.

Measured Relative Displacements
(Between Deck and Abutment; and Deck and Tower)



	Earthquake Excitation	Direc-tion	Without Dampers				With Dampers			
			Abutment	Tower	Tower	Abutment	Abutment	Tower	Tower	Abutment
1	1979 Imperial Valley E.Q. Array #. 5,6	L T	±5 ±8	±2 ±8	±2 12, 3	±2 ±8	0 ±1	±2 ±1	±0.5 ±0.5	0 ±1
2	1940 El Centro Earthquake	L T	±4 ±32	±2 ±24	4, 2 36, 28	3 16	±2 ±2	±4 ±4	±4 ±4	±2 ±4
3	Japanese Earthquake Level 1	L T	±4 ±16	±2 ±16	3, 2 28, 4	±4 ±16	±1 ±1	±1 ±4	±4 ±2	±1 ±1
4	Japanese Earthquake Level 2	L T	±2 ±32	±8 ±20	3, 1 12, 16	±8 ±16	±1 ±2	±4 ±4	±6 ±5	±1 ±3
5	Japanese Earthquake Level 3	L T	±2 ±16	±2 ±16	±2 12, 8	±9 ±16	±1 ±2	±2 ±6	±2 ±1	±0.5 ±1
6	Random Motion	L T	±6 ±10	±3 ±9	±4 ±7	±5 ±9	±1 ±1	±1 ±1	±2 ±2	±0.5 ±2

L = Longitudinal Direction
T = Transverse Direction
Units are 1/32 of an inch

Fig. 1 General schematic diagram showing the bridge model, the USC two shake tables and the data acquisition system.

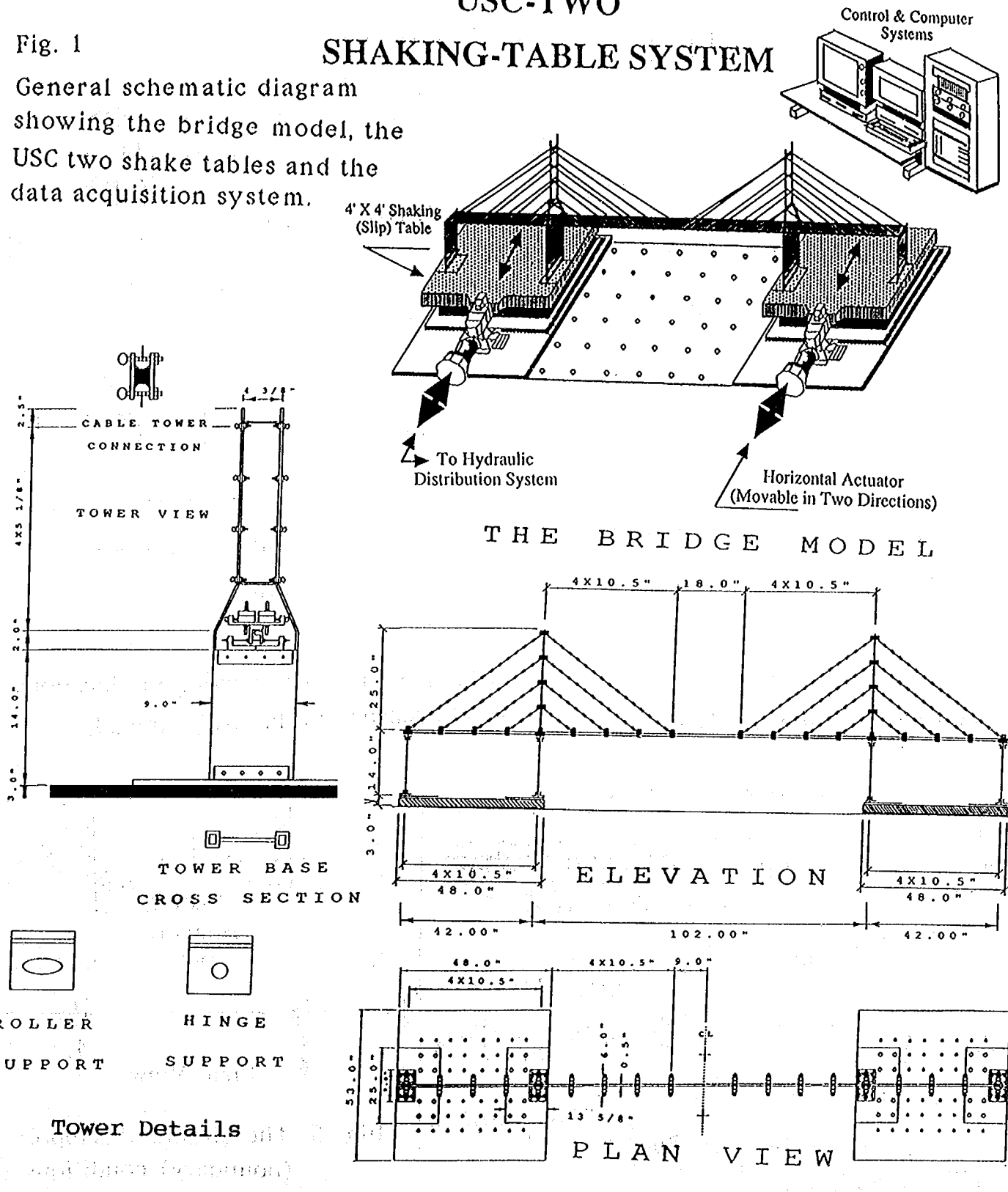


Fig. 2 Structural details and dimensions of the 1/100 reduced-scale bridge model.

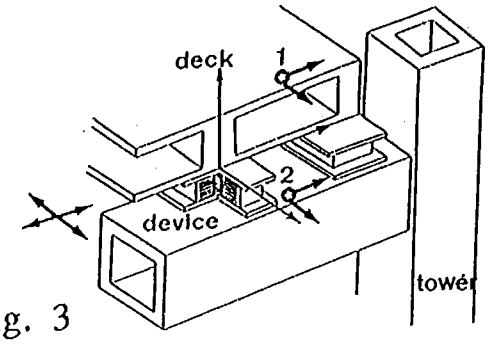
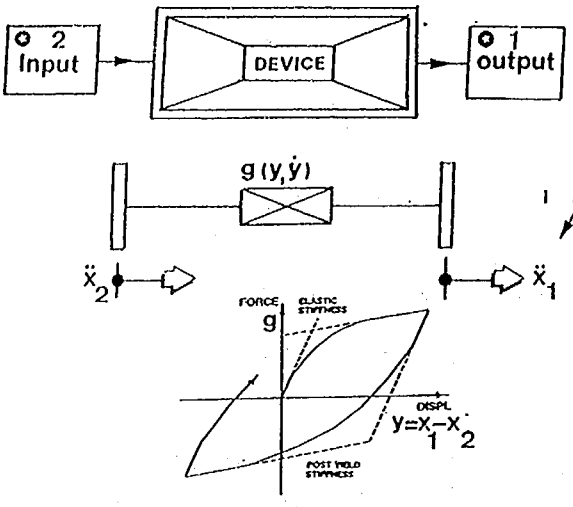


Fig. 3

Sketch showing the tower-deck connections with the hysteretic energy- dissipation bearings.



Hysteretic-Type Device

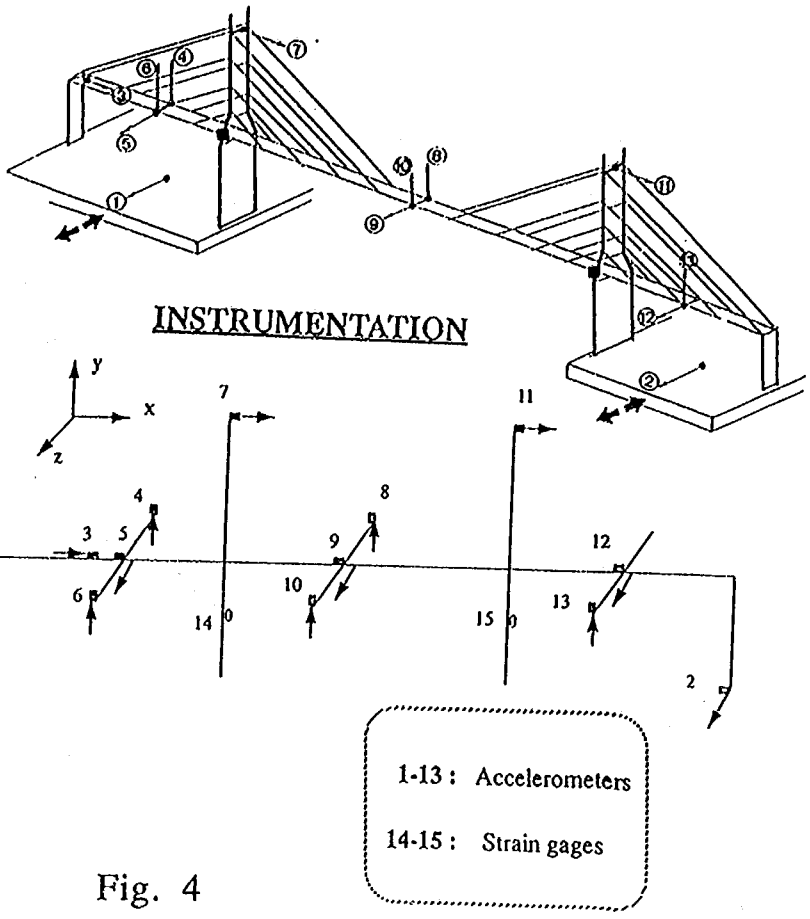


Fig. 4

Schematic diagram showing the locations of the sensors on the bridge model.

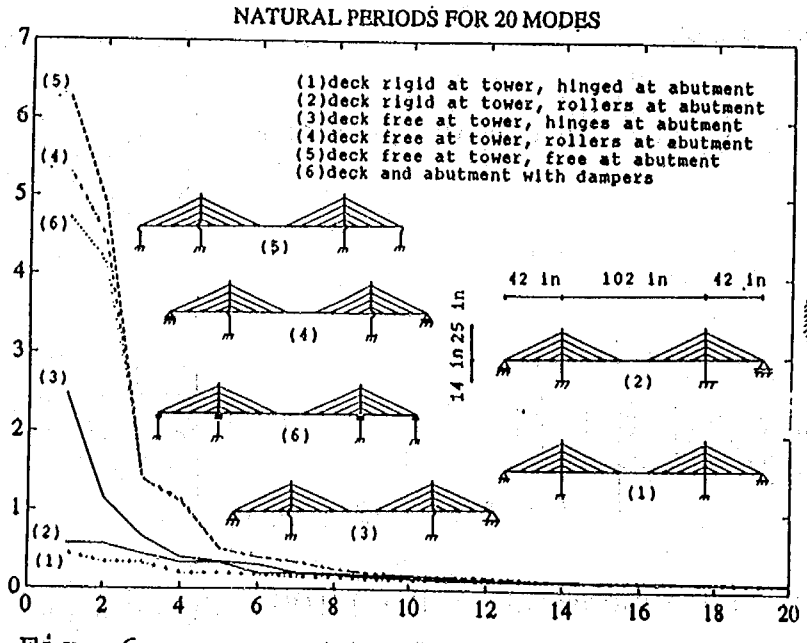


Fig. 6

Effect of support conditions on natural period of cable- stayed bridges

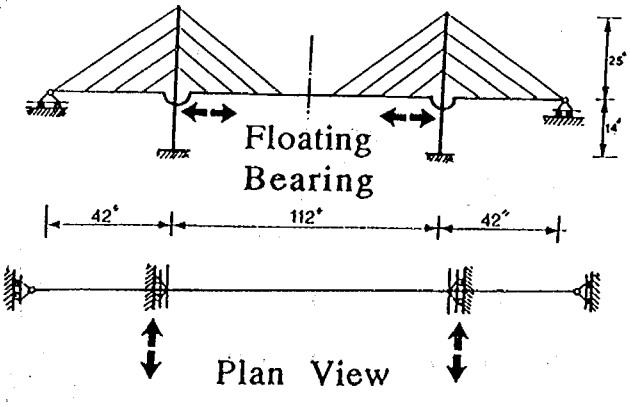
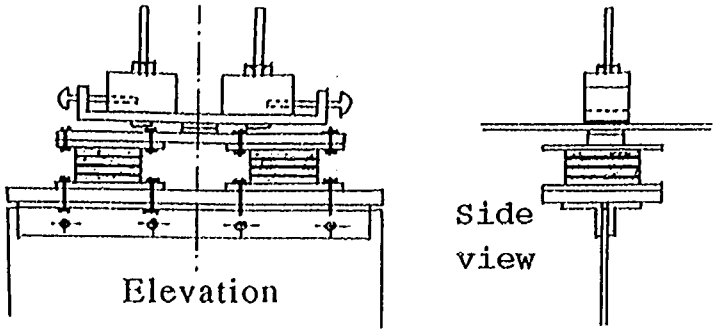
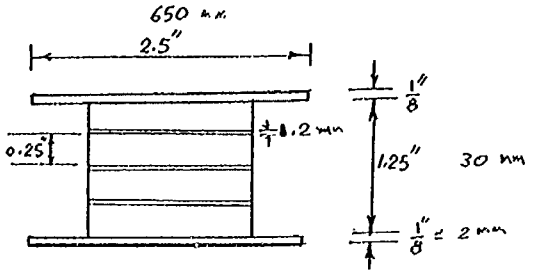


Fig. 5 The structural support (boundary) conditions of the floating connections



Pier-deck connection with damper



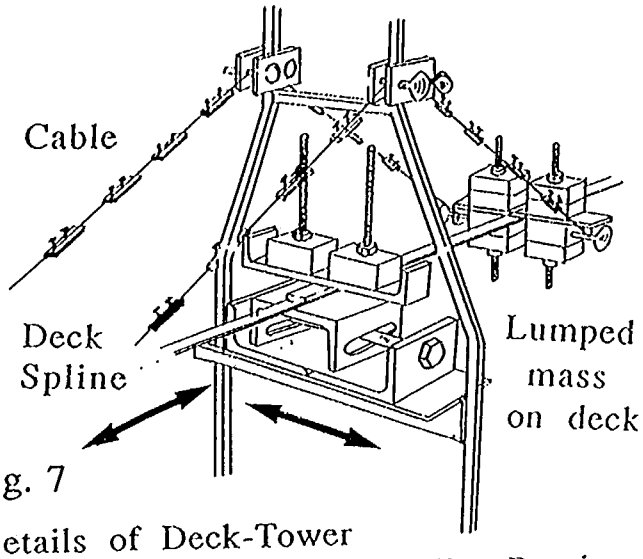
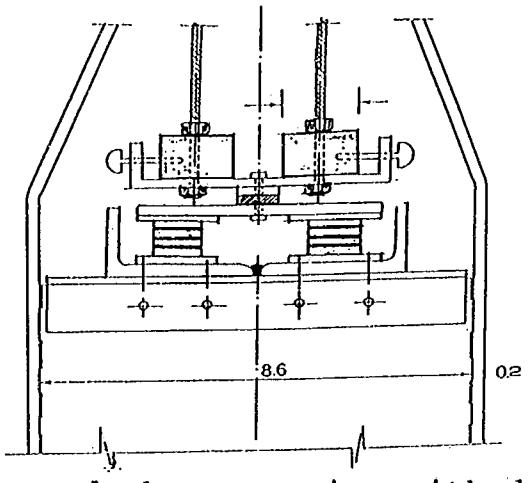
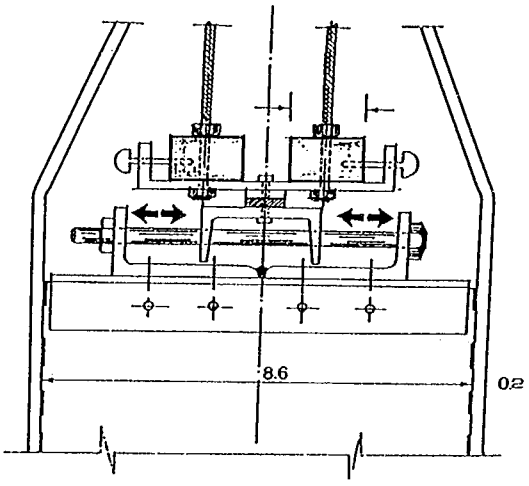


Fig. 7

Details of Deck-Tower Connection (Floating or Roller Bearings)



Tower-deck connection with damper



(floating or roller bearings)

Elevation of the Deck-Tower Connection

Fig. 8 Sketch showing the tower-deck and the pier-deck connections with the hysteretic energy-dissipation bearings.

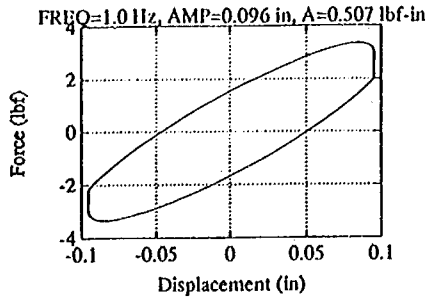


Fig. 9 A typical hysteresis loop of the damper

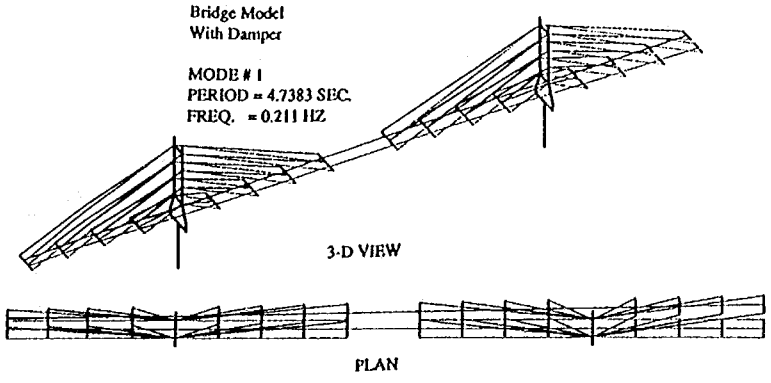


Fig. 10 Calculated first mode with damper

IMPROVEMENT OF EARTHQUAKE RESISTANCE OF PRESTRESSED CONCRETE CABLE-STAYED BRIDGES BY HYSTERESIS DAMPER

Toshimichi ICHINOMIYA[1], Tetsuo TAKEDA[1] and Katsuhisa KANDA[2]

[1] Civil Engineering Dept. I, Kajima Technical Research Institute, Tokyo, Japan

[2] Kobori Research Complex, Kajima Corporation, Tokyo, Japan

SUMMARY

This paper presents the results of an analytical study conducted in order to understand how the displacement of the girder and the bending moment of the main tower of PC cable-stayed bridges would be reduced by connecting the main girder with the main and the end piers by hysteresis dampers. It has been found that use of the hysteresis damper effectively reduces the displacement of the girder and the bending moment of the tower in comparison with floating system, and that there exists optimum stiffness and yield strength of the damper, which transmits the inertia force of the girder to the main and the end piers and absorbs hysteretic energy and reduces the response of the structure most effectively.

INTRODUCTION

Prestressed concrete (PC) cable-stayed bridges have come into the spotlight as being suited for long span bridges, and many bridges of this type are already completed or under planning at various part of the would. In order to construct PC cable-stayed bridges with longer span in seismically active regions such as Japan and United States, it is important to ensure their adequate earthquake resistant performance.

Introduction of a floating system (in which the girder is not supported by bearing supports but by stay cables only) to long-span (PC) cable-stayed bridges results in longer natural periods. This often improves their earthquake resistant performance in longitudinal direction.

In the case of floating type PC cable-stayed bridges, however, longitudinal displacement of the girder may become greater and its inertia force may be transmitted through the stay cables to the tower. The floating system, therefore, is not necessarily superior in earthquake resistant performance to a fixed system (in which the girder is horizontally connected with the main pier).

In this study, the earthquake resistant performance of a damper system (in which the girder is connected with the main and the end piers by hysteresis dampers) is compared with those of a floating and a fixed systems. Then, the damper type PC cable-stayed bridges, with various stiffness and yield strength, are analyzed.

CONCEPT OF APPLICATION OF HYSTERESIS DAMPERS

Fig. 1 shows conceptional distribution of bending moment of the tower and the main pier of a floating type and a fixed type PC cable-stayed bridges when subjected to the inertia force of the girder.

Bending moment of the tower of the floating type bridge is larger than that of the fixed type bridge because the inertia force of the girder is transmitted to the tower through the stay cables. On the contrary, the bending moment of the main piers of the fixed type bridge is larger than that of the floating type bridge because the inertia force of the girder of the fixed type bridge is larger than that of the floating type bridge.

When the girder is connected with the main piers by adequate springs, bending moment distribution of the tower and the main pier will be between those of the floating and the fixed type bridge. If the end piers can bear a portion of the inertia force of the girder, the bending moment of the tower and the main pier can be reduced by connecting the girder with the end piers by springs. Moreover, if some damping is added to the structure, the inertia force of the girder itself can be reduced.

A hysteresis damper is a spring system that is generally represented by a bilinear model and absorbs earthquake energy through looping motion.

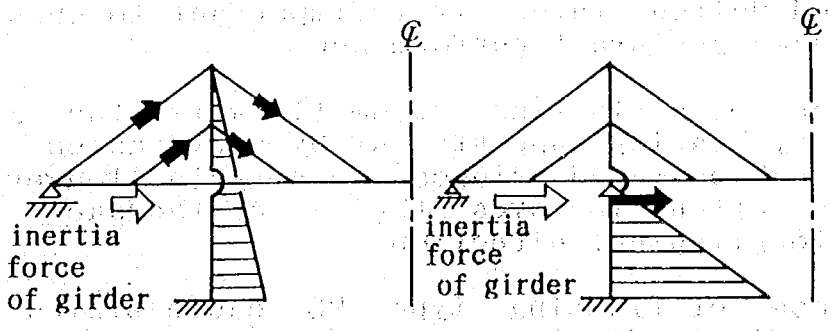


Fig. 1 Conceptional Distribution of Bending Moment of Tower and Main Pier

The goal of this study is to achieve the following effects by applying hysteresis dampers in floating type PC cable-stayed bridges, that is, to connect the girder with the main piers and the end piers by hysteresis dampers:

a) To control the displacement of the girder with the springs of the hysteresis dampers

b) To reduce the sectional force of the tower by letting the hysteresis dampers transmit part of the inertia force of the girder directly to the main and the end piers

c) To reduce the inertia force of the girder by letting the hysteresis dampers absorb earthquake energy.

In this method, the ratio between the inertia force of the girder to be imposed upon the main piers and that upon the end piers can be adjusted by changing stiffness and yield strength of the hysteresis dampers installed at the main piers and the end piers. Thus, there are various possible conditions of the sectional forces.

A lead rubber bearing and a high damping rubber bearing are two of hysteresis dampers, and have already been applied to girder bridges. In the case of PC cable-stayed bridges, the degree of freedom in the design of hysteresis dampers is high because they don't have to support the weight of the girder.

OUTLINE OF THE ANALYSIS

ANALYTICAL MODEL

A three-span continuous floating type PC cable-stayed bridge, as shown in Fig. 2, was analyzed. Table 1 shows the primary structural data of the bridge.

The bridge was modeled as a multi-mass spring system as shown in Fig. 3, and was assumed to be linear. Seventeen stay cables are modeled as four bundled cables. The basic vibration properties, however, are close to those of the prototype. Table 2 shows the structural data of the model.

Table 3 shows the results of eigen value analysis of the model, and Fig. 4 shows its vibration mode shape.

The hysteresis damper was expressed as a bilinear model as shown in Fig. 5, in which the ratio of primary stiffness to secondary stiffness was 1:10.

Table 4 shows the types of structure considered and the

corresponding mechanisms of girder connection. The stiffness of the dampers installed at the end piers was assumed to be 1/2 of that of the dampers installed at the main piers.

ANALYTICAL METHOD

A time history response analysis was performed. The standard input wave for time history response analysis (for Class I ground) defined in "Specifications for Highway Bridges, Part V Earthquake Resistant Design", was used as the input wave (Fig. 6)..

The damping of the structure was assumed to be proportional to the strain energy. A damping ratio of 5% was used for the girder, the towers and the piers, and 2% for the stay cables.

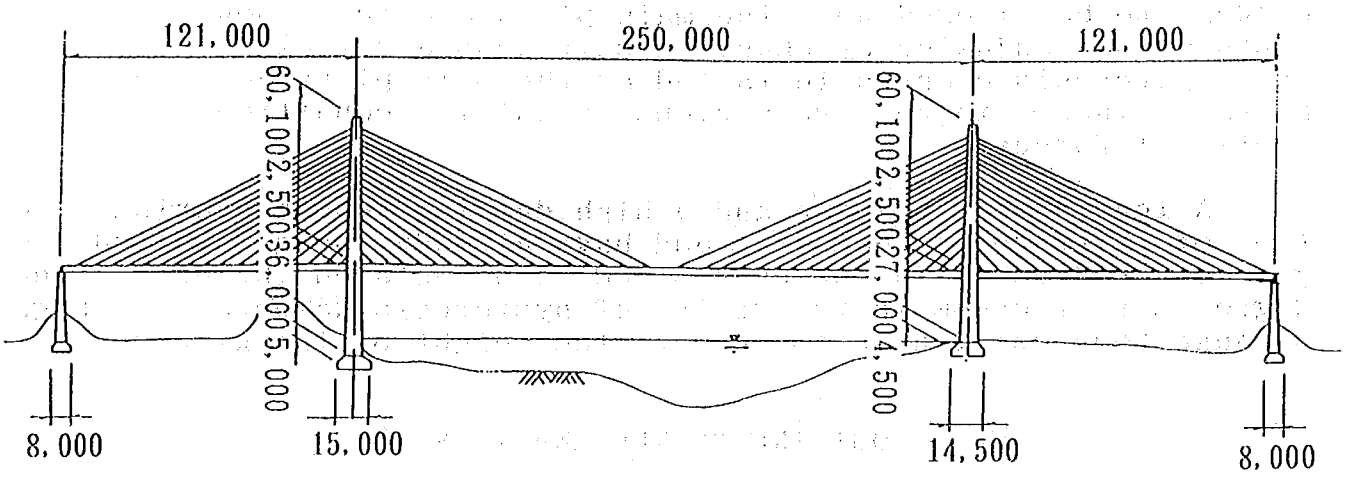


Fig. 2 PC Cable-Stayed Bridge for Analysis

Table 1 Structural Data of the Bridge for Analysis

Type of Structure	3-span continuous prestressed concrete cable-stayed bridge (floating type)
Type of Foundation	Spread foundation
Span	121.0m+250.0m+121.0m=492.0m
Effective Width	10.9m
Height of Pier and Tower	41.0m+62.6m=103.6m
Length of Stay Cables	16.1m ~135.8m

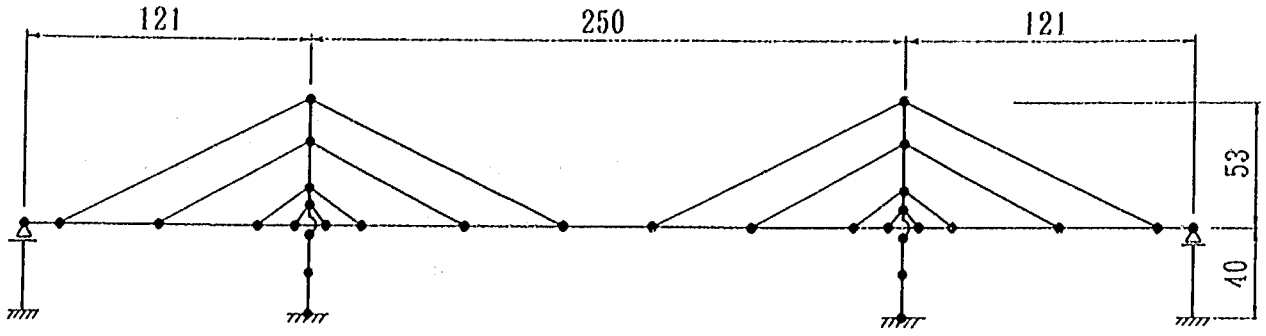


Fig. 3 Analytical Model

Table 2 Data of Analytical Model

	Young's modulus E (tf/m^2)	Sectional area A (m^2)	Geometrical moment of inertia (m^4)	Weight (tf/m^3)
Main girder	3.5×10^6	7.0	4.0	3.0
Main tower	3.5×10^6	15.0	20.0	2.5
Main pier	3.0×10^6	70.0	350.0	2.5
End pier	3.0×10^6	35.0	175.0	2.5
Stay cable (the top)	1.86×10^7	0.034	0.0	10.0
Stay cable (the second)	1.86×10^7	0.034	0.0	10.0
Stay cable (the third)	1.86×10^7	0.026	0.0	10.0
Stay cable (the bottom)	1.86×10^7	0.012	0.0	10.0

* Concentrated mass for lateral beam along the tower
  - at the top stay cable 313 tf
  - at the bottom stay cable 125 tf

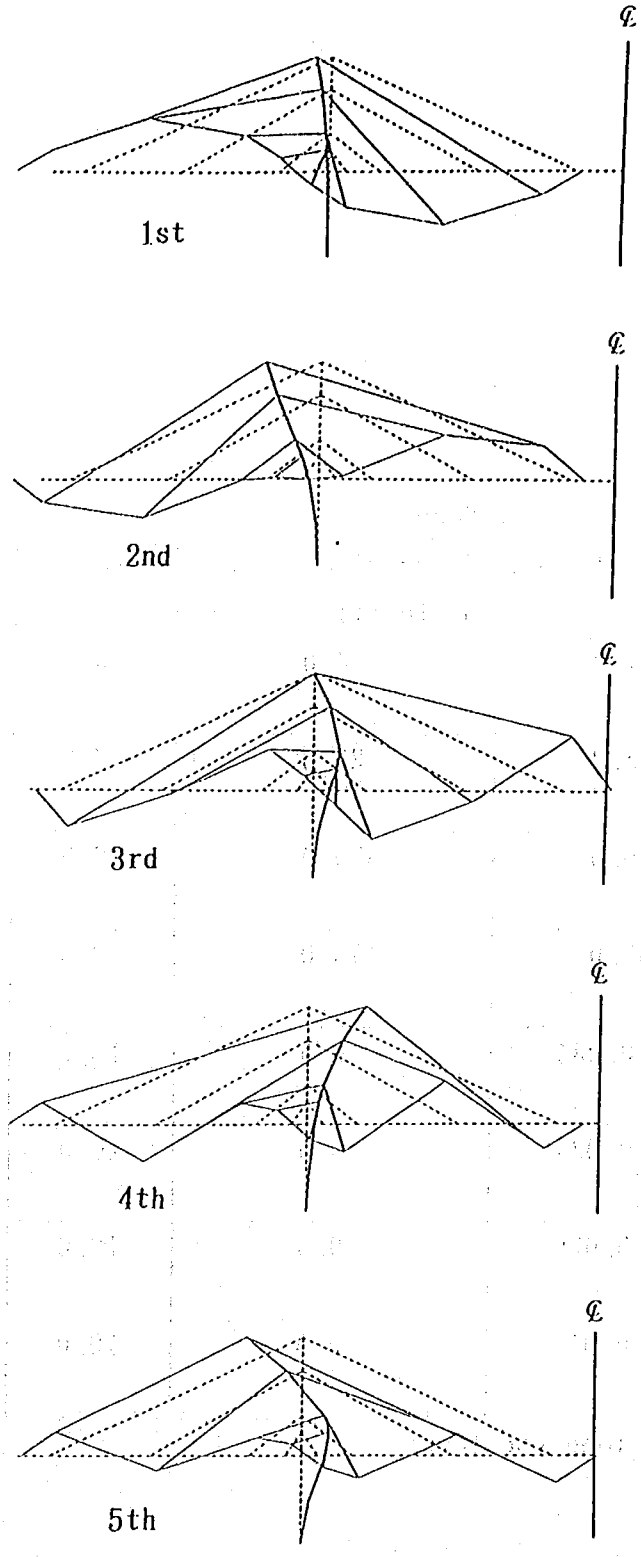
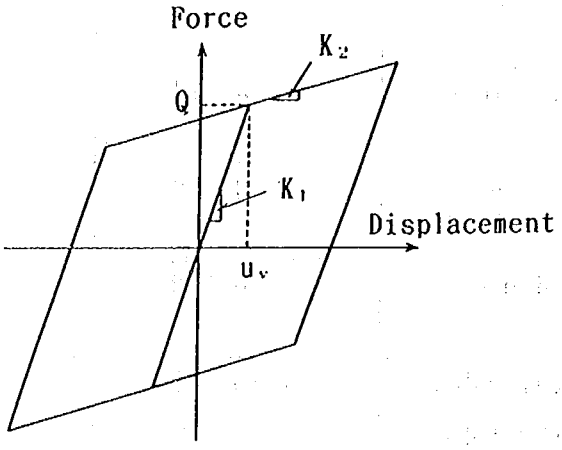


Fig. 4 Vibration Mode Shape

Table 3 Results of Eigen Value Analysis

Mode No.	Natural Period T (sec)	Participation Factor
1	3.16	0.74
2	1.75	1.13
3	0.75	0.59
4	0.41	0.19
5	0.40	0.83



u_y :Yield displacement
Q :Yield strength
K_1 :Primary stiffness
K_2 :Secondary stiffness

Fig. 5 Force-Displacement Relationship of Hysteresis Damper

Table 4 Conditions of Girder Connection

	Main Pier	End Pier
Floating system	Free	Roller
Fixed system	Pin	Roller
Damper system	Bilinear damper	Bilinear damper

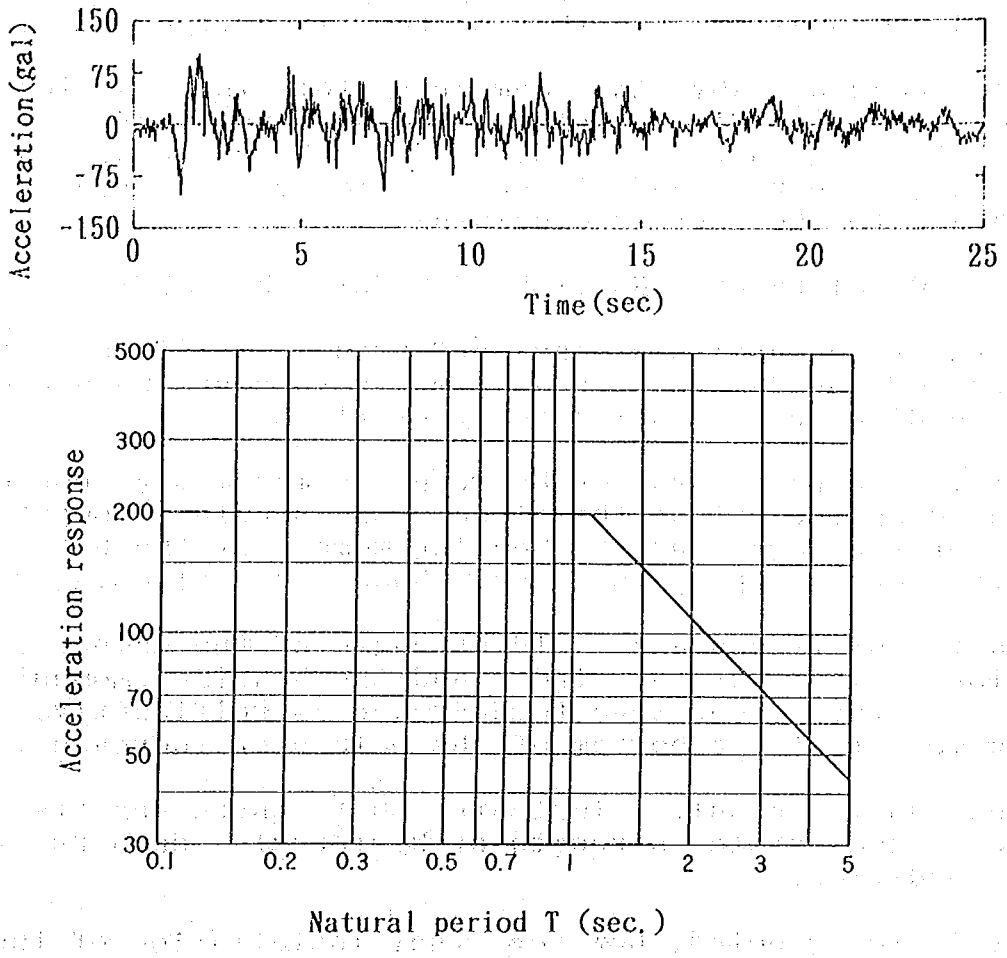


Fig. 6 Input Wave and Acceleration Response Spectrum

RESULTS AND DISCUSSIONS

COMPARISON WITH FLOATING SYSTEM AND FIXED SYSTEM

If a damper to be installed at each main pier has a primary stiffness of 200 tf/cm and yield strength of 200 tf, the maximum response of longitudinal displacement of the girder is 6.9 cm, which is approximately 63% of that in a floating type bridge(11 cm).

The distribution of the maximum bending moment of the towers and the main piers of a floating type and a fixed type bridges were compared in Fig. 7.

The bending moment of the tower of the fixed type bridge is smaller than that of the floating type bridge, and that of the damper type bridge is the smallest. The bending moment of the pier of the floating and the damper type bridges are almost the same, and are smaller than that of the fixed type bridge.

The reasons why the damper system is superior to the floating and the fixed systems are, 1) a part of the inertia force of the girder is transmitted to the end piers through the hysteresis dampers, and 2) the inertia force of the girder is reduced due to the increased damping.

INFLUENCE OF STIFFNESS AND YIELD STRENGTH OF DAMPER

Parametric analysis was performed. Stiffness and yield strength of the damper were adopted as varying parameters with the yield displacement being constant (1 cm).

Fig. 8 shows the ratios between the maximum response values of the displacement of the girder, the bending moment at the bottom of the tower and the bending moment at the bottom of the main pier for a damper system and those for a floating system.

As the stiffness and yield strength of the damper increases, the displacement of the girder and the bending moment at the bottom of the tower tend to decrease significantly, and the bending moment at the bottom of the main pier increases.

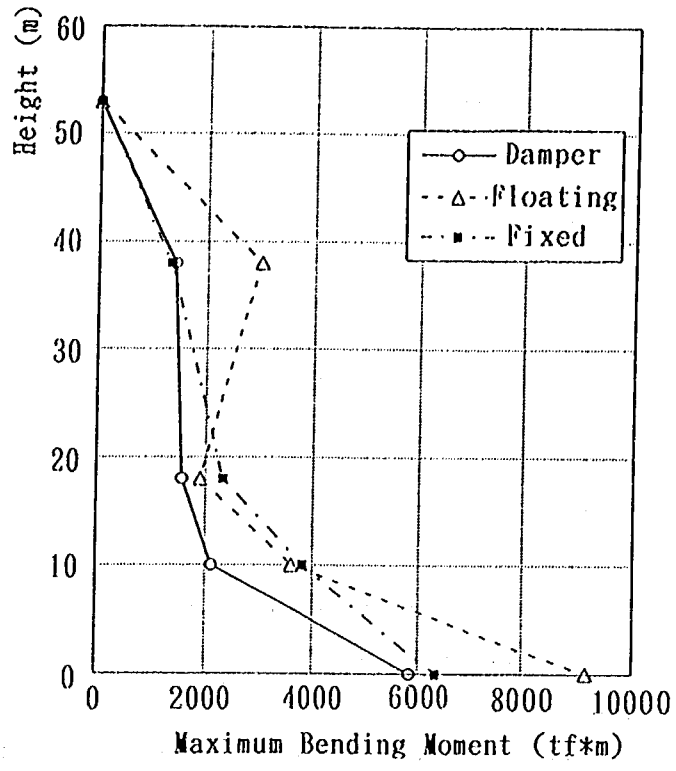
The above results indicate that there exists optimum stiffness and yield strength of hysteresis dampers for each design condition.

It is to be noted, however, that installation of the damper at the main and the end piers may result in increase of bending moment of the main and the end piers caused by creep and drying shrinkage (displacement at the end of the girder is about 10 cm) and temperature variation (displacement at the end of the girder is about 2.5 cm with temperature variation of 10 °C). It is therefore necessary to consider such influences in determining optimum stiffness and yield strength of hysteresis dampers.

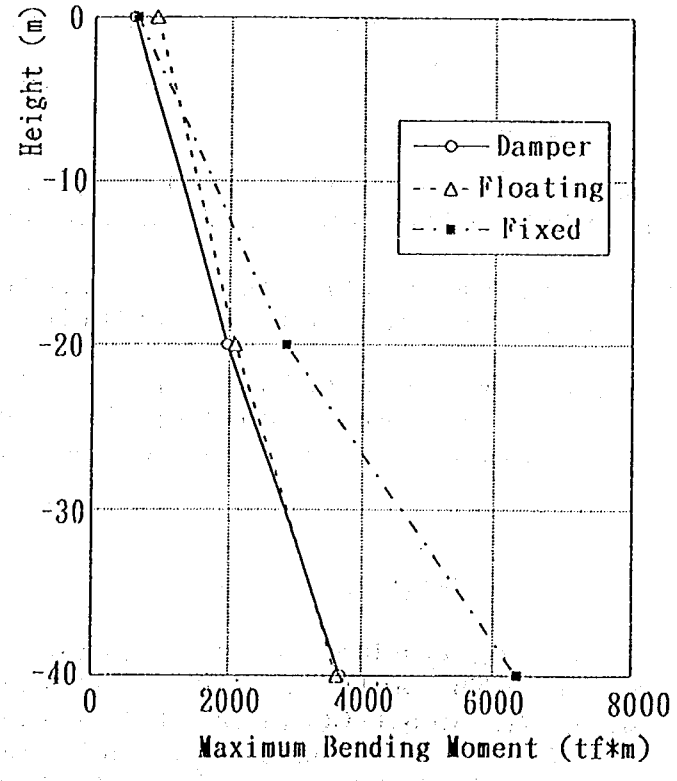
CONCLUSIONS

From above analyses following conclusions are drawn:

a) Use of hysteresis dampers improves the distribution of the



(b) Tower



(a) Main Pier

Fig. 7 Distribution of Maximum Bending Moment

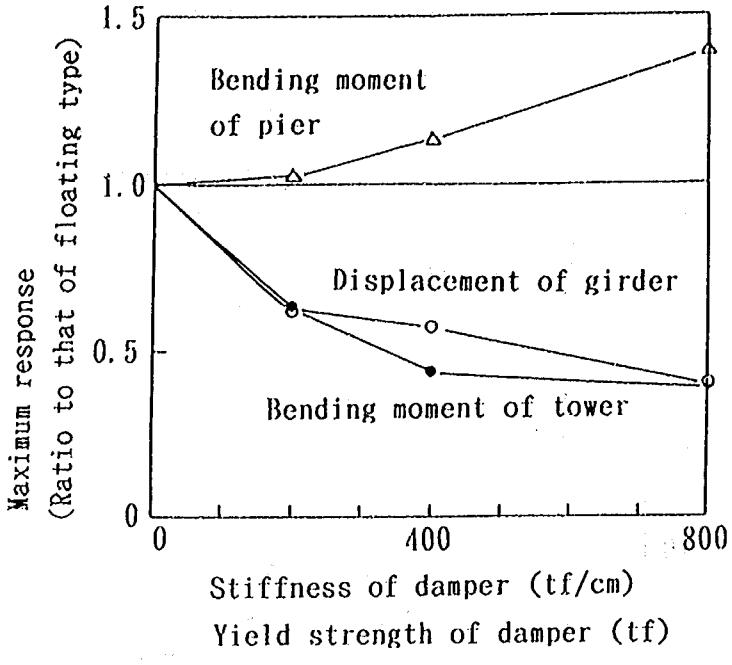


Fig. 8 Maximum Response vs.
Stiffness and Yield Strength of Hysteresis Damper

bending moment of the tower and the main pier in comparison with that of the floating type and the fixed systems, therefore, improves earthquake resistant performance of long span PC cable-stayed bridges.

b) Hysteresis dampers decrease the displacement response of the girder in comparison with that of floating type bridges.

c) There exists optimum stiffness and yield strength of hysteresis dampers for each design condition.

Following problems are now being studied: 1) the nonlinear behavior in the case of large earthquake motion; and 2) maintenance and interchange of hysteresis dampers.

ACKNOWLEDGEMENT

This study has been conducted as a part of CUREe-Kajima joint research project. The authors wish to express their hearty thanks to Professor A. M. Abdel-Ghaffar of University of Southern California, Dr. T. Kobori of Kobori Research Complex and the other members of this project for their invaluable guidance.

DEVELOPMENT OF JOINTLESS SYSTEM WITH MENSHIN BEARING FOR EXISTING SIMPLE-SPANNED STEEL BRIDGES

Toshihiko NAGANUMA, Shuji MIZOBUCHI
Maintenance Engineering Division, Maintenance & Facility Design Department,
Hanshin Expressway Public Corporation.
Hiroshige UNO
Deputy Manager of Research and Development Division, Sogo Engineering Inc. Osaka.

SUMMARY

The "Steel Girder Connecting Jointless Method" is one of techniques which have been proposed and examined in "Road Traffic Anti-vibration Measure Study Commitee" from 1987 till 1989. In this method, the seismic force run-off, dispersion and interference effects of vibration are expected by means of connecting the existing simple girders for continuance and replacing the existing bearings with elastic ones (Menshin). Furthermore, the reduction of higher harmonics caused by expansion joint as well as impact brought by travelling vehicles are aimed by the continuation of pavement. Since the service ability of the method has been convinced through analytical examinations up to now, based on the results of which a prototype indoor experiment has been carried out to check both of safety and durability for various traffic loads, its practical application for an existing bridge has been realized at this opportunity.

INTRODUCTION

As one of preventive measures against traffic vibrations and noises brought by travelling vehicles on an elevated bridge, Hanshin Expressway Public Corporation is now promoting development/research activities for so-called "Jointless Method", where the expansion joints will disappear on the travelling surface at all. The buried joint method is one of its practical fruits which can be applied for RC or PC girders with span length of 25m or shorter, and the construction works have been completed now on more than 1,000 traffic lanes, where the actual effects have been convinced so far. As for the buried joint method, the corporation is exerting itself as well to improve its workability and durability by means of practicing and repeating numerous material and working tests for modification ever since.

Meanwhile, in the case of jointless method for steel girders, a method to continue upper flange of simple I-girders and RC floor slab and to pave continuous pavement has been used. In this case, taking earthquake into consideration, it is constructed so as to attain even distribution of lateral seismic force by replacing the existing fixed bearing with a movable one,

and by fitting a viscous oil damper. It is designed to function as a simple girder for live loads, and on the behaviour for the temperature fluctuation, it is intended to work as if it was a continuous beam.

This method is featured by minimizing structural modification for the existing simple girder as possible to facilitate the work execution, and its practical execution results have been enjoyed for three bridges as a matter of fact. However, it was found to be rather difficult to adopt the method for a routine regulated work because it did require not only a large scale chopping work for floor slab with big working noises but also a long working term, which caused problems to be solved.

It is the very "Steel Girder Connecting Jointless Method" to liquidate those problems and to promote the mitigation of vibrations and noises still more, which we had a chance to apply for in-service routes last year. The text presents the outline of "Steel Girder Connecting Jointless Method".

OUTLINE OF STEEL GIRDER CONNECTING JOINTLESS METHOD

This is, as shown in Fig.1, a method to connect adjacent main girder-ends with splice plates and simultaneously to replace the rigid bearing with the elastic one to continue the pavement alone. Key points of this method are as follows:

① Connection of adjacent main girders enables to reduce deflection angle at girder-ends and to distribute the load to respective adjacent main girders at the same time, which mitigates the lower harmonics eventually by bringing vibration nature close to continuous girder. (Continuation)

② Removal of joints and continuation of pavement liquidate surface inharmony to mitigate higher harmonics. (Jointless)

③ Replacement of the existing rigid bearing with the elastic one prevents fatigue failure of splice plates and integrates those adjacent two bearings into a unit so as to function as a support for the continuous girder. Furthermore, a decrease of seismic inertia force has been contrived by means of Menshin bearing, and the anti-seismic property has been improved eventually. (Elastic <Menshin> Bearing)

This method is a technique, of which a hint was received from connecting continuous beam of precast segmental pretension T-girders, and the construction designing viewpoints to connect and to continue in-service steel simple girders are as follows:

① Since overall dead load is supported by simple girders as it is, no camber adjustment is required.

② The negative bending moment at the intermediate support caused by live loads in continuous beam system is so small that the continuation can be attained only by connecting adjacent steel girders.

③ Since the connection is restricted to steel girders, no unnatural force is yielded to slab concrete.

④ Since the intermediate supports are replaced with elastic bearings, it does not restrain girder rotation.

⑤ Similarly, it does not restrict girder expansion as well.

⑥ Application of Menshin bearing enables to reduce seismic inertia force and to decrease the number of fixed piers.

Taking the case of connecting three simple girders, the structural systems for superstructure and substructure may change as shown in Fig.2 and 3 respectively.

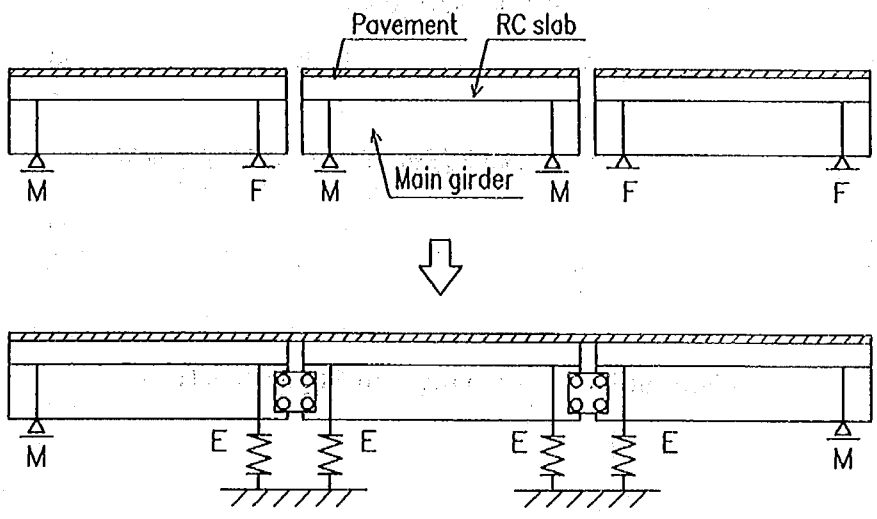


Fig.1 Concept of Connecting Jointless Method

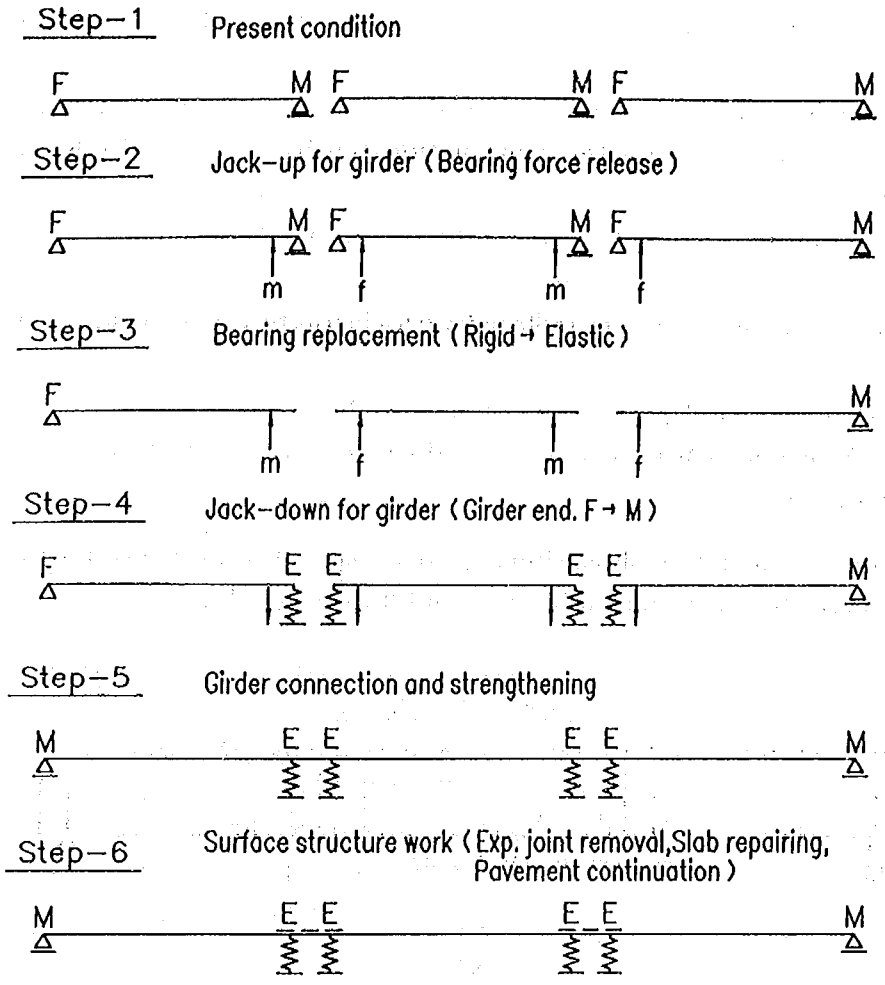
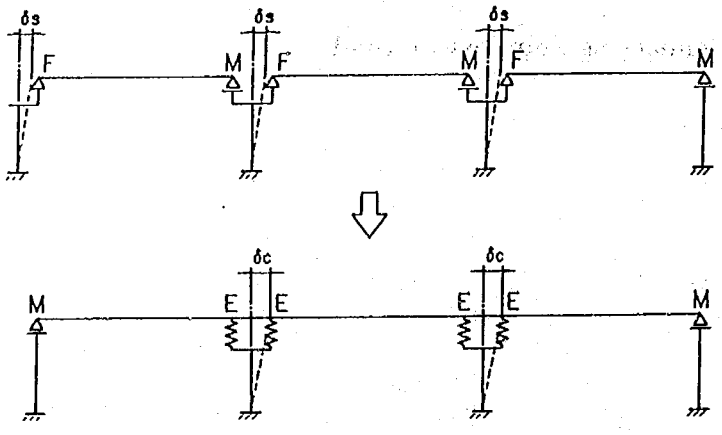


Fig.2 Structural Changes in Superstructure



Due to anti-seismic design for simple girders, the superstructure has been fixed by three piers, however, it can be changed to an intermediate two pier fixing.

The weight of superstructure affecting to fixing piers increases up to one and a half times, with which the reduction in response acceleration attained by Menshin bearing can cope.

Fig.3 Structural Changes in Substructure

IN DOOR EXPERIMENT WITH PROTOTYPE MODEL

Two kinds of joint construction, Type-A and Type-B were provided for the experimented girder as shown in Fig.4. The restrictions of experimental equipments allocated an overall length of approx. 7.4m for the experimented girder, which was connected by means of "Torshear type high strength bolts" (M22) after it had been carrid in laboratory. SS400 materials have been used for base metal and switch clip, and upper flange: 320x19mm, lower flange: 280x19mm and web: 1700x9mm have been applied. And for floor slab, those of 1500mm width, 210mm thickness and 51mm haunch height have been used. As for the used concrete, the compressive strength was 470kgf/cm^2, tensile strength: 38kgf/cm^2 and Young's modulus E=281,000kgf/cm^2.

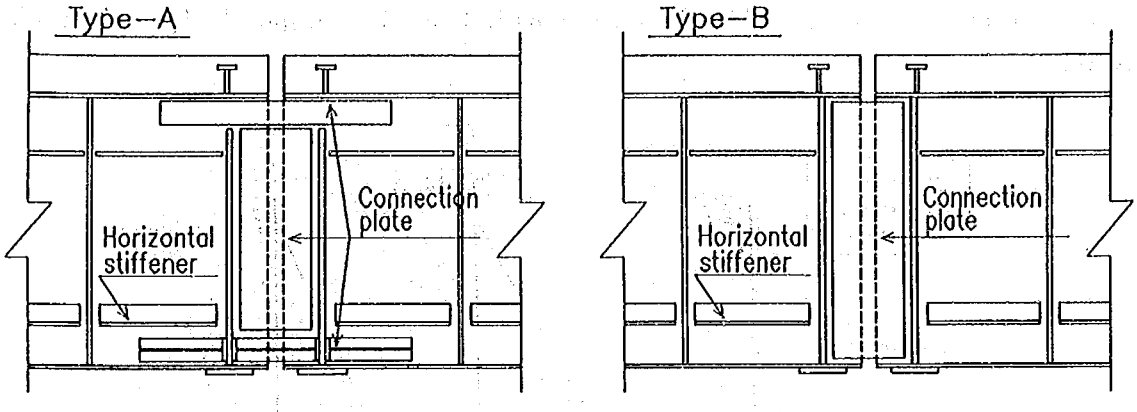


Fig.4 Joint Construction of Experimental Girder

Fig.5 illustrates the load bearing method for the experimental girder. Rigid bearings have been used both for the intermediate support and the reaction support in the experiment, which has been practiced with statically determinate structures.

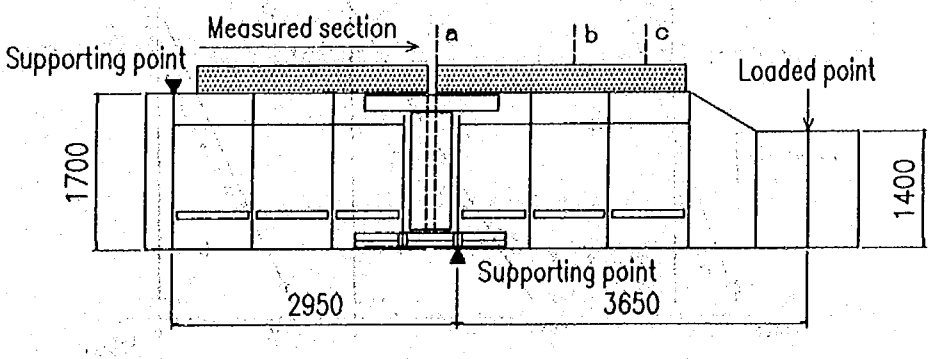


Fig.5 Load Bearing Method for Experimental Girder

First of all, the load test has been carrid out at 27tf maximum (within elastic region) in the experiment, where the distortion and deflection at respective parts have been measured. Subsequently, a fatigue test (2 million times) has been implemented at loading amplitude of 25tf (2～27tf) and loading frequency of 3Hz. During the fatigue test, those static load experiments have been conducted for every 10,000, 50,000, 100,000 and 250,000 times, where the changes taken place in distortion and deflection have been checked. Finally, in order to examine behaviours within the plastic region, the load test has been performed up to the full load capacity for the testing unit and the frame (Max. 80tf).

Since no damages such as fatigue cracks were broken out in joints and base metal, and no remarkable changes in distortion and deflection have been observed as well in respective parts in spite of the development of fatigue test, the stress distribution in joints obtained in static load tests shall be indicated here in this case. Fig.6 shows normal stress distributions for longitudinal direction at the load of 25tf in three sections indicated in proposals Type-A and Type-B respectively.

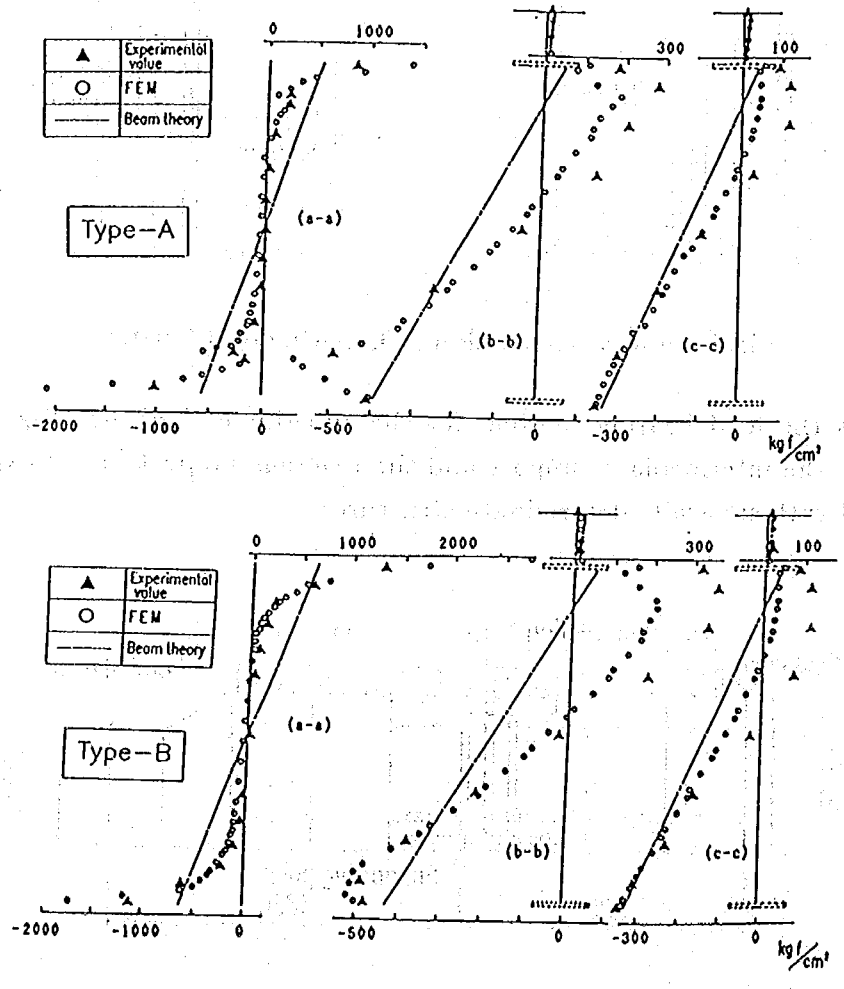


Fig.6 Comparison of Stress Distribution by means of Static Load Experiment and FEM Analysis (at the load of 25tf)

In FEM analysis, the three panels being adjacent to the joint have been analysed as a problem of plane stress. For the loading conditions, a nordal force corresponding to bending stress distribution and shearing force distribution for a built-up beam obtained in accordance with beam theory has been given to both girder ends as an external force. In addition, it was supposed that the floor slab and steel girder had been completely jointed and the connection plate and web plate had been integrated in a body by means of high strength bolts. Judging from the stress distribution shown in Fig.6, so far as those within the elastic region are concerned, it is found that the analysis as a problem of plane stress is inclined to offer rather excellent accuracy.

Meanwhile, it is also turned out that the difference between the experimental value and the design value based on beam theory is considerablly large in web plates for joint section a-a and adjacent panel section b-b. Since the stress at the upper and lower edge in the middle of connection plate (section a-a) may be increased well enough, it is necessary for us to pay much attention toward this point at the time of designing for an actual bridge. Since the comparison of both plans has brought us to consider that Type-A is rather excellent in view of stress flow from the switch clip to flange, and as to buckling of web plate in the lower of part of the adjacent panel in joint (compression side), Type-A is more effective as well, we have decided to adopt this plan.

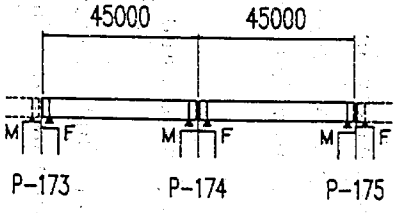
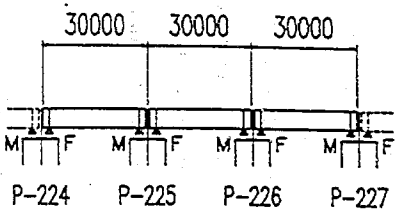
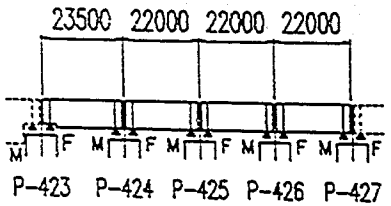
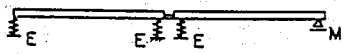
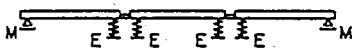
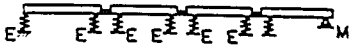
APPLICATION TO EXISTING BRIDGES

The "Steel Girder Connecting Jointless Method" has been applied already for two bridges in Moriguchi Route in Hanshin Expressway, where another one bridge is now under construction also in Sakai Route. In order to apply to existing bridges, those blocks provided with the following conditions have been selected in view of its nature as a test case:

1) The holizontal alignment shall be as close to a straight line as possible, and with less gradient.
2) The piece number, height and position of connected main girders shall be coincided.
3) The span length shall be that of small-to-medium size (30～40m or so), which is close to uniform span length.
4) The type and shape of substructure shall be nearly the same.
5) The above-mentioned condtions shall be satisfied subsequently in an interval covering 3～5 spans at least.
6) A district where the vibration caused by travelling vehicles is relatively large and the loadside pollusion abatement is required.

The major technical data (specifications) for an applicating bridge shall be enumerated in Table-1.

Table.1 Description of Bridges Applied Jointless Work in Hanshin Expressway (Osaka)

Location	Moriguchi (1)	Moriguchi (2)	Sakai
Side-view			
Bearing conditions after connecttion			
Width	17.6m (4-lanes)	17.6m (4-lanes)	17.6m (4-lanes)
Type of structure	Simple supported composite steel girder (2-spans)	The same as the left (3-spans)	The same as the left (4-spans)
Depth & number of main girder	h=2.4m, n=5	h=1.7m, n=5	h=1.4m, n=5
Type of bearing	roller and pin	bearing plate	bearing plate
Type of structure	RC T-shaped pier (19m height)	RC T-shaped pier (13m height)	RC portal bracing pier (9m height)
Type of foundation	cast-in-place concrete pile 1m diameter, 19m length	caisson 6m diameter, 25m length	cast-in-place concrete pier 1m diameter, 11m length
Type of soil profile	alluvium	alluvium	alluvium

The working procedures are as shown in Fig.2. In the case of Moriguchi Route, the operation up to girder connection has been executed under in-service conditions, whereras, the surface structure work including removal of expansion joint and so on has been treated during the working term for a large scale repairing. Meanwhile, as for Sakai Route, all works shall be performed under in-service conditions firmly based on the aforesaid achievements, and the surface treatment is slated to be done only under lane regulation so far.

The construction diagram of joint shall be indicated in Fig.7 and that for the floor Slab Concrete in Fig.8.

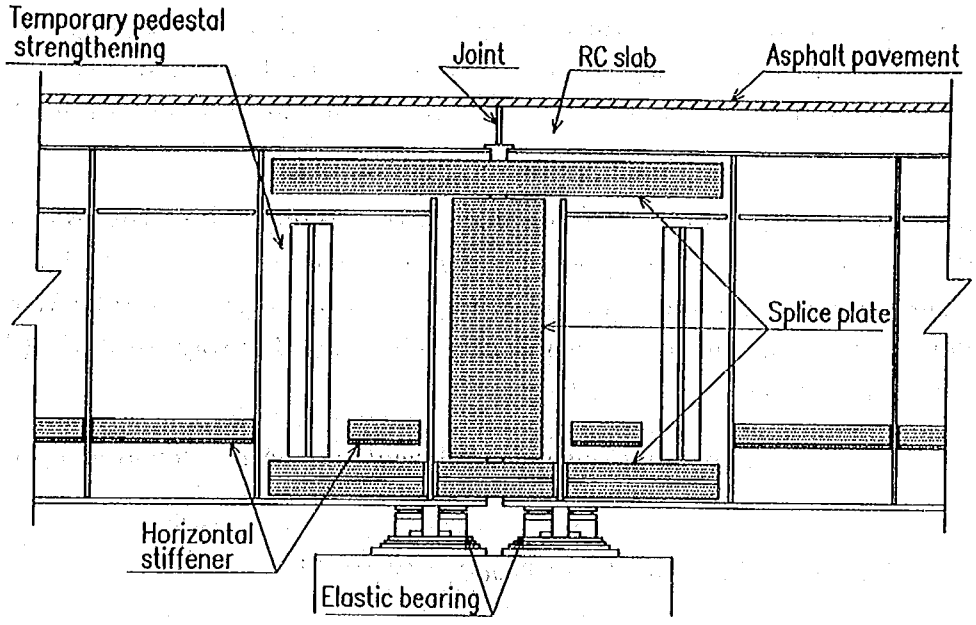


Fig.7 Joint Construction Diagram

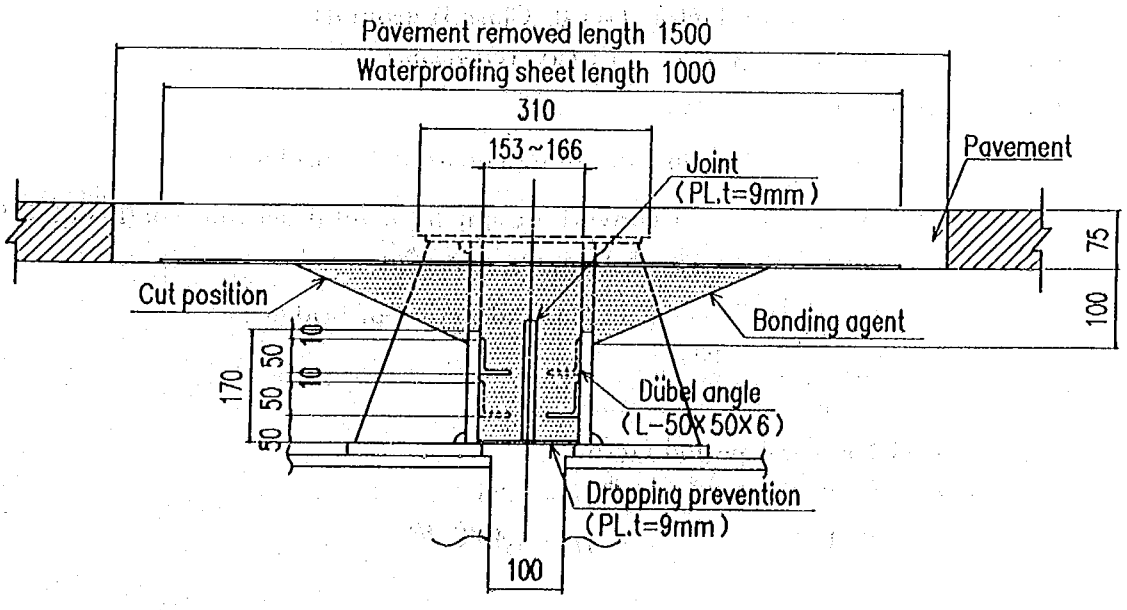


Fig.8 Construction Diagram for Floor Slab Concrete

DESIGN FOR MENSHIN BEARING

Because a simple beam turns to continuous one through connecting steel girders, the pier and foundation may be affected by this, to say nothing of superstructure or bearing. Above all, the strengthening for pier and foundation is scarcely possible as a matter of fact. Therefore, it is necessary for us to restrain the affection within a range of load carrying capacity for the existing bridge. For this reason, the Layered Rubber Bearing comprizing a lead plug (LRB), for which we can expect a reaction force dispersion at the time of earthquake as well as a reduction in inertia force caused by high damping, has been adopted.

For the construction, it is an elastic bearing integrated with a lead plug embeded in the center of layered rubber, which enjoys both of layered rubber bearing function (vertical load supporting and horizontal spring) and energy absorption function brought by lead plug plastic deformation.

The designing has been practiced in accordance with, "Handbook of Highway Bridge Bearing" (Japan Road Association) not to speak of, "Study Report of Highway Bridge Menshin System Development" (commercial joint study of Ministry of Construction, Public Works Research Insititute, 1990) and "Guideline of Menshin Designing for Highway Bridge" (draft) (Land Development Technical Research Center, 1988).

In this case, the design horizontal seismic coefficient has been calculated by means of formula <1>.

$$Kh = C_z \cdot C_G \cdot C_I \cdot C_D \cdot C_{Th} \cdot C_{TI} \cdot K_{hIO} \cdots\cdots\cdots\cdots <1>$$

where Kh : Design horizontal seismic coefficient

K_{hIO} : Standard design horizontal seismic coefficent for Level 1 (=0.2)

C_z : Seimic zone factor (=1.0 Osaka Prefecture)

C_G : Ground condition factor (=1.0 Class II ground)

C_I : Importance factor (=1.0 1st grade)

C_D : Damping constant factor

$$C_D = \frac{1.5}{40 \times hr + 1} + 0.5$$ (hr : damping constant for bridge)

C_{Th} : modification factor to convert design horizontal seismic coefficent into a value being equivalent to 5% of damping constant

$$C_{Th} = \frac{1}{\frac{1.5}{\frac{40 \times 0.04}{T} + 1} + 0.5}$$ (T: Natural period of bridge)

C_{TI} : Level 1 natural period factor

0.2sec $\leqq$ T $\leqq$ 1.3sec $C_{TI} = 1.25$

1.3sec $<$ T $C_{TI} = 1.49T^{-2/3}$

Furthermore, the lower limit value for design horizontal seismic coefficient has been set at 4/5 of the standard seismic coefficient (0.2), that is, 0.16 as specified in "Guideline for Menshin Designing".

Taking the case of three span connecting beam in Moriguchi Route as an example, a part of the design results shall be illustrated in Table-2, and a detailed diagram of Menshin Bearing in Table-9. In particular, since the Menshin bearings are to take over the place of the existing bearing plate (BP) shoes, both of plane dimension and height has been designed under serious restricted conditions.

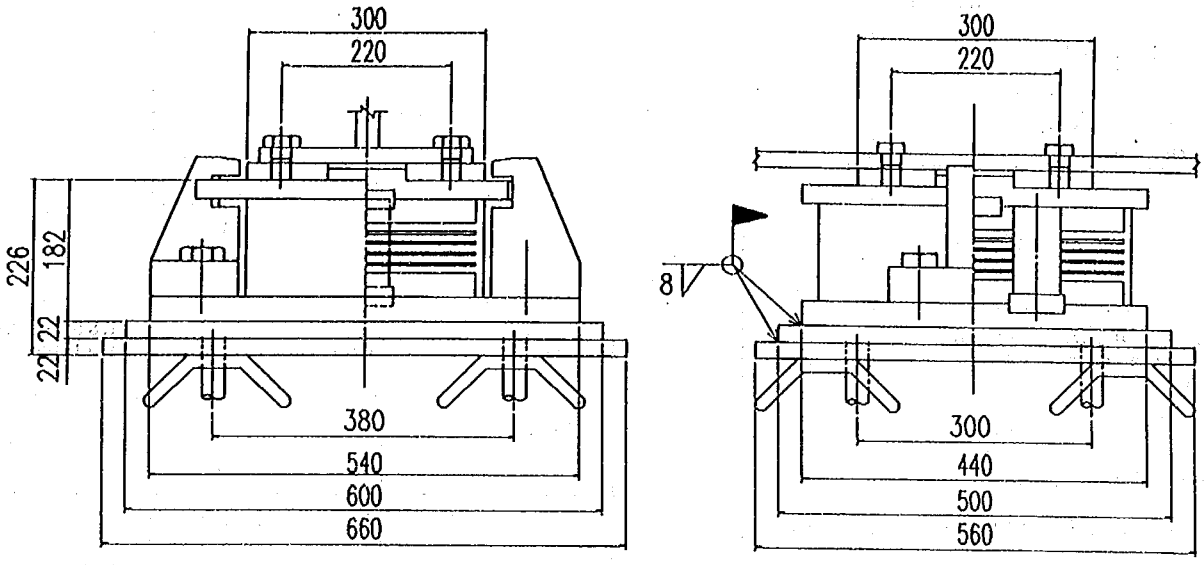


Fig.9 Construction Diagram for Menshin Bearing

Table-2 Characteristic Value of LRB and Bridge, Load-carring Capacity of LRB and Calculation for Dispersion

Name	Code	Unit	P 225	P 226	Reference
① LRB characteristic value (per pier)					
Secondary rigidity	K_{2i}	tf/m	1570	1574	
Primary rigidity	K_{1i}	tf/m	10205	10232	
Equivalent rigidity	K_{Bi}	tf/m	2370	2382	
Damping constant	h_{Bi}	%	19.50	19.57	
② Bridge characteristic value					
Bridge natural period	T	sec	1.282		
Bridge damping constant	h_T	——	16.36		
Compensating rate	C_D	——	0.699		() refer
	C_{Th}	——	1.0 (0.857)		
	C_{Ti}	——	1.25		
Design horizontal seismic coefficient	K_h	——	0.175		=assumpted value
③ LRB load-carrying capacity (per bearing)					
Vertical load	R_{Di}	tf	58.0	58.0	
Design displacement	U_{Bi}	cm	6.01	5.95	
Effective area for rubber	A_{Ri}	cm2	839.2	840.9	
Degree of bearing stress	σ_{bi}	kgf/cm^2	69.1	69.0	
Shearing strain (Compressive)	γ_c	%	127.5	127.2	
Shearing strain (Displacement)	γ_s	%	109.3	108.2	≦ 150
Shearing strain Total	γ	%	236.7	235.4	≦ 333
④ Calculation for dispersion (per pier)					
Superstructure displacement	U_T	cm	7.14		
Inertia force	P_i	tf	142.43	141.8	
Piertop displacement	U_{Pi}	cm	1.13	1.19	
LRB displacement	UB_i	cm	6.01	5.95	
Shearing strain	γ_i	%	109.3	108.2	

VERIFICATION BY MEANS OF DYNAMIC ANALYSIS

In the foregoing paragraph, the analysis has been developed, using design horizontal seismic coefficient calculated in the seismic coefficient method in view of damping. In order to verify the results, a time history response analysis (dynamic analysis) has been applied by means of the model shown in Fig.10.

In the dynamic analysis, three kinds of seismic wave, say, ① modified Itajimabashi, ② Tokachi-oki, and ③ El · Centro were used. Amplitude adjustment has been applied for those seismic waves either for them so as to conform to acceleration response spectrum S at the maximum acceleration of 250 gal as specified in "Highway Bridge Specifications".

The analysis results for three span connecting beam shall be shown in Table-3. As shown in the figure, the results of dynamic analysis indicates smaller figures on the whole compared with those of seismic coefficient method, and taking the convenience in designing into consideration, we believe that no problem could be caused by using the calculation results attained in the seismic coefficient method.

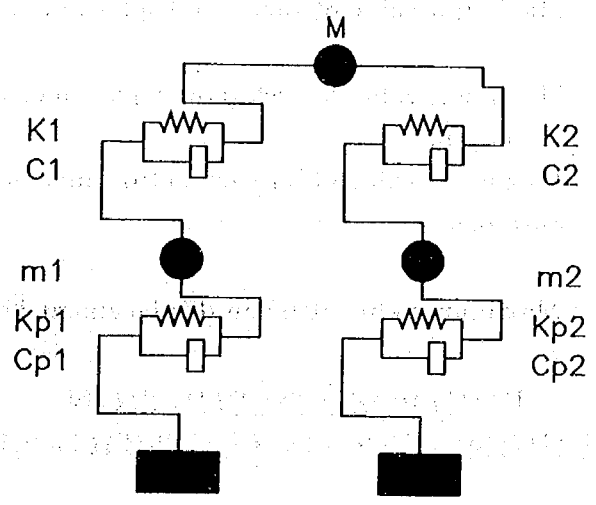


Fig.10 Diagram for Dynamic Analysis Model

Table-3 Comparison between Dynamic Analysis and Static Analysis in Three Span Connecting Girder

Input seismic wave	Pier No.	Displacement (mm)		Relative displacement. (mm)		Force(tf)		Beam displacement(mm)	
		D.A.	S.A.	D.A	S.A.	D.A.	S.A.	D.A.	S.A.
Modified Itagimabashi	P225	4.6	11.3	20.9	60.1	56	142.4	24.4	71.4
	P226	4.8	11.9	20.7	59.5	56	141.8		
Tokachi-oki	P225	11.9	11.3	59.4	60.1	155	142.4	70.4	71.4
	P226	12.5	11.9	58.8	59.5	154	141.8		
EL CENTRO	P225	9.4	11.3	45.6	60.1	117	142.4	54.5	71.4
	P226	9.9	11.9	45.1	59.5	116	141.8		

D.A. = Dynamic analysis (maximum acceleration of input waves; 250gal)
S.A. = Static analysis

where, Displacement: Maximum value of pier top displacement against ground
Relative displacement: Maximum value for relative displacement between girder and pier
Force : Maximum value of superstructure inertia force affecting onto pier
Girder displacement : Maximum value of beam displacement for ground

PRE/POST-EXECUTION ENVIRONMENTAL INVESTIGATION

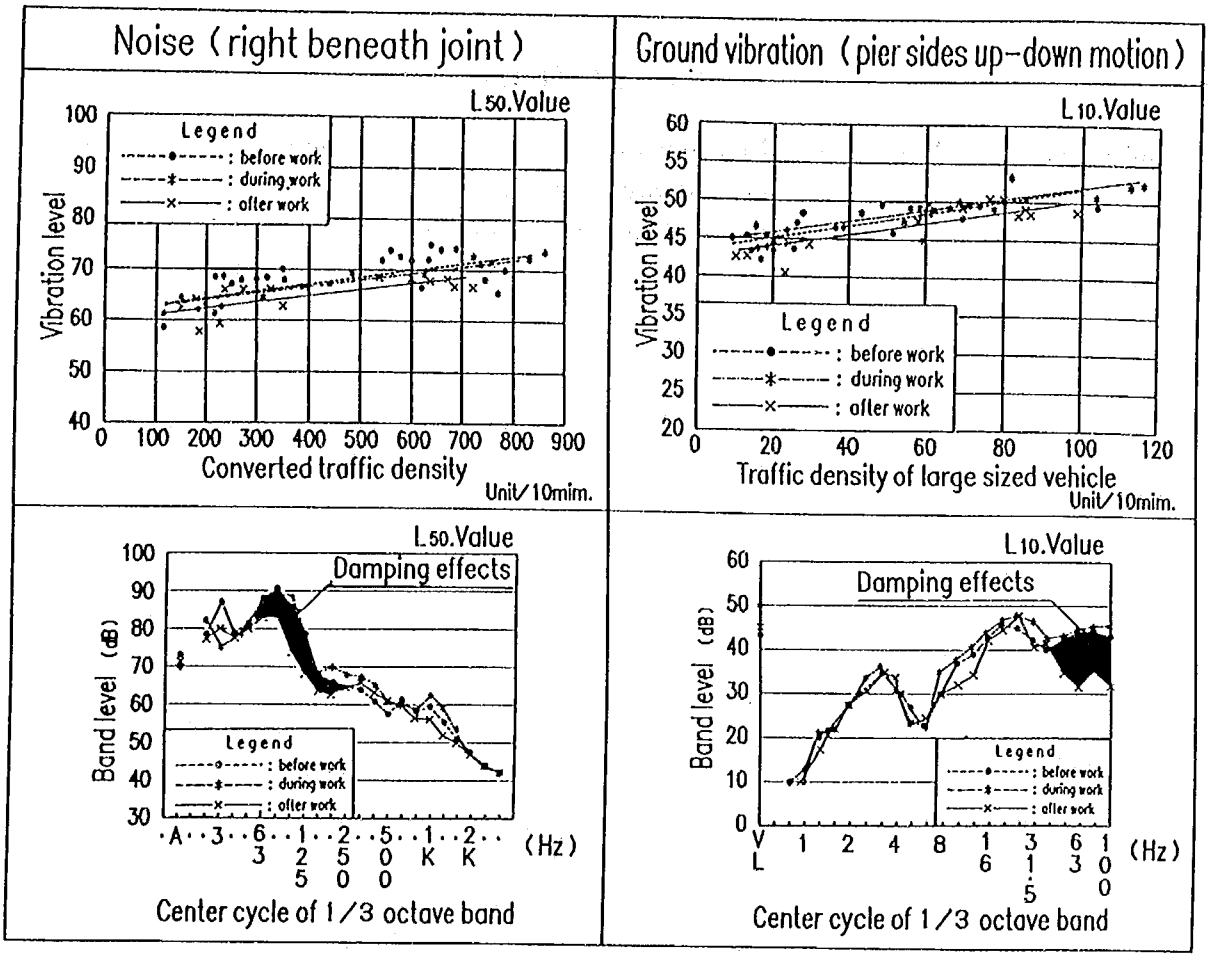
In order to verify effects of the method affecting to roadside environment, noise examination and ground vibration examination have been implemented at those respective time points, such as before, during (after replacement with elastic bearing) and after consruction. The damping effects (a typical example) of noise (right beneath the joint) and ground vibration (up and down motion at pier sides) shall be illustrated in Table-4.

The noise just under the joint can be reduced for 2.5dB or so in L50 value due to jointless method, whereas, the run-off effect has gotten no further than 1 dB or so in State-people boundary (10m point). Furthermore, the run-off effect has been inclined to remain stagnant at 1.5 dB or so in L50 value in pier sides ground due to introduction of jointless method, and so at 0.5 dB level in State- people boundary. It seems reasonable to assume that this is because, as have been clarified by the frequency analysis results and so forth, the frequency band

reduced by connecting jointless method was within a range of 31.5～250Hz, which underwent a negative compensation largely through hearing and feeling compensation circuits, and its overall level contribution ratio became smaller.

Judging from the fact that no suspected mal-inffluence of replacement with elastic bearing has been observed, we consider that no problem is expected in the further application as a Menshin bearing.

Table-4 Run-off Effect of Noise/Vibration



POSTSCRIPT

It was confirmed that the "Steel Girder Connecting Jointless Method" attempted this time had not brought any considerable overstress to the existing structures. This widely depends upon the fact that the design of the bearing provided with such damping fuctions as those not to largely fluctuate the seismic inertia force at the time of construction has been accomplished.

Moreover, in the practical working aspect, it has enabled the execution under the routine regulation conditions (lane per day), which is easier for a road controller to adopt, and the environmental improvement in the vicinity of an elevated bridge has been conviced as well. Above all, the impact vibration run-off associated by the introduction of jointless technique is enjoying a big psychological effect toward inhabitants in a sense of prevention against "Vibration as a Sound", therefore, we believe that it would be applicable enough as one of further vibration-proof measures. Last but not least, the author is grateful to Professor Kajikawa in Kanazawa University for his valuable guidance in this study as well as investigation.

REFERENCE

1)Tomita. Tanaka. Miyahara : Non-jointification of simply supported girders on elevated expressways in service.
Proceedeings of the Forth U.S Japan bridge workshop
(1988.5)

Session-8

Dynamic Characteristics of Base-Isolated Bridges

J-17) Vibration Tests of A Menshin Designed Prestressed Concrete Bridge
(Goto, Y., Kikuchi, T., Ina, Y. and Sakakibara, N.)

J-18) Report on Vibration Experiments for an Actual Steel Bridge Supported with Menshin-Type Bearings
(Komatsu, I., Yasuda, F. and Nishibayashi, M.)

J-19) Response Analysis of Miyagawa Bridge Based on A Measured Acceleration Record
(Kawashima, K., Nagashima, H., Masumoto, S., and Hara, K.)

VIBRATION TESTS OF A MENSHIN DESIGNED PRESTRESSED CONCRETE BRIDGE

Yozo GOTO*1 Toshio KIKUCHI*1
Yoshinao INA*2 Naoki SAKAKIBARA*2

*1) Technical Research Institute, Obayashi Corporation, Kiyose-shi, Tokyo, Japan
*2) Civil Engineering Division, Obayashi Corporation, Chiyoda-ku, Tokyo, Japan

SUMMARY

Karasaki Bridge is the first prestressed concrete bridge for which the Menshin Design was adapted in Japan, having a 2-span structure of 76.95m length and 11.2m width. It was originally designed by the conventional seismic coefficient method and then the earthquake resistance was enhanced by the Menshin Design. In order to know the vibration characters of the Menshin-designed bridge, Karasaki Bridge was tested by a forced vibration method. Although the test was in a limited amplitude range smaller than that of a large earthquake, the following results are obtained ; (1) The vibration of the girder is simplified to that of a one-mass system by the Menshin Design. (2) The stiffness and the damping of the Menshin bearing determine the fundamental frequency and damping ratio of the bridge. (3) Vibration due to traffic load is also isolated to the abutment and the pier by the Menshin bearing.

INTRODUCTION

There are 45 or more base isolated bridges in New Zealand and over 10 completions are accounted in the U.S.A.. In Japan, in the field of building constructions, about 50 base isolated structures have been completed. But, as Japanese highway bridges have a combination of large earthquake load, much soft ground and a big volume of traffic, Japanese bridge engineers have pursued the development of Menshin Design which places emphasis in increasing energy dissipating capability and in distribution of lateral force to many piers and abutments.

In 1989, the Technology Research Center for National Land Development established a proposal entitled "Guidelines for Base Isolation of Highway Bridges"[1] as a result of three-year research. In 1992, the Public Works Research Institute and 28 private firms completed "Manual for Menshin Design of Highway Bridges

(Draft)"[2] as one of the final accomplishments of their three-year joint research program. Basing upon these research accomplishments, the Japanese first Menshin-designed bridge, the Miyagawa Bridge in Shizuoka prefecture (a 3-span continuous steel plate girder bridge) was completed in March 1991.

Obayashi Corporation also designed and constructed the Karasaki Bridge which is the first Menshin-designed prestressed concrete bridge in Japan. The Karasaki Bridge was completed in July 1991, and just after the completion, forced vibration tests using a mechanical shaken and a heavy motor car were carried out in order to know the fundamental performance of the Menshin-designed bridge. An instrumented observation of response due to natural earthquake is also being carried out.

The forced vibration tests were based on vibrations of small amplitude, and therefore did not fully reproduce the conditions of a strong earthquake. They however could make the fundamental vibration characters of the Menshin-designed bridge clear. This paper describes the features of the Menshin device introduced to the Karasaki Bridge, and discusses the results of the forced vibration tests.

OUTLINE OF KARASAKI BRIDGE AND MENSHIN SYSTEM

Outline of Bridge

The Karasaki Bridge is a prestressed concrete girder highway bridge of 2 spans, acrossing a river on land belonging to the Soma Kyodo Power Company Ltd in Fukushima prefecture. The view of the bridge is shown in Figures 1 and 2. The 2-spans are connected to be continuous one by ϕ 32mm high tensile steel bars and a reinforced concrete deck as shown in Figure 3.

Ground Conditions

The soil profile below G.L.-20m～-25m consists of silty layers (Tertiary deposits) on top of which are deposited fine sandy layers (Alluvial layers). The ground conditions at the middle of the bridge are shown in Figure 4. The layer below G.L.-22m has a measured V_s value of 560 m/s and is considered suitable for engineering baserock.

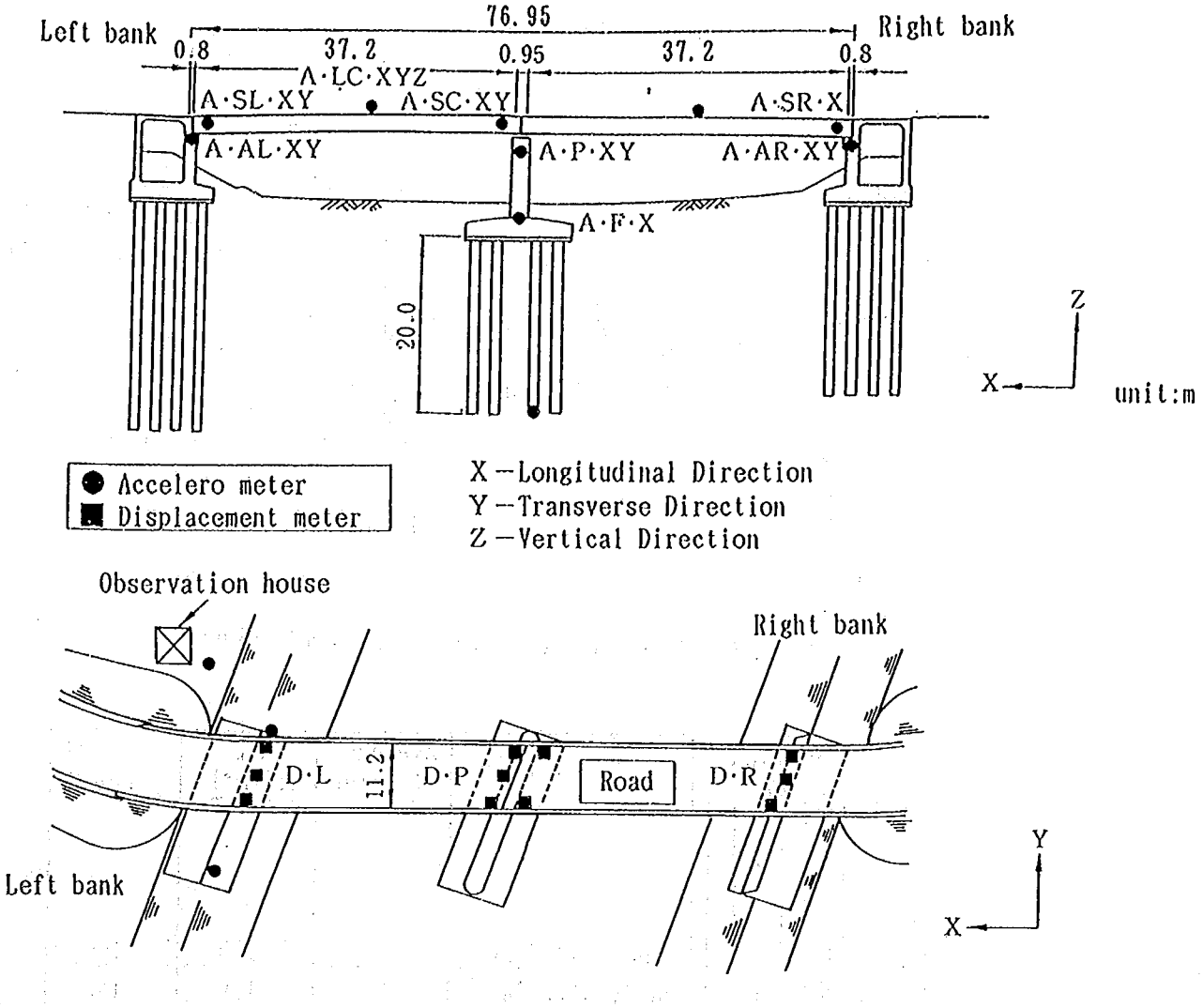


Fig.1 Bridge-profile and Locations of Meters

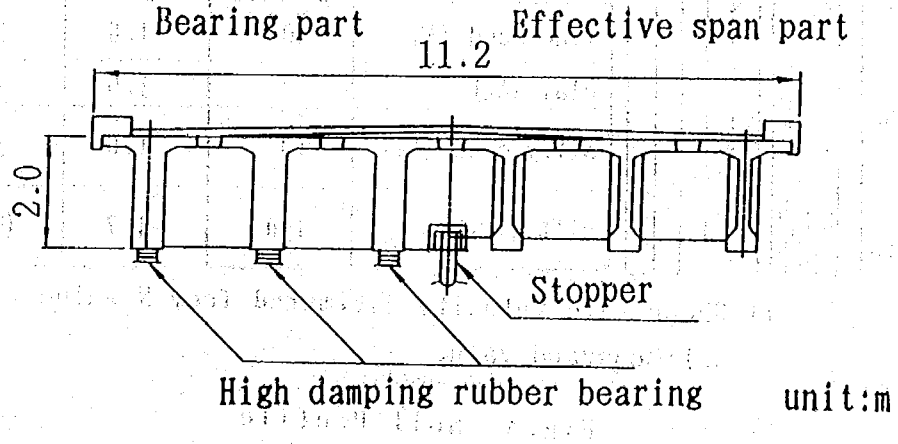


Fig.2 Disposition of Menshin Bearing and Stopper

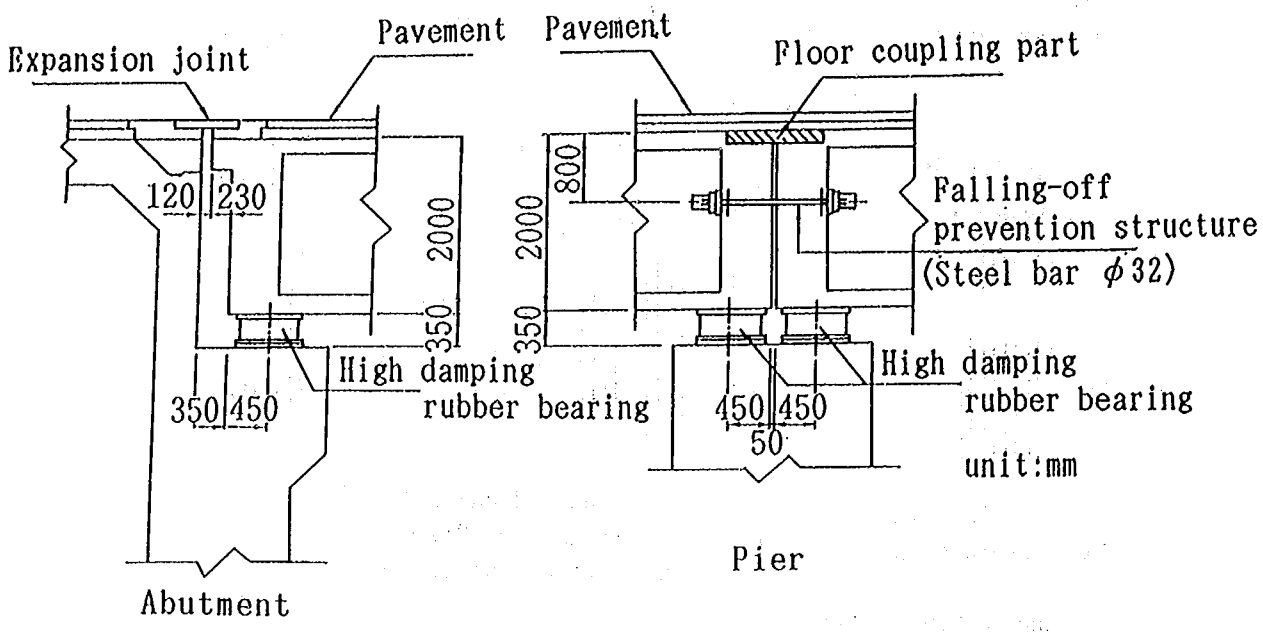
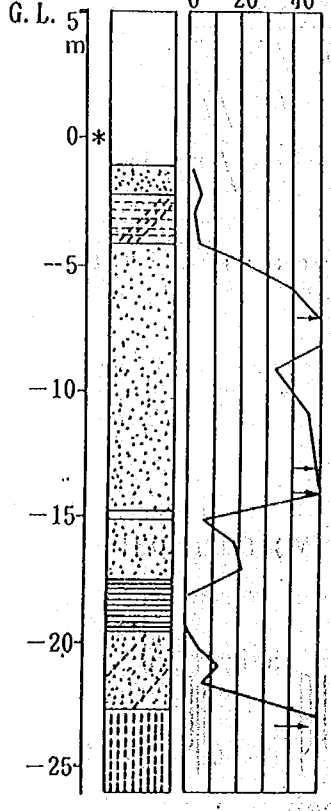


Fig.3 Profile of Abutment and Pier



Soil	Average N-value	γ_t (tf/m³)	*1 V_s (m/s)
fine sand (F_s)	2	1.8	100
sandy silt (A_{c1})	3	1.6	140
fine sand (A_{s1})	40 ～ 50	1.9	250
clay (A_c)	8	1.5	200
fine sand (A_{s2})	20	1.8	220
clay (A_c)	2	1.5	130
silty sand (A_{s2})	10	1.6	170
silt (T_{s1})	150	1.7	(560)

*1 Shear wave velocity estimated from N-value

( ):Measured value

Fig.4 Soil Profile

Menshin Design

(1) Design policy

Karasaki Bridge is a highway bridge having the common abutments and pier with the neighboring belt conveyor bridge. The dead load and the live load of the highway bridge are large in comparison to those of the belt conveyor bridge. Menshin devices were therefore adopted to the highway bridge in order to improve the seismic stability of the bridges as a whole. (The Menshin design is not used in the transverse direction of the bridge.) The natural period of the ground during strong earthquake was analyzed using the equivalent linear method, and was estimated to be T=0.65～0.89sec. The natural period of the bridge being equiped with Menshin device was designed to be T=1.4sec so as not to coincide with that of the ground. Two levels of earthquake load were posited : strong earthquake level(Level 1, here after) and sever earthquake level(Level 2, here after).

(2) Bearings

The bearings consist of high damping laminated rubber and was designed to be stable against Level 2 earthquake.

(3) Stopper for transverse direction

In order to restrain displacement of the girder in the transverse direction of the bridge, stoppers were installed to the abutments and pier. High damping rubber with slider pad was inserted between the girders and the stoppers to absorb shocks. The girders and the stoppers are free to slide in the longitudinal direction of the bridge.

(4) Gap between abutment and girder

The gap clearance between the abutments and the main girders is 350mm, which is sufficient to prevent collision even at loads above Level 1.

(5) Expansion joints

The gap between bridge deck and the abutment top was determined from the calculated displacement in the longitudinal direction of the bridge at the Level 1 earthquake load. As the clearance was determined to be 119 mm, so rubber expansion joints were adopted. The rigidity of these expansion joints is around 1/100 that of the Menshin bearings.

(6) Knock-off device

A knock-off device was installed to prevent the heavy damage from the collision between the deck of the bridge and the abutments when a load greater than Level 1 is applied. The profiles of the knock-off device are shown in Figure 5. At the designing, overturning and slippage of the knock-off element caused by T-load(16tf) and H-load(starting or stopping load) were checked

respectively.

(7) Continuous deck and coupling device:

As a falling-off prevention device in the longitudinal direction of the bridge, the two series of girders are linked at the middle support by ϕ 32 high tensile steel bars. The decks of the two spans were connected by a reinforced slab to keep the road surface smooth and to distribute the lateral forces.

Results of Design

Results of the Menshin Design are compared to that of the conventional design. The natural periods, the design lateral force coefficients, and the stress responses of the piers together with pile reaction forces are compared in Table 1. It is also confirmed that the number of piles required could be reduced.

Table 1 Effect of Menshin Design

Items		Conventional Design	Menshin Design
Natural Period	T (sec)	0.32	1.44
Design Lateral Force Coefficient	k_h	0.25	0.17
Stress of Pier	σ_c (kgf/cm^2)	67	40
	σ_s (kgf/cm^2)	2230	950
Pile Reaction	R_{max} (tf/pile)	234	190
	R_{min} (tf/pile)	-9	35
Pile Number		32	28

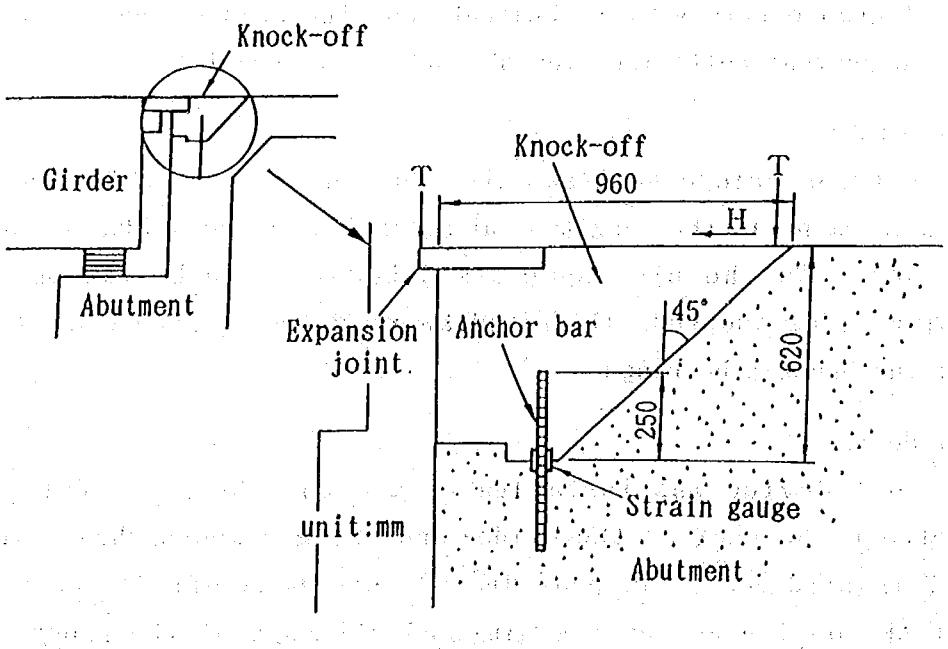


Fig. 5 Knock-off Device

VIBRATION TESTS

Method of Experiment

(1) Forced vibration test using shaker

The shaker used for the test was driven by a servo motor to push and pull a mass of 15 tons in a horizontal direction (Figure 6). In case of continuous operation, the maximum excitation force was approximately 3tf. The shaker was set up on the bridge deck near the left side abutment. The frequencies of the excitation applied were 0.20Hz～7Hz.

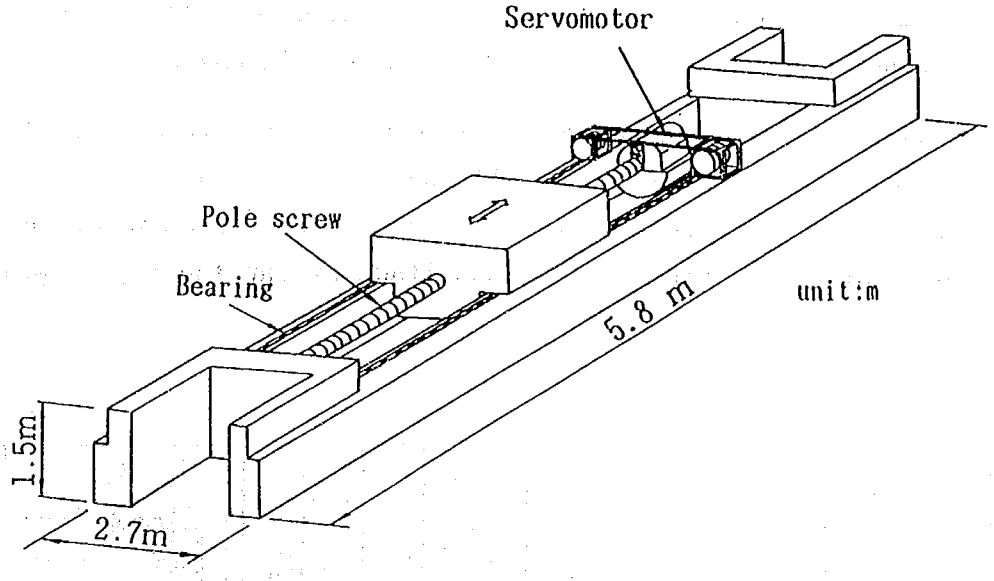


Fig.6 shaker

(2) Motortruck travelling test

A truck weighting approximately 25 tons was used as a test vehicle. The vibrations of the girders, abutments and pier were measured when the truck started, stopped, and ran at a constant speed.

(3) Travelling test on knock-off device

In order to verify the stability of the knock-off device during the heavy motortruck travelling, the strain occurring in the anchor bar of the knock-off device was measured. As same as the truck travelling tests, measurements were made when the vehicle started, stopped and ran at constant speed.

Experimental Results

(1) Forced vibration test with shaker

The resonance and phase curves at representative measuring points are shown in Figures 7～10. Figure 7 shows the resonance and phase curves at a point in the

center of the left side span. The resonance curve in the longitudinal direction of the bridge is a simple curve with a peak of 0.22cm/tf at 2.3Hz. The resonance curve for the transverse direction showed no obvious peak, indicating that the stopper is effective in restricting displacement in the transverse direction. In the vertical direction, the response curve shows a peak at 3.1Hz. From the mass and the flexual rigidity of the girders, the natural frequency of the girders in the vertical direction can be calculated. If the girders are taken to be a beam fixed at one end and simply supported at the other, the frequency is calculated to be 3.5Hz(2.2Hz for a simple beam), which is close to the measured value. This shows that the connecting of the 2 span deck is half way between a hinge and a fixed joint, and that the Karasaki Bridge is structurally equivalent to a continuous 2 spans bridge as far as the holizontal displacement is concerned.

Figure 8 shows the resonance and phase curves in the longitudinal direction at pier top, abutment and footing. They all show a large peak at 2.3Hz. This peak comes from the resonance of the girders. However, the amplitude of the abutment is only 1/30 of that of the girder. The amplitude of the footing is around 1/40.

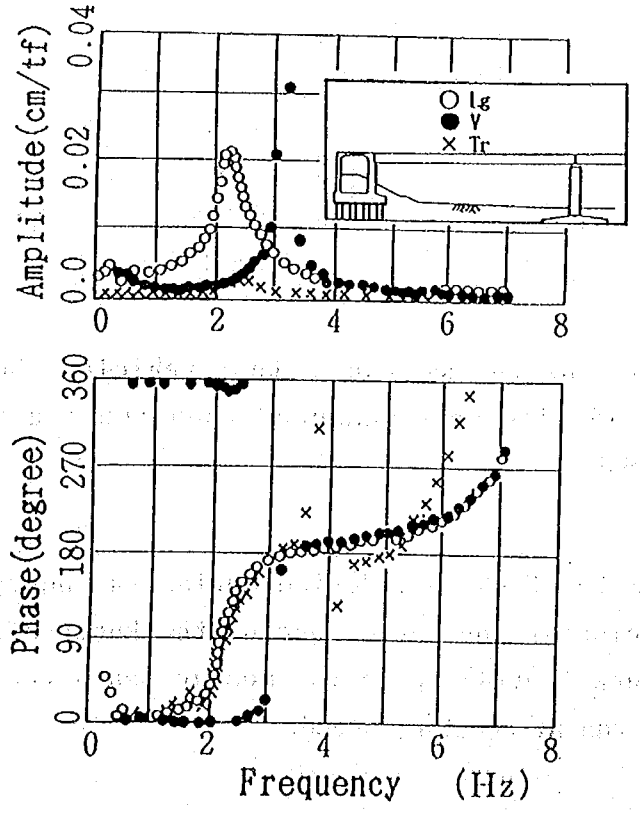


Fig.7 Resonance Curves of the Girder

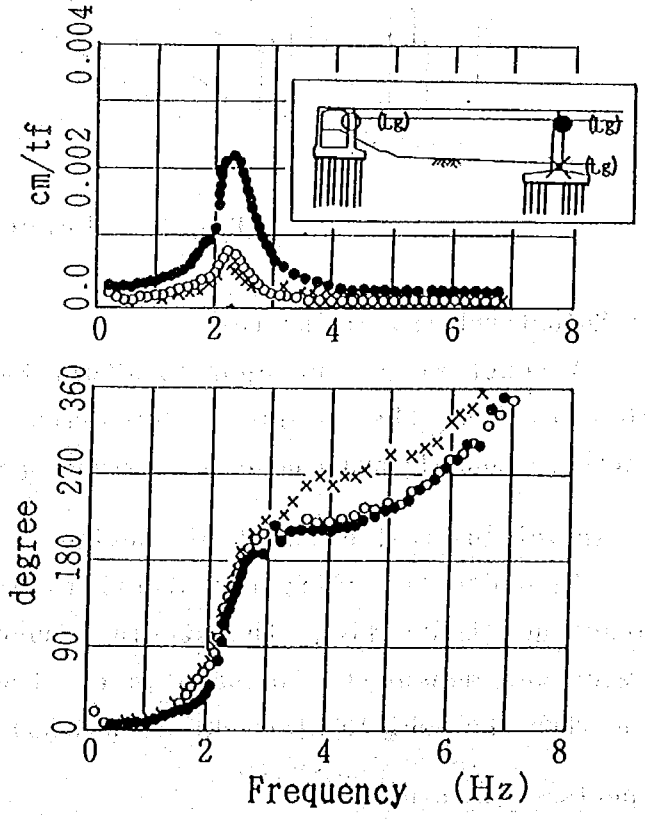


Fig.8 Resonance Curves of the Abutment & Pier

Figure 9 shows the resonance and phase curves for relative displacement between the girder and pier top. Relative displacements in all cases show an obvious peak at 2.3Hz, while amplitude, at 0.02cm/tf, is virtually the same as the absolute value for the girder amplitude. These results agree with those of Figure 8, and show that the most part of the horizontal displacement occurs in the bearings.

Figure 10 shows the resonance and phase curves at the ground surface near the left abutment. The resonance frequency of the ground is approximately 1.8Hz.

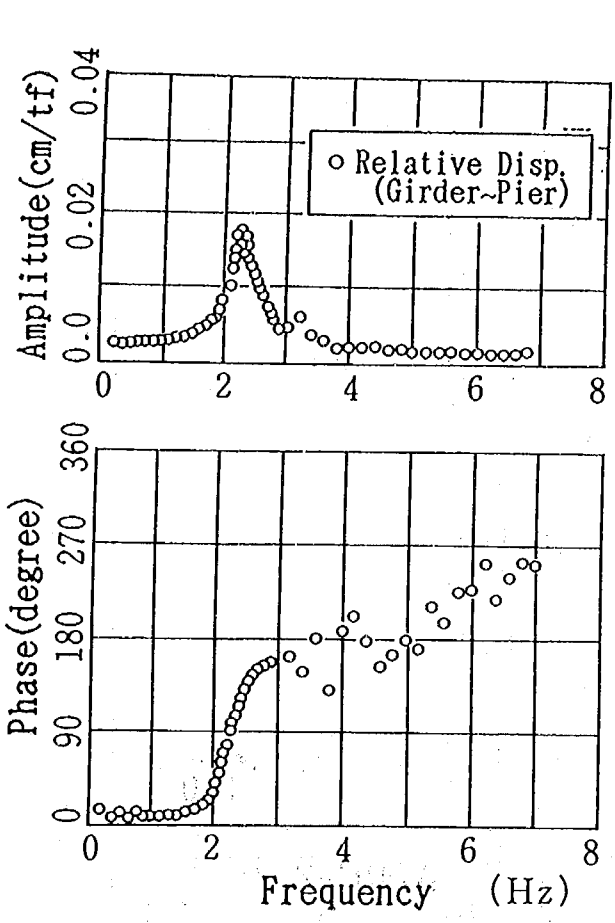


Fig.9 Resonance Curves of Relative Displcement (Between girder and pier)

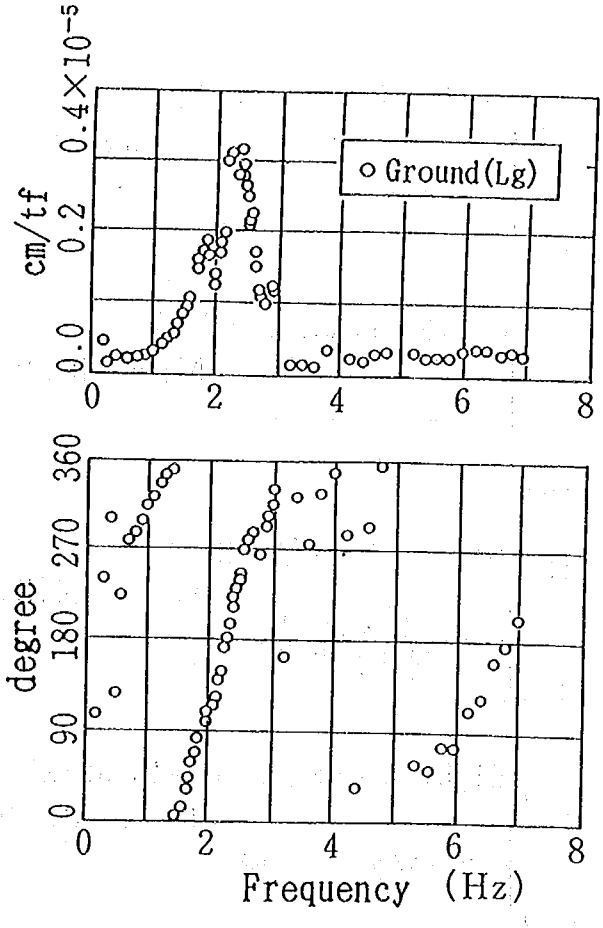


Fig.10 Resonance Curves of the neighforing Ground

(2) Motortruck travelling tests

Figure 11 shows recorded acceleration waves and its Fourier spectrum on the girders during the truck travelling test. The maximum acceleration for girders and abutments are shown in Table 2. From this figure and table, it may be seen that maximum acceleration of the longitudinal direction of the bridge is greater for starting and stopping than for travelling at constant speed. The maximumacceleration of abutments and piers are low at 1/7 and 1/10～1/20 relative to the girders respectively, indicating the effect of the high damping laminated rubber bearings. The Fourier spectrum for the girders shows a peak around 2.5 ～

2.7Hz, which is presumably the natural frequency of the bridge in the longitudinal direction. The maximum acceleration in the transverse direction is small compared to that of the longitudinal direction. This would appear to indicate the effectiveness of the stoppers. Vibration in the vertical direction is the greatest for starting, smallest for constant speed travelling, being about 14 gal for starting. The Fourier spectrum of the girder shows large peaks at 2.5～2.7Hz and 3.2 ～3.3Hz, as if the natural frequencies in longitudinal and vertical direction combined.

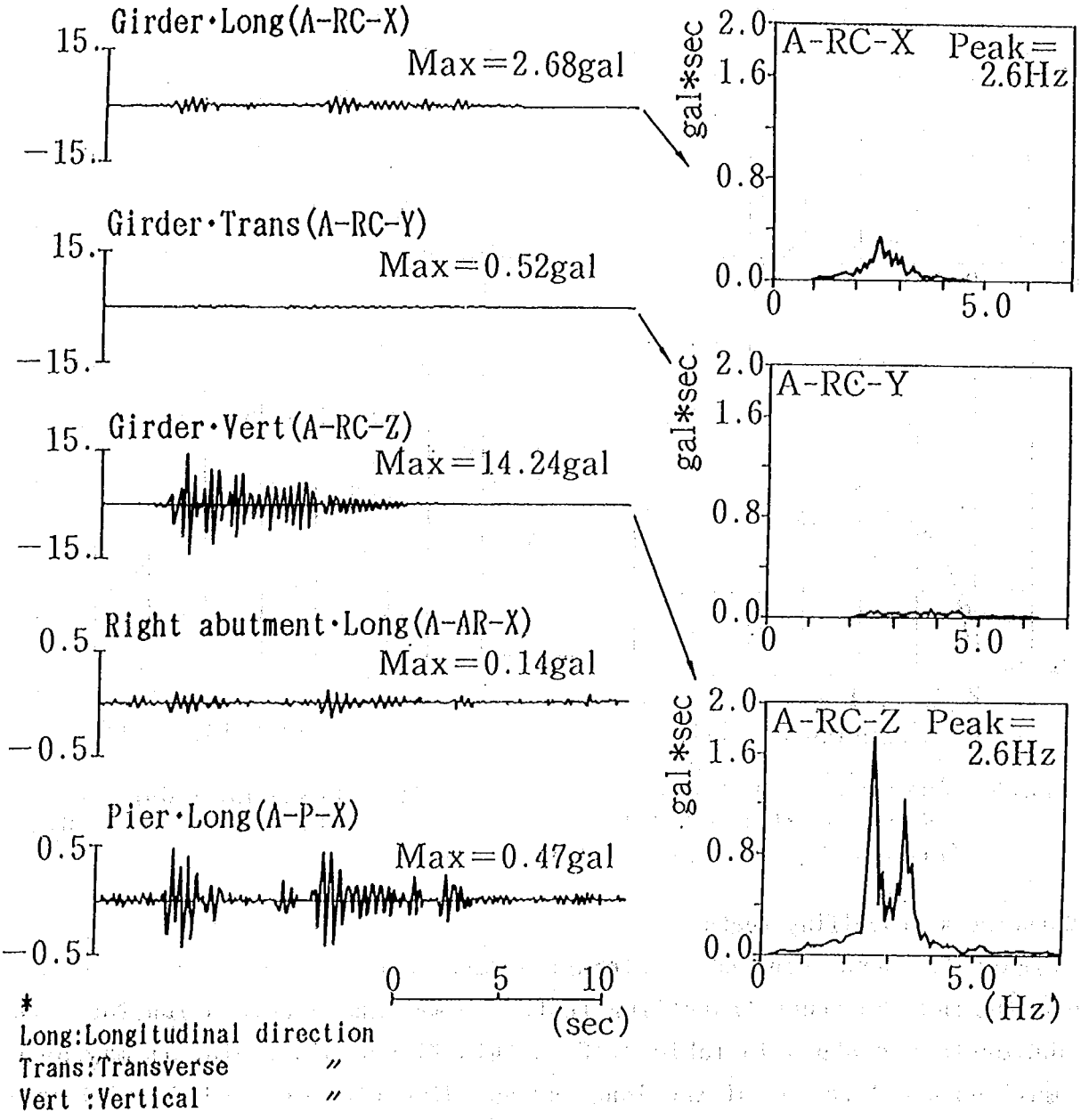


Fig. 11 Waves and Fourier Spectrum

Table 2 Maximum Accelerations by Travelling Test

unit:gal

Measured piont / Item	Longitudinal					Transverse				Vertical	
	Girder (1)	Girder (2)	Abut. Left	Abut. Right	Pier	Girder (1)	Girder (2)	Abut. Right	Pier	Girder (1)	Abut. Left
Constant (30km/h)	1.92	1.83	0.17	0.23	0.27	0.74	0.51	0.13	0.10	7.63	9.58
Start	3.13	2.68	0.19	0.14	0.47	0.78	0.52	0.09	0.15	12.00	0.51
Stop	2.73	2.69	0.16	0.13	0.44	0.84	0.72	0.10	0.16	6.27	0.58

*Girder(1) : Between left abutment and pier
Girder(2) : Between right abutment and pier

(3) Travelling test on knock-off device

Figure 12 shows an example of the strain that occurs in the steel anchor bars of the knock-off device. Strain is a low 5 ~10μ in each of the travelling patterns, and even in terms of stress works out at only around 11 ~21kgf/cm^2. The knock-off device is evaluated as having adequate stability for heavy traffic.

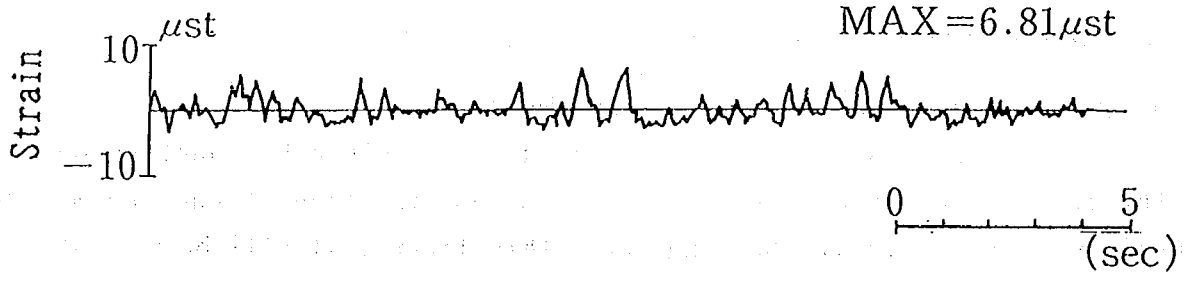


Fig.12 Strain Wave

ANALYSIS

Spring and Damping Factors of Bearings

(1) Spring factor obtained from loading test on single bearing

The loading test involved a constant vertical load and applied a horizontal load of 0.5Hz to top of the bearing. Figure 13 shows a representative example of the load-displacement diagram. The loading test applied loads to the point where a deformation occurred such as seen in large earthquakes. However, in order to obtain a value applicable to the analysis of the vibration test where the displacement was small, the spring factor was calculated from the relationship between the load and a small horizontal displacement of ± 1mm. The obtained value was approximately 10.6tf/cm.

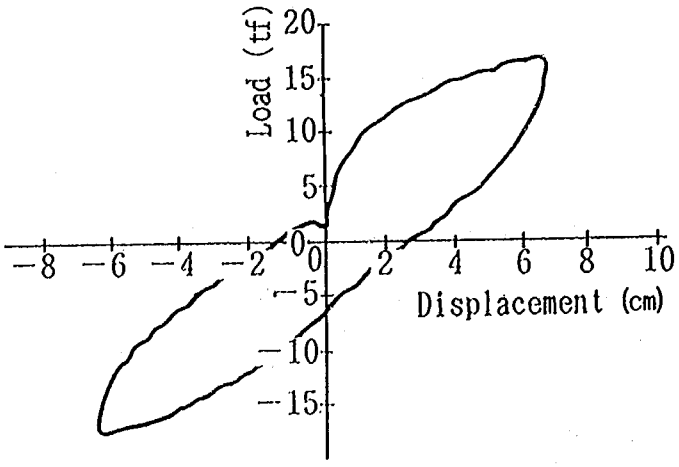


Fig.13 Load-Displacement Diagram

(2) Damping factor

The damping factor obtained by the $1/\sqrt{2}$ method from the resonance curve of the girder is h= 7～10%. As the displacement of the girders is almost due to the deformation of the bearings, it is reasonable to assume that the dampingfactor is determined by the characteristics of the bearings. But, the relativedisplacement was around± 0.6mm, and at this small amplitude, the damping effect of the high damping laminated rubber bearing is not fully exploited.

(3) Spring factor obtained from forced vibration test

Figure 14 shows the spring factor which is obtained by counting backward from the force (excitation force + inertia force of girders) and the measured relative displacement of the bearing. From this figure, it will be seen that the spring factor at the resonance frequency is 11～15tf/cm. Compared with the spring factor of 10.6tf/cm obtained from a single bearing loading test, the factor obtained from the experimental results is relatively large. Given the difference between the amplitude in the loading test of a single bearing and that in the vibration tests, it may be taken to depend on the strain related rigidity of the bearing.

Simulation of Experimental Results by Mass-Spring Model

(1) Analytical model

Figure 15 shows the analytical model. The girders, abutments, piers and footing were represented by using beam elements and the footing was taken rotational inertia into account. The pile foundations and ground were represented by a rotational spring and a horizontal spring, and the spring factor of these were calculated using the V_s value method. The bearings were represented by a single element in the model and their shear rigidity was set on the basis of the spring

factor obtained from the forced vibration tests. The damping factor was assumed to be 8%. The nodal points of abutments and pier were constrained in the vertical direction. The excitation force was applied at the same point (end of the girders of the left span) as during the vibration tests.

(2) Results of analysis

Figures 16 to 18 show the comparison of analysis and experimental results. From these figures, it will be seen that the analytical model provides a good coincidence of the experimental results.

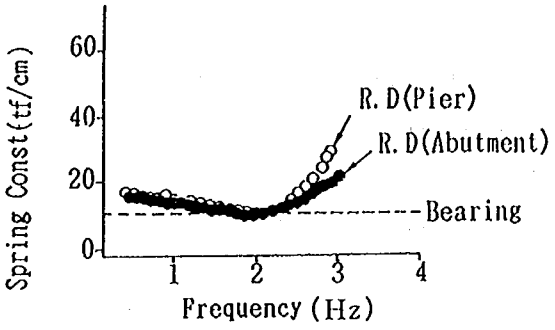


Fig.14 Comparison of Spring Constant

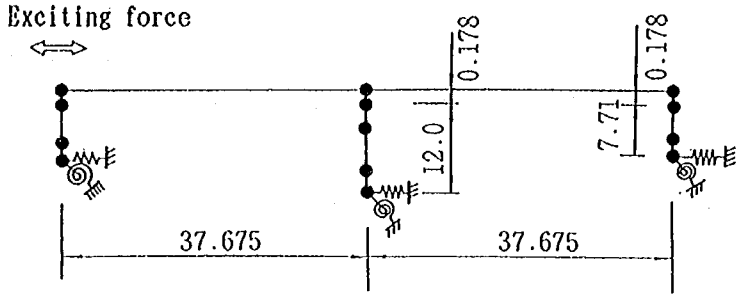


Fig.15 Analytical Model

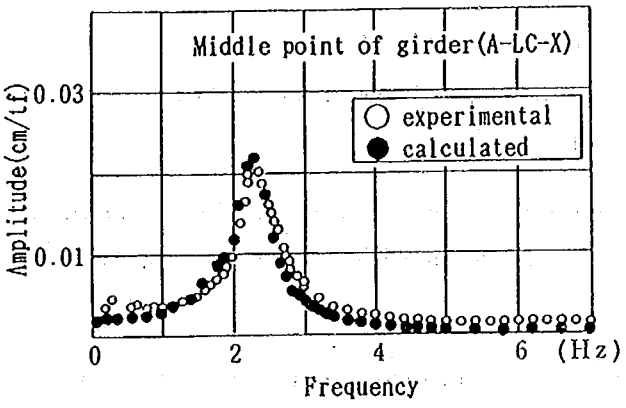


Fig.16 Comparison of Resonance Curves (Girder)

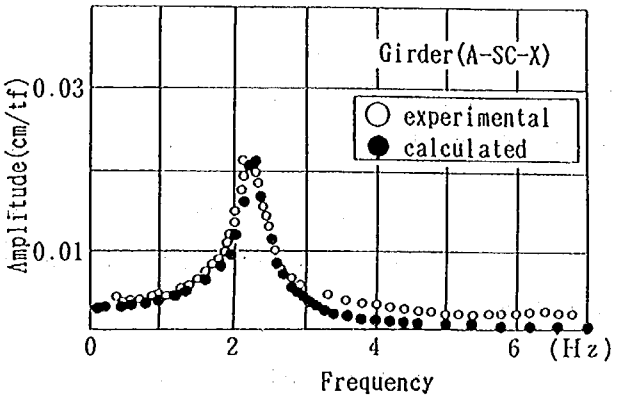


Fig.17 Comparison of Resonance Curves (Girder)

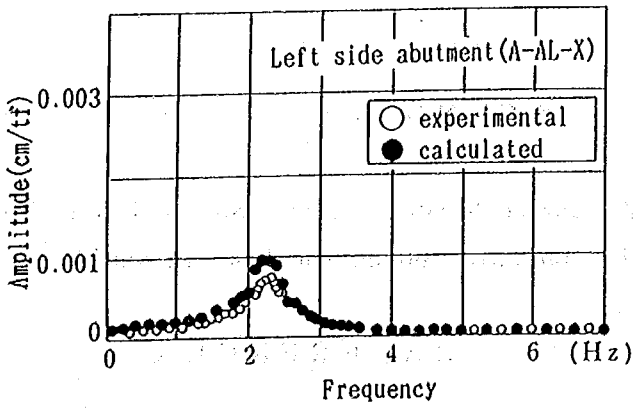


Fig.18 Comparison of Resonance Curves (Abutment)

CONCLUDING REMARKS

(1) A Menshin Design was adopted to the Karasaki Bridge such that the natural period of the bridge became 1.4 sec for an input load of design earthquake Level 1. The clearances between main girders and abutments, and the clearances of the expansion joints were designed to be 35cm and 12cm respectively. Incorporation of the Menshin Design the design lateral force coefficient was reduced by 30%.

(2) It is found from the vibration test that natural frequency and damping factor of the girders are determined by the rigidity and damping factor of the Menshin bearings. Though, it was not possible to apply a large deformation in the vibration test, the rigidity and damping of each single bearing was verified and approved by the factory test generating a displacement equivalent to a large earthquake. As the design of the Karasaki Bridge is based on these results, it is concluded that the Menshin Design will function according to expectation in even a large earthquake.

(3) Given the natural frequency of deflection of the girders, it was concluded that the deck of the two girders are joined by an appropriate rigidity.

(4) As no significant stress was recorded in the anchor bars of the knock-off device when a load vehicle ran over it, it can be assumed that this type of knock-off device is safe for normal traffic loads.

(5) It was verified that the girders are prevented from moving in the transverse direction of the bridge by the stoppers, but are free to slide in the longitudinal direction.

(6) When a load vehicle ran over the bridge, the vibration of the girders in the longitudinal direction is damped by the Menshin devices and is reduced to 1/7 at the top of the pier. Accordingly, the effect of traffic vibration to the belt conveyor bridge which shares abutments and piers with the highway bridge is negligible.

ACKNOWLEDGEMENT

The owner of Karasaki Bridge is the Souma Kyodo Karyoku Co. Ltd, who is greatly thanked for his appreciation on the Menshin Design and the vibration tests.

REFERENCES

1) Technology Research for National Land Development : Guidelines for Base

Isolation of Highway Bridges, Final Report of A Committee for Study of Aplication of Base Isolation to Seismic Design of Highway Bridges, March 1989

2) Public Works Research Institute and 28 Private Firms : Manual for Menshin Design of Highway Bridges (Draft), March 1992, Joint Research Report, Public Works Research Institute(in Japanese).

3) Japan Road Association : Part V Seismic Design Specifications for Highway Bridges, February 1990

4) Public Works Research Institute and 29 Private Firms : "Development of Menshin Systems of Highway Bridges-Report No.1", PWRI Joint Research Reports No.44, March 1990 (in Japanese)

5) Public Works Research Institute and 28 Private Firms : "Development of Menshin Systems of Highway Bridges Report No.2", PWRI Joint Research Reports No.60, July 1991 (in Japanese)

6) Ina,Y., Shoji,H. and Anzai,K. : "Menshin Design and Construction of the PC Highway Bridge", Proceeding of the 47th Annual Conference of the Japan Society of Civil Engineer, September 1992 (in Japanese).

7) Kikuchi,T., Anzai,K. and Goto,Y. : "Vibration Test of Prestressed Concrete Road Bridge Designed by Applying The Menshin Method", Proceeding of the 47th Annual Conference of the Japan Society of Civil Engineer, September 1992(in Japanese)

REPORT ON VIBRATION EXPERIMENTS FOR AN ACTUAL STEEL BRIDGE SUPPORTED WITH MENSHIN-TYPE BEARINGS

Ikuo KOMATSU, Furitsu YASUDA and Motohiko NISHIBAYASHI
Hanshin Expressway Public Corporation

SUMMARY

This paper summarizes the highlights of vibration experiments which were conducted for a steel box-girder bridge on the Bay Route of Hanshin Expressway in Osaka. The bridge adopts Menshin-type bearings, which are elastomeric rubber bearings with damping function, for the first time in the Hanshin Expressway, and, therefore, it becomes important to measure and confirm the vibration properties of the bridge before recognizing such bearing as an effective supporting device for seismic resistance.

In this field experiments, the entire girders were vibrated by means of large-sized exciter and hydraulic jack. Thereby their natural vibration characteristics were identified.

A three-dimensional frame model for the entire bridge is developed for the purpose of conducting vibrational analysis of the bridge corresponding to the experiments. The main purpose of this analysis is to evaluate a possibility to simulate the real dynamic vibration characteristics by using a simple model.

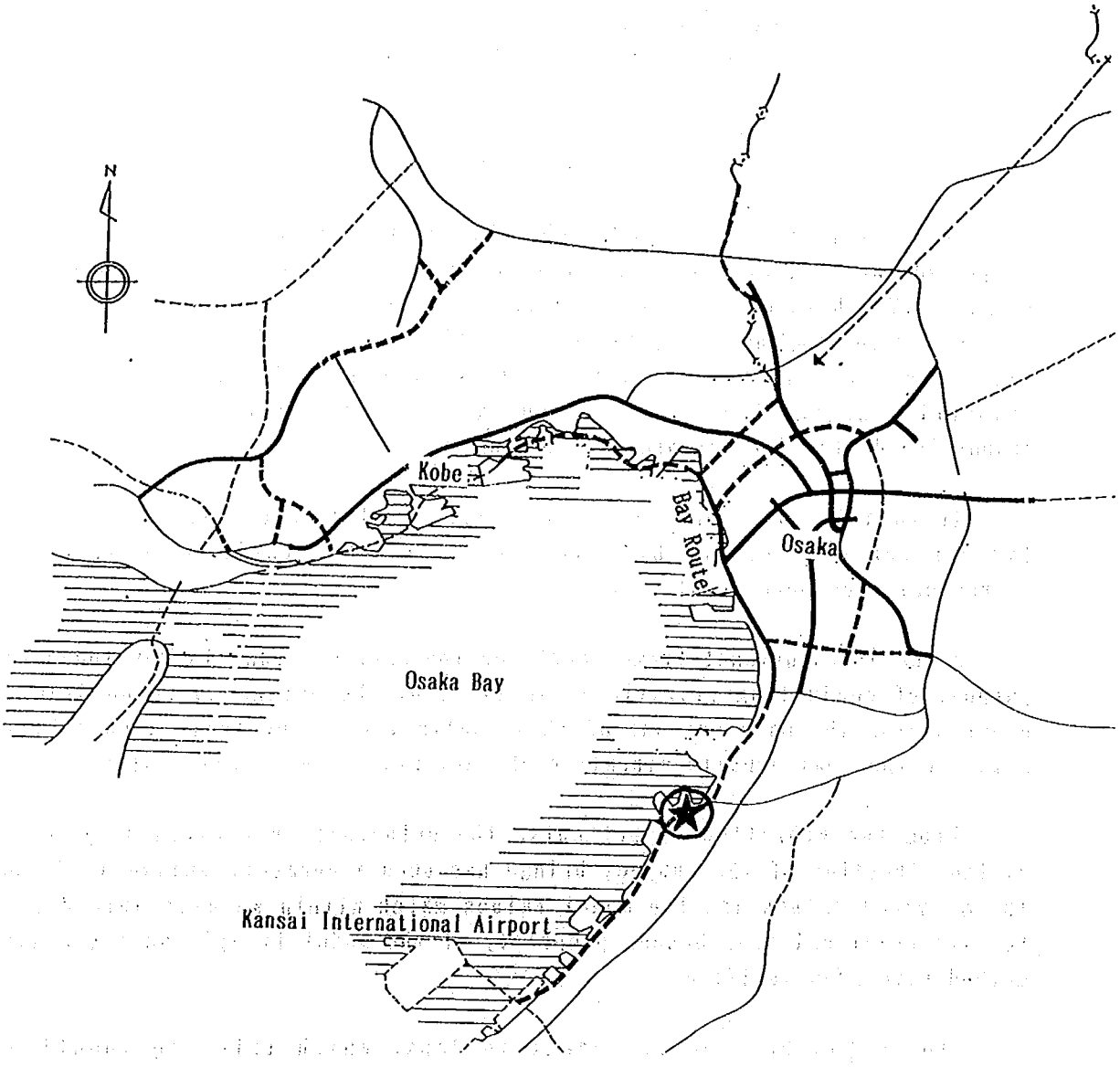
From the vibration experiments, the principal characteristics of short-cycled vibration of the subject bridge has been accurately measured. Meanwhile, the measured values and the model values match within an allowable difference for its practical use. Hence, propriety of the model itself and its analytical method have been verified.

There has been no precedent in Japan which tries to identify real characteristics of Menshin bearings after their installation. It is expected that the results will provide useful basic data for the design of similar Menshin bridges in the future.

INTRODUCTION

Hanshin Expressway is an intra-city highway network in Osaka region. Currently, among its ongoing projects, the highest priority is on carrying forward the Bay Route project. The route is an access highway linking the new second international airport to Osaka and Kobe, two major cities in the region. Menshin-type bearings, whose function are to disperse seismic force and reduce the degree of seismic response of the superstructure, are adopted to a 4-spanned continuous non-composite steel box-girder bridge located at the southern part of the Bay Route. (see Map-1)

This bearing is made of elastomeric rubber with lead components in between It works as a base isolator as well as a damper. There have been quite a few



Map-1 Location of the Bridge Under Study

examples of application of such Menshin bearing to bridges or viaducts in Japan, and this is the first case for the Hanshin Expressway. When practising such a new aseismic device, it is often necessary to verify its actual performance. One of the most effective method is to actually vibrate a real bridge with Menshin bearings and to evaluate whether they can function as designed in case of an earthquake.

Therefore, field vibration experiments of the subject bridge is conducted, and its natural frequencies, oscillation modes and modal damping ratio, which are three parameters representing the bearing's seismic characteristics, are measured. The experiments use large-sized vibration exciter and hydraulic jack. The former gives a continuous vibration in sine waves, and the latter considers a damped free vibration when load is abruptly released.

In the next step, natural vibration analysis using a frame model of the entire bridge structure is conducted. Then, the outcomes are compared with those of the experiments in order to clarify the simulation ability of the model and to establish an effective dynamic design method of Menshin bridges.

This paper is focused on the vibration experiments and comparison with the model analysis. Based on these results, the safety of Menshin bridges against an unprecedented earthquake is evaluated. The evaluation is briefly described in the end.

OUTLINES OF THE EXPERIMENTED BRIDGE

The bridge subjected to the tests is, as illustrated in Fig. 1, 211.5m in length, 21.94m in total width, and with a radius of carvature of 560m. The experiments had been executed before decks were installed on the girders. Total steel weight of the superstructure at the time of the tests was about 1,450 tons. Menshin-type bearings are mounted on three middle piers (B, C and D). Bearings for both end piers(A and E) are conventional roller bearings. Menshin bearings used here are lead rubber type (LRB) which incorporates lead plugs within stratified rubber plates. 12 pieces of LRB (750 X 1050 X 201mm) are used in total taking the two pieces as one unit for a girder support. Configuration and principal dimensions of the bearing are indicated in Fig. 2 and Table-1 respectively.

Installing such Menshin device, the bridge does not positively consider its expected effects for safer and more economical aseismic designing. Here, the bridge was originally designed with the seismic coefficient method prescribed in the Specifications for Highway Bridges, Japanese equivalent of AASHTO. Therefore, advantages of the Menshin bearings are limited to further improvement on seismic safety of the bridge. Meanwhile, in designing Menshin bearings themselves, their principal dimensions are determined so as to meet all the safety requirements prescribed in the draft of "Guidelines for the Menshin Design Methods of Highway Bridges" which was prepared in 1989 by the Hanshin Expressway Public Corporation.[1] Here, design conditions of Menshin bearing contain the maximum vertical supporting capacity of 1,254 tonf and the maximum allowable horizontal displacement of 100mm (equal to about 80% of shear strain). The bearing's deformation characteristics from micro-deformation to maximum deformation had been measured at factory in advance.

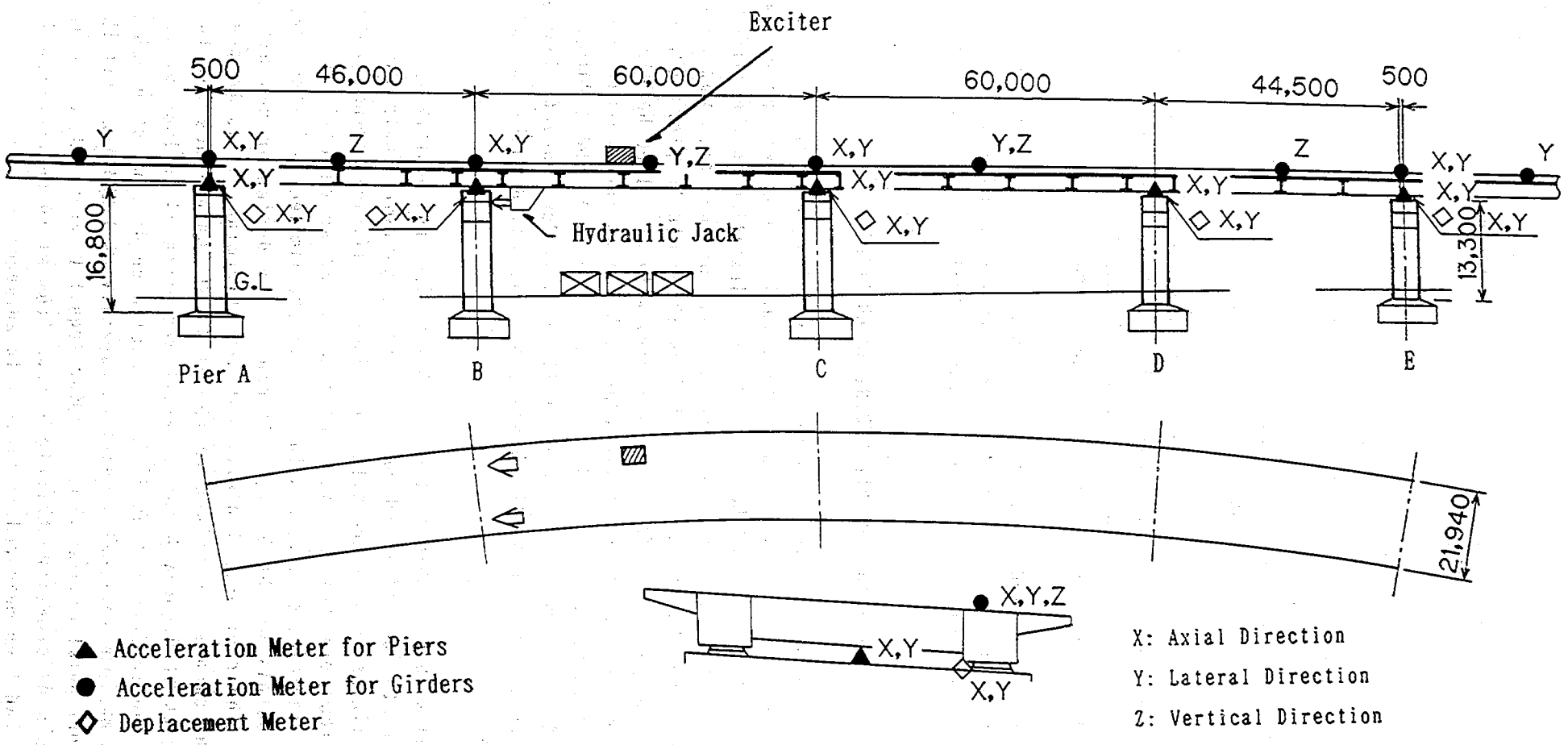


Fig. 1 Configuration of the Experimented Bridge and Arrangement of the Experimental Deveices

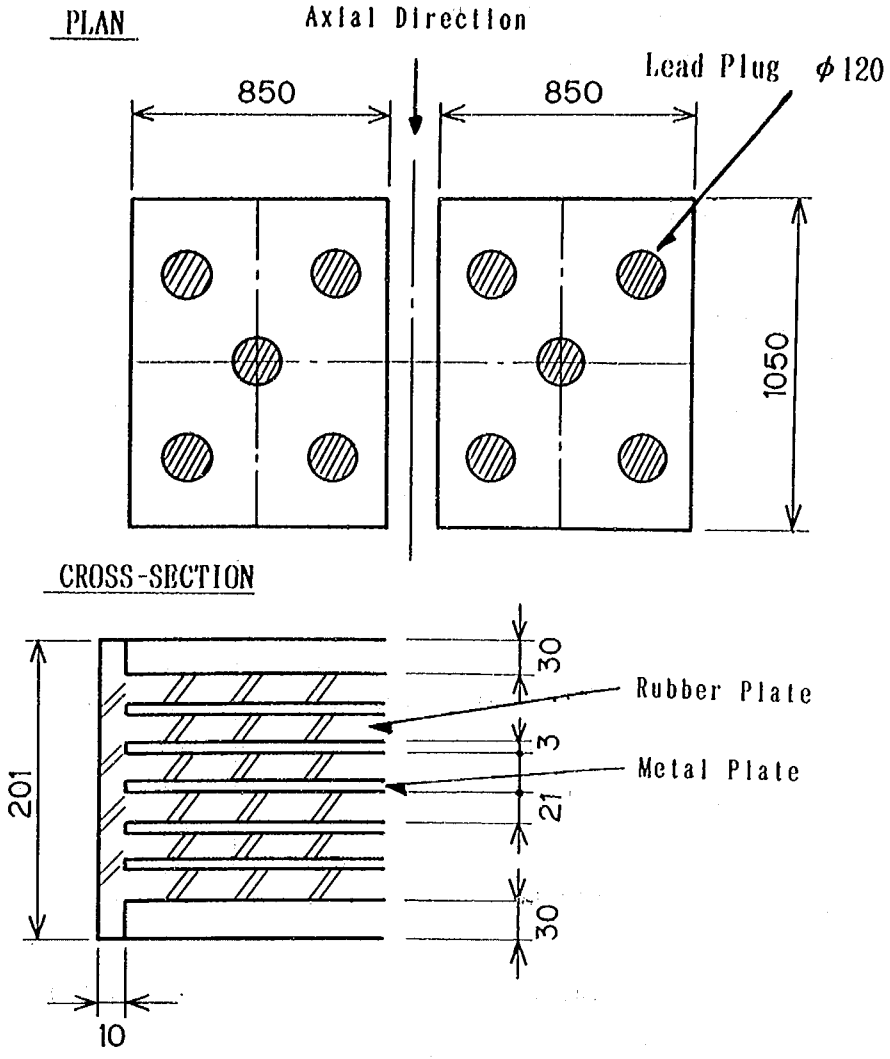


Fig. 2 Rough Configuration of LRB

Table-1 Principal Dimensions of LRB

		Designed Dimension
Size	Plane Size (cm)	1 0 3 × 8 3 × 2 set
	Effective Area (cm^2)	7 9 8 3 . 5 × 2 set
	Lead Plug Diameter (cm)	5 × 1 2 × 2 set
	Effective Rubber Thickness (cm)	6 × 2 . 1
	Total Height (cm)	2 0 . 1
Rubber Properties	Shear Modulus of Rigidity (kgf/cm^2)	8 . 0
	Shape Factor	1 0 . 2 2
	Compressive Rigidity (tf/m)	6 9 9 . 8 × 10^3
	Horizontal Rigidity (tf/m)	1 0 1 3 . 8
Yield Strength (tf)		8 8 . 2
Primary Rigidity (tf/m)		1 2 1 9 0
Secondary Rigidity (tf/m)		1 8 7 5 . 5

EXPERIMENT METHODS

Single Pier Excitation

Pier B had been vibrated under its self-standing state before steel girders were erected to measure the dynamic stiffness of its lower part. A small-sized vibration exciter (electro-hydraulic actuater type, maximum exciting force is 5 tonf) was installed on the top of the pier, It vibrated the pier in constant sine waves along the bridge's and pier's axis. Then, by servo-typed meters, horizontal acceleration in the exciting direction at the top and bottom of the pier, and rotational acceleration at the bottom of the pier were measured.

Girder Excitation by Exciter

After the Menshin bearings had been installed and steel girders had been erected, the entire bridge was vibrated by a large-sized exciter generating sine waves within a range of 0.5～ 5.0 Hz. The exciter is EX-6300H-VF type for horizontal vibration with maximum exciting force of 20 tonf and owned by the Public Works Research Institute of the Ministry of Construction. It is installed on the girder as shown in Fig.1. The bridge was excited in both axiak and lateral directions to the bridge.

Girder Excitation by Hydraulic Jack

6 sets of hydraulic jack were mounted near the crest of the pier B. They are owned by the laboratory of the Japan Highway Public Corporation and have loading capacity of 180 tons with rapid-release valves. The jacks are used for a damped free vibration experiment in which the jacks are abruptly released after forcedly deflecting the bridge in the axial direction. With such a loading process, bearings on pier B, C, D do not take an uniform share of total loads by the hydraulic jacks. Instead, the ratio is about 2:1:1.

Measuring Methods

The measured factors of the two experiments are: acceleration at girders and the top of pier, and the relative displacement between girder at bearing part and the top of pier. Meters for these two measurements are respectively servo-type speed meter and dial-gauge type displacement meter. Their arrangement is shown in Fig.1. Besides, signals for exciting force of the exciter and the generated load by the hydraulic jacks are measured as a standard parameter of input factors.

RESULTS OF THE EXPERIMENTS

Single Pier Excitation

Satisfactory sinusoidal response data of piers have been obtained in the axial and longitudinal direction. As its typical example, response curves in the axial direction at pier's top are illustrated in Fig.3. (a) shows amplitude response curve per 1 ton of excited force, and (b) shows a phase curve according to the degree of excited force.

Parameters representing the pier's natural vibration characteristics were obtained from the test results. Table-2 shows natural frequencies and modal damping ratio of the pier. Its oscillation modes are indicated in Fig.4 from which it is clear that major portion of the horizontal displacement at pier's

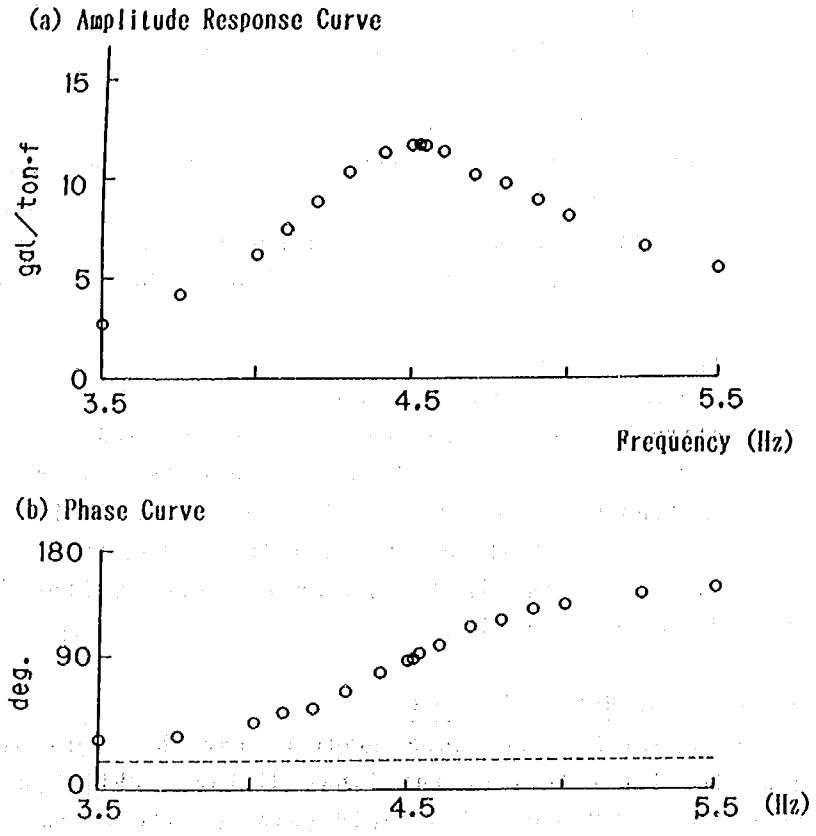


Fig. 3 Sinusoidal Response Curves by Single Pier Excitation (axial direction, obtained from pier's top)

Table-2 Natural Frequency and Modal Damping Ratio of a Pier

Exciting Direction	Natural Frequency (Hz)		Modal Damping Ratio (%)
	Measured Value	Estimated value	Measured Value
Axial	4.53	4.51	9.2
Lateral	4.19	4.14	5.4

top is caused from rotational movement at pier's bottom.

Based on the measured parameters, fixed coefficient of ground reaction at per's bottom was determined by the following process: natural vibration analysis with a single pier model is carried out by varying two coefficients of ground reaction (horizontal coefficient K_{H} and rotational coefficient K_{R}). Then optimized values of the coefficients are calculated so that the estimated natural frequency and the oscillation mode can be in the best conformance with their measured values. Table-2 and Fig.4 show the estimated values with the fixed coefficients and their comparison with the measured values.

This process resulted in overestimation of the coefficients compared with those prescribed in the Specifications for Highway Bridges: estimated K_{H} and K_{R} are respectively 5.2 and 3.1 times as high as the specified values. This difference is considered to be caused by the premise that the former is based on the frequent vibration with micro-amplitude level, while the latter is considering a major turbulence by a rare big earthquake.

Girder Excitation by Exciter

As an example of the results of exciter experiment, response curves of the pier B in the axial direction in case of 5-ton excitation level is shown in Fig.5. (a) and (b) are spectral amplitude curve and phase curve respectively with same definition as Fig.2. Meanwhile, (c) is the modal circle indicating in polar coordinates the relationship between amplitude and phase of the response simultaneously. Resonance point can be easily found with this circle. The right half of Fig.5 is resonance curves when the excition level is doubled. Here, there is a clear difference compared with the original level: drop of the peak frequency and distorted resonance curve can be seen when amplitude becomes greater. This is considered to be mainly due to non-linearity of the bearing's behaviours. The natural frequencies of the entire bridge are obtained from the given relationship between the maximum responsed amplitude and the phase. Furthermore, oscillation modes and modal damping ratio are determined according to the relative amplitude of each measuring point and the shape of resonance curve respectively.

Girder Excitation by Hydraulic Jack

Fig.6 illustrates a typical example of wave form in the damped free vibration state by a hydraulic jack. It is found that, in case of 500-ton loading, maximum relative displacement at bearing portion is about 36mm. This value is equivalent to the absolute displacement of the Menshin bearings on pier B. Right after load is released, the relative displacement at bearing portion is immediately decreased up to almost the neutral position. However, rather evident free damping wave form in which axial oscillation mode excels appears subsequently, and the residual displacement after the free damping is relatively small. The same performance is observed with a smaller load. Moreover, the wave form of relative displacement of bearings at pier A indicates a response wave form of absolute displacement of the entire bridge, since they are fixed roller bearings. Also, it can be said that acceleration wave forms at girders and pier's top includes high frequency components caused by a shock wave at the time of load release. Given these results, other values of natural frequency, oscillation mode and damping constant were obtained.

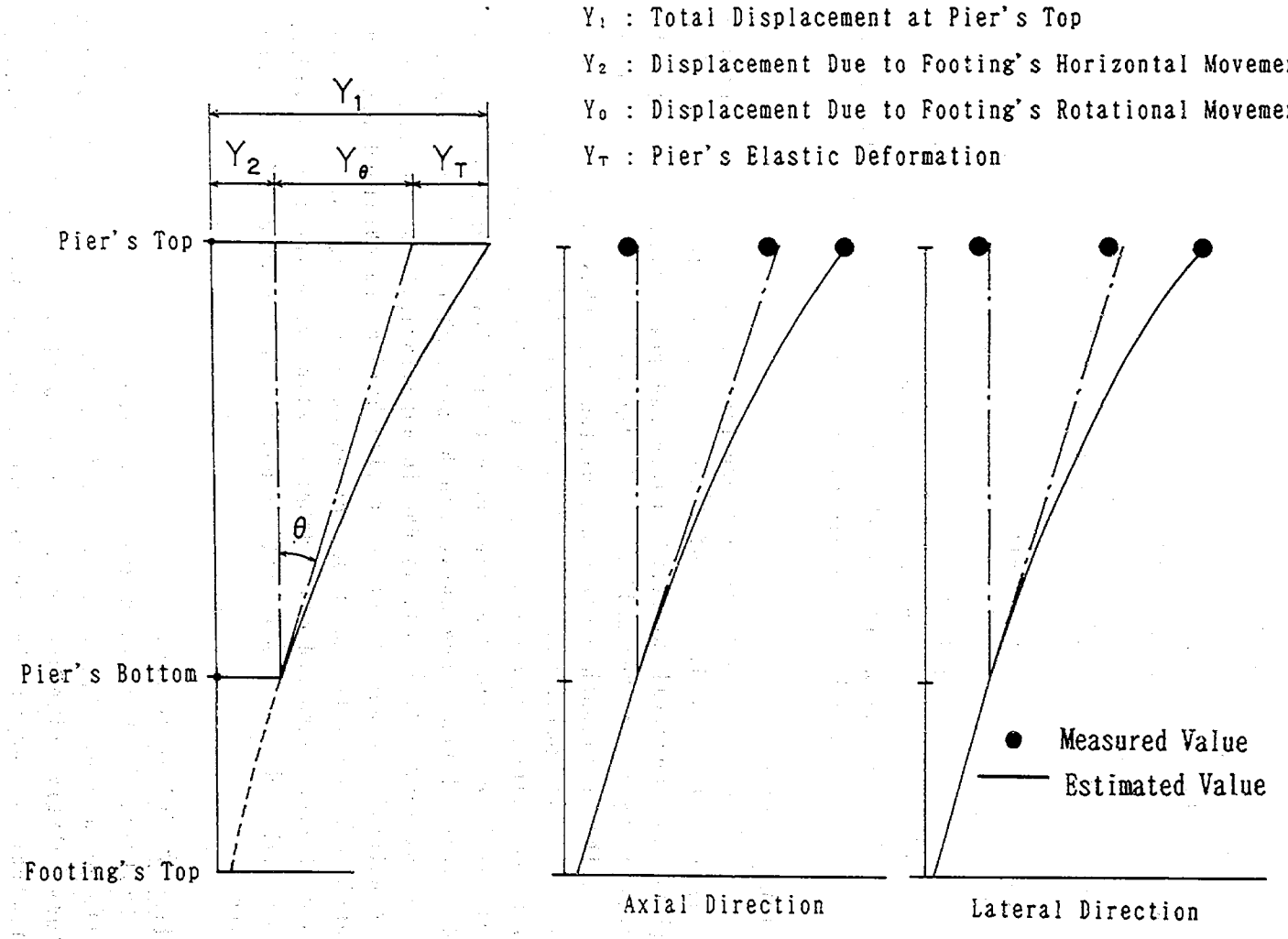


Fig. 4 Measured and Estimated Values of the Pier's Vibration Modes

Measuring Point: Girder's Upper Flange above Pier 8

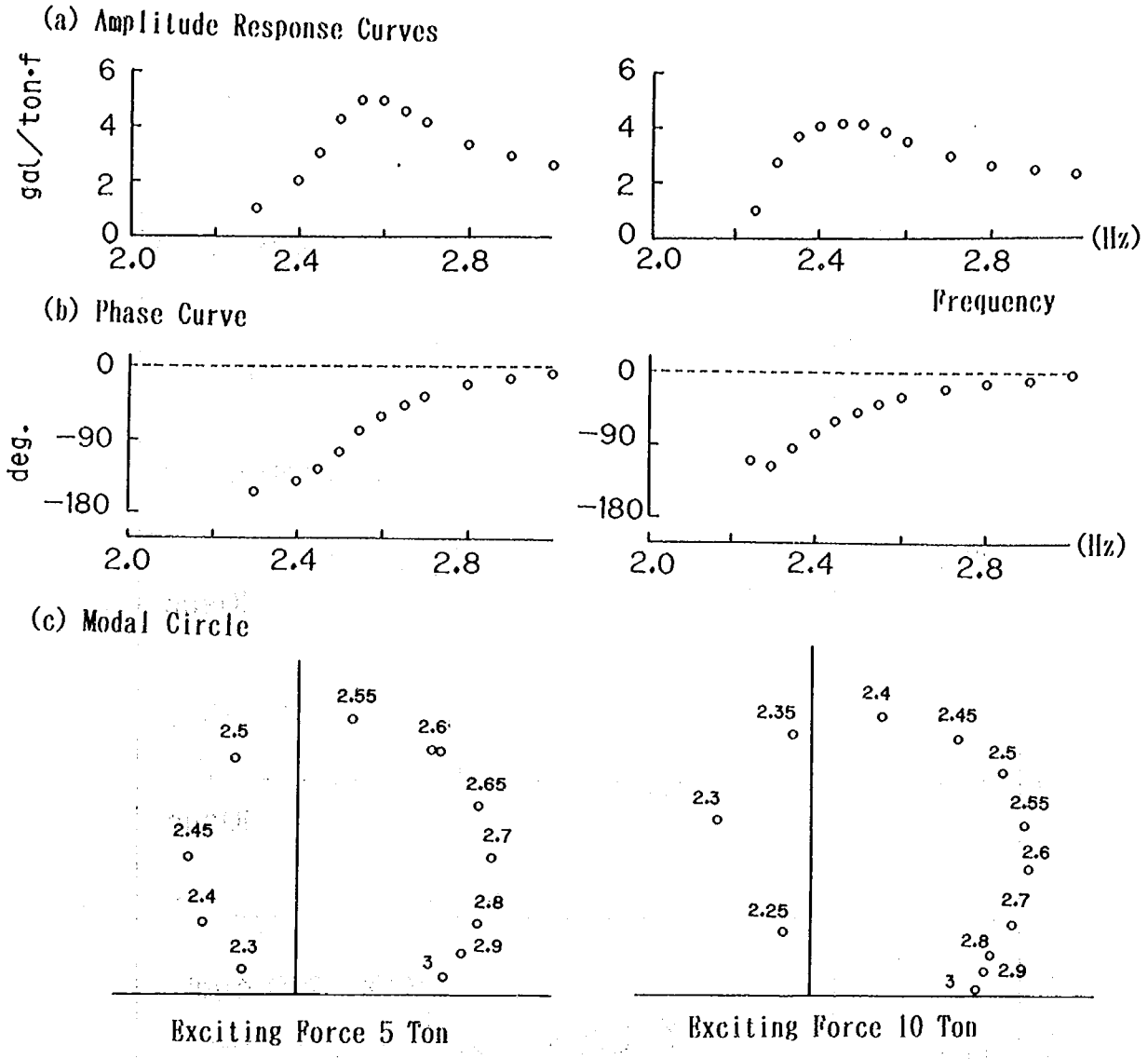


Fig. 5 Response Curves from Girder Excitaion by Exciter
(Excitation to Axial Direction)

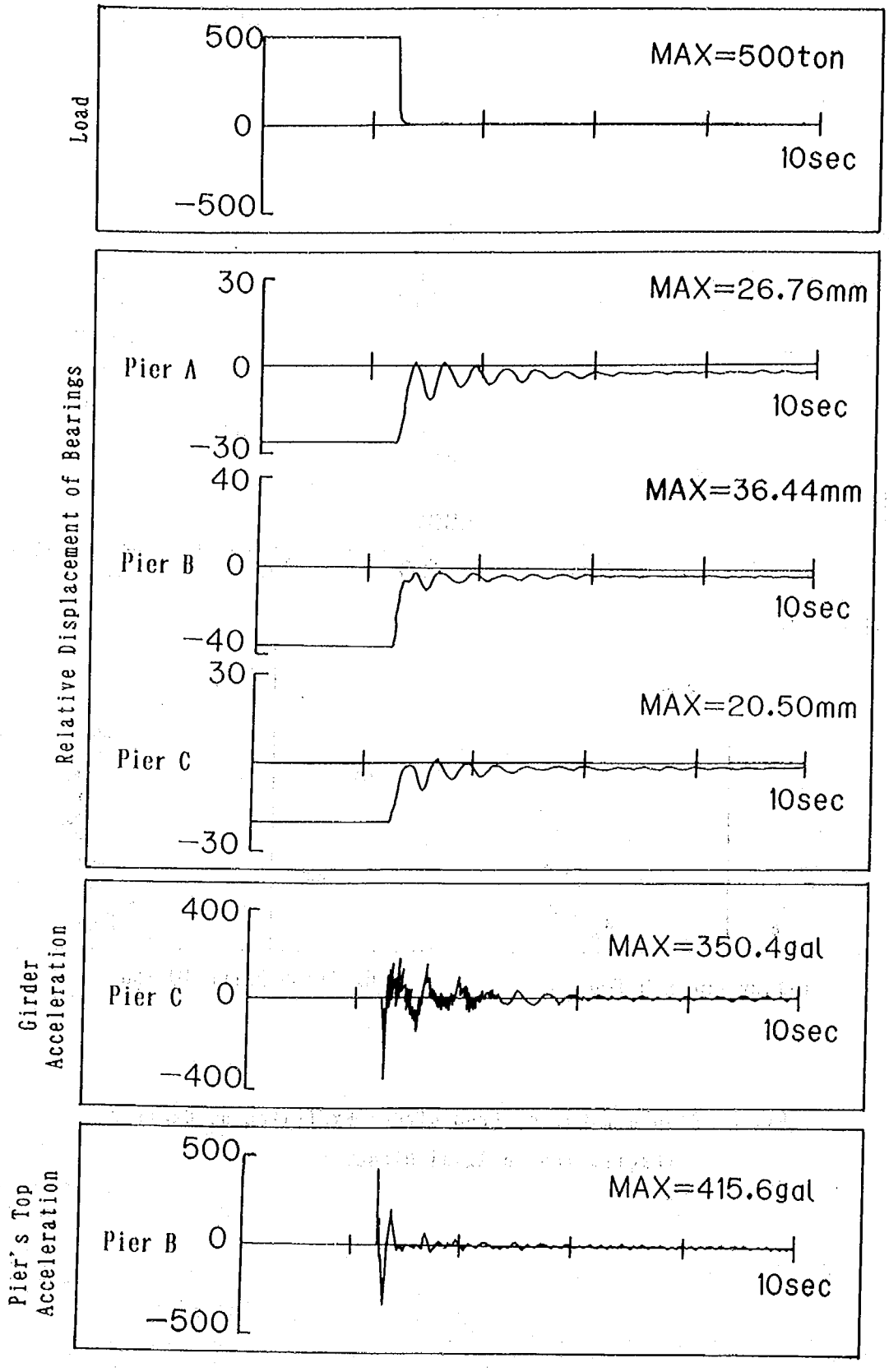
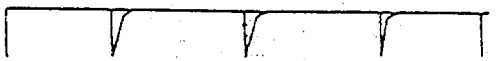
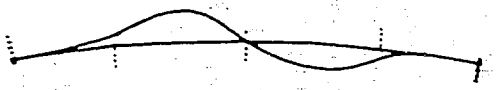
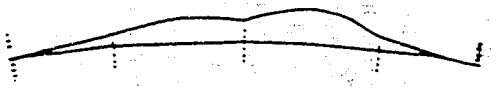
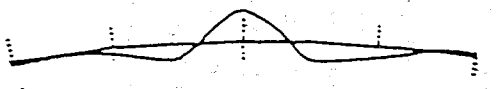
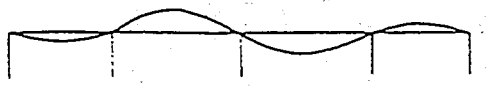


Fig.6 Wave Forms from Girder Excitation by Hydraulic Jack
(Immediate Load Release after 500-ton Loading)

Table-3 Summary of Measurement Results of Vibrational Characteristics

Vibrating Direction	Exciting Method (Exciting Direction)	Vibration Order	Oscillation Mode	Natural Frequency (Hz)	Modal Damping Ratio (%)	Girder's Maximum Amplitude (One-sided)	
						Acceleration (gal)	Displacement (mm)
Axial	Exciter (Axial)	1	 (profile)	2.55 (Exciting Force 5 ton) 2.40 (Exciting Force 10 ton)	5.8 7.8	25.0 41.9	1.0 1.8
	Hydraulic Jack (Axial)	1	(same as above)	2.86 (200t Loading) 2.30 (500t Loading)	6.5 * 7.3 *	——	2.6 12.5
Lateral	Exciter (Lateral)	1	 (plan)	1.97	1.2 *	34.0	2.2
		2	 (plan)	2.23	1.8	54.6	2.8
		3	 (plan)	3.72	3.0	14.0	0.3
Vertical	Exciter (Axial)	1	 (Profile)	2.22	0.5 *	30.0	1.5

* The figures are obtained from damped free state. Otherwise, they are obtained by half-power method from the given resonance curves.

Summary of the Results

The parameters values of the bridge's natural vibration characteristics measured by the aforementioned two experiments are summarized in Table-3. The bottom column of the table, which indicates the case of excitation in the longitudinal direction, is considered to be induced by the girder's moment component from vertical vibration when excited in the axial direction. In case of oscillation mode in the axial direction, in which Menshin bearings are largely deformed, natural frequency and modal damping ratio is in proportion to the degree of amplitude. On the contrary, in case of lateral mode, where there is little bearing deformation, they are independent from the amplitude level. Also, 1st and 3rd modes, which are composed of the elastic deformation of the main girders, appears at relatively lower frequency. It is because that deck slabs had not been placed at the time of experiment, and lateral rigidity of the girder was then lower than the actual composition. Therefore, after the deck placement, such elastic deformation is supposed to disappear.

MODEL ANALYSIS OF NATURAL VIBRATION

As shown in Fig.7, the analytical model of the bridge uses three-dimensional frame structure in order to express the structural detail as realistically as possible. Stiffness of Menshin bearing, K_M had been predetermined by the factory experiment data. Fig.8 illustrates three force-deflection loops of the bearings. They show that the relationship between the input force and the bearing's response greatly varies according to the magnitude of the given amplitude level of the bearings. In particular, in case of small amplitude level which is equivalent to that of the vibration experiment, the loop does not form so-called bilinear shape.

In order to compare the model analysis with the vibration experiments, effective stiffness of Menshin bearing is determined by the average slope of the given force-deflection loop at same small amplitude level as for the field experiments. Frequency and oscillation mode are estimated by the natural vibration analysis with coefficients of ground reaction estimated by the single pier excitation experiment. Then, by taking account of damping effects on each part of the bridge, the model's modal damping ratio are calculated in the following modal damping equation:[2)]

$$h_i = \frac{\Sigma \phi_{ij}^T \times h_j \times K_j \times \phi_{ij}}{\phi_i^T \times K \times \phi_i}$$

Where,

ϕ_{ij}: modal vector of element j in ith mode
h_j : modal damping ratio of element j
K_j : stiffness matrix of element j
ϕ_i : modal vector of the entire structure in ith mode
K : stiffness matrix of the entire structure

Here, modal damping ratio at steel structures and ground spring are presumed to be 0.5% and 10% respectively by referring to the results of the field experiments indicated in Table-3. The value for Menshin bearings is fixed to be 5.8% from the closed area of the loop in Fig.8 (a).

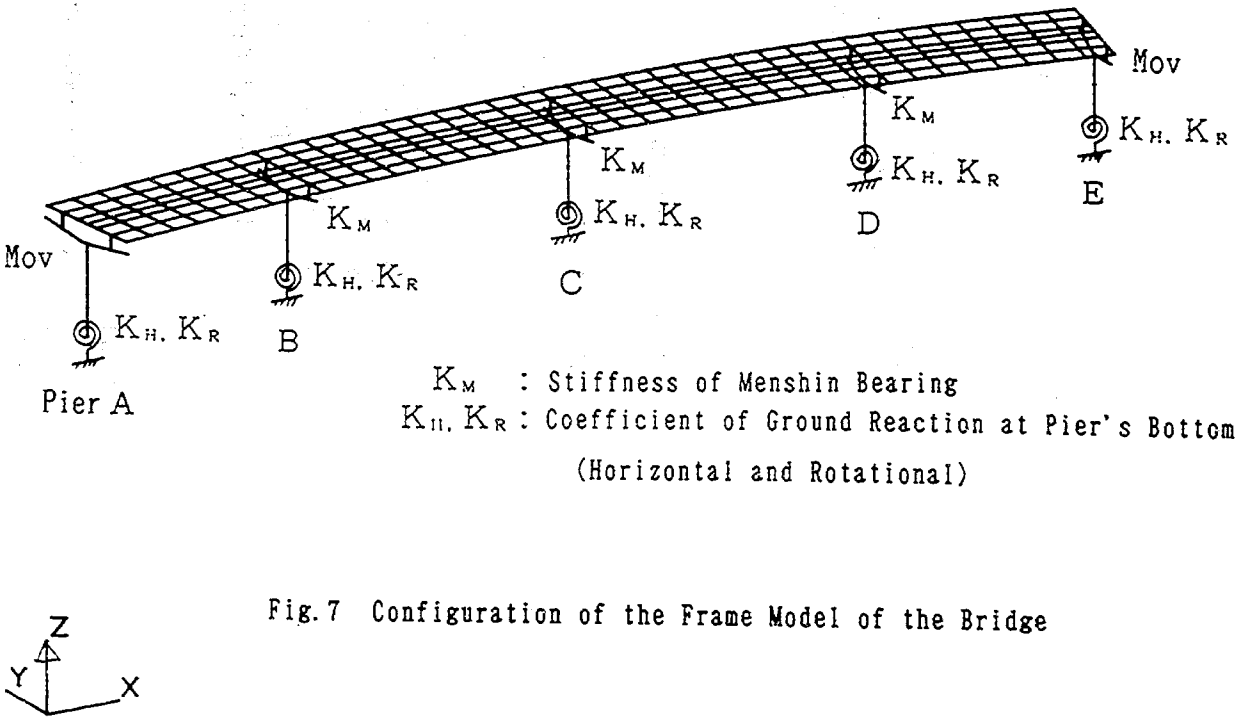


Fig. 7 Configuration of the Frame Model of the Bridge

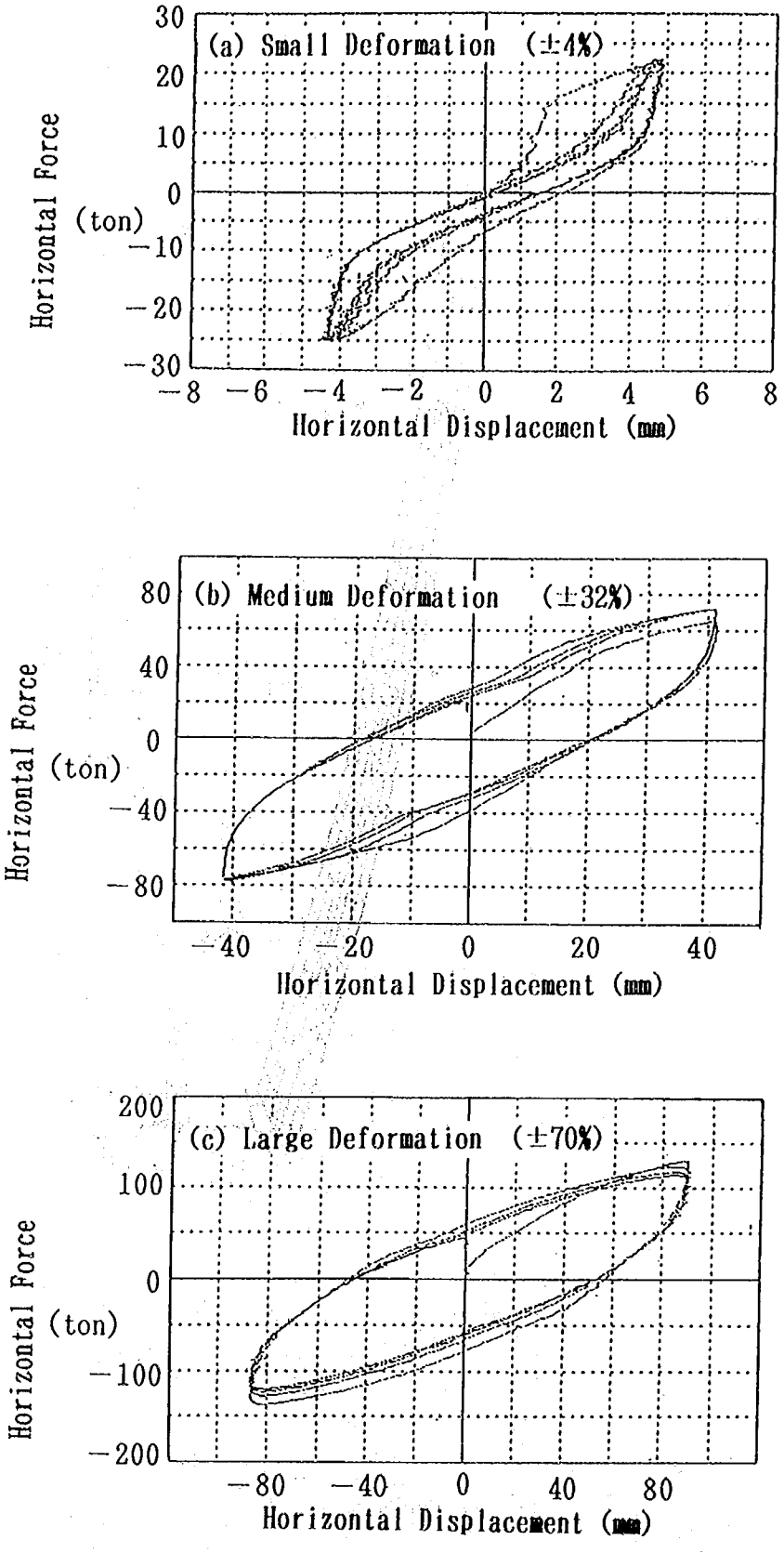


Fig. 8 Force-Deflection Loops of Menshin Bearing by Factory Experiment

The results of the model analysis and those of the exciter experiment are compared in Table-4. It shows that the measured and calculated natural frequencies are agreed with satisfactory accuracy in all modes. Damping constant is a little overestimated in most modes, though it is considered to be an allowable difference for the model's practical use. Moreover, the comparison of oscillation mode illustrated in Fig.9 clarifies that the model values precisely simulate the experiment values in all modes.

From these results, it can be considered that natural vibration characteristics in a low-level vibration of the entire bridge, which is supposed to be important as the basis for the Menshin design, can be estimated by this developed model with sufficient accuracy for its practical use.

As a result of the model analysis corresponding to the hydraulic jack loading experiment, static deformation in case of 500-ton loading is shown in Fig.10, which is the comparison between the experiment values and the model values with respect to relative displacement at five supporting points. Here, a non-linear analysis is conducted with non-linear stiffness of the Menshin bearings, which is estimated by the 32% deflection loop indicated in Fig.8. The experiment values are a little greater than the model values. But their difference is within 10%, which is allowable as an accurate estimation.

The model analysis corresponding to the rapid release experiment by a hydraulic jack is not conducted here, since transitional load/deformation characteristics of the Menshin bearing at the time of abrupt load decrease have not yet been clarified. At present, investigations are being made to obtain accurate data on the transitional characteristics for the future model analysis.

CONCLUSION

With field vibration experiments, vibration characteristics of the actual bridge incorporating Menshin bearings can be measured with desirable accuracy. Moreover, model analysis is proved to have a satisfactory simulation ability in many cases, and effectiveness of this analytical method can be recognized to some degree.

This series of experiment and model analysis take account of small-scaled vibration. If the analytical method is proved to be adequate, then it can be applied to larger amplitude level for regular seismic design, because Menshin bearings work most effectively when the bridge is struck by major earthquakes. Since such large deformation could not be realized in the vibration experiments, dynamic analysis has been conducted instead by applying the prescribed seismic waves to the developed bridge model. The Specifications for Highway Bridges provide these seismic waves which are applicable to the geological conditions of the construction site. Table-5 summarizes the results of the analysis along with the designed values for comparison. The actual design was based on the conventional static method. In all aspects, the model estimates that the values are about 40% less than those in design.

Although Menshin bearings can significantly reduce the seismic effects, they just reinforce its seismic safety in addition to other aseismic

Table-4 Comparison between Measured and Model Values

Exciting Direction		Natural Frequency (Hz)		Modal Damping Ratio (%)	
		Measured V.	Model Value	Measured V.	Model Value
Axial	1	2.55 (5ton) 2.40 (10ton)	2.52	5.8 7.8	7.0
Lateral	1	1.97	1.95	1.2	1.5
	2	2.23	2.17	1.8	3.2
	3	3.72	3.83	3.0	2.6
Vertical	1	2.22	2.12	0.5	0.7

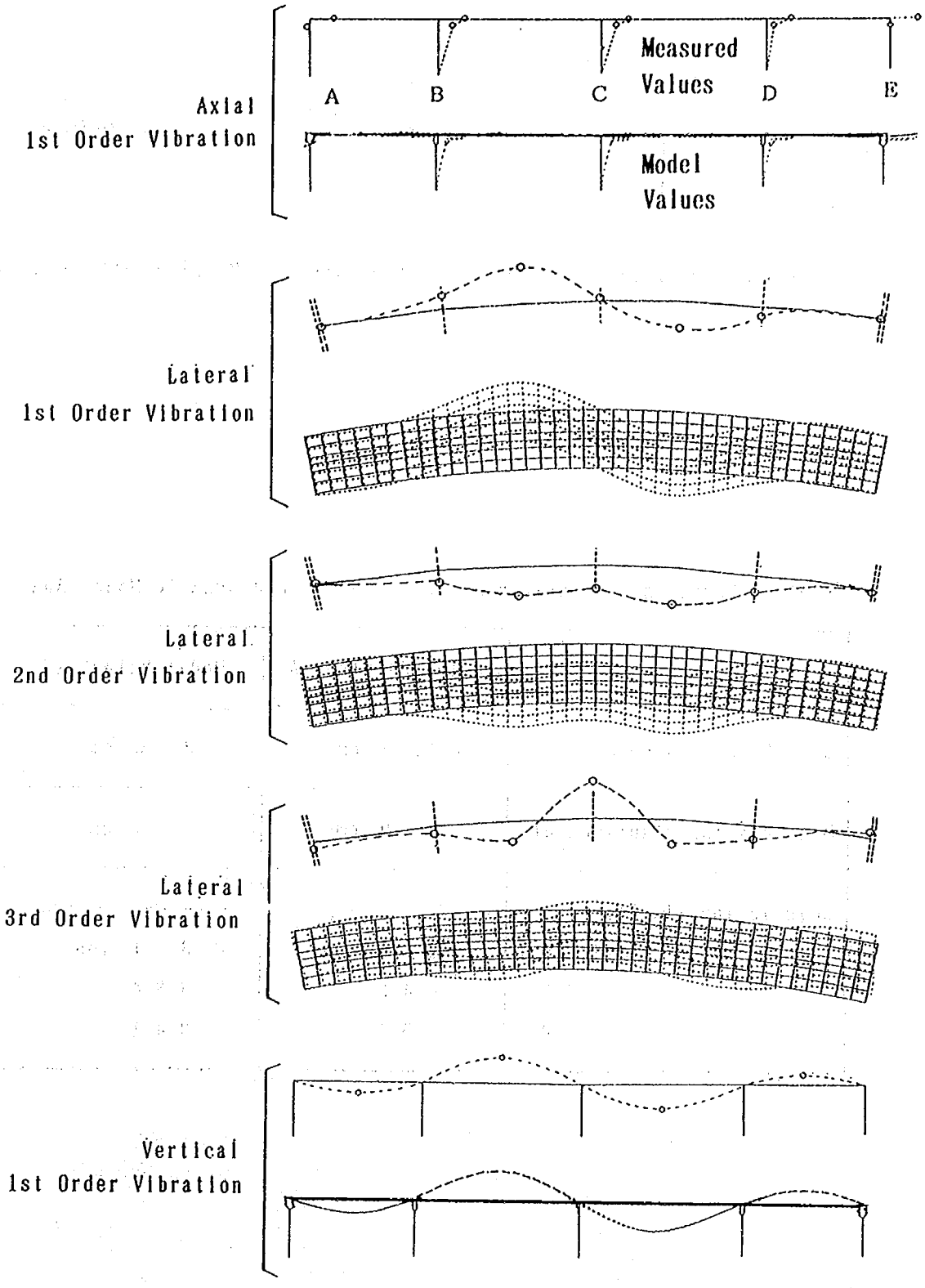


Fig. 9 Comparison of Oscillation Modes

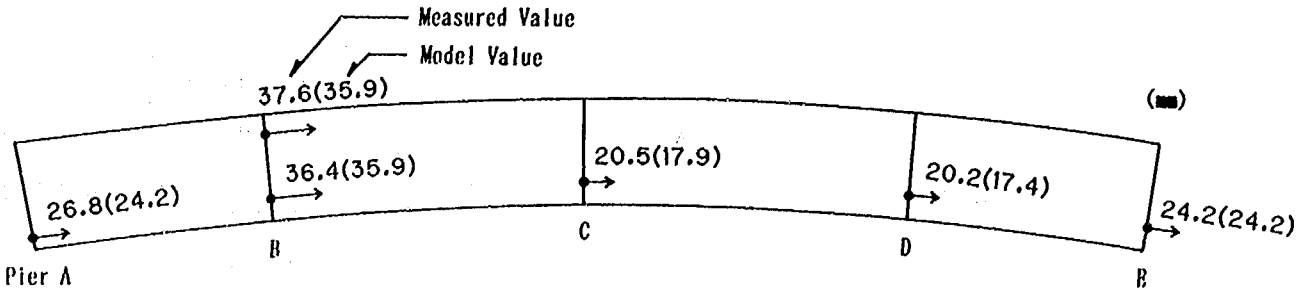


Fig. 10 Comparison of Static Deformation of Menshin Bearings (500-ton Loading)

Table-5 Comparison of Static Aseismic Design and Dynamic Model Analysis

	Designed Value (A)	Model Value (B)	B／A
Max. Bridge Movement	12.3 cm	8.0 cm	0.65
Max. Bearing Displacement	9.9 cm	6.1 cm	0.62
Seismic Inertia Force			
at Pier B	530 ton	331 ton	0.62
C	543	334	0.62
D	551	341	0.62

considerations. Hence, design of the bridge did not deal with the efficient use of the bearings, such as for reducing the size of foundations and/or piers. Reflecting more positively the effects of Menshin bearings, as clarified in this report, in the more economical design of other regular bridges is a possible next step in the future.

ACKNOWLEDGEMENTS

We greatly appreciate numerous technical guidances and advices given by members of Aseismic Design Sub-Committee in the Technical Council and the Committee With Respect To The Practical Use Of Menshin Bridges, both of which are organized by the Hanshin Expressway Public Corporation. Furthermore, we thank the joint ventures of the steel girder erection works of the bridge under study for their cooperation which enabled the smooth execution of both the experiments and analyses.

REFERENCES

1) Hanshin Expressway Public Corporation. "Dourokyo no Menshin Sekkeiho Gaidorain (An), (in Japanese, 'Guidelines for the Menshin Design Methods of Highway Bridges (Draft)')". March, 1989.

2) Japan Road Association. "Dourokyo Shihosho, V: Taishin Sekkei Hen, (in Japanese 'Specifications for Highway Bridges, Chapter V: Aseismic Design')". February, 1990.

RESPONSE ANALYSIS OF MIYAGAWA BRIDGE BASED ON A MEASURED ACCELERATION RECORD

Kazuhiko Kawashima[I], Hiroyuki Nagashima[II], Shuji Masumoto[III] and Kohji Hara[IV]

I Head, Earthquake Engineering Division, Earthquake Disaster Prevention Department, Public Works research Institute, Ministry of Construction
II Panning Department, Kanto Regional Construction Bureau, Ministry of Construction
(Formerly, Research Engineer, Earthquake Engineering Division, ditto)
III Director, Road Construction Department, Shizuoka Ken
IV Second Design Office, Numazu Construction Office, Shizuoka Ken

ABSTRACT

This paper presents an analysis of a measured acceleration record at Miyagawa Bridge, the first seismically isolated bridge in Japan. Amplification of the peak accelerations is examined between the deck, pier and ground motions. Seismic isolation effect can be clearly observed. Dynamic response analysis using the analytical model adopted for seismic design is made assuming the acceleration recorded at underground as the input ground motion. Response acceleration computed at the deck is quite similar with the measured acceleration although peak acceleration is larger in the analysis.

INTRODUCTION

Miyagawa Bridge is the first seismically isolated bridge in Japan, and is located on National Highway No. 362 in Shizuoka ken[1)2)]. It completed in March 1991. Strong motion observation has been made since the completion. Because the first record was obtained by an earthquake with magnitude 4.9, which took place close to the site, an analysis was made for verifying the effectiveness of Menshin Design[3)]. This paper presents the seismic behavior of Miyagawa Bridge based on the analysis of the recorded accelerations.

STRONG MOTION OBSERVATION AT MIYAGAWA BRIDGE

As was reported in the previous paper[1)2)], the Menshin Design (seismic isolation design) of Miyagawa Bridge was made in accordance with the

Guidelines of Menshin Design of Highway Bridges[2]. In the Menshin Design, the Menshin devices are designed by both the Seismic Coefficient Method and the Bearing Capacity Method. In both methods, the lateral force is statically applied to the bridge, and the seismic safety is examined based on the allowable stress design approach in the Seismic Coefficient Method and the bearing capacity considering ductility in the Bearing Capacity Method.

The lateral force coefficient was not, however, reduced at the Miyagawa Bridge from the design value specified in the Specifications of Design of Highway Bridges[4], because it was the pilot project for verifying the effectiveness of the Menshin Design. The lateral force coefficient is therefore ? in both longitudinal and transverse directions.

Lead rubber bearings[5] were adopted so that damping ratio of 0.12 can be obtained for the first mode of the bridge. Natural period of the bridge in longitudinal direction was assumed as 0.76 second in the Seismic Coefficient Method and 1.0 second in the Bearing Capacity Method. Because of the deformation dependence of the stiffness of the lead rubber bearings, the natural period is not the same for the Seismic Coefficient and the Bearing Capacity Method.

Soil condition at the site is I-group (stiff) based on the classification of ground condition specified in the Seismic Design Specifications of Highway Bridges[4].

Three 3-components feed-back servo type strong motion accelerometers were placed on the deck and pier crest at pier 1 (P1) and 10 m below the ground surface 10 m apart from the abutment 1 (A1) as shown in **Fig. 1**. The data are recorded on the analog magnetic type recording system when the ground acceleration larger than the triggering level is developed.

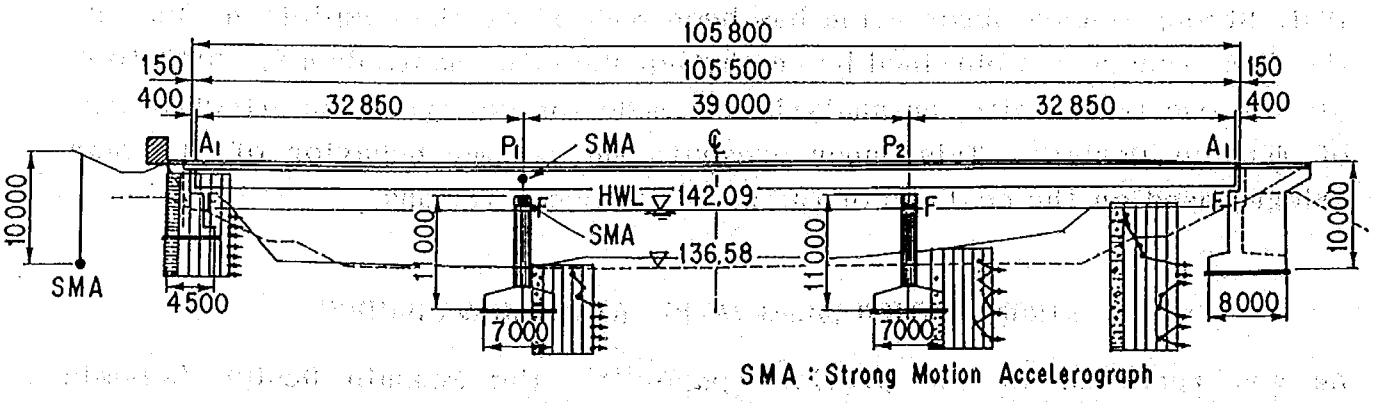
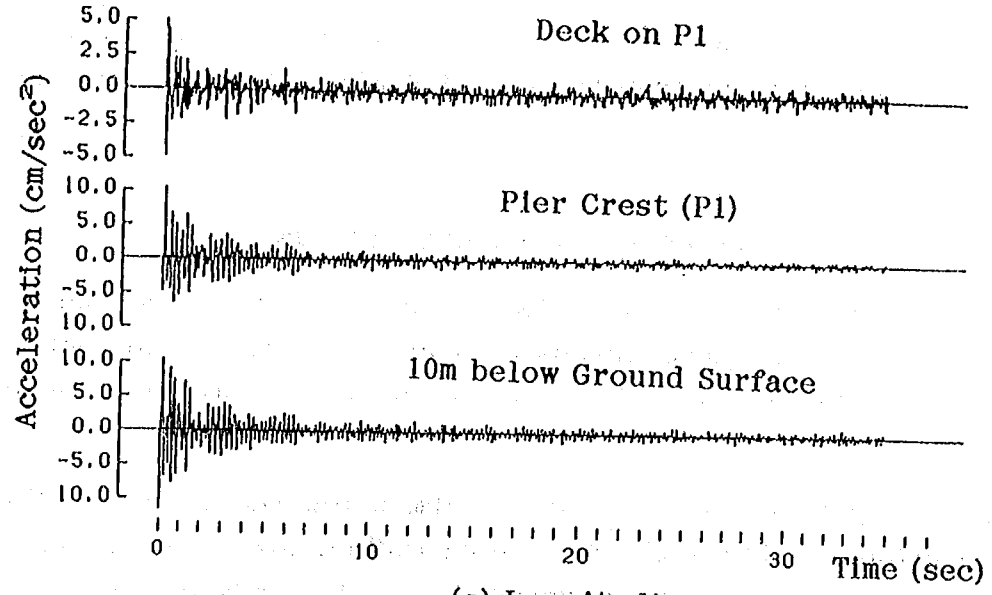
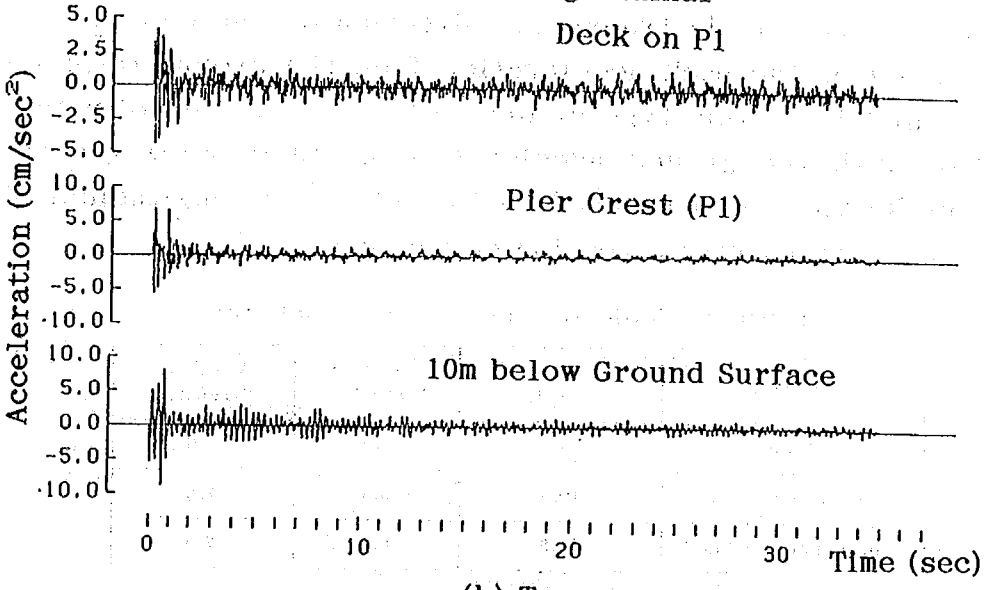


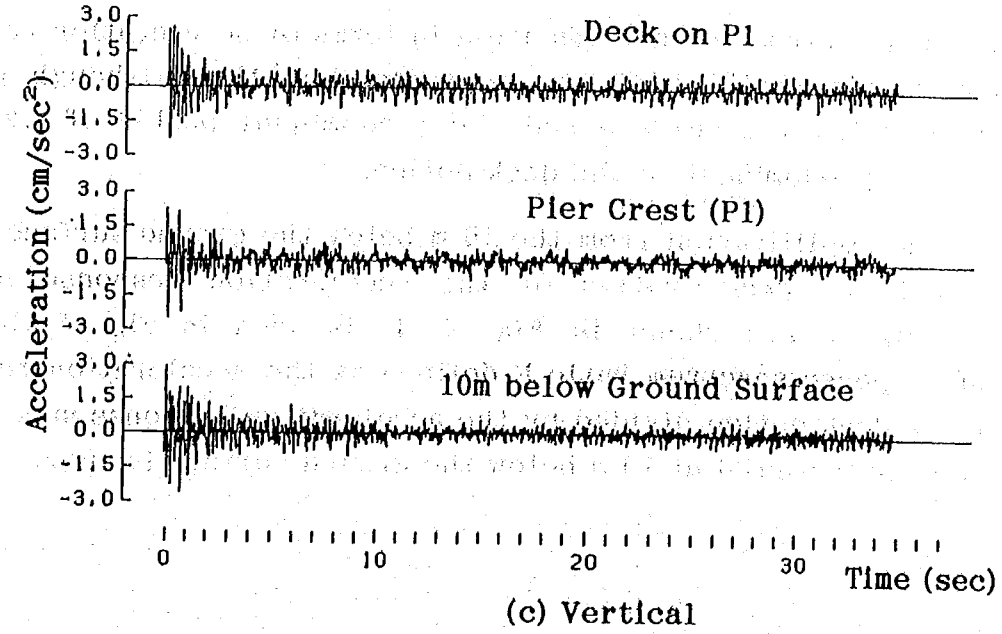
Fig. 1 Miyagawa Bridge and Location of Accelerometers



(a) Longitudinal



(b) Transverse



(c) Vertical

Fig. 2 Measured Accelerations

The first record was obtained by an earthquake with magnitude 4.9 which took place about 30 km north east from the site. Seismic Intensity of Japanese Methodological Agency was II.

ANALYSIS OF MEASURED RECORDS

Fig. 2 shows the accelerations recorded at the deck, pier crest and 10m below the ground surface. Because intensity was so small, first part of the response could not be recorded. But main part could be successfully recorded.

Table 1 shows the peak acceleration. At 10m below the ground surface, the peak acceleration was 11.6 cm/sec^2 in longitudinal direction and 8.9 cm/sec^2 in transverse direction. This decreased to 10.4 cm/sec^2 in longitudinal direction and 6.6 cm/sec^2 in transverse direction on the pier crest. Because the amplification of the peak acceleration from the ground to pier crest is generally about 2.5 for this type of bridges[8], the decrease of pier response in comparison with the ground acceleration at 10 m below the surface is apparent. Furthermore, it decreased to 5.0 cm/sec^2 in longitudinal direction and 4.3 cm/sec^2 in transverse direction on the deck.

Table 1 Peak Accelerations Measured

Location	Longitudinal Direction	Transverse Direction	Vertical Direction
Deck on P1	5.0	4.3	2.6
Pier Crest of P1	10.4	6.6	2.5
10 m underground	11.6	8.9	2.9

Fig. 3 shows such decrease of amplification in terms of acceleration response spectra with damping ratio of 0.05. It is apparent that although ground motion at 10 m below the surface had the predominant period of 0.2 ~ 0.3 second, it is not predominant in the deck motion.

For studying the amplification from the 10 m below the ground surface to the pier crest and the deck, ratios of the acceleration response spectra presented in **Fig. 3** are shown in **Fig. 4**. It is seen in **Fig. 4** that the acceleration response spectrum ratio R defined as the acceleration response spectrum of the deck motion divided by the acceleration response spectrum of the ground motion measured at 10 m below the ground surface is approximately

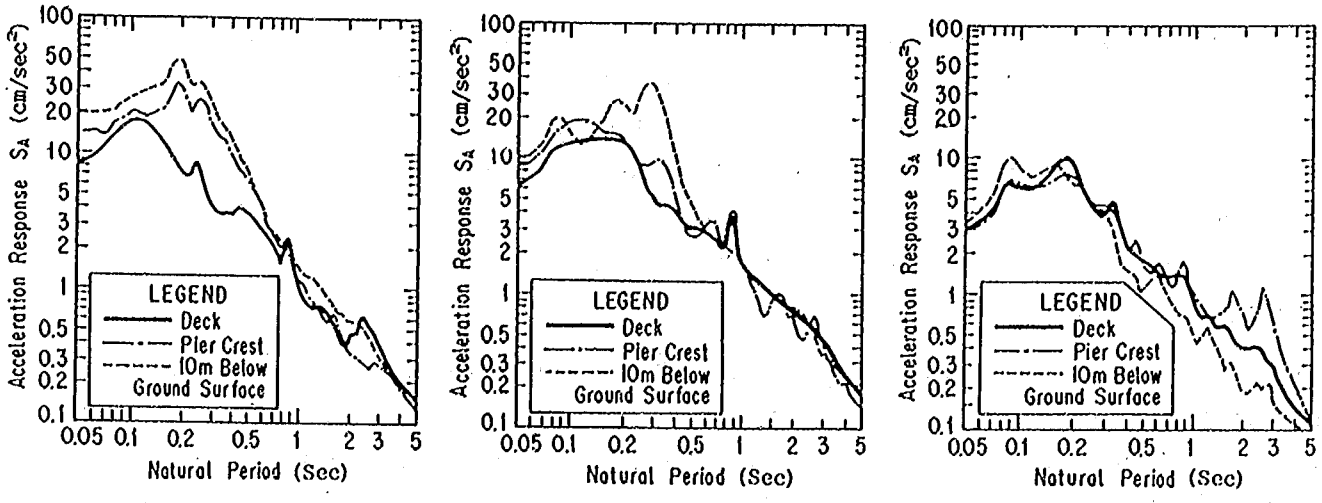


Fig. 3 Acceleration Response Spectra of Measured Acceleration Record (Damping Ratio of 0.05)

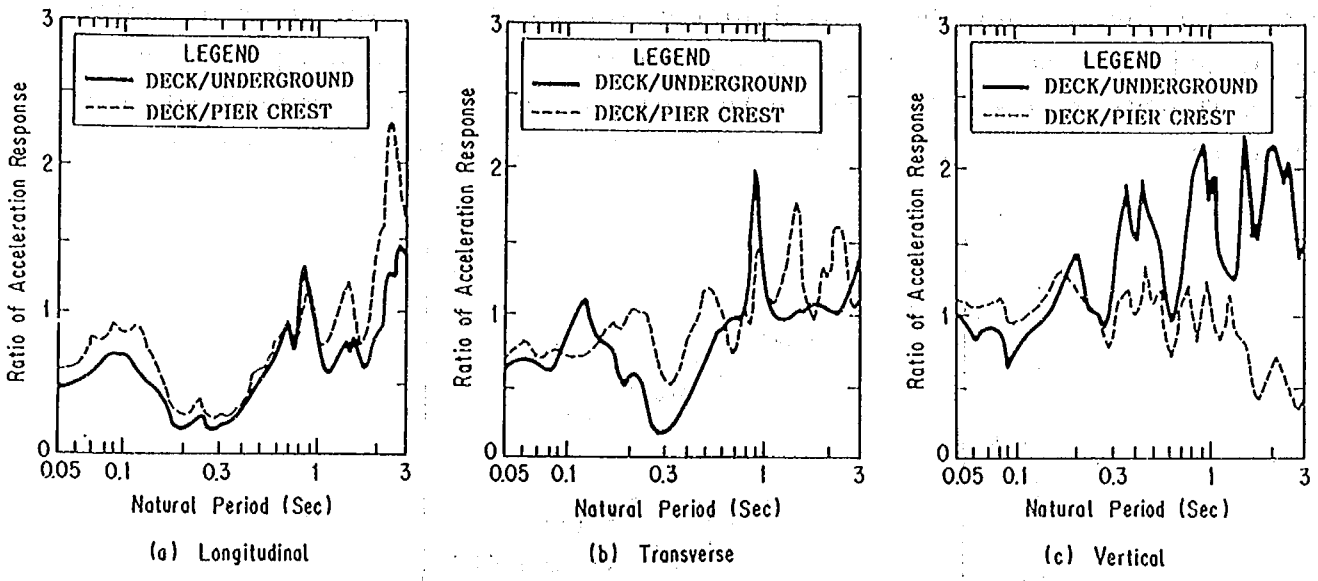


Fig. 4 Ratios of Acceleration Response Spectra

0.2 at natural period of 0.2～0.3 second. The motion at this period is filtered out at the deck due to the effect of seismic isolation.

On the other hand, the ratio R defined as the acceleration response spectrum of the deck motion divided by the acceleration response spectrum of the ground motion measured 10 m below the ground surface increases to 1.4 in longitudinal direction and 2.0 in transverse direction at natural period of

about 0.85 second. Reminding the fact that the natural period assumed in the Seismic Coefficient Method was 0.76 second, this represents the amplification of deck response due to resonance of the first mode. Reflecting the fact that the deformation of LRBs developed during the earthquake is much smaller than that assumed in the design by means of the Seismic Coefficient Method, stiffness of LRBs is approximately 25 % higher than that assumed in the design.

The LRBs were designed so that yielding of the lead plug be developed for the lateral force coefficient over 0.12. Of course, because the response during the earthquake was much smaller that this level, bilinear behavior of LRBs seems not significant. However it should be noted that LRBs show high energy dissipation capability from small displacement. **Fig. 5** shows the equivalent damping ratio of the LRBs obtained from the full size test[7]. Although the equivalent damping ratio for shear strain smaller than 20 % is not presented here, it is known that the equivalent damping ratio for smaller shear range can be approximately evaluated by extrapolating the relation presented in **Fig. 5.** Therefore it may be assumed that the equivalent damping ratio of LRBs was approximately 30 % for the shear strain developed during the earthquake.

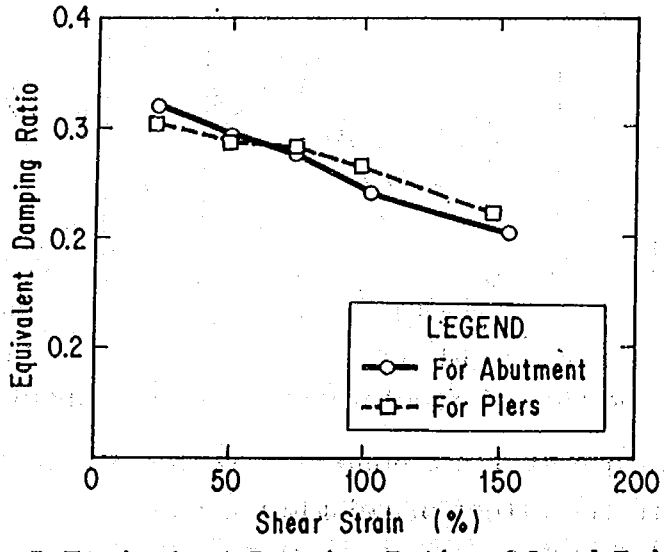


Fig. 5 Equivalent Damping Ratio of Lead Rubber Bearings Based on Full Model Tests

STUDY OF THE RECORD BY DYNAMIC RESPONSE ANALYSIS

Because dynamic response analysis was made at the design stage for Miyagawa Bridge, it was decided to adopt the same analytical model as shown in **Fig. 6** for studying the record. The acceleration recorded at 10 m below the ground

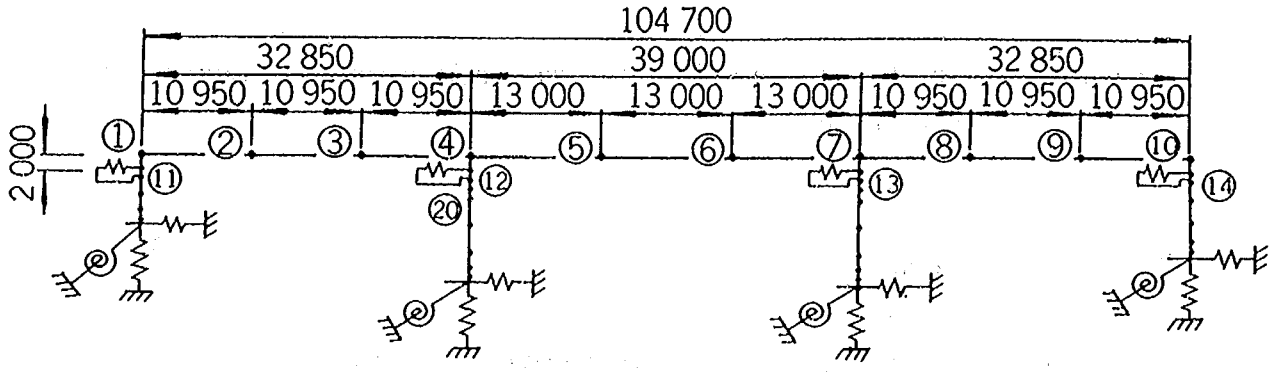


Fig. 6 Dynamic Response Analysis Model of Miyagawa Bridge for Design Purpose

surface was regarded as the input ground motion and the response of the deck and substructure were computed and compared with the recorded accelerations. Because the footings of P1 and P2 are almost on the same level with the down-hole accelerometer placed 10 m below the ground surface (refer to **Fig. 1**), it was considered appropriate to apply the acceleration measured at 10 m below the ground surface to the footings. Although the footing of two abutments, A1 and A2, is slightly higher in level than the down-hole accelerometer, it was disregarded in the analysis because it would cause only minor difference.

Analysis was made by the equivalent linear analysis. Because the deformation of the LRBs was quite small during the earthquake, the first stiffness k_1 was assumed as the equivalent stiffness of LRBs as

$$k_1 = 6.5\ k_2 \tag{1}$$

$$k_2 = \frac{F - Q_d}{u_B} \tag{2}$$

$$Q_d = A_P \cdot q_o \tag{3}$$

$$F = A_R \cdot G \cdot \gamma + A_P \cdot q \tag{4}$$

$$q = -283.6\ \gamma^2 + 183.8\ \gamma + 85.0 \tag{5}$$

where

k_1 :1st stiffness of LRB (kgf/cm)
k_2 :2nd stiffness of LRB (kgf/cm)
Q_d :yielding force of lead (kgf)
q_o :shear stress of yielding of lead plug (= 85.0 kgf/cm^2)
G :shear modulus of rubber (kgf/cm^2)
F :shear force of LRB (kgf)
u_B :design displacement (cm)

γ :shear strain

Modal damping ratio h of the bridge was computed by means of the energy-proportional damping method as[4]

$$h = \frac{\sum_{j=1}^{n} \phi_{ij}^{T} h_j K_j \phi_{ij}}{\Phi_i^{T} K \Phi_i} \qquad (6)$$

where

ϕ_{ij} :mode vector of j-th structural component for i-th mode
h_j :damping ratio of j-th structural component
K_j :stiffness matrix of j-th structural component
Φ_i :mode vector of bridge for i-th mode
K :stiffness matrix of bridge

Eq. (6) is effective to evaluate the modal damping ratio of bridges based on an experimental study[5]. Damping ratio of structural components was assumed in design as shown in **Table 2.** Because the deformation developed in LRBs is small during the design earthquake assumed in the Seismic Coefficient Method, it was assumed in the design that the damping ratio of LRBs is zero in the Seismic Coefficient Method. It may be therefore good to assume zero damping ratio for LRBs for the consistency with the seismic design. However it became apparent that zero damping ratio for LRBs gives appreciably lager bridge response than the measured values. Therefore it was assumed as 0.3 based on the above described full model test results on the damping characteristics of LRB.

Table 2 Damping Ratio Assumed in Seismic Design of Miyagawa Bridge

Structural Components		For Design		For this Analysis
		Seismic Coefficient Method	Bearing Capacity Method	
Super structure		0.03	0.03	0.03
Piers and Abutments		0.05	0.05	0.05
Foundations		0.1	0.1	0.1
Menshin Bearings	A1	0	0.177	0.3
	P1	0	0.137	0.3
	P2	0	0.139	0.3
	A2	0	0.199	0.3

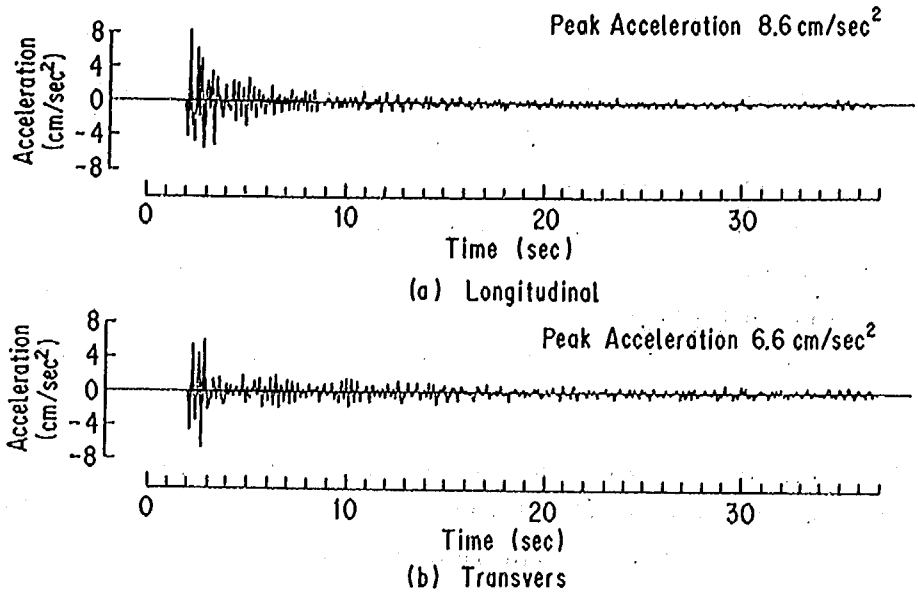


Fig. 7 Computed Deck Acceleration

Fig. 7 shows the response acceleration of the deck thus computed. Although the computed acceleration is 1.5 ~ 1.7 times larger in amplitude than the measured response, overall characteristics of the computed response is similar with the measured acceleration. Overestimation of response acceleration of the deck may be attributed to the fact that the damping ratio of the foundation is underestimated in the dynamic analysis. This is for the sake of giving safe-side result for design purpose.

CONCLUSION

The first record obtained at the Miyagawa Bridge, the first Menshin bridge in Japan, was analyzed to study the seismic behavior of Menshin bridges. The following conclusions may be deduced based on the analysis presented herein :

1) The deck acceleration is about 50 % in amplitude of the underground acceleration at 10 m below the ground surface. This clearly shows the effectiveness of the seismic isolation.

2) When amplification of the response from the 10 m below the ground surface to the deck is represented in terms of the acceleration response ratio with damping ratio of 0.05, the acceleration response ratio R defined as the response acceleration of the deck motion divided as the response

acceleration of ground motion measured at 10 m below the ground surface is only 0.25 at natural period of 0.2 ~ 0.3 second which is the predominant period of the ground motion. However the acceleration response ratio R defined as the response acceleration of the deck motion divided by the response acceleration of ground motion measured at 10 m below the ground surface is 1.4 ~ 2.0 at 0.85 second which is the fundamental natural period of the bridge. Therefore selection of the natural period in consideration with the predominant period of ground motion is very important in the Menshin Design.

3) The dynamic response analysis model which was adopted for the seismic design of Miyagawa Bridge can realistically simulate the response of the deck although the analysis overestimates the measured acceleration.

REFERENCES

1) Matsuo, Oishi, Hara, K. and Yamashita, : Design and Construction of Miyagawa Bridge, Bridges and Foundations, Vol. 91-2, 1991
2) Matsuo, Y and Hara, K. : Design and Construction of Miyagawa Bridge -First Menshin Bridge in Japan-, 1st U.S.-Japan Workshop on Earthquake Protective Systems of Highway Bridges, National Center for Earthquake Engineering Research, Buffalo, N.Y., U.S.A., September 1991
3) Technology Research Center for National Land Development : Guidelines for Base Isolation of Highway Bridges, 1989
4) Japan Road Association : Part V Seismic Design of Design Specifications of Highway Bridges, 1990
5) Robinson, W.H. : Lead Rubber Hysteretic Bearings Suited for Protecting Structures during Earthquakes, Earthquake Engineering and Structural Dynamics, Vol. 10, 1982
6) Kawashima, K. : A State of the Arts of Earthquake Engineering Research for Application to Seismic Design of Bridge Foundations, Technical Report, No. 2385, Public Works Research Institute, July 1986
7) Makiguchi, Y., Matsuo, and Hara, H. : Performance Test of Lead Rubber Bearings for Miyagawa Bridge, Annual Meeting of the Japan Society of Civil Engineers, Part I, 1991
8) Kawashima, K., Nagashima, H. and Iwasaki, H. : Effectiveness of the Energy Proportional Method for Evaluating Modal Damping Ratio of Menshin Bridges, Civil Engineering Journal, 1992

Session–9

Active and Hybrid Control for Bridges

J–20) Effectiveness of the Variable Damper for Reducing Seismic Response of Highway Bridges
(Kawashima, K., Unjoh, S., Iida, H. and Mukai, H.)

J–21) Active Control of Seismic Response of Structures with Base Isolation System
(Sato, T. and Toki, K.)

U–9) Use of Variable Dampers for Earthquake Protection of Bridges
(Shinozuka, M. and Ghanem, R.)

U–10) Hybrid Control of Sliding Isolated Bridges
(Reinhorn, A. M., Nagarajaiah, S., Riley, M. A. and Subramaniam, R.)

EFFECTIVENESS OF THE VARIABLE DAMPER FOR REDUCING SEISMIC RESPONSE OF HIGHWAY BRIDGES

Kazuhiko KAWASHIMA, Shigeki UNJOH, Hiroyuki IIDA
and Hidetoshi MUKAI

Earthquake Engineering Division, Public Works Research Institute

SUMMARY

Presented are analytical and experimental studies on the dynamic characteristics of a variable damper developed at the Public Works Research Institute. Effectiveness of the variable damper for reducing seismic response of highway bridges is analytically investigated. A prototype model of the variable damper is developed and the dynamic characteristics obtained through the dynamic loading tests is also presented.

INTRODUCTION

Because integration of functions of a damper-stopper and a energy dissipator is effective for increasing seismic safety of highway bridges, the applicability and practicability of the variable damper, in which the damping characteristics is variable depending on the response of highway bridges, has been studied at the Public Works Research Institute[1)-8)].

This paper presents analytical and experimental studies on the dynamic characteristics of the variable damper. Simple analytical results are described for presenting the effectiveness of the variable damper for reducing seismic response of highway bridges. A prototype model of the variable damper is developed and the load-displacement characteristics and the controllability obtained through the dynamic loading tests are also presented.

FUNCTIONS OF THE VARIABLE DAMPER

The variable damper is a viscous damper in which the viscous damping force is variable depending on the response of highway bridges as shown in

Fig.1. That is:

1) The damping coefficient of the variable damper is taken large during a small deck vibration so that the damper have the same function as a fixed bearing support against the braking load of vehicles. It is movable against actions with low-velocity such as an elongation of deck by temperature change.

2) When the amplitude of deck vibration becomes larger up to a certain level during an earthquake, the damping coefficient is decreased so that the energy dissipation be optimum and the inertia force of a superstructure to substructures be decreased appropriately.

3) Furthermore, when the vibration amplitude of the deck becomes excessive, the damping coefficient is gradually increased in order to suppress the excessive amplitude. Therefore, the damper has a function as a stopper with a shock absorber function. This is to prevent the impact response by the sudden operation of the stopper[5].

Therefore, the variable damper has the advantages of an usual viscous damper-stopper[6)-8], a passive energy dissipator and a stopper with a shock absorber function.

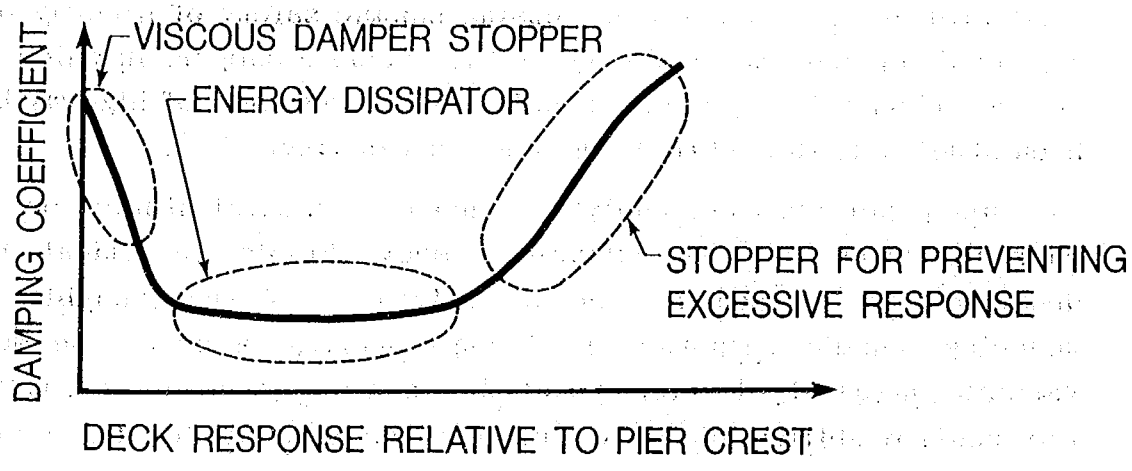


Fig.1 Basic Concept of Variable Dampers

The concept of the variable damper, in which the damping characteristics can be variable depending on the situation, has been effectively adopted in a field of mechanical engineering, in particular in a suspension system for an aircraft and an automobile. An active suspension to improve driving comfortability and stability of the automobile is one of the examples[9)10].

However, it is a new idea to apply the variable damper for highway bridges based on the concept of distributing the inertia force of a superstructure to substructures.

Although various types of the variable damper can be made, the simplest one may be as shown in **Fig.2**. The basic component is an cylinder-type viscous damper. A by-pass pipe is installed between the cylinder-cells divided by the piston. The damping characteristics can be controlled by varying the amount of flow of viscous material which passes through the by-pass. Since various technology for controlling such material flow has been developed, the variable damper is most promising and near to the practical use. Furthermore, the external energy required for the operation is significantly smaller in the variable damper than in active control devices[1].

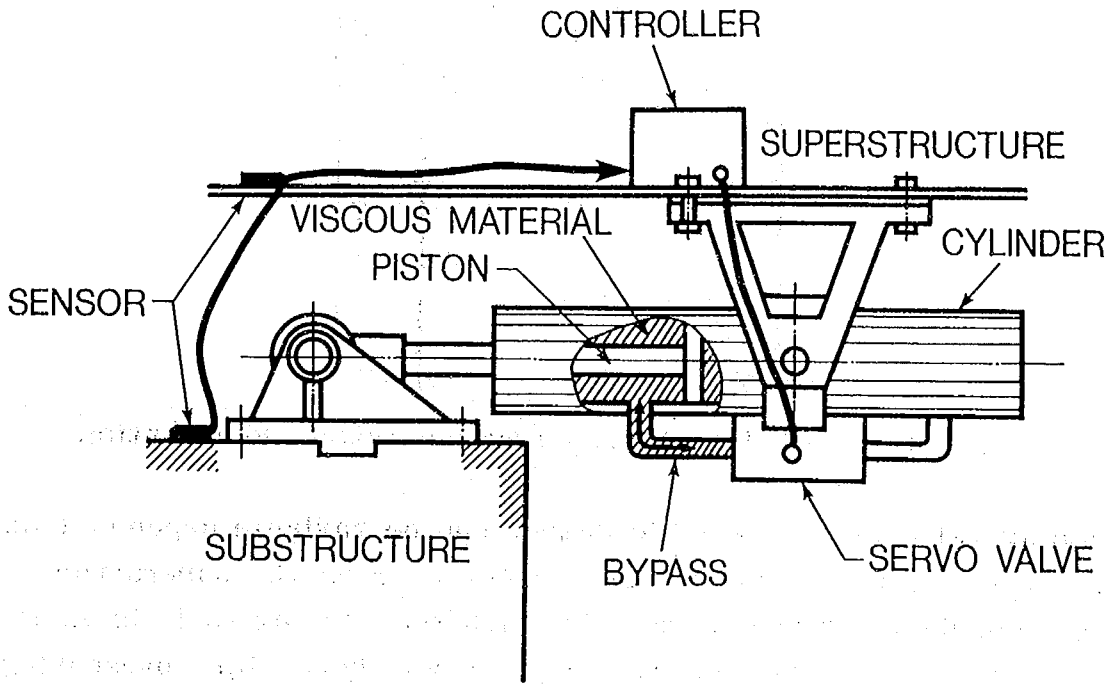


Fig.2 Variable Damper

SEISMIC RESPONSE ANALYSES OF HIGHWAY BRIDGES WITH VARIABLE DAMPERS

In order to investigate the effectiveness of the variable damper, a simple span girder bridge, as shown in **Fig.3**, with a span length of 30m is analyzed[8]. The response in longitudinal direction is considered. Although the variable damper has better applicability for multi-span continuous girder bridges, the simple span girder bridge is taken as an analytical model here for simplicity.

The superstructure of the model is supported by elastic isolators in longitudinal direction and the variable dampers are assumed to be installed between the superstructure and the pier top. The weight of the superstructure and spring stiffness of elastic isolator are assumed as 241.5tf and 640tf/m, respectively. The flexural stiffness of piers is assumed so that the fundamental natural period of the model be 0.5sec when the both bearing supports are hinged. The stiffness of isolators results in the fundamental natural period of 1sec for the model with elastic isolators.

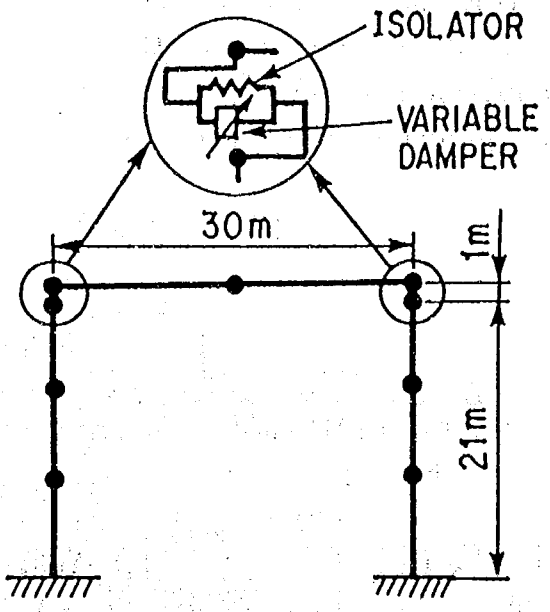


Fig.3 Highway Bridge Analysed and Analytical Idealization

Damping ratio of the variable damper can be variable dependent on both relative velocity and relative displacement between the superstructure and the pier top. Only analytical cases in which the damping ratio is varied with the relative deck displacement are shown here for presenting the effectiveness of the variable damper.

Fig.4 shows the control method of the damping coefficient of the variable damper so that it has the functions as a damper-stopper, a energy dissipator and a stopper with a shock absorber function. The displacement, at which the stopper function for preventing excessive displacement initiates to work, is assumed as 2/3 of the peak relative displacement d_u and the damping ratio is increased from h_1 to h_3. The displacement d_u is defined hereafter as a design displacement of the variable damper. For suppressing small deck displacement

the damping ratio of the variable damper is increased from h_1 to h_2 in the range of the relative displacement from $-1/6d_u$ to $1/6d_u$. The design displacement d_u, damping ratio h_1, h_2 and h_3 are assumed here as 6.34cm, 0.5, 3 and 3, respectively. These values are determined through the parametric analyses to obtain appropriate ones for the model bridge with the variable damper[3].

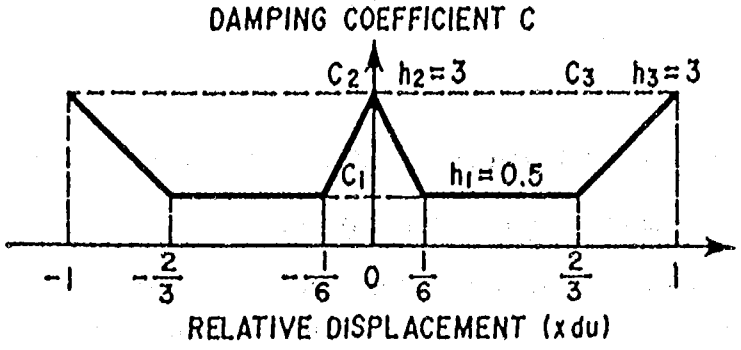


Fig.4 Displacement Dependent Damping (d_u=6.34cm)

The acceleration recorded on the ground around the Tsugaru Bridge during the Nihonkai-Chubu Earthquake of 1983 was used as an input acceleration. The acceleration was modified so that the response spectrum matches with the target spectrum. The acceleration spectrum, which is specified in "Part V Seismic Design" of the "Design Specifications for Highway Bridges", is assumed as the target spectra. The target spectra is used for the check of bearing capacity of reinforced concrete piers on soft soil site (ground condition Ⅲ).

When the variable damper is not provided, the modal damping ratio of the model bridge is assumed to be 2% of critical.

Table 1 compares the peak responses of the model bridge with and without control. If the variable damper with $h_1 = 0.5$ and $h_2 = h_3 = 3$ is provided, peak deck displacement and peak deck acceleration decrease to 25% and 43% of those with no control, respectively. The maximum bending moment at the pier bottom decreases to 46% of that. The required damping force and peak stroke of the variable damper are 62.6tf × 2 = 125tf and 5.78cm, respectively. The variable damper with this specification can be designed within the current scope of damper technology.

Table 1 Peak Response of the Bridge and the Variable Damper

Analytical Cases	Deck		Pier		Variable Damper		
	Displacement (cm)	Acceleration (cm/s^2)	Shear Force (tf)	Bending Moment (tf·m)	Damping Force (tf)	Relative Displacement (cm)	Total Energy (tf·m)
No Control	33.04	1,300	166.9	3,297	---	---	---
Displacement Dependent Damping	8.38	555	81.2	1,528	62.6	5.78	77.4

DEVELOPMENT OF A PROTOTYPE MODEL OF THE VARIABLE DAMPER

Outline of A Prototype Model of the Variable Damper

Fig.5 and **Photo.1** show a design plan and a view of the variable damper developed. The model is designed so that the maximum damping force be 20tf, maximum relative displacement of damper piston be within ± 10cm. The control of the damping ratio is arbitrarily made by a personal computer depending on relative displacement and velocity developed between deck and substructures.

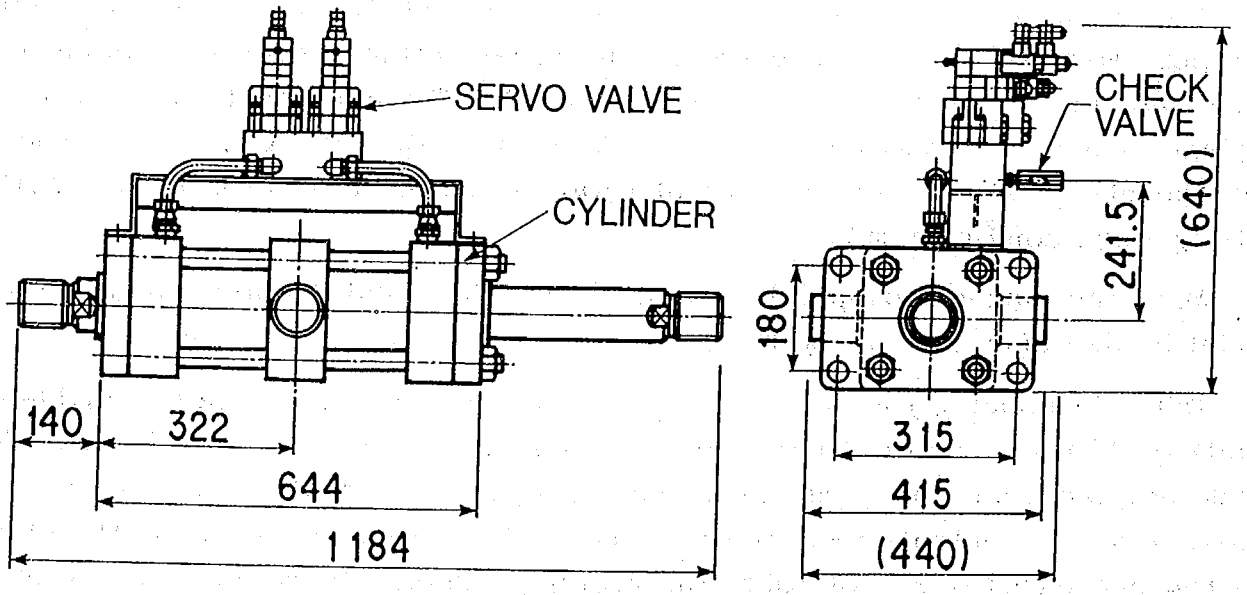


Fig.5 Prototype Model of Variable Damper

The piston-cylinder has the total length of 1,184mm, the pressure area of the piston is 137.4cm^2 and the maximum stroke of the piston is ± 13cm. A steel pipe by-pass with servo valves is installed between the cylinder-cells

divided by the piston. The servo valve is a D.C. proportional relief valve. When the oil pressure through the valve increases to specified one, the pore oil pressure is relieved. This pressure is defined hereafter as control pressure. Therefore, damping force of the piston is developed by the difference of the pressure between two cells in the cylinder. The damping force increases up to when the pressure reaches the specified one, then becomes constant after the pressure exceeds the specified one. Therefore, if the control pressure of the servo valve is assumed to be constant, the damping force is dependent on neither displacement nor velocity of the piston. Therefore, friction type damping force is developed.

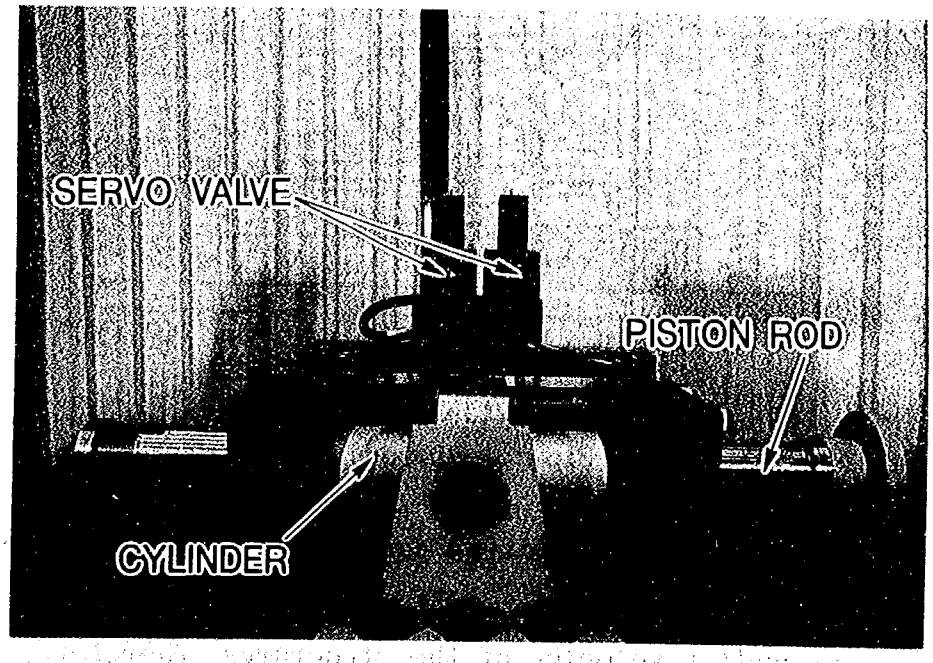


Photo 1 Prototype Model of Variable Damper

The input voltage from a servo amplifier to the servo valve is designed in the range of 0 to 5V. The control pressure is 0 at the input voltage of 0V and increases with increase of the input voltage. The viscous material used for the variable damper is an usual oil for a dynamic loading actuator. The variable damper also has a fail-safe function for an emergency condition such as power failure. The control pressure can be fixed at arbitrary one for such cases.

Fig.6 shows the flow of the viscous material in the variable damper. The damper piston can move in the left and right directions accompanying with the deck response. When the piston moves in the left side, the viscous material

flows from the left cell of the cylinder to the light one through the by-pass and the servo valves. The difference of the pressure in the two cells is adjusted as specified one by servo valves. When the piston moves in the opposite direction, damping force is controlled in the same manner.

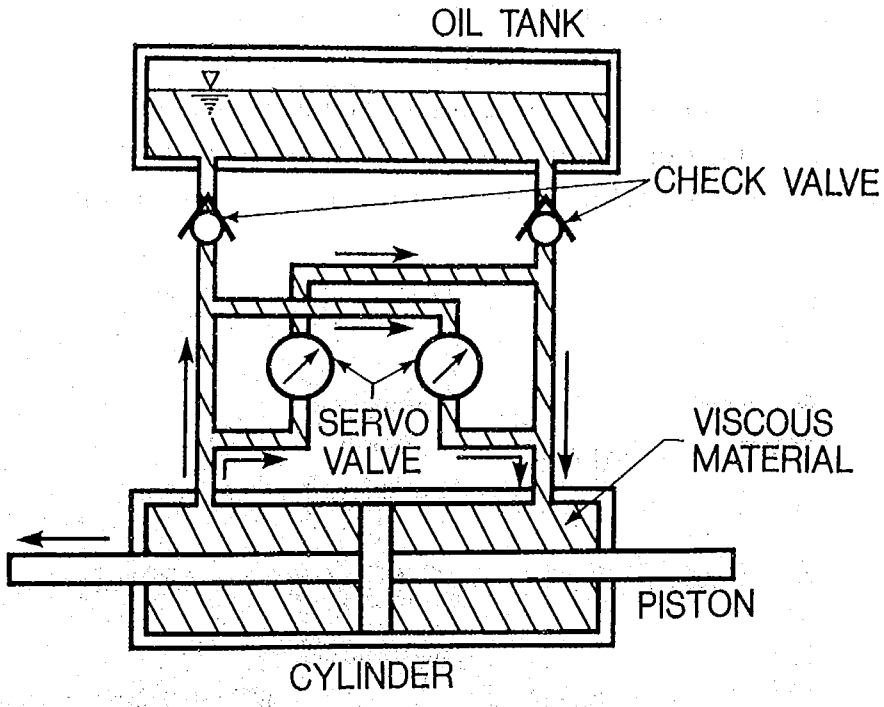


Fig.6 Flow of Viscous Material

Dynamic Loading Tests of the Prototype Model of the Variable Damper

The variable damper can vary the damping characteristics depending on the displacement and/or velocity of the structures. Therefore, in order to provide the variable damper with the required damping characteristics it is necessary to know the basic dynamic characteristics. The damping characteristics of the variable damper is controlled by the control pressure of the servo valve and it is controlled only by the input voltage to the servo valve from the servo amplifier. Therefore, in order to arbitrarily control the damping force of the variable damper developed, the relation between the input voltage to the servo valve and damping characteristics of the variable damper is essential.

Fig.7 shows the set-up of the dynamic loading tests. Under the condition that the control pressure of the servo valve is kept to be constant, the loading was applied to the piston by a dynamic actuator under the

displacement control. The input voltage to the servo valve, reaction force and stroke of the piston are measured. The loading is assumed as harmonic and repeated by 10 cycles for each loading displacement.

Table 2 shows the experimental cases. Case 1 is to measure the friction force of the damper piston. Static loading was made with loading frequency of 0.05Hz and loading displacement of ± 100mm. The input voltage of the variable damper is assumed to be 0V so that the control pressure be 0. Case 2 is to obtain the relation between input voltage to the servo valve and damping force of the variable damper. Loading frequency, loading displacement and input voltage are varied. It should be noted here that the loading, in which the maximum loading velocity exceeded 7cm/sec, was not made because of the capability of a loading apparatus.

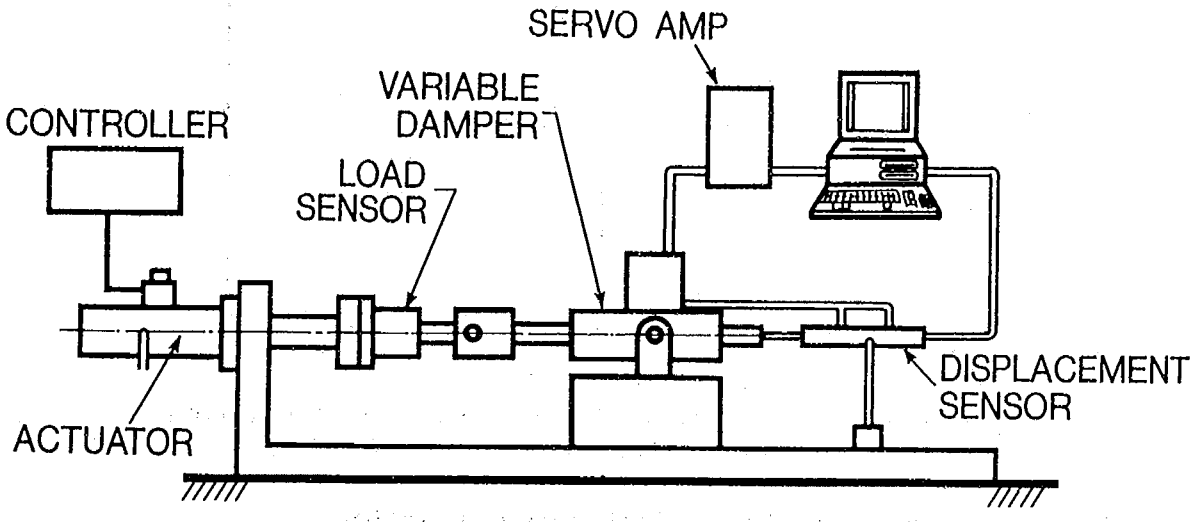


Fig.7 Set Up of Loading Test

Table 2 Experimental Cases

Case	Objective	Loading Frequency (Hz)	Loading Displace-ment (cm)	Input Voltage (Volt)
1	Measurement of Friction Force of Damper-stopper	0.05	±100	0
2	Relation between Damping Force and Input Voltage	0.1~1.0	±2~±100	0~5

Performance of the Prototype Model of the Variable Damper

(1) Friction force of the damper-piston

Fig.8 shows hysteresis loops of the load-displacement relation when the damper is loaded with the loading frequency of 0.05Hz and loading displacement of ± 100mm to obtain the friction force of the damper-piston. The load-displacement relation shows almost rectangular shape. It means that the typical friction type load-displacement relation is obtained. The hysteresis is stable for a number of loading cycles. The average friction force is about 1tf.

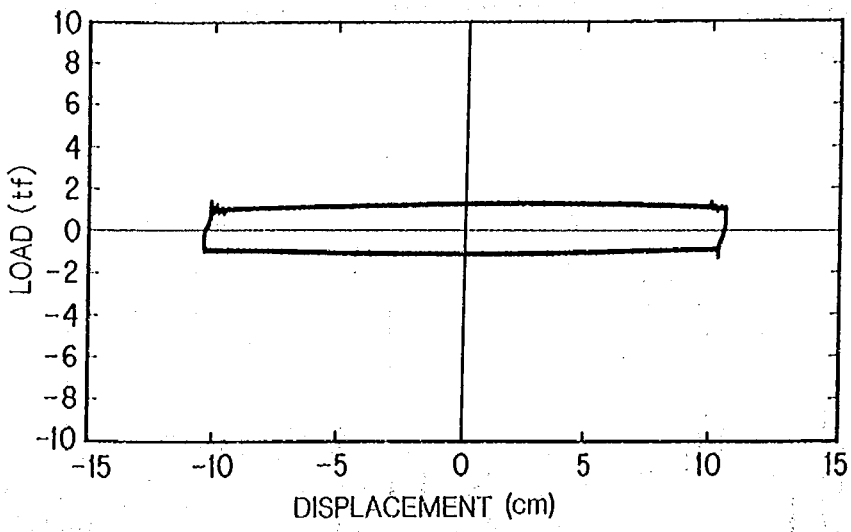
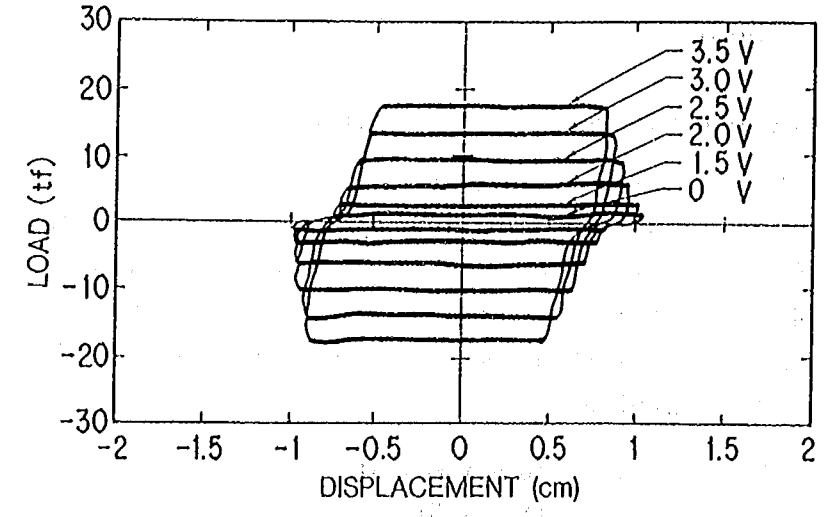


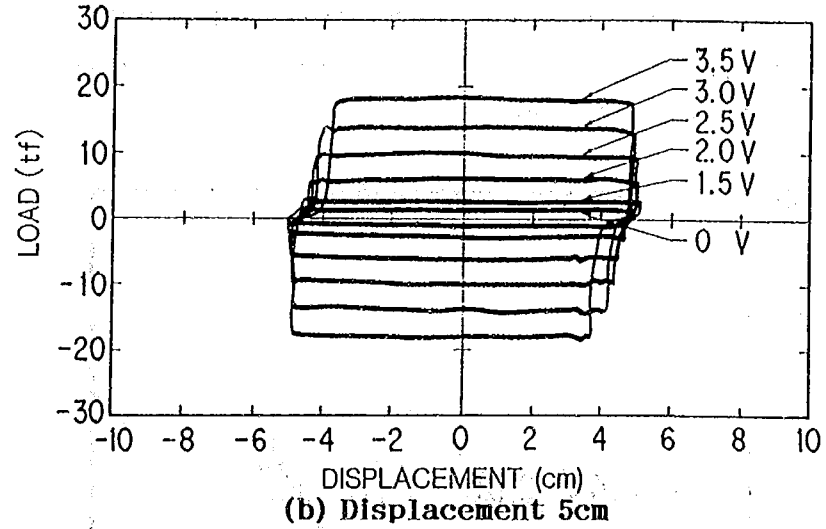
Fig.8 Hysteresis Loops of Load-Displacement Relation (Displacement = 10cm, Frequency = 0.05Hz)

(2) Hysteresis Loops of the Load-displacement Relation

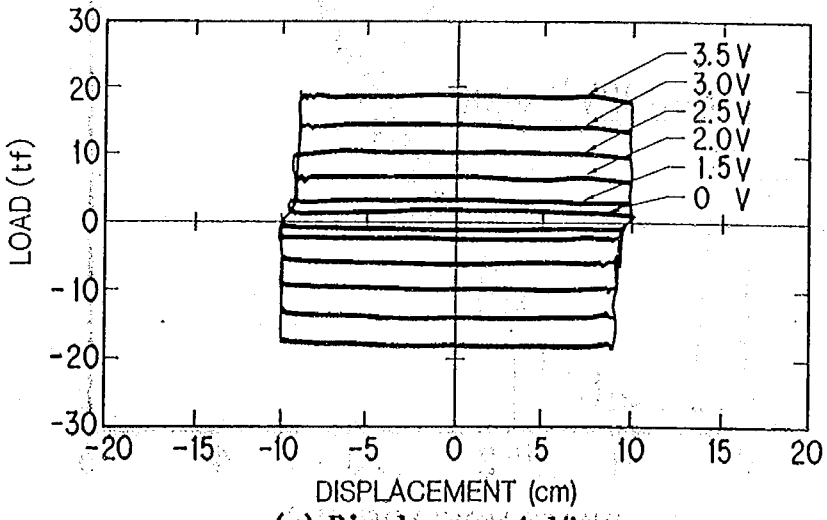
Fig.9 shows some of hysteresis loops of the load-displacement relation obtained. The hysteresis loops are shown for the loading frequency is 0.1Hz and loading displacement of ± 1cm, ± 5cm and ± 10cm. The variation of hysteresis loops with the input voltage are also shown in **Fig.9**. The hysteresis loops have the rectangular shape which means that the variable damper has the typical friction type hysteresis loops as designed. Although the damping force instantaneously decreases from specified one to 0 at the instance when the direction of movement of the piston changes at maximum displacement, the time-lag is found at the standing of the damping force. This is because increase of the oil pressure from 0 to specified one takes some time. Turbulence is also found at the instance when the damping force reaches specified one. This may be because the pressure wave motion is developed by



(a) Displacement 1cm



(b) Displacement 5cm



(c) Displacement 10cm

Fig.9 Hysteresis Loops of Load-Displacement Relation (Frequency = 0.1Hz)

sudden standing of the pressure.

(3) The relation between the input voltage and damping force

Fig.10 shows the relation between the damping force and the input voltage. The empirical equation obtained by a least square method is also shown in **Fig.10.** The damping force varies as a power function of the input voltage when the input voltage is lower than 1.8V. When the input voltage is greater than 1.8V the relation becomes almost linear. Therefore, the empirical equation is assumed as

$$F = \begin{cases} 0.42V^{3.7} + 1.0 & (0 \leqq V \leqq 1.8) \\ 8.14V - 9.95 & (V > 1.8) \end{cases} \qquad (1)$$

where, F and V represent damping force (tf) and input voltage (Volt), respectively. In Eq.(1), the constants are determined as averaged values of those obtained in each loading case.

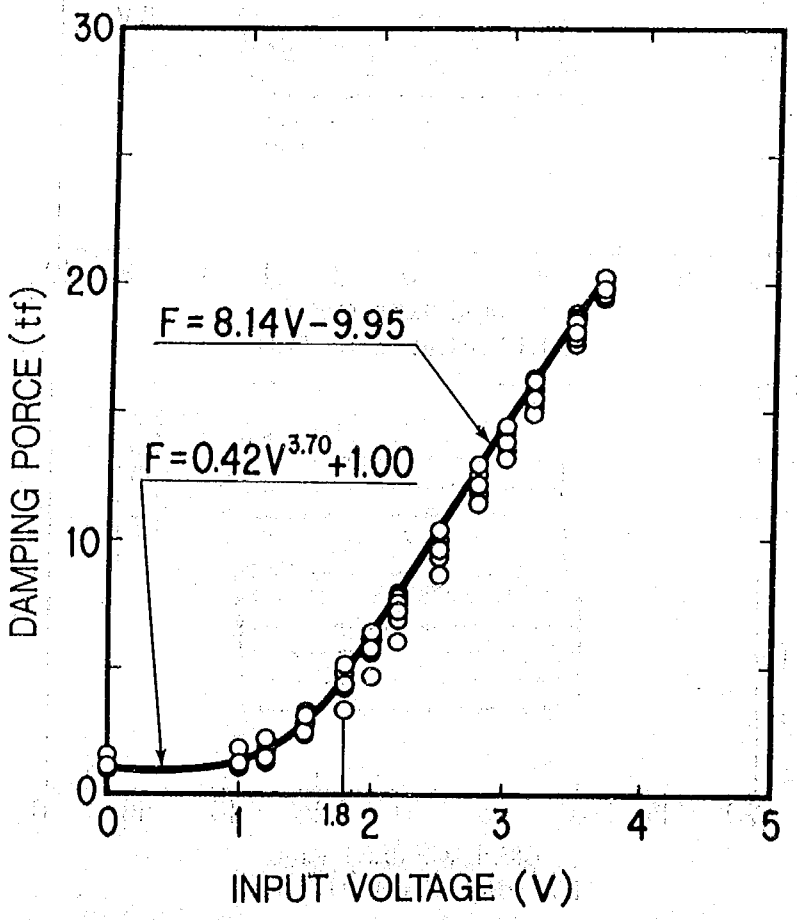
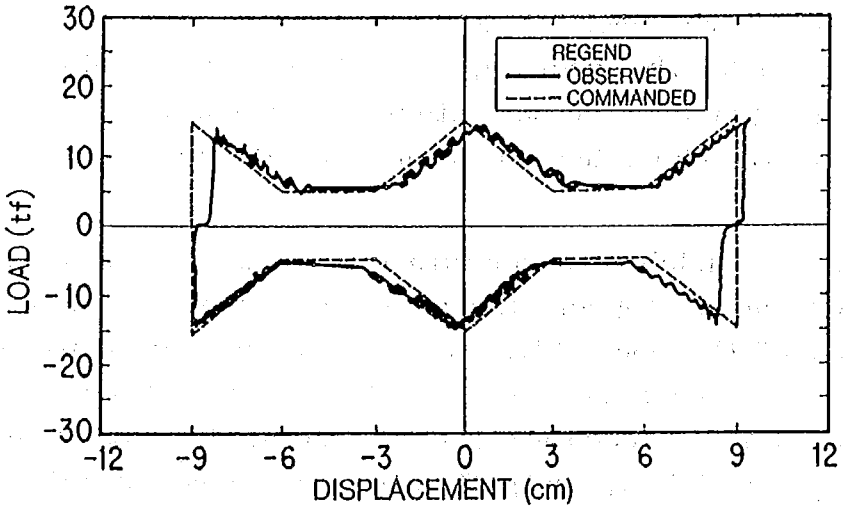


Fig.10 Damping Force vs. Input Voltage Relation

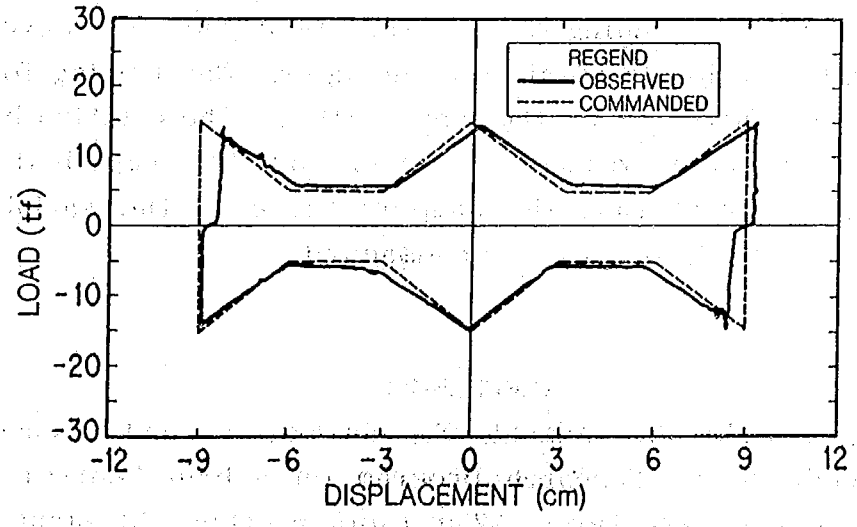
(4) Controllability of the Variable Damper

Based on the above experimental results, the damping force is controlled by the input voltage using Eq.(1). The controllability of the variable damper so as to control damping force as shown in **Fig.1** is tested. The control of the variable damper is made by control signal from a personal computer according to the displacement and/or velocity obtained by sensors.

Fig.11 shows hysteresis loops of load-displacement relation to show the controllability of the variable damper. The commanded damping force and the



(a) Sampling Time 0.1sec



(b) Sampling Time 0.01sec

Fig.11 Controllability of the Variable Damper Developed

measured one are shown in **Fig.11. Fig.11(a)** and **(b)** show the cases when the sampling time of displacement is assumed as 0.1sec and 0.01sec, respectively. The damping force is found to be controlled almost as commanded. When the sampling time is 0.1 sec, corrugation is found when the damping force is varied with the displacement. Therefore, it is required to use the appropriate sampling time in order to precisely control in consideration with the loading velocity.

CONCLUDING REMARKS

The applicability and controllability of the variable damper developed for reducing seismic response of highway bridges are analytically and experimentally studied. The prototype model of the variable damper was developed and the performance was studied through the dynamic loading tests. According to the above investigations the following conclusions may be deduced:

1) By providing the variable damper with functions of a damper-stopper, an energy dissipator and a stopper, the peak deck displacement and the peak deck acceleration of the model highway bridge were reduced to 25% and 43%, respectively. The peak bending moment at the pier bottom decreased to 46%. The required peak damping force and peak stroke of the variable damper were 62.6tf × 2=125tf and 5.78cm, respectively. The peak damping force is equivalent with 52% of the deck weight. These capability of the damper can be designed within the current scope of damper technology.

2) Based on the dynamic loading tests of the prototype model developed, the load-displacement relation is obtained as designed. The damping force of the variable damper is controlled by the input voltage. The relation between the damping force and input voltage is given by the empirical equation. Furthermore, it is found that the damping force of the variable damper developed can be controlled almost as commanded.

REFERENCES

1) Taguchi, J., Iwasaki, T., Adachi, Y., Sasaki, Y. and Kawashima, K. : U.S.-Japan Cooperative Research Program on Hybrid Control of Seismic Response of Bridge Structures, 22nd Joint Meeting, U.S.-Japan Panel on Wind and Seismic Effects, UJNR, Gaithersburg, Maryland, USA, May, 1990

2) Kawashima, K., Unjoh, S., Nagashima, H. and Shimizu, H. : Current Research

Efforts in Japan for Passive and Active Control of Highway Bridges Against Earthquakes, 23rd Joint Meeting, U.S.-Japan Panel on Wind and Seismic Effects, UJNR, Tsukuba, May, 1991

2) Kawashima, K., Unjoh, S. and Shimizu, H. : Seismic Response of Highway Bridges by Variable Damper, 24th Joint Meeting, U.S.-Japan Panel on Wind and Seismic Effects, UJNR, Gaithersburg, Maryland, May, 1992

3) Liu, S., C., Lagorio, H., J. and Chong, K., P. : Status of U.S. Research on Structural Control Systems, 23rd Joint Meeting, U.S.-Japan Panel on Wind and Seismic Effects, UJNR, Tsukuba, May, 1991

4) Kawashima, K., Hasegawa, K. and Nagashima, H. : Experiment and Analysis on Seismic Response of Menshin Bridges, Proc. 1st U.S.-Japan Workshop on Earthquake Protective Systems of Highway Bridges, National Center for Earthquake Engineering Research, Buffalo, N.Y., U.S.A., September 1991

5) Fukuoka, S. : Design of Multi-span Continuous Girder Bridge using Viscous Shear Stopper, Bridge, pp.22-29, February, 1980 (in Japanese)

6) Izeki, H. : Viscous Shear Stopper, Proposal to the Multi-Continuous Girder Bridge, Bridge, pp.30-33, February, 1980 (in Japanese)

7) Matsumura, S., Fukuoka, S, Mizumoto, Y. and Nakata, T. : Seismic Design of Multi-Span Continuous Girder Bridge using Damper Stopper, Bridge and Foundation, pp.31-37, May, 1982 (in Japanese)

8) Milliken, Jr., W., F. : Lotus Active Suspension System, Proceedings of 11th International Conference on Experimental Safety Vehicles, pp.467-475, Washington D.C., May, 1987

9) Sugawara, F. : Electronically Controlled Shock Absorber System Used as a Road Sensor which Utilizes Super Sonic Waves, Proceedings of Society of Automotive Engineers, pp.6.15-6.25, 1986

10) Kawashima, K., Unjoh, S. and Shimizu, H. : Optimum Seismic Response Control of Highway Bridges by Active Mass Damper, Civil Engineering Journal, Vol.33, No.9, pp.61-68, November, 1991 (in Japanese)

11) Kawashima, K., Unjoh, S. and Shimizu, H. : Earthquake Response Control of Highway Bridges by Variable Damper, Proceedings of Colloquium on Control of Structures, Japan Society of Civil Engineers, Part. B, pp.221-224, July, 1991 (in Japanese)

12) Feng, Q. and Shinozuka, M. : Use of A Variable Damper for Hybrid Control of Bridge Response Under Earthquake, U.S. National Workshop on Structural Control Research, University of Southern California, CA., U.S.A., October, 1990

13) Shinozuka, M., Feng, Q. and Kawamura, S. : New Perspectives for Sliding

Base Isolation Systems, Proceedings of International Workshop on Recent Developments in Base-Isolation Techniques for Buildings, Tokyo, Japan, 27-30 April, 1992

14) Kawashima, K., Unjoh, S. and Shimizu, H. : Earthquake Response Control of Highway Bridges by Variable Damper, Transactions of the Japan National Symposium on Active Structural Response Control, Japan Science Council, pp.311-317, March, 1992 (in Japanese)

15) Kawashima, K., Unjoh, S. and Shimizu, H. : Experimental Study on Dynamic Characteristics of Variable Damper, Transactions of the Japan National Symposium on Active Structural Response Control, Japan Science Council, pp.311-317, March, 1992 (in Japanese)

ACTIVE CONTROL OF SEISMIC RESPONSE OF STRUCTURES WITH BASE ISOLATION SYSTEM

Tadanobu SATO and Kenzo TOKI

Disaster Prevention Research Institute, Kyoto University, Uji, Kyoto 611, Japan

SUMMARY

The effectivity of hybrid control system consisting of a base isolation system connected with active tendon control device is main theme of this paper. To realize a practical hybrid control system for high-raise buildings we developed a new closed-open-loop optimal control algorithm that has been derived by minimizing the sum of the quadratic time-dependent performance index and the dynamic energy input to the structural system. Three types of input energy are considered that are the seismic energy, control force energy and the sum of both energy. This new control law provides feasible control algorithms that can easily be implemented for hybrid control system and applications to seismic-excited structures. This optimal algorithm is simple and reliable for on-line control operations because control force does not depend on the rigidity of structural system. The control efficiency affected by two weighting matrices included in the performance index is investigated in detail. Numerical examples are worked out to demonstrate the control efficiency of the proposed algorithms.

INTRODUCTION

Using base isolators for aseismic design of structures has attracted considerable attention in recent years. A number of base isolation systems have been developed, and used for protection of buildings, nuclear power plants, bridges, and other structures. Extensive reviews of base isolation devices were provided by Kelly [1,2]. On the other hand the application active control system to reduce the earthquake-induced vibration of tall buildings and long-span bridges has also become an area of considerable interest both theoretically and experimentally in recent years. Detail reviews of recent advancement in active control of civil engineering structures were made by Yang [3] and Soong [4].

Classical active control theories of structures were applications of optimal regulator problems. Every regulator problem is converted into a feedback algorithm optimized with respect to a quadratic performance index that includes product terms between the state and control values [5]. The feedback, therefore, does not include the non-homogeneous term that is a result of the earthquake excitation. Furthermore, the performance index is given by the integration of quadratic evaluation functions over the time interval from 0 to t_f, a duration defined as longer than that of the earthquake; consequently, the input excitation in that interval must be known a priori in order to calculate the state and control values.

Linear control laws are derived for open-loop and open-closed loop control schemes; but, the closed-loop control algorithms are widely used for earthquake-excited structures. This is the special case in which the control force is regulated by the response state vector and the Riccati matrix. It has been pointed out that because external excitation is

ignored in the derivation of the Riccati equation, the closed-loop control law is not truly optimal. If the excitation term is included in the Riccati equation, its solution requires a priori knowledge of the loading history. This generally is not possible for excitations such as earthquakes. To overcome this difficulty several control algorithms have been proposed; the pole assignment method [6], the instantaneous optimal control [7], and the pulse control [8].

We proposed a new instantaneous closed-open-loop control which takes into account the energy of earthquake motion input to the structure [9]. A time-dependent performance index similar to that defined in [7] was used to obtain the control vector. The instantaneous optimal control algorithms proposed in [7] were classified as open-loop, closed-loop and open-closed-loop controls; but, the control efficiencies were identical because the same performance index was minimized. This was referred to as Yang's optimal control algorithm. We defined a new objective function of which minimization results in different efficiencies for the three control algorithms [9]. We here examine the efficiency of proposed algorithm and give theoretical back ground for the feedforward term in the control algorithm.

It has been shown that a combined use of active and passive control systems, referred to as the hybrid control system, is more effective for reducing the seismic response structures [10]. Based on the concept of proposed algorithm, the optimal control of hybrid system is formulated in this paper.

CONTROL ALGORITHM TAKING INTO ACCOUNT INPUT ENERGY TO STRUCTURE

A structure that is idealized by an n-degree of freedom system is subjected to a one-dimensional earthquake ground acceleration $\ddot{X}_0(t)$. The matrix equation of motion is expressed as

$$M\ddot{x}(t) + C\dot{x}(t) + Kx(t) = -m\ddot{X}_0(t) + Hu(t) \tag{1}$$

in which M, C, K are the mass, damping and stiffness matrices, u the r-dimensional control vector, and H a $(2n \times r)$ matrix specifying the location of active controllers. The state space description of Eq.(1) is given by

$$\dot{z}(t) = Az(t) + Bu(t) + W_1\ddot{X}_0(t) \tag{2}$$

in which

$$A = \begin{bmatrix} 0 & I \\ -M^{-1}K & -M^{-1}C \end{bmatrix} \quad B = \begin{bmatrix} 0 \\ M^{-1}H \end{bmatrix} \quad W_1 = \begin{bmatrix} 0 \\ -M^{-1}m \end{bmatrix} \tag{3}$$

The solution of Eq.(2) is

$$z(t) = e^{A\Delta t}z(t-\Delta t) + e^{At}\int_{t-\Delta t}^{t}\{Bu(\tau) + W_1\ddot{X}_0(\tau)\}e^{-A\tau}d\tau \tag{4}$$

Using a trapezoidal approximation for the integral term, $z(t)$ is rewritten

$$z(t) = D(t-\Delta t) + \frac{\Delta t}{2}[Bu(t) + W_1\ddot{X}_0(t)] \tag{5}$$

in which

$$D(t-\Delta t) = e^{A\Delta t}\{z(t-\Delta t) + \frac{\Delta t}{2}[Bu(t-\Delta t) + W_1\ddot{X}_0(t-\Delta t)]\} \tag{6}$$

To take into account the seismic energy input into the structure, the following integration formula of equation of motion is considered

$$\int_{t-\Delta t}^{t} \dot{x}^T(\tau)M\ddot{x}(\tau)d\tau + \int_{t-\Delta t}^{t} \dot{x}^T(\tau)C\dot{x}(\tau)d\tau + \int_{t-\Delta t}^{t} \dot{x}^T(\tau)Kx(\tau)d\tau$$

$$= -\int_{t-\Delta t}^{t} \dot{x}^T(\tau)m\ddot{X}_0(\tau)d\tau + \int_{t-\Delta t}^{t} \dot{x}^T(\tau)Hu(\tau)d\tau \tag{7}$$

The first term on the left side of this equation is the kinetic energy of the system, the second the energy absorbed by system damping, the third the strain energy during time interval from $t-\Delta t$ to t . The first term of right hand side is the total seismic energy input to the structure system and the second the total energy input by the control force in the same time interval. By integrating Eq.(7) is decomposed into the term related to the values at time t and $t-\Delta t$

$$\dot{x}^T(t)\frac{1}{2}M\dot{x}(t) - \dot{x}^T(t-\Delta t)\frac{1}{2}M\dot{x}(t-\Delta t) + \dot{x}^T(t)\frac{\Delta t}{2}C\dot{x}(t)$$

$$+\dot{x}^T(t-\Delta t)\frac{\Delta t}{2}C\dot{x}(t-\Delta t) + x^T(t)\frac{1}{2}Kx(t) - x(t-\Delta t)\frac{1}{2}Kx(t-\Delta t)$$

$$= -\dot{x}^T(t)\frac{\Delta t}{2}m\ddot{X}_0(t) - \dot{x}^T(t-\Delta t)\frac{\Delta t}{2}m\ddot{X}_0(t-\Delta t)$$

$$+\dot{x}^T(t)\frac{\Delta t}{2}Hu(t) + \dot{x}^T(t-\Delta t)\frac{\Delta t}{2}Hu(t-\Delta t) \tag{8}$$

Rearranging the terms at time t and expressing the terms related to values at time $t-\Delta t$ as $E(t-\Delta t)$ Eq.(8) can be rewritten.

$$z^T(t)Q_1z(t) = -z(t)W_2\ddot{X}_0(t) + z(t)H_wu(t) + E(t-\Delta t) \tag{9}$$

in which

$$E(t-\Delta t) = \dot{x}^T(t-\Delta t)\frac{1}{2}M\dot{x}(t-\Delta t) - \dot{x}^T(t-\Delta t)\frac{\Delta t}{2}C\dot{x}(t-\Delta t)$$

$$+x(t-\Delta t)\frac{1}{2}Kx(t-\Delta t) - \dot{x}^T(t-\Delta t)\frac{\Delta t}{2}m\ddot{X}_0(t-\Delta t) + \dot{x}^T(t-\Delta t)\frac{\Delta t}{2}Hu(t-\Delta t)$$

$$Q_1 = \begin{bmatrix} \frac{K}{2} & 0 \\ 0 & \frac{M}{2} + \frac{\Delta t}{2}C \end{bmatrix} \quad W_2 = \begin{Bmatrix} 0 \\ \frac{\Delta t}{2}m \end{Bmatrix} \quad H_w = \begin{bmatrix} 0 \\ \frac{\Delta t}{2}H \end{bmatrix}$$

The three types of closed-open-loop optimal control algorithms can be established based on the definition of three types of energy input to the structure.

Control law taking into account control force energy (type 1)

The control force energy input to the structure is given by the second term of right hand side of Eq.(7). We, therefore, assume the following time-dependent performance index $J_N(t)$

$$J_N(t) = \int_{t-\Delta t}^{t} \{z^T(\tau)Qz(\tau) + u^T(\tau)Ru(\tau) + \alpha \dot{x}^T(\tau)Hu(\tau)\}d\tau \tag{10}$$

The first and second term of right hand side of Eq.(10) are the quadratic terms of state variable and control force. The third term is control force energy input to the structure and α is a parameter rating the input energy effect. Applying trapezoidal integration for the first and second term and using Eq.(8), Eq.(10) can be written

$$J_N(t) = z^T(t)Q'z(t) + u^T(t)R'u(t) + \alpha z^T(t)W_2\ddot{X}_0(t) + E_1'(t-\Delta t) \tag{11}$$

in which

$$E_1'(t-\Delta t) = z^T(t-\Delta t)Q'z(t-\Delta t) + u^T(t-\Delta t)R'u(t-\Delta t) + \alpha z^T(t-\Delta t)W_2\ddot{X}_0(t-\Delta t)$$

$$Q' = \frac{\Delta t}{2}Q + \alpha Q_1 \qquad R' = \frac{\Delta t}{2}R \tag{12}$$

To minimize the performance index $J_N(t)$ given by Eq.(11) under the constraint in Eq.(5), the generalized performance index $\tilde{J}_N$ with the Lagrangian Multiplier vector Λ is defined by

$$\tilde{J}_N = z^T(t)Q'z(t) + u^T(t)R'u(t) + \alpha z^T(t)W_2\ddot{X}_0(t) + E_1'(t-\Delta t)$$

$$+\Lambda[z(t) - D(t-\Delta t) - \frac{\Delta t}{2}\{Bu(t) + W_1\ddot{X}_0(t)\}] \tag{13}$$

The necessary conditions for minimizing the performance index $\tilde{J}_N$ are

$$\frac{\partial \tilde{J}_N}{\partial z} = 0 \quad (14a), \qquad \frac{\partial \tilde{J}_N}{\partial u} = 0 \quad (14b)$$

Upon substituting Eq.(13) into Eqs.(14a,b), we obtain

$$(Q'^T + Q')z(t) + \alpha W_2\ddot{X}_0(t) + \Lambda = 0 \tag{15}$$

$$2R'u(t) - \frac{\Delta t}{2}B^T\Lambda = 0 \tag{16}$$

The control vector $u(t)$ can be obtained from Eqs.(15) and (16)

$$u(t) = -\frac{\Delta t}{4}R^{-1}B^T(Q^T + Q)z(t) - \frac{\alpha}{2}R^{-1}B^T(Q_1^T + Q_1)z(t) - \frac{\alpha}{2}R^{-1}B^TW_2\ddot{X}_0(t) \tag{17}$$

As seen in Eq.(17) the control vector consists of a feedback of the state at time t and a weighted input ground acceleration at that time; hence, this control law is referred to as the optimal closed-open-loop control. The first feature of this control law is that the control force generated by feedback term is increased due to the influence of matrix Q_1.

The second is the control force based on the feedforward term is in opposite phase of input seismic motion.

Control law taking into account seismic input energy (type 2)

The time-dependent performance index $J_N(t)$ introducing the seismic energy input to structure is defined by

$$J_N(t) = \int_{t-\Delta t}^{t} [z^T(\tau)Qz(\tau) + u^T(\tau)Ru(\tau) + \alpha\{-\dot{x}^T(\tau)m\ddot{X}_0(\tau)\}]d\tau \tag{18}$$

As the result of trapezoidal integration of Eq.(18) we obtain

$$J_N(t) = z^T(t)Q'z(t) + u^T(t)R'u(t) - \alpha z^T(t)W_2\ddot{X}_0(t) + E_2'(t-\Delta t) \tag{19}$$

in which

$$E_2'(t-\Delta t) = z^T(t-\Delta t)Q'z(t-\Delta t) + u^T(t-\Delta t)R'u(t-\Delta t) - \alpha z^T(t-\Delta t)W_2\ddot{X}_0(t-\Delta t)$$

$$Q' = \frac{\Delta t}{2}Q \qquad R' = \frac{\Delta t}{2}R \tag{20}$$

Minimizing the performance index under the constraint in Eq.(5), the optimal control force is

$$u(t) = -\frac{\Delta t}{4}R^{-1}B^T(Q^T + Q)z(t) + \frac{\alpha}{2}R^{-1}B^TW_2\ddot{X}_0(t) \tag{21}$$

This control law has also the closed-open-loop formula. The feedback term, however, is not affected by structural rigidity and the feedforward term is in same phase of input seismic motion in contrast to the type 1 formula. Note that the Yang's optimal control algorithm [4] is obtained by putting α to be 0.

Control law taking into account the total input energy (type 3)

Because the total input energy to the structural system is expressed by the left hand side of Eq.(7) we here define the following time-dependent performance index $J_N(t)$

$$J_N(t) = \int_{t-\Delta t}^{t} [z^T(\tau)Qz(\tau) + u^T(\tau)Ru(\tau) + \alpha\{-\dot{x}^T(\tau)m\ddot{X}_0(\tau) + \dot{x}(\tau)Hu(\tau)\}]d\tau \tag{22}$$

Integrating Eq.(22) and using the relation given in Eqs.(8)and (9) we obtain

$$J_N(t) = z^T(t)Q'z(t) + u^T(t)R'u(t) - \alpha z^T(t)W_2\ddot{X}_0(t) + \alpha z^T(t)H_\omega u(t) + E_3'(t-\Delta t) \tag{23}$$

in which

$$E_3'(t-\Delta t) = z^T(t-\Delta t)Q'z(t-\Delta t) + u^T(t-\Delta t)R'u(t-\Delta t)$$
$$-\alpha z^T(t-\Delta t)W_2\ddot{X}_0(t-\Delta t) + \alpha z^T(t-\Delta t)H_\omega u(t-\Delta t)$$

$$Q' = \frac{\Delta t}{2}Q \qquad R' = \frac{\Delta t}{2}R \tag{24}$$

Based on the Lagrangian multiplier method we can minimize the performance index given by Eq.(23) and obtain the control force

$$u(t) = -(2R' + \alpha\frac{\Delta t}{2}B^T H_w)^{-1} \cdot (\alpha H_w^T + \frac{\Delta t}{2}B^T Q')z(t)$$

$$+(2R' + \alpha\frac{\Delta t}{2}B^T H_w)^{-1} \cdot \alpha\frac{\Delta t}{2}B^T W_2 \ddot{X}_0(t) \qquad (25)$$

The control force consists of the feedback and feedforward terms. The effect of the parameter expressing rate of input energy power α is included in both terms. When α increases, therefore, not only the control force based on the feedforward term but also that of feedback term increases.

EFFECT OF FEEDFORWARD TERM ON CONTROL EFFICIENCY

To demonstrate the difference of control efficiencies of three control algorithms, a three-story building was modeled as shown in Fig.1. The parameters for this model are given in Table 1. Active tendon controllers are assumed to be installed in every story unit. The accelerogram at El Centro (NS,1940) was used.

To examine the effects of the weighting matrices Q and R, and parameter α on active control, we partitioned Q as follows:

$$Q = \begin{bmatrix} Q_{11} & Q_{12} \\ Q_{21} & Q_{22} \end{bmatrix} \qquad (26)$$

in which the order of matrices Q_{ij} is (3×3). Note that the submatrices Q_{11} and Q_{12} do not contribute to the active forces because the matrix B which appears in Eq.(3) contains 0 matrix. However Q must be positive semi-definite matrix we therefore assume the conditions of $Q_{11} = 100 \cdot Q_{22}$ and $Q_{12} = 10 \cdot Q_{22}$. For simplicity, Q_{21} is considered to be equal to $10 \cdot Q_{22}$, and we assigned the unit matrix multiplied by r to R. The appropriate assignment of the elements of Q_{21} and Q_{22} to achieve maximum control efficiency have not been investigated because it requires a two stage optimization technique that is beyond the scope of the research reported here. We use the following matrix based on several trial and error to select a appropriate Q_{22} matrix [9].

$$Q_{22} = q \cdot \begin{bmatrix} 1.0 & 0.75 & 0.4 \\ 0.75 & 0.7 & 0.4 \\ 0.4 & 0.4 & 0.35 \end{bmatrix} \qquad (27)$$

The respective relative velocity responses of top floor for the control algorithm without and with feedforward term (type 2 algorithm) are shown in Fig.2(a) and (b). The corresponding required control forces from the top and bottom controllers are depicted in Fig.2(c), (d), (e) and (f). To check the efficiency of both control algorithms, the same weighting matrices Q and R were used in the calculation of the control forces. The maximum velocity response caluculated using the algorithm with feedforward term is controlled at 60% of response obtained by the algorithm without feedforward term. The time history of the control force at the bottom actuator obtained by type 2 algorithm is very similar to the input accelerograms, and the maximum control force at the top actuator is 40% smaller than that obtained by control algorithm without feedforward term. This means

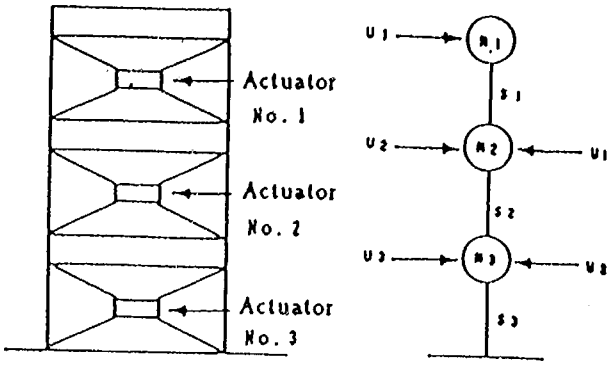
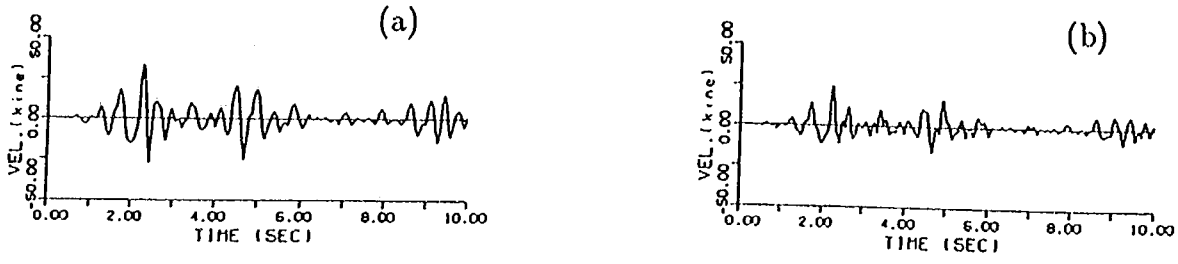


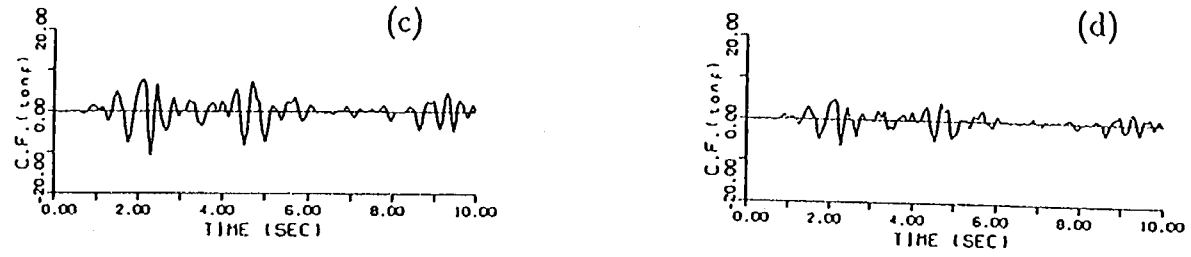
Figure 1. Model of the structural system.

Active Tendon Control		
No.	Mass (ton)	Stiffness (tonf/cm)
1	0.048	
2	0.048	23.66
3	0.048	42.59
		47.32

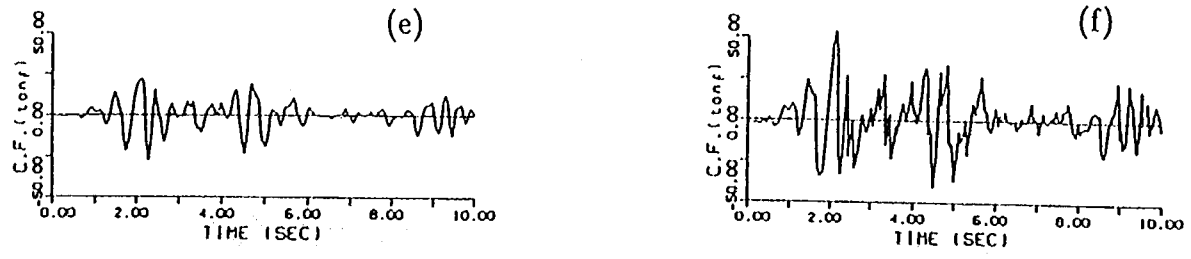
Table 1.
Structural properties of a linear model.



Velocity response of the top floor



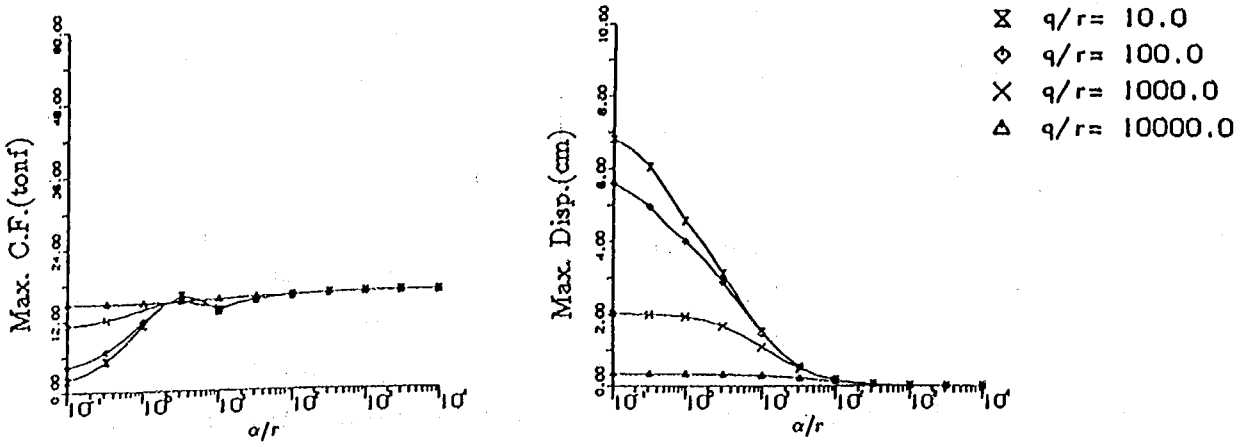
Control force (Top actuator)



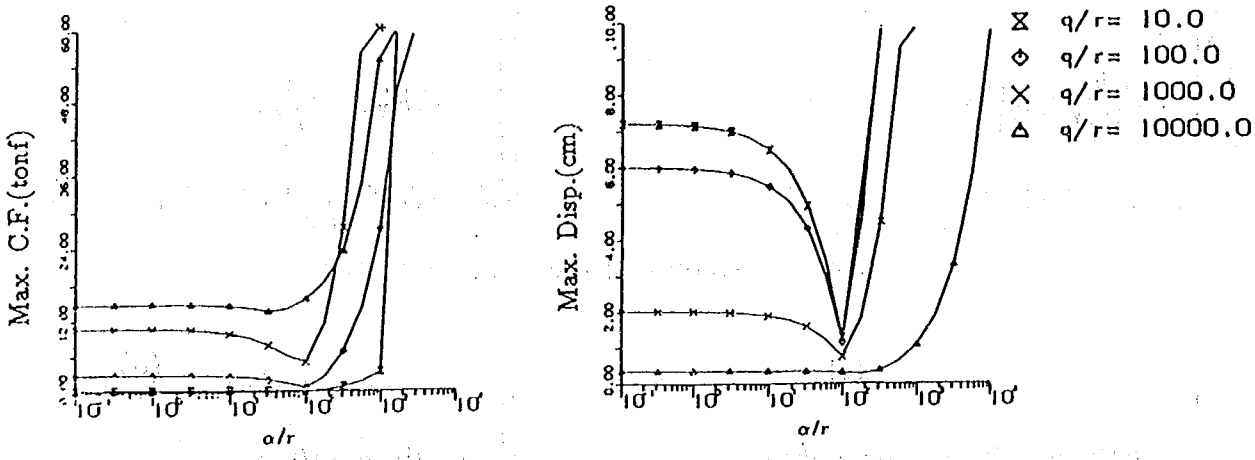
Control force (Bottom actuator)

(without feedforward term) (with feedforward term)

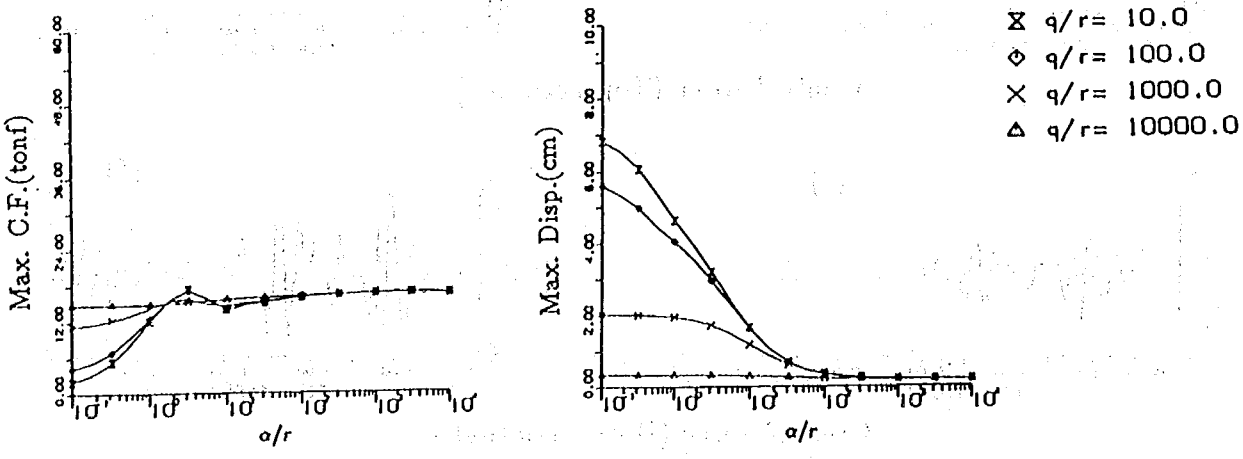
Figure 2. Time history of velocity response and actuators.



(a) For the case using Type 1 evaluation function.



(b) For the case using Type 2 evaluation function.



(c) For the case using Type 3 evaluation function.

Fig 3. Relation of α/r to the maximum relative displacement of the top floor and the maximum control force of the top actuator.

that the type 2 algorithm generates a rather large control force for the base controller that corresponds to the input acceleration and reduces the seismic energy input to the upper floors.

The maximum relative displacements of the top floor and the control forces of the top actuator for three different control algorithms (type 1, 2 and 3) are shown in Fig.3 as functions of α/r for several different q/r values. The value of q/r can be used to represent the effect of $R^{-1}Q$ on control efficiency. When the α/r is selected to be zero the structural response decreases consistently as q/r increases; whereas, the required active control force increases. At the q/r of infinity the response becomes zero and the control force approaches to a fixed value.

When we use control algorithms of type 1 and type 3 general trend of control force and maximum relative displacement at top floor changing with α/r value are almost same. Although there are some fluctuations in control force around α/r value of 5.0, the required active control force increases as α/r increases, whereas the structural response decreases consistently. At the α/r of infinity the response becomes zero and the control force approaches to a fixed value for a wide range of q/r values. Peculiar trends can be seen for the case using type 2 algorithm. The maximum relative displacement and control force have minimum values at about $\alpha/r = 10^2$ for a wide range of q/r values. The decrease of the response is very sharp for small q/r values; hence, the proposed control algorithm has a high efficiency for cases in which low capacity actuators are implemented.

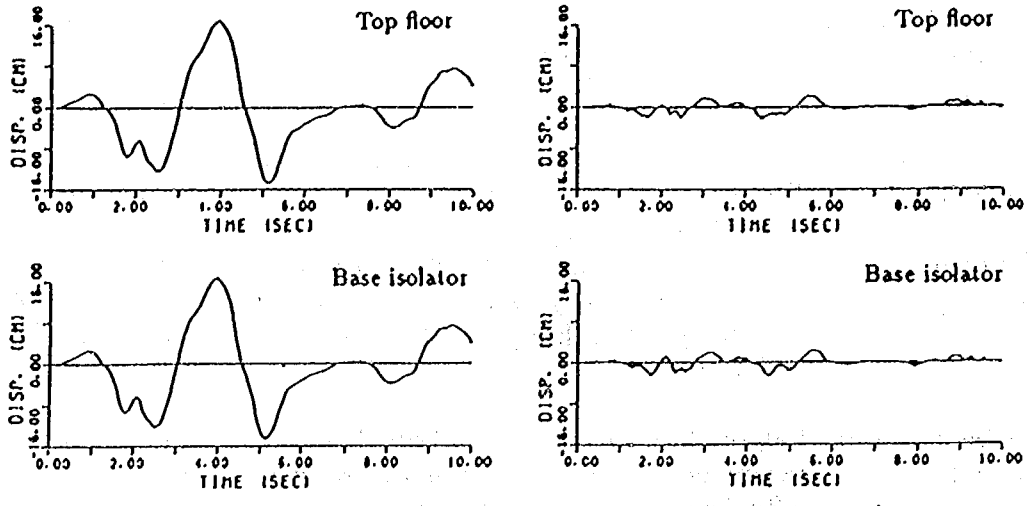
OPTIMAL CONTROL OF A BASE-ISOLATED STRUCTURE

A three-story building resting on laminated rubber bearings with a lead core is modeled. Because the effect of the rubber isolator introduces a soft story with inelastic characteristics, the superstructure behaves like a rigid body and the relative displacement between stories become very small; whereas, the relative displacement between the superstructure and the ground becomes very large. Active tendon control is introduced to limit the relative displacement of the rubber isolator to avoid instability failure as well as the relative displacement of the superstructure. The dynamic characteristics of the superstructure are assumed to be linear elastic (Table 1); whereas, the rubber isolator has bilinear elastic-plastic behavior. The elastic stiffness of the base isolator is assigned as 2.2 tonf/cm and the post-elastic stiffness 0.44 tonf/cm. Yielding is assumed to occur at a relative displacement of 0.5 cm. As the total system has been modeled as a four-degree-of-freedom system we use matrix Q_{22} as defined by .

$$Q_{22} = q \begin{bmatrix} 1 & 0.7 & 0.4 & 0.2 \\ 0.7 & 0.7 & 0.4 & 0.2 \\ 0.4 & 0.4 & 0.4 & 0.2 \\ 0.2 & 0.2 & 0.2 & 0.2 \end{bmatrix} \tag{28}$$

The values of q/r and α/r are assigned as 100 and 60.

The controlled and uncontrolled relative displacements of the top floor and base isolator with respect to the ground are shown in Fig.4. The hysteresis loops of the elastic-plastic restoring shear forces in the base isolator are shown in Fig.5; (a) represents a case with control and (b) without it. These figures show that the active tendon control system markedly reduces not only the superstructure response but the deformation of the base isolator as well. As a check on increases in the relative displacement between stories, the force-relative displacement relation of the top spring is given in Fig.6. Even if the control



(a) without control (b) with control

Fig 4. Relative displacement to the ground.

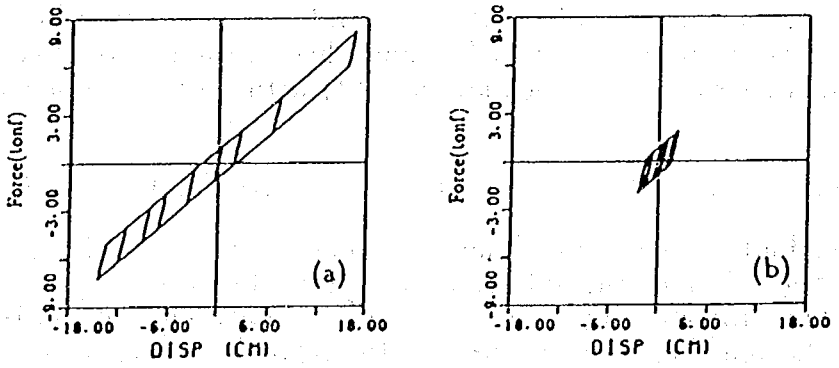


Fig 5. Hysteresis loops of the base isolator.
(a)without,(b)with control

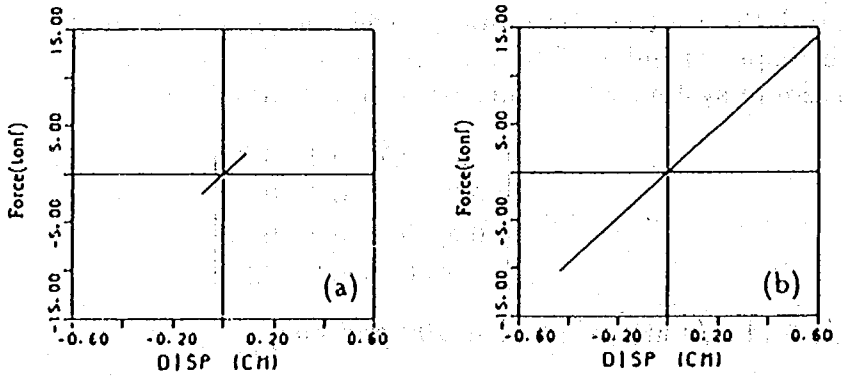


Fig 6. Force-displacement relation of the top spring.
(a)without,(b)with control

force is applied to the structural system, the relative displacement between the top and second floors is kept very small. The base isolation system is used to absorb a large deformation and to dissipate input energies such that smaller excitations are transmitted to the superstructure. This system, however, must be protected against severe damage or instability failure. This is achieved by the ability of our proposed optimal control algorithm to reduce deformation of the base isolator and to maintain a small relative displacement between the stories.

CONCLUDING REMARKS

We have developed a new closed-open-loop active control algorithm which takes into account the input seismic energy to the structure system. We investigated the efficiency of our proposed control algorithm by applying it to linear structural systems with a tendon control system. We analyzed seismic response characteristics of the hybrid control system combined a base isolation system with the active tendon system. The principle results and conclusions of our study are

(1)To derive the closed-open-loop control algorithm three different types input energy to the structure were considered for defining the time-dependent performance index. The control force obtained through performance index taking into account the seismic energy input to the structure was not affected by structural rigidity, hence, this algorithm is simple and applicable even to the structure system with nonlinearity.

(2) The effect of control parameters on the system response are expressed by two independent variables; one controls the level of feedback, the other reflects the level of input excitation. For a given structural system we found that there were appropriate control parameters to maximize control efficiencies.

(3)The combination of passive and active control systems is of use in preventing the failure of the base isolator while simultaneously keeping the relative displacement of the superstructure parts small. Because a base isolator absorbs seismic input and behaves nonlinearly, the optimal algorithm we have developed, which includes the effect of seismic excitation, is very efficient for the control of a building with a base isolation system.

REFERENCES

1. Kelly, J.M., Aseismic Base Isolation, Shock Vib. Dig., Vol.14, pp.17-25, 1982.
2. Kelly, J.M., Aseismic Base Isolation: Review and Bibliography, Soil Dyn. Earthquake Engng., Vol.5, pp.202-216, 1986.
3. Yang, J.N. and Soong, T.T., Recent Advancement in Active Control of Civil Engineering Structures, Journal of Probabilistic Engineering Mechanics, vol.3, No.4, pp.179-188, 1988.
4. Soong, T.T., Active Structural Control: Theory and Practice, Longman Scientific and Technical, New York, 1990.
5. Leipholz, J.N. (1980), Structural Control, North-Holland Publishing Company, Amsterdam, The Netherlands.
6. Bryson, A.E. Hr and Ho, Y.C., Applied Optimal Control, John Wiley and Sons, New York, U.S.A., 1975.

7. Yang, J.N. Akbarpour, A. and Ghaemmaghami, P., New Optimal Control Algorithms for Structural Control, Journal of Engineering Mechanics, ASCE, Vol.113, No.9, 1987, pp.1369-1386.

8. Udwadia, F.E. and Tabaie, S., Pulse Control of Structural and Mechanical Systems, Journal of Engineering Mechanics, ASCE, Vol.107, No.6, 1981, pp.1011-1028.

9. Sato, T. and Toki K., Active Control of Seismic Response of Structures, Journal of Intelligent Material Systems and Structures, Vol.1, No.4, 1990, pp.447-475.

10. Yang, J.N., Li, Z. and Danielians A., Hybrid Control of Seismic-Excited Nonlinear and Inelastic structural systems, National Center for Earthquake Engineering Research, Technical Report NCEER-91-0020, 1991.

Use of Variable Dampers for Earthquake Protection of Bridges

M. Shinozuka* and R. Ghanem†

Abstract

This paper demonstrates the applicability of variable dampers to the protection of bridges against earthquakes. Its beneficiary effects are demonstrated through computer simulations. One and two-degree-of-freedom models of bridges are used in the simulations, and various functional variations in the damping forces are explored.

Introduction

Recent technological developments have made feasible the implementation of variable dampers into large scale structural systems. These developments stem either from the declassification of military applications, or from a renewed interest in smart materials such as Electro-Rheological (ER) fluids. Clearly, variable damping is a particular form of active control since the restoring force is actively changed to meet some performance criterion and an optimal control approach must be followed if the optimal variation of the restoring force is to be obtained. For a number of reasons an optimal control is not sought in this investigation, neither in a passive nor in an active form. Firstly, non-active optimal control would incorporate knowledge about the excitation into the optimality criterion. In the case of earthquakes, even statistical characterization represents at best a rough approximation, therefore placing the significance of such optimality in suspect. As for active (or adaptive) optimal control, its robustness is still questionable, and a certain amount of basic research is still needed before its implementation into earthquake resistant design can be safely recommended. Such research must focus on coupling system identification (Ghanem et.al, 1991, 1992) with control in order to track the structural response into the nonlinear range. Short of this, the optimality of the control will be questionable, as it will be with respect to a linear reference model. In view of the above, the approach followed in the present paper is to perform extensive computer simulations to determine a near-optimal functional form for the variable damper. This simulation is not completely ad-hoc and is guided by a knowledge of the expected behavior of the structure.

*Department of Civil Engineering, Princeton University Princeton, NJ. USA
†Department of Civil Engineering, SUNY, Buffalo, NY. USA

This paper demonstrates, through various computer simulations, the potential of variable dampers to the vibration isolation of structural systems subjected to earthquake excitations. Both discrete state and continuous state dampers are implemented, reflecting the variety of damping devices that are both available and projected in the near future. Discrete state dampers can be realized using dampers with multiple orifices to switch back and forth between a discrete number of damping force levels. These dampers have been known and implemented in classified military applications for some time. Continuous state dampers can be thought of as the limit of discrete state dampers as the number of states becomes very large. These can be realized using smart materials. In particular, electro-rheological fluids seem to be good candidates for such implementations. Further research is currently underway to implement the electrical and rheological properties of E-R fluids into the control algorithm.

Dynamical System and Variable Damping

The equation of motion for a typical dynamical system considered in this investigation is given by

$$\mathbf{M}\ddot{\mathbf{x}} + \mathbf{C}\dot{\mathbf{x}} + \mathbf{K}\mathbf{x} = \mathbf{f}(t) \tag{1}$$

where $\mathbf{f}(t)$ represents the base acceleration, and $\mathbf{M}$, $\mathbf{C}$, and $\mathbf{K}$ represent respectively, the mass, damping, and stiffness matrices. The implementation of variable dampers implies that the damping matrix $\mathbf{C}$ can be written as the sum of a passive and a variable component in the form

$$\mathbf{C} = \mathbf{C}_p + \mathbf{C}_v(\mathbf{x}, \dot{\mathbf{x}}) . \tag{2}$$

In the case of a multi-stage variable damper, $\mathbf{C}_v$ would be a piecewise constant function of the state of the structure. Alternatively, $\mathbf{C}_v$ can be made to have any desired continuous functional dependence on the state of the structure. A simple relationship that can be implemented with reliable hardware is of course desirable. Due to the permanent presence of the $\mathbf{C}_p$ component, it is seen that if the active component fails for some reason, the system will still be able to resist external loads, though not necessarily without sustaining some level of damage.

Two simplified models of a bridge are used in the analysis. The first model consists of a single-degree-of-freedom oscillator. Its equation of motion simplifies to

$$m\ddot{x} + (c_p + c_v(\dot{x}, \dot{x}))\dot{x} + kx = f(t) . \tag{3}$$

Values of m, c_p and k are taken equal to $3,000\text{Ns}^2/\text{m}$, $10,309\text{Ns/m}$ and $462,794\text{N/m}$, respectively. These values correspond to a natural frequency equal to 12.4 rd/sec, and a

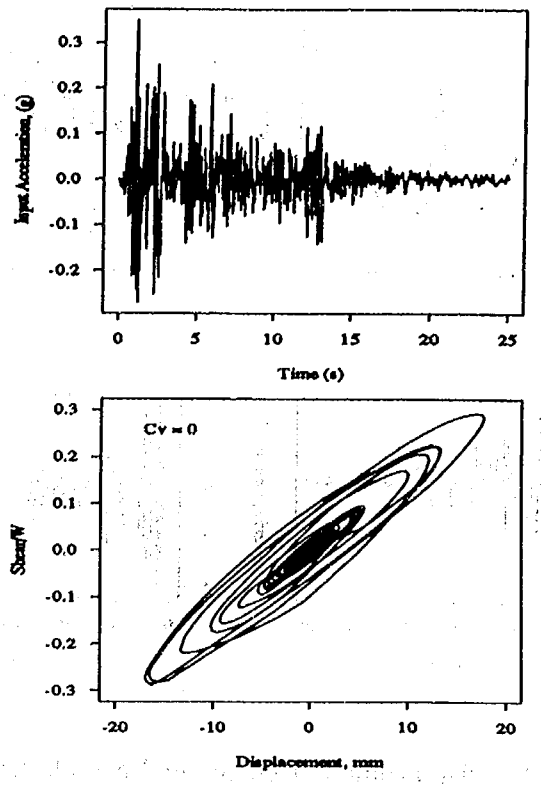


Figure 1: Input Acceleration, and Response with no Variable Damper.

damping ratio equal to 14% of critical. The coefficient $c_v(x, \dot{x})$ is allowed to vary as a function of the state variables x and $\dot{x}$. Both discrete variation and continuous variation are implemented. The continuous models feature a number of different functional relationships between the damping coefficients and either the displacement or the velocity of the structure. The relationships aim at providing low damping levels at intermediate values of the state variables while providing for large damping at very low and high values. This philosophy for variable damping was suggested by Kawashima et.al (1991, 1992). In this way, the damper can act as an energy absorber at intermediate levels of motion, while acting as a motion stopper for very large and very small levels. The results associated with applying only the passive damping at the level of 14% of critical to this system are shown in Figure (1). This figure also shows the input acceleration record (1940 El Centro N-S).

Figure (2) shows the results from implementing a displacement dependent variable damper with the above mentioned characteristics. The variation of the damping coefficient with displacement is depicted as well as the variation of the damping force, and the base shear. Figure (3) shows the results from implementing a velocity-dependent variable

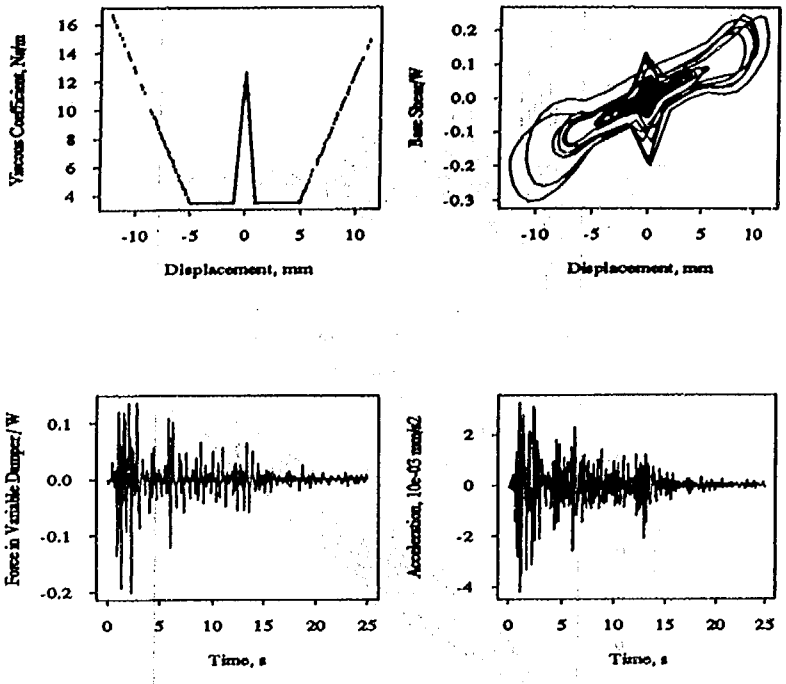


Figure 2: Displacement Dependent Variable Damping.

damper.

In addition to the continuously varying damper, a two-stage damper is also implemenetd. This damper, shown in Figure (4) was recently constructed at the Seismic Laboratory of The State University of New York at Buffalo, and will soon be tested on a model structure. The passive component of this damper was fixed at 14% of critical. The variable component, on the other hand, was allowed to take either of two values, 0 and c_{max}, depending on the form of the control algorithm. This arrangement is effectively equivalent to a bang-bang control algorithm with velocity-proportional controls. A number of different values of c_{max} as well as different control algorithms were implemented. The resulting parametric study provides insight into the sensitivity of the response of the structure to various control parameters. Specifically, four values of c_{max} were used corresponding to $2c_p$, $3c_p$, and $4c_p$, respectively. Furthermore, the control algorithms used are given by the following equations

$$c_v = \begin{cases} 0 & x < x_m \\ c_{max} & x \geq x_m \end{cases} \tag{4}$$

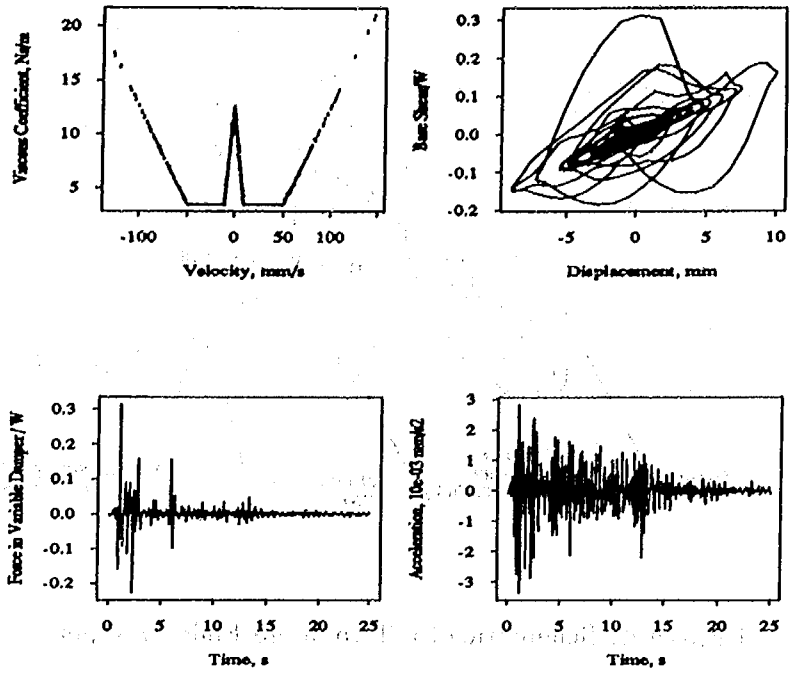


Figure 3: Velocity Dependent Variable Damping.

$$c_v = \begin{cases} 0 & s < s_m \\ c_{max} & s \geq s_m \end{cases} \tag{5}$$

$$c_v = \begin{cases} 0 & \dfrac{x}{x_m} < \dfrac{s}{s_m} \\ c_{max} & \dfrac{x}{x_m} \geq \dfrac{s}{s_m} \end{cases} \tag{6}$$

$$c_v = \begin{cases} 0 & \dfrac{x}{x_m} < \dfrac{\ddot{x}}{\ddot{x}_m} \\ c_{max} & \dfrac{x}{x_m} \geq \dfrac{\ddot{x}}{\ddot{x}_m} \end{cases} \tag{7}$$

In the above equations, s denotes the base shear, and is given as the sum of the forces in the dampers and the spring, while x_m, s_m, and $\ddot{x}_m$ denote reference values for the displacement,

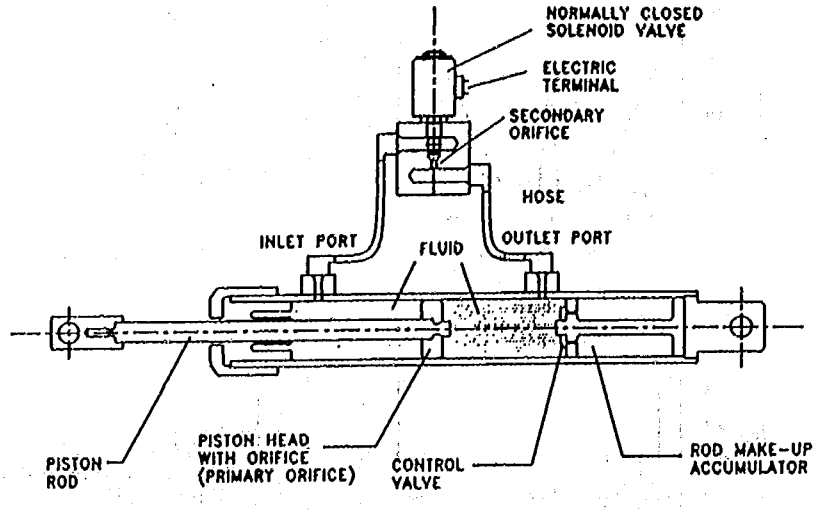


Figure 4: Schematic of a Two Stage Fluid Damper.

the base shear, and the acceleration, respectively. These values were taken to correspond to a fraction of the maximum displacement and shear with no variable damping and the identical (El Centro) input motion, and were equal to 10mm, 40kN, and 0.04m/s^2 respectively. Some of the control algorithms given in the above equations have been suggested by various researchers (Shinozuka et.al 1992; Feng and Shinozuka, 1992). Various computer simulations were performed for a number of different levels of damping coefficient. Figures (5)-(8) show the results associated with the control algorithms given in equations (4)-(7).

The second model is a two-degree-of-freedom system. Its equation of motion is given by the equation

$$\begin{bmatrix} m_1 & 0 \\ 0 & m_2 \end{bmatrix} \begin{Bmatrix} \ddot{x}_1 \\ \ddot{x}_2 \end{Bmatrix} + \begin{bmatrix} c_1 + c_2 & -c_2 \\ -c_2 & c_2 \end{bmatrix} \begin{Bmatrix} \dot{x}_1 \\ \dot{x}_2 \end{Bmatrix} + \begin{bmatrix} k_1 + k_2 & -k_2 \\ -k_2 & k_2 \end{bmatrix} \begin{Bmatrix} x_1 \\ x_2 \end{Bmatrix} = \begin{Bmatrix} 0 \\ f(t) \end{Bmatrix}. \tag{8}$$

In this equation, each of c_1 and c_2 consists of two components, one passived and the other variable. These are denoted with subscripts, p and v, respectively.

The two-stage variable damper was implemented for the two-degree-of-freedom model of a bridge. The effect of varying the damping coefficients at both the ground level and at the deck-pier joint was investigated. Control algorithms for varying the damping levels were utilized that are identical with those for the one-degree-of-freedom model. Similar effectiveness of the variable dampers was observed although not reported here due to lack of space.

Analysis of the Results

From the parametric study detailed above, a number of conclusions could be drawn that

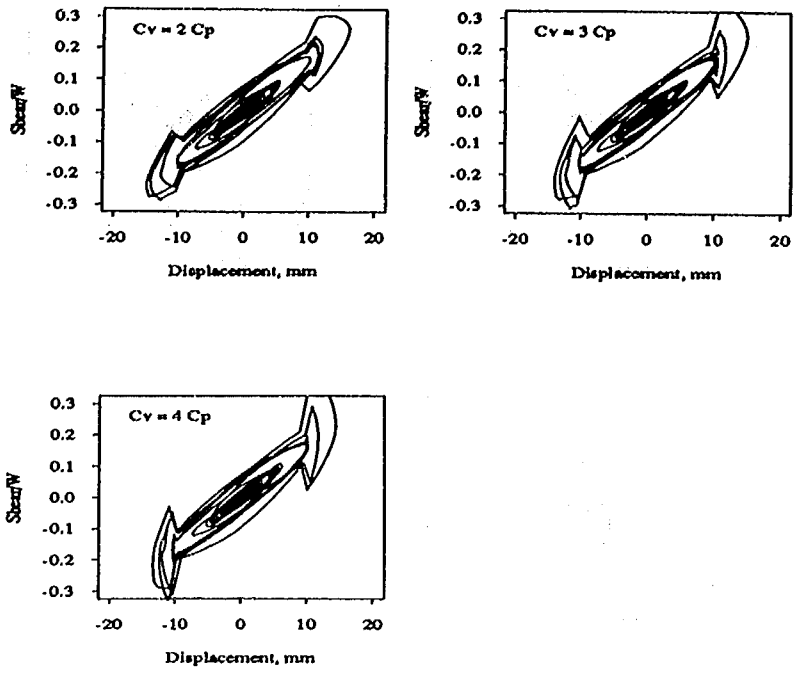


Figure 5: System with Variable Damper: Equation (4)

only emphasize the importance of damping at vibration suppression. For the continuously variable dampers, it was observed that for a given level of control force, the displacement dependent variable dampers were better at reducing the vibration of the system than the velocity dependent dampers. While the numerical results are not reported in this paper, the effect of increasing the damping force for small displacement or velocity levels was not noticeable. For the discretly variable damper, the effect of the particular strategy for switching between levels was significant. This warrants further research into developing optimal or near-optimal criteria for the activation of the dampers. Such criteria would have to accommodate the uncertainties associated with modelling large degrading structures, with parameters that are varying with time and load level. Based on the parameteric study reported in this paper, it appears that the criterion given by equation (5) is the most suitable for the system under consideration. Both maximum displacement and shear were significantly reduced for the levels of damping used. The control given by equation (4), while effective at somewhat reducing the displacement, it increases the maximum shear level. This is however accompanied by greater energy dissipation as witnessed by the wider

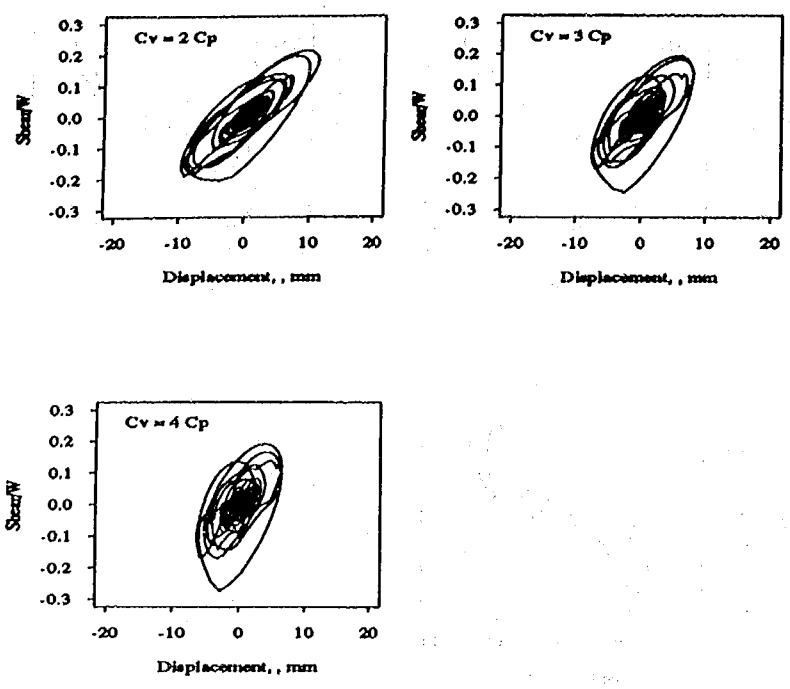


Figure 6: System with Variable Damper: Equation (5)

hysteresis loop. The control given by equation (6) does not seem to be effective for reducing either the displacement or the base shear. Finally, the control given by equation (7) results in an interesting behavior: while the bulk of the shear-displacement curve has shrunk, a single loop has expanded with the level of damping applied. This can be explained by the fact that beyond a certain level, additional damping increases the transmission of force into the system.

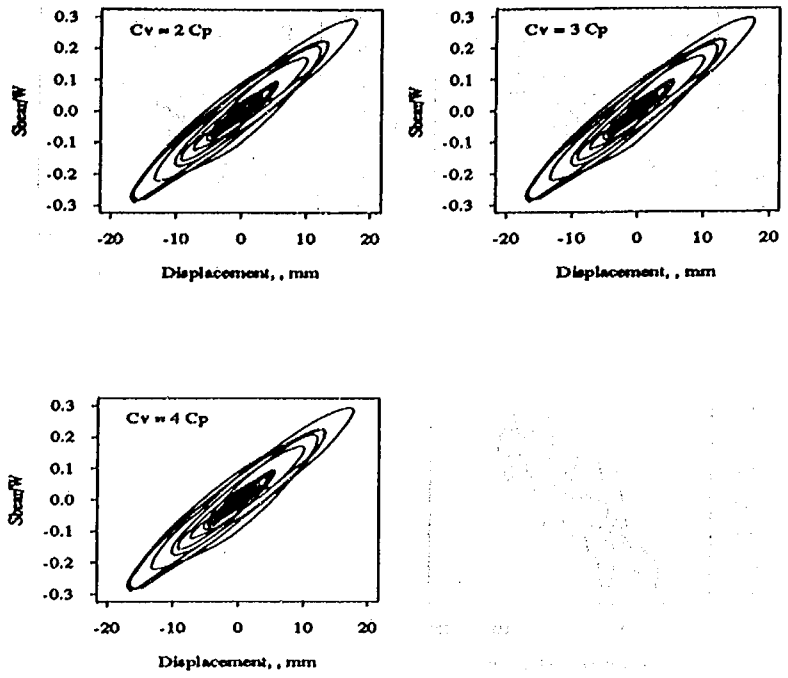


Figure 7: System with Variable Damper: Equation (6)

Acknowledgments

This work was partially supported by the National Center for Earthquake Engineering Research (NCEER) under grant number 915411A, and 925001F, and by the Center for Infrastructure Research and Development (CIRD).

Bibliography

[1] M.Q. Feng, and M. Shinozuka, "Control of seismic response of bridge structures using variable dampers," *Journal of Intelligent Material Systems and Structures,* (to appear) 1992.

[2] R. Ghanem, M. Shinozuka, and H. Gavin, "Recursive system identification in earthquake engineering," *10th World Conference on Earthquake Engineering,* July 1992.

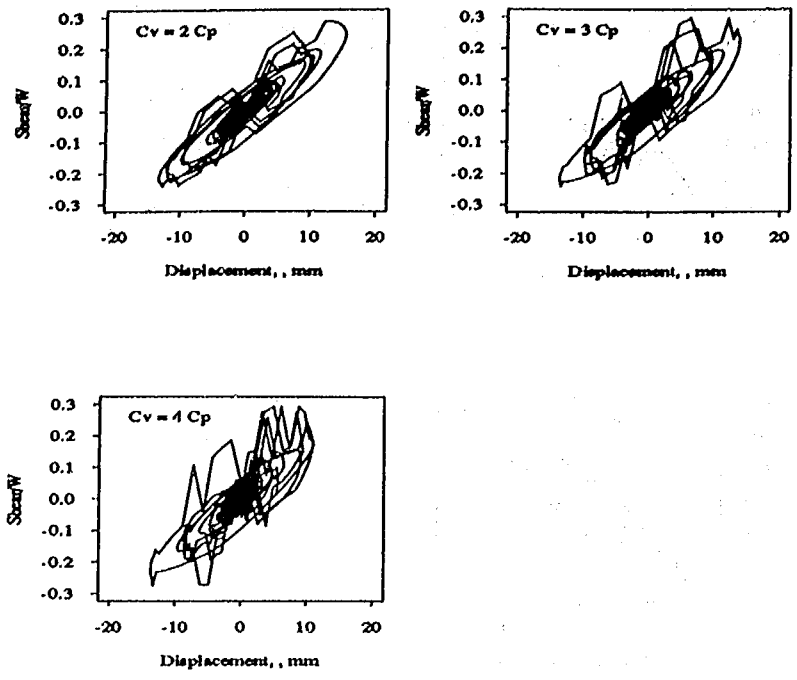


Figure 8: System with Variable Damper: Equation (7)

[3] R. Ghanem, M. Shinozuka, and H. Gavin, "Experimental verification of a number of system identification algorithms," NCEER Technical Report 91-0024, 1991.

[4] Kawashima, K., Hasegawa, K., Unjoh, S., Nagashima, H., and Shimizu, H., "Current research efforts in Japan for passive and active control of highway bridges against earthquake," 23rd *Joint Meeting, U.S.-Japan Panel on Wind and Seismic Effects,* UJNR, Tsukuba, May 1991.

[5] Kawashima, K., Unjoh, S., and Shimizu, H., "Earthquake response control of highway bridges by variable damper," *Proceedings of the Japan National Symposium in Structural Response Control,* Science Council of Japan, Tokyo, March 1992, pp. 311-324.

[6] Shinozuka, M., Constantinou, M., and Ghanem, R., "Passive and active fluid dampers in structural applications," *U.S./China/Japan Workshop on Structural Control,* Shanghai, China, October 1992.

HYBRID CONTROL OF SLIDING ISOLATED BRIDGES

Andrei M. Reinhorn, Satish Nagarajaiah, Michael A. Riley, and Ravi Subramaniam

Department of Civil Engineering
State University of New York at Buffalo
Buffalo, New York 14260

ABSTRACT

The seismic response of bridges can be improved by isolating the structure with aseismic sliding bearings. Specialized passive devices are commonly used to complement these bearings, to control the displacement of the structure during large magnitude events, and to restrict a build-up of drift. Active servo-hydraulic actuators are used herein to supplement the conventional sliding bearings creating a hybrid active-passive protective system. The control system is capable of minimizing the inertial forces in the structure, while providing higher damping ratios and better displacement control when necessary. This paper presents three control algorithms for the hybrid system. Two of these algorithms are verified experimentally, and the third is verified with an analytical model. The results show that the hybrid system is capable of significantly improving the seismic response of the bridges.

INTRODUCTION

Sliding isolation systems have been used to protect bridges from damage during earthquakes. The sliding isolation systems decouple the motion of the bridge from the ground motion, significantly reducing the forces transmitted to the bridge deck; however, the sliding isolators by themselves cannot control the potentially large relative displacements and do not provide any recentering forces. For this reason, passive devices are usually used to control the displacement in the isolation system, increase the energy dissipation, and provide recentering forces [1]. These passive systems have been shown to improve the structural response in experimental tests [1], but they have limitations. In particular, the friction forces will always affect the bridge deck response and some offset in the final position of the system is possible.

Active and hybrid control systems offer the possibility of further improving the seismic response of the system. One previously developed hybrid control system uses active variable friction bearings to adjust the level of friction in the isolation system [2].

A hybrid system is proposed, using an active control system with the sliding isolators, instead of passive displacement control devices. This hybrid system is advantageous, since the active controller can be used to push against the friction force, minimizing or completely negating the friction forces that affect the structure. The active system can be used to control the relative displacement more effectively than the standard displacement control devices, and to dissipate more energy if necessary. After a seismic event has ended, the active device can be set to automatically return the bridge deck to its original position. The hybrid nature of this system makes it more reliable than a purely active system, since the passive isolators will still protect the structure from serious damage if the active portion were to fail. An idealized sketch of a bridge superstructure protected by this system is shown in Figure A.

Three control algorithms have been developed for the hybrid system, and a model of a rigid sliding bridge has been tested with the active controller. An overview of the control algorithms and a summary of the experimental and analytical results that were obtained are present below.

DEVELOPMENT

The proposed hybrid system consists of a hydraulic servo-actuator mounted between the bridge deck and foundation. During large magnitude seismic events, the actuator will apply a control force to offset the friction forces in the sliding isolation system, which will minimize the forces entering the bridge deck. In addition, the control system will control the relative displacement of the bridge deck, limiting the peak motion to less than the limits imposed by the bearings. Theoretically, if the control force is equal to the friction forces, this hybrid system will bring the inertial forces in the bridge deck to zero and it will remain stationary with respect to an absolute reference.

Three algorithms have been developed to control this system, the friction force control algorithm and an instantaneous optimal control algorithm using absolute acceleration feedback have been tested experimentally. A fuzzy control algorithm has been tested with an analytical model.

The friction force control algorithm is based on an enhancement of dynamic linearization control. Dynamic linearization is based on choosing an ideal system with favorable response characteristics, and producing a control force that will make the actual system respond like the ideal system [6]. In the case of the hybrid sliding structure, the ideal system is a structure on frictionless isolators. Based on the equation of motion of a rigid bridge deck without any restoring or damping forces:

$$m\,\ddot{x}_i(t) \;=\; u(t) \;-\; F_f(t) \tag{1}$$

The absolute acceleration of the rigid bridge deck, $\ddot{x}_i(t)$, will be zero when the control force, $u(t)$, is equal to the friction force, $F_f(t)$.

Unfortunately, errors in the physical system, due to time delays in the control and inaccuracies in the estimate of the systems state, will cause a difference between the ideal control force and the control force which is actually applied. This difference will cause some acceleration of the bridge deck to occur, but since the acceleration is proportional to the errors in the control, the response of the bridge deck can be minimized by using an acceleration feedback to compensate for some of the original error. The control force will now be [4]:

$$\hat{u}(t) \;=\; \hat{c}\,\dot{\hat{x}}(t) \;+\; \hat{k}\,\hat{x}(t) \;+\; \hat{F}_f(t) \;-\; G_a\,\hat{m}\,\ddot{\hat{x}}_i(t) \tag{2}$$

Where, the symbol ^ indicates that the variable is an estimate of the exact value or state, containing some error, the variables $\hat{c}$ and $\hat{k}$ are a virtual damping and stiffness, which are added to the control force to influence the relative displacement, and G_a is a non-dimensional gain factor for the acceleration term.

The second control algorithm [3] is based on the instantaneous optimal control laws [7], using absolute acceleration feedback. Here, the motion of the sliding system can be formulated in state-space as:

$$\dot{\mathbf{z}}(t) = \mathbf{A}(t)\,\mathbf{z}(t) + \mathbf{B}\mathbf{u}(t) + \mathbf{W}(t) \tag{3}$$

Where, $\mathbf{z}(t) = \{x_t, \dot{x}_t\}^T$ is the state of the system, $\mathbf{A}(t)$ is the system matrix, $\mathbf{B}$ is the control force location matrix, and $\mathbf{W}(t)$ is the excitation matrix. The time dependent performance index is now used to develop the control force vector [3]:

$$\mathbf{u}(t) = -\mathbf{R}^{-1}\,\mathbf{B}^T\,\mathbf{Q}\,\dot{\mathbf{z}}(t) \quad \text{with:} \quad \mathbf{R} = \mathbf{I}, \quad Q(2,2) = 100.62 \tag{4}$$

Here, R and Q are the weighting matrices that were found for the experimental system. All of the terms in Q are zero, except as mentioned above.

The third control algorithm [5] is based on fuzzy logic, with the control gain determined by fuzzy set theory. The equation of motion for the rigid structure with a restoring force, $k\,x(t)$, and a damping force, $c\,\dot{x}(t)$, is:

$$m\,\ddot{x}_t(t) + c\,\dot{x}(t) + k\,x(t) = u(t) - F_f(t) \tag{5}$$

Accounting for the time delay, δt, in the system, the fuzzy control force is defined as:

$$u(t) = G(t)\,\ddot{x}_t(t - \delta t) \tag{6}$$

Where, $G(t)$ is a non-linear function of the state of the system, which is calculated through fuzzy set theory.

EXPERIMENTAL RESULTS & ANALYTICAL SIMULATIONS

A hybrid system, shown in Fig. A, was built and tested with the hybrid control system on a shaking table. The model weighed 4.9 kips, and was controlled with a single 5.5 kip actuator. The rigid bridge model was isolated through four steel and Teflon bearings, located at the four corners. The friction forces in the isolators were modeled using a velocity dependent model [1] with the peak friction coefficient varying from 0.17 to 0.22 as the bearings wore.

The hybrid system was tested with several earthquake excitations including: the S00E component of the El Centro record (1940 Imperial Valley earthquake); the N21E component of the Taft record (1952 Kern County earthquake), scaled to 200% of the original excitation; the East-West component of the Hachinohe record (1968 Tokachi-Oki earthquake); and an artificial motion that was developed by filtering the Imperial Valley earthquake. The system was tested with the rigid bridge model fixed to the ground, with the model free to slide with no control, and with the model controlled by the friction force control and instantaneous optimal control algorithms. Problems with the test setup caused the passive system to respond improperly, so an analytical model was used to estimate the passive response of the system. The experimental results are shown in Table 1 and in Fig. D. These results have been filtered to remove the signal noise above 12.5 Hz. The effectiveness of the fuzzy control algorithm was demonstrated using an analytical model of the system. Results have been generated for each of the four excitations used to excite the experimental model.

DISCUSSIONS AND CONCLUSIONS

The results in Table 1 indicate a reduction of the peak accelerations in all cases by using sliding bearings only and further reductions using the hybrid system. The additional reductions are more evident in the RMS response that characterizes the entire motion. The absolute peak displacements are maintained to levels of same order of magnitude as the ground displacements (see the fixed base case) with associated small relative displacements.

Based on the results of this investigation it can be concluded that the concept of hybrid control of sliding isolated bridges is feasible with existing technology. The hybrid system is able to significantly reduce the seismic response of the sliding system. The fuzzy control algorithm was most effective at reducing the peak accelerations in the basemat, while the friction force control was most effective at reducing the intensity of the acceleration over the entire time history. The instantaneous optimal control algorithm reduced both the intensity and the peak acceleration significantly. The instantaneous optimal control was shown to be stable when the Q matrix is properly chosen.

The hybrid system is able to improve the response of the bridge to seismic excitation, providing better earthquake protection than the passive isolation system; however, the response of the control system was limited by the time delay in the control system, and by the limitations in the response of the control actuator. Additional analytical and experimental studies are underway to improve the efficiency and response of the hybrid system.

ACKNOWLEDGEMENTS

This research was supported in part by the National Center for Earthquake Engineering Research Grant No. NCEER-91-5111. The support is greatly acknowledged. Special acknowledgments are due to Mr. M. Pitman and D. Walch from the Seismic Simulation Laboratory at the University of Buffalo.

REFERENCES

1. Constantinou, M. C., Kartoum, A., and Reinhorn, A. M. (1992). "Sliding Isolation System for Bridges: Experimental Study", *Earthquake Spectra*, Vol. 8, No. 3, pp. 321-44.

2. Feng, Q., Shinozuka, M., Fujii, S., and Fujita, T. (1991). "A Hybrid Isolation System for Bridges", *Proc. 1st US-Japan Workshop on Earthquake Protection Systems for Bridges*, Buffalo, NY.

3. Nagarajaiah, S., Riley, M. A., Reinhorn, A. M., and Shinozuka, M. (1992). "Hybrid Control of Sliding Isolated Bridges", *Proc. of the 1992 ASME Pressure Vessels and Piping Conference*, New Orleans, LA. PVP-237, Vol. 2, pp. 83-89.

4. Riley, M. A. (1992). "Hybrid Control of Motion in Sliding Systems through Active Forces." MS Thesis, State University of New York at Buffalo, Buffalo, N.Y.

5. Subramaniam, R., Reinhorn, A. M., and Nagarajaiah, S. (1993). "Application of Fuzzy Set Theory to the Active Control of Base-Isolated Structures", *Proc. Second IEEE International Conference on Fuzzy Systems*, San Francisco, CA.

6. Yang, J. N., and Li, Z. (1992). "Control of Base-Isolated Building Structures", *Innovative Large Span Structures, IASS-CSCE International Congress 1992*, Toronto, Canada.

7. Yang, J. N., Li, Z., Danielians, A., and Liu, S. C. (1992). "Aseismic Hybrid Control of Nonlinear Hysteretic Structures I", *Journal of Engineering Mechanics*, ASCE, Vol. 118, No. 7, pp. 1423-40.

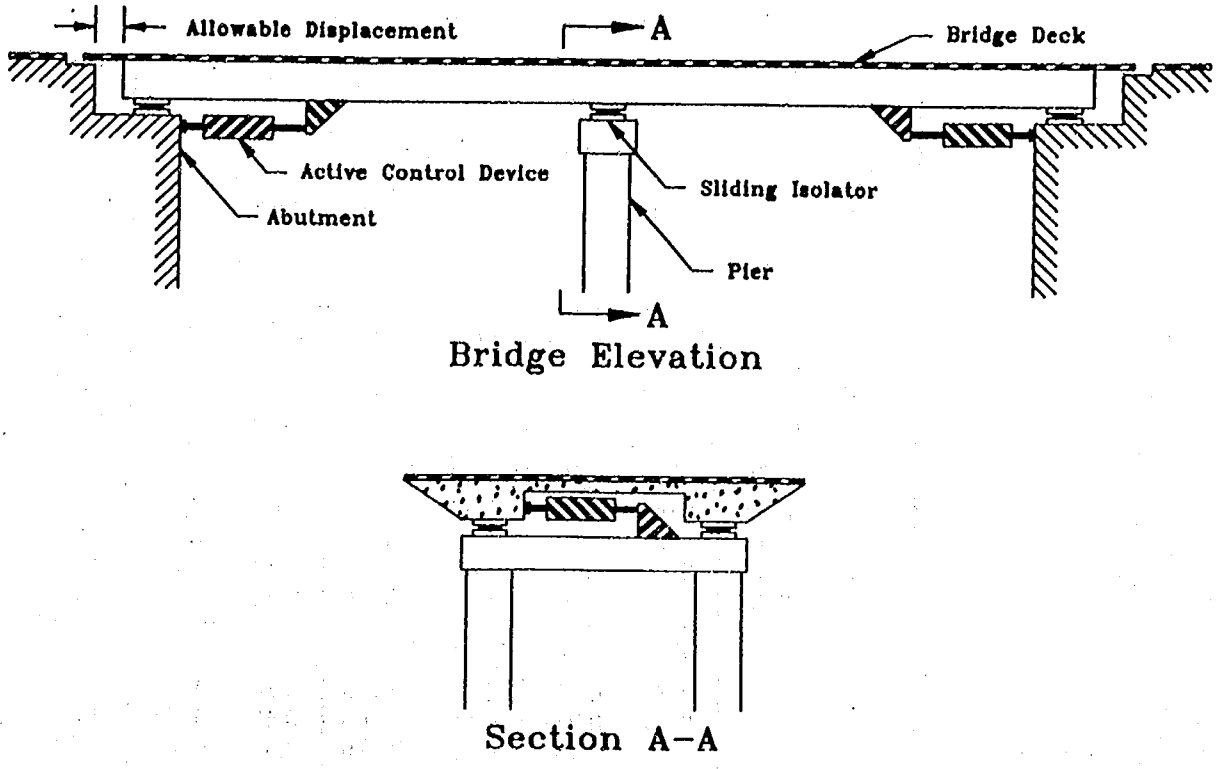


Figure A. Bridge Structure Isolated with Hybrid System

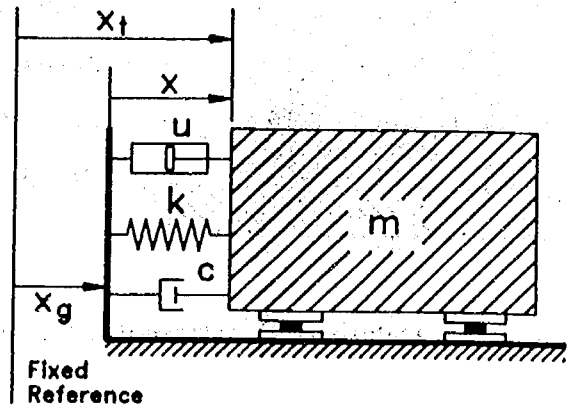


Figure B. Idealized System

Table 1. Response of Experimental Model

Name (1)	Base Fixed (Experiment) Peak (2)	Base Fixed (Experiment) RMS (3)	Passive Isolation (Analytical) Peak (4)	Passive Isolation (Analytical) RMS (5)	Instantaneous Optimal Control (Experiment) Peak (6)	Instantaneous Optimal Control (Experiment) RMS (7)	Friction Force Control (Experiment) Peak (8)	Friction Force Control (Experiment) RMS (9)	Fuzzy Control (Analytical) Peak (10)	Fuzzy Control (Analytical) RMS (11)
Basemat Acceleration (G's)										
El Centro S00E	0.327	0.051	0.192	0.061	0.175	0.044	0.201	0.033	0.133	0.052
Taft 200%	0.357	0.062	0.188	0.074	0.151	0.053	0.245	0.039	0.123	0.060
Hachinohe EW	0.195	0.041	0.180	0.050	0.134	0.039	0.141	0.031	0.121	0.045
Artificial Motion	0.416	0.060	0.230	0.069	0.175	0.052	0.207	0.041	0.139	0.058
Absolute Basemat Displacement (inches)										
El Centro S00E	1.77	0.37	2.03	0.49	1.92	0.40	1.65	0.34	1.92	0.38
Taft 200%	2.19	0.41	2.04	0.48	1.98	0.45	1.88	0.38	2.39	0.55
Hachinohe EW	3.74	1.03	3.77	1.01	3.68	1.04	3.70	1.06	3.96	1.03
Artificial Motion	3.49	0.70	4.71	0.79	3.16	0.68	3.24	0.64	2.74	0.71
Relative Basemat Displacement (inches)										
El Centro S00E	-	-	0.53	0.318	0.76	0.199	0.76	0.184	1.72	0.164
Taft 200%	-	-	0.46	0.277	0.45	0.166	0.46	0.175	1.02	0.338
Hachinohe EW 100%	-	-	0.18	0.130	0.77	0.176	0.84	0.316	0.80	0.172
Artificial Motion	-	-	0.64	0.299	1.40	0.195	1.30	0.324	2.08	0.384

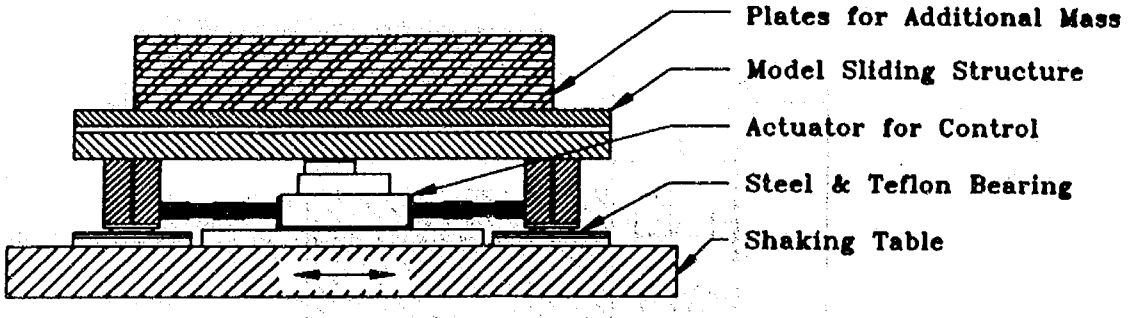


Figure C. Details of Experimental Model

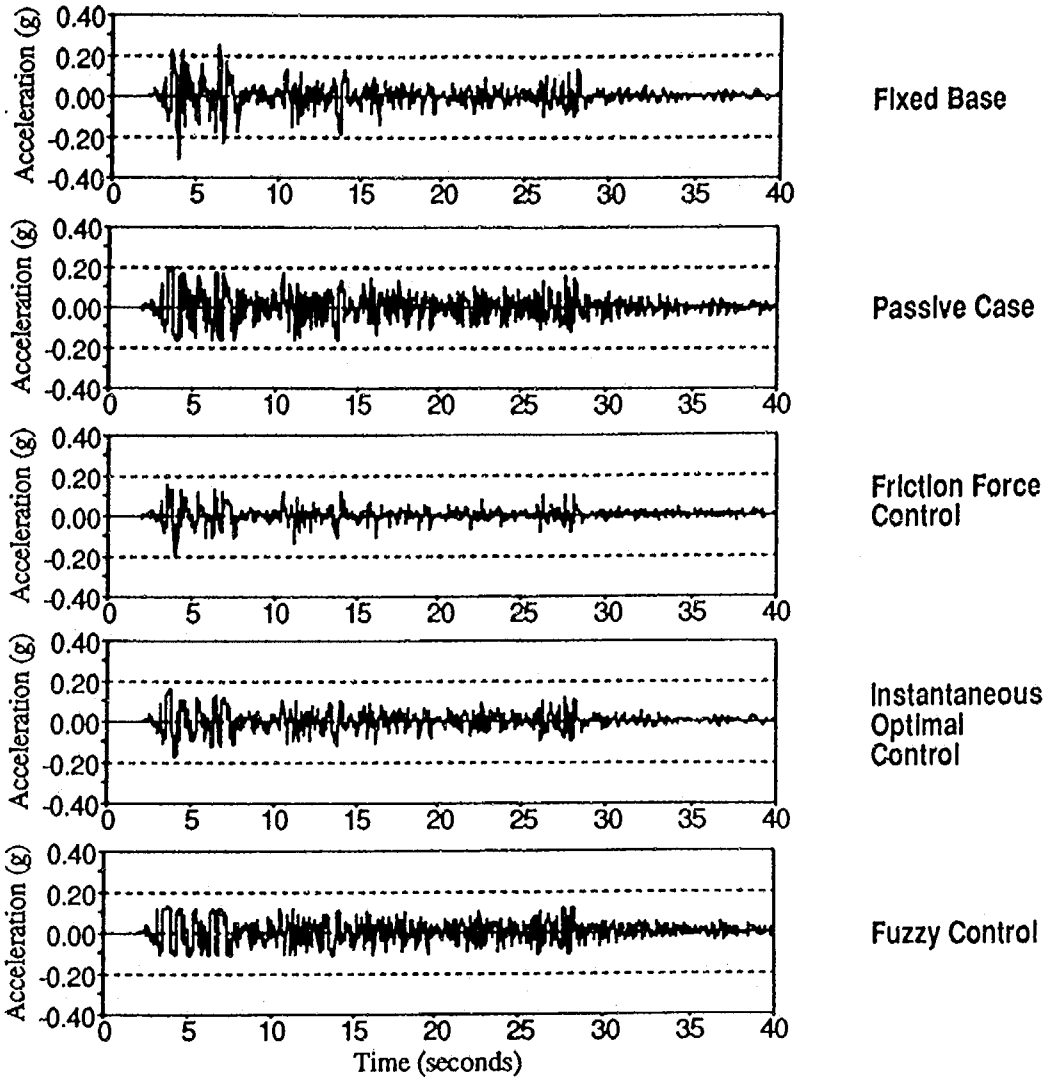


Figure D. Acceleration Response of Hybrid System To El Centro S00E Excitation

Session-10

Comparative Design Example

U-11) Bridge Design Example-1
(Mayes, R. L.)

U-12) Bridge Design Example-2
(Constantinou, M. C., Tsopelas, P. C. and Ozaki, D.)

J-22) Design Example of A Highway Bridge Based on The Manual for Menshin Design of Highway Bridges
(Kawashima, K., Okado, M. and Horikawa, M.)

Bridge Design Example-1

by

Ronald L. Mayes
President Dynamic Isolation Systems
2855 Telegraph Avenue, Suite 410
Berkeley, CA 94705, USA

ELASTOMERIC BEARING DESIGN EXAMPLES
(Metric Units)

The design example was performed for a lead rubber system (LRB) and a system using the nonlinearity of the elastomer with an assumed 10% value of equivalent viscous damping. (These so called HDR systems have damping values that vary between 10–15%). The designs were also performed for a two and four bearing configuration.

TABLE 1

ISOLATION SYSTEM	NO. OF ISOLATORS	BASE SHEAR F/W	COLUMN DEFLECTION		EFFECTIVE PERIOD	ISOLATOR SIZE
			ISOLATOR DEFLECTION	MINIMUM COLUMN DESIGN FORCE		
LEAD RUBBER	2	0.15	160	0.06	2.1	S660-200-190
	2	0.34	70	0.16	0.9	S940-130-300
	4	0.16	150	0.06	1.95	S530-200-130
	4	0.34	70	0.16	0.95	S660-130-220
10% NON-LINEAR RUBBER	2	0.13	225	0.03	2.7	S690-280-0
	2					
	4					
	4					

ELASTOMERIC BEARING DESIGN EXAMPLES

The design example was performed for a lead rubber system (LRB) and a system using the nonlinearity of the elastomer with an assumed 10% value of equivalent viscous damping. (These so called HDR systems have damping values that vary between 10–15%). The designs were also performed for a two and four bearing configuration.

TABLE 1

ISOLATION SYSTEM	NO. OF ISOLATORS	BASE SHEAR F/W	COLUMN DEFLECTION		EFFECTIVE PERIOD	ISOLATOR SIZE
			ISOLATOR DEFLECTION	MINIMUM COLUMN DESIGN FORCE		
LEAD RUBBER	2	0.15	6.2	0.06	2.1	S26-8-7.5
	2	0.34	2.8	0.16	0.9	S37-5-12
	4	0.16	5.8	0.06	1.95	S21-8-5
	4	0.34	2.8	0.16	0.95	S26-5-8.5
10% NON-LINEAR RUBBER	2	0.13	8.8	0.03	2.7	S27-11-0
	2					
	4					
	4					

OVERALL SEISMIC PERFORMANCE : SEGMENT 1

Seismic performance is calculated assuming rigid substructures and a rigid structure above the bearings. If the substructures are flexible then the estimated effective period will be less than the actual effective period. The assumption of rigid substructures is a conservative method of calculating maximum earthquake forces. The values of effective period, maximum displacement and elastic force coefficient are based on the DIS Non-Linear response spectra for the specified acceleration level and soil type. This is a single mode spectral analysis method assuming that the dominant mode is the deformation of the bearings and the force coefficient is calculated from the period of this mode. The non-linear spectra allow the additional damping from the lead cores to be accounted for in calculating forces and displacements. The reduction factor listed is the ratio between the peak acceleration on the response spectrum and the elastic force coefficient using isolation.

DESIGN LEVEL : 0.40 g Soil Type 2 (Qd 0.056)
(AASHTO Guide Specifications Spectral Shape)

Effective Period (secs)	:	2.08
Maximum Displacement (inches)	:	6.15
Elastic Force Coefficient	:	0.146
Reduction Factor from Peak	:	6.9

PERFORMANCE FOR OTHER ACCELERATION LEVELS :

		EARTHQUAKE G LEVEL				
		0.20G	0.30G	0.40G	0.50G	0.60G
Effective Period (secs)	:	1.72	1.93	2.08	2.19	2.26
Maximum Displacement (inches)	:	2.82	4.28	6.15	8.10	10.08
Elastic Force Coefficient	:	0.096	0.118	0.146	0.173	0.201
Reduction Factor from Peak	:	5.2	6.4	6.9	7.2	7.5
Effective Damping %	:	32.667	28.007	23.280	19.835	17.225

EARTHQUAKE EFFECTIVE STIFFNESS

	EARTHQUAKE G LEVEL				
	0.20G	0.30G	0.40G	0.50G	0.60G
S26-8-7.50					
Earthquake Displacement :	2.82	4.28	6.15	8.10	10.08
Effective Stiffness (kip/in) :	30.87	24.73	21.14	19.16	17.93
Factor of Safety for :					
Strain Limit :	3.22	2.76	2.21	1.71	1.26
Buckling :	8.60	8.03	7.31	6.55	5.78
Rollover :	7.77	5.11	3.56	2.70	2.17

BEARING PROPERTIES (Sheet 1 of 1) Units Kips, In.

S26-8-7.50

DIMENSIONAL PROPERTIES

Shape Factor	:	16.67
Gross Bonded Area	:	625.00
Plug Area	:	44.18
Net Bonded Area	:	580.82
Rubber Thickness	:	4.500

STRENGTH AND STIFFNESS PROPERTIES

Yielded Stiffness	:	12.91
Elastic Stiffness	:	160.47
Characteristic Str.	:	50.63
Yield Strength	:	55.05
Yield Displacement	:	0.343
Inner Layer Stiff.	:	224343
Outer Layer Stiff.	:	199745
Vertical Stiffness	:	15747

VERTICAL LOAD CAPACITIES

Maximum Rotation on Bearing		
At 0% Strain	:	1682.6
At R+S+T	:	1367.9
At EQ Disp.	:	1323.1
Zero Rotation on Bearing		
At 0% Strain	:	1682.6
At R+S+T	:	2243.4
At EQ Disp.	:	1988.2

VERTICAL STRESSES AND DEFLECTIONS

Dead Load	Stress	:	1.437
	Deflection	:	0.057
	Rotation (deg)		0.261
D+L	Stress	:	1.826
	Deflection	:	0.072
	Rotation (deg)		0.332

LIMIT STATES

Rollover Displ.	:	21.893
Buckling Load Longl.	:	8683.5
Buckling Load Trans.	:	8683.5

OVERALL SEISMIC PERFORMANCE : SEGMENT 1

Seismic performance is calculated assuming rigid substructures and a rigid structure above the bearings. If the substructures are flexible then the estimated effective period will be less than the actual effective period. The assumption of rigid substructures is a conservative method of calculating maximum earthquake forces. The values of effective period, maximum displacement and elastic force coefficient are based on the DIS Non-Linear response spectra for the specified acceleration level and soil type. This is a single mode spectral analysis method assuming that the dominant mode is the deformation of the bearings and the force coefficient is calculated from the period of this mode. The non-linear spectra allow the additional damping from the lead cores to be accounted for in calculating forces and displacements. The reduction factor listed is the ratio between the peak acceleration on the response spectrum and the elastic force coefficient using isolation.

DESIGN LEVEL : 0.40 g Soil Type 2 (Qd 0.144)
(AASHTO Guide Specifications Spectral Shape)

Effective Period (secs)	:	0.91
Maximum Displacement (inches)	:	2.78
Elastic Force Coefficient	:	0.340
Reduction Factor from Peak	:	2.9

PERFORMANCE FOR OTHER ACCELERATION LEVELS :

	EARTHQUAKE G LEVEL				
	0.20G	0.30G	0.40G	0.50G	0.60G
Effective Period (secs) :	0.71	0.83	0.91	0.97	1.01
Maximum Displacement (inches) :	1.08	1.83	2.78	3.77	4.77
Elastic Force Coefficient :	0.218	0.272	0.340	0.410	0.480
Reduction Factor from Peak :	2.3	2.8	2.9	3.1	3.1
Effective Damping % :	35.943	30.874	25.479	21.481	18.516

EARTHQUAKE EFFECTIVE STIFFNESS

	EARTHQUAKE G LEVEL				
	0.20G	0.30G	0.40G	0.50G	0.60G
S37-5-12.00					
Earthquake Displacement :	1.08	1.83	2.78	3.77	4.77
Effective Stiffness (kip/in) :	183.58	133.93	109.72	97.42	90.26
Factor of Safety for :					
Strain Limit :	10.45	9.18	7.64	6.11	4.66
Buckling :	96.33	94.25	91.63	88.89	86.14
Rollover :	23.77	13.98	9.20	6.77	5.36

BEARING PROPERTIES (Sheet 1 of 1) Units Kips, In.

S37-5-12.00

DIMENSIONAL PROPERTIES		
Shape Factor	:	24.00
Gross Bonded Area	:	1296.00
Plug Area	:	113.10
Net Bonded Area	:	1182.90
Rubber Thickness	:	1.875

STRENGTH AND STIFFNESS PROPERTIES		
Yielded Stiffness	:	63.09
Elastic Stiffness	:	880.56
Characteristic Str.	:	129.60
Yield Strength	:	139.60
Yield Displacement	:	0.159
Inner Layer Stiff.	:	946070
Outer Layer Stiff.	:	798692
Vertical Stiffness	:	128384

VERTICAL LOAD CAPACITIES		
Maximum Rotation on Bearing		
At 0% Strain	:	4927.4
At R+S+T	:	3584.9
At EQ Disp.	:	4247.5
Zero Rotation on Bearing		
At 0% Strain	:	4927.4
At R+S+T	:	5908.4
At EQ Disp.	:	6860.5

VERTICAL STRESSES AND DEFLECTIONS			
Dead Load	Stress	:	0.693
	Deflection	:	0.007
	Rotation (deg)		0.022
D+L	Stress	:	0.880
	Deflection	:	0.009
	Rotation (deg)		0.028

LIMIT STATES		
Rollover Displ.	:	25.569
Buckling Load Longl.	:	89076.5
Buckling Load Trans.	:	89076.5

Bridge Design Example-2

by

M.C. Constantinou and P.C. Tsopelas
Dept. of Civil Engineering
State University of New York
Buffalo, NY 14260, USA

and

D. Ozaki
Technology Planning Department
Taisei Corporation, Japan

1. INTRODUCTION

The project description is shown in Table 1. Design specifications are limited to performance criteria and they do not include minimum limits on design displacements. It was assumed that the design could be based on nonlinear dynamic analysis. For this purpose, the mathematical model used in the dynamic analysis was verified by comparison to shake table test results of a large scale bridge model. The earthquake input was represented by simulated motions compatible with the specified design spectra.

A detailed design was developed for the 0.4g, soil type 2 AASHTO spectrum. Furthermore, a design was developed for the Japanese Level 2, Ground Condition 2 bridge design spectrum, anchored at 0.4g peak ground acceleration. Both designs are based on the performance criterion of minimum isolation system displacement with pier force less than 40% of the supported weight.

2. EARTHQUAKE INPUT

Figure 1 shows the design spectra of AASHTO and Japanese bridge design code for soil type 2 (or G.C. 2) and PGA=0.4g. For comparison, Figure 1 includes the Japanese spectra for G.C. 1 (stiff soil) and G.C. 3 (very soft soil), also for PGA=0.4g.

Figures 2 and 3 show two simulated motions compatible with the AASHTO spectrum. These motions have PGA=0.4g, PGV=600mm/sec and PGD=325 and 420 mm. The authors consider them representative of the design spectrum.

Figure 4 shows time histories of simulated motions used in Japan for bridge design. The spectra of the motions are shown in Figure 1. The motion for Level 2, Ground Condition 2 has been used for the analyses of the designed isolation system.

3. SEISMIC ISOLATION SYSTEM

The isolation system consists of sliding bearings, rubber restoring force devices and fluid viscous dampers. This system has been recently tested at U. Buffalo and results are presented at the workshop (paper by Okamoto, Constantinou, Tsopelas, Fujii and Ozaki). The attached NCEER publication provides an overview of the research program. The layout of the isolation system is shown in Figures 5 and 6.

Each sliding bearing carries a load of 4000 kN. The sliding interface will consist of polished stainless steel and a woven composite with PTFE included in its matrix. The composite has approximately the frictional properties of PTFE but substantially more bearing capacity (rated at 275 MPa) and wear life. The frictional properties of the interface are shown in Figure 7. The bearing pressure will be 23 MPa, for which the coefficient of friction at large velocity of sliding is 0.10. Alternatively,

glass filled Teflon at 15% by weight under bearing pressure of 13.8 MPa may be used. It can deliver a friction coefficient of 0.10.

The restoring force devices will shaped in a manner similar to the one used in the shake table testing at U. Buffalo (see attached NCEER publication and paper by Okamoto). The devices are designed to deliver linear stiffness of 1790 kN/m each up to displacements of $\pm 100\,mm$ for the AASHTO motion and $\pm 200\,mm$ for the Japanese motion. Beyond this limit, they exhibit large stiffness and act as displacement restrainers.

The fluid dampers represent standard equipment typically used in the U.S. in military applications. Over 13,000 of these devices are currently in service in the U.S.. They employ fluidic control orifices and passive thermostats which allow operation over the temperature range of $-40°$ to $70°\ C$ (see attached paper by Shinozuka, Constantinou and Ghanem). The fluid dampers are designed to have a damping constant equal to 1.37 kN-sec/mm, displacement capacity of $\pm 100\,mm$ and rated load capacity of 450 kN for the AASHTO motion, and $\pm 200\,mm$ and 588 kN for the Japanese motion.

4. MATHEMATICAL MODEL OF BRIDGE

The mathematical model for nonlinear dynamic analysis is shown in Figure 8. It accounts for the nonlinear characteristics of the isolation and for the pier flexibility. It neglects higher mode effects of the pier, deck flexibility, pier rotation and soil flexibility.

Despite its simplicity, the model is capable of capturing well the response of the tested bridge model with similar dynamic characteristics. Figure 9 shows the tested bridge model (quarter length scale). In one testing configuration, the model had $T_{PIER}=0.1\,secs$, $T_{ISO}=1.4\,secs$, $\mu=0.14$ and $\xi_{ISO}=0$ or 0.47, thus very similar to the designed isolated bridge.

Test and simulation results with input being the Japanese Level 2, G.C. 2 (scaled at 75%) motion are shown in Figures 10 and 11.

5. RESPONSE OF DESIGNED ISOLATED BRIDGE

The peak response of the isolated bridge for the AASHTO motion is presented in Table 2. Analyses were performed for coefficient of friction equal to 0.10 and 0.12. The latter case is used to obtain upper bounds on the design forces, while the former case is used to obtain upper bounds on displacements.

Furthermore, Table 2 presents the peak response for the Japanese Level 2, Ground Condition 2 motion. From these results the design values were determined and presented in Table 3. Evidently, the design satisfies the limit of 0.4 times the carried weight of shear in the pier while displacements are, respectively 71 mm and 175 mm for the AASHTO and Japanese motions.

Details of the designed sliding bearings, rubber restoring force devices and fluid dampers for the AASHTO motions are shown in Figures 12 to 14. The displacement capacity of the system

(for AASHTO motion) is 40% more than the calculated response. This was thought to be necessary for accommodating bidirectional motions, unanticipated stronger motions and thermal movements (estimated at $\pm 5mm$ for $\pm 25°C$ temperature changes).

Detail of the design for the Japanese motion are not presented. However, the results of Table 3 provide the necessary information for the detailing of the isolation elements.

TABLE 1

PROPOSED BRIDGE DESIGN EXAMPLES

SECOND US-JAPAN WORKSHOP ON PROTECTIVE SYSTEMS FOR BRIDGES

Bridge Geometry:	Single span segment of a long bridge Span length = 40 m Clear height at support = 10 m Width of superstructure = 14 m Depth of superstructure = 2 m Weight of superstructure = 200 kN/m
Bridge Materials:	Reinforced concrete
Bridge Substructure:	Could be single column or multiple column
Foundation:	Spread footing on moderate soil US Soil Type 2 (a stiff clay or deep cohesionless conditions greater than 60m in depth)
Peak Ground Acceleration:	0.4 g
Spectral Shape:	2 design spectra, one US the other Japanese, anchored to the above peak ground acceleration
Isolation Performance Criteria:	2 designs are required for each of the above 2 spectra to provide: (a) minimum forces in the substructure OR (b) minimum displacements in the superstructure provided the force in the substructure does not exceed 40% of the supported weight

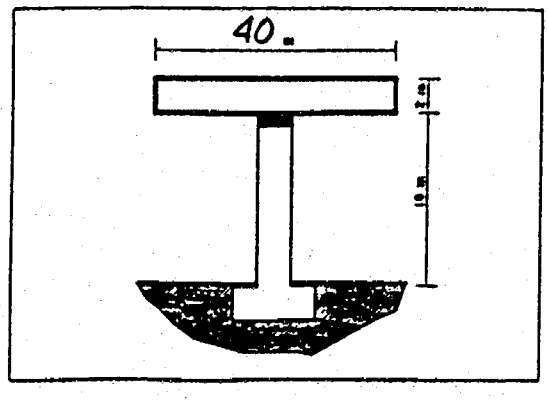


Table 2 : Peak Response of Isolated Bridge

EXCITATION	DAMPERS / FRICTION	BEARING DISPL. (mm)		ISOLATION SYSTEM FORCE / WEIGHT		PIER TOP ACCEL. (g)		PIER SHEAR / WEIGHT		DAMPER FORCE (EACH kN)	
		NO	YES	NO	YES	NO	YES	NO	YES	NO	YES
AASHTO #1	0.10	109	71	0.148	0.177	0.76	0.77	0.229	0.266	0	423
	0.12	80	52	0.156	0.195	0.89	0.85	0.263	0.302	0	433
AASHTO #2	0.10	88	64	0.138	0.172	0.84	0.86	0.268	0.267	0	414
	0.12	87	64	0.160	0.190	0.94	0.84	0.307	0.295	0	412
JAPANESE LEVEL 2 G.C.2 (0.4 g)	0.10	242	175	0.208	0.258	0.91	0.84	0.267	0.324	0	564
	0.12	233	145	0.223	0.257	1.13	0.93	0.306	0.324	0	523

Table 3 : Design Values. Value in Parenthesis is Capacity of Designed System

SPECTRUM	BEARING DISPL. (mm)	ISOLATION SYSTEM FORCE / WEIGHT	PIER SHEAR / WEIGHT	DAMPER FORCE (kN)
AASHTO 0.4 g, S2	71 (100)	0.195	0.302	433 (670)
JAPANESE LEVEL 2 G.C.2	175 (200)	0.258	0.324	564 (890)

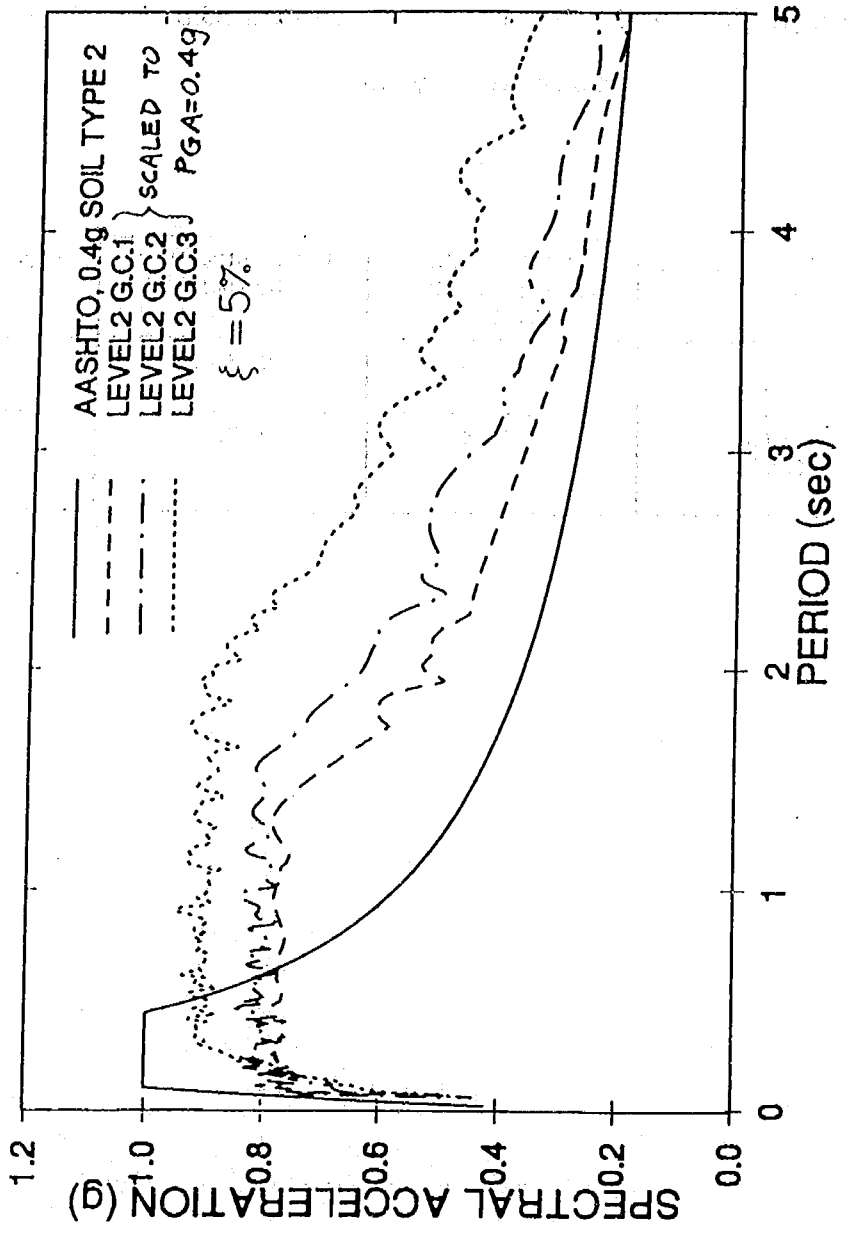

AASHTO, 0.4g SOIL TYPE 2
LEVEL2 G.C.1
LEVEL2 G.C.2
LEVEL2 G.C.3
SCALED TO PGA=0.4g
ξ = 5%
SPECTRAL ACCELERATION (g)
PERIOD (sec)
0.0
0.2
0.4
0.6
0.8
1.0
1.2
0
1
2
3
4
5

FIGURE 1

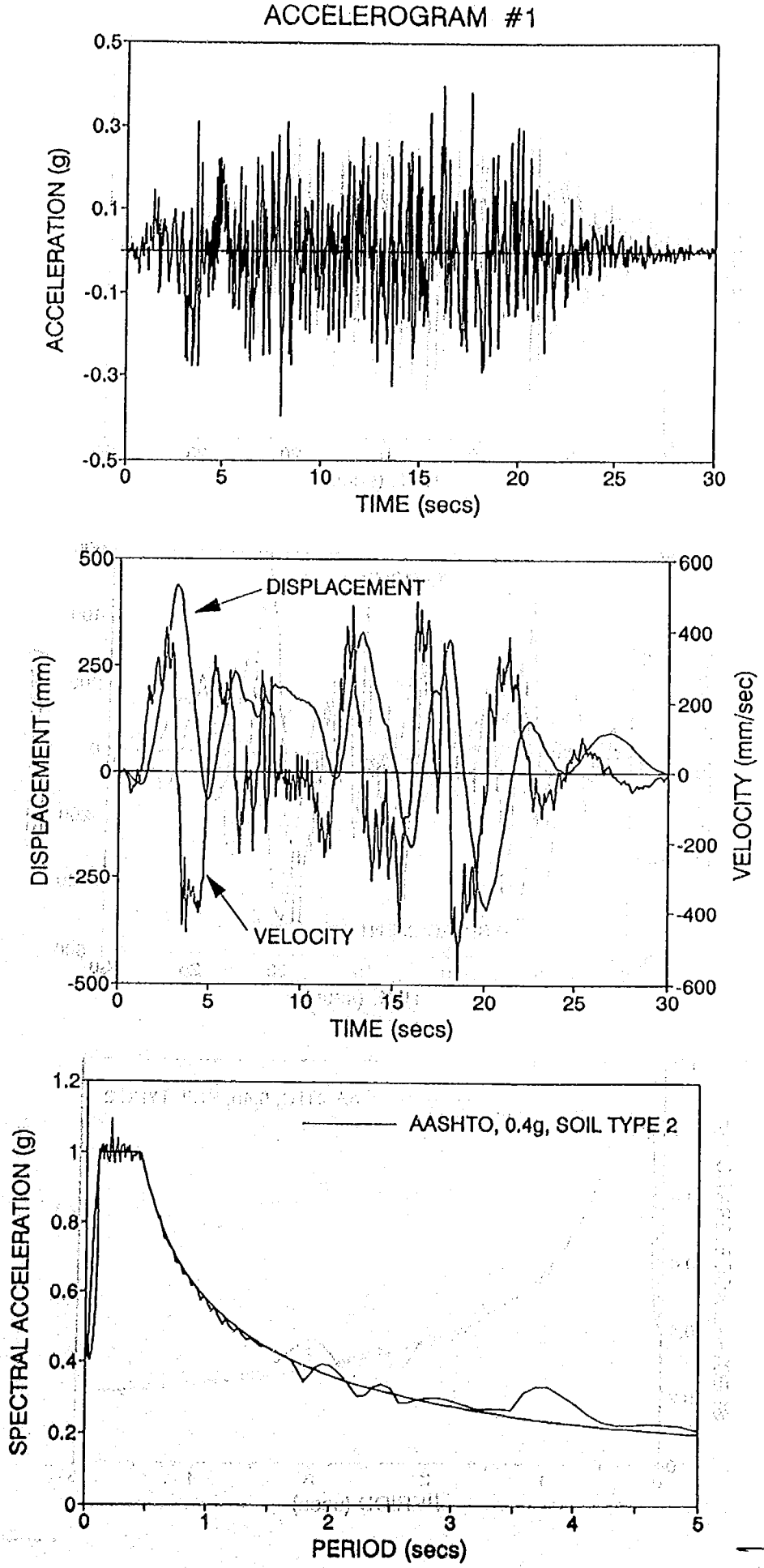

ACCELEROGRAM #1
ACCELERATION (g)
0.5
0.3
0.1
-0.1
-0.3
-0.5
0
5
10
15
20
25
30
TIME (secs)
DISPLACEMENT
VELOCITY
DISPLACEMENT (mm)
VELOCITY (mm/sec)
500
250
0
-250
-500
600
400
200
0
-200
-400
-600
TIME (secs)
AASHTO, 0.4g, SOIL TYPE 2
SPECTRAL ACCELERATION (g)
1.2
1
0.8
0.6
0.4
0.2
0
1
2
3
4
5
PERIOD (secs)

FIGURE 2

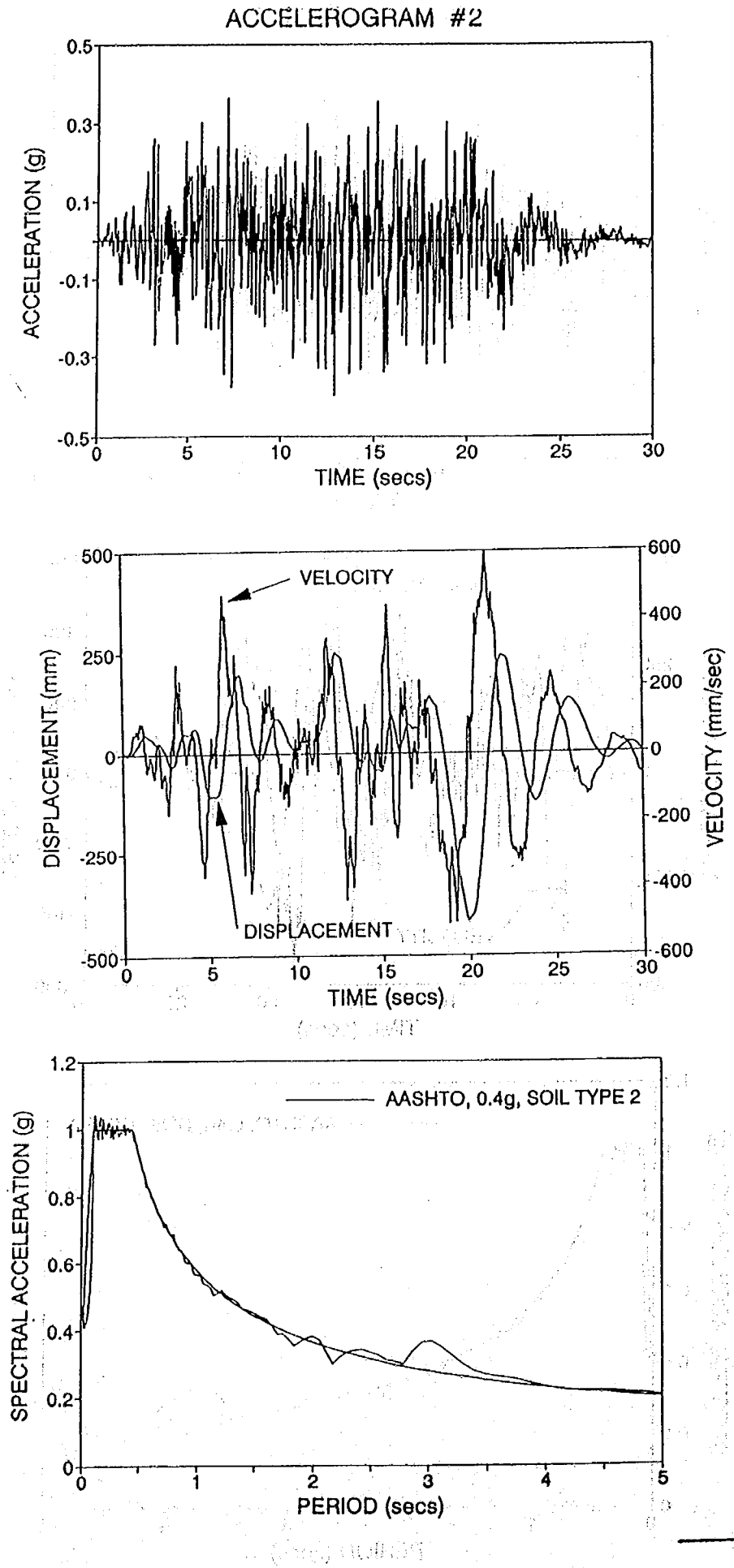

ACCELEROGRAM #2
ACCELERATION (g)
0.5
0.3
0.1
-0.1
-0.3
-0.5
0
5
10
15
20
25
30
TIME (secs)
VELOCITY
DISPLACEMENT
DISPLACEMENT (mm)
VELOCITY (mm/sec)
500
250
0
-250
-500
600
400
200
0
-200
-400
-600
TIME (secs)
AASHTO, 0.4g, SOIL TYPE 2
SPECTRAL ACCELERATION (g)
1.2
1
0.8
0.6
0.4
0.2
0
1
2
3
4
5
PERIOD (secs)

FIGURE 3

JAPANESE BRIDGE DESIGN MOTIONS

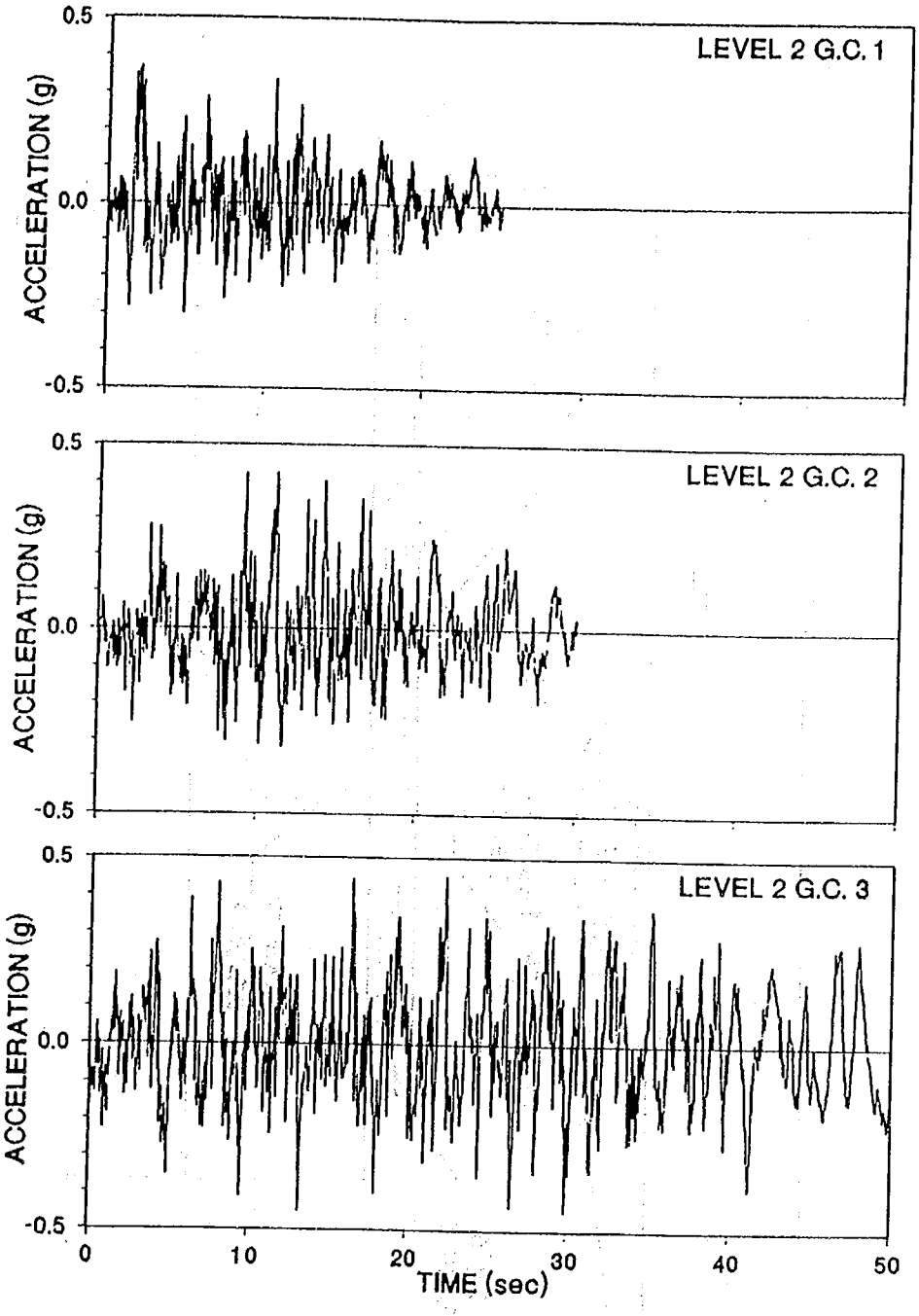


FIGURE 4

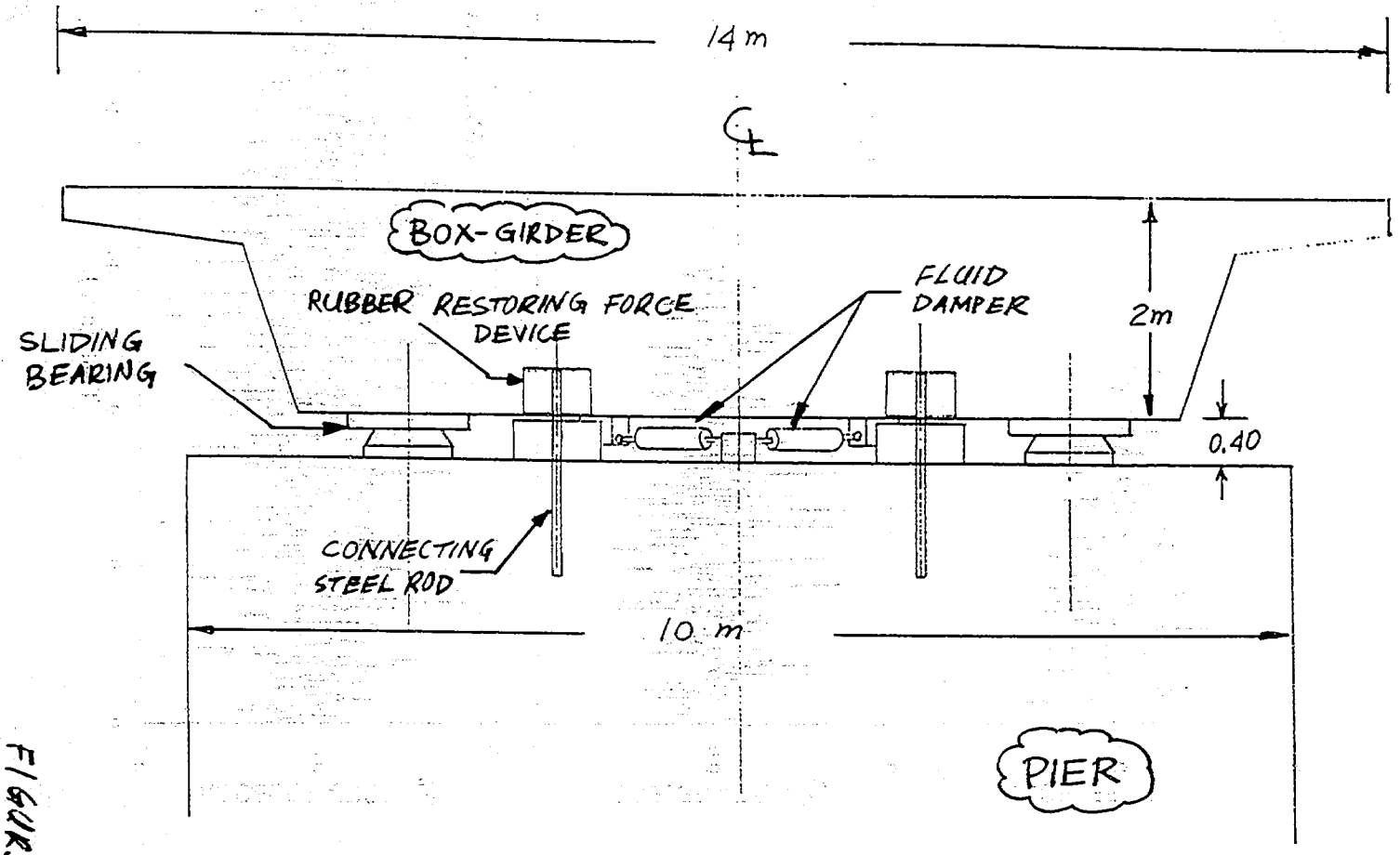

14 m
BOX-GIRDER
RUBBER RESTORING FORCE DEVICE
FLUID DAMPER
SLIDING BEARING
2m
0.40
CONNECTING STEEL ROD
10 m
PIER

FIGURE 5

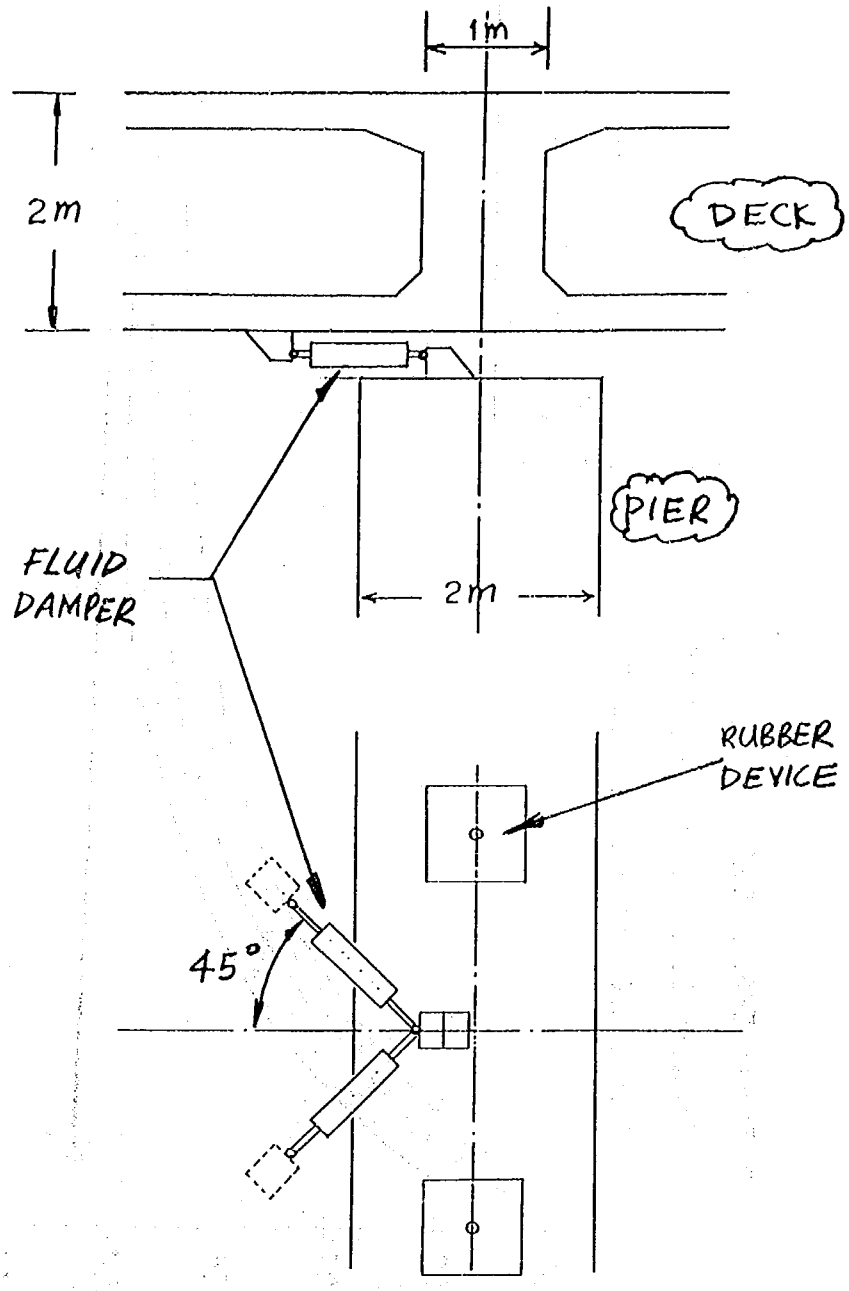


FIGURE 6

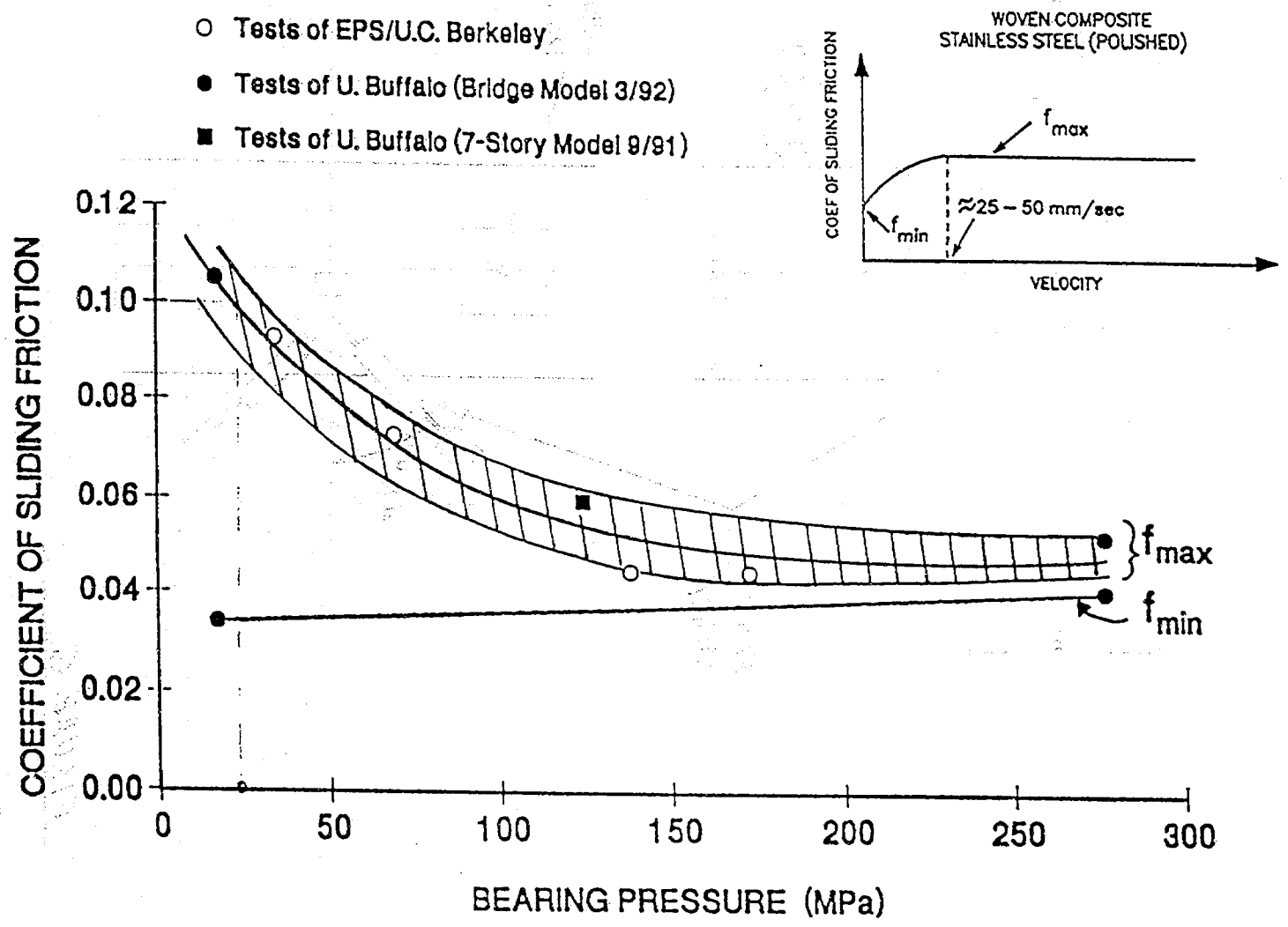
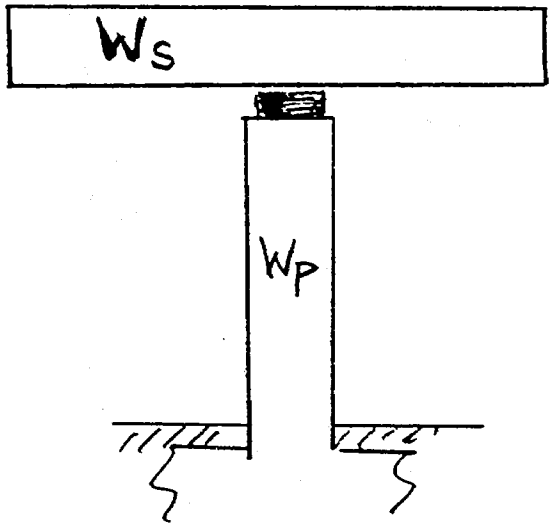
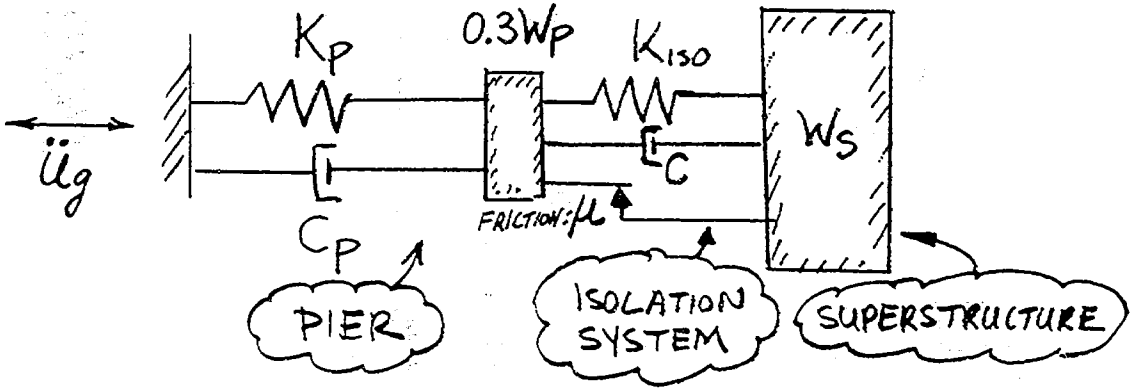


FIGURE 7

Frictional Properties of Woven Composite-Stainless Steel Sliding Interface





$$\xi_P = \frac{C_P}{2\sqrt{K_P m_P}} = 0.05$$

$$\xi_{iso} = \frac{C}{2\sqrt{K_{iso} m_S}} = 0.4$$

$$T_{PIER} = 2\pi\sqrt{\frac{0.3W_P}{g K_P}} = 0.2 \text{ secs}$$

$$T_{iso} = 2\pi\sqrt{\frac{W_S}{g K_{iso}}} = 3 \text{ secs}$$

$W_S = 8000$ kN , $m_S = W_S/g$

$W_P = 4703$ kN

$0.3W_P = 1411$ kN , $m_P = 0.3W_P/g$

$K_P = 147000$ kN/m

$K_{iso} = 3580$ kN/m

$\mu = 0.10$

FIGURE 8

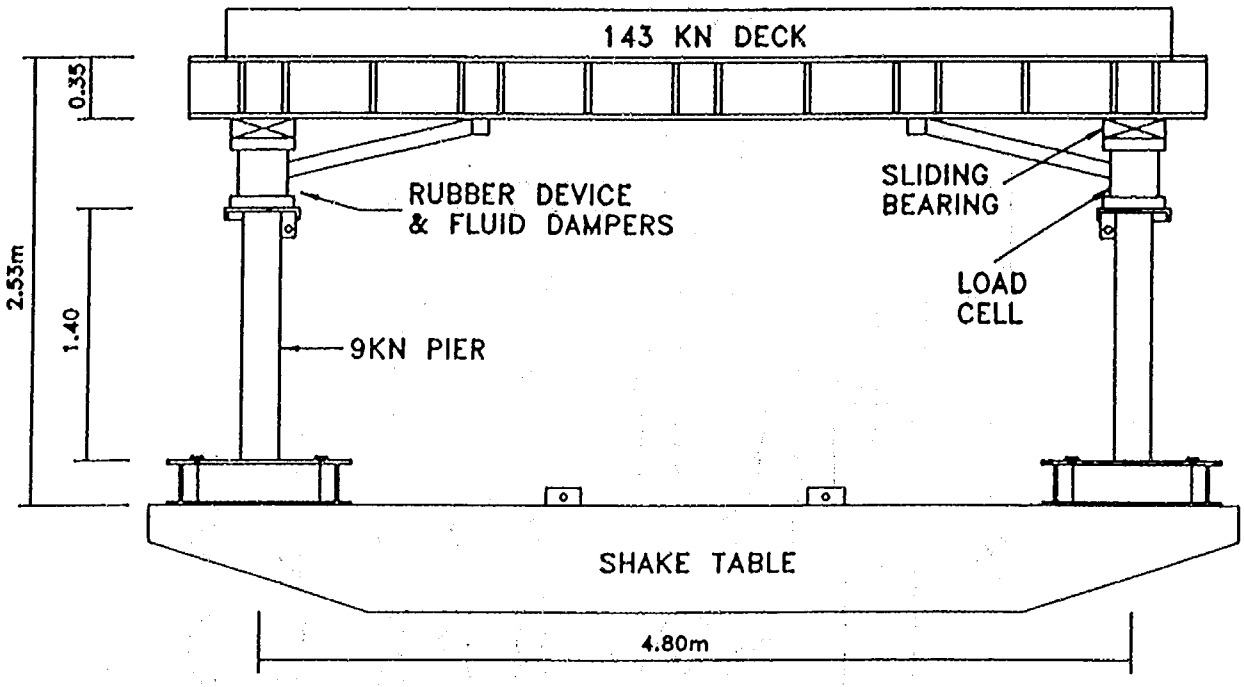
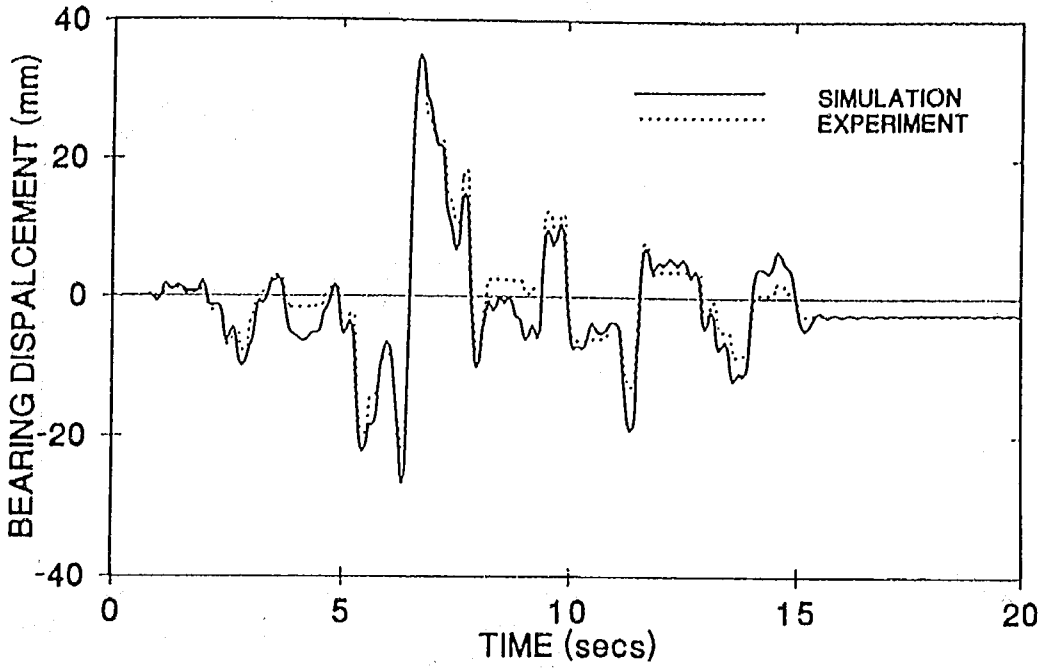

143 KN DECK
0.35
2.53m
1.40
RUBBER DEVICE
& FLUID DAMPERS
SLIDING
BEARING
LOAD
CELL
9KN PIER
SHAKE TABLE
4.80m

FIGURE 9

BRIDGE MODEL ($S_{LENGTH} = 4$), INPUT = JAPANESE LEVEL 2 G.C. 2, 75%

$\mu = 0.14$, T = 1.4secs (RUBBER DEVICE)



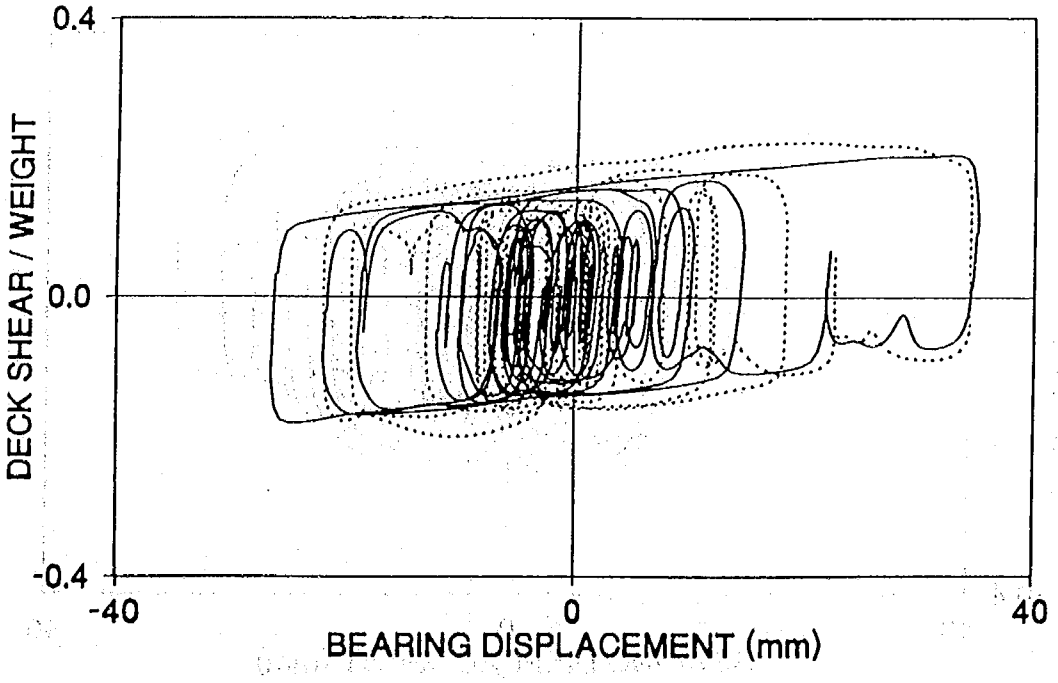
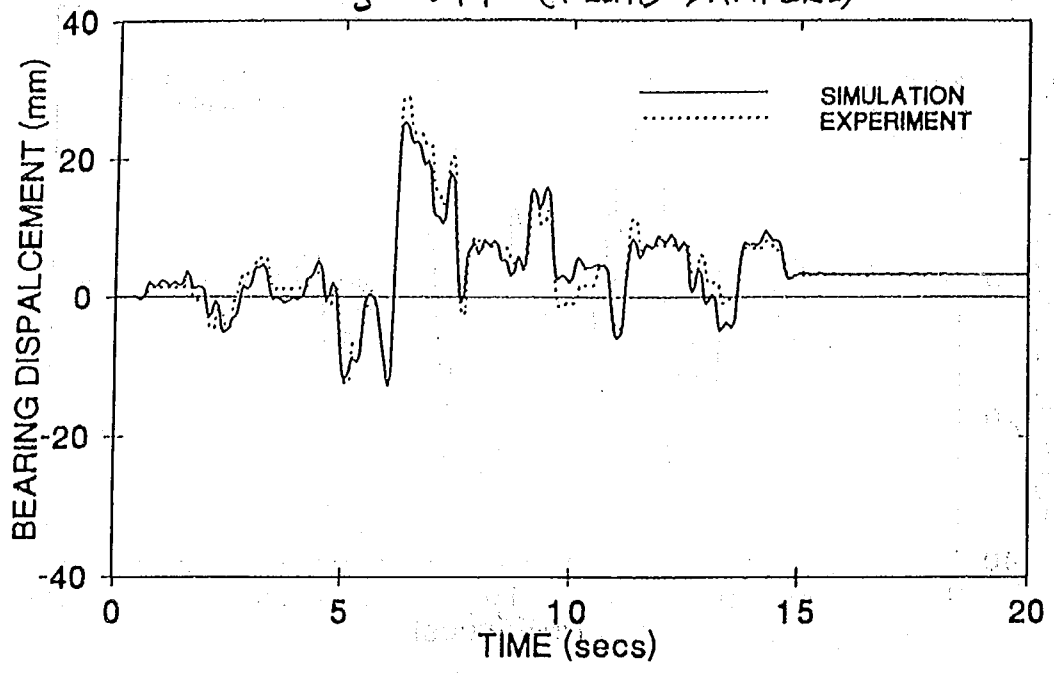


FIGURE 10

BRIDGE MODEL ($S_L = 4$), INPUT = JAP. LEVEL 2
G.C. 2, 75%
$\mu = 0.14$, $T = 1.4$ secs (RUBBER DEVICE)
$\xi = 0.47$ (FLUID DAMPERS)



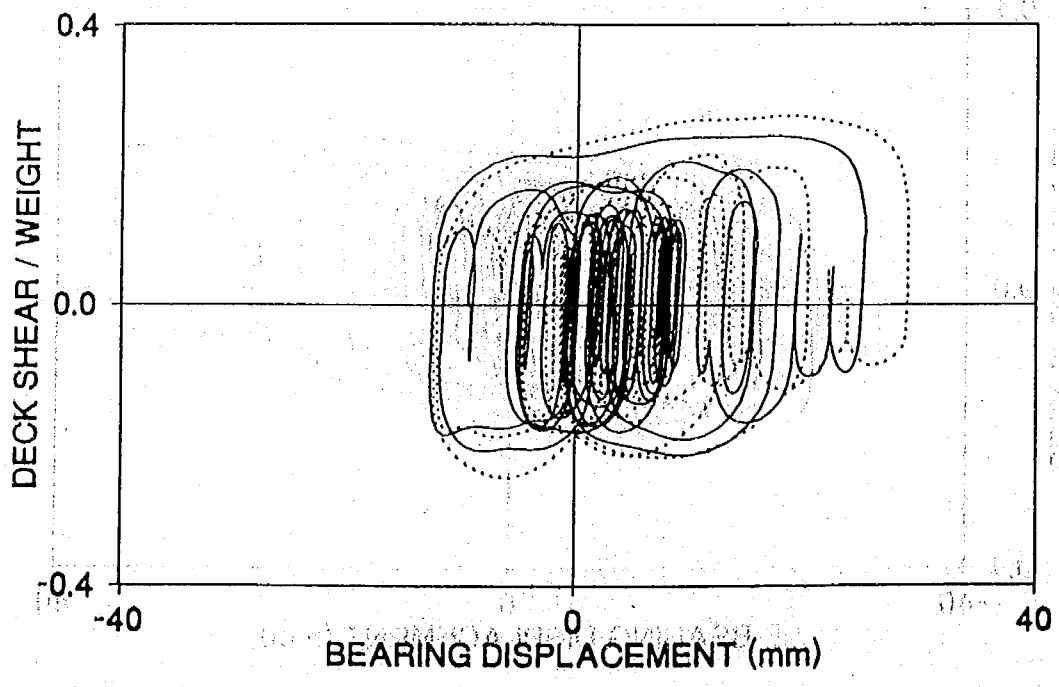
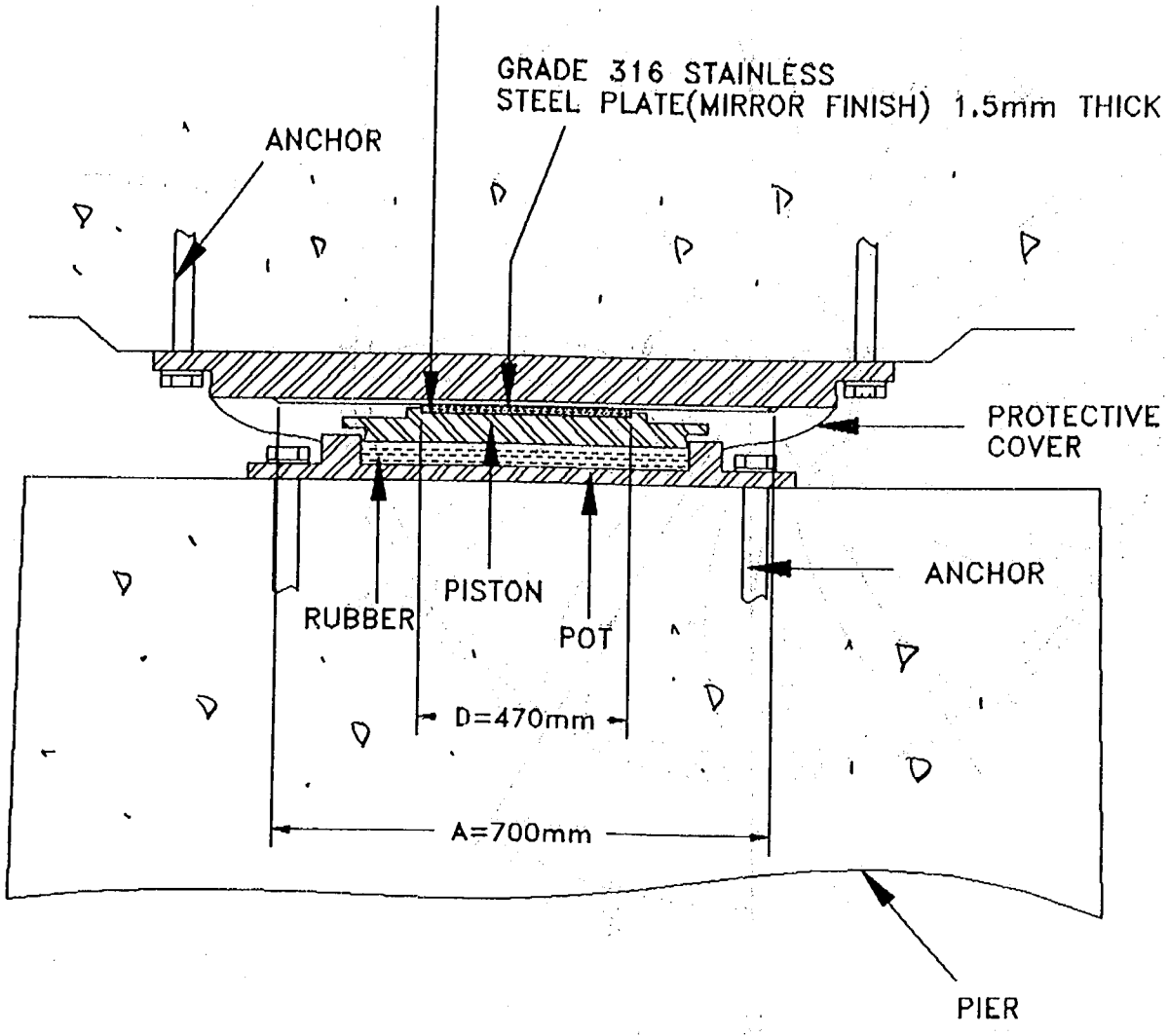


FIGURE 11

SLIDING BEARING (FOR AASHTO MOTION)

WOVEN COMPOSITE BEARING MATERIAL BONDED TO STEEL



NOTES: 1. POT MAY BE REPLACED BY SPHERICAL OR DISC SUPPORTING PART
2. A VARIETY OF MANUFACTURERS PRODUCE SLIDING BEARINGS. ANY BEARING IS ACCEPTABLE PROVIDED IT SATISFIES THE DIMENSIONAL AND MATERIAL CONSTRAINTS OF THIS DRAWING
3. PROTECTIVE COVER IS REQUIRED

FIGURE 12

RUBBER RESTORING FORCE DEVICE (FOR AASHTO MOTION)

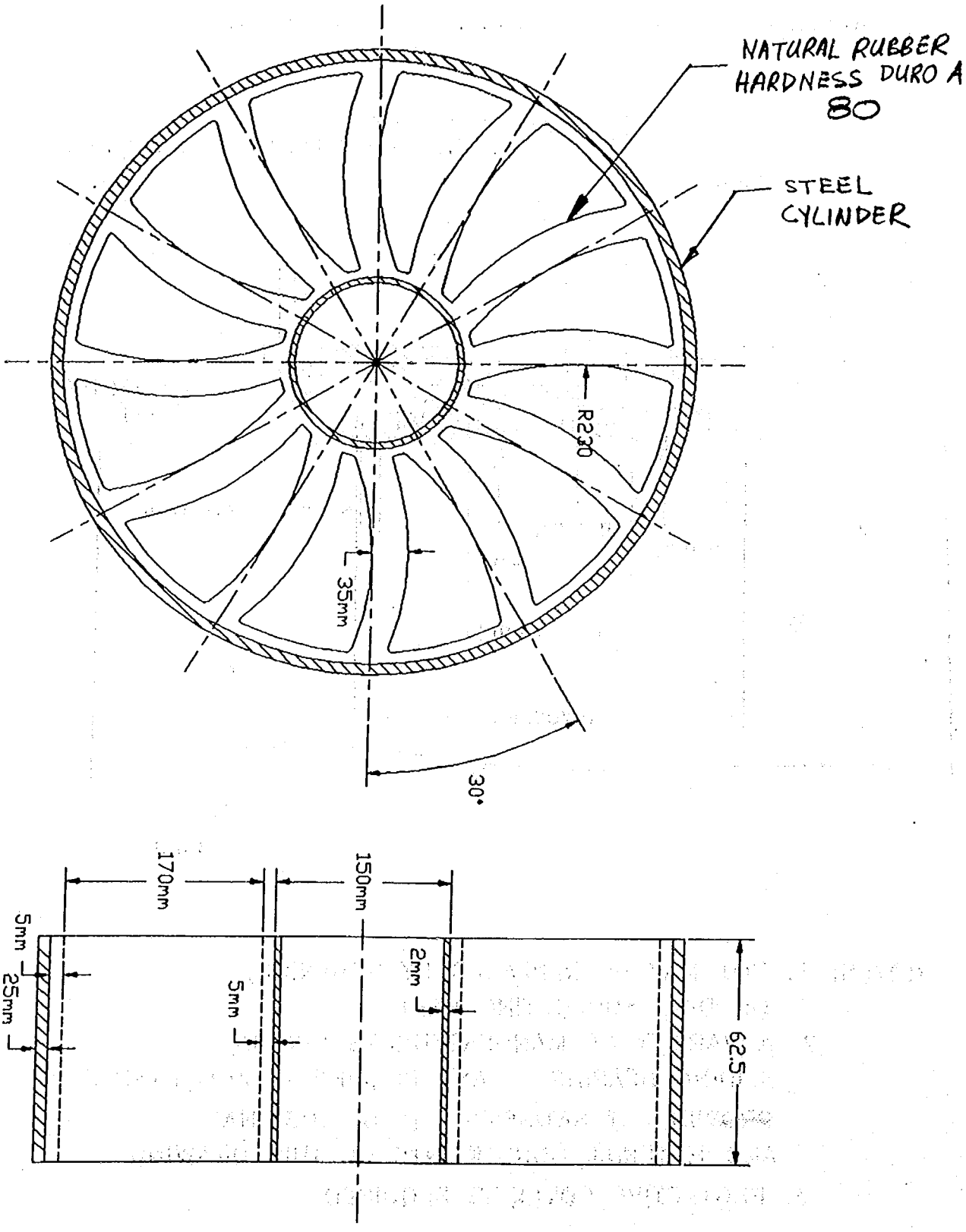
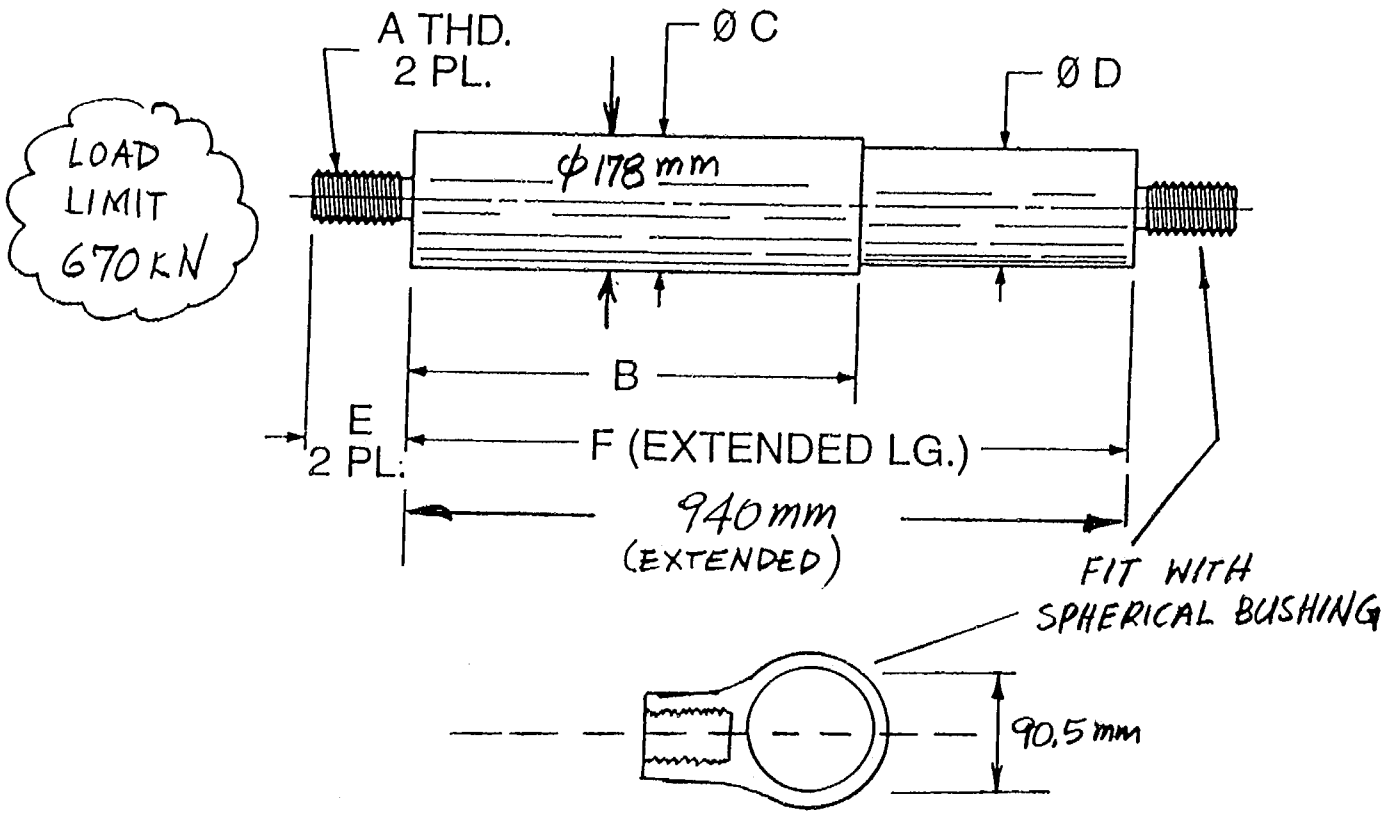


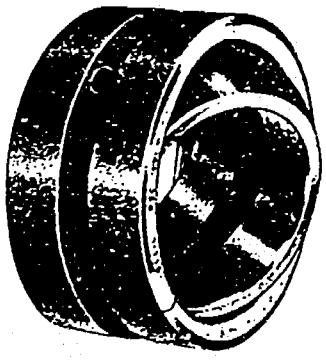
FIGURE 13

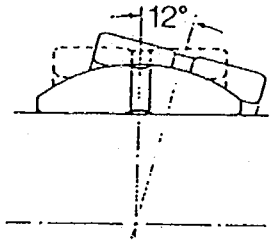
FLUID DAMPER (FOR AASHTO MOTION)



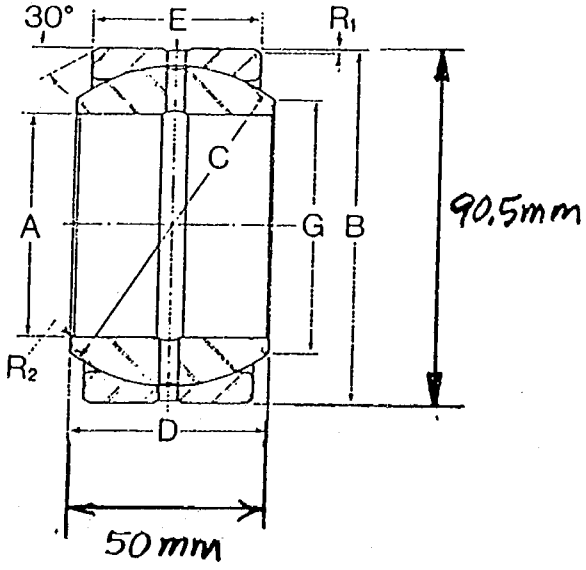
Self-Aligning Radial Bushings

Heavy Duty, Single Fractured, Self-Contained





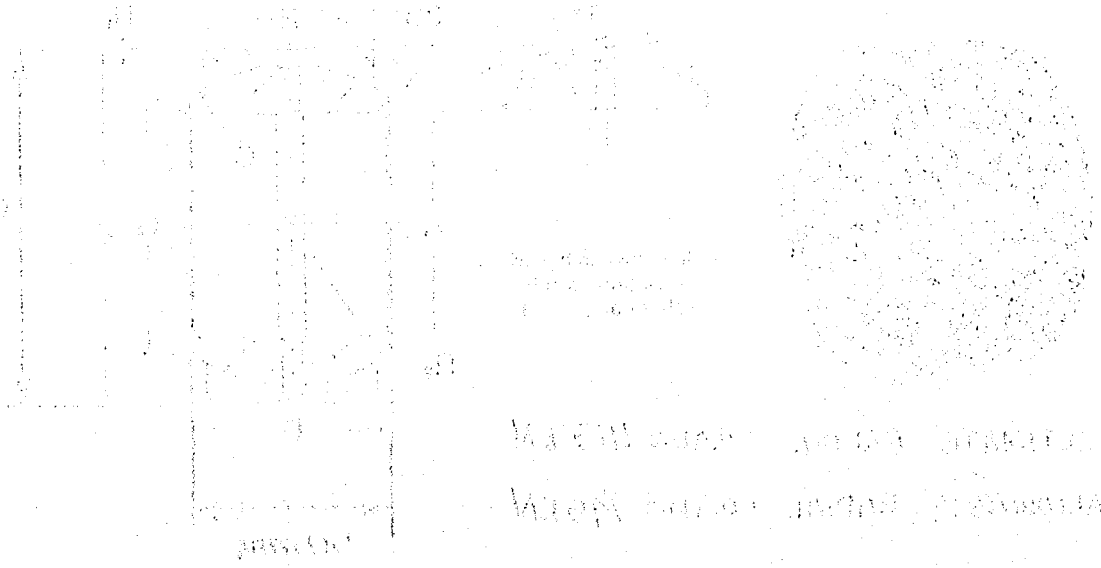
Angle shown is based on maintaining full spherical contact.



ULTIMATE RADIAL LOAD= 1115 kN

ALLOWABLE RADIAL LOAD= 745 kN

FIGURE 14



DESIGN EXAMPLE OF A HIGHWAY BRIDGE BASED ON THE MANUAL FOR MENSHIN DESIGN OF HIGHWAY BRIDGES

Kazuhiko KAWASHIMA[1], Mitsuo OKADO[2] and Michihiro HORIKAWA[3]

1) Head, Earthquake Engineering Division, Earthquake Disaster Prevention Department, Public Works research Institute, Ministry of Construction, Tsukuba, Japan
2) Assistant Manager, Design Department, New Structural Engineering Ltd., Chiyoda-ku, Tokyo
3) Chief, Design Department, New Structural Engineering Ltd., Chiyoda-ku, Tokyo

ABSTRACT

Presented is a design example of a base isolated bridge with a span length of 40 m and a clear height of 10 m. Design was made in accordance with the Manual of Menshin Design of Highway Bridges. Effect of Menshin design is discussed.

INTRODUCTION

A design was made for the same design condition with the U.S. group for comparing the seismic isolation design of bridges. Two types of Menshin devices were considered in this example calculation. First is the lead rubber bearings[1] (LRB) and the other is the high damping rubber bearing (HDR). Design was made in accordance with the Manual for Menshin Design of Highway Bridges[2] which was compiled in March 1992 as the final accomplishment of the Five Year Research Program between the Public Works Research Institute and 28 private firms on the "Development of Menshin Systems of Bridges". The design is not the detailed design but the rough estimation of approximate size and reinforcement.

DESIGN CONDITION

A bridge with multi-span continuous prestressed concrete girder with a weight of 200 kN/m (20.4 tf/m) as shown in Fig. 1 is considered. Only a single span segment is designed. The span length and the width of the superstructure are assumed as 40 m and 14 m, respectively. The girder depth is 2 m. The clear height is assumed as 10m. Soil condition is assumed as a stiff clay with N-value of the Standard Penetration Test of 30 or more. Thickness of this layer is about 60 m. Those are the design conditions specified for the common condition between U.S. and Japan. Table 1 summarizes those conditions.

Because the soil is of stiff clay with N-value of 30 or more, it may be diluvial clay layer. The soil condition is classified by the characteristics value as defined by

$$T_G = \Sigma \frac{4 H_i}{V_{si}} \qquad (1)$$

where,

T_G : characteristics value (sec)
H_i : thickness of i-th sub layer (m)
V_{Si} : shear wave velocity of i-th sub layer (m/sec)

Because the shear wave velocity of the diluvial clayey layer may be over 400 m/sec, the soil condition may be classified as the 1st group in accordance with the "Part V Seismic Design" of the "Design Specifications of Highway Bridges"[2].

The foundation type is therefore assumed as a spread foundation (direct foundation). The bearing capacity, which is the most critical in design of foundation, is assumed as 60 tf/m^2. In actual design, the detailed soil survey is required. Table 2 shows the design condition of the foundation based on the Design Specifications of Highway Bridges. Assuming that the covering depth is 1.5 m, the pier height from the surface of the footing to the pier crest is 11.5 m.

It is assumed that the bridge is located in the seismically active area. And also it is assumed that the bridge is categorized as the "important" bridge.

Then based on the Manual the design lateral force coefficient in the Seismic Coefficient Method is as[2]

$$k_h = c_Z \cdot c_G \cdot c_I \cdot c_T \cdot c_E \cdot k_{h0} \geqq 0.1 \quad (2)$$

where

$$c_T \cdot c_E \geqq 0.8 \quad (3)$$

where,

k_h : seismic coefficient in the Seismic Coefficient Method
c_Z : modification factor for zone (= 1.0, seismically active area)
c_G : modification coefficient for ground condition (= 0.8, 1st group)
c_I : modification factor for importance (= 1.0, important bridge)
c_T : modification of structural response, and shall be computed by Table 3
c_E : modification factor for damping ratio of bridge, and shall be determined by Table 4
k_{h0} : standard design lateral force coefficient for Seismic Coefficient Method(= 0.2)

In the Bearing Capacity Method, the lateral force coefficient shall be as[2]

$$k_{he} = \frac{k_{h0}}{\sqrt{2\mu - 1}} \geqq 0.3 \quad (4)$$

$$k_{h0} = c_Z \cdot c_I \cdot c_R \cdot c_E \cdot k_{h00} \quad (5)$$

where,

k_{he} : equivalent lateral force coefficient for Bearing Capacity Method
k_{h0} : lateral force coefficient in the Bearing Capacity Method

c_Z : modification factor for zone (= 1.0, seismically active area)
c_I : modification factor for importance (= 1.0 , important bridge)
c_R : modification factor for structural response, and shall be computed by Table 5
c_E : modification factor for damping ratio of bridge, and shall be obtained by Table 6
k_{hc0} : standard lateral force coefficient for Bearing Capacity Method (= 1.0)
μ : allowable ductility for reinforced concrete piers

The modification coefficients c_E, c_T and c_R have to be determined based on the natural period and damping ratio of the bridge.

Because in seismic design the bridge is critical in longitudinal (bridge axis) direction, major attention was paid in seismic design in longitudinal direction.

DESIGN OF MENSHIN DEVICES

Design Requirements

The design displacement of the Menshin device is an important parameter for designing the Menshin devices, and is defined as

$$u_B = \frac{k_h \cdot W_u}{K_B} \quad \text{(Seismic Coefficient Method)} \tag{6}$$

$$u_B = \frac{k_{hc} \cdot W_u}{K_B} \quad \text{(Bearing Capacity Method)} \tag{7}$$

where,

u_B : design displacement of Menshin device (cm)
K_B : equivalent stiffness (kgf/cm^2)
k_h : seismic coefficient in the Seismic Coefficient Method, and shall be computed by Eq. (2)
k_{hc} : lateral force coefficient in the Bearing Capacity Method, and shall be computed by Eq. (5)
W_U : weight of superstructure supported by the Menshin device (kgf)

It should be noted in Eq. (7) that the lateral force coefficient by Eq. (5) is used for design of the Menshin device. Therefore the reduction of lateral force considering the ductility of the pier is not considered for evaluating the lateral force for design of the Menshin device.

Following items are required to be checked for the Menshin devices :

(a) Check against Vertical Pressure

$$\sigma_{max} \leq \sigma_{max,a} \tag{8}$$

$$\sigma_{max} - \sigma_{min} \leqq \Delta\sigma_a \quad (9)$$

$$\sigma_{max} = R_{max} / A_{RO} \quad (10)$$

$$\sigma_{min} = R_{min} / A_R \quad (11)$$

where,

σ_{max} : maximum vertical stress (kgf/cm^2)

$\sigma_{max,a}$: allowable maximum vertical stress (= 80.0 kgf/cm^2)

σ_{min} : minimum vertical stress (kgf/cm^2)

$\Delta\sigma_a$: allowable amplitude of compression stress (= 50 kgf/cm^2)

R_{max} : maximum vertical force (dead weight + maximum active load)

R_{min} : minimum vertical force (dead weight + minimum active load)

A_R : sectional area of Menshin device (cm^2)

A_{RO} : effective sectional area of deformed Menshin device (cm^2)

(b) Check against Lateral Displacement

$$u_O \leqq \gamma_{Oa} \cdot \Sigma t_e \quad (12)$$

$$u_B \leqq \gamma_{Ba} \cdot \Sigma t_e \quad (13)$$

where,

u_O : design displacement of Menshin device against normal load such as creep, shrinkage and temperature change (cm)

γ_{Oa} : allowable shear strain of rubber against normal load (±0.7)

u_B : design displacement of Menshin device against normal load and seismic effects (cm)

γ_{Ba} : allowable shear strain of rubber against normal load and seismic effects, and shall be 1.5 in the Seismic Coefficient Method and 2.5 in the Bearing Capacity Method

Σt_e : total thickness of rubber (cm)

(c) Check against Buckling

$$\sigma_o \leqq \sigma_{cRa} \quad (14)$$

where,

σ_o : averaged vertical stress (kgf/cm^2)

σ_{cRa} : allowable vertical stress for safety against buckling (kgf/cm^2), and shall be determined as

$$\sigma_{cRa} = G \cdot S \cdot \alpha / f_S \quad (15)$$

where,

G : shear modulus of rubber (kgf/cm^2)

S : coefficient depending on shape, and shall be obtained in the square bearings as

$$S = \frac{A_R}{2(a+b)\,t_e} \quad (16)$$

A_R : sectional area of rubber (cm^2)

a , b : effective length and width of rubber (cm)

t_e : thickness of one rubber layer (cm)

$\alpha = a / \Sigma t_e$ or $b / \Sigma t_e$

Σt_e : total thickness of rubber (cm)
f_s : safety factor (= 2.5)

(d) Check against Local Shear Strain

$$(\gamma_c + \gamma_R + \gamma_s) \leqq \gamma_u / f_s \quad (17)$$

where,
γ_c : local shear strain due to vertical load
γ_R : local shear strain due to rotation of bearing
γ_s : local shear strain due to lateral displacement
γ_u : rupture strain of rubber and shall be determined by Table 7
f_s : safety factor for local shear strain, and is 2.5 for normal load and 1.8 and 1.2 for seismic design by means of the Seismic Coefficient Method and Bearing Capacity Method, respectively

(e) Check against Stress of Internal Steel Plate

$$\sigma_s \leqq \sigma_{sa} \quad (18)$$

$$\sigma_s = \sigma_c \frac{t_e}{t_s} \quad (19)$$

where,
σ_s : stress in tension of the plate (kgf/cm^2)
σ_{sa} : allowable stress of steel in tension (kgf/cm^2)
t_s : thickness of steel plate (cm)
σ_c : maximum vertical stress induced in Menshin device (kgf/cm^2)
t_e : thickness of one rubber layer (cm)

Design Requirement of LRB

In the LRB, natural rubber with the shear modulus of 8.0 kgf/cm^2 was adopted. The equivalent stiffness and the equivalent damping ratio is obtained as

$$K_B = \frac{A_R \cdot G \cdot \gamma + A_P \cdot q}{u_{Be}} \quad (20)$$

$$h_B = \frac{2 Q_d \{u_{Be} + Q_d / (K_2 - K_1)\}}{\pi u_{Be} (Q_d + u_{Be} K_2)} \quad (21)$$

where,
K_B : equivalent stiffness (kgf/cm^2)
h_B : equivalent damping ratio
u_{Be} : effective design displacement of Menshin device (cm)
Q_d : yield force of lead, and can be determined as

$$Q_d = A_P \cdot q_0 \quad (22)$$

A_p : sectional area of lead plug (cm^2)
q_0 : yielding shear stress of lead (85 kgf/cm^2)

A_R : sectional area of rubber (cm^2)
G : shear modulus of rubber (kgf/cm^2)
γ : shear strain
q : shear stress of lead, and shall be obtained as

$$q = \begin{cases} -283.6\gamma^2 + 183.8\gamma + 85.0 & (0 \leqq \gamma \leqq 0.5) \\ 28.3\gamma^2 - 128.1\gamma + 163.0 & (0.5 < \gamma \leqq 2.0) \\ 20 & (2.0 < \gamma \leqq 2.5) \end{cases} \quad (23)$$

K_1, K_2 : first and second stiffness of LRB (kgf/cm^2)

The shape of the lead plug needs to be as

$$1.25 \leqq \frac{H_P}{D_P} \leqq 5.1 \quad (24)$$

where,
H_P : height of lead plug (cm)
D_P : diameter of lead plug (cm)

Design Requirements of HDR

In the HDR, the equivalent stiffness and the equivalent damping ratio are evaluated as

$$K_B = \frac{A_R \cdot G(\gamma)}{\Sigma t_e} \quad (25)$$

$$G(\gamma) = \begin{cases} 45.3 - 72.7\gamma_e + 57.3\gamma_e^2 - 19.0\gamma_e^3 + 2.18\gamma_e^4 & (0 < \gamma e \leqq 2.0) \\ 12.2 & (2.0 < \gamma_e \leqq 3.0) \end{cases} \quad (26)$$

$$h_B = 0.154 + 0.0383\gamma_e - 0.0445\gamma_e^2 + 0.00858\gamma_e^3 \quad (0 < \gamma_e \leqq 3.0) \quad (27)$$

where,
K_B : equivalent stiffness (kgf/cm^2)
h_B : equivalent damping ratio
G : shear modulus of the high damping rubber (kgf/cm^2)
A_R : sectional area of rubber (cm^2)
γ_e : effective shear strain
Σt_e : total thickness of rubber

Design of LRB and HDR

The natural period of the Menshin bridge is recommended in the Manual to set about twice as long as the one of the bridge with usual bearing condition (non-Menshin bridge). Because the natural period of the non-Menshin bridge was estimated as 0.58 second, it was aimed to design LRB and HDR so that the natural period of the Menshin bridge becomes approximately 1.1 second. It should be noted that effect of soils was considered in computing the natural period by a set of soil springs as shown in Table 8. Because the soil is stiff, effect of soil was insensitive for the natural period.

Because the equivalent stiffness of LRB and HDR depends on the deformation developed in the device, the natural period of the bridge is not the same depending on the device and the Menshin design method. The natural period of the bridge was evaluated as 1.23 second (LRB) and 0.95 second in the Seismic Coefficient Method, and 1.91 second (LRB) and 1.44 second (HDR) in the Bearing Capacity Method. The damping ratio was evaluated as

$$h = \frac{\Sigma K_{Bi} \cdot u_{Bi}^2 \cdot c_{hi}}{\Sigma K_{Bi} \cdot u_{Bi}^2 \cdot c_i} \tag{28}$$

$$c_{hi} = h_{Bi} + \frac{h_{Pi}}{K_{Pi}} + \frac{h_{Fui}}{K_{Fui}} + \frac{h_{F\theta i} \cdot H^2}{K_{F\theta i}} \tag{29}$$

$$c_i = 1 + \frac{K_{Bi}}{K_{Pi}} + \frac{K_{Bi}}{K_{Fui}} + \frac{K_{Bi} \cdot H^2}{K_{F\theta i}} \tag{30}$$

where

h	: Modal damping ratio of bridge
h_{Bi}	: Damping ratio of i-th damper
h_{Pi}	: Damping ratio of i-th pier/abutment
h_{Fui}	: Damping ratio of i-th foundation associated with translational movement
$h_{F\theta i}$	: Damping ratio of i-th foundation associated with rotation
K_{Pi}	: Equivalent stiffness of i-th pier/abutment
K_{Fui}	: Translational stiffness of i-th foundation
$K_{F\theta i}$	: Rotational stiffness of i-th foundation
u_{Bi}	: Design displacement of i-th menshin device
H	: Height from the bottom of pier to the gravity center of deck

The damping ratio of structural components including the LRB and HDR was assumed as shown in Table 9. The damping ratio of the bridge for the first mode was evaluated by Eq. (28) as 0.21 (LRB) and 0.13 (HDR) in the Seismic Coefficient Method and 0.12 (LRB) and 0.11 (HDR) in the Bearing Capacity Method. The design displacement u_B was 3.1 cm (LRB) and 2.3 cm (HDR) in the Seismic Coefficient Method and 33.0 cm (LRB) and 18.5 cm (HDR) in the Bearing Capacity Method.

The modification factor for damping ratio of bridge c_E, which was evaluated from Tables 4 and 6 based on the above described damping ratio of the bridge, is shown in Table 10. Table 11 shows the modification factor for structural response c_T (Seismic Coefficient Method) and c_R (Bearing Capacity Method). The lateral force coefficient becomes 0.17 (LRB) and 0.18 (HDR) in the Seismic Coefficient, and 0.45 (LRB) and 0.55 (HDR) in the Bearing Capacity Method.

It should be noted that if the non-Menshin bridge has the natural period of 0.58 second, the modification factor for structural response c_T and c_R is

1.25, and that the reduction of the lateral force coefficient by means of the modification factor for damping ratio of bridge c_E can not be considered. A comparison of the lateral force coefficient between the Menshin bridge and the non-Menshin bridge is shown in Table 12. In the Menshin bridge the lateral force coefficient is 15 % (LRB) and 10 % (HDR) in the Seismic Coefficient Method and 36 % (LRB) and 21 % (HDR) in the Bearing Capacity Method less than the non-Menshin bridge.

Fig. 2 shows the LRB and HDR designed based on those conditions. Although there was some interaction between the design of Menshin device and the design of substructure which will be described later, the final shape of the devices determined is presented here. The most critical factor for determining the dimension of the Menshin devices was the check against the lateral displacement in the Bearing Capacity Method by Eq. (13). The shear strain of the rubber is 250 % and 231 % in LRB and HDR, respectively, while the allowable shear strain γ_{Ba} in Eq. (13) is 250 %.

Table 13 summarizes the design of LRB and HDR.

SEISMIC DESIGN OF SUBSTRUCTURES

Seismic Design of Pier

Seismic design of pier was made by the Seismic Coefficient Method. Fig. 3 shows the analytical model for the pier and the foundation. For designing the pier, the distance in longitudinal direction from the edge of the pier to the front edge of the bearing has to be larger than the following seat length to avoid the spalling of the concrete at the pier crest during an earthquake :

$$S = 20 + 0.5l \qquad (31)$$

where,

S : seat length from the edge of pier to the edge of bearing (cm)

l : span lengt (m)

Because the span length is 40 m, 40 cm is required for the seat length S. The seat length has to be provided both side of the bearing in longitudinal direction. Because the length of the Menshin device is 95 cm (LRB) and 89 cm (HDR), two times of the seat length S plus the length of the Menshin device is 175 cm (LRB) and 169 cm (HDR). Therefore, the depth of the pier (length in longitudinal direction) was determined as about 2 m. The width of the pier (length in transverse direction) was determined so that the stress of the concrete and that of the reinforcement become in good proportion.

The strength of the concrete is 240 kgf/cm^2, and the grade of the reinforcement is the SD 345 (deformed bars). As shown in Table 2, the allowable stress is 120 kgf/cm^2 in concrete and 3,000 kgf/cm^2 in the reinforcement.

Table 14 shows the force used for seismic design of pier and the stress computed. Because the bottom of the pier is the most critical in seismic design, the design calculation was made for this section. It can be said that the selected section is in good proportion, because the stress developed in the concrete and the reinforcement is close with their allowable stress and both the concrete and the reinforcements are effectively used.

After the dimension of the pier and the reinforcement was determined, the check of bearing capacity was made by the Bearing Capacity Method. Some increase of the depth and the reinforcement was required.

Fig. 4 shows the section thus determined. The size off the column is 2.2 m in longitudinal direction and 3 m in transverse direction. When LRB is adopted, 38 reinforcements with the diameter of 29 mm are required along the face in axial direction, and 24 reinforcements with diameter of 19 mm along the face in transverse direction are required. The total area of the reinforcements is 313.0 cm^2, and this corresponds to 0.47 % of the concrete section (main reinforcement ratio = 0.47 %). One the other hand, when HDR was adopted, the diameter of main reinforcement along the face in longitudinal direction were required to increase one grade, and 38 reinforcements with diameter of 32 mm were provided. The reinforcement along the face in transverse direction was the same with the previous case. The total area of the reinforcement is 370.6 cm^2, and the main reinforcement ratio is 0.56 %.

Seismic Design of Foundation

Design of foundation was made by the Seismic Coefficient Method. Safety against sliding, overturning and bearing capacity of supporting soil was checked. Table 15 summarizes the design of the foundation. The size of the footing is 7.5 m x 7.5 m when the LRB was adopted and 7.7 m x 7.7 m when the HDR was adopted.

CONCLUDING REMARKS

The preceding pages presented a design example of a bridge supported by LRB and HDR. By adopting the Menshin devices, 10 % ~ 15 % decrease and 21 %~ 36 % decrease of the lateral force could be made in the Seismic Coefficient Method and the Bearing Capacity Method, respectively. The bridge designed seems in good shape and reasonable.

REFERENCES

1) Robinson, W.H. : Lead-rubber Hysteretic Bearings Suitable for Protecting Structures during Earthquakes, Earthquake Engineering and Structural Dynamics, Vol. 10, 1982
2) Manual for Menshin Design of Highway Bridges, Public Works Research Institute and 28 Private Firms, Bulletin of PWRI, Vol. 59, Public Works Research Institute, March 1992
3) Japan Road Association : Design Specifications of Highway Bridges, 1990

Table 1 Design Conditions

Structure	Multi-span Continuous Prestressed Concrete Girder
Span Length	40m
Width	14m
Clear Heigth	10m
Dead Weight of Superstructure	20.4tf/m (200KN/m)
Soile Condition	N=30, Depth=60m

Table 2 Design Condition for Foundation

Allowable Stress	Steel	σ_{sa}	3,000kgf/cm^2(SD345)
	Concrete	σ_{ca}	120kgf/cm^2(σ ck=240kgf/cm^2)
Allowable Bearing Capacity q_a			60tf/m^2
Safty Factor for Sliding			1.2
Safty for Overturning			Combined force of Axial force and lateral force should be applied within 1/3 of the width of footing

Table 3 Modification Factor for Structural Response c_T

Ground Group	Structural Response Coefficient c_T		
Group I	$T < 0.1$ $c_T = 2.69T^{1/3} \geqq 1.00$	$0.1 \leqq T \leqq 1.1$ $c_T = 1.25$	$1.1 < T$ $c_T = 1.33T^{-2/3}$
Group II	$T < 0.2$ $c_T = 2.15T^{1/3} \geqq 1.00$	$0.2 \leqq T \leqq 1.3$ $c_T = 1.25$	$1.3 < T$ $c_T = 1.49T^{-2/3}$
Group III	$T < 0.34$ $c_T = 1.80T^{1/3} \geqq 1.00$	$0.34 \leqq T \leqq 1.5$ $c_T = 1.25$	$1.5 < T$ $c_T = 1.64T^{-2/3}$

Table 4 Modification Factor for Damping Ratio c_E

Damping Ratio h	Modification Factor c_E
$h < 0.1$	1.0
$h \geqq 0.1$	0.9

Table 5 Modification Factor for Structural Response c_R

Ground Group	Structural Response Coefficient c_R		
Group I	$T_{EQ} \leqq 1.4$ $c_R = 0.7$		$1.4 < T_{EQ}$ $c_R = 0.876T_{EQ}^{-2/3}$
Group II	$T_{EQ} < 0.18$ $c_R = 1.51T_{EQ}^{1/3} \geqq 0.7$	$0.18 \leqq T_{EQ} \leqq 1.6$ $c_R = 0.85$	$1.6 < T_{EQ}$ $c_R = 1.16T_{EQ}^{-2/3}$
Group III	$T_{EQ} < 0.29$ $c_R = 1.51T_{EQ}^{1/3} \geqq 0.7$	$0.29 \leqq T_{EQ} \leqq 2.0$ $c_R = 1.0$	$2.0 < T_{EQ}$ $c_R = 1.59T_{EQ}^{-2/3}$

Table 6 Modification Factor for Damping Ratio c_E

Damping Ratio h	Modification Factor c_E
$h < 0.1$	1.0
$0.1 \leqq h < 0.12$	0.9
$0.12 \leqq h < 0.15$	0.8
$0.15 \leqq h$	0.7

Table 7 Rupture Strain of Rubber

Type of Rubber	Shear Modulus $G(kgf/cm^2)$	Rupture Strain $\gamma u(\%)$
Natural Rubber	8.0	500
	10.0	500
	12.0	400
Chloroprene Rubber	8.0	400
	10.0	400

Table 8 Spring Stiffness of Soils

	LRB	HDR
Stiffness for Translation	2.88×10^5 tf/m	2.99×10^5 tf/m
Stiffness for Rotation	4.04×10^6 tf/m	4.51×10^6 tf/m

Table 9 Damping Ratio Assumed in Design for Structural Components

Superstructures			0.03
Menshin Device	SCM	LRB	0.28
		HDR	0.16
	BCM	LRB	0.15
		HDR	0.14
Pier/Columns			0.05
Footing			0.1

Table 10 Modification Factor c_E for the Bridge Designed

	LRB	HRD
SCM	0.9	0.9
BCM	0.8	0.8

Table 11 Modification Factor c_T and c_R for the Bridge Designed

	LRB	HRD
SCM	0.9	1.0
BCM	0.8	0.8

Table 12 Comparison of Lateral Force Coefficient between Menshin Bridge and Non-Menshin Bridge

Design Method	SCM		BCM	
	LRB	HDR	LRB	HDR
① Menshin Design	0.17	0.18	0.45	0.55
② Non-Menshin Design	0.20		0.7	
①／②	85 %	90 %	64 %	79 %

Table 13 Design of LRB and HDR

Characteristic Values			LRB		HDR	
			SCM	BCM	SCM	BCM
Lateral Force		k_h	0.17	0.45	0.18	0.55
Natural Period		T(s)	1.23	1.91	0.95	1.44
Design Displacement		u_B(cm)	3.1	33.0	2.3	18.5
Effective Displacement		u_{Be}(cm)	2.1	23.1	1.6	13.0
Damping Ratio		h_T	0.21	0.12	0.14	0.12
Equivalent Stiffness		K_B(tf/m)	4,775	1,132	6,403	2,374
Equivalent Damping Ratio		h_B	0.28	0.15	0.16	0.14
Lateral Force		F(tf)	105.9	261.4	144.0	448.0
Local Shear Strain	Vertical Strain	γ_c	0.24	1.09	0.60	1.62
	Lateral Strain	γ_s	0.75	2.50	0.28	2.31
	Total Strain	γ_T	0.99	3.59	0.88	3.93

Table 14 Design Force and Check of Seismic Safety of Pier

Characteristics		LRB	HDR
Force Developed at Pier Bottom	Axial Force F	1,062tf	1,062tf
	Bending Moment M	1,564tfm	1,656tfm
	Shear Force Q	136tf	144tf
Diameter of Main Reinforcement and Interval		D29@150mm	D32@150mm
Seismic Design Method	Stress of Concrete σ_c	108kgf/cm^2	106kgf/cm^2
	Stress of Reinforcement σ_s	2,838kgf/cm^2	2,643kgf/cm^2
Bearing Capacity Method	Bearing Capacity considering Ductility	186tf	219tf
	Lateral Force considering Ductility $k_{he} \cdot W$	165tf	203tf

Table 15 Design of Foundation

	LRB	HDR	Allowable Values
Bearing Capacity	54.6tf/m^2	53.2tf/m^2	60.0tf/m^2
Safety Factor for Sliding	6.8	6.6	$\geqq$ 1.2
Safety for Overturning (Eccentricity from Center of Footing)	1.23m	1.28m	$\leqq$ 2.5～2.6

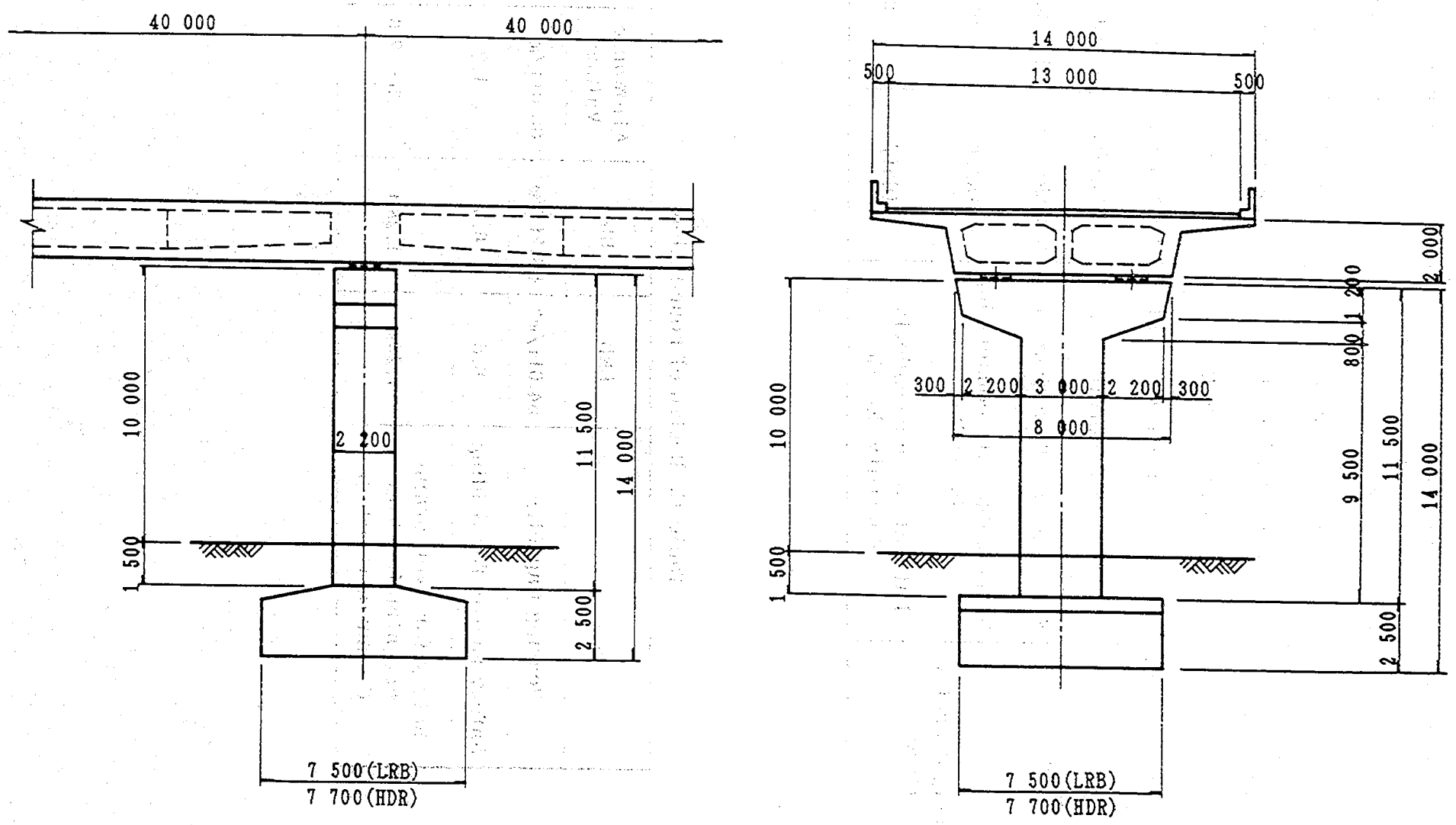
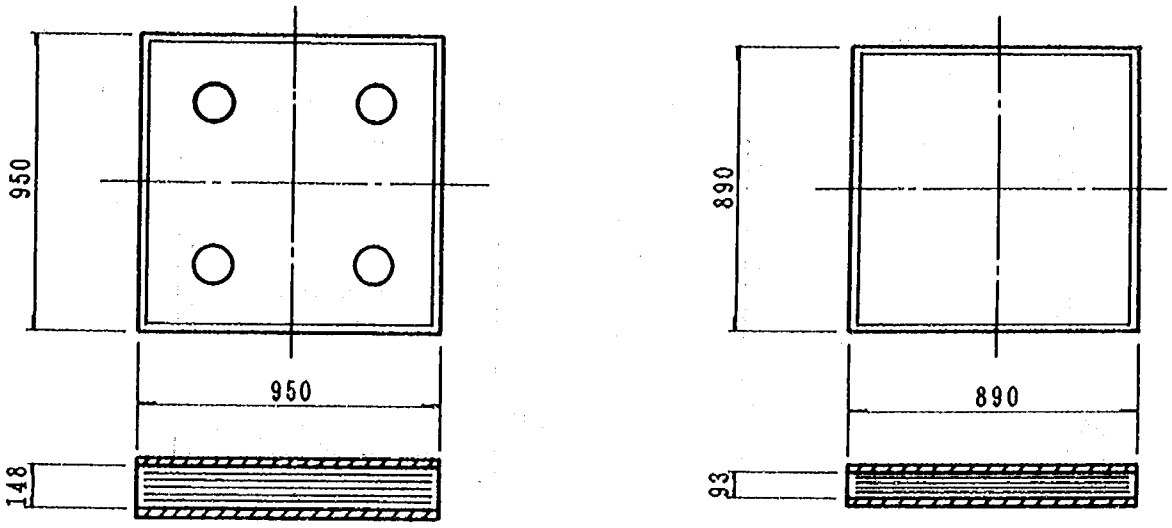


Fig.1 Bridge Considered in Design



(a) LRB (b) HDR

Fig. 2 LRB and HDR

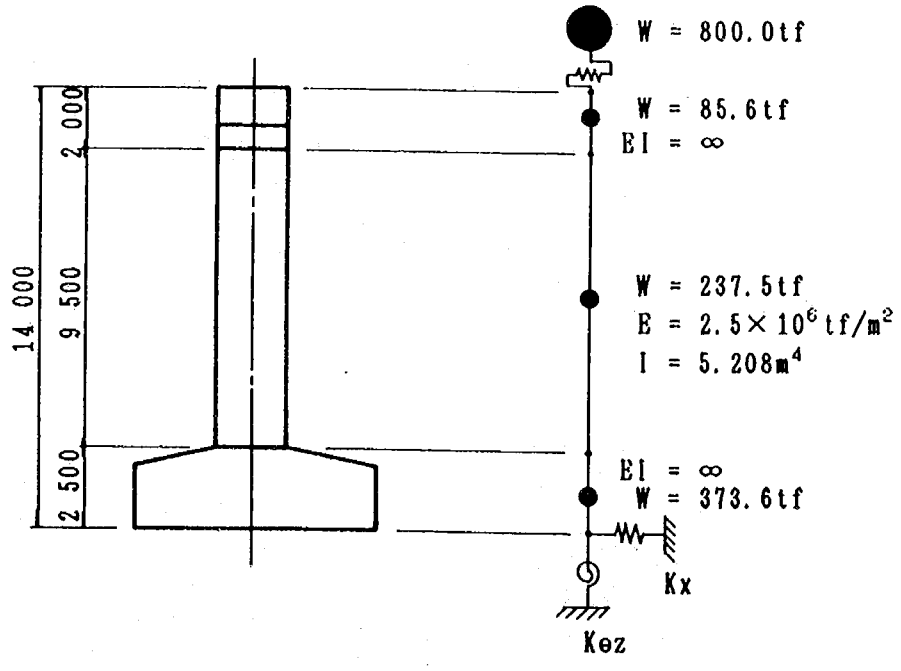


Fig. 3 Analytical Model in Design

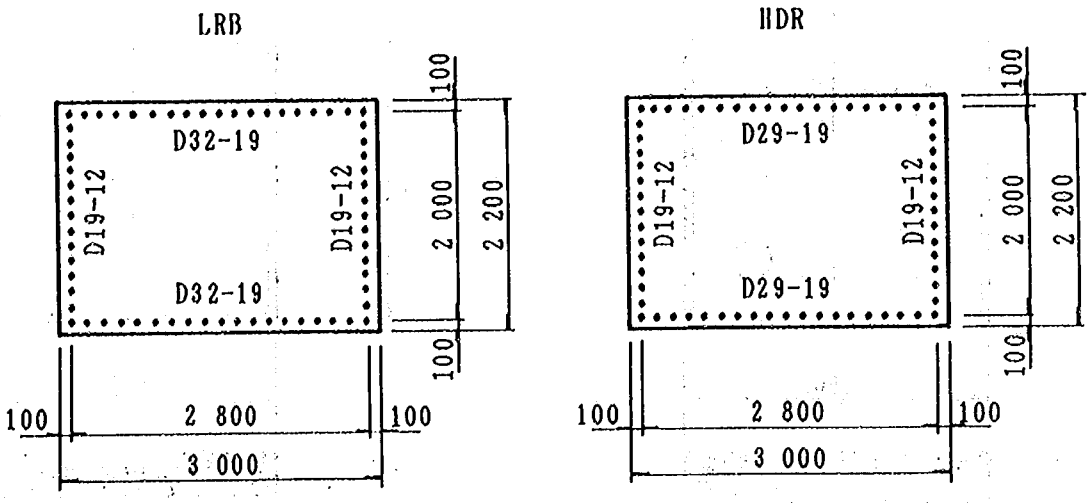


Fig. 4 Section of Pier and Main Reinforcement

Directory of Seismially Isolated Bridges in North America

Directory of Seismically Isolated Bridges in North America

BRIDGE	LOCATION	GEOMETRY	OWNER	YEAR ISOLATED	EQUIVALENT DESIGN SPECTRUM	SUPER-STRUCTURE TYPE	REMARKS
Sierra Point Overhead (Retrofit)	So. San Francisco, CA (U.S. 101 over SP Railroad, etc.)	Length = 616' Width = 117' 10 simple spans, max span 100'	Caltrans	1985	Caltrans A = 0.6g 0 - 10' alluvium	Longitudinal, steel plate girders; transverse, steel plate girder bent caps	3' diameter, 25' tall columns were protected by reducing elastic seismic forces, by a factor of 6, to levels well within their elastic capacity.
Santa Ana River Bridge (Retrofit)	Riverside, CA (10' diameter steel water pipe over Santa Ana River)	Length = 1010' 13 spans, max span 180'	MWDSC (Metro. Water Dist. of So. CA)	1986	ATC A = 0.4g Soil Profile Type II	Three 180' simple span through trusses; ten steel girder approach spans	Replacement of vulnerable steel bearings reduced elastic forces to levels within the elastic capacity of the existing concrete wall piers and certain truss members that were overstressed.
Main Yard Vehicle Access Bridge (Retrofit)	Long Beach, CA (former railroad bridge over Long Beach Freeway)	Length = 256' Width = 32' 2 equal simple spans, 58° skew	LACTC (Los Angeles County Trans. Comm.)	1987	Caltrans A = 0.5g 10 - 80' alluvium	Two 128' simple span, steel through plate girders; steel floor beams, concrete deck	Replacement of vulnerable steel bearings eliminated the potential for shear failure in the columns of the 2-column bent with in-fill wall. Forces on the tall abutments were also reduced.
Eel River Bridge (Retrofit)	Rio Dell, CA (U.S. 101 over Eel River)	Length = 606' Width = 26' 2 equal simple spans	Caltrans	1987	Caltrans A = 0.5g >150' alluvium	Two 300' steel through truss, simple spans	Replacement of vulnerable steel bearings provided protection for the non-ductile wall piers.
All-American Canal Bridge (Retrofit)	Winterhaven, Imperial County, CA (I-8 over All-American Canal)	Length = 410' Width = 41' 3 continuous spans	Caltrans	1988	Caltrans A = 0.6g >150' alluvium	Continuous, steel plate girders (replacing former steel deck trusses)	Use of isolation on the superstructure replacement eliminated the need to replace the columns and foundations or strengthen them under water.
Sexton Creek Bridge (New)	Alexander County, IL (Illinois Route 3 over Sexton Creek)	Length = 394' Width = 40' Max. span 154' Slight horizontal curvature	Illinois DOT	1990	AASHTO A = 0.2g Soil Profile Type III	3-span, continuous, steel plate girders	Overall seismic force input was reduced by a factor of 3, and the isolation design redistributed much of the lateral seismic and non-seismic forces from the wall piers and piled foundations to the abutments.

Revised, November 1992

BRIDGE	LOCATION	GEOMETRY	OWNER	YEAR ISOLATED	EQUIVALENT DESIGN SPECTRUM	SUPER-STRUCTURE TYPE	REMARKS
Toll Plaza Road Bridge (New)	Montgomery County, PA (Approach to toll plaza over Hwy. LR145)	Length = 176' Width varies, 150' to 210' Single span	Pennsylvania Turnpike Commission	1990	AASHTO A = 0.1g Soil Profile Type II	176' simple span, composite steel plate girder	Some overall seismic benefit, plus transverse thermal capability of isolation bearings on such a very wide bridge was an important consideration.
Lacey V. Murrow Bridge West Approach (Retrofit)	Seattle, WA (Approach to original Lake Washington Floating Bridge)	Length = 1128' 8 spans	Washington State DOT	1991	AASHTO A = 0.25g Soil Profile Type II	3-span, continuous, concrete, box girders; 3-span, continuous deck trusses; simple span, tied arch (similar tied arch span at east end also retrofitted)	Seismic isolation saved the existing piers and foundations, thus avoiding the need to replace the whole structure.
Deas Slough Bridge (Retrofit)	Richmond, British Columbia (Hwy. 99 over Deas Slough)	Length = 320' Width = 58' 3 spans, max. span 140' 38° skew	British Columbia Ministry of Trans. and Hwys.	1990	AASHTO A = 0.2g Soil Profile Type III	3-span continuous, riveted, haunched, steel plate girders	An isolation design focusing on redistribution of lateral forces away from the fixed pier made it possible to accomplish seismic upgrade by replacing the bearings.
Cache River Bridge (Retrofit)	Alexander County, IL (Illinois Rte. 3 over Cache River Diversion Channel)	Length = 280' 3 spans, max. span 108' 21° skew	Illinois DOT	1991	AASHTO A = 0.2g Soil Profile Type III	3-span, continuous, steel plate girders	Seismic isolation/force redistribution design enabled re-use of the existing pier in this superstructure replacement project.
Wabash River Bridge (New)	Terra Haute, Vigo County, IN (US 40 over Wabash River)	Dual Structures Length = 880' Width = 41' 7 spans, max. span 150'	Indiana DOT	1991	AASHTO A = 0.1g Soil Profile Type II	7-span, continuous, steel plate girders	Isolation design maximized seismic protection at least cost for the hammerhead wall piers and piled foundations.
SB I-170/EB I-70 Bridge (New)	St. Louis, MO (Metrolink Light Rail over SB I-170/EB I-70)	Dual Structures (one per track) Length = 910' Width = 12' per track 7 spans, max. span 196' Partially curved	Bi-State Development Agency	1991	AASHTO A = 0.1g Soil Profile Type I	Span 1: 120' simple span, steel box girder; Spans 2-4: 280', 3-span, continuous, haunched, concrete box girder; Spans 5-7: 510', 3-span, continuous, curved, steel box girder	Isolation design facilitated distribution of longitudinal forces among the substructures for optimum economy while providing some seismic benefit.

Revised, November 1992

BRIDGE	LOCATION	GEOMETRY	OWNER	YEAR ISOLATED	EQUIVALENT DESIGN SPECTRUM	SUPER-STRUCTURE TYPE	REMARKS
East Campus Drive Bridge (New)	St. Louis, MO (Metrolink Light Rail over East Campus Drive)	Dual Structures (one per track) Length = 417' 4 spans, max. span 114' Slight horizontal curvature	Bi-State Development Agency	1991	AASHTO A = 0.1g Soil Profile Type I	4-span, continuous, haunched, concrete box girder	(See SB I-170/EB I-70)
UMSL Garage Bridge (New)	St. Louis, MO (Metrolink Light Rail over access to UMSL Garage)	Dual Structures (one per track) Length = 286' 3 spans, max. span 100'	Bi-State Development Agency	1991	AASHTO A = 0.1g Soil Profile Type I	3-span, continuous, haunched, concrete box girder	(See SB I-170/EB I-70)
Geiger Road Bridge (New)	St. Louis, MO (Metrolink Light Rail over Geiger Road)	Dual Structures (one per track) Length = 832' 8 spans, max. span 115'	Bi-State Development Agency	1991	AASHTO A = 0.1g Soil Profile Type I	Equal, continuous units; one tangent, one curved; each 416' long, 4-span, haunched, concrete box girder	(See SB I-170/EB I-70)
Springdale Bridge (New)	St. Louis, MO (Metrolink Light Rail over Springdale Road)	Dual Structures (one per track) Length = 221' 3 spans, max. span 85' 31° skew	Bi-State Development Agency	1991	AASHTO A = 0.1g Soil Profile Type I	3-span, continuous, haunched, concrete box girder	(See SB I-170/EB I-70)
Ramp 26 Bridge (New)	St. Louis, MO (Metrolink Light Rail over Ramp 26)	Dual Structures (one per track) Length = 292' 4 spans, max. span 81' 50° skew	Bi-State Development Agency	1991	AASHTO A = 0.1g Soil Profile Type I	4-span, continuous, haunched, concrete box girder	(See SB I-170/EB I-70)
NB I-170 Bridge (New)	St. Louis, MO (Metrolink Light Rail over NB I-170)	Dual Structures (one per track) Length = 288' 4 spans, max. span = 114'	Bi-State Development Agency	1991	AASHTO A = 0.1g Soil Profile Type I	2-span, continuous, steel box girder flanked by short, simple span, steel box girders	(See SB I-170/EB I-70)
West Street Overpass (Retrofit)	Harrison, Westchester County, NY (West St. over I-95 New England Thruway)	Length = 172' Width = 33' 4 spans, max. span 54.5'	New York State Thruway Authority	1991	AASHTO A = 0.19g Soil Profile Type III	Four simple-span, steel beam structures	Replaced vulnerable steel bearings in two center spans over Thruway traffic lanes to prevent collapse and relieve forces on center pier.

Revised, November 1992

BRIDGE	LOCATION	GEOMETRY	OWNER	YEAR ISOLATED	EQUIVALENT DESIGN SPECTRUM	SUPER-STRUCTURE TYPE	REMARKS
Route 161 Bridge (New)	St. Clair County, IL (Illinois Rte. 161 over Dutch Hollow Road, CSX Railroad and Schoenberger Creek)	Dual Structures Length = 356' Width = 46' 4 spans, max. span 96' 26° skew	Illinois DOT	1991	AASHTO A = 0.14g Soil Profile Type III	4-span, continuous, steel plate girder	Isolation reduced overall seismic force input and mitigated disparity in pier stiffnesses by redistributing lateral forces.
Pequannock River Bridge (New)	Morris and Passaic Counties, NJ (I-287 over Pequannock River, Paterson-Hamburg Turnpike, and NY Susquehanna & Western Railroad)	Dual Structures Length = 854' Width = 63' 8 spans, max. span 123' Slight horizontal curvature	New Jersey DOT	1991	AASHTO A = 0.12g Soil Profile Type II	Three continuous, steel plate girder units of 2, 3, and 3 spans	Isolation design reduced overall seismic force input and mitigated disparity in pier stiffnesses by redistributing lateral forces.
I-80 Bridges B764E & W (Retrofit)	Verdi, Washoe County, NV (I-80 over Truckee River and a local roadway)	Dual Structures Length = 443' Width = 43' 6 spans, max. span 101' Slight horizontal curvature	Nevada DOT	1992	AASHTO A = 0.37g Soil Profile Type I	Simple span, composite steel plate girders or rolled beams	Isolation and force redistribution design reduced seismic forces to within the elastic capacity of the 3 column bents and mitigated the disparity in pier stiffnesses. Simple spans were tied together to make superstructure respond as a diaphragm.
Squamscott River Bridge (New)	Exeter, NH (Relocated NH Rte 101 over Squamscott River)	Length = 874' Width = 52' 6 spans, max. span 156'	New Hampshire DOT	1992	AASHTO A = 0.15g Soil Profile Type III	6-span, continuous, steel plate girders	Isolation and force redistribution design resulted in a net savings of $160,000.00 (4%) in the overall cost of the bridge due to reduction in the size of the "fixed" pier and the number of piles.
Blackstone River Bridge (New)	Woonsocket, RI (Woonsocket Industrial Hwy. over Blackstone River, Providence & Worcester Railroad, and local roads)	Length = 1000' Width = 86' 4 spans, max. span 280'	Rhode Island DOT	1992	AASHTO A = 0.1g Soil Profile Type II	4-span, continuous composite steel plate girders	Isolation design reduced overall seismic force input and mitigated disparity in pier stiffnesses.

Revised, November 1992

BRIDGE	LOCATION	GEOMETRY	OWNER	YEAR ISOLATED	EQUIVALENT DESIGN SPECTRUM	SUPER-STRUCTURE TYPE	REMARKS
Olympic Blvd. Separation (New)	Walnut Creek, CA (SB I-680 Flyover Ramp over Olympic Blvd.)	Length = 700' Width = 32' 4 spans, max. span 210' Curved	Caltrans	1992	Caltrans A = 0.6g 10 - 80 ft. alluvium	4-span, continuous, steel plate girders	Isolation design enabled elastic design of the single column hammerhead piers and saved 38% in the cost of the foundations.
Carlson Blvd. Bridge (New)	Richmond, CA (part of 23rd St. Grade Separation Project)	Length = 153' Width = varies 49'-57' Single span, 45° skew	City of Richmond, CA	1992	Caltrans A = 0.7g 80 - 150 ft. alluvium	Simple span, multi-cell concrete box girder	Isolation design reduced the elastic force coefficient to 0.45 (factor of 3 from peak), a design advantage for the wall abutments.
Clackamas Connector (New)	Milwaukie, OR (part of Tacoma St. Interchange)	Length = 1005' Width = 36' 8 spans, max. span 135' 12.5° Horizontal curve through 80° central angle	Oregon DOT	1992	AASHTO A = 0.29g Soil Profile Type III	8-span, continuous, post-tensioned concrete, trapezoidal box girder	Isolation design resulted in a net savings of $400,000 (12%) due to reduction in foundation size and will protect the tapered single column bents from damage in an earthquake.
Cedar River Bridge (New)	Renton, WA (I-405 over Cedar River and BN Railroad)	Dual Structures Length = 521' Width varies 72' to 86' 4 spans, max. span 196' Horizontal curve	Washington State DOT	1992	AASHTO A = 0.25g Soil Profile Type II	4-span, continuous, steel plate girders	Isolation used for initial economy and assurance of serviceability after an earthquake.
Poplar St. East Approach Bridge #082-0005 (Retrofit)	East St. Louis, IL (carrying I-55/70/64 over railroad yard to Poplar St. Bridge across Mississippi River	Length = 856' Width varies 112' to 165' 6 spans, max. span 161'	Illinois DOT	1992	AASHTO A = 0.12g Soil Profile Type III	Two dual, steel plate girder units (5-span, continuous, and 1 simple, span); supported on multi-column or wall piers; piled foundations	Isolation as a seismic upgrade was implemented by change order to an existing rehabilitation contract.
Dog River Bridge (New)	Mobile County, AL	Dual Structures Length = 462' Width = 37' 3 spans, max. span 180'	Alabama Highway Dept.	1992	AASHTO Category A	3-span, continuous, steel plate girders	Isolation avoided extra restraints to meet 0.2g Category A requirement and satisfied owner's quest for a multi-directional, maintenance free device.
US 51 over Minor Slough (New)	Ballard County, KY	Length = 371' Width = 47' 3 equal spans, 45° skew	Kentucky Transportation Cabinet	1992	AASHTO A = 0.25g Soil Profile Type II	Three 121' simple span, prestressed concrete I-girders with continuous deck	Seismic forces were reduced by a factor of 3.5 and then redistributed to minimize the forces on the piers.

Revised, November 1992

BRIDGE	LOCATION	GEOMETRY	OWNER	YEAR ISOLATED	EQUIVALENT DESIGN SPECTRUM	SUPER-STRUCTURE TYPE	REMARKS
Relocated NH Rte 85 over NH Rte 101 (New)	Towns of Exeter-Stratham, Rockingham County, NH	Length = 170' Width = 76' 2 equal spans, 16° skew	New Hampshire DOT	1992	AASHTO A = 0.15g Soil Profile Type I	2-span, continuous, steel plate girders	Seismic forces were reduced by a factor of 4.5 and then redistributed to further reduce the forces on the 34' high wall abutments.
Ompompanoosuc River Bridge (Retrofit)	Rte 5, Norwich, VT	Length = 251' Width = 31' 3 equal spans, 45° skew	Vermont Agency of Transportation	1992	AASHTO A = 0.10g Soil Profile Type III	3-span, continuous, steel plate girders	Seismic forces were reduced by a factor of 2.5 and then redistributed to minimize the forces on the piers.
Providence Viaduct (Retrofit)	Rte I-95, Providence, RI	Dual structures Length = 1290' Width = 45' 8 spans, max. span 210'	Rhode Island DOT	1992	AASHTO A = 0.32g Soil Profile Type III	Two steel plate girder, simple spans and Two 3-span, continuous, haunched, steel plate girder units	Two-level criteria calling for serviceability after an A = 0.16g event and no collapse in an A = 0.32g event. Isolation was the cost-effective solution, and the viaduct will remain in service after the higher level event.

Resolutions

RESOLUTIONS

Background

The second U.S.–Japan Workshop on Earthquake Protective Systems for Bridges was held in Tsukuba, Japan on December 7 and 8, 1992 under the auspices of Task Committee G on "Passive, Active and Hybrid Control Systems" of the UJNR Panel on Wind and Seismic Effects with the cooperation of Task Committee J "Wind and Earthquake Engineering for Transportation Systems". The workshop was attended by 13 U.S. and 93 Japanese participants. In addition, one participant from New Zealand also attended. U.S. sponsorship for the meeting was provided by the National Science Foundation and the National Center for Earthquake Engineering Research (NCEER) which is headquartered on the campus of the State University of New York at Buffalo. The organizer and sponsor for the Japan–side was the Public Works Research Institute (PWRI) of the Ministry of Construction.

This comprehensive workshop comprised the presentation and discussion of 10 U.S., 1 New Zealand, 22 Japanese papers which covered a wide range of topics including seismic isolation hardware, the testing of isolated bridges and components, active control and hybrid systems, design issues and applications, long span bridges, seismic retrofit and new construction. Fruitful discussion on many issues of common concern took place. Of continuing interest was the difference in philosophy between menshin design in Japan and seismic isolation as practiced in the United States. The need to lengthen the period of vibration is not so important (in Japan) as is the requirement to keep joint clearances small. Other issues included joint design, displacement restraint devices, and durability of isolation hardware in the field.

In conjunction with the workshop, a Study Tour of seismic isolated bridges in Japan was undertaken by the United States participants. The purpose was to obtain first–hand knowledge about Japanese practice concerning the use of seismic isolation for seismic retrofit and the construction of new bridges.

Resolutions

1. There are many topics of common interest related to the development and implementation of these earthquake protective systems. It is therefore resolved that continued cooperation between researchers and bridge engineers in both countries be actively encouraged. The free exchange of research and design experience, in both the laboratory and field, will facilitate the advancement of this technology and its practical implementation in both countries.

2. In view of the success of this workshop, the importance of this technology and the rapidly advancing state-of-the-art, it is resolved that a third U.S.-Japan Workshop on Earthquake Protective Systems for Bridges be held in United States in late 1993 or early 1994.

3. It is further resolved that the third workshop be oriented towards research and application rather than state-of-the-art reviews. Topics to be covered should include: (1)innovative protective systems; (2)design methods for seismic isolated/menshin bridges; (3)full-scale verification of performance; (4)comparative design examples. As passive protective systems have begun to be implemented in both countries, increased emphasis on active and hybrid systems and on the use of smart and high-performance structural materials and systems will be made in this workshop.

Appendices

THE 2ND U.S.-JAPAN WORKSHOP ON EARTHQUAKE PROTECTIVE SYSTEMS FOR BRIDGES

DECEMBER 7 AND 8, 1992

PUBLIC WORKS RESEARCH INSTITUTE, TSUKUBA, JAPAN

WORKSHOP PROGRAM

December 7 (MON)

8:10 Leave Hotel Sunroute Tsukuba

8:30 Registration

9:00 **Opening Session**

(Chairmen : Unjoh, S. and Shinozuka, M.)

Addressed by Mr. Sumiyoshi, Y., Assistant Director-General, Public Works Research Institute

Addressed by Dr. Liu, S. C., Program Director, National Science Foundation

Addressed by Dr. Kawashima, K., Head, Earthquake Engineering Division, Public Works Research Institute

Addressed by Dr. Buckle, I. G., Deputy Director, National Center for Earthquake Engineering Research

---

9:30 **Session-1 Testing of Seismic Isolation Hardware-1**

(Chairmen : Toki, K. and Abdel-Ghaffar, A. M.)

J-1) Approving Test Procedure for Menshin Devices
(Kawashima, K., Makiguchi, Y., Suizu, Y. and Endo, K.)

U-1) Mechanical Characteristics of Elastomeric Seismic Isolation Bearings
(Aiken, I. D., Clark, P. W., Kelly, J. M.)

J-2) Approving Test Results on Four High Damping Rubber Bearings
(Kawashima, K. Endo, K., Doro, N., Sudoh, C. and Nishikawa, I.)

10:30 Break

10:50 **Session-2 Testing of Seismic Isolation Hardware-2**

(Chairmen : Iwasaki, T. and Robinson, W. H.)

J-3) Hybrid Earthquake Loading Tests of Various Types of Base Isolation Bearings
(Iemura, H., Yamada, Y., Tanzo, W. and Nanjo, A.)

U-2) Seismic Response Variability of Bridges on Friction-Controllable Isolators
(Feng, M. Q.)

J-4) Shake Table Test of A Model Bridge with Sliding Isolation System
(Okamoto, S., Constantinou, M. C., Tsopelas, P. C., Fujii, S. and Ozaki, D.)

11:50 Lunch

12:30 Japanese Cultural Exhibition (Flower Arrangement beside the 8th Floor Conference Room)

13:00 **Session-3 Testing of Seismic Isolation Hardware-3**

(Chairmen : Kuribayashi, E. and Aiken, I. D.)

J-5) Evaluation of Shear Modulus of High Damping Rubber Bearings and Lead Rubber Bearing during Low-Rate Load Reversals
(Kawashima, K., Koshitoge, M., Sudo, C., Makiguchi, Y. and Endo, K.)

J-6) Loading Facilities for Menshin Devices
(Makiguchi, Y., Endo, K., Kawai, N., Suizu, Y., and Nishikawa, I.)

J-7) Temperature-Dependency of Base-Isolated Bearings
(Nakano, O., Nishi, H., Shirono, T. and Kumagai, K.)

J-8) Load Durability Test for Highway Bridge Rubber Bearing Pads
(Matsuda, T., Maeda, Y. and Murayama, A.)

14:20 Break

14:50 **Session-4 Seismic Isolation Design-1**
(Chairmen : Iemura, H. and Nagarajaiah, S.)

NZ-1) Seismic Isolation of Bridges in New Zealand
(Robinson, W. H.)

J-9) Manual for Menshin Design of Highway Bridges
(Kawashima, K.)

U-3) Application of AASHTO Seismic Isolation Design and Analysis Requirements to Bridges
(Mayes, R. L.)

15:50 Break

16:10 **Session-5 Seismic Isolation Design-2**
(Chairmen : Tokida, K. and Mayes, R. L.)

U-4) Stability of Elastomeric Base Isolators
(Buckle, I. G. and Liu, H.)

J-10) Development of Expansion Joint, Stopper and Knock-off Abutment for Menshin Bridges
(Goto, Y., Kikuchi, T., Kimishima, A., Matsumoto, S., Ozaki, D. and Tsukamoto, A.)

U-5) Development and Applications of Simple Analytical Models of Lead Rubber Base Isolated Bridges
(Maragakis, E. and Saiidi, M.)

J-11) Design of 9-Span Continuous Prestressed Concrete Girder Bridge with Base Isolators
(Kubota, N., Shikauchi, S., Osaki, H., Mitake, Y. and Arai, H.)

17:30 Adjourn
17:50 Leave PWRI
18:05 Arrive Hotel Sunroute

19:00 Reception Hosted by Director-General, PWRI
(Hou-oh Room on the 2nd Floor at Hotel Sunroute)

December 8 (TUE)

8:30 Leave Hotel Sunroute Tsukuba and Hotel Ground Shinonome

9:00 **Session-6 Design Applications-1**
(Chairmen : Fujiwara, M. and Cooper, J.)
U-6) Simplified Preliminary Design Approach for Base-Isolated Bridges
(Mahin, S. A.)
J-12) Preliminary Analysis of the Effects of Spatially Correlated Input Motions on the Response of Multiple-Span Continuous Bridges
(Tokida, K., Tamura, K. and Fukada, H.)
U-7) Recent Developments in Seismic Isolation at CALTRANS
(Yashinsky, M.)
J-13) Seismic Design of the Trans-Tokyo Bay Highway Bridges
(Shioi, Y., Yoshida, O. and Honma, M.)

10:20 Break

10:35 **Session-7 Design Applications-2**
(Chairmen : Iida, Y. and Maragakis, E. M.)
J-14) Menshin Design and Construction of Multi-Span Continuous Prestressed Concrete Bridge
(Uzuka, T., Kawakami, K. and Kumakura, K. and Tani, H.)
U-8) Two Shake Table Experimental Studies of the Effectiveness of Damping-Augmentation Devices in Cable-Stayed Bridges
(Abdel-Ghaffar, A., Masri, S. F. and Ali, H.)
J-15) Improvement of Earthquake Resistance of Prestressed Concrete Cable-Stayed Bridges by Hysteresis Damper
(Ichinomiya, T., Takeda, T. and Kanda, K.)
J-16) Development of Jointless System with Menshin Bearing for Existing Simple-Spanned Steel Bridges
(Naganuma, T., Mizobuchi, S. and Uno, H)

11:55 Memorial Group Photo
12:00 Lunch

13:00 **Session-8 Dynamic Characteristics of Base-Isolated Bridges**
(Chairmen : Sato, T. and Yashinsky, M.)
J-17) Vibration Tests of A Menshin Designed Prestressed Concrete Bridge
(Goto, Y., Kikuchi, T., Ina, Y. and Sakakibara, N.)
J-18) Report on Vibration Experiments for an Actual Steel Bridge Supported with Menshin-Type Bearings
(Komatsu, I., Yasuda, F. and Nishibayashi, M.)
J-19) Response Analysis of Miyagawa Bridge Based on A Measured Accelerations Record
(Kawashima, K., Nagashima, H., Masumoto, and Hara, K.)

14:00 Break

14:10 **Session-9 Active and Hybrid Control for Bridges**
(Chairmen : Okahara, M. and Feng, M. Q.)

J-20) Effectiveness of the Variable Damper for Reducing Seismic Response of Highway Bridges
(Kawashima, K., Unjoh, S., Iida, H. and Mukai, H.)

J-21) Active Control of Seismic Response of Structure with Base Isolation System
(Sato, T. and Toki, K.)

U-9) Use of Variable Dampers for Earthquake Protection of Bridges
(Shinozuka, M. and Ghanem, R.)

U-10) Hybrid Control of Sliding Isolated Bridges
(Reinhorn, A. M., Nagarajaiah, S., Riley, M. A. and Subramaniam, R.)

15:30 Break

15:40 **Session-10 Comparative Design Example**
(Chairmen : Nakano, O. and Mahin, S.)

U-11) Bridge Design Example-1
(Mayes, R. L.)

U-12) Bridge Design Example-2
(Constantinou, M. C., Tsopelas, P. C. and Ozaki, D.)

J-22) Design Example of A Highway Bridge Based on Manual of Menshin Design of Highway Bridges
(Kawashima, K. and Okado, M. and Horikawa, M.)

16:40 Visit to Laboratories
a) Shaking Table Laboratory
(Shaking Table Test of A Model Bridge with Variable Damper)
b) Earthquake Engineering Laboratory

17:30 **Closing Session**
(Chairmen : Kawashima, K. and Buckle, I. G.)

18:00 Closure
18:05 Leave PWRI
18:20 Arrive Hotel Sunroute

19:00 Reception Hosted by U.S. Side
(Restaurant Isami)

TECHNICAL STUDY-TOUR

December 9 (WED)

9:00	Leave Hotel at Tsukuba Science City for Yama-age Bridge (by Bus)
11:00	Visit to Yama-age Bridge Yama-age Bridge (Base Isolated Bridge under Construction. Forced Excitation Test will be made at the time of visit.)
12:00	Lunch
13:00	Forced Excitation Test
15:00	Leave the Site for Tokyo (by Bus)
17:30	Arrive at Tokyo (Check in Hotel, Ginza Dai-ichi Hotel)

December 10 (THU)

9:00	Leave Hotel
10:00	Visit to Construction Site of A Base-Isolated Bridge by Metropolitan Expressway Public Corporation (MEPC) (by Bus)
12:00	Lunch
14:00	Visit to a Base Isolated Bridge of MEPC (by Bus)
15:00	Visit to Construction Site of a Suspension Bridge of MEPC (by Bus)
17:00	Arrive at Hotel (Ginza Dai-ichi Hotel)

December 11 (FRI)

9:00	Leave Hotel
10:00	Visit to a Construction Site of A Cable-Stayed Bridge of MEPC (by Bus)
12:00	Lunch
13:30	Kawasaki St.
14:00	Visit to a Construction Site of Trans-Tokyo Bay Highway (Bay Cruise)
17:00	Kawasaki St.
18:00	Arrive at Hotel (Ginza Dai-ichi Hotel)

PARTICIPANTS IN THE WORKSHOP

PARTICIPANTS FROM THE U.S. SIDE

Prof. Ahmed Abdel-Ghaffar
Professor of Civil Engineering
Kaprielian Hall
University of Southern California
Los Angeles, CA 90089-2531

Dr. Ian D. Aiken
Earthquake Engineering Research Center
University of California
1301 South 46th Street
Richmond, CA 94804

Prof. Ian G. Buckle
Professor of Civil Engineering
105 Red Jacket Quadrangle
State University of New York at Buffalo
Buffalo, NY 14261

Mr. James Cooper
Acting Chief
Structures Division
Federal Highway Administration(HNR-10)
6300 Georgetown Pick
McLean, VA 22101

Prof. Maria Q. Feng
Professor of Civil Engineering
University of California
Irvine, CA 92717

Dr. S.-C. Liu
Program Director
Earthquake Hazard Mitigation
National Science Foundation
1800 G Street, N.W., Room 1132
Washington, DC 20550

Prof. Stephen A. Mahin
Professor of Civil Engineering
771 Davis Hall
University of California
Berkeley, CA 94720

Prof. Emmanuel (Manos) Maragakis
Professor of Civil Engineering
University of Nevada
Reno, NV 89557

Dr. Ronald L. Mayes
President
Dynamic Isolation Systems
2855 Telegraph Avenue, Suite 410
Berkeley, CA 94705

Dr. Satish Nagarajaiah
243 Ketter Hall
State University of New York at Buffalo
Buffalo, NY 14260

Dr. W. H. Robinson
New Zealand Institute for Industrial Research and Development
PO Box 31 310, Lower Hutt,
New Zealand

Mr. Michael Robinson
New Zealand Institute for Industrial Research and Development
PO Box 31 310, Lower Hutt,
New Zealand

Mr. Harry (Tripp) Shenton
Research Structural Engineer
Building 226, Room B158
National Institute of Standards and Technology
Gaithersburg, MD 20899

Prof. Masanobu Shinozuka
Professor of Civil Engineering
Princeton University
Princeton, NJ 08544

Mr. Mark Yashinsky
Division of Structures
California Department of
Transportation
P.O.Box 942874
Sacramento, CA 94274-0001

(In alphabetical order)

PARTICIPANTS FROM THE JAPAN SIDE

Mr. Hisakazu OHISHI
Director
Road Disaster Prevention Section
Planning Division
Road Bureau
Ministry of Construction Proper
Kasumiga-seki Chiyoda-ku, Tokyo,
Japan, 100

Mr. Ryoji HATTORI
Assistant Director
Road Disaster Prevention Section
Planning Division
Road Bureau
Ministry of Construction Proper
Kasumiga-seki Chiyoda-ku, Tokyo,
Japan, 100

Mr. Kakihiko KAWATA
Chief Official
Road Disaster Prevention Section
Planning Division
Road Bureau
Ministry of Construction Proper
Kasumiga-seki Chiyoda-ku, Tokyo,
Japan, 100

Mr. Yoshikazu KITAGAWA
Director
International Institute of Seismology
and Earthquake Engineering
Building Research Institute
Ministry of Construction
1, Tatehara, Tsukuba-shi, Ibaraki,
Japan, 305

Mr. Yukihiko SUMIYOSHI
Director-General
Public Works Research Institute
Ministry of Construction
1, Asahi, Tsukuba-shi, Ibaraki,
Japan, 305

Mr. Hiroshi KONO
Deputy Director-General
Public Works Research Institute
Ministry of Construction
1, Asahi, Tsukuba-shi, Ibaraki,
Japan, 305

Dr. Takashi IIJIMA
Assistant Director-General
Public Works Research Institute
Ministry of Construction
1, Asahi, Tsukuba-shi, Ibaraki,
Japan, 305

Mr. Hiroaki KOJIMA
Director of General Affairs
Public Works Research Institute
Ministry of Construction
1, Asahi, Tsukuba-shi, Ibaraki,
Japan, 305

Mr. Masahide TAMURA
Director of Planning and Research
Administration Department
Public Works Research Institute
Ministry of Construction
1, Asahi, Tsukuba-shi, Ibaraki,
Japan, 305

Mr. Tadahiko FUJISAWA
Research Coordinator for Advanced
Technology
Planning and Research Administration
Department
Public Works Research Institute
Ministry of Construction
1, Asahi, Tsukuba-shi, Ibaraki,
Japan, 305

Mr. Akira FUJIMOTO
Coordinator for International Cooperation
Planning and Research Administration Department
Public Works Research Institute
Ministry of Construction
1, Asahi, Tsukuba-shi, Ibaraki,
Japan, 305

Mr. Nobuhiko TANIGUCHI
Bridge Instructor
Planning and Research Administration Department
Public Works Research Institute
Ministry of Construction
1, Asahi, Tsukuba-shi, Ibaraki,
Japan, 305

Mr. Nozomu MORI
Head
Planning Division
Planning and Research Administration Department
Public Works Research Institute
Ministry of Construction
1, Asahi, Tsukuba-shi, Ibaraki,
Japan, 305

Mr. Kenji SUZUKI
Assistant Head
Planning Division
Planning and Research Administration Department
Public Works Research Institute
Ministry of Construction
1, Asahi, Tsukuba-shi, Ibaraki,
Japan, 305

Mr. Noriaki AOYAMA
Chief
International Research Section
Planning Division
Planning and Research Administration Department
Public Works Research Institute
Ministry of Construction
1, Asahi, Tsukuba-shi, Ibaraki,
Japan, 305

Mr. Hiroo KANZAKI
Director of Road Department
Public Works Research Institute
Ministry of Construction
1, Asahi, Tsukuba-shi, Ibaraki,
Japan, 305

Mr. Yutaka ANZAKI
Research Coordinator for Road Traffic
Road Department
Public Works Research Institute
Ministry of Construction
1, Asahi, Tsukuba-shi, Ibaraki,
Japan, 305

Mr. Tetsuo MATSUMURA
Research Coordinator for Traffic Safety
Road Department
Public Works Research Institute
Ministry of Construction
1, Asahi, Tsukuba-shi, Ibaraki,
Japan, 305

Mr. Minoru FUJIWARA
Director of Structure and Bridge Department
Public Works Research Institute
Ministry of Construction
1, Asahi, Tsukuba-shi, Ibaraki,
Japan, 305

Dr. Michio OKAHARA
Head
Foundation Engineering Division
Structure and Bridge Engineering Department
Public Works Research Institute
Ministry of Construction
1, Asahi, Tsukuba-shi, Ibaraki,
Japan, 305

Dr. Hiroshi SATOH
Head
Structure Division
Structure and Bridge Engineering Department
Public Works Research Institute
Ministry of Construction
1, Asahi, Tsukuba-shi, Ibaraki,
Japan, 305

Mr. Kazuhiro NISHIKAWA
Head
Bridge Division
Structure and Bridge Engineering Department
Public Works Research Institute
Ministry of Construction
1, Asahi, Tsukuba-shi, Ibaraki,
Japan, 305

Mr. Yutaka IIDA
Director of Earthquake Disaster Prevention Department
Public Works Research Institute
Ministry of Construction
1, Asahi, Tsukuba-shi, Ibaraki,
Japan, 305

Mr. Ken-ichi TOKIDA
Head
Ground Vibration Division
Earthquake Disaster Prevention Department
Public Works Research Institute
Ministry of Construction
1, Asahi, Tsukuba-shi, Ibaraki,
Japan, 305

Dr. Kazuhiko KAWASHIMA
Head
Earthquake Engineering Division
Earthquake Disaster Prevention Department
Public Works Research Institute
Ministry of Construction
1, Asahi, Tsukuba-shi, Ibaraki,
Japan, 305

Dr. Keiichi TAMURA
Senior Research Engineer
Ground Vibration Division
Earthquake Disaster Prevention Department
Public Works Research Institute
Ministry of Construction
1, Asahi, Tsukuba-shi, Ibaraki,
Japan, 305

Mr. Yoshio NINOMIYA
Senior Research Engineer
Ground Vibration Division
Earthquake Disaster Prevention Department
Public Works Research Institute
Ministry of Construction
1, Asahi, Tsukuba-shi, Ibaraki,
Japan, 305

Mr. Masuo KONDOH
Research Engineer
Ground Vibration Division
Earthquake Disaster Prevention Department
Public Works Research Institute
Ministry of Construction
1, Asahi, Tsukuba-shi, Ibaraki,
Japan, 305

Mr. Seitaroh YOSHIMI
Research Engineer
Ground Vibration Division
Earthquake Disaster Prevention Department
Public Works Research Institute
Ministry of Construction
1, Asahi, Tsukuba-shi, Ibaraki,
Japan, 305

Mr. Hidemi FUKADA
Assistant Research Engineer
Ground Vibration Division
Earthquake Disaster Prevention Department
Public Works Research Institute
Ministry of Construction
1, Asahi, Tsukuba-shi, Ibaraki,
Japan, 305

Mr. Takuo AZUMA
Assistant Research Engineer
Ground Vibration Division
Earthquake Disaster Prevention Department
Public Works Research Institute
Ministry of Construction
1, Asahi, Tsukuba-shi, Ibaraki, Japan, 305

Mr. Shigeki UNJOH
Senior Research Engineer
Earthquake Engineering Division
Earthquake Disaster Prevention Department
Public Works Research Institute
Ministry of Construction
1, Asahi, Tsukuba-shi, Ibaraki, Japan, 305

Mr. Hideki SUGITA
Research Engineer
Earthquake Engineering Division
Earthquake Disaster Prevention Department
Public Works Research Institute
Ministry of Construction
1, Asahi, Tsukuba-shi, Ibaraki, Japan, 305

Mr. Junichi HOSHIKUMA
Research Engineer
Earthquake Engineering Division
Earthquake Disaster Prevention Department
Public Works Research Institute
Ministry of Construction
1, Asahi, Tsukuba-shi, Ibaraki, Japan, 305

Mr. Tomoru NAKAJIMA
Research Engineer
Earthquake Engineering Division
Earthquake Disaster Prevention Department
Public Works Research Institute
Ministry of Construction
1, Asahi, Tsukuba-shi, Ibaraki, Japan, 305

Mr. Hiroyuki IIDA
Research Engineer
Earthquake Engineering Division
Earthquake Disaster Prevention Department
Public Works Research Institute
Ministry of Construction
1, Asahi, Tsukuba-shi, Ibaraki, Japan, 305

Mr. Hidetoshi MUKAI
Assistant Research Engineer
Earthquake Engineering Division
Earthquake Disaster Prevention Department
Public Works Research Institute
Ministry of Construction
1, Asahi, Tsukuba-shi, Ibaraki, Japan, 305

Mr. Kazuhiro NAGAYA
Assistant Research Engineer
Earthquake Engineering Division
Earthquake Disaster Prevention Department
Public Works Research Institute
Ministry of Construction
1, Asahi, Tsukuba-shi, Ibaraki, Japan, 305

Mr. Ryoichi KUROSAKI
Earthquake Disaster Prevention Department
Public Works Research Institute
Ministry of Construction
1, Asahi, Tsukuba-shi, Ibaraki, Japan, 305

Ms. Yoriko MORI
Earthquake Disaster Prevention Department
Public Works Research Institute
Ministry of Construction
1, Asahi, Tsukuba-shi, Ibaraki, Japan, 305

Ms. Misako IKEDA
Earthquake Engineering Division
Earthquake Disaster Prevention Department
Public Works Research Institute
Ministry of Construction
1, Asahi, Tsukuba-shi, Ibaraki, Japan, 305

Ms. Kyoko SAITOH
Earthquake Engineering Division
Earthquake Disaster Prevention Department
Public Works Research Institute
Ministry of Construction
1, Asahi, Tsukuba-shi, Ibaraki, Japan, 305

Prof. Kenzoh TOKI
Professor
Disaster Prevention Research Institute
Kyoto University
Kyoto, Japan, 611

Prof. Tadanobu SATOH
Associate Professor
Disaster Prevention Research Institute
Kyoto University
Kyoto, Japan, 611

Prof. Hirokazu IEMURA
Associate Professor
Department of Civil Engineering
Kyoto University
Yoshida-hon-machi, Sakyo-ku,
Kyoto-Shi, Japan, 606

Prof. Eiichi KURIBAYASHI
Professor
Department of Civil Engineering
Toyohashi University of Science and Technology
Toyohashi, Japan, 440

Prof. Masanori HAMADA
Professor
School of Marine Science and Technology
Tokai University
3-20-1 Orido, Shimizu-shi, Shizuoka, Japan, 424

Dr. William T. TANZO
Research Associate
Department of Construction Engineering
Saitama University
255, Shimo-ohkubo, Urawa-shi, Saitama, Japan, 338

Dr. Toshio IWASAKI
Advisor
Highway Industry Department Organization
1-25-5 Toranomon, Minato-ku, Tokyo, Japan, 105

Mr. Osamu NAKANO
Head
Structures Section
Structures Division
Civil Engineering Research Institute
Hokkaido Developing Agency
1-3, Hiragishi, Toyohira-ku,
Sapporo, Japan, 062

Mr. Hiroaki NISHI
Research Engineer
Structures Section
Structures Division
Civil Engineering Research Institute
Hokkaido Developing Agency
1-3, Hiragishi, Toyohira-ku,
Sapporo, Japan, 062

Mr. Hiroshi HARA
Chief Engineer
Numazu Construction Office
Shizuoka Prefectural Government
Numazu, Shizuoka, Japan, 410

Mr. Norio UZUKA
Manager
Road Construction Division
Department of Public Works,
Tochigi Prefectural Government
Utsunomiya, Tochigi, Japan, 320

Mr. Kazuhiko KAWAKAMI
Chief
Road Construction Division
Department of Public Works,
Tochigi Prefectural Government
Utsunomiya, Tochigi, Japan, 320

Mr. Kazuomi KUMAKURA
Senior Officer
Road Construction Division
Department of Public Works,
Tochigi Prefectural Government
Utsunomiya, Tochigi, Japan, 320

Mr. Tetsuo MATSUDA
Head
Bridge Section
Research Institute of Japan Highway
Public Corporation
1-4-1, Tadao, Machida-shi, Tokyo,
Japan, 194

Mr. Akira MURAYAMA
Bridge Section
Research Institute of Japan Highway
Public Corporation
1-4-1, Tadao, Machida-shi, Tokyo,
Japan, 194

Mr. Hirofumi ANDOH
Bridge Section
Research Institute of Japan Highway
Public Corporation
1-4-1, Tadao, Machida-shi, Tokyo,
Japan, 194

Mr. Nobuo KUBOTA
Manager
Design Division
Bay-Shore Route Construction Bureau
Metropolitan Expressway Public
Corporation
1-11-11, Shiba, Minato-ku,
Tokyo, Japan, 105

Mr. Yuzuru MITAKE
Design Division
Bay-Shore Route Construction Bureau
Metropolitan Expressway Public
Corporation
1-11-11, Shiba, Minato-ku,
Tokyo, Japan, 105

Mr. Atsushi NANJO
Chief Engineer
Design Section
Engineering Division
Hanshin Expressway Public
Corporation
4-1-3 Kyutaro-cho Chuo-ku,
Osaka, Japan, 541

Mr. Motohiko NISHIBAYASHI
Engineer
Design Section
Engineering Division
Hanshin Expressway Public
Corporation
4-1-3 Kyutaro-cho Chuo-ku,
Osaka, Japan, 541

Mr. Ikuo KOMATSU
Engineer
Design Section
First Osaka Construction Division
Hanshin Expressway Public
Corporation
4-1-3 Kyutaro-cho Chuo-ku,
Osaka, Japan, 541

Mr. Furitsu YASUDA
Engineer
Shin-Yodogawa Construction Office
Third Osaka Construction Division
Hanshin Expressway Public Corporation
4-1-3 Kyutaro-cho Chuo-ku,
Osaka, Japan, 541

Mr. Syuji MIZOBUCHI
Engineer
Maintenance Engineering Section
Maintenance & Facility Design Division
Hanshin Expressway Public Corporation
4-1-3 Kyutaro-cho Chuo-ku,
Osaka, Japan, 541

Dr. Yukitake SHIOI
General Manager
Design and Engineering Department
Trans-Tokyo Bay Highway Corp.
15-5 Ichibancho, Chiyoda-ku, Tokyo,
Japan, 102

Mr. Osamu YOSHIDA
Manager
Bridge Design Division,
Design Department
Trans-Tokyo Bay Highway Corp.
15-5 Ichibancho, Chiyoda-ku, Tokyo,
Japan, 102

Mr. Masayuki HONMA
Assistant Manager
Bridge Design Division,
Design Department
Trans-Tokyo Bay Highway Corp.
15-5 Ichibancho, Chiyoda-ku, Tokyo,
Japan, 102

Dr. Hideyo SUZUKI
Chief Researcher
Architecture Department
Engineering Research Center
Tokyo Electric Power Co. Inc.
r2-4-1 Nishi-tutujigaoka, Chofu-shi,
Tokyo, Japan, 182

Mr. Yozo GOTO
Manager
The 5 th Civil Engineering Division
Technical Research Institute
Obayashi Corporation
4-640, Shimokiyoto, Kiyose-shi,
Tokyo, Japan, 204

Mr. Toshio KIKUCHI
Chief Researcher
The 5 th Civil Engineering Division
Technical Research Institute
Obayashi Corporation
4-640, Shimokiyoto, Kiyose-shi,
Tokyo, Japan, 204

Mr. Syun-ichi HIGUCHI
Researcher
Technical Research Institute,
Obayashi Corporation
4-640, Shimokiyoto, Kiyose-shi,
Tokyo, Japan, 204

Mr. Susumu OKAMOTO
Research Engineer
Earthquake Engineering Team
Earthquake & Wind Engineering Research Group
Technology Research Center
Taisei Corporation
344-1, Nasemachi, Totsuka-ku,
Yokohama, Japan, 245

Mr. Atsuyuki TSUKAMOTO
Engineer(Bridges)
Civil Engineering Design Dept.
Civil Engineering Div.
Taisei Corporation
1-25-1, Nishishinjuku Shinjuku-ku,
Tokyo, Japan, 163-06

Mr. Tetsuo TAKEDA
Chief Earthquake Engineering Section
Civil Engineering Department I
Kajima Technical Research Institute
Kajima Corporation
2-19-1, Tobitakyu, Choufu-shi,
Tokyo, Japan, 182

Mr. Toshimichi ICHINOMIYA
Research Engineer
Civil Engineering Department
Kajima Technical Research Institute
Kajima Corporation
2-19-1, Tobitakyu, Chofu-shi,
Tokyo, Japan, 182

Mr. Katsuhisa KANDA
Research Engineer
Earthquake & Soil Dynamics
Kobori Research Complex
Kajima Corporation
6-5-30, Akasaka, Minato-ku
Tokyo, Japan

Mr. Yoshitake SAWAUCHI
Assistant Manager
Engineering Development Department
Civil Engineering Design Division
Kajima Corporation
6-5-30, Akasaka, Minato-ku
Tokyo, Japan, 107

Mr. Katsuyuki DEWA
Manager
Design Department of Civil Engineering Division
Shimizu Corporation
1-2-3, Shibaura, Minato-ku
Tokyo, Japan, 105-07

Mr. Minoru SHIMADA
Design Chief
Design Department of Civil Engineering Division
Shimizu Corporation
1-2-3, Shibaura, Minato-ku
Tokyo, Japan, 105-07

Mr. Michio SUGIMOTO
Chief Research Engineer
Takenaka Technical Research Institute
Takenaka Corporation
2-5-14, Minamisuna, Koto-ku
Tokyo, Japan, 136

Mr. Takashi HIRAI
Research Engineer
Takenaka Technical Research Institute
Takenaka Corporation
2-5-14, Minamisuna, Koto-ku
Tokyo, Japan, 136

Mr. Hiroshi TUNEKAWA
Research Engineer
Takenaka Technical Research Institute
Takenaka Corporation
2-5-14, Minamisuna, Koto-ku
Tokyo, Japan, 136

Mr. Isao KAMEKO
Research Engineer
Research Department of Civil Structures
Institute of Construction Technology
Kumagai Gumi Co., Ltd.
1043 Shimoyama, Onigakubo
Tsukuba-shi, Ibaraki , Japan, 300-22

Mr. Yositaka ADACHI
Research Engineer
Research Department of Civil Structures
Institute of Construction Technology
Kumagai Gumi Co., Ltd.
1043 Shimoyama, Onigakubo
Tsukuba-shi, Ibaraki , Japan, 300-22

Dr. Masaaki YOSHIKAWA
Manager
Technical Management Section
Tukuba Research Institute
Okumura Corporation
387 Ohsuna, Tsukuba-shi, Ibaraki,
Japan, 300-33

Mr. Katsumi MATSUBARA
First Research Department
Hazama Corporation
4-17-23, Honmachi-Nishi
Yono-shi, Saitama
Japan, 338

Mr. Hideo ARAI
Deputy Manager
Section 2
Civil Engineering Department
Construction & Engineering Division
Civil Engineering Operations
Sumitomo Construction Co., Ltd.
13-4, Araki, Shinjyuku-ku
Tokyo, Japan, 160

Mr. Hiroshi MASUKO
Assistant Manager
Section 2
Civil Engineering Department
Construction & Engineering Division
Civil Engineering Operations
Sumitomo Construction Co., Ltd.
13-4, Araki, Shinjyuku-ku
Tokyo, Japan, 160

Mr. Takashi TAMURA
Civil Engineer
Design Section 2
Civil Engineering Design Div.
Mitusi Construction Co., Ltd.
3-10-1, Iwamoto-cho, Chiyoda-ku,
Tokyo, Japan, 101

Mr. Tamotsu TAMURA
Civil Engineer in Earthquake
Engineering
Research and Development Division
Engineering Research Institute
Penta-Ocean Construction Co., Ltd.
1-11-25 Higashi-oki,
Shinagawa-ku, Tokyo, Japan, 140

Mr. Akio KIMIJIMA
Assistant General Manager
Engineering Design Dept.
Engineering Division
Nippon Chuzo K K.
2-1, Shiroishi-Cho, Kawasaki-ku
Kawasaki-shi, Kanagawa, Japan, 210

Mr. Shin-ichi IZUMA
Manager
Engineering Design Dept.
Engineering Division
Nippon Chuzo K K.
2-1, Shiroishi-cho, Kawasaki-ku
Kawasaki-shi, Kanagawa,
Japan, 210

Mr. Jiro MATSUDA
Deputy Manager
Second Group
Forgings & Castings Sales Dept.
The Japan Steel Works, Ltd.
1-1-2, Yuuraku-cho, Chiyoda-ku
Tokyo, Japan, 100

Dr. Tatsumasa TAKATU
General Manager
Bridge Construction &
Engineering Dept.
NKK Corporation
2-1, Suehiro-cho Tsurumi-ku, Yokohama,
Japan, 230

Mr. Kazuo ENDOH
Chief Engineer
Construction Materials Dept.
The Yokohama Rubber Co., Ltd.
2-1, Oiwake, Hiratsuka-shi
Kanagawa, Japan, 254

Mr. Masahiro KOSHITOGE
Testing Division
MB Material Development Dept.
The Yokohama Rubber Co., Ltd.
2-1, Oiwake, Hiratsuka-shi
Kanagawa, Japan, 254

Mr. Michio ASAMI
Project Manager
Construction Materials Dept.
The Yokohama Rubber Co., Ltd.
2-1, Oiwake, Hiratsuka-shi
Kanagawa, Japan, 254

Mr. Norio KAWAI
Manager
Chemical/Industrial Products Division
Technical Department
Toyo Tire & Rubber Co., Ltd.
302 Sasayamagahara, Irima-shi,Saitama,
Japan, 358

Mr. Yoritaka SASAKI
Manager
Chemical/Industrial Products Division
Technical Department
Toyo Tire & Rubber Co., Ltd.
302 Sasayamagahara, Irima-shi,Saitama,
Japan, 358

Mr. Yoji SUIZU
Senior Research Engineer
Research & Development
Bridgestone Corporation
3-1-1, Ogawa-higashi-machi
Kodaira-shi, Tokyo
Japan, 187

Mr. Kengo GODA
Research & Development
Bridgestone Corporation
3-1-1, Ogawa-higashi-machi
Kodaira-shi, Tokyo
Japan, 187

Mr. Hiroshi KAWAKAMI
Manager
Seismic Isolation Bearing
Development Group
Bridgestone Corporation
1, Kashi-cho, Totsuka-ku
Yokohama, Japan, 244

Mr. Chiaki SUDOH
Engineer
New Products Development
(Seismic Isolation)
Bridgestone Corporation
1, Kashi-cho, Totsuka-ku
Yokohama, Japan, 244

Mr. Nobuo MUROTA
Engineer
Seismic Isolation Bearing Development
Bridgestone Corporation
1, Kashi-cho, Totsuka-ku
Yokohama, Japan, 244

Mr. Seiich KONDOH
Engineer
New Products Development
Bridgestone Corporation
1, Kashi-cho, Totsuka-ku
Yokohama, Japan, 244

Mr. Yutaka MAKIGUCHI
Staff Manager
Technical Development Dept. 2
Oiles Corporation
8, Kirihara-cho, Fujisawa-city
Kanagawa, Japan, 252

Mr. Ikuo SHIMODA
Manager
Development Section
Structural Equipment Division
Oiles Corporation
8, Kirihara-cho, Fujisawa-city
Kanagawa, Japan, 252

Mr. Takehiro SHIROSAKI
Manager
Research & Development Sec. 1
Research & Development Dept.
Oiles Corporation
8, Kirihara-cho, Fujisawa-city
Kanagawa, Japan, 252

Dr. Mituaki SAEKI
Director
Earthquake Disaster Mitigation
Section
Civil Engineering Dept.
Japan Engineering Consultants
Co., Ltd.
5-33-11, Hon-cho, Nakano-ku, Tokyo,
Japan, 164

Mr. Iwao KAWASAKI
Assistant Manager
Bridge & Structural Design Section
Civil Engineering Dept.
Japan Engineering Consultants Co., Ltd.
5-33-11, Hon-cho, Nakano-ku, Tokyo, Japan, 164

Mr. Takamura IGUCHI
Manager
Engineering Department
B. B. M. Corporation
1-3-3, Yaesu, Chuo-ku
Tokyo, 103

Mr. Hidero HAINO
Chief Engineer
Bridge Design Section
B. B. M. Corporation
1-3-3, Yaesu, Chuo-ku
Tokyo, 103

Mr. Kenji TANAKA
Assistant Manager
Bridge Design Section
B. B. M. Corporation
1-3-3, Yaesu, Chuo-ku
Tokyo, 103

Mr. Ichiro NISHIKAWA
Manager
Metal Research & Development Dept.
Showa Electric Wire & Cable Co., Ltd.
4-1-1, Minami-hashimoto, Sagamihara
Kanagawa, Japan, 229

Mr. Yoshitaka MURAMASHU
Functional Materials 2nd Lab.
Metal Research & Development Dept.
Showa Electric Wire & Cable Co., Ltd.
4-1-1, Minami-hashimoto, Sagamihara
Kanagawa, Japan, 229

Mr. Keiichi TAKAYAMA
Manager
Engineering Section
Mold & Vibration Isolation System Dept.
Showa Electric Wire & Cable Co., Ltd.
4-1-1, Minami-hashimoto, Sagamihara
Kanagawa, Japan, 229

Mr. Naoki KATOH
Engineering Section
Mold & Vibration Isolation System Dept.
Showa Electric Wire & Cable Co., Ltd.
4-1-1, Minami-hashimoto, Sagamihara
Kanagawa, Japan, 229

Mr. Akio HAYASHI
Registered Consulting Engineer
Pacific Consultants Co., Ltd.
7-5, Sekido 1-chome, Tama-shi, Tokyo, Japan, 206

Mr. Hiroshige UNO
Deputy Manager
Research and Development Division
Sogo Engineering Inc.
3-5-9 Higashi Nakajima
Higashiyodogawa-ku, Osaka, Japan, 533

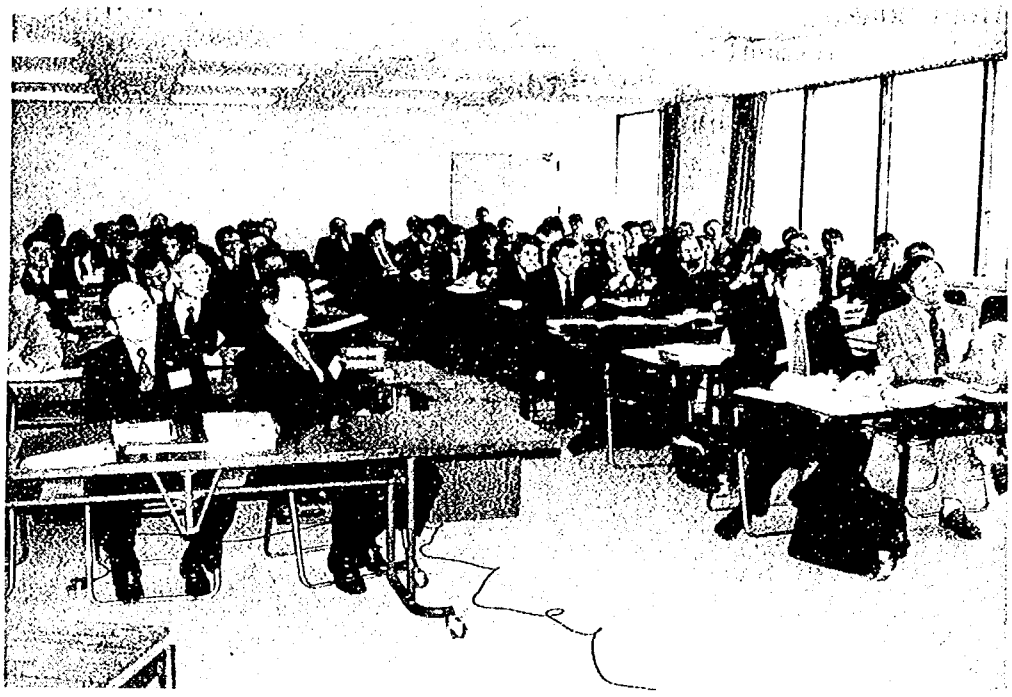
Mr. Mitsuo OKADO
Assistant Manager
New Structural Engineering Co., Ltd.
12, Niban-cho, Chiyoda-ku, Tokyo, Japan, 102

Mr. Michihiro HORIKAWA
New Structural Engineering Co., Ltd.
12, Niban-cho, Chiyoda-ku, Tokyo, Japan, 102

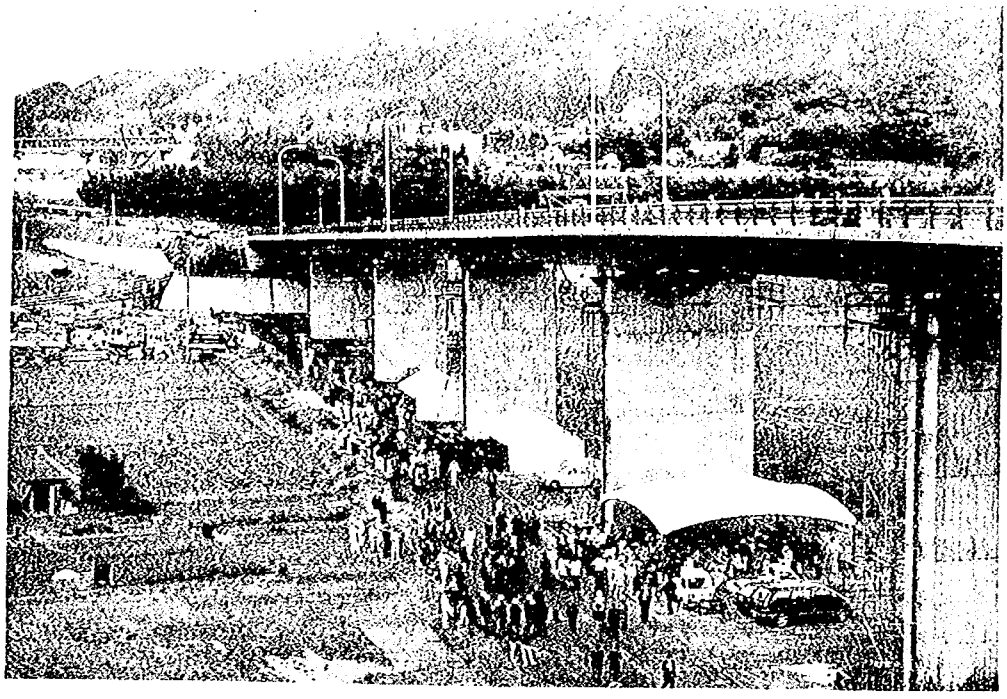
Mr. Yoshifumi UNO
Chief Engineer
Kawaguchi Metal Industries Co., Ltd.
No.7-18 2-Chome Shibata, Kita-ku, Osaka, Japan, 533

Mr. Kelichi HONMA
Engineering Department
Kawaguchi Metal Industries Co., Ltd.
18-19, Miya-cho, Kawaguchi-shi,
Saitama, Japan, 332

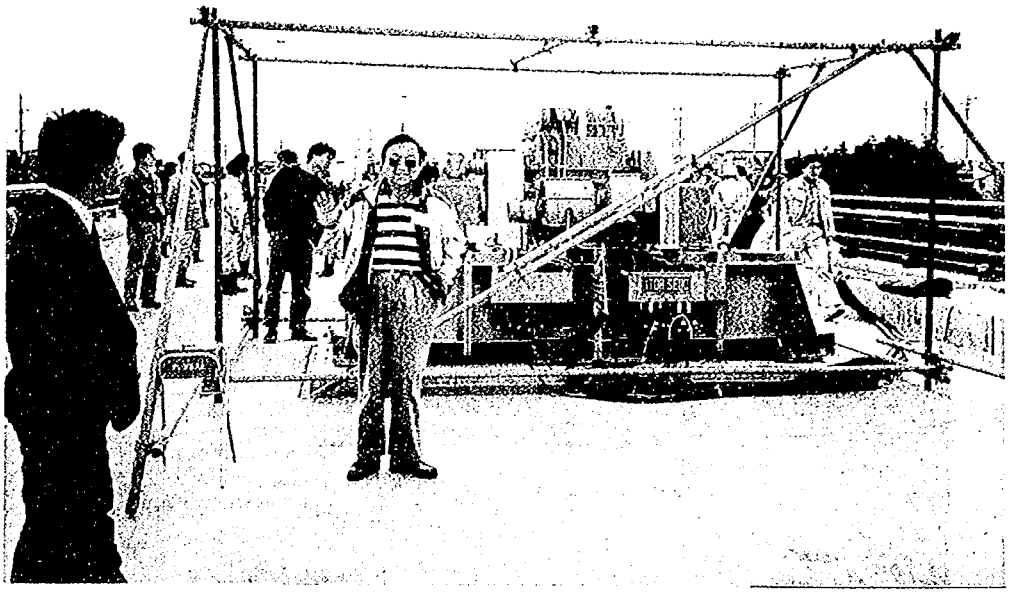


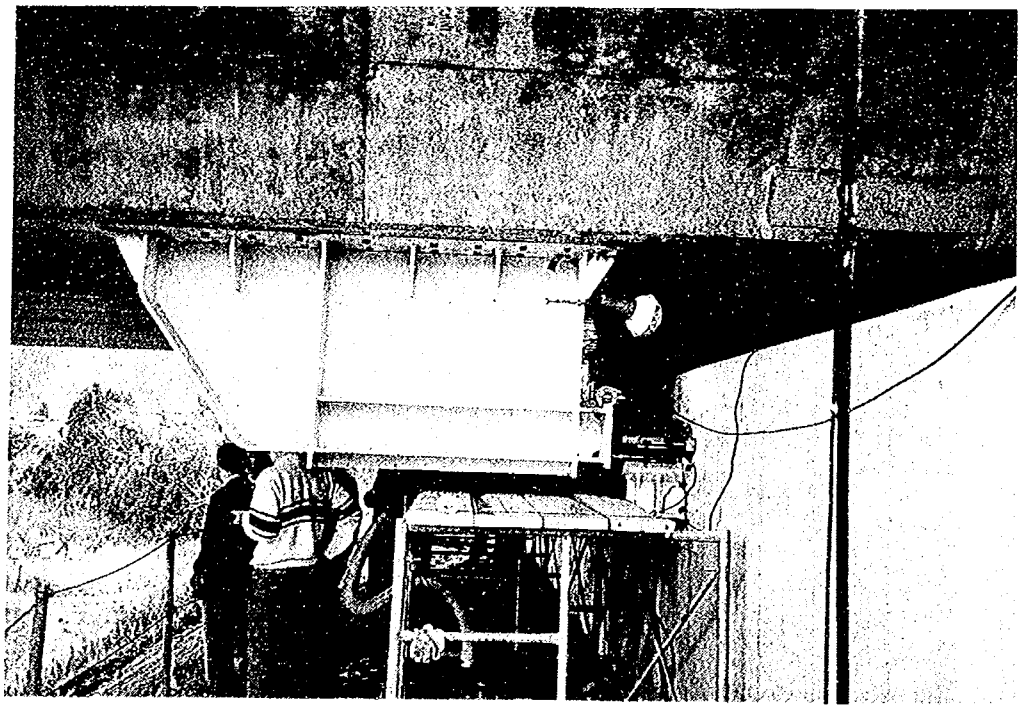


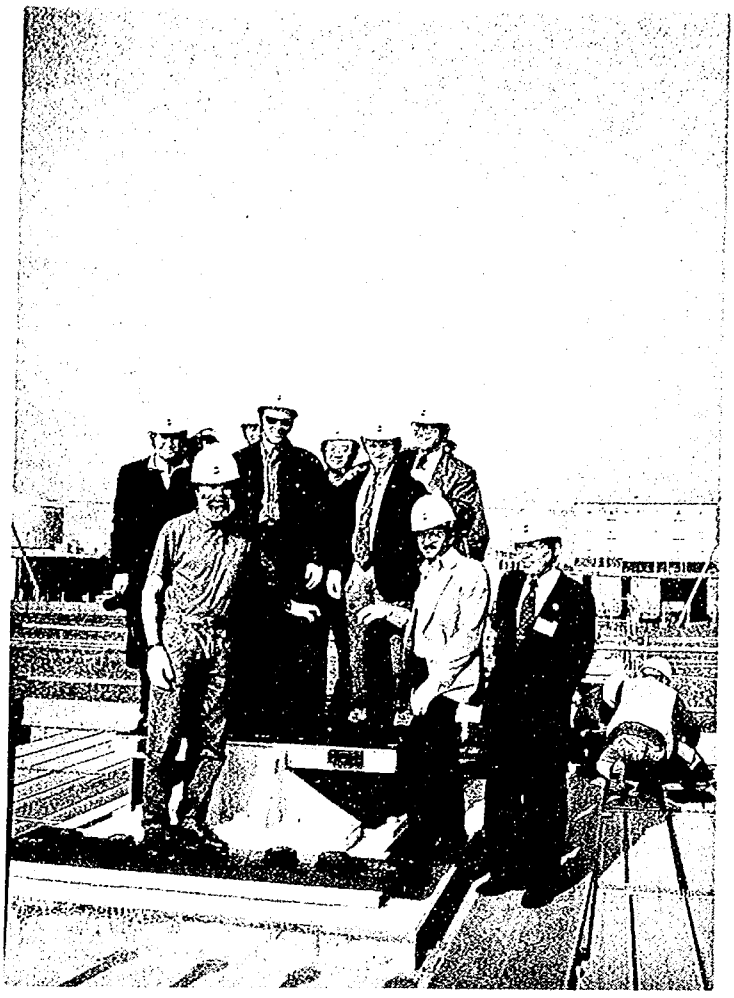






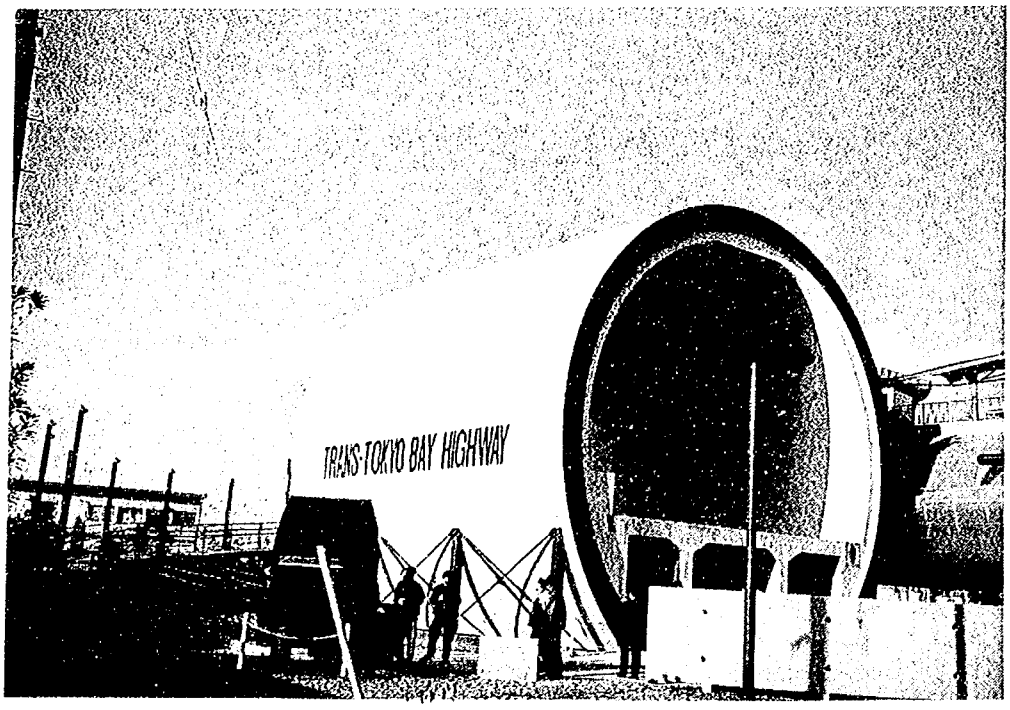











TRANS-TOKYO BAY HIGHWAY

PROCEEDING OF THE SECOND U.S.-JAPAN WORKSHOP ON EARTHQUAKE PROTECTIVE SYSTEMS FOR BRIDGES

ISSN 0386-5878
Technical Memorandum of PWRI No. 3196

Kazuhiko Kawashima, Shigeki Unjoh, Hiroyuki Iida and Hidetoshi Mukai

This proceedings document the results of the Second U.S.-Japan Workshop on Earthquake Protective Systems for Bridges. The workshop was held at PWRI in Tsukuba Science City, Japan, between December 7 and 8, 1992, and was organized by the task Committee G "Passive, Active and Hybrid Control Systems", Panel on Wind and Seismic Effects, UJNR.

郵便はがき

Postage stamp

〒305-□□

建設省土木研究所地震防災部耐震研究室
〒305 茨城県つくば市大字旭1番地

Earthquake Engineering Division,
Public Works Research Institute
Tsukuba Science City
Japan 305

No. 889

No. 889

配布先氏名

配布先住所

Receipt of

Technical Memorandum of PWRI No. 3196

Name .....

Address .....

.....